

Studies in Systems, Decision and Control 338

Alla G. Kravets
Alexander A. Bolshakov
Maxim Shcherbakov *Editors*

Cyber-Physical Systems: Modelling and Intelligent Control

 Springer

Studies in Systems, Decision and Control

Volume 338

Series Editor

Janusz Kacprzyk, Systems Research Institute, Polish Academy of Sciences,
Warsaw, Poland

The series “Studies in Systems, Decision and Control” (SSDC) covers both new developments and advances, as well as the state of the art, in the various areas of broadly perceived systems, decision making and control—quickly, up to date and with a high quality. The intent is to cover the theory, applications, and perspectives on the state of the art and future developments relevant to systems, decision making, control, complex processes and related areas, as embedded in the fields of engineering, computer science, physics, economics, social and life sciences, as well as the paradigms and methodologies behind them. The series contains monographs, textbooks, lecture notes and edited volumes in systems, decision making and control spanning the areas of Cyber-Physical Systems, Autonomous Systems, Sensor Networks, Control Systems, Energy Systems, Automotive Systems, Biological Systems, Vehicular Networking and Connected Vehicles, Aerospace Systems, Automation, Manufacturing, Smart Grids, Nonlinear Systems, Power Systems, Robotics, Social Systems, Economic Systems and other. Of particular value to both the contributors and the readership are the short publication timeframe and the world-wide distribution and exposure which enable both a wide and rapid dissemination of research output.

Indexed by SCOPUS, DBLP, WTI Frankfurt eG, zbMATH, SCImago.

All books published in the series are submitted for consideration in Web of Science.

More information about this series at <http://www.springer.com/series/13304>

Alla G. Kravets · Alexander A. Bolshakov ·
Maxim Shcherbakov
Editors

Cyber-Physical Systems: Modelling and Intelligent Control

 Springer

Editors

Alla G. Kravets
Volgograd State Technical University
Volgograd, Russia

Alexander A. Bolshakov
Peter the Great St. Petersburg Polytechnic
University
St. Petersburg, Russia

Maxim Shcherbakov 
Volgograd State Technical University
Volgograd, Russia

ISSN 2198-4182

ISSN 2198-4190 (electronic)

Studies in Systems, Decision and Control

ISBN 978-3-030-66076-5

ISBN 978-3-030-66077-2 (eBook)

<https://doi.org/10.1007/978-3-030-66077-2>

© The Editor(s) (if applicable) and The Author(s), under exclusive license to Springer Nature Switzerland AG 2021

This work is subject to copyright. All rights are solely and exclusively licensed by the Publisher, whether the whole or part of the material is concerned, specifically the rights of translation, reprinting, reuse of illustrations, recitation, broadcasting, reproduction on microfilms or in any other physical way, and transmission or information storage and retrieval, electronic adaptation, computer software, or by similar or dissimilar methodology now known or hereafter developed.

The use of general descriptive names, registered names, trademarks, service marks, etc. in this publication does not imply, even in the absence of a specific statement, that such names are exempt from the relevant protective laws and regulations and therefore free for general use.

The publisher, the authors and the editors are safe to assume that the advice and information in this book are believed to be true and accurate at the date of publication. Neither the publisher nor the authors or the editors give a warranty, expressed or implied, with respect to the material contained herein or for any errors or omissions that may have been made. The publisher remains neutral with regard to jurisdictional claims in published maps and institutional affiliations.

This Springer imprint is published by the registered company Springer Nature Switzerland AG
The registered company address is: Gewerbestrasse 11, 6330 Cham, Switzerland

Preface

The main focus of cyber-physical systems development is related to improving approaches for its modelling and control. New types of systems combining physical and digital components as well as everywhere data collecting push to rethinking about procedures for creating, controlling, maintenance, and support during all lifecycle. The contribution of the book is in presenting scientific research results in the field of applications for cyber-physical systems design and intelligent control in different domains.

The book contains 28 original chapters where authors discuss the results covering both theoretical and practical aspects. The part Cyber-Physical Systems Modelling includes chapters with fundamental scientific research improving the design stage of cyber-physical systems. The part Cyber-Physical Systems Intelligent Control covers theoretical impacts to control theory regarding systems of Industry 4.0. Excellent results for space cyber-physical systems presented in the third part of the book named Modelling and Intelligent Control for Space Exploration. The last part discusses interesting results on the implementation of a novel design approach and intelligent control approach for such domain as hybrid electric vehicle design, design of agriculture robots, telecommunication systems, aircraft manufacturing, complex equipment control, and so on.

The book is directed to researchers and practitioners in artificial intelligence and machine learning, as it describes results that can be applied in cyber-physical systems design and intelligent control.

Edition of the book is dedicated to the 130th Anniversary of Kazan National Research Technological University and the 35th Anniversary of Computer-Aided Department at Volgograd State Technical University. Also, it is technically supported by the Project Laboratory of Cyber-Physical Systems of Volgograd State Technical University.

Volgograd, Russia
St. Petersburg, Russia
Volgograd, Russia
January 2021

Alla G. Kravets
Alexander A. Bolshakov
Maxim Shcherbakov

Contents

Cyber-Physical Systems Modeling

Numerical Simulation of Distributed Devices for the Processing of UltraWideband Information	3
Sergey L. Chernyshev and Igor B. Vlasov	
Significant Uniformity Digital Models on the Set of Probabilistic Points	11
Valery Kuznetsov, Valery Pesoshin, Artyom Gumirov, and Darya Shirshova	
The Multiplicative-Isolating Principle of Significantly Nonlinear Mathematical Models Creation	23
Rudolf Neydorf, Anatoly Gaiduk, and Nikita Gamayunov	
Numerical Approaches to Solving a Non-linear System of Schrödinger Equations	33
Airat Sakhabutdinov, Vladimir Anfinogentov, Oleg Morozov, and Robert Gubaydullin	
Research of the Boundary Value Problem for the Sophie Germain Equation in a Cyber-Physical System	51
Andrey Ushakov	
Modeling of Vibration Separation of Bulk Materials Based on the Theory of Random Processes	65
Fail Akhmadiev, Renat Gizzyatov, and Ilshat Nazipov	
Cyber-Physical Systems Intelligent Control	
Forecast Evaluation Techniques for I4.0 Systems	79
Andrey Davydenko, Cuong Sai, and Maxim Shcherbakov	

Classification of the Technological Process Condition Based on Hybrid Neural Networks	103
Andrey Puchkov, Maxim Dli, and Yekaterina Lobaneva	
Fuzzy Rules Reduction in Knowledge Bases of Decision Support Systems by Objects State Evaluation	113
Maria Dagaeva and Aleksey Katasev	
Conversion of CGA Models to Jordan Controlled Form for Design Significantly Nonlinear Control Systems	125
Rudolf Neydorf, Anatoly Gaiduk, Sergey Kapustyan, and Nikita Kudinov	
Searching and Selection of a Flexible Manufacturing System by Means of Frame Model	139
J. F. Mammadov, K. S. Abdullaev, U. H. Agaev, I. R. Aliev, and G. G. Huseynova	
Robust Autonomous Control of a Multiply Connected Technological Object with Input Delays	153
I. V. Gogol, O. A. Remizova, V. V. Syrokvashin, and A. L. Fokin	
Bee-Inspired Algorithm for Groups of Cyber-Physical Robotic Cleaners with Swarm Intelligence	167
Oleg Yu. Maryasin	
Modeling the Highly Effective Object for Continuous Compaction Control of the Cyber-Physical Road-Construction System	179
Andrey Prokopen, Zhasurbek Nabizhanov, Rurik Emelyanov, and Vladimir Ivanchura	
Modelling and Intelligent Control for Space Exploration	
Creation of a Simulation Model of Spacecrafts' Navigation Referencing to the Digital Map of the Moon	193
Alexey Andreev, Natalya Demina, Yury Nefedyev, Natalya Petrova, and Arthur Zagidullin	
Information Technology Concept of Integration of Computing Resources and Physical Processes in Cyber-Physical Systems for Personalized Information About the Potential Danger of an Emergency Situation in High-Altitude Flight	205
Nikolai Markov, Alexey Bogomolov, Anatoly Shishov, and Mikhail Dvornikov	
The Use of the Synthetic Method of Harmonic Analysis for Investigating the Structure of Space Natural Bodies	215
Natalya Demina and Alexey Andreev	

The Study of Geodynamic Parameters on the Basis of Adaptive Regression Modeling 225
 Yury Nefedyev, Regina Mubarakshina, Alexey Andreev, and Natalya Demina

The Use of Huber’s Method for Estimating Libration Selenographic Parameters 237
 Konstantin Churkin and Yury Nefedyev

Cyber-Physical Resolution Evaluation System for Digital Aerophotographic Systems 247
 Evgeniy Chausov and Andrey Molchanov

Modelling and Intelligent Control Implementation

Configuring Systems Based on Petri Nets, Logic-Probabilistic, and Simulation Models 257
 Irina Bondareva, Anna Khanova, and Yulya Khanova

Intelligent Robots Coalition Formation in Cyberphysical Space for Emergency Response 267
 Alexander Smirnov, Nikolay Teslya, and Anna Motienko

Aircraft Flight Safety Control Methodology 283
 Aleksey Kulik

The Applying of the Formalism of Cyber-Physical Systems in the Description of Hydrodynamic Cavitation in a Direct-Flow Valve 295
 A. B. Kapranova, A. E. Lebedev, A. M. Melzer, S. V. Neklyudov, and A. S. Brykalov

Analysis of Conjectural Variations in Nonlinear Stackelberg Duopoly Model for Cyber-Physical Systems in Telecommunications Markets 309
 Mikhail Geraskin

Functional Model for the Formation of Individual Metal Control Programs of Boiler Equipment 323
 V. D. Belov and E. R. Moshev

Statistical Precision-Recall Curves for Object Detection Algorithms Performance Measurement 335
 Anna A. Kuznetsova

YOLOv5 versus YOLOv3 for Apple Detection 349
 Anna Kuznetsova, Tatiana Maleva, and Vladimir Soloviev

Cyber-Physical Systems Modeling

Numerical Simulation of Distributed Devices for the Processing of UltraWideband Information



Sergey L. Chernyshev and Igor B. Vlasov

Abstract A mathematical model of a smooth irregular line with distributed parameters is considered, on which ultra-wideband information is recorded in the form of a change in wave parameters. The numerical solution of the differential equation makes it possible to determine the law of this change. As a result, when an ultra-wideband signal is input to such a line, the reflected signal carries the recorded information.

Keywords Ultrawideband signal · Irregular distributed line · Wave parameters · Reflection coefficient · Numerical solution · Mathematical model

1 Introduction

Ultrawideband (UWB) technologies are gaining increasing application [1–7]. The relative frequency band of ultra-wideband signals exceeds 50% [8]. The IEEE 802.15.4a/b standard provides ultra-wideband wireless communications at speeds up to 500 Mbps [9, 10]. UWB devices are also used when processing signals in radar [11, 12] and when creating antennas [13–15]. In these cases, it is possible to use digital processing if the frequency band occupied by the signal allows the use of an ADC. In the case of a wider frequency band, when such ADCs do not exist, either a stroboscopic signal processing method or UWB irregular distributed lines are used, on which the necessary information is recorded. The characteristics of such lines are formed on the basis of cyber-physical principles, due to distributed parameters [16]. Such lines must be synthesized according to a given frequency dependence of the reflection coefficient [17]. However, one of the main difficulties in creating devices on such lines is the need to solve a differential equation that describes such lines [18]. This equation has the form of Riccati and does not have a general analytical solution.

S. L. Chernyshev (✉) · I. B. Vlasov
Bauman Moscow State Technical University, 5, 2nd Baumanskaya Str, Moscow, Russia
e-mail: chernshv@bmstu.ru

I. B. Vlasov
e-mail: vlasovbmstu@mail.ru

In the particular case, after presentation through power series [19], this solution can be found, however, a direct solution to this equation is possible only numerically. This chapter is devoted to this numerical solution and numerical simulation.

2 The Differential Equation of an Irregular Line

Figure 1 shows the dependence of the wave parameters ($\rho(x)$ —wave resistance, $\beta(x)$ —propagation constant) on the longitudinal coordinate in an irregular distributed line. An electromagnetic wave propagating along this line receives numerous reflections, and as a result, a reflected wave is formed that carries information about the line configuration.

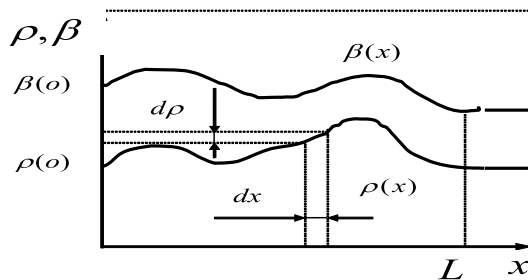
Creating of the necessary configuration allows to record information on the line that the incident ultra-wideband signal will read. When information is entered into the incident signal, its corresponding processing in such a line will occur. However, to record information on an irregular line, it is necessary to develop a method for synthesizing this line, as a result of which the desired dependence is found. Information recording consists in providing the required frequency dependence of the complex reflection coefficient from the input of the line. For such a synthesis, it was required to find the dependence of the internal parameters of the irregular line with this reflection coefficient. The conducted studies consisted in finding a mathematical model of an irregular line in the form of a differential equation. For such a synthesis, it was required to find the dependence of the internal parameters of the irregular line with this reflection coefficient. The conducted studies consisted in finding a mathematical model of an irregular line in the form of a differential equation.

A Riccati-type differential equation describing an irregular non-dissipative transmission line has the form [18]:

$$\frac{\partial \ln(\partial F_{11}(\omega, x)/\partial S_{11}(\omega, x))}{\partial S_{11}(\omega, x)} = 2 \left(\frac{1}{S_{11}^*(\omega, x)} - S_{11}(\omega, x) \right)^{-1}, \quad (1)$$

where $S_{11}(\omega, x)$ —is the reflection coefficient from the input of the line with a length x , ω —is the circular frequency, $F_{11}(\omega, x)$ —is the function depending on the internal

Fig. 1 The dependence of the wave parameters of an irregular line from the longitudinal coordinate



parameters of the line:

$$F_{11}(\omega, x) = \int_0^x N(y) \exp \left[-2j \int_0^y \beta(\omega, z) dz \right] dy,$$

where $N(x) = \frac{1}{2} \frac{d \ln \rho(x)/\rho(0)}{dx}$ —the so-called local reflection function.

Equation (1) represents the differential equation at the partial complex variable. In this case, the variable depends on two arguments, of which the argument ω is fixed, and the differentiation of functions is carried out by the argument x . Equation (1) can be converted into the following form, more convenient for synthesis:

$$\frac{\partial^2 F_{11}(\omega, \tau)}{\partial S_{11}^2(\omega, \tau)} = \frac{2S_{11}^*(\omega, \tau)}{1 - |S_{11}(\omega, \tau)|^2} \frac{\partial F_{11}(\omega, \tau)}{\partial S_{11}(\omega, \tau)}. \quad (2)$$

Differentiation of complex functions in this equation is carried out in a new private argument

$$\tau = 2x/V_f(x),$$

where $V_f(x)$ —is the phase velocity of the wave propagating in the line. With this definition, the variable represents the delay time of the wave reflected from the cross section of the irregular line with coordinate x .

The general form of the solution of Eq. (2) has the form

$$F_{11}(\omega, \tau) = \int_0^\tau \frac{\partial S_{11}(\omega, t)}{\partial t} \exp \left[\int_0^t \frac{2S_{11}^*(\omega, v)}{1 - |S_{11}^2(\omega, v)|} \frac{\partial S_{11}(\omega, v)}{\partial v} dv \right] dt. \quad (3)$$

This expression implies integration and differentiation with respect to the current coordinate, while the integrands assume knowledge of the line configuration, which is not possible in advance. This fact leads to the need for a numerical solution and the development of an appropriate synthesis algorithm.

3 Description of the Algorithm

The algorithm assumes the following sequence of actions.

1. The search for the necessary line configuration is carried out as a result of synthesis. The criterion of optimality is to provide input line reflection coefficients $S_{11}(\omega_n, \theta)$ given at reference frequencies ω_n with a given accuracy.
2. The solution to Eq. (2) is to find the function $F_{11}(\omega, \tau)|_{\tau=\theta}$, where $\theta = 2L/V_f(L)$ —double wave delay at full line length L .

3. This function, as shown in [17, 18], allows one to find the function of local line reflections through the inverse Fourier transform:

$$4. N(\tau) = \frac{1}{2\pi} \int_{-\infty}^{\infty} F_{11}(\omega, \theta) e^{j\omega\tau} d\omega, \quad \tau = [0; \theta]. \quad (4)$$

5. The necessary law for changing the wave resistance of an irregular line that implements a given frequency dependence of the complex reflection coefficient $S_{11}(\omega, \theta)$ is determined as follows:

$$6. \rho(\tau) = \rho(0) e^{2 \int_0^\tau N(t) dt}.$$

Thus, the described algorithm for synthesizing an irregular line from a given frequency dependence of the complex reflection coefficient includes a solution to Eq. (2), which does not have an analytical solution and requires a numerical solution.

In the numerical solution, we use the Newton-Raphson method. When iterating closer to the solution, the function $F_{11}(S_{11})$ will take values $F_{11(k)}(S_{11})$, where k is the iteration number $k = 1, 2, \dots$. By expanding the function $F_{11(k)}(S_{11})$ in a series around the point $F_{11(k-1)}(S_{11})$ and restricting ourselves to a second-order term, we obtain

$$\begin{aligned} F_{11(k)}(S_{11}) &= F_{11(k-1)}(S_{11}) + \left. \frac{\partial F_{11}}{\partial S_{11}} \right|_{k-1} (S_{11}(\omega_n, \theta) - S_{11(k-1)}) \\ &\quad + \frac{1}{2} \left. \frac{\partial^2 F_{11}}{\partial S_{11}^2} \right|_{k-1} (S_{11}(\omega_n, \theta) - S_{11(k-1)})^2. \end{aligned}$$

If we express the second derivative from Eq. (2), we obtain

$$\begin{aligned} F_{11(k)}(S_{11}) &= F_{11(k-1)}(S_{11}) + \left. \frac{\partial F_{11}}{\partial S_{11}} \right|_{k-1} (S_{11}(\omega_n, \theta) - S_{11(k-1)}) \\ &\quad \left[1 + \frac{S_{11(k-1)}^*}{1 - |S_{11(k-1)}|^2} (S_{11}(\omega_n, \theta) - S_{11(k-1)}) \right], \quad (5) \end{aligned}$$

where $S_{11}(\omega_n, \theta)$ is the specified value of the coefficient of reflection from the line at the reference frequency ω_n $n = 1, 2, \dots M$.

Iterative procedures (5) are carried out at each of the reference frequencies ω_n .

For such a solution, it is necessary to set some dependence as the initial dependence $N_0(\tau)$. We find this initial approximation based on the equality found in [19] $F_{11}(\omega, \theta) = e^{j\varphi_{11}(\omega, \theta)} \text{Arth}|S_{11}(\omega, \theta)|$, where $\varphi_{11}(\omega, \theta) = \arg S_{11}(\omega, \theta)$, and applying Eq. (2). For this line configuration, using chain theory methods we find $S_{11(0)}(\omega, \tau)$ —the reflection coefficient from the line of initial.

Note that the derivative in (5) can be found from expression (3) by differentiating its left and right parts:

$$\left. \frac{\partial F_{11}(\omega_n, \tau)}{\partial S_{11}(\omega_n, \tau)} \right|_{k-1} = \exp \left[\int_0^\tau \frac{2S_{11(k-1)}^*(\omega, t)}{1 - |S_{11(k-1)}(\omega, t)|^2} \frac{\partial S_{11(k-1)}(\omega, t)}{\partial t} dt \right].$$

The integral in this equation is calculated numerically, since the dependence $S_{11(k-1)}(\omega_n, \tau)$, which is the complex reflection coefficient of the line with the length τ at the $(k - 1)$ -th iteration, is determined for the dependence $N_{k-1}(\tau)$ that was found earlier at the same iteration.

The numerical solution occurs relatively quickly, at 3–4 iterations, which is explained by the choice of a good initial approximation, which is so necessary for the Newton-Raphson method, which is one of the fastest among nonlinear optimization methods.

The optimality criterion for this algorithm is to minimize the residuals and fall into the acceptability region $\sum_{n=1}^N |S_{11(k)}(\omega_n, \theta) - S_{11}(\omega_n, \theta)|^2 < \varepsilon$, where ε = is the given accuracy.

Figure 2 shows a simplified block diagram of the described algorithm.

After finding the function $F_{11}(\omega, \tau)|_{\tau=\theta}$, we find the local reflection function $N(\tau)$ using transformation (4). Knowing $N(\tau)$, we find the law of change in the wave resistance of an irregular distributed line, which allows you to implement the information recorded on the line.

As an example, Fig. 3 shows the dependence of the width of a microstrip irregular distributed line on a substrate 1 mm high with a dielectric constant of 9.8, synthesized from a given frequency dependence, the amplitude-frequency and phase-frequency characteristics of which are shown in Fig. 4a, b.

4 Conclusion

The distributed nature of irregular lines implementing the cyberphysical principles of processing ultra-wideband information required the solution of a non-linear Riccati-type equation and the implementation of an algorithm for its numerical solution. Such a numerical model made it possible to synthesize irregular lines in order to record the necessary ultra-wideband information.

The information that must be recorded on an irregular line is the aforementioned frequency dependence of the complex reflection coefficient $S_{11}(\omega, \theta)$, which provides the conversion of the signal incident on the line.

So, if the spectrum of the incident ultra-wideband signal is equal $a(\omega)$, then the reflected signal will have a spectrum $b(\omega) = S_{11}(\omega)a(\omega)$, and in the time domain the signal $b(t) = \int_0^t g_{11}(\tau)a(t - \tau)d\tau$ will be reflected, where $g_{11}(t)$ is the impulse response of the reflection line. The synthesis of such irregular lines based on the

Fig. 2 The simplified scheme of the algorithm

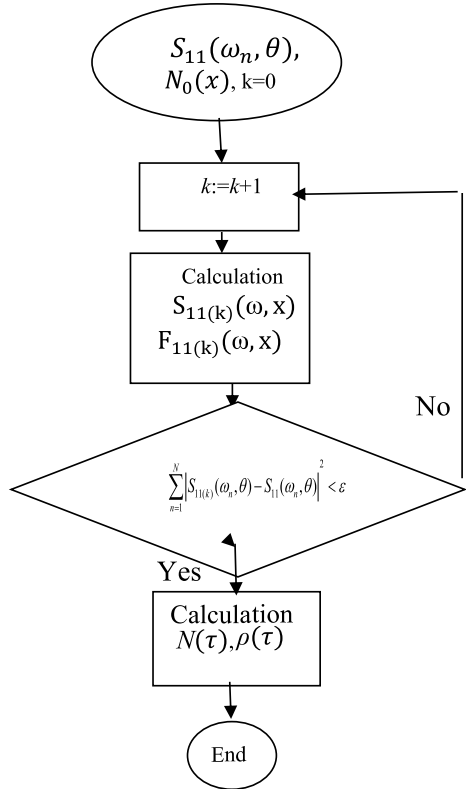
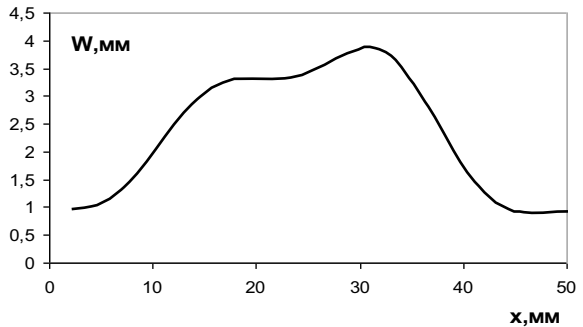
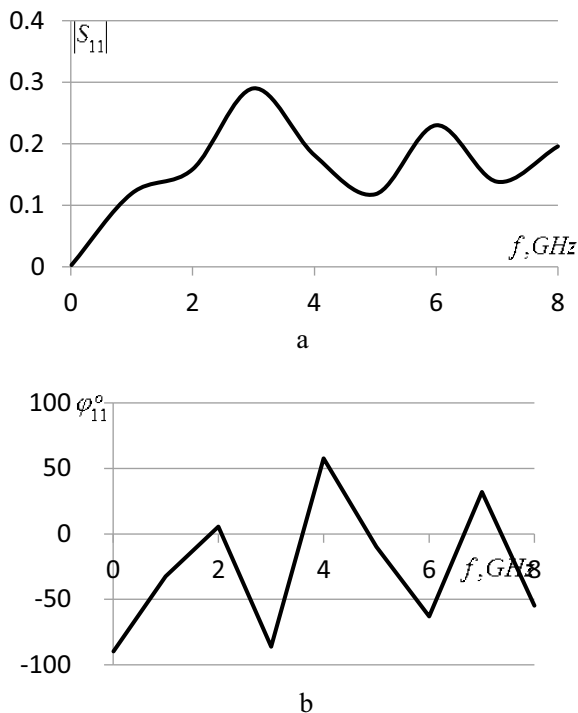


Fig. 3 The dependence of the width of the synthesized microstrip line



numerical solution of differential Eq. (2) allows the processing of information of ultra-wideband signals.

Fig. 4 Frequency dependences: **a** amplitude-frequency, **b** phase-frequency



References

1. Russian SCRF Decision # 09-05-02 dated 15 Dec 2009
2. US Federal Communications Commission (FCC) Decision № FCC 02-48 from 02.14.2002
3. Taylor, J.D.: Introduction to ultra-wideband radar systems. CRC Press LLC. 1995
4. Ghavami, M., Michael, L.B. Kohno, R.: UWB signals and systems in communication engineering, 354 p. Wiley publishing, London (2006)
5. Scholtz, R.A., Pozar, D.M.: Won namgoong. Ultra wideband radio. EURASIP J. Appl. Sign. Process. Hindawi Publishing Corporation, pp. 252–272 (2005)
6. Hirt, W.: Ultra-wideband radio technology: overview and future research. Comput. Commun. **26**(1), 46–52 (2003)
7. Recommendation ITU-R SM.1755-0. Characteristics of ultra-wideband technology (2006) www.itu.int
8. Aiello, R., Batra, A.: Ultra wideband systems. Newnes-Elsevier, 341 p (2006)
9. Meschanov, V.P., Metelnikova, I.V., Tupikin, V.D., Chumaevskaya, G.G.: A new structure of microwave ultra-wideband differential shifter. IEEE Trans. Autom. Contr. **MTT-42**(5), 762 (1994)
10. Roy, S., Foerster, J.R., Somayazulu, V.S., Leeper, D.G.: Ultrawideband radio design: the promise of high-speed, short-range wireless connectivity. Proc. IEEE **92**(2), 295–311 (2004)
11. Mroue, A., Heddebaut, M., Elbahhar, F., Rivenq, A., Rouvaen, J.-M.: Automatic radar target recognition of objects falling on railway tracks. Meas. Sci. Technol. (2012). <https://doi.org/10.1088/0957-0233/23/2/025401>
12. Chernyshev, S.L.: Applying matched filtering for processing ultra-wideband signals. Sci. Educ. Sci. Publ. BMSTU **10**, 315–324 (2013)

13. Chernyshev, S.L., Vilenskiy, A.R.: Development and research of a modified Vivaldi antenna as part of an X-band flat broadband antenna array. *Sci. Educ. Sci. Publ. BMSTU* **11**, 44 (2011)
14. Liang, X.L.: Ultra-wideband antenna and design. *IntechOpen*. <https://doi.org/10.5772/47805> (2012)
15. Chernyshev, S.L., Vilenskiy, A.R.: Investigation of balanced printed slot antennas as part of a traveling-wave broadband antenna array X-band. *Radio Eng.* **11**, 118–122 (2013)
16. Chernyshev, S.: Cyber-physical principles of information processing in ultra-wideband systems. *Stud. Syst. Decis. Contr.* **260**, 3–10 (2020)
17. Isaev, V.M., Semenchuk, V.V., Meshchanov, V.P., Shikova, L.V.: UltraWideband fixed phase shifters based on coupled transmission lines with stubs. *J. Commun. Tech. Electron.* **60**(6), 566–571 (2015)
18. Chernyshev, S.L., Vilenskiy, A.R.: Analysis and synthesis of ultra-wideband devices in the frequency domain. *Bulletin of the Moscow State Technical University named after N.E. Bauman. Series: Instrument Making, No. A. P.* 150 (2009)
19. Chernyshev, S.L.: The synthesis of ultra-wideband devices in frequency domain. In: *Proceedings of 4th International Conference on Ultrawideband and Ultrashort Impulse Signals, Sevastopol, Ukraine, pp. 207–209. Sept 2008*

Significant Uniformity Digital Models on the Set of Probabilistic Points



Valery Kuznetsov , Valery Pesoshin, Artyom Gumirov,
and Darya Shirshova

Abstract The applicability of the statistical method for determining the significant homogeneity of binary sequences under probabilistic moments of any finite order for solving problems of mathematical modeling of stochastic objects is proved. Approaches to the construction of the homogeneity criterion in the framework of various ways of setting probabilistic moments are described. Significant differences between the Central probabilistic moments' initial decompositions for systems of random events of homogeneous character and digital models of processes are revealed. Brief theses of methods for finding the critical length of samples within which binary sequences have significant homogeneity over the specified raw or central probabilistic moments are presented. Areas of application of the concept of homogeneity of random sequences in classical simulation and creation of objects of cyber-physical systems are noted.

Keywords Simulation · Probabilistic moment · Raw moment · Central moment · Significant homogeneity · Homogeneity criterion · Cyber-physical system

1 Introduction

Traditionally, methods of statistical testing and simulation modeling in modern settings [1] require the formation of multi-dimensional ensembles of random

V. Kuznetsov (✉) · V. Pesoshin · A. Gumirov · D. Shirshova
Kazan National Research Technical University Named After A.N. Tupolev, 10 K.Marx St., Kazan,
Tatarstan 420111, Russia
e-mail: kuznet_evm@mail.ru

V. Pesoshin
e-mail: pesoshin-kai@mail.ru

A. Gumirov
e-mail: neporebrik@mail.ru

D. Shirshova
e-mail: einstein@mail.ru

sequences both in terms of the power of the set-theoretic representation in the space of discrete States, and in terms of the complexity of distributions of durations of all components in the clock time dimension [2, 3]. In response to the development of the theory and expansion of the practice of machine experiments in all areas of activity of individual societies and society as a whole, the phenomenon of global digitalization has emerged. This was reflected in the info-communication activity of a person in the areas of management, maintenance, design, production, and operation of cyber-physical objects, which was formed by the concept of “industry 4.0” [4, 5]. Typical, however, biased by the concepts of “digital doppelganger” and “digital shadow” had well-known components of the simulation experiment in the form of digital models of objects and processes oriented to modern technology development and production implementation of business projects. The mentioned paradigm of a symbiosis of applied modeling and production organization significantly increases the requirements for the adequacy of similarity to real objects and processes that exhibit, as a rule, random behavior [6–8]. The resulting uniqueness of the necessary probability and correlation properties of processes forces developers of computer simulation experiments to select programs that are adequate to these algorithms or develop new ones.

The simplest ways to meet the requirements of the problem setters are implemented by the developers of the machine experiment by selecting a minimum set of sequences based on the Bernoulli independent test scheme. Technically, this is achieved by implementing deterministic algorithms for obtaining pseudo-random numbers [3, 9, 10] or hardware generation of truly random sequences [9, 11–14], which reproduce the known postulates of Golomb S.W. [9, 15], which approximate the artificial nature of the generated sequences to the ideal model of a random signal like “white noise” [11, 12, 14].

Kolmogorov A. N. and Uspensky V. A. gave a strict mathematical form for describing the Bernoulli properties of binary sequences [16]. They defined three properties of randomness in terms of set-theoretic representation and algorithmic computability: typicality, randomness, and stochasticity. Understanding the General sample as a sequence of infinite length, the authors of the algorithmic randomness theory attributed these three properties to a particular sample in the form of a chain of finite length as a fragment of an infinite sequence.

Parallelization of algorithms for pseudo-random sequence generators by organizing multi-core, vector, cluster, and multiprocessor processing certainly reduces the time costs of simulation, but it comes at the cost of hardware resources of very expensive computers. The question arises, is it not possible to use the finiteness factor of samples of simulating sequences to simplify the algorithms for their formation and, due to this, combine several different sequences into one?

Indeed, the shorter the sample, the wider the dispersion spread of statistical estimates of probabilistic parameters of different random sequences, among which it is possible to establish the fact of indistinguishability of two or more samples with lengths not exceeding a certain critical value, with a given confidence.

2 Statistically Significant Sequence Uniformity

The task of determining the homogeneity of two sequences of probabilistic-statistical nature $\langle a \rangle$ and $\langle b \rangle$ the selected qualifying parameters is set. These parameters can be, for example, the mathematical expectations of the base and alternative sequences (BS and AS). For binary sequences, they coincide with the probabilities of occurrence of one, respectively, P_a and P_b . We show the universality of the probability of elementary and complex events as a qualifying parameter when testing for homogeneity in moments of not only the first but also higher finite order.

The main independent variable n is the length of the partial retrieval. The simulation model takes the probability from the BS P_a in the form of statistical estimates at the time of implementation of the n model tact, i.e. $P_a \rightarrow P_a^*(n)$. Same for AS: $P_b \rightarrow P_b^*(n)$. We provide for restrictions of the form τ_{\max} when investigating the homogeneity of autocorrelation properties, via second-order moment functions, and a limit n_{\max} for n . From the conditions of the paradigm adopted in machine modeling of a particular class of stochastic objects, a typical level of significance of the homogeneity criterion α is set, as the probability of an error of the first kind.

The approach used in nonparametric criteria [17–19] is based on calculations of empirical statistics that are directly proportional to the average values of discrepancies of qualifying parameters and inversely proportional to the value of the variance spread of estimates of discrepancies. The final procedure of the criterion is to test the hypothesis of homogeneity by comparing the value of the obtained statistics with a critical level that takes into account the specified significance.

This problem provides for multiple tests of hypotheses based on statistics in the form of the ratio of functions of the expected differs in probability estimates $\Delta P^* \rightarrow P_a^*(n) - P_b^*(n)$ and the estimate of the standard deviation of this difference depending on n , i.e.

$$t_{emp}(n) \rightarrow M_{\Delta P^*}^*(n) / \sqrt{D_{\Delta P^*}^*(n)} \quad (1)$$

The empirical material for this statistics is provided by forming a sufficient set of samples of elements of the difference sequence of the form:

$$\langle d \rangle_n = \langle a \rangle_n - \langle b \rangle_n, \quad (2)$$

length n in ascending order from 1 to n_{\max} . The obtained numerical values (1) are compared with some critical value $t_{cr}(\alpha)$ that gives basis to accept or reject the null hypothesis H_0 about the homogeneity of the tested objects or, rejecting it, chooses a competing hypothesis H_1 , according to the conditions:

$$\left\{ \begin{array}{l} |t_{emp}| < t_{cr}, H_0, \max [n(|t_{emp}| < t_{cr})] = n_{cr}, \\ |t_{emp}| \geq t_{cr}, H_1, n = \overline{1, n_{max}}. \end{array} \right. \quad (3)$$

The meaningful result of the test is: “Both sequences on the sample length $n_{cr} = \max \lfloor n(|t_{emp}| < t_{cr}) \rfloor$ (or at least n_{\max}) are statistically homogeneous (belong to the same General population) with a degree of significance α ”.

Let’s consider the applicability of classical probabilistic moments of finite orders, paying special attention to binary structured digital models of processes in the form of binary sequences.

3 Raw Probabilistic Moments

It is accepted [17, 18] to represent the raw probability moment of order r of a discrete random variable A as

$$\nu_r(A) = \sum_{i=1}^u a_i^r \cdot p_i, \quad (4)$$

where u is the number of discreteness levels, p_i —is the probability of taking the value A of a_i —level, and the order of r is defined on the set of natural numbers.

The minimum value $u = 2$ corresponds to the binary character of the value A . Reducing by unit both summation limits in (4) and defining the alphabet $a_i \in \{0, 1\}$ for $i = 0, 1$, we present the following probability distribution: $\mathbf{P}\{A = 0\} = p_0$ and $\mathbf{P}\{A = 1\} = p_1$.

If to put $0^r = 0$ and $1^r = 1$, then it is true for any arbitrarily high finite order r in the form of a natural number:

$$\nu_r(A) = \nu_1(A) = \mathbf{M}[A] \text{ and } \mathbf{M}[A] = \mathbf{P}\{A = 1\} = p_1. \quad (5)$$

The system of k random discrete quantities A_1, A_2, \dots, A_k of the multilevel type ($u > 2$) is characterized by a mixed raw moment

$$\nu_r(A_1, A_2, \dots, A_k) = \sum_{i_1=0}^{u-1} \sum_{i_2=0}^{u-1} \dots \sum_{i_k=0}^{u-1} a_{1i_1}^{r_1} a_{2i_2}^{r_2} \dots a_{ki_k}^{r_k} p_{i_1 i_2 \dots i_k}, \quad (6)$$

where $r = \sum_{j=1}^k r_j$ is the order of the moment r_j as the sum of the r_j orders of the system elements A_j .

For a system of random binary quantities (at $u = 2$), the fixation of elementary components $r_j = 1$ for all $j = \overline{1, k}$ is obvious, which ensures that the dimension of the system is equal to its order, i.e. $r = k$. Then the mixed raw moment [20] of the binary system can be expressed based of the expression (6) in the form

$$\nu_r(A_1, A_2, \dots, A_r) = \sum_{i_1=0}^1 \sum_{i_2=0}^1 \dots \sum_{i_r=0}^1 a_{1i_1} a_{2i_2} \dots a_{ri_r} p_{i_1 i_2 \dots i_r}$$

or through mathematical expectation and probability of occurrence of a set of r units: $\nu_r(A_1, A_2, \dots, A_r) = \mathbf{M}[A_1 A_2 \dots A_r]$ and

$$\mathbf{M}[A_1 A_2 \dots A_r] = \mathbf{P}\{A_1 = 1, A_2 = 1, \dots, A_r = 1\} = p_{11\dots 1}. \quad (7)$$

The described moment is focused on single values of binary variables. However, along with the moment of the form (7), raw moments that allow inverse values of binary variables have the right to be used independently, for example, for $r = 4$:

$$\nu_4(A_1, \bar{A}_2, A_3, A_4) = \mathbf{P}\{A_1 = 1, A_2 = 0, A_3 = 1, A_4 = 1\} = p_{1011}. \quad (8)$$

Such binary combination systems and corresponding r -order probabilistic moments in 2^r quantity form a complete group of events.

4 The Relation Between Central Probabilistic Moments and Raw Moments

The simulation model, as an object of using random sequences, may require uniformity, not for the raw, but the central probability moment of the r th order of the general form $\mu_r(A) = \sum_{i=1}^u (a_i - v_1)^r p_i$ [14, 18]. In this case, binary forms of elementary variables in the central moment event $\mu_r(A) = \sum_{i=0}^1 (a_i - v_1)^r p_i$ do not allow one to reduce the homogeneity testing procedure to the same simple and technological actions with probabilities, as is achieved when specifying qualifying parameters by raw moments. However, using the expression of the central moment via the mathematical expectation operator $\mu_r(A) = \mathbf{M}[(A - v_1)^r]$, it is possible to obtain its decomposition into some raw moments of r th and smaller orders. So, in the literature on probability theory [17, 18], examples of decomposition of several central moments of small order into raw ones are given:

$$\mu_2 = v_2 - v_1^2, \quad \mu_3 = v_3 - 3v_1v_2 + 2v_1^3, \quad \mu_4 = v_4 - 4v_1v_3 + 6v_1^2v_2 - 3v_1^4. \quad (9)$$

The general expression of the central moment through the raw is well known:

$$\mu_r = \sum_{s=0}^r (-1)^s C_r^s v_{r-s} v_1^s. \quad (10)$$

In this case, random events in the abstract form of the probability-theoretic description assume full equality with each other, i.e. each element of the system experiences interdependence of all the others.

To processes the events of interest to us A_j , where $j = \overline{1, r}$, are separated by unidirectional discrete time τ , which disciplines the formation of a system of random binary quantities in the form of a chain $A_1 \longrightarrow \tau A_2 \longrightarrow \tau \dots, \longrightarrow \tau A_r$.

Also, for the completeness of the description of the sequence property by mixed probabilistic moments, it is necessary to introduce time distance control factors in the form of shifts of elements relative to each other by multiples of τ steps. One of the options for setting non-analyzed positions of binary combinations is implemented by the condition's validity $r_j = 0$. However, in this case, the binary alphabet of the sequence elements for the raw moments will trigger a formally undefined "zero to zero degree" action. To eliminate uncertainty, we change the membership r_j from the set of natural numbers (in particular, from a fixed value of 1) to the set of non-negative integers 0 and 1, which will allow us to mean $0^0 = 1$ and $0^1 = 0$.

Mutual relations between the events of the sequence are determined by different time distances ($\tau, 2\tau, 3\tau, \dots$), which violates their equal relations. However, a General representation of the sequence, as in the case of the formation of sets of abstract events decomposition of the central moment of r th order according to the formula (10), helps single ($C_r^0 = 1$) joining the initial point $v_r = p_{\underbrace{11\dots 1}_r}$ of the same

order as the term. So, for example, under $r = 2$ this $v_2 = p_{11}$. The formal invariance of the decomposition (10) also has the last two terms $s = r - 1, r$ in the form, which gives an invariable $(r - 1)$ -multiple occurrence of the r th degree of probability of appearance of 1 with a minus sign or plus sign depending on the parity/odd order of r . For example, for $r = 3$ this $2p_1^3$, and $r = 4$ gives $-3p_1^4$.

5 Analysis of Decompositions of Central Moments into Raw Moments for Binary Sequences

The insufficiency of describing the central moments of the sequence in (9) and (10) is manifested in $r \geq 3$ and $1 \leq s \leq r - 2$. In these cases, it is necessary to include no more than $(C_r^s - s - 1)$ -multiple probabilities of combinations of binary variables collected in the system of elements with the organization of step time skips that violate the density of the set of analyzed variables.

The introduced redefinition of elementary orders with $r_j = 1$ on $r_j \in \{0, 1\}$ allows setting the product $r_1 \cdot r_2 \dots r_j \dots r_r = 1$ for dense r th-sets and the product $r_1 \dots r_2 \dots r_j \dots r_r = 0$ for sparse ones. The general form of formulas for determining mixed moments, both raw and central, to binary values r_j and A_j , is represented as:

$$v_{r'}(A_1, A_2, \dots, A_r) = \sum_{(i_1 i_2 \dots i_r)=0}^{2^r-1} \prod_{j=1}^r a_{j i_j}^{r_j} p_{i_1 i_2 \dots i_r} = \mathbf{M}[A_1^{r_1} A_2^{r_2} \dots A_r^{r_r}], \quad (11)$$

$$\mu_{r'}(A_1, A_2, \dots, A_r) = \sum_{(i_1 i_2 \dots i_r)=0}^{2^r-1} \prod_{j=1}^r (a_{j i_j} - v_1)^{r_j} p_{i_1 i_2 \dots i_r} = \mathbf{M}[A_1^{\circ r_1} A_2^{\circ r_2} \dots A_r^{\circ r_r}], \quad (12)$$

where $\langle i_1 i_2 \dots i_r \rangle$ —is r th-bit binary integer; $r' = \sum_{j=1}^r r_j$ is the partial (actual) order of the moment as the sum of unit values r_j ; $A_1^{\circ}, A_2^{\circ}, \dots, A_r^{\circ}$ is centered values A_1, A_2, \dots, A_r relative to the general expectation $v_1 = p_1$. Each zero value r_j removes an element A_j (or A_j°) from the complex combination, increases the time space between the remaining elements by one step, and reduces by unit the actual order of the entire probability moment within $1 \leq r' \leq r$.

For example, when $r = 3$ the second term in the expansion (10) for μ_3 causes a 3-fold occurrence v_2 . For an abstract event system A_{j-1}, A_j, A_{j+1} , this situation is provided by the combinations $A_{j-1} A_j, A_j A_{j+1}$ and $A_{j-1} A_{j+1}$. In a sequence (if it is stationary), the first two combinations give a component $2p_{11}$, the third combination corresponds to the raw moment of the second order, which is generally different from the moments of the first two combinations of the same second order. Let's denote this raw moment $p_{1 \cdot 1}$ as the probability of coincidence of two variables by 1, separated by two steps of the sequence implementation in discrete time due to the determine of $r_j = 0$.

It is easy to show that the real random variable A is equivalent to an abstract system A_1, A_2, \dots, A_k of equal events if the binary alphabet applies to them. According to (5), the expression $v_r = p_1$ is true on condition that $r \geq 1$. Then the decomposition (10) of central moments into raw ones will be written in the following probabilistic form:

$$\mu_r = p_1 \left[1 + \sum_{s=1}^{r-1} (-1)^s C_r^s p_1^s \right] + p_1^r. \tag{13}$$

Specific types of relationships of the central probabilistic moments of the first four orders with the raw moments for the binary variable and for r th binary sequence system presented in Table 1. The table shows that these expansions differ significantly for $r \geq 3$ with terms written in sums at positions between p_1 or $p_{11\dots 1}$ and $(r - 1)p_1^r$.

To numerically determine the central moment of the r th order of a binary sequence, you need to find all 2^{r-1} the raw moments of partial orders from 1 to r . For example, for $r = 4$ you need to determine $2^{4-1} = 8$ probabilities

$$\underbrace{p_{1111}}_{v_4}, \underbrace{\overbrace{p_{111}}^{-2}, p_{1 \cdot 11}, p_{11 \cdot 1}}_{v_3}, \underbrace{\overbrace{p_{11}}^3, \overbrace{p_{1 \cdot 1}}^2, p_{1 \cdot \cdot 1}}_{v_2}}_{v_2}, \underbrace{\overbrace{p_1}^{-4 \rightarrow -3}}_{v_1} \text{ and in multiple}$$

Table 1 Expression of central moments through raw moments ($r = 1, 4$)

μ_r	For binary A	For binary system A_1, A_2, \dots, A_r
μ_1	0,	0,
μ_2	$p_1 - p_1^2,$	$p_{11} - p_1^2,$
μ_3	$p_1 - 3p_1^2 + 2p_1^3,$	$p_{111} - (2p_{11} + p_{1 \cdot 1}) p_1 + 2p_1^3,$
μ_4	$p_1 - 4p_1^2 + 6p_1^3 - 3p_1^4$	$p_{1111} - (2p_{111} + p_{1 \cdot 11} + p_{11 \cdot 1}) p_1$ $+ (3p_{11} + 2p_{1 \cdot 1} + p_{1 \cdot \cdot 1}) p_1^2 - 3p_1^4$

Table 2 Binary combinations of complex events in determining the relation between the raw moments and the central moments for $r = \overline{2, 6}$

r	Partial order $r' = \overline{1, r}$					
	1	2	3	4	5	6
2	1	11	–	–	–	–
3	–	1 · 1	111	–	–	–
4	–	1 · · 1	1 · 11 11 · 1	1111	–	–
5	–	1 · · · 1	1 · · 11 11 · · 1 1 · 1 · 1	1 · 111 11 · 11 111 · 1	11111	–
6	–	1 · · · · 1	1 · · · 11 1 · · 1 · 1 1 · 1 · · 1 11 · · · 1	1 · · 111 1 · 1 · 11 1 · 11 · 1 11 · · 11 11 · 1 · 1 111 · · 1	1 · 1111 11 · 111 111 · 11 1111 · 1	111111

quantities include them into μ_4 as summands and subtracts (see upper brackets), which indicates that the well-known representation (9) and in General form (10) does not apply to the considered sequential events.

Sets of characters 1 and indeterminate characters (marked with dots) that form the necessary complex events of the sequence for determining the raw moments that are included in the central moment up to the 6th order are shown in Table 2. The central moment μ_r , along with $\nu_r = p_{11\dots 1}$, includes sets of all smaller orders.

The Central point μ_r , along with $\nu_r = p_{11\dots 1}$, includes sets of all smaller orders.

6 Formation of Complex Events for a Criterion of Homogeneity

It should be emphasized that the homogeneity criterion for probabilistic moments does not require calculating the numerical values of the moments, for example, in the form of estimates of the corresponding probabilities.

According to the selected first probabilistic moment it is sufficient to form a difference sequence type $\langle a \rangle_n - \langle b \rangle_n = \langle d \rangle_n$ (2) of identically formed groups of elementary random variables BS and AS and to form a number of statistics (1) criterion of homogeneity for all partial sample of dimension n from to a critical value using mean values and standard deviations of the set of partial sums of the elements of the difference $\langle d \rangle_n$. It is algorithmically obvious to use the described probabilities

of elementary and complex events $v_1 = p_1$ and $v_r = \mathbf{P}\{A_1, A_2, \dots, A_r\}$ as raw probabilistic moments of finite order as qualifying parameters P_a or P_b , statistical criteria defined by expressions (1)–(3).

Sequentially generated random samples $A_{j-1}, A_j, A_{j+1} \dots$ that take binary values are combined by conjunction into groups that form complex events (7) and/or (8), taking into account the delays between them and inversions. Examples of hardware formation of 4th order events for representing the raw moments are shown using the diagrams in Fig. 1.

Sample testing steps. Given the order r and a specific type of raw probability moment, we determine the necessary transformation function of the form (7) of both sequences based on the operations of shifts, conjunctions, and, in the necessary cases for the form (8), inversions. The probability of the resulting combinations of binary variables represents the specified starting point. From the sequences of events received from both test sequences, we form a difference sequence, the elements of which are used as input data for the statistical criterion. We perform a series of iterations to calculate statistics, the values of which are compared with the critical level, forming tests of hypotheses. The result of these iterations is a chain (3) of accepting the null hypothesis, classifying the homogeneity property of the tested sequences with a given significance by a given raw probability moment.

Using the mathematical expectation operator (11), we obtain a decomposition of a given mixed central moment of r th order into a set of raw moments 2^{r-1} , the type of which is defined in Table 2 as the contents of cells with single sets of partial orders. We define all the necessary functions for converting the types of raw moments with the dimension of partial orders from 1 to r that are included in the given central moment. We carry out the necessary number of iterations of statistical calculations for all generated raw moments using the above method. As a result of the complete series of test iterations, a set of values of critical lengths is formed, the minimum value of which is the desired critical value. Outside of it, the test sequences are interpreted as non-uniform for a given central probability moment.

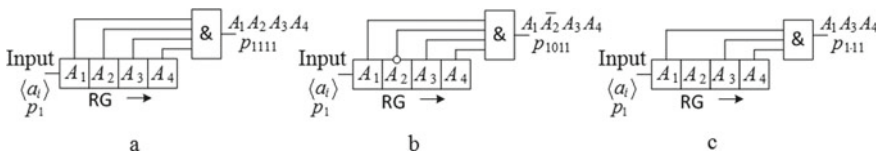


Fig. 1 The formation of events for the coincidence of straight lines (a), with the participation of inverse (b) and with the inclusion of indefinite (c) values of symbols

7 Conclusion

Proofs for the applicability of the statistical method for determining significant homogeneity to binary sequences for probabilistic moments of any finite order are obtained.

The choice of the raw moment as the main qualifying homogeneity constraint allows for a single chain of hypothesis tests. If the central moment is selected, the criterion operation is significantly complicated by the need to check the homogeneity for all orders from 1 to r inclusive. The full analytical form of the connection of the central moment of the r th order with the raw ones for the binary sequence has not yet been established. However, the logic of filling in the table obtained in the work 2 at the algorithmic level completely replaces the mathematical expression in the problem of practical implementation of the criterion.

Analyzing the contents of Table 2, it is not difficult to conclude that the central probabilistic moment of the $r \geq 2$ order includes autocorrelation dependencies in the domain of the argument definition $\tau = \bar{1}, r - \bar{1}$, provided that the probability is uniform p_1 . This allows one to use autocorrelation function values as the initial qualifying data of the criterion along with probabilistic moments.

The procedure for determining the statistical homogeneity of random sequences applies both to problems of classical simulation modeling and objects of cyber-physical systems. Providing a time domain for the existence of significant homogeneity in the conditions of given probabilistic moments increases the objectivity of analyzing the properties of digital models in a comparative comparison of several business projects in a real full-scale production environment.

Of practical interest are also private hardware solutions for digital specialized tools embedded in a physical object, such as in [5], to improve the safety of aircraft control. The material given in the chapter is supposed to be used for the synthesis of information security tools of the expert system of radio identification “friend-foe”.

The mathematical formulation of the problem of statistical indistinguishability of digital models of processes in General, with a multi-valued alphabet, can become the formal basis of the algorithm for significant certification of digital doubles [4]. An obvious condition is the inclusion of a time factor in the matrix of target indicators and resource constraints used in the synthesis of digital models at the development stage, and to maintain their adaptive and predictive abilities during the practical implementation of the project.

Acknowledgements The work was carried out with the financial support of the RFBR and the RT Academy of Sciences (Grant 18 47 160001).

References

1. Sovetov, B., Ya., Yakovlev, S.A.: System modeling (3rd edn) reprint and add, 343 p. M.: Vyssh. Shk. (2001) (In Russian)
2. Forrester, J.W.: Industrial Dynamics, 464 p. Productivity Press, Portland, OR (1961)
3. Knuth, D.E.: The art of computer programming: stminumtrical algorithms (3rd edn), 782 p. Addison-Wesley (1997)
4. Petrov, A.V.: Simulation modeling as the basis of digital doubles technology. *Vestnik Irstu* **10**, 56–66 (2018)
5. Bolshakov, A., Kulik, A., Sergushov, I., Scripal, E.: Decision support algorithm for parrying the threat of an accident. In: A. G. Kravets et al.: (eds.) *Cyber-Physical Systems: Industry 4.0 Challenges, Studies in Systems, Decision and Control*, 260, pp. 237–247. Springer Nature Switzerland AG (2020)
6. Bangsow, S.: Manufacturing simulation with plant simulation and sim talk usage and programming with examples and solutions, 300 p. Springer (2010)
7. Robert, C.P., Casella, G.: Monte Carlo statistical methods (2nd edn). 683 p. Springer (2004)
8. Amann, H.: Monte-Karlo methoden und lineare randwerprobleme. *ZAMM* **48**, 109–116 (1968)
9. Schneier, B.: Applied cryptography. protocols, algorithms, and source code in C, 758 p. Wiley, New York (1996)
10. Neuman, F.: Autocorrelation peaks in congruential pseudorandom number generators. *IEEE Trans. Comput.* **25**(5), 457–460 (1976)
11. Johnston, D.: Random number generators—principles and practices: a guide for engineers and programmers, 439 p. DEG Press (2018)
12. Fischer, V., Drutarovsky, M.: True random number generator embedded in reconfigurable hardware. In: *Cryptographic Hardware and Embedded Systems - CHES 2002*, Redwood Shores, CA, USA, 2002, Revised Papers, ser. LNCS, vol. 2523, pp. 415–430. Springer (2002)
13. Dichtl, M., Golic, J.: High-speed true number generation with logic gates only. In: *Cryptographic Hardware and Embedded Systems—CHES 2007*, Vienna, Austria, Proceedings, ser. LNCS, vol. 4727, pp. 45–61. Springer (2007)
14. Turan, M.S., Barker, E., Kelsey, J., McKay, K.A., Baish, M.L., Boyle, M.: Recommendation for the entropy sources used for random bit generation, 84 p. NIST Special Publication, Computer Science Published (2018)
15. Golomb, S.W.: Shift register sequences, 224 p. Holden Day, San Francisco (1967)
16. Kolmogorov, A.N., Uspenskij, V.A.: Algorithms and randomness. *Prob. Theor. Appl.* **XXXII**(3), 425–455 (1987)
17. Dodge, Y.: *The Concise Encyclopedia of Statistics*, 616 p. Springer Science + Business Media, LLC (2008)
18. Kremer, N.Sh.: *Theory of Probability and Mathematical Statistics*, 543 p. M.: Yuniti-Dana (2002)
19. Pishro-Nik, H.: *Introduction Probability, Statistics and Random Processes*, 747 p. Kappa Research, LLC <https://www.probabilitycourse.com>. (2014)
20. Petrov, A.V.: To the issue of standardization of probabilistic characteristics. *Vestnik IrTU* **1**, 56–64 (2016)

The Multiplicative-Isolating Principle of Significantly Nonlinear Mathematical Models Creation



Rudolf Neydorf, Anatoly Gaiduk, and Nikita Gamayunov

Abstract A new principle of mathematical models creation for the technical and other objects which are characterized by essential nonlinearity of interdependence of variables is substantiated. It is shown that the use of special analytical functions with a number of unique properties for the multiplicative transformation of fragmented mathematical models that approximate certain parts of the modeled dependencies allows us to obtain new functions that are analytically isolated in their domain of definition. The analyticity of these functions makes it possible additively to combine them into a single analytical function that approximates the simulated dependence in the entire area of its description. In this case, the total approximation error of the mathematical model of the studied object does not exceed the largest error of fragmentary approximating functions. The unique properties of multiplicatively isolating functions provide an almost “seamless” additive union of fragments. This chapter is dedicated to the study and proof of these properties, which are illustrated by examples.

Keywords Nonlinear dependence · Mathematical model · Experimental data · Approximation · Analytical function · Multiplicative isolation

1 Introduction

Modern control systems for various processes and technical objects are usually created based on their mathematical models (MM). This approach, in particular, is

R. Neydorf · N. Gamayunov
Don State Technical University, Gagarin Sq 1, Rostov on Don 344000, Russia
e-mail: ran_pro@mail.ru

N. Gamayunov
e-mail: mangal.harry@yandex.ru

A. Gaiduk (✉)
Southern Federal University, 44 Nekrasovsky, Taganrog 347928, Russia
e-mail: gaiduk_2003@mail.ru

characteristic when using analytical methods for the synthesis of control systems [1–4]. Currently, such analytical methods are widely used as linearization by feedback [5, 6], the passification method [7–9], the trajectory-positional approach [10, 11], the method of quasilinear models [12], and the Jordan controlled form method [13] and others. In these cases, the required control law is found by solving some systems of equations that are created on the basis of the requirements for the synthesized system taking into account the control object’s MM properties. However, analytical methods of synthesis can be implemented if only the object MM is analytical, i.e. the functions of its equations are continuous and differentiable. This requirement is due to the fact that each analytical method for the control systems synthesis implies some mathematical transformations possibility of the MM equations of both objects and control systems.

On the other hand, the modern systems quality requirements have increased so that they can be satisfied only taking into account the nonlinearities that are inherent in almost all controlled objects. Therefore, the MM of real control objects are nonlinear [12–14]. Most often, these MMs are determined experimentally by applying some test actions to the object and fixing its reaction to these actions. The tables obtained as a result contain experimental point data on the dependence of the object’s variables from the trial actions and other variables. Very often, these dependencies are very complex and cannot be described quite accurately by continuous analytical functions in the entire range of arguments. They have a pronounced fragmentary character, and neighboring fragments can have different slopes and curvature [14, 15].

Therefore, to obtain MM, these data are approximated at separate intervals by changes in variables by suitable analytical functions. However, the fragmented MM of the nonlinear object obtained in this way is not analytical, which does not allow the use of most of the known methods for the nonlinear controls synthesis.

An example of such a two-dimensional nonlinear dependence $f(x_1, x_2)$, having a fragmentary structure with respect to the variable x_1 , is shown in Fig. 1. As seen here in the interval $x_1 \in [0 \div (4 - 0, 333x_2)]$ derivative $\partial y / \partial x_1$ is positive, and when $x_1 \in [(4 - 0, 333x_2) \div 6]$ this derivative is negative, i.e. at the boundary of these

Fig. 1 Two-dimensional dependence $y = f(x_1, x_2)$

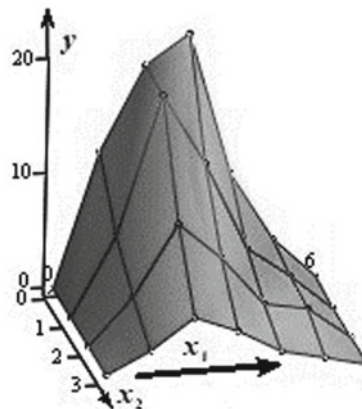
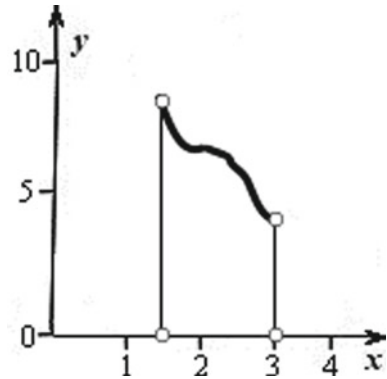


Fig. 2 Function fragment $f_0(x)$



intervals there is a “kink” of nonlinearity. In such cases, methods are used that can describe the “kink” with the necessary accuracy. The simplest and most effective is the piecewise (fragmentary) description [14], which provides any accuracy.

In Fig. 2 shows a fragmentary description $y = f_0(x)[1(x - 1.5) - 1(x - 3)]$ of the nonlinearity of one variable x by some function $f_0(x)$, but only on the interval $1.5 \leq x \leq 3$. Here, step function $1(x)$ is used, but it is not differentiable, therefore the MM is nonlinearity (Fig. 2) but is not analytic, since it has gaps in the derivatives on the points of the fragments joining, that excludes a possibility of analytical transformations of such models. The spline approximation also gives a fragmentary description, but it is also inconvenient for analytical transformations of MM [14, 15]. In addition to the “fragment-oriented” methods, methods are known that are oriented to the construction of analytical MMs: regression analysis [16], polynomial decompositions [17], methods of radial basis functions [18], and others. But they do not provide the necessary accuracy for approximating nonlinearities with kinks, gaps, and multi-extremums.

In order to overcome these difficulties, Professor R.A. Neydorf developed a multiplicative-isolating principle for the MM creation of essentially nonlinear controlled objects. The algorithmic basis of this principle is the original multiplicatively isolating function (MIF) developed by him. It allows one to obtain a common analytical MM of the controlled object using the Cut-Glue approximation method, which provides an additive “seamless” combination of fragments of experimental point data [12, 19, 20].

The aim of this work is to study the properties of MIF as the core of the multiplicative-isolating principle of creating essentially nonlinear MMs.

2 Multiplicative-Isolating Principle

The multiplicative-isolating principle is a fundamentally new approach to solving the problem of approximating experimental data, which, due to significant nonlinearity, need fragmentation to achieve the required approximation accuracy. It has two functionally different stages: the stage of preparation and primary processing of experimental data, as well as the stage of final processing with creation of the approximating MM. The experimental data array is split into fragments at the preparatory stage. Then each fragment is subjected to mathematical description by locally approximating functions. These functions are usually found in the class of analytic functions. The local approximation process is implemented using well-known classical methods [16–18].

At the stage of final processing, the experimental data undergo a multiplicative transformation using multiplicatively isolating functions. On the one hand, MIFs isolate the fragments created at the first stage, and on the other hand, they combine these fragments into a single analytical function. These operations are schematically

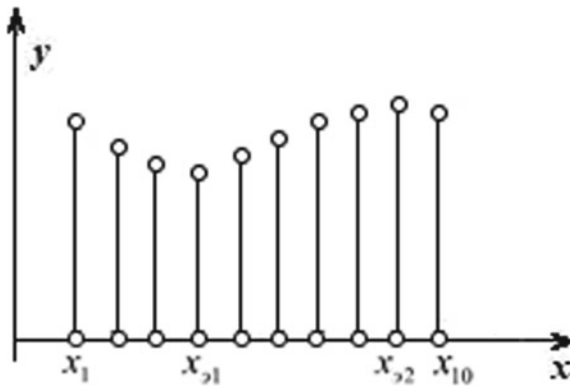


Fig. 3 Point array of experimental data

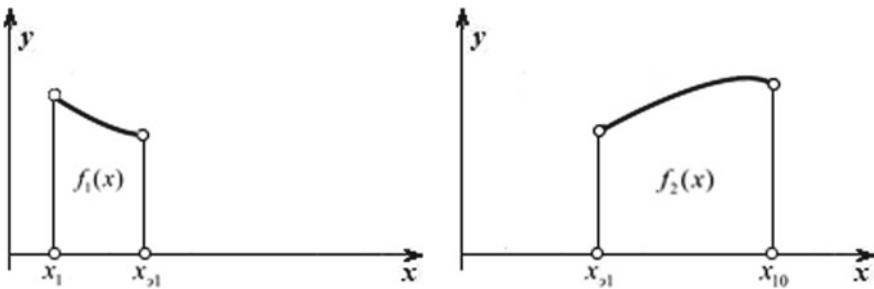
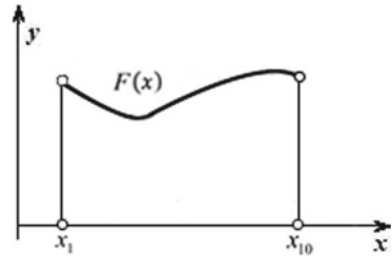


Fig. 4 Results of multiplicative transformation (1)

Fig. 5 The resulting single function $F(x)$



shown in Figs. 3, 4 and 5. In this case, two fragments are cut from the point experimental data as shown in Fig. 3. Each of these fragments is approximated by a suitable analytic function (Fig. 4), which are then combined (are glued) into a single continuous function (Fig. 5). These operations are an essential, distinctive feature of the multiplicative-isolating principle, which determines its approximating capabilities and uniqueness.

Thus, the processing of experimental data in accordance with the multiplicative-isolating principle consists in “cutting” them into separate fragments, local approximation of these fragments and then these fragments are glued into a single continuous function with analytical properties. Therefore, the practical implementation of this principle was called the “Cut-Glue Approximation” (CGA) method. Further we will consider in more detail the main stages of the multiplicative-isolating principle implementation.

The initial array of experimental data on a certain object, the model of which must be created, is represented by point values $y(x_1) - y(x_{10})$, shown in Fig. 3. The entire array of experimental data does not lend itself to sufficiently accurate approximation by known methods. This is caused by multi-extremums (minimum at the point $x_{\beta 1}$ and maximum at the point $x_{\beta 2}$), and also a rather sharp “kink” of nonlinearity at the point $x_{\beta 1}$. Therefore, the array is cut, in this case, into two fragments. Values $y(x_1) - y(x_{\beta 1})$ refer to the first fragment, and values $y(x_{\beta 1}) - y(x_{10})$ to the second fragment.

Each of the shown fragments is described with a sufficiently high accuracy by the analytical locally approximating functions $\varphi_1(x)$ and $\varphi_2(x)$. This operation corresponds to the application of the well-known piecewise approach to the approximating nonlinear data problem [14, 16]. However, the paradigm of the multiplicative-isolating principle is to obtain the final result—MM, in the form of a function with analytical properties. This condition implies additional steps to combine (glue) the approximating functions of the selected fragments.

For this purpose, approximating functions of each individual fragment of experimental data is exposed to the isolating transformation. The essence of this transformation lies in the fact that the approximation created within the limits of the experimental data region limited by the fragment is preserved, and outside the fragment boundaries the multiplicatively isolating function provides practically zero value.

The result of the isolating transformation is new analytical functions— $f(x)$, which are formed from $\varphi(x)$ by multiplying each $\varphi(x)$ on a special function $E(x)$:

$$f_1(x) = \varphi_1(x)E_1(x), \quad f_2(x) = \varphi_2(x)E_2(x). \quad (1)$$

This operation determined the use of the term “multiplicatively”. Figure 4 shows the functions $f_1(x)$ and $f_2(x)$, obtained as a result of applying the multiplicative operation (1).

Finally, the functions $f_1(x)$ и $f_2(x)$ are glued together into one analytical expression by simple summation:

$$F(x) = f_1(x) + f_2(x). \quad (2)$$

The result of their addition—function $F(x)$, is a single continuous curve, which is shown in Fig. 5.

As can be seen from expressions (1) and (2), the function $E_i(x)$ performs two operations simultaneously: (1) multiplicatively selects each fragment $\varphi(x)$, keeping the values of the approximating function in its definition domain; (2) multiplicatively “zeroes out” all values of this locally approximating function $\varphi(x)$ outside the fragment, forming new multiplicatively transformed functions $f(x)$. This provides the actual fragment “isolation” $\varphi(x)$ in the experimental data array. Therefore the function $E_i(x)$ from (1) is called the multiplicatively isolating function.

The transformed functions (1) are independent from each other and from other fragments. Thus, the operation addition of the multiplicatively transformed functions $f_1(x)$ and $f_2(x)$ (2) becomes correct both in the mathematical sense and in the sense of the multiplicative-isolating principle’s paradigm.

Thus, the multiplicatively isolating function (MIF) is the most essential element of the multiplicative-isolating principle implementation, so we pass on to a detailed consideration of its properties.

3 Properties of the Multiplicatively Isolating Function

This function should have the following ideal properties as a means of implementing the multiplicative-isolating principle. First, it should have a value ideally equal to 1, on the segment of its argument $[x_{i-1}, x_i]$, i.e.

$$\forall x \in [x_{i-1}, x_i] \rightarrow E_i^I(x) = 1. \quad (3)$$

Secondly, in the rest of its definition area, the condition of its values (ideally, exact zeroing) tending to zero must be fulfilled, i.e.

$$\forall x : x_{i-1} > x > x_i \rightarrow E_i^I(x) = 0. \quad (4)$$

Function $E_i(x)$ at the interval boundary points x_{i-1} and x_i should ideally have an average value between its minimum and maximum values throughout the fragment, i.e. 0.5. Then, when adding and at the edge points of the segments, values equal to

1 will be obtained. Therefore, the function $E_i^I(x)$ must, in addition to the argument x , contain additional parameters—area coordinates to be cut out, here called the “fragment”. In this way

$$E_i^I(x, \dots) = E_i^I(x, x_l, x_r), \quad (5)$$

where x_l , x_r are the left and right fragment boundaries, “cut out” from the experimental data array. Accordingly, function $E_i^I(x)$ (5) should ideally be described by the following conditional-logical expression:

$$E_i^I(x, x_l, x_r) = \begin{cases} 1, & \forall x \in (x_l, x_r); \\ 0.5, & \forall x = x_l, x_r; \\ 0, & \forall x_l > x > x_r. \end{cases} \quad (6)$$

The real function $E_i(x)$ was developed and presented in works [13, 19, 20] and many others. In the general case, it is described by the following expression:

$$E_i(x, S) = \frac{\left[x - x_l + \sqrt{(x - x_l)^2 + \varepsilon_l^2} \right] \cdot \left[x_r - x + \sqrt{(x_r - x)^2 + \varepsilon_r^2} \right]}{4 \cdot \left[\sqrt{(x - x_l)^2 + \varepsilon_l^2} \right] \cdot \left[\sqrt{(x_r - x)^2 + \varepsilon_r^2} \right]}. \quad (7)$$

The main argument of function (7) is the coordinate variable x , and the set S contains parametric settings that provide the functional of the multiplicative-isolating principle.

In the one-dimensional case (x —scalar) MIF (7) contains the minimum number of parametric settings required for multiplicative processing $S = \{s_i | i = \overline{1, 4}\}$. Here $s_1 = x_l$, $s_2 = x_r$ —left and right boundaries of the approximated fragment; $s_3 = \varepsilon_l$, $s_4 = \varepsilon_r$ —parameters of the experimental data fragment left and right boundaries approximation error, respectively.

Settings x_l and x_r ensure the formation of the one-dimensional fragment boundaries when it is “cut out”, and $\varepsilon_l = \varepsilon_r$ —the fulfillment of the conditions for the MIF existence [19]. The study of function (7) as a multiparameter dependence shows that it really has all the properties important for the multiplicative-isolating principle implementation. It should be noted that, provided $\varepsilon_l = \varepsilon_r$, function (7) has symmetric left and right fronts of the “cut out” fragment, therefore the function $E_i(x, S)$ with $\varepsilon_l = \varepsilon_r$ is called “symmetric”. Accordingly, function (7) with $\varepsilon_l \neq \varepsilon_r$ is called “asymmetric” [19, 20].

Let us consider the main features and properties of multiplicatively isolating function (7):

- (1) MIF (7) in the interval (x_l, x_r) takes values close to one. Moreover, the proximity of its values to one is effectively adjusted by the parameters $\varepsilon_l, \varepsilon_r$. In ranges $(-\infty, x_l)$ and (x_r, ∞) MIF (7) takes on values as close to zero as desired.

Moreover, both the proximity of the function value to zero and the proximity to the edge points are also adjusted by the parameters $\varepsilon_l, \varepsilon_r$.

This MIF property is illustrated in Fig. 6, which shows the MIF (7) graph at $x_l = 14, x_r = 21$ and at $\varepsilon_l = \varepsilon_r = \varepsilon$. It is clearly seen: the smaller value of ε , the MIF values in the interval $x \in (x_l, x_r)$ closer to 1, and if $x \notin (x_l, x_r)$, then the values of $E_i(x, x_l, x_r, \varepsilon)$ (7) are closer to zero. In this case, the graph of function $E_i(x, x_l, x_r, \varepsilon)$ (7) is symmetrical about point $x_m^s = 17.5$, which in this case is the midpoint of the interval (x_l, x_r) .

- (2) Function (7) symmetric at $\varepsilon_l = \varepsilon_r$ about the middle of the interval (x_l, x_r) and has a single maximum at point $x_m^s = (x_r + x_l)/2$ [19, 20]. This is also clearly seen in Fig. 6, where point $x_m^s = 17.5$.
- (3) At boundary points x_l, x_r MIF (7) takes a value from 0.25 to 0.5, which, in turn, depends on the width of the fragment $|x_r - x_l|$ and value $\varepsilon_l, \varepsilon_r$ [20].
- (4) Function (7) of the asymmetric MIF has a single maximum at point x_m^a , which is shifted to boundary x_l or x_r , which has a smaller parameter ε_l or ε_r . This MIF property is illustrated in Fig. 7 by graphs $E_1(x, S)$ and $E_2(x, S)$ where $x_l = -0.5, x_r = 0.5$ and $\varepsilon_{l1} = 0.1, \varepsilon_{r1} = 1.0, \varepsilon_{l2} = 0.3, \varepsilon_{r2} = 0.01$.

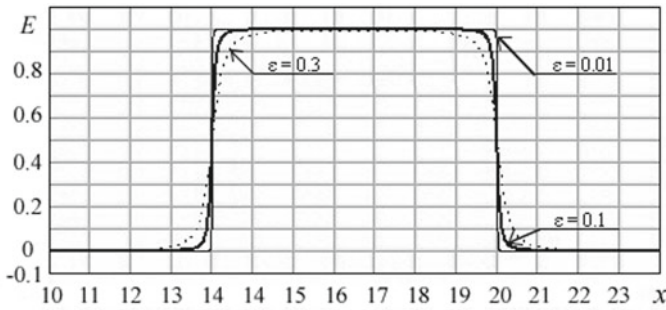


Fig. 6 Symmetric MIF with different values ε

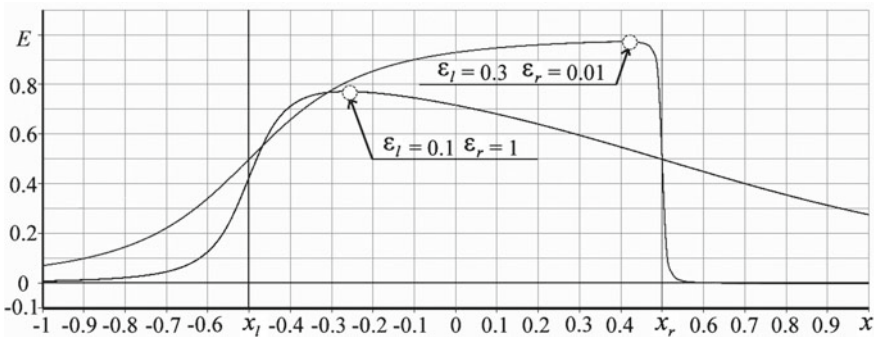


Fig. 7 Asymmetric MIFs

As you can see in Fig. 7, the MIF curves are essentially non-symmetric. The extremum point x_m^a of function $E_1(x, S)$ really shifts towards a lower value ε_l or ε_r . So, if $\varepsilon_{l1} = 0.1$, $\varepsilon_{r1} = 1.0$, then extremum $E_1(x, S)$ corresponds to the point $x_m^a = -0.265$, if $\varepsilon_{l2} = 0.3$, $\varepsilon_{r1} = 0.01$, then the extremum corresponds to point $x_m^a = 0.403$. Extreme function value $E(x, S)$ becomes much less than 1 with an increase in the average value $(\varepsilon_l + \varepsilon_r)/2$ and approaches to 1 as this value decreases.

(5) MIF (7) is infinitely differentiable, like any radical-fractional function.

Examples of creating mathematical models based on the multiplicative-isolating principle can be found in [12, 19] and others.

4 Conclusion

The multiplicative-isolating principle of creation of mathematical nonlinear models based on experimental data is an effective approach that has no analogues in world practice. A practical implementation of this principle is the Cut-Glue approximation method, in which the fundamental properties of the multiplicatively isolating functions are used. This method is perspective and, that is important, an effective way of the mathematical description of experimental data, and also the subsequent creation of analytical models of significantly nonlinear objects. The features of the multiplicative-isolating principle are considered above allow to solve the problems of minimization of approximation error and increase in accuracy of the description of experimental data.

Acknowledgements Chapter is prepared on the results of the projects creation with support of the RFBR grants No. 18-08-01178/20 in DG TU and No. 19-08-01226 in LLC “SRI MVUS”.

References

1. Moothedath, S., Chaporkar, P., Belur, M.N.: Minimum cost feedback selection for arbitrary pole placement in structured systems. *IEEE Trans. Autom. Contr.* **63**(11), 3881–3888 (2018)
2. Kotenko, I., Parashchuk, I.: Determining the parameters of the mathematical model of the process of searching for harmful information. In: Kravets, A.G., Bolshakov, A.A., Shcherbakov, M.V. (eds.) *Cyber-Physical Systems: Industry 4.0 Challenges*, vol. 260, pp. 225–236. Springer, New York (2019)
3. Mei, W., Friedkin, N.E., Lewis, K., Bullo, F.: Dynamic models of appraisal networks explaining collective learning. *IEEE Trans. Autom. Contr.* **63**(9), 2898–2912 (2018)
4. Kersting, S., Buss, M.: Direct and indirect model reference adaptive control for multivariable piecewise affine systems. *IEEE Trans. Autom. Contr.* **62**(11), 5634–5649 (2017)
5. Yang, G., Liberzon, D.: Feedback stabilization of switched linear systems with unknown disturbances under data-rate constraints. *IEEE Trans. Autom. Contr.* **63**(7), 2107–2122 (2018)
6. Voevoda, A.A., Filiushov, VYu.: Feedback linearization: inverted pendulum. *Trans. Scient. Papers Novosibirsk State Tech. Univ.* **3**(85), 49–60 (2016)

7. Madeira D. de S., Adamy, J.: Feedback control of nonlinear systems using passivity indices. In: Proceedings of IEEE Conference on Control Applications, pp. 263–268. Sydney, Australia, (2015)
8. Byrnes, C., Isidori, A., Willems, J.: Passivity, feedback equivalence and the global stabilization of minimum phase nonlinear systems. *IEEE Trans. Automat. Contr.* **36**, 1228–1240 (1991)
9. Xia, M., Rahnama, A., Wang, S., Antsaklis, P.J.: Control design using passivation for stability and performance. *IEEE Trans. Contr.* **63**(9), 2987–2993 (2018)
10. Pshikhopov, V.Kh., Chernukhin, Yu.V., Medvedev M., Yu.: Structural synthesis of dynamic regulators for position-trajectory adaptive mobile robot control system on base of mini-airships. In: Proc. of VII Intern. SAUM Conf. on Systems, Automatic Control and Measurements, pp. 64–69. Vrnjachka Banja, Yugoslavia (2001)
11. Li, I.H., Chen, Y.H., Wang, W.Y., Kao, Y.F.: Hybrid intelligent algorithm for indor path planning and trajectory-tracking control of wheeled mobile robot. *Int. J. Fuzzy systems* **18**(4), 595–608 (2016)
12. Gaiduk, A.R., Neydorf, R.A., Kudinov, N.V.: Application of cut-glue approximation in analytical solution of the problem of nonlinear control design. In: *Cyber-Physical Systems: Industry 4.0 Challenges*, pp. 117–132. Springer (2020)
13. Gaiduk, A.R.: Nonlinear control systems design by transformation method. *Mekhatronica, Avtomatizatsiya, Upravlenie* **19**(12), 755–761 (2018)
14. António, M.G., Ghanbari, P., Ghanbari, M.: Piecewise approximation of contours through scale-space selection of dominant points. *IEEE Trans. Image Process.* **19**(6), 1442–1450 (2010)
15. De Boor C.: A practical guide to splines, 357 p. Springer (1978)
16. Khan, Md, Shaw, J.: Multilevel logistic regression analysis applied to binary contraceptive prevalence data. *J. Data Sci.* **9**(1), 22–31 (2011)
17. Totik, V.: Orthogonal polynomials. *Surv. Approx. Theor.* **1**, 70–125 (2005)
18. Light, W., Wayne, H.: Error estimates for approximation by radial basis functions. In: Singh S.P. (eds) *Approximation Theory, Wavelets and Applications*. NATO Science Series (Series C: Mathematical and Physical Sciences), vol. 454. Springer, Dordrecht (1995)
19. Neydorf, R., Neydorf, A.: Technology of cut-glue approximation method for modeling strongly nonlinear multivariable objects. *Theoretical Bases and Prospects of Practical Application*. SAE Technical Paper 2016–01–2035 (2016). <https://doi.org/10.4271/2016-01-2035>
20. Gamayunov, N., Neudorf, R.: Properties of overarching symmetric multiplicative-isolating functions in the «cut-glue» approximation method. In: Bolshakov, A.A. *Mathematical methods in equipment and technologies: works collection of the international scientific conference: in 12 t. T. 8*, vol. 8, pp. 72–76. Polytechnic Publishing House, SPb (2020)

Numerical Approaches to Solving a Non-linear System of Schrödinger Equations



Airat Sakhabutdinov , Vladimir Anfinogentov , Oleg Morozov ,
and Robert Gubaydullin

Abstract The chapter considers an approach to numerical integration of the second kind nonlinear coupled Schrödinger equation system, written taking into account second-order dispersion and Raman scattering, which differs from the often-used approach based on the method of splitting into physical processes. The main advantages of the proposed method are its absolute stability through the use of an implicit computing scheme, an integrated mechanism for refining the solution at each step; automatic selection of integration step. Besides, there is a noticeable performance gain (or time resolution) up to three or more orders of magnitude because there is no need to produce direct and inverse Fourier transforms at each integration step, as is required in the method of splitting according to physical processes, which is very important for cyber-physical systems with minimum time response requirement. An additional advantage of the proposed method is the ability to calculate the interaction with an arbitrary number of propagation modes in the fiber.

Keywords Polarization maintaining optical fiber · Few-mode propagation · System of coupled nonlinear Schrodinger equations · System of coupled nonlinear Schrödinger equations · Kerr effect · Raman scattering · Dispersion · Implicit numerical computing scheme

A. Sakhabutdinov (✉) · V. Anfinogentov · O. Morozov · R. Gubaydullin
Kazan National Research Technical University Named After A.N. Tupolev-KAI, Karl Marx str.
10, Kazan 420008, Russia
e-mail: kazanboy@yandex.ru

V. Anfinogentov
e-mail: v.anfinogentov@yandex.ru

O. Morozov
e-mail: microoil@mail.ru

R. Gubaydullin
e-mail: diablogrr@gmail.com

1 Introduction

The propagation of light in optical fiber is described by the nonlinear Schrödinger equation, where the nonlinearity arises due to the Kerr effect. In particular, this is the task of delivering an ultrashort optical pulse of high power [1–4]. Nonlinearity is also a problem when transmitting information over long distances with the currently used modulation formats in fiber optic communication. Directly proportional to a signal intensity increase, its nonlinear distortions due to crosstalk also increase, which limits the possibility of restoring the transmitted information at the receiver input [5–7]. Researchers are faced with the task of compensating for nonlinear effects in order to provide a high speed of information transfer. So far, two main approaches to solving this problem have been proposed: the first consists in mitigating nonlinear effects by special methods [8], the second in special coding of information in the eigenmodes of the nonlinear channel [9], which is based on the integration of the nonlinear Schrödinger equation.

The propagation of light, taking into account its polarization dynamics, is described by the Manakov equations, which are valid for modern fiber-optic communication lines under certain conditions. These equations are a special case of the Schrödinger equations [10–12].

The most common method for solving the system of nonlinear Schrödinger equations is the method of splitting into physical processes [13–15], which consists of a mixed numerical-analytical approach and is a numerical integration of the equation system. The method of splitting into physical processes is based on the assumption that when the optical field propagates over a short length, dispersive and nonlinear effects can act independently [15]. The method consists in the fact that with a small integration step, it is assumed that the propagation of a perturbation can be divided into two steps, wherein the first step only non-linear effects act, and in the second—only dispersion effects. The solution at each step of integration is found as the result of the inverse Fourier transform of the product of the analytical solution for the linear term multiplied by the Fourier transform of the nonlinear part, where the Fourier transform is calculated in the time domain in either case [16].

Thus, the splitting method into physical processes from the point of view at the numerical methods and finite-difference schemes can be characterized as a method having the first order of accuracy in the integration step and using data of the previous integration step to calculate the values at the current integration step. The latter gives grounds to classify the splitting method according to physical processes as an explicit finite-difference method with all its inherent shortcomings, such as the conditional stability of a method. The computational complexity of the splitting method into physical processes is determined mainly by the computational complexity of the algorithms of direct and inverse Fourier transforms, which must be carried out at each step of integration.

Replacing the splitting method into physical processes by the method of direct numerical integration using an implicit finite-difference scheme allows eliminating

several shortcomings of the splitting method. As the two most important disadvantages, the following should be noted. Firstly, it is an ability to ensure the absolute stability of the integration method through the use of the implicit finite-difference scheme. Secondly, this is a reduction in the computational complexity of the method due to the replacement at each step of the integration of two (direct and inverse) Fourier transforms by solving a system of linear equations by the sweep method. The remaining, no less important, but less obvious benefits of the proposed method of direct numerical integration are presented in the conclusion to the chapter.

2 Formulation of the Problem

A model of a fiber optic channel with distributed nonlinearity and linear distortions due to chromatic dispersion can be represented using the Manakov system of nonlinear equations [10, 17–19]:

$$\begin{cases} \frac{\partial E_1}{\partial \xi} = -i \cdot \frac{\beta_2}{2} \cdot \frac{\partial^2 E_1}{\partial \tau^2} + i\gamma \cdot \frac{8}{9} \cdot (|E_1|^2 + |E_2|^2) \cdot E_1 + \frac{\alpha}{2} \cdot E_1 \\ \frac{\partial E_2}{\partial \xi} = -i \cdot \frac{\beta_2}{2} \cdot \frac{\partial^2 E_2}{\partial \tau^2} + i\gamma \cdot \frac{8}{9} \cdot (|E_1|^2 + |E_2|^2) \cdot E_2 + \frac{\alpha}{2} \cdot E_2 \end{cases}$$

$$E_1 = E_1(\xi, \tau), \quad E_2 = E_2(\xi, \tau) \tag{1}$$

where ξ —a spatial coordinate along a central axis of the optical fiber, τ —time, E_1 and E_2 —polarizations, each of which is a complex function, i —the imaginary unit, α, β_2, γ —given process constants. Under given boundary conditions in the form:

$$\begin{aligned} E_1(L, \tau) = E_{01}(\tau), \quad E_1(\xi, 0) = E_1(\xi, T_0) = 0, \\ E_2(L, \tau) = E_{02}(\tau), \quad E_2(\xi, 0) = E_2(\xi, T_0) = 0. \end{aligned} \tag{2}$$

where L —the length of an optical fiber cable, T_0 —the propagation time. The boundary conditions at the end of L are specified as functions $E_{01}(\tau)$ and $E_{02}(\tau)$, specified in discrete-time samples as values of functions $E_{01}(\tau_n)$ and $E_{02}(\tau_n)$, with $n = \tau_0 + \Delta\tau_n, \Delta\tau = T_0/N, n = 0, N$.

The task is to find a solution for backscattering, [5] in the form of dependencies:

$$E_1(0, \tau) \text{ u } E_2(0, \tau), \tag{3}$$

which can also be determined at discrete points in time.

3 Equation System

To change from the formulation of the problem (1) in dimensional quantities to dimensionless quantities, the variables were changed:

$$x = \frac{E_1}{\sqrt{P}}, \quad y = \frac{E_2}{\sqrt{P}}, \quad t = \frac{\tau}{T_0}, \quad z = -\frac{\xi}{L}, \quad P = \frac{|\beta_2|}{\frac{8}{9}\gamma T_0^2}, \quad L = \frac{2T_0^2}{|\beta_2|}. \quad (4)$$

where L and T_{02} are related by $L = 2T_{02}/|\beta_2|$.

The system of equations in dimensionless quantities will be written as (5):

$$\begin{cases} i \frac{\partial x}{\partial z} = \frac{\partial^2 x}{\partial t^2} + 2\Phi(x, y)x \\ i \frac{\partial y}{\partial z} = \frac{\partial^2 y}{\partial t^2} + 2\Phi(x, y)y \end{cases}, \quad (5)$$

where the nonlinear term is written in the form of the product of the desired function to the nonlinear part, for which the notation is introduced (6):

$$\Phi(x, y) = i\alpha + |x|^2 + |y|^2. \quad (6)$$

The boundary conditions, in this case, will take the form:

$$\begin{aligned} x(-1, t) = x_0(t), \quad x(z, 0) = x(z, 1) = 0, \\ y(-1, t) = y_0(t), \quad y(z, 0) = y(z, 1) = 0. \end{aligned} \quad (7)$$

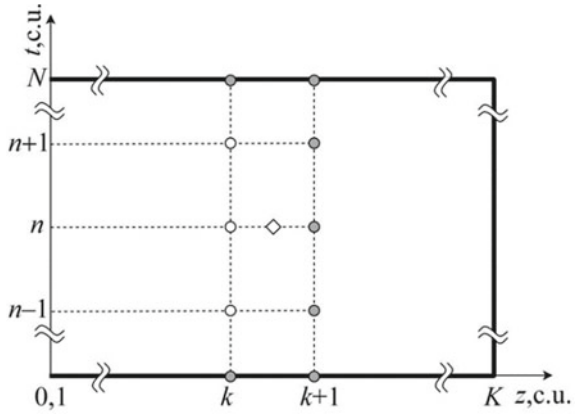
The formulation of the problem in terms of the initial conditions is initially given on a discrete set of points, it is logical and the solution would be to look numerically, writing the initial relations in a finite-difference form.

4 Difference Scheme

The classical implicit difference scheme Crank-Nicolson (Fig. 1) was used to write Eq. (5) in the finite-difference form. The choice of the difference scheme is due to the fact that it is implicit, which makes it absolutely stable. Another advantage of the Crank-Nicolson scheme is that when integrating the equations of mathematical physics with the first derivative with respect to one and the second derivative with respect to another variable, it leads to the need to solve a system of linear equations with three diagonal matrices at each integration step, which is performed by a simple tridiagonal matrix algorithm [6].

In the Crank-Nicolson scheme, the coordinate grid is used in space and time, in the scheme in Fig. 1, the variable n is used to designate the layers in time and

Fig. 1 The finite-difference scheme used to solve the system of equations: the rhombus in the figure indicates the point for which the equality of the system of equations is written; circles—nodes of a finite-difference scheme



the variable k in space. The parameters on the $k + 1$ layer of the coordinate grid are considered known, at the same time, the known values should be the initial and boundary values for $k = K$ ($z = -1$), $n = 0$ ($t = 0$), $n = N$ ($t = 1$). In Fig. 1, the known values are indicated by gray circles, the values that need to be determined are the unfilled circles.

For the system of Eqs. (5), the integration scheme, written in a completely implicit form, not only does not lead to the three-diagonal system of linear equations but does not even lead to a linear system of equations. Let us write the system of Eq. (5) in the finite-difference form, using the six-point Crank-Nicolson scheme, having entered two parameters σ and θ , changing in the range $[0, 1]$, the defining position of a shift for writing the finite-difference relations between the two (known and unknown) layers of integration.

The parameter σ is responsible for the implicit record of the linear part of Eqs. (5), and the parameter θ is separately allocated for the implicit record of a nonlinear multiplier $\Phi(x, y)$. The first derivative in space is written by first-order precision relations for a node $(k + 1/2, n)$. The first derivative with respect to the variable z for the node $(k + 1/2, n)$ is approximated by the central difference, which has a second approximation order.

$$\left\{ \begin{aligned} & \frac{i \cdot (x_{k+1}^n - x_k^n)}{\Delta z} - \frac{\sigma \cdot (x_k^{n-1} - 2x_k^n + x_k^{n+1}) + (1-\sigma) \cdot (x_{k+1}^{n-1} - 2x_{k+1}^n + x_{k+1}^{n+1})}{\Delta t^2} \\ & = 2 \cdot (\theta \Phi_k^n + (1-\theta) \Phi_{k+1}^n) \cdot (\sigma x_k^n + (1-\sigma)x_{k+1}^n) \\ & \frac{i \cdot (y_{k+1}^n - y_k^n)}{\Delta z} - \frac{\sigma \cdot (y_k^{n-1} - 2y_k^n + y_k^{n+1}) + (1-\sigma) \cdot (y_{k+1}^{n-1} - 2y_{k+1}^n + y_{k+1}^{n+1})}{\Delta t^2} \\ & = 2 \cdot (\theta \Phi_k^n + (1-\theta) \Phi_{k+1}^n) \cdot (\sigma y_k^n + (1-\sigma)y_{k+1}^n) \end{aligned} \right. \quad (8)$$

To record the finite-difference relations of the second time derivative on each spatial layer, the first-order accuracy relations are used, which are written in the grid nodes as (k, n) and $(k + 1, n)$. By setting the σ (8) parameter to a value of $1/2$, the second time derivative and the linear multiplier on the right-hand side of the nonlinear term can be agreed, also for the node $(k + 1/2, n)$. The combined

explicitly-implicit difference Crank-Nicolson integration scheme (8) at each node of the finite-difference grid can be rewritten as (9), for the tridiagonal matrix algorithm:

$$\begin{aligned} a_n \cdot x_k^{n-1} + b_n \cdot x_k^n + c_n \cdot x_k^{n+1} &= d_n^x, \quad k = \overline{1, K}, \quad n = \overline{1, N}. \\ a_n \cdot y_k^{n-1} + b_n \cdot y_k^n + c_n \cdot y_k^{n+1} &= d_n^y, \end{aligned} \quad (9)$$

where:

$$\begin{aligned} a_n &= -\sigma, \\ b_n &= 2 \cdot \sigma - \frac{i \cdot \Delta t^2}{\Delta z} - 2 \cdot \sigma \cdot (\theta \cdot \Phi_k^n + (1 - \theta) \cdot \Phi_{k+1}^n), \\ c_n &= -\sigma, \\ d_n^x &= (1 - \sigma)(x_{k+1}^{n-1} - 2x_{k+1}^n + x_{k+1}^{n+1}) - \frac{i \Delta t^2}{\Delta z} x_{k+1}^n \\ &\quad + (1 - \sigma)(\theta \Phi_k^n + (1 - \theta) \Phi_{k+1}^n) x_{k+1}^n, \\ d_n^y &= (1 - \sigma)(y_{k+1}^{n-1} - 2y_{k+1}^n + y_{k+1}^{n+1}) - \frac{i \Delta t^2}{\Delta z} y_{k+1}^n \\ &\quad + (1 - \sigma)(\theta \Phi_k^n + (1 - \theta) \Phi_{k+1}^n) y_{k+1}^n \end{aligned} \quad (10)$$

In order to match the recording of the nonlinear multiplier in (8) for the same node of the difference grid ($k + 1/2, n$), it is also necessary to give the parameter θ in (8) the value equal to $1/2$, which leads to the fact that system of Eq. (9) with respect to unknown quantities becomes nonlinear. To avoid such a problem helps the choice of the parameter θ equal to zero. The simultaneous choice of parameters $\sigma = 1/2$ and $\theta = 0$ provides practical stability of the finite-difference scheme with the simultaneous possibility of reducing the system of equations at each integration step to a system of linear equations solved by the tridiagonal matrix algorithm [6].

The final system of equations takes the form (9) with the values of the tridiagonal matrix coefficients in the form (11):

$$\begin{aligned} a_n &= -\sigma, \quad b_n = 2 \cdot \sigma - \frac{i \cdot \Delta t^2}{\Delta z} - 2 \cdot \sigma \cdot \Phi_{k+1}^n, \quad c_n = -\sigma, \\ d_n^x &= (1 - \sigma)(x_{k+1}^{n-1} - 2x_{k+1}^n + x_{k+1}^{n+1}) - \frac{i \Delta t^2}{\Delta z} \cdot x_{k+1}^n + (1 - \sigma) \cdot \Phi_{k+1}^n \cdot x_{k+1}^n, \\ d_n^y &= (1 - \sigma)(y_{k+1}^{n-1} - 2y_{k+1}^n + y_{k+1}^{n+1}) - \frac{i \Delta t^2}{\Delta z} \cdot y_{k+1}^n + (1 - \sigma) \cdot \Phi_{k+1}^n \cdot y_{k+1}^n \end{aligned} \quad (11)$$

For the coefficients at the edges, it is necessary to take into account the boundary conditions (7), and correct the coefficients b , which in general terms can be written as:

$$db_1^x = d_1^x - a_1 \cdot x_k^0, \quad db_{N-1}^x = d_{N-1}^x - c_{N-1} \cdot x_k^N,$$

$$db_1^y = d_1^y - a_1 \cdot y_k^0, \quad db_{N-1}^y = d_{N-1}^y - c_{N-1} \cdot y_k^N. \quad (12)$$

For (9) and (11), the integration is carried out along the spatial coordinate, and the system of equations is solved on each spatial layer.

Thus, the obtained difference scheme is a generalization of a special case of the Crank-Nicolson difference scheme, in which all linear terms of the equations are written according to an implicit finite-difference scheme, and the nonlinear term is taken from the previous computational layer. The integration is carried out in layers, from $k + 1$ to the k -th layer along the z coordinate.

5 Initial and Boundary Conditions

The initial conditions for solving the system of Eqs. (9) with (11), (12) are the given values of the x and y arrays at $k = K$ ($z = -1$) for all values of $n = 1, N$. In terms of the problem statement, the initial conditions (given values of the distribution of x and y as a function of time at the remote end of the optical fiber at $z = 1$) determine the shape of the optical signal received at the remote end [20]. Let's set, for example, at the remote end of reception of the ideal signal in the form of 16QAM with switching the information signal for x and for y . The system of Eq. (1), even if written in the discrete-difference form (9) with (11), (12), requires that the desired functions x and y be continuous, along with their second derivatives with respect to time and first derivatives with respect to space. Switching the information signal to 16QAM implies a discontinuity of both the function itself and its derivative. The use of a knowingly discontinuous function as initial conditions for solving the system of equations formulated for continuous functions immediately leads to unreliable results. In order to avoid the problem of breaking the initial data curves, the smooth joining technique of two discontinuous curves was used. The classical function that is conveniently used for these purposes is the hyperbolic tangent [21]:

$$S(t, p, q) = \frac{1 - \tanh(q(t - p))}{2}, \quad (13)$$

where t —an abscissa, along which it is necessary to sew two functions on the interval $[t_0, t_N]$; p —a point from the interval $[t_0, t_N]$, determines the location of the joining; q —parameter responsible for the degree of smoothness of the joining.

For single switching information signal, the initial distribution and for the x and y represents the joining four functions in the interval $[t_0, t_N]$. The first interval is $x(t) = 0, y(t) = 0$ for $t_0 < t \leq t_B$; the second segment is $x(t) = 16\text{QAM}_{i1}(t), y(t) = 16\text{QAM}_{j1}(t)$ for $t_B < t \leq t_M$; the third segment is $x(t) = 16\text{QAM}_{i2}(t), y(t) = 16\text{QAM}_{j2}(t)$ for $t_M < t \leq t_E$; the fourth segment is $x(t) = 0, y(t) = 0$ for $t_E < t \leq t_N$. The initial and final parts specified by zero values of x and y are determined by the requirements of the boundary conditions (7).

The initial distribution is given by discrete samples:

$$\begin{aligned}
 x_n &= A_{\max} e^{-j\omega t_n} \\
 &\times (S(t_n, p_M, q_M) QAM_{16}(i_B) + (1 - S(t_n, p_M, q_M)) QAM_{16}(i_E)) \\
 &\times (1 - S(t_n, p_B, q_B)) S(t_n, p_E, q_E) \\
 n &= \overline{1, N}
 \end{aligned}
 \tag{14}$$

In (14), the first multiplier forms the unmodulated carrier frequency, the second multiplier describes the switching at the pM point of the 16QAM signal from the value determined by the iB index to the value determined by the iE index, with the smoothing parameter qM. The third factor in (14) determines the switching of signals with zero boundary values at the points pB and pE with the corresponding smoothing parameters qB and qE.

Figure 2 shows the dependence of signal intensity x on time for its real part at the remote end of the fiber. The imaginary part of x, as well as the distribution for the real and imaginary parts of y, are not shown in Fig. 2, since the imaginary and real parts of the signal are shifted relative to each other by a quarter of the period, and the distribution for y is similar to the distribution for x.

A fragment of the graph illustrating ensuring continuity when switching the 16QAM information signal is shown in the inset of Fig. 2. This shows that the smoothing technique provides both the continuity of the function itself and its derivative. In the places where switching from the information signal to the zero value, similar requirements of the continuity of the sought functions are provided together with their derivatives.

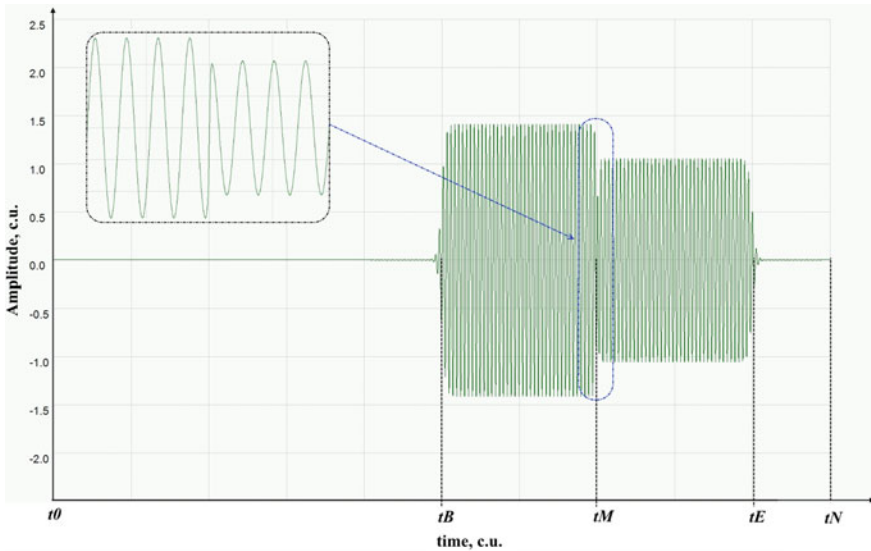


Fig. 2 The initial conditions for the real part x at the remote end of the optical fiber: the initial distribution and switching of the information signal from “0000” to “1001”

6 Ensuring the Necessary Accuracy of the Integration

Two layers along the spatial coordinate are the values of the sought functions on the k and $k + 1$ layers for all values of $n = 1, N$ over which integration is performed at each computational moment. Despite the absolute stability of the implicit Crank-Nicolson scheme, it is necessary to be sure that during the transition from layer to layer there is no loss of calculation accuracy and accumulation of error, which can become significant with a sufficiently large number of integration steps along the spatial coordinate. In addition, it is necessary not to lose sight of the fact that the scheme proposed above does not use a purely implicit, but a mixed Crank-Nicolson scheme. There is an approach that helps to minimize the disadvantage that the nonlinear addend is used in the scheme in an explicit form.

The transition at each integration step from k to $k + 1$ layers in space is carried out according to the following algorithm. The first step of the algorithm is to calculate the values of the sought functions x and y on the k -th unknown layer, using the values for the implicit multiplier (6) with $k + 1$ of the calculated layer from the explicit scheme. Denote the calculated values of the functions on the k -th layer:

$$(x_k^n)_i \text{ and } (y_k^n)_i \text{ for } n = \overline{1, N}, \tag{15}$$

where i —an iteration number taken after the first iteration step is a value equal to one.

Further, an iterative process is organized to find the desired functions x and y on the k -th unknown layer at the $i + 1$ iteration. In this case, the implicit multiplier (6) in the computational scheme is corrected each time as if its value on the k -th layer is already known. The value on the k -th layer itself is taken as the half-sum of the values on the k -th and $k + 1$ layers, but calculated at the previous iteration:

$$(\Phi_k^n)_{i+1} = \frac{(\Phi_k^n)_i + (\Phi_{k+1}^n)_i}{2}, \text{ for } n = \overline{1, N} \tag{16}$$

The iteration process is carried out until the maximum difference between the values calculated on the i and $i + 1$ iterations is less than the predetermined error:

$$\max(\max |(x_k^n)_{i+1} - (x_k^n)_i|, \max |(y_k^n)_{i+1} - (y_k^n)_i|) < \varepsilon, \text{ for } n = \overline{1, N} \tag{17}$$

The proposed iterative process is rapidly converging and requires 3–7 iterations, depending on the specified error value.

7 Integration with a Variable Step

Another factor that allows increasing the accuracy of calculations is the mechanism for automatic selection of the integration step. In this case, it is the automatic choice of the integration step by the spatial coordinate— Δz . The use of a variable integration step allows us to take into account the behavior of the solution and reduce the total number of steps while maintaining the required accuracy of the approximate solution. Thus, the amount of work and machine time can be reduced and the growth of computational error is slowed down [22].

The algorithm for automatic selection of the integration step is traditional, where two sets of values of the sought functions are compared in the norm—the calculated two integration steps with a step Δz_j , and the calculated one integration step with a double step $2\Delta z_j$. In case the norm is lower than the specified error, the integration step is increased 1.1–1.3 times, and the current values are recorded. At the norm above the specified error, the integration step decreases by 0.7–0.9 times, and the integration steps are recalculated.

Combining integration with variable steps and an iterative process that levels the use of the explicit-implicit scheme gives quite good results.

8 Numerical Results

To implement the proposed numerical method, a computer program was written in the C++ programming language. Figure 3 shows screenshots of the working area of the program, at all time points at different distances from the remote end of the optical fiber. In the left part of the program working area, the dependencies of the sought functions x and y on time are displayed at different distances. On the upper right graph, the distribution of the perturbation of the function x (real—blue and imaginary—red parts) along with the fiber from the time at point 0.45 sr. units from the beginning of the fiber counted from the beginning of one. Service messages are displayed in the lower right part of the program, control buttons are located and calculation parameters are set.

Despite the fact that the discussion of the results of calculations is beyond the scope of the objectives of this chapter, below are some analysis results of this work. First, there is a noticeable influence of nonlinear distortions, which consist of a blurring of wavefront and the distortion of the switching front of the information signal for 16QAM. Figure 3 shows a noticeable shift of the signal to the beginning of the time axis, with increasing distance from the far end of the optical fiber, which agrees well with the physical conditions for the propagation of optical disturbance in the fiber. The boundary conditions in the form of (2) or (7) determine that there was no disturbance in the entire fiber at the initial and final moments of time, in other words, there was a complete absence of a signal. However, the initial perturbation indicates that all perturbation is inside the fiber section. Therefore, the numerical

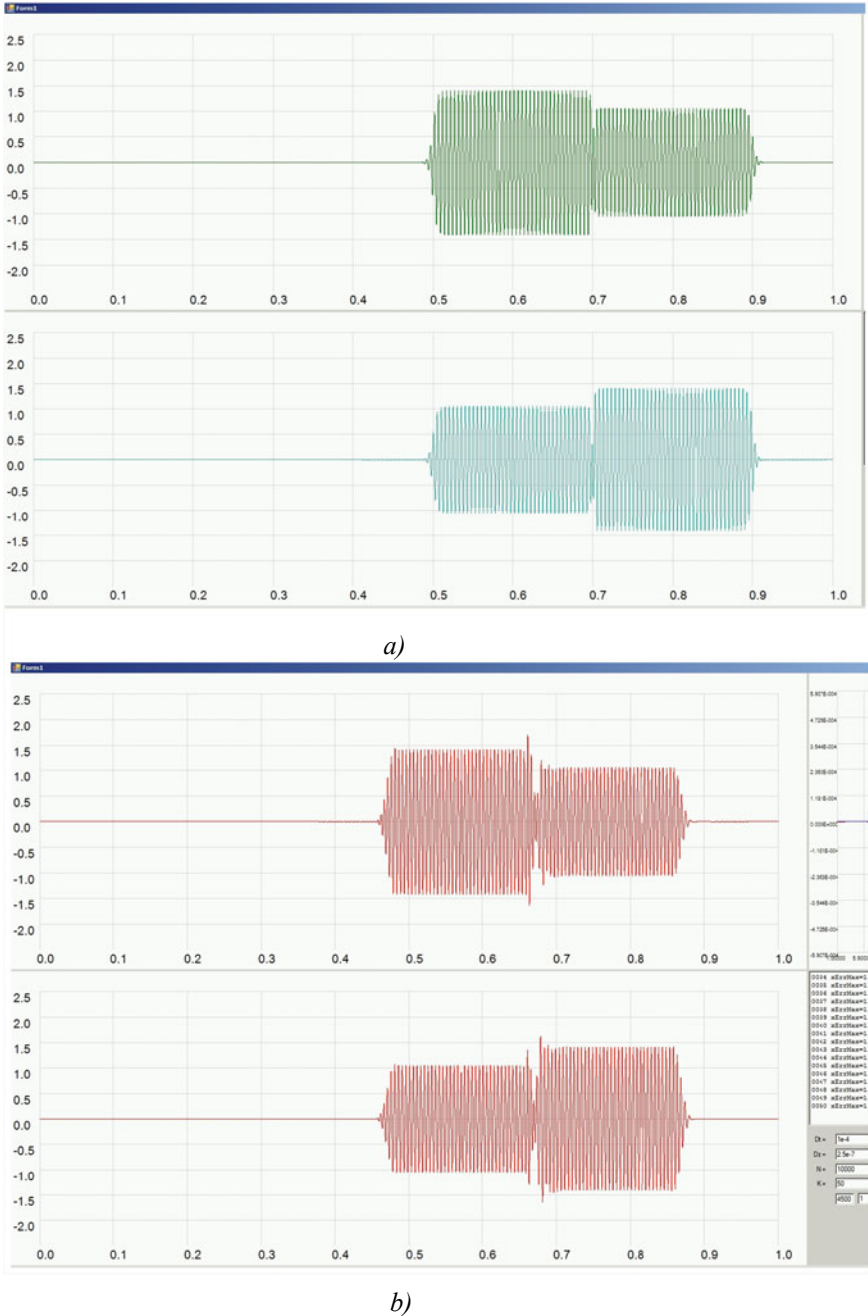
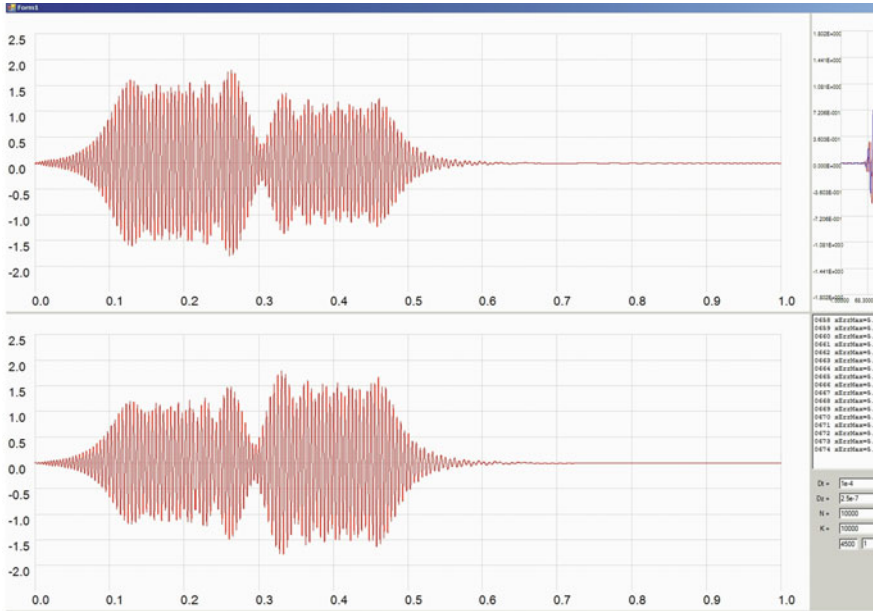
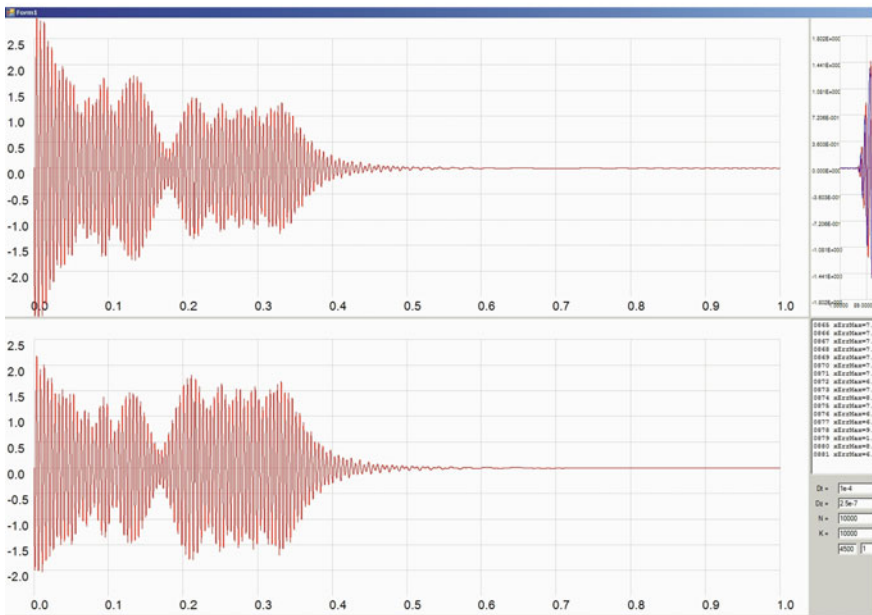


Fig. 3 The working screen of the numerical integration program of the equation system (5) for different values of the fiber length: **a** at the fiber end (initial distribution); and at a distance: **b** $50 \times \Delta z$, **c** $674 \times \Delta z$, **d** $881 \times \Delta z$ from the remote end. The task parameters are: $\Delta t = 10^{-4}$, $\Delta z = 2.5^{-7}$, $N = 10,000$, $\sigma = 0.5$



c)



d)

Fig. 3 (continued)

calculation is possible only up to the moment when the signal was introduced into the optical fiber. Figure 3b) shows that with continued integration beyond the fiber section in which the perturbation is introduced, the perturbation is reflected from the beginning of time $t = 0$, which leads to results explained from a physical point of view.

Figure 4 shows the calculations for the initial conditions, describing a single Gauss of a similar pulse in time, given only for the real part of the function x . The initial values of the imaginary part of the function x and the real and imaginary parts of the function y are set equal to zero.

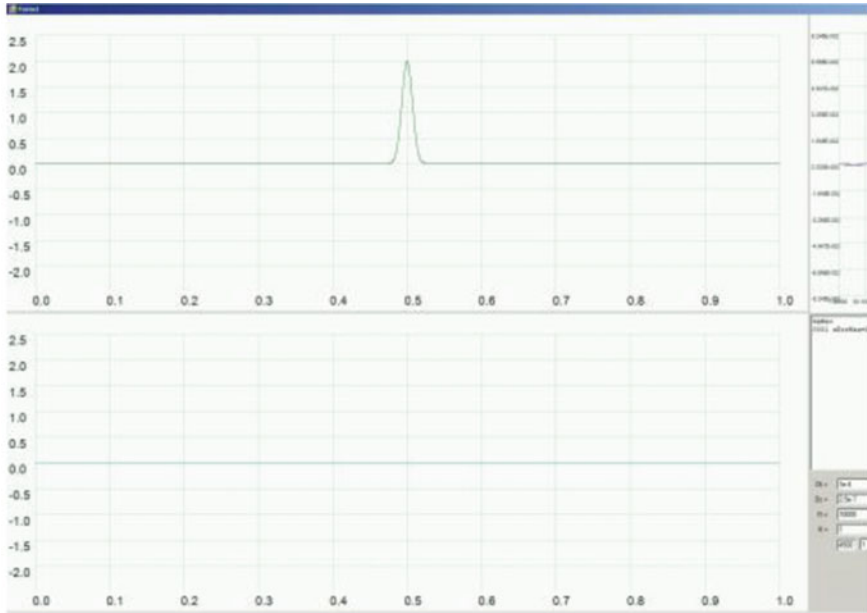
The shape of the deformation signal of the similar Gaussian, the nature and form of the appearance of its imaginary part, corresponds to the results outlined in the works of other authors [7], which further indicates the correctness of the assumptions made, the chosen integration methods and the correctness of the results obtained.

9 Calculations for a Long Section of Optical Fiber

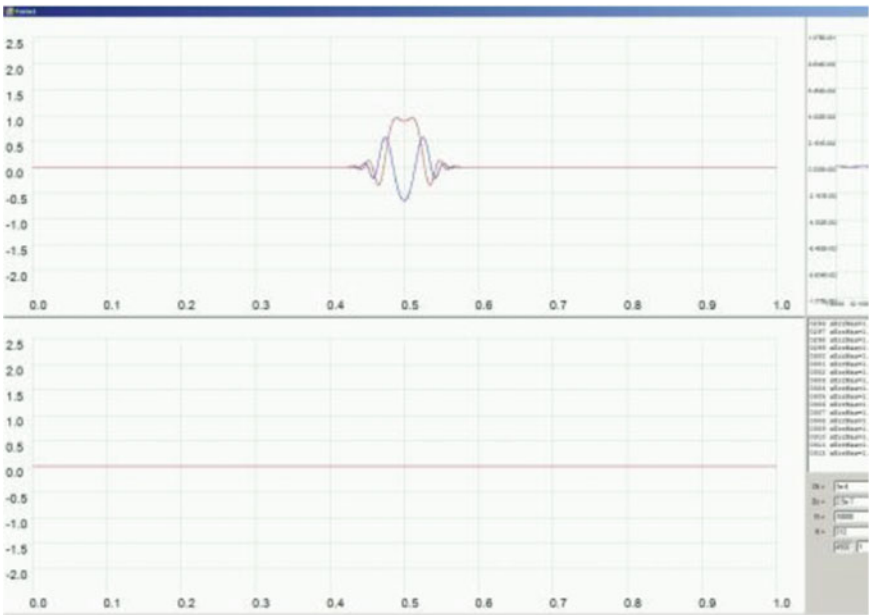
Distribution of the disturbance along the time axis from its current position to the beginning of the time reference point imposes a restriction on the possibility of calculations for extended sections of optical fiber. Combating this restriction directly leads to the need to dramatically increase the length of the arrays used to store information of the time interval containing all the disturbances from the beginning to the end while ensuring that there isn't the disturbance in the entire fiber at the initial and final points in time.

However, there is an approach that can provide continuous integration for long sections of optical fiber. For this purpose, it is necessary to consider a time segment with a sliding integration window [23]. Figure 5 shows a diagram-explanation, which makes it possible to implement calculation algorithms for long sections of optical fiber without the need to increase the size of arrays.

The one-dimensional array that forms the sought functions on the k -th and $k + 1$ spatial layers contain discrete samples with the values of the sought functions along the time axis. The initial distribution of the disturbance at the remote end looks like a dependence shown in Fig. 5, bounded by a red frame (state A), and located in the array x from the first to the last (N) element. At the same time, with an increase in the distance traveled, the disturbances shift relative to the array indices and at some point, further integration will be difficult as the disturbance approaches the left border of the array—the blue frame in Fig. 5 (state B). As soon as such a moment has arrived, it is sufficient to shift the perturbation curve with respect to the array, returning it to state A. With such a re-indexing (displacement of the perturbation relative to the array indices), the values of the sought functions in the initial part of the array (in Fig. 5 indicated by a blue dot-and-dash line) will be undefined. However, this disadvantage is easily remedied by smoothly stitching a part of the values in the array region that falls into both states (A and B) with the zero function. The values on the right-hand side (falling into state B, but not falling into state A) may be considered unnecessary.



a)



b)

Fig. 4 The working screen of the program of numerical integration of the equation system (5) for the single Gauss of the similar pulse: **a** at the end of the fiber (initial distribution), **b** at a distance of $312 \times \Delta z$ from the remote end of the fiber

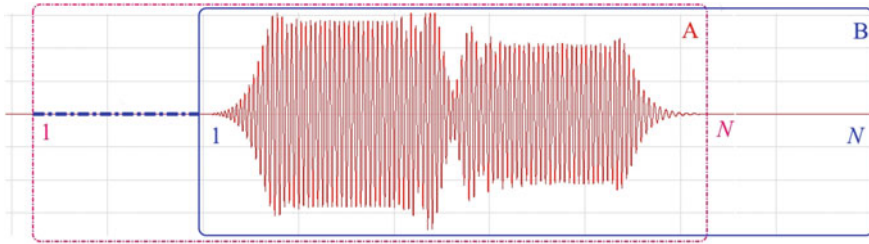


Fig. 5 Scheme explanation for the implementation of the calculation algorithms for long sections of optical fiber

10 Conclusions

Finding an approximate solution to the Schrödinger equation system related to the modeling of optical communication lines based on multimode fibers can be carried out using the combined explicitly-implicit numerical integration scheme based on the Crank-Nicholson scheme with writing the nonlinear term in the finite-difference form, which was obtained in the previous integration step.

The direct numerical integration method according to the combined explicitly-implicit finite-difference scheme in comparison with the splitting method into physical processes has a number of advantages. Firstly, it is the ability to ensure the absolute stability of the integration method due to the implicit finite-difference scheme. Secondly, this is the reduction in the computational complexity of the method due to the replacement at each step of the integration of two (direct and inverse) Fourier transforms by solving the system of linear equations by the sweep method. Thirdly, the inclusion in the method of the refinement solution algorithm at each integration step, which makes it possible to level the lack of recording of the nonlinear term taken from the previous integration step. Fourth, the algorithm for automatic selection of the integration step provides a higher integration speed, which reduces the computational complexity of the method. Fifthly, the displacement algorithm allows one to calculate the propagation of disturbances for extended sections of fiber.

The results of test calculations and comparisons of the results of calculations with the data of other authors allow concluding that the development of this algorithm is expedient and promising in the future.

Funding The reported study was funded by RFBR, project numbers 19-37-90057 and 19-57-80006.

References

1. Pouysegur, J., Guichard, F., Weichelt, B., Delaigue, M., Zaouter, Y., Hönninger, C., Mottay, E., Georges, P., Druon, F.: Single-stage Yb: YAG booster amplifier producing 2.3 mJ, 520 fs pulses at 10 kHz. *Advanced Solid State Lasers*, OSA Technical Digest (online), paper AW3A.5 (2015)
2. Tianprateep, M., Tada, J., Kannari, F.: Influence of polarization and pulse shape of femtosecond initial laser pulses on spectral broadening in microstructure fibers. *Opt. Rev.* **12**, 179–189 (2005). <https://doi.org/10.1007/s10043-005-0179-7>
3. Stingl, A.: Femtosecond future. *Nat. Photon.* **4**, 158 (2010)
4. Sibbett, W., Lagatsky, A.A., Brown, C.T.A.: The development and application of femtosecond laser systems. *Opt. Expr.* **20**(7), 6989–7001 (2012)
5. Zhou, X., Nelson, L.E., Isaac, R., Magill, P.D., Zhu, B., Borel, P., Carlson, K., Peckham, D.W.: 12,000 km transmission of 100 GHz spaced, 8495-Gb/s PDM time-domain hybrid QPSK-8QAM signals. *Optical Fiber Communication Conference and Exposition and the National Fiber Optic Engineers Conference (OFC/NFOEC)*. Anaheim, 2013. Paper OTu2B.4. (2013). <https://doi.org/10.1364/ofc.2013.otu2b.4>
6. Ip, E., Neng, B., Yue-Kai, H., Mateo, E., Yaman, F., Ming-Jun, L., Bickham, S., Ten, S., Linares, J., Montero, C., Moreno, V., Prieto, X., Tse, V., Kit Man, C., Lau, A., Hwa-yaw, T., Chao, L., Yanhua, L., Gang-Ding, P., Guifang, L.: $88 \times 3 \times 112$ -Gb/s WDM transmission over 50 km of three-mode fiber with inline few-mode fiber amplifier. In: *37th European Conference and Exhibition on Optical Communication (ECOC)*. Geneva, 2011. Paper Th.13.C.2 (2011). <https://doi.org/10.1364/ecoc.2011.th.13.c.2>
7. Takara, H.: 1.01-Pb/s (12 SDM/222 WDM/456 Gb/s) Crosstalk-managed transmission with 91.4-b/s/Hz aggregate spectral efficiency. In: *38th European Conference and Exhibition on Optical Communication (ECOC)*. Amsterdam, 2012. Th.3.C.1 (2012). <https://doi.org/10.1364/ecoc.2012.th.3.c.1>
8. Raja, S.J., Rao, S.S., Charlcedony, R.: Design and analysis of dispersion-compensating chalcogenide photonic crystal fiber with high birefringence. *SN Appl. Sci.* **2**, 499 (2020). <https://doi.org/10.1007/s42452-020-2308-0>
9. Mecozzi, A., Antonelli, C., Shtaif, M.: Nonlinear propagation in multi-mode fibers in the strong coupling regime. *Optic. Expr.* **20**(11), 11673–11678 (2012)
10. Mumtaz, S., Essiambre, R.J., Agrawal, G.P.: Nonlinear propagation in multimode and multicore fibers: generalization of the Manakov equations. *J. Lightw. Tech.* **31**(3), 398–406 (2013). <https://doi.org/10.1109/JLT.2012.2231401>
11. Marcuse, D., Manyuk, C.R., Wai, P.K.A.: Application of the Manakov-PMD equation to studies of signal propagation in optical fibers with randomly varying birefringence. *J. Lightw. Tech.* **15**(9), 1735–1746 (1997)
12. Nakazawa, M.: Evolution of EDFA from single-core to multi-core and related recent progress in optical communication. *Opt. Rev.* **21**, 862–874 (2014). <https://doi.org/10.1007/s10043-014-0139-1>
13. Sinkin, O.V., Holzlohner, R., Zweck, J., Menyuk, C.R.: Optimization of the split-step Fourier method in modeling optical fiber communications systems. *J. Lightw. Tech.* **21**(1), 61–68 (2003)
14. Burzler, J.M., Hughes, S., Wherrett, B.S.: Split-step fourier methods applied to model nonlinear refractive effects in optically thick media. *Appl. Phys. B* **62**, 389–397 (1996). <https://doi.org/10.1007/BF01081201>
15. Long, V.C., Viet, H.N., Trippenback, M., Xuan, K.D.: Propagation technique for ultrashort pulses II: Numerical methods to solve the pulse propagation equation. *Comp. Meth. Sci. Tech.* **14**(1), 13–19 (2008)
16. Burdin, V.A., Bourdine, A.V.: Simulation of an ultrashort optical pulse propagation in a polarization-maintaining optical fiber. *Appl. Photon.* **6**(1–2), 93–108 (2019)
17. Röpke, U., Bartelt, H., Unger, S., et al.: Fiber waveguide arrays as model system for discrete optics. *Appl. Phys. B* **104**, 481 (2011). <https://doi.org/10.1007/s00340-011-4635-8>

18. Mecozzi, A., Antonelli, C., Shtaif, M.: Coupled Manakov equations in multimode fibers with strongly coupled groups of modes. *Opt. Expr.* **20**(21), 23436–23441 (2012). <https://doi.org/10.1364/OE.20.023436>
19. Mecozzi, A., Antonelli, C., Shtaif, M.: Nonlinear propagation in multi-mode fibers in the strong coupling regime. *Opt. Expr.* **20**(11), 11673–11678 (2012)
20. Fedoruk, M.P., Sidelnikov, O.S.: Algorithms for numerical simulation of optical communication links based on multimode fiber. *Comput. Tech.* **20**(5), 105–119 (2015)
21. Anfinogentov, V.I., Morozov, G.A.: The review of methods of physical and mathematical modelling of the microwave heating. In: 13th International Crimean Conference “Microwave and Telecommunication Technology”, CriMiCo 2003, Conference Proceedings, pp. 710–711 (2003)
22. Sakhabutdinov, Zh.M.: Discrete models for motion of a point, 196 p. IMM RAN (1995)
23. Ivanov, D.V.: Methods and mathematical models for studying the propagation in the ionosphere of complex decameter signals and the correction of their dispersion distortions, 266 p. MarGTU (2006)

Research of the Boundary Value Problem for the Sophie Germain Equation in a Cyber-Physical System



Andrey Ushakov

Abstract We consider the boundary value problem for an inhomogeneous biharmonic equation and extend the problem in a variational form. Also, we carry out the discretization of the considered problem by the finite element method. The continued problems, is presented in matrix form. An iterative process is formulated for an approximate solution to the original problem. The problem in matrix form is solved by method of fictitious components. Estimates of the convergence of the iterative process are given. Research of the problem being solved is reduced to a cyber-physical system. The estimates of the convergence of the absolute error do not depend on the grid steps. An algorithm is formulated for solving the investigated computer problem. To process information in the algorithm, a variation method is used. The steepest descent method is used to control computations in the iterative process. The software implementation of the algorithm uses certain elements of artificial intelligence.

Keywords Sophie Germain equation · Biharmonic equation · Boundary value problem · Fictitious component method · Cyber-physical system

1 Introduction

Let us consider a mathematical model of displacements of plate points given in the theory of elasticity. This boundary value problem is considered for a biharmonic equation under general assumptions ensuring the existence and uniqueness of the solution [1–10]. We carry out a fictitious extension of this problem in a variational form. Let us formulate a modified fictitious component method for the analytical solution of the problem under consideration. For the numerical solution of the problem, we apply the methods of finite elements and fictitious components [11–13]. The numerical solution of the problem is reduced to the numerical solution of the discrete analogue of the fourth-order elliptic boundary value problem in a rectangular domain [14–20].

A. Ushakov (✉)
South Ural State University, 76 Lenina, Chelyabinsk 454080, Russia
e-mail: ushakov_al@inbox.ru

© The Author(s), under exclusive license to Springer Nature Switzerland AG 2021
A. G. Kravets et al. (eds.), *Cyber-Physical Systems: Modelling and Intelligent Control*, Studies in Systems, Decision and Control 338,
https://doi.org/10.1007/978-3-030-66077-2_5

We implement a numerical method for solving the problem in the form of an iterative algorithm. In the algorithm, we indicate a method for automatically selecting iterative parameters and criteria for stopping the iterative process. Research of the original problem will be reduced to a cyber-physical system. Note that the considered problem is linear and stationary. However, the method for solving the problem is non-linear and non-stationary.

2 Mathematical Model of Displacements of Plate Points Ina Physical System

Consider bounded domains $\Omega, \Omega_\alpha \subset R^2, \alpha \in \{I, II\}$ on the plane that have piecewise-smooth boundaries without self-intersections and self-tangencies:

$$\Omega_I, \Omega_{II} \subset \Omega, \bar{\Omega}_I \cup \bar{\Omega}_{II} = \bar{\Omega}, \Omega_I \cap \Omega_{II} = \emptyset, \partial\Omega_I \cap \partial\Omega_{II} = \Gamma_{I,0} \cap \Gamma_{II,3} = \bar{S} \neq \emptyset, \partial\Omega_\alpha = \bar{s}_\alpha, s_\alpha = \Gamma_{\alpha,0} \cup \Gamma_{\alpha,1} \cup \Gamma_{\alpha,2} \cup \Gamma_{\alpha,3}, \Gamma_{\alpha,i} \cap \Gamma_{\alpha,j} = \emptyset, i \neq j, i, j = 0, 1, 2, 3,$$

$$\partial\Omega = \bar{s}, s = \Gamma_0 \cup \Gamma_1 \cup \Gamma_2 \cup \Gamma_3, \Gamma_i \cap \Gamma_j = \emptyset, i \neq j, i, j = 0, 1, 2, 3.$$

The unions of a finite number of disjoint open arcs of smooth curves give parts of the boundaries of these domains $\Gamma_i, \Gamma_{\alpha,i}, i = 0, 1, 2, 3$.

Consider the boundary value problem and its zero extension under four types of boundary conditions on the corresponding domains $\Omega_\alpha, \alpha \in \{I, II\}$,

$$\Delta^2 \tilde{u}_\alpha + a_\alpha \tilde{u}_\alpha = \tilde{f}_\alpha, a_I = 0, a_{II} \geq 0, \tilde{f}_{II} = 0, \quad (1)$$

$$0) \tilde{u}_\alpha \Big|_{\Gamma_{\alpha,0}} = \frac{\partial \tilde{u}_\alpha}{\partial n_\alpha} \Big|_{\Gamma_{\alpha,0}} = 0, \quad (2)$$

$$1) \tilde{u}_\alpha \Big|_{\Gamma_{\alpha,1}} = l_{\alpha,1} \tilde{u}_\alpha \Big|_{\Gamma_{\alpha,1}} = 0, \quad (3)$$

$$2) \frac{\partial \tilde{u}_\alpha}{\partial n_\alpha} \Big|_{\Gamma_{\alpha,2}} = l_{\alpha,2} \tilde{u}_\alpha \Big|_{\Gamma_{\alpha,2}} = 0, \quad (4)$$

$$3) l_{\alpha,1} \tilde{u}_\alpha \Big|_{\Gamma_{\alpha,3}} = l_{\alpha,2} \tilde{u}_\alpha \Big|_{\Gamma_{\alpha,3}} = 0. \quad (5)$$

Here we use the differential operators on the boundary

$$l_{\alpha,1} \tilde{u}_\alpha = (1 - \sigma_\alpha) n_{\alpha,1} n_{\alpha,2} \tilde{u}_{\alpha,xy} - n_{\alpha,2}^2 \tilde{u}_{\alpha,xx} - n_{\alpha,1}^2 \tilde{u}_{\alpha,yy}, \quad (6)$$

$$l_{\alpha,2}\tilde{u}_\alpha = \frac{\partial \Delta \tilde{u}_\alpha}{\partial n_\alpha} + (1 - \sigma_\alpha) \frac{\partial}{\partial s_\alpha} (n_{\alpha,1}n_{\alpha,2}(\tilde{u}_{\alpha yy} - \tilde{u}_{\alpha xx}) + (n_{\alpha,1}^2 - n_{\alpha,2}^2)\tilde{u}_{\alpha xy}),$$

n_α are external normals to the corresponding boundaries $\partial\Omega_\alpha$, $n_{\alpha,1} = -\cos(n_\alpha, x)$, $n_{\alpha,2} = -\cos(n_\alpha, y)$, σ_α is Poisson's ratio, \tilde{u}_α are displacements of the points of the plate and its extension. We consider the problem and its extension with a finite number of the points, where the type of the boundary condition is changed.

Introduce the bilinear forms

$$\begin{aligned} \Lambda_\alpha(\tilde{u}_\alpha, \tilde{v}_\alpha) = & \int (\sigma_\alpha \Delta \tilde{u}_\alpha \Delta \tilde{v}_\alpha + \\ & + (1 - \sigma_\alpha)(\tilde{u}_{\alpha xx} \tilde{v}_{\alpha xx} + 2\tilde{u}_{\alpha xy} \tilde{v}_{\alpha xy} + \tilde{u}_{\alpha yy} \tilde{v}_{\alpha yy}) + a_\alpha \tilde{u}_\alpha \tilde{v}_\alpha) d\Omega_\alpha. \end{aligned}$$

Consider the boundary value problem and its zero extension in the variational form

$$\tilde{u}_\alpha \in \tilde{H}_\alpha : \Lambda_\alpha(\tilde{u}_\alpha, \tilde{v}_\alpha) = g_\alpha(\tilde{v}_\alpha) \quad \forall \tilde{v}_\alpha \in \tilde{H}_\alpha, \quad \alpha \in \{1, \text{II}\}. \tag{7}$$

Here we use the function spaces and functionals of the right parts:

$$\begin{aligned} \tilde{v}_\alpha \in \tilde{H}_\alpha = \tilde{H}_\alpha(\Omega_\alpha) = W_2^2(\Omega_\alpha) : \tilde{v}_\alpha \Big|_{\Gamma_1 \cap \Gamma_0} = \frac{\partial \tilde{v}_\alpha}{\partial n_\alpha} \Big|_{\Gamma_{\alpha,0} \cup \Gamma_{\alpha,2}} = 0, \\ g_\alpha(\tilde{v}_\alpha) = \left(\tilde{f}_\alpha, \tilde{v}_\alpha \right) = \int \tilde{f}_\alpha \tilde{v}_\alpha d\Omega_\alpha. \end{aligned}$$

For such problems, the assumptions that ensure the existence and uniqueness of solution to each of the problem are quite common:

$$\exists c_1, c_2 > 0 : c_1 \|\tilde{v}_\alpha\|_2^2 \leq \Lambda_\alpha(\tilde{u}_\alpha, \tilde{v}_\alpha) \leq c_2 \|\tilde{v}_\alpha\|_2^2 \quad \forall \tilde{v}_\alpha \in \tilde{H}_\alpha.$$

Here, for functions, we use the norms of Sobolev spaces $\|\tilde{v}_\alpha\|_2 = \|\tilde{v}_\alpha\|_{W_2^2(\Omega_\alpha)}$.

3 Analytical Computing System. Modified Method of Fictitious Components for Finding Displacements of Plate Points

Consider the bilinear form

$$\Lambda(\tilde{u}, \tilde{v}) = \Lambda_1(\tilde{u}, \tilde{v}) + \Lambda_{\Pi}(\tilde{u}, \tilde{v}) \quad \forall \tilde{u}, \tilde{v} \in \tilde{V}.$$

Here the function space has the norm

$$\tilde{v} \in \tilde{V} = \tilde{V}(\Omega) = W_2^2(\Omega) : \tilde{v} \Big|_{\Gamma_0 \cup \Gamma_1} = \frac{\partial \tilde{v}}{\partial n} \Big|_{\Gamma_0 \cup \Gamma_2} = 0, \quad \|\tilde{v}\|_{\tilde{V}} = \sqrt{\Lambda(\tilde{v}, \tilde{v})},$$

n is the external normal to $\partial\Omega$. We assume that the following inequalities hold:

$$\exists c_1, c_2 > 0 : c_1 \|\tilde{v}\|_{W_2^2(\Omega)}^2 \leq \Lambda(\tilde{u}, \tilde{v}) \leq c_2 \|\tilde{v}\|_{W_2^2(\Omega)}^2 \quad \forall \tilde{v} \in \tilde{V}.$$

Define the subspaces of functions $\tilde{V}_1 = \left\{ v_1 \in \tilde{V} : \tilde{v}_1 \Big|_{\Omega \setminus \Omega_1} = 0 \right\}$, $\tilde{V}_3 = \left\{ \tilde{v}_3 \in \tilde{V} : \tilde{v}_3 \Big|_{\Omega \setminus \Omega_{\Pi}} = 0 \right\}$, $\tilde{V}_1 \oplus \tilde{V}_3 = \tilde{V}_0$,

$$\tilde{V}_2 = \left\{ \tilde{v}_2 \in \tilde{V} : \Lambda(\tilde{v}_2, \tilde{v}_0) = 0 \quad \forall \tilde{v}_0 \in \tilde{V}_0 \right\}, \quad \tilde{V}_0 \oplus \tilde{V}_2 = \tilde{V}.$$

Here we consider the direct sum of subspaces in the scalar product generated by the bilinear form $\Lambda(*, *)$. Introduce the operators of projection of the space on subspaces: $I_j: \tilde{V} \rightarrow \tilde{V}_j : \tilde{V}_j = im I_j$, $I_j = I_j^2$, $j = 0, 1, 3$, $I_0 = I_1 + I_3$.

Extend the considered problem and write the problem in the variational form—:

$$\tilde{u} \in \tilde{V} : \Lambda_1(\tilde{u}, I_1 \tilde{v}) + \Lambda_{\Pi}(\tilde{u}, \tilde{v}) = g_1(I_1 \tilde{v}) \quad \forall \tilde{v} \in \tilde{V}. \quad (8)$$

In view of the possibility to extend functions under the same norm in the corresponding Sobolev spaces, we consider the assumption about the extension of the functions $\exists \tilde{\beta}_1 \in (0; 1]$, $\exists \tilde{\beta}_2 \in (\tilde{\beta}_1; 1]$: $\tilde{\beta}_1 \Lambda(\tilde{v}_2, \tilde{v}_2) \leq \Lambda_{\Pi}(\tilde{v}_2, \tilde{v}_2) \leq \tilde{\beta}_2 \Lambda(\tilde{v}_2, \tilde{v}_2) \quad \forall \tilde{v}_2 \in \tilde{V}_2$. to be satisfied. In order to solve the problem written in the variational form, we formulate the modified method of fictitious components:

$$\begin{aligned} \tilde{u}^k \in \tilde{V} : \Lambda(\tilde{u}^k - \tilde{u}^{k-1}, \tilde{v}) \\ = -\tau_{k-1}(\Lambda_1(\tilde{u}^{k-1}, I_1 \tilde{v}) + \Lambda_{\Pi}(\tilde{u}^{k-1}, \tilde{v}) - g_1(I_1 \tilde{v})) \quad \forall \tilde{v} \in \tilde{V}, \end{aligned}$$

$$\tau_0 = 1, \tau_{k-1} = 2/\tilde{\beta}_1 + \tilde{\beta}_2, k \in \mathbb{N} \setminus \{1\} \forall \tilde{u}^0 \in \tilde{V}_1. \tag{9}$$

For the modified method of fictitious components, the convergence estimate is known:

$$\begin{aligned} \|\tilde{u}^k - \tilde{u}\|_{\tilde{V}} &\leq \varepsilon \|\tilde{u}^0 - \tilde{u}\|_{\tilde{V}}, \quad \varepsilon = cq^{k-1}, \quad c \in [0; +\infty), \quad k \in \mathbb{N}, \\ q &= (\tilde{\beta}_2 - \tilde{\beta}_1) / (\tilde{\beta}_1 + \tilde{\beta}_2) < 1, \quad c = \sqrt{\|I_1\|_{\tilde{V}}^2 - 1}. \end{aligned}$$

Note that the estimate of the iterative process convergence is optimal. If the norm of the projection operator is equal to unity, then the iterative process converges in one iteration.

4 Computing System. Numerical Method of Fictitious Components for Finding Displacements of Platepoints

Consider the extended problem under the additional assumptions:

$$\Omega = (0; b_1) \times (0; b_2), \quad b_1, b_2 \in (0; +\infty), \quad \partial \Omega = \bar{s}, \quad s = \Gamma_1 \cup \Gamma_2, \quad \Gamma_0, \Gamma_3 = \emptyset,$$

$$\Gamma_1 = \{b_1\} \times (0; b_2) \cup (0; b_1) \times \{b_2\}, \quad \Gamma_2 = \{0\} \times (0; b_2) \cup (0; b_1) \times \{0\}.$$

Select a grid with nodes at points of the rectangular domain Ω

$$(x_i; y_j) = ((i - 0, 5)h_1; (j - 0, 5)h_2), \quad h_1 = b_1 / (m + 0, 5), \quad h_2 = b_2 / (n + 0, 5),$$

$$i = 1, 2, \dots, m, \quad j = 1, 2, \dots, n, \quad m, n \in \mathbb{N}.$$

Let $v_{i,j} \in R$ be the values of functions of discrete arguments at grid nodes. Introduce the subspace of functions with the norm

$$\tilde{V} = \left\{ \tilde{v} : \tilde{v} = \sum_{i=1}^m \sum_{j=1}^n v_{i,j} \Phi^{i,j}(x; y) \right\} \subset \tilde{V}, \quad \|\tilde{v}\|_{\tilde{V}} = \sqrt{\Lambda(\tilde{v}, \tilde{v})}.$$

Here we use the known functions

$$\Phi^{i,j}(x; y) = \Psi_{1,i}(x)\Psi_{1,j}(y), \quad i = 1, 2, \dots, m, \quad j = 1, 2, \dots, n,$$

$$\Psi_{1,i}(x) = E(1/i)\Psi(x/h_1 - i + 3) + \Psi(x/h_1 - i + 2) - E(i/m)\Psi(x/h_1 - i),$$

$$\Psi_{2,j}(y) = E(1/j)\Psi(y/h_2 - j + 3) + \Psi(y/h_2 - j + 2) - E(j/n)\Psi(y/h_2 - j),$$

$$\Psi(z) = \begin{cases} 0, 5z^2, & z \in [0; 1], \\ -z^2 + 3z - 1, 5, & z \in [1; 2], \\ 0, 5z^2 - 3z + 4, 5, & z \in [2; 3], \end{cases}$$

$\Psi(z) = 0$, $z \notin (0; 3)$, $E(*)$ is the function that gives the integer part of a number. Additionally, we assume that all basis functions have the property

$$\Phi^{i,j}(x; y) = 0, (x; y) \notin \Omega, i = 1, 2, \dots, m, j = 1, 2, \dots, n.$$

Define the subspaces of functions $\tilde{V}_1 = \{ \tilde{v}_1 \in \tilde{V} : \tilde{v}_1|_{\Omega \setminus \Omega_1} = 0 \}$, $\tilde{V}_3 = \{ \tilde{v}_3 \in \tilde{V} : \tilde{v}_3|_{\Omega \setminus \Omega_{II}} = 0 \}$, $\tilde{V}_1 \oplus \tilde{V}_3 = \tilde{V}_0$,

$$\tilde{V}_2 = \{ \tilde{v}_2 \in \tilde{V} : \Lambda(\tilde{v}_2, \tilde{v}_0) = 0 \forall \tilde{v}_0 \in \tilde{V}_0 \}, \tilde{V}_0 \oplus \tilde{V}_2 = \tilde{V}.$$

Here we consider the direct sum of subspaces in the scalar product generated by the bilinear form $\Lambda(*, *)$. The previously introduced projection operators act similarly on the corresponding finite-dimensional subspaces

$$I_j : \tilde{V} \rightarrow \tilde{V}_j : \tilde{V}_j = im I_j, I_j = I_j^2, j = 0, 1, 3, I_0 = I_1 + I_3.$$

The extended problem is written on the finite-dimensional subspace:

$$\tilde{u} \in \tilde{V} : \Lambda_1(\tilde{u}, I_1 \tilde{v}) + \Lambda_{II}(\tilde{u}, \tilde{v}) = g_1(I_1 \tilde{v}) \forall \tilde{v} \in \tilde{V}. \quad (10)$$

In view of the possibility to extend functions under the same norm in the corresponding Sobolev spaces, we consider the assumption about the extension of the functions on finite-dimensional subspaces

$\exists \tilde{\beta}_1 \in (0; 1], \exists \tilde{\beta}_2 \in (\tilde{\beta}_1; 1] : \tilde{\beta}_1 \Lambda(\tilde{v}_2, \tilde{v}_2) \leq \Lambda_{II}(\tilde{v}_2, \tilde{v}_2) \leq \tilde{\beta}_2 \Lambda(\tilde{v}_2, \tilde{v}_2) \forall \tilde{v}_2 \in \tilde{V}_2$ to be satisfied. In order to solve the problem on a finite-dimensional subspace, we formulate the modified method of fictitious components:

$$\begin{aligned} \tilde{u}^k \in \tilde{V} : \Lambda(\tilde{u}^k - \tilde{u}^{k-1}, \tilde{v}) = \\ = -\tau_{k-1}(\Lambda_1(\tilde{u}^{k-1}, I_1 \tilde{v}) + \Lambda_{II}(\tilde{u}^{k-1}, \tilde{v}) - g_1(I_1 \tilde{v})) \forall \tilde{v} \in \tilde{V}, \\ \tau_0 = 1, \tau_{k-1} = 2/(\tilde{\beta}_1 + \tilde{\beta}_2), k \in \mathbb{N} \setminus \{1\} \forall \tilde{u}^0 \in \tilde{V}_1. \end{aligned} \quad (11)$$

For the modified method of fictitious components on a finite-dimensional subspace, the following convergence estimate takes place:

$$\begin{aligned} \left\| \bar{u}^k - \bar{u} \right\|_{\bar{V}} &\leq \varepsilon \left\| \bar{u}^0 - \bar{u} \right\|_{\bar{V}}, \varepsilon = cq^{k-1}, c \in [0; +\infty), k \in \mathbb{N}, \\ q &= (\bar{\beta}_2 - \bar{\beta}_1) / (\bar{\beta}_1 + \bar{\beta}_2) < 1, c = \sqrt{\|I_1\|_{\bar{V}}^2 - 1}. \end{aligned}$$

Note that the estimate of the iterative process convergence may not depend on the discretization parameters under the appropriate construction of the projection operator I_1 .

If we number the values of the discrete functions, the coefficients of the basis functions at the corresponding nodes of the grid, then we obtain the vectors

$$\begin{aligned} \bar{v} &= (v_1, \dots, v_N) \in R^N, N = mn, v_{n(i-1)+j} = v_{i,j} \in \mathbb{R}, \\ & i = 1, 2, \dots, m, j = 1, 2, \dots, n. \end{aligned}$$

When discretizing the extended problem by the finite element method, we obtain the system of linear algebraic equations

$$\bar{u} \in R^N : B\bar{u} = \bar{g}, \bar{g} \in R^N. \tag{12}$$

Here the matrix of the system and the vector of the right-hand side are defined as follows:

$$\begin{aligned} \langle B\bar{u}, \bar{v} \rangle &= \Lambda_1(\bar{u}, I_1\bar{v}) + \Lambda_{II}(\bar{u}, \bar{v}) \quad \forall \bar{u}, \bar{v} \in \bar{V}, \\ \langle \bar{g}, \bar{v} \rangle &= g_1(I_1\bar{v}) \quad \forall \bar{v} \in \bar{V}, \quad \langle \bar{u}, \bar{v} \rangle = (\bar{u}, \bar{v})h_1h_2, \end{aligned}$$

(\bar{u}, \bar{v}) is the usual scalar product of vectors. Consider the case when the operator of projection on the first finite-dimensional subspace zeros the coefficients of the basis functions, which carriers are not contained in the first domain. Formulate a modified method of fictitious components at the matrix level, which in this case coincides with the method of fictitious components:

$$\begin{aligned} \bar{u}^k \in R^N : \Lambda(\bar{u}^k - \bar{u}^{k-1}) &= -\tau_{k-1}(B\bar{u}^{k-1} - \bar{g}), \\ \tau_0 &= 1, \tau_{k-1} = 2 / (\bar{\beta}_1 + \bar{\beta}_2), k \in \mathbb{N} \setminus \{1\} \quad \forall \bar{u}^0 \in \bar{V}_1, \end{aligned} \tag{13}$$

$\bar{V}_1 \subset R^N$ is the subspace corresponding to the subspace $\tilde{V}_1 \subset \tilde{V}$, Λ is a matrix, which we define as follows:

$$\langle \Lambda\bar{u}, \bar{v} \rangle = \Lambda(\bar{u}, \bar{v}) \quad \forall \bar{u}, \bar{v} \in \bar{V}.$$

Introduce the norms

$$\|\bar{v}\| = \sqrt{\langle \bar{v}, \bar{v} \rangle}, \|\bar{v}\|_{\Lambda} = \sqrt{\langle \Lambda\bar{v}, \bar{v} \rangle}, \|\bar{v}\|_{\Lambda^2} = \sqrt{\langle \Lambda^2\bar{v}, \bar{v} \rangle}.$$

For the iterative process, the following estimates of convergence take place:

$$\begin{aligned} \|\bar{u}^k - \bar{u}\|_A &\leq \varepsilon \|\bar{u}^0 - \bar{u}\|_{A^2}, \quad \|\bar{u}^k - \bar{u}\|_A \leq \varepsilon \|\bar{g}^0 - \bar{g}\|, \\ \varepsilon &= cq^{k-1}, \quad c \in (0; +\infty), \quad q = (\tilde{\beta}_2 - \tilde{\beta}_1) / (\tilde{\beta}_1 + \tilde{\beta}_2) < 1, \quad \bar{g}^0 = \Lambda \bar{u}^0, \\ c &\approx 8\pi^{-2}(b_1^{-2} + b_2^{-2})^{-1}, \quad h_1, h_2 \rightarrow 0. \end{aligned}$$

In particular, for $\bar{u}^0 = \bar{0}$

$$\|\bar{u}^k - \bar{u}\|_A \leq \varepsilon \|\bar{u}\|_{A^2}, \quad \|\bar{u}^k - \bar{u}\|_A \leq \varepsilon \|\bar{g}\|.$$

From the above estimates, it is possible to obtain estimates of the relative error of the iterative process in the energy norm, but the obtained estimates depend on the specific solution and the discretization parameters.

First, we number the values of discrete functions and the coefficients for the basis functions at the corresponding grid nodes:

$$v_{n(i-1)+j} = v_{i,j} \in R, \quad i = 1, 2, \dots, m, \quad j = 1, 2, \dots, n.$$

Next, first of all, we enumerate the coefficients of the basis functions, which carriers are contained in the first domain. Second, we enumerate the coefficients of the basis functions, which carriers intersect the boundaries of the first and second domains. Third, we enumerate the coefficients of the basis functions, which carriers are contained in the second domain. For example, the new numbering reduces the structure of previously arising matrices and vectors as follows:

$$A = \begin{bmatrix} \Lambda_{11} & \Lambda_{12} & 0 \\ \Lambda_{21} & \Lambda_{22} & \Lambda_{23} \\ 0 & \Lambda_{32} & \Lambda_{33} \end{bmatrix}, \quad B = \begin{bmatrix} \Lambda_{11} & \Lambda_{12} & 0 \\ 0 & \Lambda_{02} & \Lambda_{23} \\ 0 & \Lambda_{32} & \Lambda_{33} \end{bmatrix}, \quad \bar{v} = \begin{bmatrix} \bar{v}_1 \\ \bar{v}_2 \\ \bar{v}_3 \end{bmatrix} \in R^N.$$

The vectors of the desired solution and the right-hand side after zero extension, zero approximation, approximate solution, and iterative process errors are written as follows:

$$\bar{u} = \begin{bmatrix} \bar{u}_1 \\ \bar{0} \\ \bar{0} \end{bmatrix}, \quad \bar{g} = \begin{bmatrix} \bar{g}_1 \\ \bar{0} \\ \bar{0} \end{bmatrix}, \quad \bar{u}^0 = \begin{bmatrix} \bar{u}_1^0 \\ \bar{0} \\ \bar{0} \end{bmatrix}, \quad \bar{u}^k = \begin{bmatrix} \bar{u}_1^k \\ \bar{u}_2^k \\ \bar{u}_3^k \end{bmatrix}, \quad \bar{\psi}^k = \begin{bmatrix} \bar{\psi}_1^k \\ \bar{\psi}_2^k \\ \bar{\psi}_3^k \end{bmatrix}.$$

Define the subspaces of vectors

$$\bar{V}_1 = \{\bar{v} \in R^N : \bar{v}_2 = \bar{0}, \bar{v}_3 = \bar{0}\}, \quad \bar{V}_3 = \{\bar{v} \in R^N : \bar{v}_1 = \bar{0}, \bar{v}_2 = \bar{0}\},$$

$$\bar{V}_1 \oplus \bar{V}_3 = \bar{V}_0 = \{ \bar{v} \in R^N : \bar{v}_2 = \bar{0} \},$$

$$\bar{V}_2 = \{ \bar{v} \in R^N : \Lambda_{11}\bar{v}_1 + \Lambda_{12}\bar{v}_2 = \bar{0}, \Lambda_{32}\bar{v}_2 + \Lambda_{33}\bar{v}_3 = \bar{0} \}, \bar{V}_0 \oplus \bar{V}_2 = R^N.$$

Here we consider the direct sum of the subspaces of vectors in the scalar product $\langle \Lambda*, * \rangle$. It follows from the iterative process that

$$\begin{aligned} \Lambda(\bar{\psi}^1 - \bar{\psi}^0) &= -\Lambda_{11}\bar{\psi}_1^0, \quad \Lambda(\bar{\psi}^1 - \bar{\psi}^0)\Lambda(\bar{\psi}^1 - \bar{\psi}^0) = \Lambda_{11}\bar{\psi}_1^0\Lambda_{11}\bar{\psi}_1^0, \\ \Lambda\bar{\psi}^1\Lambda\bar{\psi}^1 - 2\Lambda\bar{\psi}^1\Lambda\bar{\psi}^0 + \Lambda\bar{\psi}^0\Lambda\bar{\psi}^0 &= \Lambda_{11}\bar{\psi}_1^0\Lambda_{11}\bar{\psi}_1^0. \end{aligned}$$

Take into account that

$$\Lambda\bar{\psi}^0\Lambda\bar{\psi}^0 \geq \Lambda_{11}\bar{\psi}_1^0\Lambda_{11}\bar{\psi}_1^0,$$

and obtain

$$\begin{aligned} \Lambda\bar{\psi}^1\Lambda\bar{\psi}^1 - 2\Lambda\bar{\psi}^1\Lambda\bar{\psi}^0 &\leq 0, \quad \Lambda\bar{\psi}^1\Lambda\bar{\psi}^1 \leq 2\Lambda\bar{\psi}^1\Lambda\bar{\psi}^0, \\ (\Lambda\bar{\psi}^1\Lambda\bar{\psi}^1)^2 &\leq 4(\Lambda\bar{\psi}^1\Lambda\bar{\psi}^0)^2. \end{aligned}$$

Apply the inequality for the scalar product of vectors

$$(\Lambda\bar{\psi}^1\Lambda\bar{\psi}^1)^2 \leq 4(\Lambda\bar{\psi}^1\Lambda\bar{\psi}^0)^2 \leq 4(\Lambda\bar{\psi}^1\Lambda\bar{\psi}^1)(\Lambda\bar{\psi}^0\Lambda\bar{\psi}^0).$$

As a result of reduction, we have

$$\begin{aligned} (\Lambda\bar{\psi}^1\Lambda\bar{\psi}^1) &\leq 4(\Lambda\bar{\psi}^0\Lambda\bar{\psi}^0), \quad \|\bar{\psi}^1\|_{\Lambda^2} \leq 2\|\bar{\psi}^0\|_{\Lambda^2}, \\ \|\bar{u}^1 - \bar{u}\|_{\Lambda^2} &\leq 2\|\bar{u}^0 - \bar{u}\|_{\Lambda^2}. \end{aligned}$$

Note that

$$\begin{aligned} \exists K(h_1, h_2) \in (0; +\infty) : (\Lambda\bar{\psi}^1, \bar{\psi}^1) &\leq K^2(h_1, h_2)(\Lambda\bar{\psi}^1\Lambda\bar{\psi}^1), \\ K(h_1, h_2) \rightarrow K \in (0; +\infty), \quad h_1, h_2 &\rightarrow 0 : \\ \sum_{i,j=1}^{+\infty} \lambda_{i,j}^2 c_{i,j}^2 &= (\Delta^2\bar{\psi}^1, \bar{\psi}^1) \leq K^2(\Delta^2\bar{\psi}^1, \Delta^2\bar{\psi}^1) = K^2 \sum_{i,j=1}^{+\infty} \lambda_{i,j}^4 c_{i,j}^2. \end{aligned}$$

Let us use

$$\bar{\psi}^1 = \sum_{i,j=1}^{+\infty} c_{i,j}\bar{\varphi}_{i,j}, \quad (\bar{\varphi}_{i,j}, \bar{\varphi}_{i,j}) = 1, \quad (\bar{\varphi}_{i,j}, \bar{\varphi}_{k,l}) = 0, \quad (i, j) \neq (k, l), \quad k, l \in \mathbb{N},$$

$$\bar{\varphi}_{i,j} \in \tilde{V}([0; b_1] \times [0; b_2]) : -\Delta\bar{\varphi}_{i,j} = \lambda_{i,j}\bar{\varphi}_{i,j}, \quad \bar{\varphi}_{i,j} \neq 0, \quad i, j \in \mathbb{N},$$

$$\lambda_{i,j} = 0, 25\pi^2((2i-1)^2 b_1^{-2} + (2j-1)^2 b_2^{-2}).$$

Then, we have

$$K = \lambda_{1,1}^{-1} = 4\pi^{-2}(b_1^{-2} + b_2^{-2})^{-1}.$$

For the method of the fictitious components, the convergence estimate is known:

$$\|\bar{u}^k - \bar{u}\|_{\Lambda} \leq q^{k-1} \|\bar{u}^1 - \bar{u}\|_{\Lambda}, \quad k \in \mathbb{N} \setminus \{1\}.$$

5 Cyber-Physical System. Algorithm for a Program Calculating Displacements of Plate Points

Consider problem (12):

$$\bar{u} \in R^N : B\bar{u} = \bar{g}, \quad \bar{g} \in R^N.$$

In order to solve the problem, we apply the method of fictitious components (13):

$$\begin{aligned} \bar{u}^k \in R^N : \Lambda(\bar{u}^k - \bar{u}^{k-1}) &= -\tau_{k-1}(B\bar{u}^{k-1} - \bar{g}), \\ \tau_0 &= 1, \quad \tau_{k-1} = 2 / (\tilde{\beta}_1 + \tilde{\beta}_2), \quad k \in \mathbb{N} \setminus \{1\} \quad \forall \bar{u}^0 \in \bar{V}_1. \end{aligned}$$

In order to select iterative parameters in the method of fictitious components, we use the method of steepest descent. Take into account that $\bar{u}^0 \in \bar{V}_1$, $\bar{\psi}^k \in \bar{V}_2$, $k \in \mathbb{N}$, \bar{V}_2 is the subspace that corresponds to the subspace \bar{V}_2 . We use that

$$\begin{aligned} \tilde{\beta}_1(\Lambda\bar{\psi}^k, \bar{\psi}^k) &\leq (B\bar{\psi}^k, \bar{\psi}^k) \leq \tilde{\beta}_2(\Lambda\bar{\psi}^k, \bar{\psi}^k), \quad \bar{\psi}^k \in \bar{V}_2, \quad k \in \mathbb{N}, \\ \langle \Lambda(\bar{u}^0 - \bar{u}^k), (\bar{u}^0 - \bar{u}^k) \rangle &\approx \langle \Lambda(\bar{u}^0 - \bar{u}), (\bar{u}^0 - \bar{u}) \rangle, \quad k \rightarrow +\infty. \end{aligned}$$

Taking into account the second variant of numbering the values of discrete functions, the coefficients of the basic functions, the components of the vectors, we obtain the following calculation algorithm.

- (1) Find the first approximation

$$\bar{u}^1 \in R^N : \Lambda\bar{u}^1 = (\Lambda - B)\bar{u}^0 + \bar{g} \quad \forall \bar{u}^0 \in \bar{V}_1,$$

$$\begin{bmatrix} \bar{u}_1^1 \\ \bar{u}_2^1 \\ \bar{u}_3^1 \end{bmatrix} \in R^N : \begin{bmatrix} \Lambda_{11} & \Lambda_{12} & 0 \\ \Lambda_{21} & \Lambda_{22} & \Lambda_{23} \\ 0 & \Lambda_{32} & \Lambda_{33} \end{bmatrix} \begin{bmatrix} \bar{u}_1^1 \\ \bar{u}_2^1 \\ \bar{u}_3^1 \end{bmatrix} = \begin{bmatrix} \bar{g}_1 \\ \Lambda_{21}\bar{u}_1^0 \\ \bar{0} \end{bmatrix} \quad \forall \begin{bmatrix} \bar{u}_1^0 \\ \bar{0} \\ \bar{0} \end{bmatrix} \in \bar{V}_1.$$

- (2) Calculate the first residual

$$\bar{r}^1 \in R^N : \bar{r}^1 = B\bar{u}^1 - \bar{g},$$

$$\begin{bmatrix} \bar{r}_1^1 \\ \bar{r}_2^1 \\ \bar{r}_3^1 \end{bmatrix} \in R^N : \begin{bmatrix} \bar{r}_1^1 \\ \bar{r}_2^1 \\ \bar{r}_3^1 \end{bmatrix} = \begin{bmatrix} \bar{0} \\ \Lambda_{02}\bar{u}_2^1 + \Lambda_{23}\bar{u}_3^1 \\ \bar{0} \end{bmatrix}.$$

- (3) Find the amendment

$$\bar{w}^{k-1} \in R^N : \Lambda\bar{w}^{k-1} = \bar{r}^{k-1}, k \in N \setminus \{1\},$$

$$\begin{bmatrix} \bar{w}_1^{k-1} \\ \bar{w}_2^{k-1} \\ \bar{w}_3^{k-1} \end{bmatrix} \in R^N : \begin{bmatrix} \Lambda_{11} & \Lambda_{12} & 0 \\ \Lambda_{21} & \Lambda_{22} & \Lambda_{23} \\ 0 & \Lambda_{32} & \Lambda_{33} \end{bmatrix} \begin{bmatrix} \bar{w}_1^{k-1} \\ \bar{w}_2^{k-1} \\ \bar{w}_3^{k-1} \end{bmatrix} = \begin{bmatrix} \bar{0} \\ \bar{r}_2^{k-1} \\ \bar{0} \end{bmatrix}, k \in N \setminus \{1\}.$$

- (4) Calculate the iterative parameter

$$\begin{aligned} \tau_{k-1} &= \langle \bar{r}^{k-1}, \bar{w}^{k-1} \rangle / \langle B\bar{w}^{k-1}, \bar{w}^{k-1} \rangle \\ &= \langle \bar{r}_2^{k-1}, \bar{w}_2^{k-1} \rangle / \langle \Lambda_{02}\bar{w}_2^{k-1} + \Lambda_{23}\bar{w}_3^{k-1}, \bar{w}_2^{k-1} \rangle, k \in N \setminus \{1\}. \end{aligned}$$

- (5) Calculate the new approximation

$$\bar{u}^k \in R^N : \bar{u}^k = \bar{u}^{k-1} - \tau_{k-1}\bar{w}^{k-1}, k \in N \setminus \{1\},$$

$$\begin{bmatrix} \bar{u}_1^k \\ \bar{u}_2^k \\ \bar{u}_3^k \end{bmatrix} \in R^N : \begin{bmatrix} \bar{u}_1^k \\ \bar{u}_2^k \\ \bar{u}_3^k \end{bmatrix} = \begin{bmatrix} \bar{u}_1^{k-1} \\ \bar{u}_2^{k-1} \\ \bar{u}_3^{k-1} \end{bmatrix} - \tau_{k-1} \begin{bmatrix} \bar{w}_1^{k-1} \\ \bar{w}_2^{k-1} \\ \bar{w}_3^{k-1} \end{bmatrix}, k \in N \setminus \{1\}.$$

- (6) Calculate the new residual

$$\bar{r}^k \in R^N : \bar{r}^k = B\bar{u}^k - \bar{g}, k \in N \setminus \{1\},$$

$$\begin{bmatrix} \bar{r}_1^k \\ \bar{r}_2^k \\ \bar{r}_3^k \end{bmatrix} \in R^N : \begin{bmatrix} \bar{r}_1^k \\ \bar{r}_2^k \\ \bar{r}_3^k \end{bmatrix} = \begin{bmatrix} \bar{0} \\ \Lambda_{02}\bar{u}_2^k + \Lambda_{23}\bar{u}_3^k \\ \bar{0} \end{bmatrix}, k \in N \setminus \{1\}.$$

- (7) Calculate a value of the same order with the square of the norm of the absolute error

$$\delta_k = \langle B\bar{\psi}^k, \bar{\psi}^k \rangle = \langle \bar{r}^k, \bar{u}^k \rangle = \langle \bar{r}_2^k, \bar{u}_2^k \rangle, k \in N \setminus \{1\}.$$

- 8) Check the condition for stopping iterations by the absolute error

$$\delta_k < \delta^2, \quad \delta \in (0; +\infty), \quad k \in \mathbb{N} \setminus \{1\}.$$

- (9) Calculate the value of the same order with the square of the relative error

$$\begin{aligned} E_k &= \delta_k / \langle \Lambda(\bar{u}^0 - \bar{u}^k), (\bar{u}^0 - \bar{u}^k) \rangle = \delta_k / \langle \Lambda(\bar{u}^k - \bar{u}^0), (\bar{u}^k - \bar{u}^0) \rangle \\ &= \delta_k / \left\langle \left[\begin{array}{c} \bar{g}_1 - \Lambda_{11}\bar{u}_1^0 \\ \Lambda_{21}\bar{u}_1^k + \Lambda_{22}\bar{u}_2^k + \Lambda_{23}\bar{u}_3^k - \Lambda_{21}\bar{u}_1^0 \\ \bar{0} \end{array} \right], \left[\begin{array}{c} \bar{u}_1^k - \bar{u}_1^0 \\ \bar{u}_2^k \\ \bar{u}_3^k \end{array} \right] \right\rangle, \quad k \in \mathbb{N} \setminus \{1\}. \end{aligned}$$

- (10) Check the condition for stopping iterations by the relative error

$$E_k < E^2, \quad E \in (0; 1), \quad k \in \mathbb{N} \setminus \{1\}.$$

Under the conditions for stopping the iterative process, $\delta \in (0; +\infty)$, $E \in (0; 1)$ are the pre-set values to obtain an approximate solution to the problem with the required accuracy.

6 Conclusion

The proposed cyber-physical system's programmable algorithm for solving the studied problem contains the possibility of automatic selection of the used iterative parameters based on the data obtained in the process of numerical solution of the problem using a computer. The algorithm contains criteria for stopping the iterative count on a computer when reaching predetermined errors of the desired solution to the problem under consideration. The algorithm implements a nonlinear, non-stationary method when obtaining as a goal a numerical approximate solution to the problem with the required accuracy. Therefore, in a cyber-physical system, in the software implementation of the algorithm, the presence of certain elements of artificial intelligence can be noted.

References

1. Aubin, J.P.: Approximation of elliptic boundary-value problems, 360 p. Wiley-Interscience, New York (1972)
2. Bjorstad, P.: Fast numerical solution of the biharmonic Dirichlet problem on rectangles. SIAM J. Numer. Anal. **20**(1), 59–71 (1983)
3. Ciarlet, P.G., Glowinski, R.: Dual iterative techniques for solving a finite element approximation of the biharmonic equation. Comput. Methods Appl. Mech. Eng. **5**(3), 277–295 (1975)
4. Girault, V., Raviart, P.A.: Finite element approximation of the Navier–Stokes equation, 210 p. Springer, New York (1981)

5. Glowinski, R.: Numerical methods for nonlinear variational problems, p. 493. Springer Verlag, New York (1984)
6. Pironneau, O.: Optimal shape design for elliptic systems. Springer, New York (1983)
7. Rice, J.R., Boisvert, R.F.: Solving elliptic problems using ELL PACK, 497 p. Springer, New York (1985)
8. Thomasset, F.: Implementation of finite element methods for Navier–Stokes equation, 164 p. Springer, New York (1981)
9. Girault, V., Raviart, P.A.: Finite element methods for Navier–Stokes equation. Theory and algorithms, 374 p. Springer, Berlin (1986)
10. Kadchenko, S.I., Soldatova, A.A., Zagrebina, S.A.: Numerical research of the Barenblatt-Zhel'tov-Kochina stochastic model. In: Bulletin of the South Ural State University. Series: Mathematical Modelling, Programming and Computer Software, Vol. 9, № 2, pp. 117–123 (2016)
11. Marchuk, G.I., Kuznetsov, Yu.A., Matsokin, A.M.: Fictitious domain and domain decomposition methods. Soviet. J. Numer. Analysis Math. Modelling, Vol. 1, №1, pp. 3–35 (1986)
12. Ushakov, A.L.: About modelling of deformations of plates. In: Bulletin of the South Ural State University. Series: Mathematical Modelling, Programming and Computer Software, Vol. 8, № 2, pp. 138–142 (2015)
13. Zhang, X.: Multilevel Schwarz method for the biharmonic Dirichlet problem. SIAM J. Sci. Comput. **15**(3), 621–644 (1994)
14. Bank, R.E., Rose, D.J.: Marching algorithms for elliptic boundary value problems. SIAM J. Numer. Anal. **14**(5), 792–829 (1977)
15. Manteuffel, T.: An incomplete factorization technique for positive definite linear systems. Math. Comput. **38**(1), 114–123 (1980)
16. Swarztrauber, P.N.: A direct method for discrete solution of separable elliptic equations. SIAM J. Numer. Anal. **11**(6), 1136–1150 (1974)
17. Swarztrauber, P.N.: The method of cyclic reduction, Fourier analysis and FACR algorithms for the discrete solution of Poisson's equations on a rectangle. SIAM Rev. **19**(3), 490–501 (1977)
18. Sweet, P.A.: A cyclic reduction algorithm for solving block tridiagonal systems arbitrary dimension. SIAM J. Numer. Anal. **14**(4), 706–720 (1977)
19. Kuznetsov, Yu.A.: Iterative methods for solution of non-compatible systems of linear equations. In: Lecture Notes in Economics and Mathematical Systems, Vol. 134, pp. 41–55. Springer, Berlin (1976)
20. Wilkinson, J.H., Reinsch, C.: Linear algebra, 441 p. Springer, Berlin, Heidelberg (1971)

Modeling of Vibration Separation of Bulk Materials Based on the Theory of Random Processes



Fail Akhmadiev , Renat Gizzyatov , and Ilshat Nazipov 

Abstract The separation of granular materials into specific fractions by size on sieve classifiers is a large and complex system both in terms of the separation process and hardware design. The separation process depends on many design and operating parameters, the shape and size of the sieve cells, the number of sieves, as well as the fractional composition, shape and particle size of the material to be separated, i.e. is a cyber-physical system (CPS). The key to CPS is the mathematical model of the separation process, which is used in the control system. A mathematical model of the process of separation of granular materials on sieve classifiers based on the theory of random processes is developed. As a random process, the linear particle density of the considered fractions on the sieve surface is considered and a system of stochastic differential equations is constructed for its determination. The obtained solutions allow us to determine the recovery coefficient and evaluate the separation efficiency. Based on the constructed mathematical model, the design and operational parameters of the classifier were optimized. The performance criteria and separation efficiency are considered as optimization criteria. All this allows us to control the process of separation of granular materials by determining the optimal values of the operating parameters of the classifier depending on the fractional composition, shape and size of the particles of the original material to be separated and its other characteristics.

Keywords Bulk material · Separation · Stochastic modeling · Optimization

F. Akhmadiev (✉) · R. Gizzyatov · I. Nazipov
Kazan State University of Architecture and Engineering, 1 Zelenaya, Kazan 420043, Russia
e-mail: akhmadiev@kgasu.ru

R. Gizzyatov
e-mail: renatgrf@mail.ru

I. Nazipov
e-mail: nilshat@inbox.ru

1 Introduction

The separation of granular materials into specific fractions by size, shape, density and other characteristics is a common technological process. Such processes can be used as an independent operation to isolate the target product of a given fractional composition, as well as an auxiliary operation to remove impurities before grinding the material. To separate bulk materials by size, vibration devices are often used, in particular, multilevel sieve classifiers [1, 2]. The processes of separation of bulk materials using similar equipment depend on a large number of design and operating parameters, the shape and size of the sieve cells, the number of sieves, as well as the fractional composition, shape and particle size of the material to be separated, i.e. It is a large and complex system both in terms of the process of separation and hardware design. Thus, the process of separating granular materials can be considered as a cyber-physical system (CPS). The key to CPS is the mathematical model of the separation process, which is used to determine the optimal design parameters of the equipment used and the operational parameters of its operation to control the process itself [3–8].

Mathematical models of the processes that occur during the separation of granular materials are the basis for the optimal design and technological calculation of the sieve classifier. In the article [1], particle motion in an oscillating medium was studied, various models of vibrational motion were considered, and dependences were obtained for the average velocity and segregation velocity. In the articles [2, 3, 5], the process of isolating target products on sieve classifiers was studied using the theory of random processes. In particular, in the article [3], the process of separating granular media on sieve classifiers was considered as a diffusion process and a change in the concentration of the number of passage particles along the thickness of a layer of granular material depending on time towards a vibrating surface was studied from the standpoint of Markov processes and described by the Kolmogorov-Fokker-Plank (K-F-P) equation.

In the article [5], the theory of Poisson processes is used to describe the separation process on screens. In many works, for example [4–7], the kinetics of the separation process on sieve classifiers has been considered. For example, in the article [6] the stochastic process of motion of small particles in a large medium in the direction of a sieve is considered on the basis of the theory of Markov chains. The work [7] is devoted to the study of segregated flows during the organization of various processes for processing granular materials. These works propose the principle of organizing technological processes with controlled segregated flows, the formation of which is accompanied by most of the processes of processing dispersed materials associated with the mutual movement of particles. In the article [8], the process of separating granular medium by density on a sieve device was studied. This device consists of a pair of mesh screens with 1 mm square apertures mounted above the surface of a vibrated fluidized bed. The upper mesh contains a large central hole referred to as a Sink-Hole. This device allows you to effectively separate bulk material with particle

sizes in the range of 2.8–8.0 mm. The Monte Carlo simulation screening probability as described in the works [9, 10].

The probabilities of sifting particles into sieve cells were studied in the articles [2, 4, 5]. The probability of passage of particles through the openings of the sieves is determined depending on the geometric dimensions and shape of the particles and the openings of the mesh sieves, as well as the speed of vibrational motion. The movement of granular materials on a vibrating surface depending on the hydrodynamic properties of the material to be separated, particle size distribution, the shape of individual particles, the presence of specific properties, etc. can be simulated both in the approximation of a single material point and on the basis of methods of mechanics of heterogeneous media [11–16]. For example, the article [15] describes the main characteristics of the state of bulk material and an overview of the physical phenomena observed by vibration, which contributes to a better understanding of the behavior of bulk material to improve separation efficiency.

Modeling of the separation of granular materials on sieves using Markov processes was carried out in the article [17]. A system of stochastic differential equations is constructed with respect to the density distribution of the number of particles on the sieve surface. This allows you to find all the interesting characteristics of the process. However, this approach makes it possible to describe the processes of separation of granular materials into only a small number of fractions with a relatively small number of tiers of the classifier. This is due to difficulties in solving a system of equations (K-F-P) of large dimension with respect to the distribution density of a random process.

The optimization of processes associated with the separation of granular materials was considered in the works [18, 19]. As optimization criteria, equipment performance, separation efficiency, and other economic indicators can be considered.

Thus, various approaches can be used to simulate the process of separating granular materials into specific fractions by size, but taking into account the random nature of the process as a whole, the stochastic approach is most preferable [2–11, 20–23].

Despite the obvious achievements in the quantitative description of the processes of separation of granular materials, which was facilitated by the development of mathematical modeling and the widespread use of computer technology based on the theory of stochastic processes and methods of mechanics of heterogeneous media, a description of these processes taking into account discreteness, stochasticity and their optimal design are not complete. It should also be noted that there are few publications related to the optimization of separation processes, especially in a multi-criteria setting. Therefore, mathematical modeling of the processes of separation of granular materials according to various criteria, taking into account stochasticity, the development of calculation methods and their optimal design are an urgent task for chemical technology and related industries.

The aim of this work is the mathematical modeling of the vibrational separation of bulk materials by size on multilevel sieve classifiers to control this process, considering it as a large and complex system.

2 Mathematical Modeling

The process of vibrational separation of bulk materials into specific fractions by size on a multi-tiered sieve classifier is considered. The working body of the multi-tiered classifier is several oscillating screening surfaces, which can be made in the form of a sieve or a bolter. Moreover, they are located one above the other, forming tiers. The initial granular material, which is characterized by a size distribution function, is fed to the beginning of the upper tier and is divided into a passage and a descent part in the process of vibrational movement. At the same time, the first largest fraction is removed from the first tier, and the product for separation at the next i -th tier is granular material sifted from the upper $i-1$ -th tier.

A description of the process of isolating target products from bulk material on a sieve classifier will be carried out taking into account the stochastic nature of such processes. As a random process, we consider the value of $N_i = N_i(x, t; d_j)$, which determines the linear density of particles with dimensions d_j at a distance x from the beginning of the i -th sieve at time t . Then the system of kinetic equations describing the process of thin-layer separation of bulk materials on a sieve classifier can be represented in the form [2]:

$$\frac{dN_i}{dt} = \frac{\partial N_i}{\partial t} + V_{iav} \frac{\partial N_i}{\partial x} = \alpha_{i-1} N_{i-1} - \alpha_i N_i + \beta_i \eta_i(t), \quad \alpha_0 \equiv 0, \quad i = \overline{1, n} \quad (1)$$

where α_i are the kinetic equation coefficients, n is the number of classifier screens, $\eta_i(t)$ —are time-delta-correlated random functions (white noise) with known numerical characteristics $M[\eta_i] = \langle \eta_i(t) \rangle = 0$ and $K[\eta_i] = \langle \eta_i(t) \eta_i(t + \tau) \rangle = \Delta_i \delta(\tau)/2$, β_i is the intensity, $\Delta_i/2$ is the spectral density of white noise. A feature of Eq. (1), which allows us to call them stochastic, is the presence of an effect in the form of white noise.

The number of particles of the selected fraction on the surface of the i -th sieve at any time $t > t_i = L_i/V_{iav}$ is determined by the expression: $\bar{N}_i(t) = \int_0^{L_i} N_i(x, t; d_j) dx$, where L_i is the length of the sieve, V_{iav} is the average speed of vibrational motion. The deviation of the number of $\bar{N}_i(t)$ particles from the average value at any time is related to the probability of sieving particles into sieve cells. The probability of sifting into a cell depends on the size and shape of the particles, the particle size distribution of the material to be separated, constraint conditions and other factors, as well as on the relative speed of the vibrational movement of the material. Therefore, the number of $\bar{N}_i(t)$ particles is considered as a random process. Approximation of the random process N_i by white noise is possible, because the correlation time of the random process is much shorter than the average residence time of the selected particles on the surface of the sieve. Taking into account the properties of white noise, process N_i is a Markov process; therefore, to study it, one can use the mathematical apparatus of the theory of Markov processes. Then the distribution density of the random process $W_i(N_1, \dots, N_i, x, t)$ is determined from the solution of the system of equations (K-F-P):

$$\frac{\partial W_i}{\partial t} = -\frac{\partial}{\partial x}(V_{i\text{av}}W_i) - \sum_{k=1}^i \frac{\partial}{\partial N_k}(F_iW_i) + \frac{1}{2} \sum_{k=1}^{i+1} \sum_{j=1}^{i+1} \frac{\partial^2}{\partial x_k \partial x_j}(B_{kj}W_i), \quad i = \overline{1, n} \tag{2}$$

where $x_k \equiv N_k$, $k = \overline{1, i}$; $x_{i+1} \equiv x$, B_{kj} —is the diffusion coefficient. Solving equations (K-F-P) for large values of n is a difficult task.

The coefficients of kinetic equations in a first approximation are calculated by the dependence:

$$\alpha_i = V_{i\text{av}}p_i/2a_i,$$

where p_i is the probability of sifting into the cell, $2a_i$ is the step of the i -th sieve. The coefficients α_i determine the number of particles passing through the cell in one second, thereby characterizing the rate of change of the random process.

The probability of sifting into the cell is considered as a complex event [2]: $p = p_g p_v$, where p_g is the probability, which depends on the size and shape of the sieve cell and particles of the material to be separated, and p_v is the probability, which depends on the relative speed of the particle on the vibrating surface. The calculation of the probability of sifting into a cell was considered in the article [2]. The probability of the speed is determined by the formulas:

$$p_v = 2 - (\Phi(z) + \Phi(z_0)), \quad z = (V_a - V_k)/\sigma, \quad z_0 = V_k/\sigma, \quad z = (V_a - V_k)/\sigma$$

where V_a is the particle velocity amplitude relative to the sieve, $\Phi(x)$ is the standard normal distribution function, V_k, σ are the parameters of the normal law, which are determined in the process of identifying the constructed models. To do this, the calculated values of the extraction coefficient are compared with the experimental values obtained at some well-defined high-speed modes of operation of the apparatus.

The vibrational motion of granular media was studied in sufficient detail in the article [1], the calculation of the average speed, the relative velocity amplitudes for some modes of vibrational motion are given in the work [2].

Consider the solution of differential Eq. (1) under the following initial and boundary conditions:

$$N_i(0, x) = 0 \text{ for } i = \overline{1, m} \text{ and } N_1(t, 0) = \overline{N}_{10}(t), \quad N_i(t, 0) = 0 \text{ for } i = \overline{2, m}. \tag{3}$$

Conditions (3) determine the supply of the material to be separated only at the beginning of the upper tier of the multilevel classifier, \overline{N}_{10} is the number of selected particles ($1/m$) that arrive at the beginning of the first sieve. Using the replacement $\tau_i = t - x/V_i$, $z = x$, Eq. (1), taking into account conditions (3), can be solved by reduction to ordinary differential equations. Then the average value of the random process N_1^j for the first sieve, taking into account conditions (3), has the form: $\overline{N}_1^j(\tau_1, z) = \overline{N}_{10}^j(\tau_1) \exp(-\alpha_1^j z/V_1)$, and the general solution of the differential

equation with respect to the average value of the random process for the i -th sieve can be written in the form:

$$\begin{aligned} \bar{N}_i^j(\tau_i, z) = & \bar{N}_{10}^j(\tau_i) \frac{\alpha_1^j \dots \alpha_{i-1}^j}{V_2 \dots V_i} [\Psi_{1,i} \exp(-\alpha_1^j z / V_1) \\ & + \dots + \Psi_{i,i} \exp(-\alpha_i^j z / V_i)] \end{aligned} \quad (4)$$

where

$$\begin{aligned} \Psi_{k,j} = & 1 / \left[(\alpha_1^j / V_1 - \alpha_k^j / V_k) \times \dots \times (\alpha_{k-1}^j / V_{k-1} - \alpha_k^j / V_k) \right. \\ & \left. \times (\alpha_{k+1}^j / V_1 - \alpha_k^j / V_k) \times \dots \times (\alpha_i^j / V_i - \alpha_k^j / V_k) \right], \quad i \geq 2 \end{aligned}$$

These results can also be obtained on the basis of the theory of Poisson processes.

In the general case, the solution of the system of equations (K-F-P) regarding the distribution density of a random process is carried out by numerical methods. When approximated by white noise, a random N_i process is normal. Therefore, knowing the numerical characteristics of the random process, we can write an approximate solution for the distribution density and transition probabilities, which are fundamental solutions to the Cauchy problem under delta-shaped initial conditions:

$$\begin{aligned} W_1^j(N_1^j, \tau_1) &= \frac{1}{\sqrt{2\pi \sigma_{N_1^j}^2(\tau_1, z)}} \exp\left(-\frac{(N_1^j(\tau_1, z) - \bar{N}_1^j(\tau_1, z))^2}{2\sigma_{N_1^j}^2(\tau_1, z)}\right), \\ W_{i/i-1}^j(N_i^j, \tau_i | N_{i-1}^j, \tau_{i-1}) &= \frac{1}{\sqrt{2\pi \sigma_{N_i^j}^2(\tau_i, z)}} \exp\left(-\frac{(N_i^j(\tau_i, z) - \bar{N}_i^j(\tau_i, z))^2}{2\sigma_{N_i^j}^2(\tau_i, z)}\right). \end{aligned}$$

For the first sieve, an analytical solution to Eq. (2) can be obtained. By replacing $\varphi = N_1 \exp(-\alpha_1 x / V_1)$, $\xi = \frac{\beta_1^2 \Delta_1}{2\alpha_1} (1 - \exp(-2\alpha_1 x / V_1))$, the equation (K-F-P) for the first sieve is reduced to the simplest diffusion equation: $\frac{\partial \tilde{W}_1}{\partial \xi} = \frac{1}{2} \frac{\partial^2 \tilde{W}_1}{\partial \varphi^2}$ and the solution of the resulting equation is written as an integral convolution:

$$\tilde{W}_1(\varphi, \xi, \tau_1) = \frac{1}{\sqrt{2\pi\xi}} \int_0^\infty \bar{W}_{10}(\theta, \tau_1) \left(\exp\left(-\frac{(\varphi - \theta)^2}{2\xi}\right) - \exp\left(-\frac{(\varphi + \theta)^2}{2\xi}\right) \right) d\theta,$$

where $\bar{W}_{10}(N_1, \tau_1)$ is the distribution density of N_1 in the initial section.

Then the general solution of the equation (K-F-P) for the first sieve has the form:

$$W_1(N_1, x, \tau_1) = \tilde{W}_1(\varphi, \xi, \tau_1) \exp(-\alpha_1 x / V_1).$$

For the remaining screens, starting from the second, obtaining an analytical solution to the equations of system (2) is a difficult task.

The coefficients of the kinetic equations of system (1) α_i^j determine the probability of passage of particles of the j -th fraction through the holes of the i -th sieve per unit time, thereby characterizing the rate of the process. Then the average value of the number of passes of the j -th fraction from the i -th sieve, taking into account solution

(4) for the time Δt_i , is determined by the formula:

$$\int_0^{\Delta t_i} \int_0^{L_i} \alpha_i^j \bar{N}_{i0}^j \exp(-\alpha_i^j z / V_i) dz dt = V_i \Delta t_i \bar{N}_{i0}^j (1 - \exp(-\alpha_i^j L_i / V_i)), \quad (5)$$

where \bar{N}_{i0}^j is the number of particles of the j -th fraction per unit length of the i -th sieve in its initial section. The expression $V_i \Delta t_i \bar{N}_{i0}^j$ in (5) determines the total number of particles of the j -th fraction entering the i -th sieve during the time Δt_i . Then, the extraction coefficient of the j -th fraction from the i -th sieve, taking into account (5), is determined by the formula:

$$\eta_i^j = \exp(-\alpha_i^j L_i / V_i), \quad i = \overline{1, n}, \quad j = i, i + 1,$$

where $j = i$ is the coarse (passing) fraction, $j = i + 1$ is the next largest (passing) fraction. The classification process will be the more effective the more you can get the extraction and less “pollute” the products. The separation efficiency on the i -th sieve is calculated by the dependence:

$$E_i = \eta_i^i (1 - \eta_i^{i+1}) \times 100\%, \quad i = \overline{1, n},$$

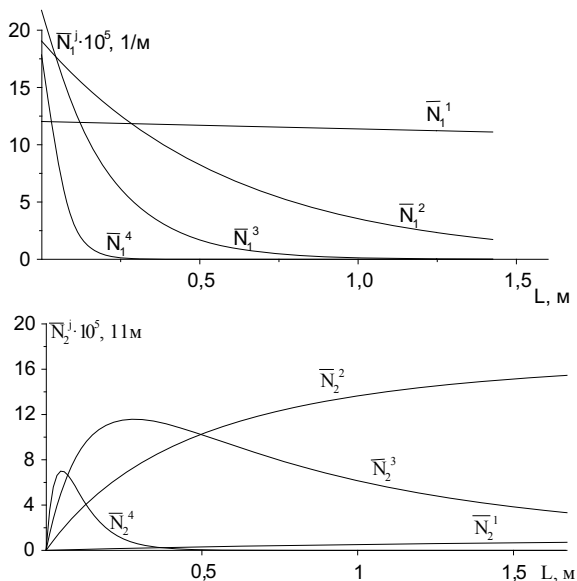
where η_i^{i+1} is the fractional fraction of the coarse fraction in the coarse fraction, which for the i -th fraction is considered as the fraction of impurities in the target product.

Figure 1 shows the results of calculations of the distribution of the linear particle density of the target products along the first and second sieves of the multilevel classifier. Based on the obtained solutions, the extraction coefficients of the target products are calculated. Also, the quality of the sieved residues from the sieves is evaluated. For this, the proportion of non-target products (small) that are in the target product is determined. Based on the constructed mathematical models to determine the optimal values of the structural and operational parameters of the classifier, it is possible to formulate and solve the optimization problem in a multi-criteria setting [19].

3 Separation Process Optimization

The efficiency of the separation process can be evaluated by various criteria [18]. Separation results can be characterized by indicators such as, for example, recovery, pollution, concentration, etc. This creates some uncertainty when evaluating the operation of the equipment used and the quality of separation. In practice, the quality of separation is most fully evaluated by two indicators—the degree of extraction of the desired fraction from the starting material and its contamination.

Fig. 1 Change in the linear particle density of the target products along the first and second sieves of the multi-tiered classifier: $\alpha_1^1 = 5.78E-3$; $\alpha_1^2 = 8.42E-2$; $\alpha_1^3 = 2.57E-1$; $\alpha_1^4 = 9.08E-1$; $\alpha_2^1 = 3.66E-4$; $\alpha_2^2 = 2.77E-3$; $\alpha_2^3 = 7.18E-1$; $\alpha_2^4 = 6.93E-1$ (sek⁻¹); $V_{cp} = 0.05$ m/sek; sizes of fractions: 1– $(0.8 \div 0.9) \cdot 10^{-3}$; 2– $(0.7 \div 0.8) \cdot 10^{-3}$; 3– $(0.6 \div 0.7) \cdot 10^{-3}$; 4– $(0.5 \div 0.6) \cdot 10^{-3}$ (m)



The processes of separation of granular materials on sieve classifiers depend on a large number of design and operating parameters, characteristics of the shared material, i.e. is a large and complex system. To control this process, on the basis of the constructed mathematical model, the optimization problem is constructed in a multi-criteria setting [19]. The optimization results will allow you to control the separation process by adjusting the operating parameters of the process depending on the fractional composition, shape and particle size of the shared material. The performance of the apparatus and the coefficients of separation efficiency on screens are considered as criteria:

$$\max Q(A, \omega, \alpha, \beta, h, B) = \rho_c h B V_{av},$$

$$\max E f_i(A, \omega, \alpha, \beta, D_i, L_i, r_i) = \eta_i (1 - R_i) \times 100\%, \quad i = \overline{1, m},$$

$$\text{under conditions: } x_j^{\min} \leq x_j \leq x_j^{\max}, \quad \varphi_k^{\min} \leq \varphi_k(A, \omega, \alpha, \beta) \leq \varphi_k^{\max}, \quad (6)$$

where x_j^{\min} , x_j^{\max} is the smallest and greatest value of the component of the vector $\bar{x} = (A, \omega, \alpha, \beta, D, L, h, r)$, φ_k are the functional limitations associated with the selected speed regime, A is the amplitude of the oscillations of the sieves, ω is the frequency of the oscillations of the sieves, α , β are the angles of inclination and vibration of the sieves, ρ_c is the bulk density, L_i is the length of the i -th sieve, B is the width of the sieve, D_i is the diameter of the cells of the i -th sieve, V_{av} is the average velocity of the granular material on the first sieve, h is the thickness of the layer of granular material at the beginning of the first sieve, R_i is the proportion of

non-target products in the target hopper, r_i —requirements for separation products, for example, $R_i < r_i$.

Optimization on a multi-criteria basis makes it possible to select design and operational parameters of equipment, taking into account several criteria necessary for the production. For example, along with efficiency, it is necessary to take into account the productivity indicator, as well as other economic indicators. But it is important to understand that for the classification process, these indicators from a certain moment, as they individually approach the extreme values, come into conflict. This is the essence of multi-criteria tasks.

The multicriteria problem (6) is solved by known methods [2, 19, 24]. For the practical organization of the classification process, depending on the type (shape) of particles, fractional composition, the type and size of the cell hole are selected, and the length of the sieves, their angle of inclination, and the amplitude of oscillations as a result of the corresponding calculations given in the article [2]. The optimal values of the angle of vibration and vibration frequency are determined from the solution of the optimization problem. The device should be able to be controlled without significant changes in design parameters by adjusting the operating parameters depending on changes in the characteristics of the material being shared.

4 Results and Discussion

A computational experiment was carried out using a complex of programs [25]. A polymer-based granular material with linear dimensions in the range of $(0.65\text{--}2.65) \times 10^{-3}$ m and the same diameters of 1.5×10^{-3} m was considered. The bulk density of the material was $\rho_c = 1160$ kg/m³, porosity – 23%. The dimensions of the first fraction are $(2.15\text{--}2.65) \times 10^{-3}$ m, the second $(1.65\text{--}2.15) \times 10^{-3}$ m. To select the first fraction, a lattice of length $L = 1.5$ m and width $B = 1.0$ m with mesh sizes of $(3.2 \times 3.2) \times 10^{-3}$ m with a circular hole of diameter $D = 2 \times 10^{-3}$ was selected. The angle of inclination of α sieves was varied within 00–50, the amplitude of the oscillations A is within $(3\text{--}5) \times 10^{-3}$ m, the height of the exit slit of the loading hopper $h = 4 \times 10^{-3}$ m, the requirement for the purity of separation $r_1 \leq 8\%$. As a result of solving the multicriteria problem, a compromise solution was obtained: $Ef_1 = 87.4\%$, $Q = 1320$ kg/h. Optimum parameter values: $\omega = 48.54$ s⁻¹ and $\beta = 10.06^\circ$. The average velocity was $V_{av} = 7.94 \times 10^{-2}$ m/s, the amplitude of the relative velocity was $V_a = 0.285$ m/s, the extraction coefficient of the first fraction was $\eta_1 = 0.95$. Thus, the constructed mathematical models make it possible to determine all the interesting characteristics of the separation process and, based on the solution of the multicriteria problem, to establish the optimal values of the design and operating parameters of the multi-tiered classifier.

5 Conclusion

The theory of random processes using the experimental results to determine the model parameters allows you to build mathematical models of the vibrational separation of bulk materials into specific fractions by size on multi-level sieve classifiers, to evaluate the separation efficiency and determine the optimal values of the design and operating parameters of the classifier. The mathematical model and the experimental results make it possible to control the separation process by adjusting its operating parameters depending on changes in the characteristics of the shared material, considering the separation process on sieves as a large and complex system.

References

1. Vaysberg, L.A., Ivanov, K.S., Mel'nikov, A.E.: Improving the approaches to mathematical modeling of vibration screening processes. *Obogashcheniye rud* **2**, 21–24 (2013)
2. Akhmadiev, F.G., Gizzyatov, R.F., Nazipov, I.T.: Hydrogasdynamics and kinetics of separation of disperse media on sieve classifiers. *J. Eng. Phys. Thermophy.* **90**, 1077–1086 (2017). <https://doi.org/10.1007/s10891-017-1659-x>
3. Nepomnyashchiy, E.A.: Kinetics of some processes of processing dispersed materials. *Theor. Found. Chem. Eng.* **7**(5), 75 (1973)
4. Gortinskiy, V.V., Demskiy, A.V., Boriskin, M.A.: Separation processes in grain processing enterprises. *Kolos, Moskov* (1973)
5. Akhmadiev, F.G., Gizzyatov, R.F.: Modeling of separation of granular materials on multiple-deck classifiers using the theory of stochastic processes. *Theor. Found. Chem. Eng.* **52**, 360–370 (2018). <https://doi.org/10.1134/S0040579518030028>
6. Ogurtsov, V.A., Fedosov, S.V., Mizonov, V.E.: Modeling the kinetics of vibration screening based on the theory of Markov chains. *Build. Mater.* **5**, 33–35 (2008)
7. Dolgunin, V.N., Ukolov, A.A., Ivanov, O.O.: Kinetic laws of segregation during the fast gravitational flow of granular materials. *Theor. Found. Chem. Technol.* **40**(4), 423–435 (2006)
8. Kumar, D., Iveson, S.M., Galvin, K.P.: Novel jamming mechanism for dry separation of particles by density. *Miner. Eng.* **148**, 106185 (2020). <https://doi.org/10.1016/j.mineng.2020.106185>
9. Beeckmans, J.M., Jutan, A.: Monte Carlo simulation of a probability screen. *Can. J. Chem. Eng.* **67**(2), 329 (1989). <https://doi.org/10.1002/cjce.5450670220>
10. Pascoe, R.D., Fitzpatrick, R., Garratt, J.R.: Prediction of automated sorter performance utilizing a Monte Carlo simulation of feed characteristics. *Miner. Eng.* **72**, 101 (2014). <https://doi.org/10.1016/j.mineng.2014.12.026>
11. Akhmadiev, F.G., Gizzyatov, R.F., Kiyamov, K.G.: Mathematical modeling of thin-layer separation of granular materials on sieve classifiers. *Theor. Found. Chem. Eng.* **47**(3), 254–261 (2013). <https://doi.org/10.1134/S0040579513030019>
12. Generalov, M.B.: *Mekhanika tverdykh dispersnykh sred v protsessakh khimicheskoi tekhnologii* (Mechanics of Solid Disperse Media in Chemical Engineering Processes). Izd. Bochkarevoi, Kaluga (2002)
13. Akhmadiev, F.G., Nazipov, I.T.: Stochastic modeling of the kinetics of processing of heterogeneous systems. *Theor. Found. Chem. Eng.* **47**(2), 136–143 (2013). <https://doi.org/10.1134/S0040579513020012>
14. Ryzhkov, A.F., Tolmachev, Y.M.: On the selection of the optimal height of the vibrated bed. *Theor. Found. Chem. Eng.* **17**(2), 206 (1983)

15. Golovanevskiy, V., Arsenyev, V., Blekhman, I., Vasilkov, V., Azbel, Y., Yakimova, K.: Vibration-induced phenomena in bulk granular materials. *Int. J. Miner. Process.* **100**(3), 79–85 (2011). <https://doi.org/10.1016/j.minpro.2011.05.001>
16. Nigmatulin, R.I.: *Fundamentals of the mechanics of heterogeneous media*, p. 336. Nauka, Moscow (1978)
17. Akhmadiev, F.G., Gizzyatov, R.F., Nazipov, I.T.: Mathematical modeling of processes of classification of granular materials on the sieve. *J. Mod. High Technol.* **12**(1), 30–35 (2019). <https://doi.org/10.17513/snt.37828>
18. Barsky, M.D.: Optimization of separation processes of granular materials, p. 168. Nedra, Moscow (1978). <https://doi.org/10.1016/B978-0-444-63919-6.00006-6>
19. Akhmadiev, F.G.: Some problems of multicriteria process optimization. *Theor. Found. Chem. Eng.* **48**(5), 574–582 (2014). <https://doi.org/10.1134/S0040579514050145>
20. Detyna, J., Bieniek, J.: Methods of statistical modelling in the process of sieve separation of heterogeneous particles. *Appl. Math. Model.* **32**(6), 992–1002 (2008)
21. Kazakov, V.A.: *Introduction to the Theory of Markov Processes and Some Radio Engineering Problems*, p. 232. Sov. Radio, Moscow (1973)
22. Tikhonov, V.I., Mironov, M.A.: *Markov Processes*, p. 488. Sovetskoe Radio, Moscow (1977)
23. Feller, W.: An introduction to probability theory and its applications 2. *Ann. Probab.* **1**(1), 193–196 (1973). <https://doi.org/10.1214/aop/1176997039>
24. Karpenko, A., Agasiev, T., Sakharov, M.: Intellectualization methods of population algorithms of global optimisation/cyber-physical systems: advances in design and modelling. *Stud. Syst. Decis. Control* **259**, 137–151 (2020). https://doi.org/10.1007/978-3-030-32579-4_11
25. Akhmadiev F.G., Gizzyatov R.F., Nazipov, I.T.: Computer simulation and optimization of the kinetics of the processing of heterogeneous media. Certificate of the State Registration of a Computer Program no. 2016661926. (2016)

Cyber-Physical Systems Intelligent Control

Forecast Evaluation Techniques for I4.0 Systems



Andrey Davydenko, Cuong Sai , and Maxim Shcherbakov 

Abstract We focus on forecast evaluation techniques that comply with the design principles of Industry 4.0 (or I4.0). The I4.0 concept refers to trends and principles attributed to the 4th industrial revolution and, in particular, assumes the following capabilities of automated systems: interoperability, decentralization, real-time processing, and service-orientation. Generally, effective forecast evaluation requires us to store both actuals and forecasts. We look at how to handle rolling-origin forecasts produced for many series over multiple horizons. This setup is met both in research (e.g., in forecasting competitions or when proposing a new method) and in practice (when tracking/reporting forecasting performance). We show how to ensure access to all the variables required for exploratory analysis and performance measurement. We propose flexible yet simple and effective data schemas allowing the storage and exchange of actuals, forecasts, and any additional relevant info. We show how to construct various tools for forecast exploration and evaluation using the schemas proposed. In particular, we present our implementation of a prediction-realization diagram showing forecasts from different methods on one plot. We propose special tools for measuring the quality of point and interval rolling-origin predictions across many time series and over multiple horizons. The workflow for using techniques proposed is illustrated using R codes.

Keywords Forecasting · Forecast evaluation · Forecasting accuracy · Forecast bias · Interval predictions · Data visualization · R · I4.0

A. Davydenko
JSC CSBI, Saint-Petersburg, Russia
e-mail: andrey@live.co.uk

C. Sai (✉) · M. Shcherbakov
Computer-aided Design Department, Volgograd State Technical University, Volgograd, Russia
e-mail: svcuonghvtqs@gmail.com

1 Introduction

Forecasting methods are used in various fields ranging from weather forecasting to supply chain management. It is important for companies to produce good forecasts in order to operate efficiently. In order to know how good a forecasting method is, we need to compare forecasts against corresponding actuals being obtained. In other words, we need empirical evaluation to assess forecast performance. A number of forecasting competitions have been held to empirically evaluate alternative methods (e.g., [1] tested 24 methods using 3003 series and recently [2] tested well-known machine learning and parametric methods using 100,000 series). These competitions have had a huge influence on the field of forecasting by focusing on forecasting performance, rather than on models design. Choosing a good metric to compare alternative forecasts is itself a challenging and controversial task (for an overview of existing approaches see, e.g., [3]).

This chapter addresses the following questions: (1) How to store forecast data in order to ensure effective forecast evaluation? (2) What tools can be used to report forecast performance in an informative and interpretable way? In particular, how to measure accuracy of point forecasts, how to measure forecast bias, and how to measure the quality of interval predictions? Some preliminary results of our research were earlier presented by us at CyberPhy-2020 conference, see [4].

We show that formats used in well-known datasets and packages do not provide some important capabilities (for example, by not allowing the storage of rolling-origin forecasts and not ensuring cross-platform and real-time capabilities). After suggesting a more suitable format we illustrate how it can be used as a basis for building forecast evaluation tools.

Generally, the solution we propose in this chapter can be seen as a statistical framework that involves the elements suggested in [5]: (i) a setup describing the tasks and requirements, (ii) principles used to ensure effective implementation, (iii) the description of tools and algorithms, (iv) codes, and (v) a workflow describing step-by-step instructions to solve the tasks identified in the setup.

The next section outlines the setup where we summarize typical settings of obtaining and evaluating forecasts and outline the principles we adopt in our solution. Then we present our view of how forecast evaluation workflow should look like. We then propose data schemas that meeting the requirements stated. Then we demonstrate how the schemas can be used to implement tools for forecast exploratory analysis and performance measurement. Data formats and tools presented can be used regardless of a scripting language or database, but our examples use R and plain csv-files. We conclude by providing a summary of our recommendations for using the tools presented.

2 Forecast Evaluation Setup, Principles, and Terminology

We propose the following forecast evaluation setup summarizing (i) what kinds of data we want to work with, (ii) what we want to obtain as a result of the analysis, (iii) under what requirements and what principles.

1. Suppose we have a set of time series. The set can contain from one to a relatively large number of series (say, millions or hundreds of thousands).
2. For each series we want to store both actuals and forecasts. In particular, we need to store out-of-sample forecasts produced from different origins (we will call them rolling-origin forecasts) over different horizons. Forecasts can be produced using alternative methods. In addition to point forecasts we may want to store prediction intervals (PIs), density forecasts, and additional information related to forecasting process (such as model structure, model coefficients, reasons for judgmental adjustments, etc.).
3. Both actuals and forecasts can be frequently and asynchronously updated as new data becomes available (this scenario is described, e.g., in [6]).

Being able to store each forecast for each horizon and each origin of interest is important because it is often not easy to reproduce forecasts for evaluation purposes. E.g., computing a single forecast can take a substantial time when using computationally intensive methods, such as MCMC, to generate posterior densities [6]. Moreover, judgmental forecasts and judgmental adjustments cannot be reproduced at all.

Given the above settings and considerations, we need convenient means to store and access (and, perhaps, to distribute or exchange) forecast data including actuals, forecasts, and other relevant info. Our aim is to find a solution that would be fast in operation (applicable in industrial settings), cross-platform, and easy to learn and to implement. In particular, we need data structures to implement a reliable and informative forecast cross-validation and a credible comparison of alternative methods. In the case of forecasting competitions, a well-defined approach to store forecasting data enables independent and objective out-of-sample evaluation of forecasting accuracy.

In our solution we aim to comply with the latest trends defined by the Industry 4.0 vision [7]. In particular, this involves interoperability, real-time capabilities, decentralization, service-orientation, and modularity. We also aim to ensure effective forecast evaluation by the use of the most appropriate error metrics and tools. We propose a forecast evaluation framework based on the following rules: (1) Use unified cross-platform data formats to store actuals and forecasts (this is needed to ensure interoperability and modularity, cross-platform data formats make it easier to exchange forecast data). (2) Use separate tables to store forecasts and actuals (this ensures effective updating of data, real-time capabilities, and objective evaluation by third parties). (3) Use well-defined and well-grounded algorithms for measuring forecasting performance (this ensures objective and reproducible forecast evaluation, see [8] for a discussion on the requirements for constructing appropriate error measurement algorithms).

We focus on numeric univariate time series, but the framework proposed is also applicable to multivariate series and to panel or longitudinal studies where observations related to various objects are collected over time. Although the chapter focuses on numeric series, the data structures proposed are capable of storing categorical data.

Some important terms we use are clarified below.

- *Forecast origin*—the most recent historical period for which data is used to obtain a forecast.
- *Forecast horizon*—the number of periods from the forecast origin to the end of the time period being forecast [9].
- *Prediction intervals (PIs)*—the bounds within which future observed values are expected to fall, given a specified level of confidence [9].
- *Prediction interval width (PIW)*—the difference between the upper and the lower bounds of a given PI.
- *Rolling-origin forecast*—a forecasting process in which forecast origin rolls forward in time [10].
- *Density forecast*—a prediction of the distribution of any given statistical object of interest [11].
- *Coverage probability*—the empirical probability that PIs contain actuals.
- *Nominal coverage probability*—the confidence level of PIs.

3 Forecast Evaluation General Workflow

Data science analysis involves not only applying a specific algorithm of interest, but also data preparation and data quality checks. Our approach is based on including these steps into a forecast evaluation framework allowing it to comply with more general methodologies, such as CRISP-DM or SEMMA.

We propose the general workflow for forecast evaluation shown on Fig. 1.

The topic of how to obtain forecasts is out of the scope of this chapter. Instead, we look at how forecast data should be stored in order to allow access to previous forecasts, to match them with actuals, and to track forecasting performance. Forecasts can be produced not only by statistical or machine learning methods but also judgmentally. It is important for a forecasting system to have the capabilities of keeping relevant information related to the reasons associated with judgmental estimates. The approach proposed in the next section is capable of keeping this kind of information as well.

The next section proposes data structures allowing the implementation of the framework shown on Fig. 1. In subsequent sections we use these structures for the exploratory analysis and performance measurement steps of the workflow.

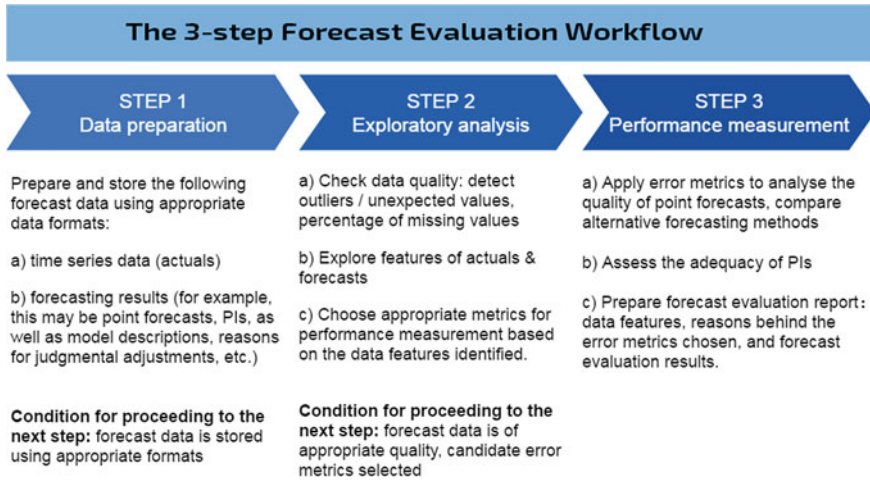


Fig. 1 Forecast evaluation workflow

4 New Data Formats

4.1 Existing Packages with Forecast Data

Some R packages contain data for forecasting competitions:

- Mcomp: Data from the M-competition and M3-competition [12];
- Tcomp: Data from the Kaggle tourism competition [13];
- tscompdata: Data from the NN3 and NN5 competitions [14];
- M4comp2018: Data from the M4-competition [15].

The above packages use objects to store forecasts and actuals. The downside of this approach is that we need to use R to access data. In other words, the approach is not cross-platform. Besides, there is no unified approach to store rolling-origin forecasts and interval forecasts.

We propose a general format based on special table schemas. The schemas we propose can be implemented in any environment, e.g., using .csv files or a SQL database.

4.2 New Approach and Its Capabilities

This section presents our approach to store forecast data in accordance with what was said in Sect. 2. More specifically, we aim to have a specification with the following capabilities (in order to comply with the I4.0 principles):

- Rolling-origin cross-validation.
- Storage of any type of forecasting results (not only point forecasts, but also interval forecasts, density forecasts, model parameters, reasons for judgmental forecasts, etc.).
- Cross-platform usage & portability.
- Ability to work with data collected for any frequency (hours, minutes, seconds, etc.) and any number of time series.
- Ease of updating actuals and forecasts, ability to store actuals separately from forecasting results, and to store forecasting results for each forecasting method separately.
- Fast access to data.
- Ease of use, understanding, and implementation.

We propose to store forecast data in plain tables (as opposed to the use of environment-specific objects, as in the above packages). This allows using a relational database (RDB) or portable files (e.g., .csv). As RDBs are widely used, companies usually have an IT infrastructure optimized to work with tabular data. DB engines and SQL statements allow accessing such data instantly ensuring real-time capabilities.

We propose the use of the following two major table schemas to store forecasts and actuals:

- Time Series Table Schema (TSTS) to store time series actuals;
- Forecast Table Schema (FTS) to store forecasting results including point forecasts, prediction intervals, and other variables of interest.

According to our approach, forecasts and actuals are stored in separate tables. To slice-and-dice forecast data easier, we may need a table containing both actuals and forecasts. To do this we propose the Actual and Forecast Table Schema (AFTS).

4.3 Time Series Table Schema (TSTS)

In this table schema each actual is stored as a separate single row (Table 1).

We may have additional columns or an additional table specifying time series features (e.g., series description, units, frequency, category, etc.). However, the schema specified by Table 1 includes the columns that are always necessary for forecast evaluation across many series. This specification does not impose any restrictions on data types, but we advise that timestamps be stored as strings. We recommend to use the ISO 8601 standard for timestamps as it allows adequate sorting of rows and correct comparison of strings containing timestamps. For example, “1997-01-20” is less than “1998-01-19” but in case of using another format this may not be the case, e.g.: “20.01.1997” > “19.01.1998”.

Table 1 Time series table schema (TSTS)

Column	Description	Example
series_id*	Time series identifier—a unique name identifying a time series	“Y1”
timestamp*	Any representation of the period to which the observation relates. We recommend the use of the ISO 8601 standard	“1997” in case of yearly data, “1997-01-20” in case of daily data, “1997-11” in case of monthly data, “1997-W03” in case of weekly data, “2018-Q2” in case of quarterly data
value	The value observed	100

*These columns form the composite key for this table schema. A composite key is a combination attributes that must not be duplicated. For this table schema it is <series_id, timestamp>. In other words, we cannot have two (or more) records relating to the same time series and the same period of observation (timestamp)

Here is how the M3-Competition data can look like in the TSTS format:

series_id	value	timestamp
Y1	3103.96	1984
Y1	3360.27	1985
Y1	3807.63	1986
Y1	4387.88	1987
Y1	4936.99	1988
Y1	5379.75	1989

In our examples below we use numeric series, but for categorical data the “value” column can store category identifiers instead of numeric values.

Panel and multivariate series can also be stored using the above schemas. To store panel data the “series_id” column can be replaced with two columns: “panel_id” and “var_id”. Alternatively, the “series_id” can be a column containing both a panel identifier and a variable identifier in one string. In the latter case columns “panel_id” and “var_id” can still be added in order to easier query data. The same relates to multivariate series.

For missing observations the corresponding rows can be omitted or corresponding values can be coded as NA’s. Sometimes it is necessary to store indications of censored data or out-of-stock events, etc. This should be specified by special rules, which we will not address in this chapter. The purpose of the above schemas is only to set out the general approach.

Table 2 Forecast table schema (FTS)

Column	Description	Example
series_id*	Time series identifier for which the forecast was calculated	“Y1”
timestamp*	Any representation of the period to which the observation relates. We recommend the use of the ISO 8601 standard	“1997” in case of yearly data, “1997-01-20” in case of daily data, “1997-11” in case of monthly data, “1997-W03” in case of weekly data, “2018-Q2” in case of quarterly data
origin_timestamp*	Origin of the forecast (provided in the same format as the timestamp)	“2000” in case of yearly data, “1997-01-23” in case of daily data, etc
horizon*	Forecast horizon	3
method_id*	Method identifier—a unique name that identifies a method by which the forecasting result was produced	“ARIMA”
forecast	Point estimate	234
lo95	The lower limit for the 95% prediction interval	178
hi95	The upper limit for the 95% prediction interval	273
lo90	The lower limit for the 90% prediction interval	162
hi90	The upper limit for the 90% prediction interval	283
...

*the composite key for this table schema is < series_id, method_id, timestamp, origin_timestamp, horizon >

4.4 Forecast Table Schema (FTS)

This schema is needed to store forecasting results. Each row contains forecasting results relating to a given time series produced using a given method for a given horizon at a given origin. Table 2 specifies the columns required. Columns containing PIs can be added or excluded.

The FTS table may be extended by adding columns to represent additional types of forecasting results (e.g., this may be textual info to store reasons for judgmental forecasts or arrays containing density forecasts). Also, if needed, we can have columns to store structured info using JSON or XML formats. Table 2 specifies typical results used in forecast evaluation.

Here is how forecasts for the M3-Competition data can look like in the FTS format:

series_id	method_id	forecast	horizon	timestamp	origin_timestamp
Y1	NAIVE2	4936.99	1	1989	1988
Y1	NAIVE2	4936.99	2	1990	1988
Y1	NAIVE2	4936.99	3	1991	1988
Y1	NAIVE2	4936.99	4	1992	1988
Y1	NAIVE2	4936.99	5	1993	1988
Y1	NAIVE2	4936.99	6	1994	1988

4.5 Actual and Forecast Table Schema (AFTS)

It is often convenient to work with a table having both actuals and forecasts in one row. By joining columns from TSTS and FTS tables based on the TSTS key fields, the Actual and Forecast Table Schema (AFTS) is obtained.

4.6 Data Preparation Process and Scenario Examples

Since the formats proposed above (TSTS and FTS) assume a table structure, the most efficient way (in terms of updating the data and accessing relevant slices) is to store forecast data within a RDBMS. When TSTS and FTS tables are stored in a RDBMS, relevant pieces of data are obtained through SQL queries. Tables containing both actuals and forecasts (formatted using the AFTS) then can be obtained using a simple INNER JOIN SQL query.

Another scenario is to use .csv files. Then actuals are stored separately from forecasts. Moreover, it is possible to store forecasts from each method in a separate file and then merge the tables for further analysis.

Of course, forecast data can be stored inside an R-package, but the idea behind our approach is still to store data as a table and not as a list of language specific data structures.

5 The Forvision Package

The forvision package for R [16] implements tools to facilitate the workflow shown on Fig. 1. The tools are implemented assuming that forecast data is stored in the TSTS and FTS formats. Our further illustrations will be based on this package, but

similar functionality and API design can be implemented in other environments (e.g., in Python or Julia).

5.1 *Downloading and Installation*

To install and use the package, run this code:

```
install.package(devtools)
devtools::install_github("forvis/forvision", build_vignettes = TRUE)
library(forvision)
```

5.2 *Data Used for Illustrations*

The package has several example datasets available as data frames. For further illustrations, we will use the following datasets:

- *m3_yearly_ts*—yearly actuals from the M3-competition (format: TSTS),
- *m3_yearly_fc*—yearly forecasts from the M3-competition (format: FTS),
- *m3_quarterly_ts*—quarterly actuals from the M3-competition formatted (format: TSTS),
- *m3_quarterly_fc_pis*—quarterly forecasts containing prediction intervals calculated for the M3-competition data (format: FTS).

The package has a special function to obtain a data frame containing both actuals and forecasts (a table in the AFTS format):

```
m3_yearly_af <- createAFTS(m3_yearly_ts, m3_yearly_fc)
```

5.3 *Visual Tools Implementation*

The forvision package contains functions implementing visual tools for exploratory analysis and performance measurement. These functions produce objects created with the use of ‘ggplot2’ and ‘dygraphs’ packages. This allows the aesthetics of graphs to be adjusted with high flexibility.

Graphical output can be improved by using rules for choosing most suitable colors and markers for producing cross-sectional plots (see [5]), but here we use default output with no special adjustments.

6 Exploratory Analysis of Forecast Data

When forecast data is stored in the appropriate format, we can define APIs and algorithms to query, slice-and-dice, and visualise forecast data.

This section presents some exploratory tools defined using the data structures we proposed above.

6.1 Prediction-Realization Diagram

The prediction-realization diagram is a scatterplot showing how forecasts correlate with actuals [17]. Here we propose plotting point forecasts and actuals relating to different series, methods, origins, and horizons on the same graph. We use different colors and symbols to denote different methods. The objective is to explore the distribution of forecast errors, to identify outliers and biases, to compare alternative forecasts.

To plot the diagram we need forecast data in the AFTS format. We can use any subset of the initial data set if needed (for example, we can use only forecasts for a specified horizon). This R-code shows the function call for constructing the diagram, Fig. 2 shows the result:

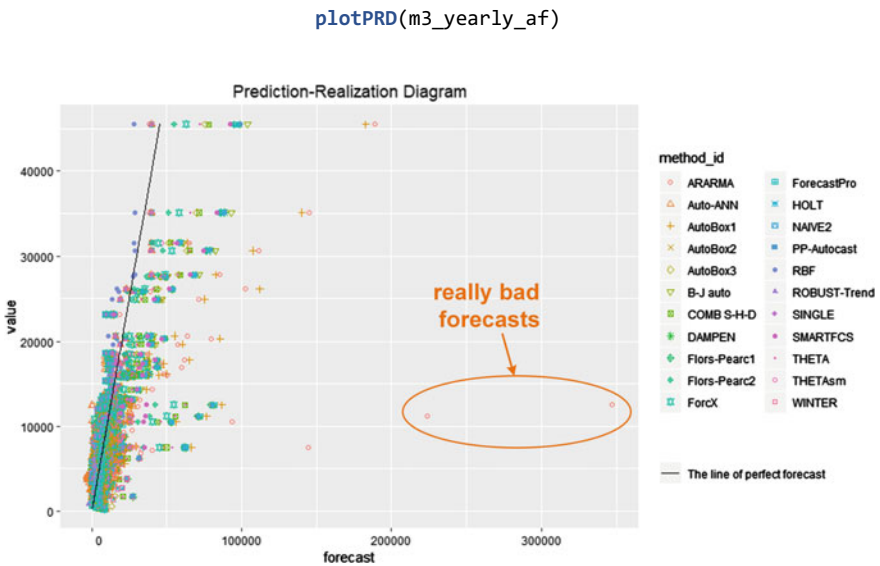


Fig. 2 Prediction-realization diagram for M3 yearly data. Different colors and marks are used to show forecasts relating to different forecasting methods. The $Y = X$ line represents perfect (zero error) forecasts

The graph on Fig. 2 spots some really unwanted cases (when forecast seriously overestimated actuals). For example, having a forecast close to 350,000 units we had actual of only about 11,000 units. We also observe some negative forecasts, but actuals are always non-negative. The distribution is skewed and in some areas points largely overlap in the bottom left corner of the graph. Using a log scale for this diagram is therefore sometimes useful, but here we will work with the raw data to keep things more simple.

Let's take a closer look at the cases spotted. With the AFTS format we can query forecast data in order to get a table with details:

```
subset(m3_yearly_af, forecast > 100000)
```

Query results indicated that the unwanted cases related to series id = "Y113". Below we illustrate how to show these forecasts on a time series graph.

6.2 Fixed Origin and Fixed Horizon Graphs

The fixed origin graph shows point forecasts produced for the same time series from the same origin, but for different horizons. It is possible to show forecasts from several methods on the same graph using different colors and symbols.

When actuals table is given in the TSTS format and forecasts table in the FTS format, we can define the following algorithm for producing the fixed origin graph. Firstly, we need to select (from the forecasts table) all point forecasts produced by the methods of interest and relating to the specified origin and specified time series. Then plot a time series graph using actuals stored in the actuals table, then plot the forecasts selected, use different colors for different methods.

Figure 3 shows the cases of poor forecasts we identified based on the prediction-realization diagram (these cases relate to series Y113 of the M3 yearly data set).

Code used to obtain the graph:

```
# Firstly, in order to use the 'dygraphs' package
# we must prepare appropriate time-based object timestamps:
library(zoo)
m3_yearly_ts$timestamp_dbo <- as.yearmon(m3_yearly_ts$timestamp, format =
'%Y')
m3_yearly_fc$timestamp_dbo <- as.yearmon(m3_yearly_fc$timestamp, format =
'%Y')

# plot fixed origin graph
plotFixedOrigin(m3_yearly_ts, m3_yearly_fc, "Y113", 1988, c("ARARMA", "HOLT",
"NAIVE2"))
```

Method "ARARMA" sometimes performs badly as it tends to extrapolate trends that do not hold. Thus, in this example the prediction-realization diagram together with the fixed origin graph helped identify the risks of using ARARMA.

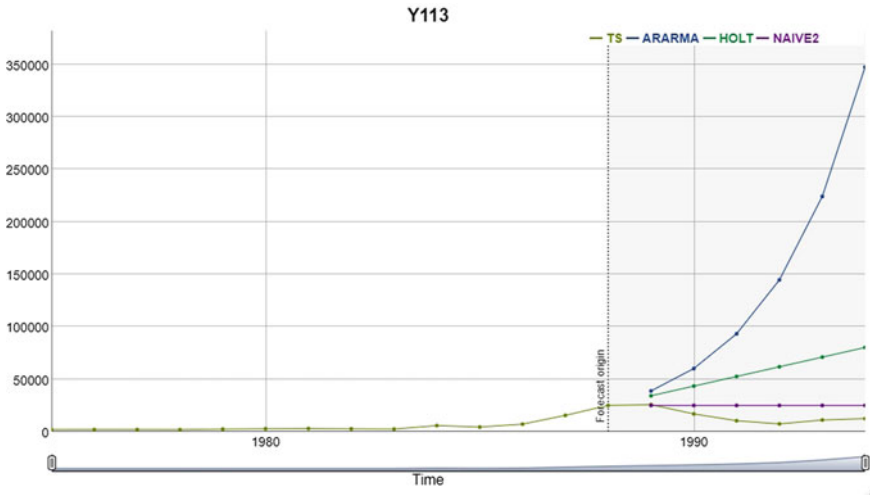


Fig. 3 Fixed origin graph

If we have a data set containing rolling-origin forecasts, the fixed horizon graph can be constructed as well. The fixed horizon graph shows point forecasts produced for the same time series, with the same horizon, but from various rolling origins. The graph is constructed in a similar manner to what we described above.

6.3 Fancharts

Fan chart shows point forecasts and prediction intervals produced for the same time series from some given fixed origin, with different horizons. Fan chart relates shows forecasts produced by only one selected method. The objectives is to visually explore PIs, to identify outliers/unexpected results, to assess the uncertainty around forecasts and adequacy of the PIs. Examples of unacceptable PIs: too wide for the practical settings, lower limit is below zero for non-negative time series, the actual coverage does not correspond to the nominal coverage, etc.

Similarly to the point forecasts graphs presented above, fan charts can be constructed given data in the TSTS and FTS formats. Figure 4 shows a fan chart produced using the forvision package.

The code below illustrates the API design based the use of the TSTS and FTS formats.

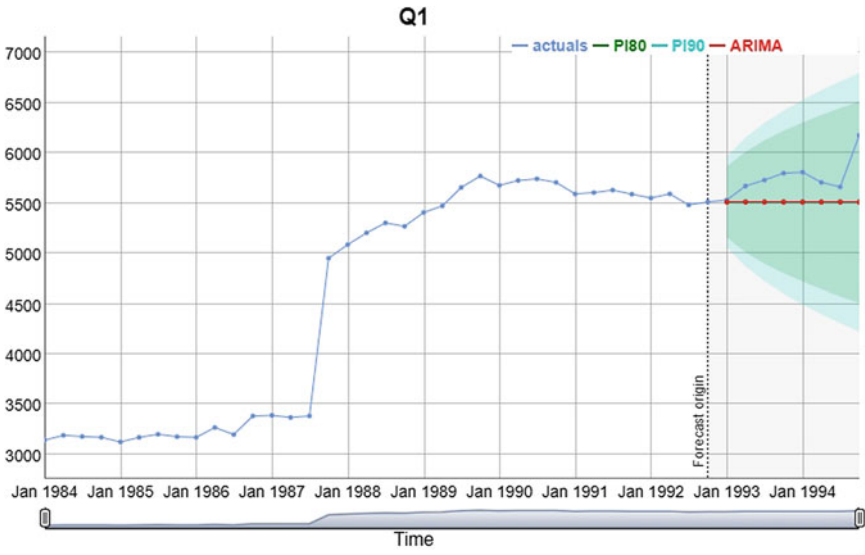


Fig. 4 Fan chart

```
# prepare appropriate time-based object timestamp columns
# for the correct use of the 'dygraphs' package
library(zoo)
m3_quarterly_ts$timestamp_dbo <- as.yearqtr(m3_quarterly_ts$timestamp, format
= '%Y-Q%q')
m3_quarterly_fc_pis$timestamp_dbo <- as.yearqtr(m3_quarterly_fc_pis$timestamp,
format = '%Y-Q%q')

# plot a fan chart
plotFan(m3_quarterly_ts, m3_quarterly_fc_pis, "Q1", "1992-Q4", "ARIMA")
```

Figure 4 shows forecasts produced from fixed origin ‘1992-Q4’ with horizons from 1 to 8. In order to show the dynamics of updating PIs, it is useful to show fan charts for different origins (one example can be found in [6, p. 17]).

By analogy with the fixed horizon graph for point forecasts, for a particular method we also can construct a graph depicting PIs for rolling-origin forecasts, but with some fixed horizon.

7 Measuring Forecasting Performance

When measuring forecast performance we can look at the accuracy and bias of point forecasts and assess the adequacy of prediction intervals. In this section we present effective tools to accomplish these tasks.

7.1 Assessing the Accuracy of Point Forecasts

In the exploratory analysis section we explored the distribution of actuals and forecasts for the M3 yearly data. We spotted zero actuals and negative forecasts, which makes some popular metrics such as MAPE (mean absolute percentage error, [18]) inapplicable. But even we have only positive actuals and forecasts, MAPE can be unreliable or even misleading [8]. Nonetheless, MAPE remains very popular. So we start with an example based on MAPE.

Having input data in the AFTS format lets us construct well-known accuracy versus horizon graphs and tables. Figure 5 shows the “MAPE versus horizon” graph for the M3 early data plotted using the following code:

```
# Exclude non-positive cases
m3_yearly_af2 <- subset(m3_yearly_af, value > 0 & forecast > 0)
# calculate MAPEs and show the “accuracy vs horizon” graph
acc <- calculateMAPE(m3_yearly_af2)
acc$plot
```

As noted above, MAPE has many flaws. It is therefore desirable to use alternatives. However, choosing the most appropriate metric remains a controversial task [19]. Sometimes researchers and practitioners are facing difficulties as the use of different metrics leads to different rankings of methods and the results become difficult to interpret [3]. Formal statistical tests for accuracy comparisons are also not always straightforward to implement.

One important property of an error measure (formulated in [8, p. 240]) is that the criteria used for optimisation of predictions must correspond to the criteria used for

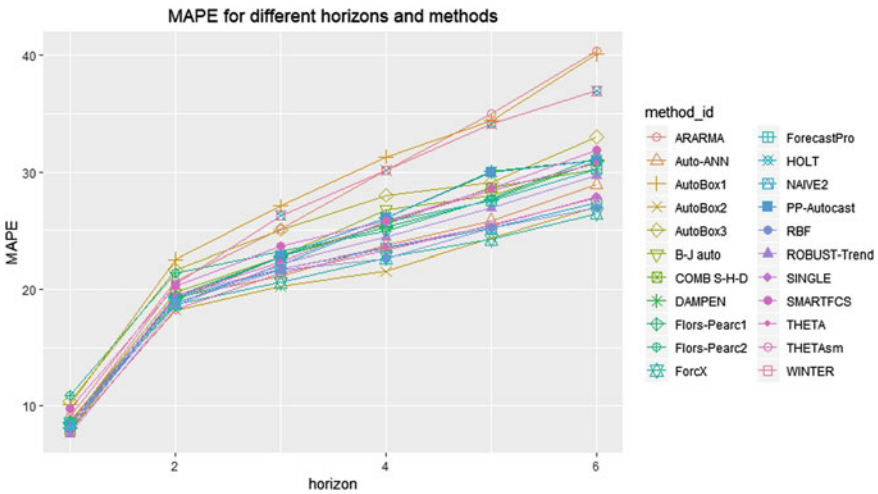


Fig. 5 Accuracy versus horizon graph

their evaluation. It is well-known [20, p. 30] that if a density forecast is available, point forecast in terms of MSE will correspond to its mean and optimal forecast in terms of MAE will correspond to its median. Usually, if density forecast is non-symmetric, original series are log-transformed, predicted, and then predictions are returned to the original scale. In this case we aim to obtain forecasts optimal in terms of MAE [8, p. 240]. If density forecast is symmetric, both MAE and MSE are suitable, but MAE is less affected by outliers.

It therefore makes sense to use out-of-sample MAE for accuracy evaluation. But this approach is applicable if we have only one time series. Importantly, metrics based on percentage errors (e.g., MAPE) are not suitable to represent accuracy in terms of linear or quadratic loss even for the case of only one time-series [19, pp. 49–53], [8, p. 241].

When it comes to measuring accuracy across series, scale-independent measures are required in order to avoid a so called “oranges versus apples comparison” [18]. Given that percentage errors are not advisable [8, 18, 19], one option is the mean scaled absolute error (MASE, [18]) where errors are scaled by MAE of the naive method. MASE, however, has some limitations [8, pp. 244–245]: it may not show relative accuracy reliably due to biases of the arithmetic mean and structural breaks in time series.

Instead, it was proposed in [3] to use the average relative mean absolute error, AvgRelMAE. This metric is based on the geometric mean of relative MAEs (RelMAEs). Suppose we have N time series, M methods, T origins from which each method produced forecasts (and corresponding outcomes are already known) with horizons from l to H . We denote forecast error as

$$e_{t+h,i,j} = Y_{t+h,i,j} - F_{t+h,i,j}, \quad (1)$$

where t —forecast origin ($t = 1 \dots T$), h —forecast horizon ($h = 1 \dots H$), i —method ($i = 1 \dots M$), j —time series ($j = 1 \dots N$), $Y_{t+h,i,j}$ —actual, $F_{t+h,i,j}$ —forecast.

MAE for a given combination of h , i , and j is

$$MAE_{h,i,j} = \frac{1}{T} \sum_{t=1}^T |e_{t+h,i,j}|. \quad (2)$$

To assess relative performances, we need to use a benchmark method (we recommend the naive method, but it can be any other method). Let B denote the index of the benchmark method. Then relative MAE (RelMAE) is:

$$RelMAE_{h,i,j} = MAE_{h,i,j} / MAE_{h,B,j}. \quad (3)$$

For a given series the RelMAE has the following interpretation: $RelMAE < 1$ means method i is better than method B in terms of the linear loss function, $RelMAE > 1$ meaning the opposite. In order to aggregate RelMAEs across series we can use

various options such as the arithmetic mean or the median, but, as explained below, the geometric mean is a better option.

The AvgRelMAE for a specified method i and horizon h is found as the geometric mean of RelMAEs:

$$AvgRelMAE_{h,i} = \left(\prod_{j=1}^N RelMAE_{h,i,j} \right)^{1/N} \quad (4)$$

Different series lengths require the use of the weighted geometric mean, as proposed in [21]. The weight of RelMAE is then the number of origins used to calculate RelMAE.

The geometric mean has the following important advantages over alternatives (such as the median or the arithmetic mean) when averaging relative forecast performances: (i) it gives equal weight to reciprocal relative changes [21, p. 61] and (ii) the resulting rankings are invariant to the choice of the benchmark [21, p. 66]. It may occur, however, that MAE becomes zero for some cases and then the above formula cannot be used directly. In these cases a special trimming procedure should be used, as proposed in [19, p. 62].

Studies of the statistical properties of the AvgRelMAE have shown that it gives a better indication of relative accuracy (compared with alternative metrics) in terms of the linear loss [19]. One important advantage of this metric is the ease of interpretation. For example, obtaining an AvgRelMAE value of 0.95 for a particular method means that this method is likely to reduce the MAE of the benchmark by 5%.

Also (as noted in [22, p. 53]) the AvgRelMAE is applicable if one wants to implement the so-called ‘forecast value added’ (FVA) concept proposed by the SAS Institute [23]. The FVA is defined as ‘the change in a forecasting performance metric that can be attributed to a particular step or participant in the forecasting process.’ [23]. So we can say that obtaining AvgRelMAE = 0.95 corresponds to the FVA of 5%.

Given its advantages, we recommend the AvgRelMAE for accuracy visualisations. By replacing MAPE with AvgRelMAE on the graph shown on Fig. 5, obtaining the ‘AvgRelMAE versus horizon’ graph is straightforward.

A corresponding ‘AvgRelMAE vs horizon’ table is also required for reporting accuracy. To make table output effective, we recommend these rules: (i) use 2 or 3 digits after the decimal point and use bold font to show best results, (ii) indicate the benchmark method used or show ranks; (iv) (optional) use asterisk (*) to indicate statistical significance of changes in accuracy. Good examples of the ‘AvgRelMAE vs horizon’ table can be found in [24, p. 253] and [25, p. 465].

When summarizing AvgRelMAE values across horizons, some researchers used MAEs containing errors for different horizons [25, p. 465]. We think this method is not desirable as accuracy becomes over-influenced by forecasts with higher horizons. We propose the following formula:

$$AvgRelMAE_i = \left(\prod_{h=1}^H AvgRelMAE_{h,i} \right)^{1/H} \quad (5)$$

By analogy to the AvgRelMAE we can define the AvgRelMSE, which indicates relative accuracy under quadratic loss [21, pp. 62–63]. Generally, if point forecasts were obtained as medians of forecast densities, it makes sense to use the AvgRelMAE [21]. And if forecast densities are non-symmetric and point forecasts were obtained as means of forecast densities, it makes sense to use the AvgRelMSE. Both the AvgRelMAE and AvgRelMSE converge to the geometric mean of relative absolute errors when T gets close to 1, which makes them biased indicators of relative accuracy [3, p. 518]. Our experiments, however, show that the AvgRelMSE is more biased compared to the AvgRelMAE, which makes the AvgRelMAE more preferable. Examples of using the AvgRelMAE and the AvgRelMSE metrics can be found in a number of recent studies (e.g., [24–27]).

The abbreviation prefix “AvgRel” to indicate averaging relative forecasting performances across time series using the geometric mean was proposed in [21] and since then this abbreviation has been used in many studies (e.g., [24–26]). Some authors used abbreviations ARMAE and ARMSE instead of the AvgRelMAE and AvgRelMSE (e.g., [27]). We do not recommend changing “AvgRel” to “ar” or “AR” in order to avoid confusion with some well-known measures for multitarget regression that are based on arithmetic mean and have the ‘ar’ prefix, such as arMAE. We propose that, if a compact notation for the “AvgRel” is needed, the “AvgRel” prefix can be replaced with the ‘Ø’ symbol. However, keeping the original “AvgRel” prefix makes measures more recognizable across studies.

When using the AvgRelMAE, one powerful tool to explore the underlying distribution is the boxplot of RelMAEs on a log scale (see Fig. 6).

This visual tool was proposed in [3, p. 520]. Examples of boxplots of log(RelMAE) can, e.g., be found in [19, p. 65] and [28, p. 18]. These plots help spot outliers and heavy tails to see if trimming is needed for a more reliable analysis. Besides, for skewed distributions additional precautions should be taken into account when applying statistical tests. For more details we refer our readers to [19].

In our package we implemented the following API for obtaining the “AvgRelMAE versus horizon” graph, table, and the log(RelMAE) boxplot:

```
# Prepare results for AvgRelMAE
acc <- calculateAvgRelMAE(m3_yearly_af2)
acc$plot      # show "AvgRelMAE vs horizon" plot
acc$accuracy # show "AvgRelMAE vs horizon" table
acc$boxplot  # show "RelMAE boxplot" (Log scale)
```

The above listing demonstrates that the schemas proposed earlier allow the effective construction of graphical and tabular output for accuracy evaluation. Any subsets of the input dataset for the evaluation can be easily constructed by standard query functions (e.g., using the ‘subset()’ function in R).

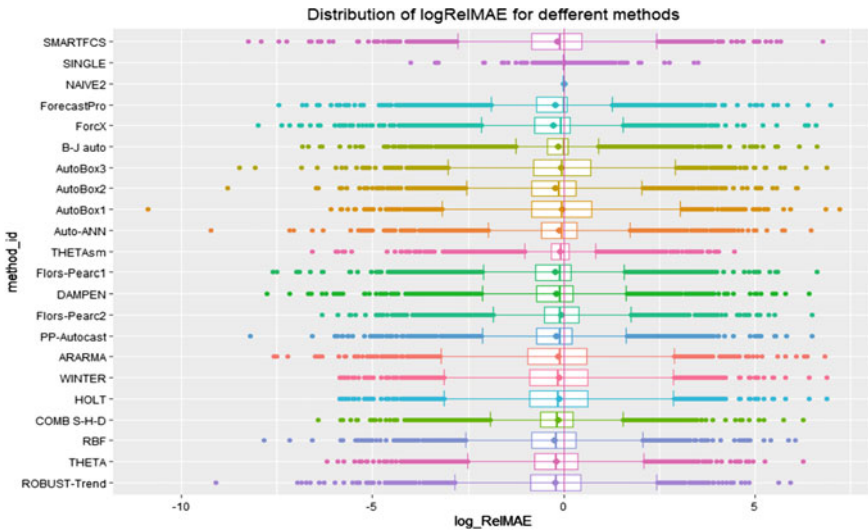


Fig. 6 Boxplots of log(ReMAEs) for M3 yearly data for different methods. Benchmark method: NAIVE2. Each boxplot shows cases for all time series and for all horizons available

7.2 Assessing the Bias of Point Forecasts

Apart from the accuracy of point forecast is often useful to see if forecasts systematically over-estimate or under-estimate actuals. The prediction-realization diagram described above is one tool to quickly explore the forecast bias. However, a more rigorous analysis requires the use of special metrics.

Usually, the term bias is used to see if the mean forecast error significantly differs from zero. However, as noted above, optimal forecasts for the linear loss correspond to the median of the forecast density. Thus, it does not make sense to evaluate forecast bias if densities are skewed and point forecasts were optimized for the linear loss. In these setting optimal forecasts will inevitably be biased [21] and reducing bias will reduce accuracy. Bias evaluation only makes sense if forecast densities are symmetric or forecasts were optimised for the quadratic loss (in this case we need to use the AvgRelMSE for accuracy evaluation).

For a single series the mean error (ME) is a good indicator of forecast bias. In order to obtain a scale-independent metric, some researchers use the mean percentage error (MPE) calculated by analogy to MAPE. One clear disadvantage of MPE is that it is vulnerable to outliers and has other limitations of MAPE. There are examples of using AvgRelMAE in combination with MPE [24, p. 253], but we do not recommend this approach due to the above reasons.

One alternative is to use the average relative absolute mean error (AvgRelAME), this metric was proposed in [21, p. 64]. Keeping the previous notation, the AvgRelAME is

$$AvgRelAME_{h,i} = \left(\prod_{j=1}^N RelAME_{h,i,j} \right)^{1/N}, \quad (6)$$

where

$$RelAME_{h,i,j} = AME_{h,i,j} / AME_{h,B,j} \quad (7)$$

and

$$AME_{h,i,j} = \left| \frac{1}{T} \sum_{t=1}^T e_{t+h,i,j} \right|. \quad (8)$$

When AvgRelAMEs for each method and each horizon are obtained, by analogy to the AvgRelMAE we can construct a ‘‘AvgRelAME versus horizon’’ graph and table. Averaging AvgRelAMEs across horizons is performed using the geometric mean, by analogy to formula (5).

7.3 Measuring the Quality of Prediction Intervals

Assessing the adequacy of PIs is based on calculating coverage probabilities and comparing them with the nominal probability. If confidence limits for the coverage probability are too wide, we can conclude there’s not enough observations to draw conclusions about the validity of PIs. Ideally, the confidence limits should be relatively narrow and include the nominal coverage. Surprisingly, very little research has been conducted in the area of validating PIs. Perhaps, most well-known attempt is [29], but it still did not provide evidence on confidence bounds for empirical coverage. Here we propose a visual tool showing both empirical coverage and corresponding error bounds.

Using the AFTS format we can implement the coverage chart shown on Fig. 7. The chart shows the coverage for ARIMA method for different forecasting horizons. The corresponding code is:

```
# show coverage chart for ARIMA forecast method
m3_quarterly_af <- createAFTS(m3_quarterly_ts, m3_quarterly_fc_pis)
plotCoverage(m3_quarterly_af, pi = 90, methods = "ARIMA")
```

By looking at the coverage chart on Fig. 7, it can be seen that the method (we used auto.arima function from the ‘forecast’ R-package to obtain PIs) tends to underestimate the uncertainty associated with the forecasts produced. Confidence limits for the actual coverage probability were obtained using the standard ‘binom.test’ function in R. If methods systematically underestimate or overestimate the uncertainty,

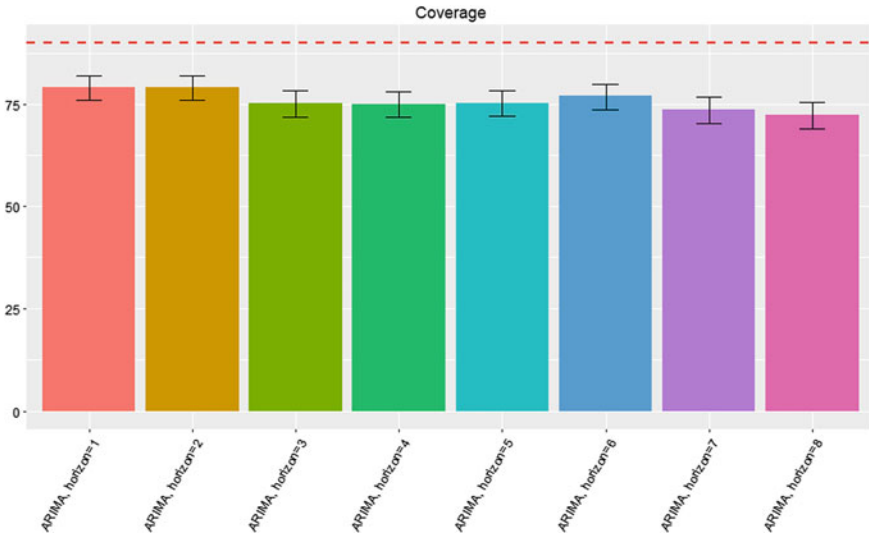


Fig. 7 Coverage chart. Error bars indicate 90% confidence intervals for coverage probabilities

this indicates the need to calibrate forecasts or apply data transformations prior to forecasting.

The coverage chart only assesses the adequacy of PIs. To compare the average width of PIs we propose the use the Average Relative Prediction Interval Width (AvgRelPIW) metric. For a specified confidence level, the AvgRelPIW is calculated by analogy to the AvgRelMAE by averaging relative PIWs across series using the geometric mean. If two methods have adequate PIs (this can be confirmed using the coverage chart) but different AvgRelPIW, the method with lower AvgRelPIW is more preferable. For example, if the task is to obtain adequate and accurate PIs for a real-time electricity consumption tracking system, we need to (1) ensure that PIs are adequate, (2) choose a model producing the lowest AvgRelPIW.

8 Recommendations Summary

In the light of the above discussion, we recommend the following algorithm for implementing the forecast evaluation workflow:

- (1) Prepare the evaluation dataset: store forecasts and actuals using the FTS and TSTS formats, respectively.
- (2) Before accuracy evaluation: produce summary of available cases, explore missing and NA values (both for forecasts and actuals), validate data integrity.
- (3) Use the prediction-realization diagram (PRD) to identify potential data issues (use log scale if needed), explore the distribution of forecasts and actuals.

- (4) If needed, use the fixed origin/fixed horizon graphs to explore time series and forecast features. Use fan charts to explore the adequacy of PIs.
- (5) Perform forecast accuracy evaluation:
 - (5.1) Choose the benchmark method (we recommend the naive method).
 - (5.2) Use the $\log(\text{RelMAE})$ boxplot to explore the distribution of RelMAEs.
 - (5.3) If no evident data flaws can be found, use the AvgRelMAE metric (here we assume forecasts are optimised for the linear loss, use the AvgRelMSE or AvgRelRMSE for the quadratic loss).
 - (5.4) Produce the “AvgRelMAE vs horizon” graph and table. Perform statistical tests to detect changes in accuracy (one possible test is described in [8, p. 62]).
 - (5.5) If needed, aggregate AvgRelMAEs across horizons.
- (6) If forecast densities are symmetric (this can be assessed using the the PRD), measure forecast bias using the AvgRelAME metric. If forecast densities are skewed, but forecasts were optimised for the quadratic loss and the AvgRelMSE was used, we can still use the AvgRelAME metric. But if forecast densities are skewed and the AvgRelMAE was used to report accuracy, measuring bias will not be informative for forecast evaluation.
- (7) Given a set of pre-defined confidence levels (say, 80, 90, and 95%) validate PIs using the coverage chart. Compare PIWs using the AvgRelPIW metric.

9 Conclusions

Having forecast data stored in a well-defined way is crucial for monitoring and evaluating forecast accuracy. In spite of the fact that a number of large-scale forecasting competitions have been conducted, at present there is no unified approach of how to store forecast data. In this chapter we proposed data schemas suitable for keeping forecast data in tables as a part of an RDB or as a portable file.

We also showed how to implement forecast evaluation based on the data structures proposed. We provided our examples in R, but, analogously, any other language (e.g., Python) can be used to implement the same approach.

The target audience for the techniques proposed involves both academics/researchers and practitioners. The framework can be applied in various scenarios. In particular, it can be used to create forecast-value-added (FVA) reports recommended by the SAS guidelines [23]. Also, separating forecast data from the evaluation algorithms and tools allows third parties to perform the forecast evaluation process, which is important to ensure objective evaluation. Finally, we showed that the framework complies with I4.0 principles [7]. We proposed RDBMS-oriented, well-defined and unified data structures, API, and visual tools ensuring the following capabilities of the framework: interoperability, decentralization, real-time operation, service-orientation, and modularity.

Acknowledgements The reported study was supported by RFBR research projects 19-47-340010_r_a.

References

1. Makridakis, S., Hibon, M.: The M3-Competition: results, conclusions and implications. *Int. J. Forecast.* **16**(4), 451–476 (2000)
2. Makridakis, S., Spiliotis, E., Assimakopoulos, V.: The M4 competition: results, findings, conclusion and way forward. *Int. J. Forecast.* **34**(4), 802–808 (2018)
3. Davydenko, A., Fildes, R.: Measuring forecasting accuracy: the case of judgmental adjustments to SKU-level demand forecasts. *Int. J. Forecast.* **29**(3), 510–522 (2013)
4. Davydenko, A., Sai, C., & Shcherbakov, M. (2020, September 14–16). Data formats and visual tools for forecast evaluation in cyber-physical system design [conference presentation]. *International scientific multiconference “Cyber-physical systems design and modelling” CyberPhy-2020*, Kazan, Russia. <https://doi.org/10.6084/m9.figshare.12981329>.
5. Davydenko, A., Charith, K. (2020, July 29–30).: A Visual Framework for Longitudinal and Panel Studies (with Examples in R) [ePoster]. IRCUWU2020. <https://doi.org/10.6084/m9.figshare.12749432>
6. Davydenko, A., Fildes, R.: A joint Bayesian forecasting model of judgment and observed data (LUMS Working Paper 2012:4). Lancaster University, The Department of Management Science (2012). https://www.researchgate.net/publication/282136270_A_joint_Bayesian_forecasting_model_of_judgment_and_observed_data
7. Industry 4.0: Definition, Design Principles, Challenges, and the Future of Employment. <https://www.cleverism.com/industry-4-0/>. Accessed 14 Jun 2020.
8. Davydenko, A., Fildes, R.: Forecast error measures: critical review and practical recommendations. In: *Business forecasting: practical problems and solutions*. Wiley, Hoboken, NJ (2016)
9. Armstrong, J.S.: *Principles of Forecasting: A Handbook for Researchers and Practitioners*. Kluwer Academic, Boston, MA (2001)
10. Hyndman, R.: Cross-validation for time series [Blog post] (2016, December 5). Retrieved from <https://robjhyndman.com/hyndsight/tscv/>
11. Glossary: Density forecast. https://ec.europa.eu/eurostat/statistics-explained/index.php/Glossary:Density_forecast. Accessed 14 Jul 2020.
12. Hyndman, R.: Mcomp: Data from the M-Competitions. R package version 2.8 (2018). CRAN.R-project.org/package=Mcomp
13. Ellis, P.: Tcomp: Data from the 2010 Tourism Forecasting Competition. R package version 1.0.1 (2018). CRAN.R-project.org/package=Tcomp
14. Hyndman, R.: tscompdata: Time series data from various forecasting competitions. R package version 0.0.1 (2018). github.com/robjhyndman/tscompdata
15. Montero-Manso, P., Netto, C., Talagala, T.: M4comp2018: Data from the M4-Competition. R package version 0.1.0 (2018). github.com/carlanetto/M4comp2018
16. Sai, C., Davydenko, A., Shcherbakov, M.: Forvision: Tools for forecast visualisation and evaluation. R package version 0.0.1 (2019). github.com/forvis/forvision
17. Theil, H.: *Applied economic forecasting*. North-Holland, Amsterdam (1996)
18. Hyndman, R., Koehler, A.: Another look at measures of forecast accuracy. *Int. J. Forecast.* **22**(4), 679–688 (2006)
19. Davydenko, A., Fildes, R.: Measuring forecasting accuracy: problems and recommendations (by the example of SKU-level judgmental adjustments). In: *Intelligent Fashion Forecasting Systems: Models and Applications*, pp. 43–70. Springer, Berlin Heidelberg (2014).

20. Zellner, A.: An Introduction to Bayesian Inference in Econometrics. Wiley Classics Library. Wiley, New York (1996)
21. Davydenko, A.: Integration of judgmental and statistical approaches for demand forecasting: Models and methods. PhD Thesis. Lancaster University, UK (2012). https://www.researchgate.net/publication/338885739_Integration_of_judgmental_and_statistical_approaches_for_demand_forecasting_Models_and_methods
22. Goodwin, P.: Profit from your Forecasting Software: A Best Practice Guide for Sales Forecasters. Wiley and SAS Business Series, Wiley, Hoboken, New Jersey (2018)
23. Gilliland, M.: Forecast value added analysis: Step-by-step. SAS Institute whitepaper (2008)
24. Ma, S., Fildes, R., Huang, T.: Demand forecasting with high dimensional data: The case of SKU retail sales forecasting with intra- and inter-category promotional information. *Eur. J. Oper. Res.* **249**(1), 245–257 (2016)
25. Huang, T., Fildes, R., Soopramanien, D.: Forecasting retailer product sales in the presence of structural change. *Eur. J. Oper. Res.* **279**(2), 459–470 (2019)
26. Fildes, R., & Goodwin, P. (2020). Stability in the inefficient use of forecasting systems: A case study in a supply chain company. *International Journal of Forecasting*. <https://doi.org/10.1016/j.ijforecast.2020.11.004>.
27. Spiliotis, E., Petropoulos, F., Kourentzes, N., & Assimakopoulos, V. (2020). Cross-temporal aggregation: Improving the forecast accuracy of hierarchical electricity consumption. *Applied Energy*, *261*, 114339. <https://doi.org/10.1016/j.apenergy.2019.114339>.
28. Chen C., Twycross J., Garibaldi J.M.: A new accuracy measure based on bounded relative error for time series forecasting. *PLoS ONE* *12*(3), e0174202 (2017). <https://journals.plos.org/plosone/article?id=10.1371/journal.pone.0174202>
29. Athanasopoulos, G., Hyndman, R.J., Song, H., Wu, D.C.: The tourism forecasting competition. *Int. J. Forecast.* **27**(3), 822–844 (2011)

Classification of the Technological Process Condition Based on Hybrid Neural Networks



Andrey Puchkov, Maxim Dli, and Yekaterina Lobaneva

Abstract The cascade architecture of neural networks, providing multichannel information processing as a part of a cyber-physical system, is presented. The architecture contains a hybrid network for aggregation of intermediate results obtained by an ensemble of deep recurrent neural networks based on fuzzy logic methods. The structure of the software which implements the presented architecture and being developed for conducting simulation experiments is described, their results are given.

Keywords Machine learning · Deep neural networks · Computer vision

1 Introduction

The improvement of the information support for cyber-physical systems now tends to be based on the use of machine learning methods which automate the procedure of extracting the necessary regularity from incoming data. Among these methods, deep neural networks gained the greatest popularity, which was facilitated by the emergence of new efficient neural network architectures and significantly increased abilities for computing technology in the middle price segment. This allowed many researchers to conduct algorithms learning and implement them in practice with the use of ready-made hardware solutions [1, 2].

The use of such solutions for complex industrial objects is faced with the need to process multi-channel technological information, therefore, in this case, ensembles of neural networks, each element of which takes into account the presentation

A. Puchkov (✉) · M. Dli · Y. Lobaneva
National Research University «Moscow Power Engineering Institute» (Branch), Energeticheskoye pryezd 1, g. Smolensk, Smolensk 2014013, Russia
e-mail: putchkov63@mail.ru

M. Dli
e-mail: MiDli@mail.ru

Y. Lobaneva
e-mail: lobaneva94@mail.ru

features and data format in a particular channel, are becoming very popular. The result combination for the work of channel neural networks for working out any generalizing solution, in this case, is carried out in the output analytical unit. The algorithms for the operation of such blocks are various, and they are based on additional cascades of neural networks [3, 4]; the following approaches are also used: fuzzy aggregation of ensemble output [5, 6]; additional information for ensemble learning [7]; self-organization of networks [8]; modifications of the Bayesian approach allowing compensation the imbalance of existing data [9]. Each of the above-mentioned approaches develops applied directions for neural networks usage taking into account a certain aspect of a particular application or presentation features and initial data form when combining the results for channel information processing. The existing wide variety of applied fields for neurotechnologies, which exist nowadays, ensures the relevance of research in this direction.

This work proposes a neural network architecture that provides multi-channel information processing as a part of a cyber-physical system in order to assess its condition. The architecture contains the input ensemble for the deep recurrent neural network (DRNN) and output hybrid neural network to aggregate the intermediate results of the presented data. Such a composition of neural networks allows predicting the parameters of a cyber-physical system due to DRNN and classifying its condition using an output hybrid (neuro-fuzzy) system which set of rules, generated automatically during learning, can be adjusted if necessary.

2 Materials and Methods

A specific feature of the applied aspect of neural networks in cyber-physical systems is the need to adapt the resulting solutions to the information-technological environment of the physical process, which is based on the experience of a developer both in the field of information and hardware. This process for neural networks consists of the analysis of the receiving result and further adjustment of network architectures and their hyperparameters (initial parameters of networks and optimization procedures which are unchanged during network training).

The absence of universal network architectures leads to the necessity to use various techniques to improve the results of data analysis. Boosting being one of them. It consists of the sequential aggregation of different algorithms in which each subsequent one uses the results of the previous ones for learning, this allows obtaining a stronger solution, high generalizing ability, and universality [10]. To a certain extent, the introduction of methods, which allow improving the understanding of how the neural network receives the result since this provides an opportunity for actions to improve it, can also be attributed to boosting. For example, in [11, in Russian] taking into account the symmetries in the incoming signals, we propose a grouping of neurons in a hidden layer according to the form of automorphism and the use of three-phase activation functions for each group. In many cases a similarity of a multi-agent approach is used: sets of relatively simple neural networks with different

hyperparameters are created, and then their outputs are analyzed according to various schemes [12].

The authors propose a hybrid architecture for the classifier of the technological process (TP) condition for the production of phosphorus from apatite-nepheline ores waste [13, in Russian], shared DRNN and ANFIS networks (adaptive neuro-fuzzy inference system is an adaptive network based on the fuzzy inference system of Takagi–Sugeno) [14]. This structure provides a mechanism to introduce into the “closed” neural network classifier the possibility of recording expert knowledge due to adjusting the rule base synthesized by the ANFIS system and allows making classification based on additional knowledge. The approach under consideration makes the understanding of classification results accessible since the output cascade of the neural networks ensemble the interpretation for the previous signals will be visible.

It should be noted, that hybrid approaches for the solver building in intelligent systems are often used in modifications of various subject areas and the ANFIS option is not the only one that can be used. One of the alternatives is the «coactive neuro-fuzzy inference system» (CANFIS), which also combines fuzzy logic and neural networks, achieving an increase in the power of intelligent systems through the use of verbal and numerical description of the subject area [15].

The proposed hybrid architecture contains the cascade inclusion of DRNN block and adaptive ANFIS networks, therefore, the output fuzzy classifier ANFIS gets a possibility to forecast the TP condition taking into account its behavior in the past due to the presence of such ability in DRNN.

Let the described architecture and its application be considered for the specific application for which it was specially created: for the processing of technological information of the system for phosphorus production from apatite-nepheline ores waste. The cyber-physical system consists of an intelligent information superstructure and three units (Fig. 1) implementing TP:

- a pelletizer (it forms raw pellets from ores waste);
- a multi-chamber indurating machine of a conveyer type (it provides high-temperature roasting of raw pellets);
- an ore-thermal furnace (pellets are melted in it with the release of gaseous phosphorus);
- The listed units are indicated in Fig. 1 as control objects CO1, CO2, and CO3, respectively.

DRNN application is justified by their ability to accumulate knowledge for some retrospective time period, which is in demand in the TP control, as it makes it possible to evaluate its condition not only by current parameters but also taking into account their past behavior. It is especially important for complex TP in which different stages are differentiated both in time and in space and implemented on various units. The DRNN ensemble provides the approximation of the historic behavior and spatial division of the controlled system into separate technological zones. The ANFIS block, in its turn, automates the receiving of final conclusions based on the results provided by recurrent networks.

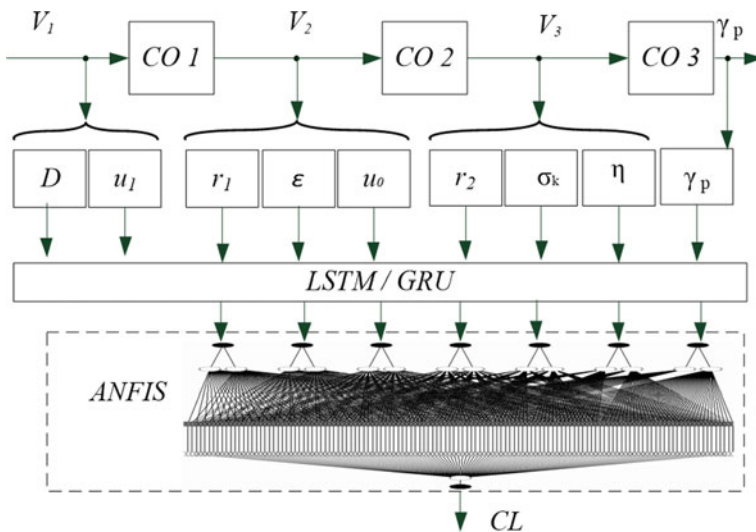


Fig. 1 The hybrid architecture of the information processing in the cyber-physical system

The application of mathematical models for transformation processes of the feed-stock into the final product by each unit makes it possible to determine the condition variables at the input/output of each unit [13]. When preparing the learning sets variables are united into row vectors:

$$V_1 = [Du_1], V_2 = [r_1 \epsilon u_0], V_3 = [r_2 \sigma_k \eta], \tag{1}$$

where D—a middle diameter for the waste particles of apatite-nepheline ores (mm); u_1 —specific humidity of ores waste (%); r_1 —a radius of a raw pellet (mm), ϵ —a pellet porosity (in fractions of the volume of the entire pellet), u_0 —pellets humidity at the exit from the granulator (%); r_2 —a radius of a roasted pellet (mm); σ_k —a pellet compressive strength (kN/pellet); η —a degree of response in decarbonization reactions (a fraction of the reacted substance from its total volume). It should be mentioned, that the output row vector V_2 of the granulator is the input one for the indurating machine, and its output row vector V_3 is the output one for the ore-thermal furnace, which output parameter is the purity of the resulting phosphorus γ_p (% from the general volume of the output fractions).

The listed parameters, taken at discrete intervals of time Δt , form an initial data matrix which is constantly updated with new values as the observation time increases. For the neural network training the data taken for a long time period, which provides a sufficient amount of the learning sample, is used. The data are stored in the form of a file with CSV format, which fragment reflecting the typical values for the TP parameters is shown in Fig. 2.

From the whole variety of DRNN for the considered architecture, two types of networks were selected, which have the best representative power and have a

Fig. 2 Data file fragment

	A	B	C	D	E	F
1	N_time, D, u1, r1, eps, u0, r2, sigma_k, etta, gamma_p					
2	0.0,1.032,0.513,11.05,0.417,12.09,10.92,2.97,0.608,34.40					
3	12.0,1.051,0.532,10.59,0.568,12.13,10.41,2.82,0.561,37.14					
4	24.0,1.049,0.501,11.10,0.612,11.43,11.12,2.71,0.483,42.65					
5	36.0,1.001,0.513,11.07,0.609,12.17,10.94,2.93,0.721,39.17					

wide range of practical applications. These networks are based on the algorithm of long short-term memory (LSTM, Long Short-Term Memory) [16, 17] and the network GRU (Gated Recurrent Unit) [18, 19], applied LSTM principles but having fewer numbers of filters and operations for calculations. LSTM and GRU layers allow coping with a problem of gradient attenuation observed in direct propagation networks with a large number of layers, as the number of layers increases, the network eventually becomes unlearning [20]. DRNN (in variants LSTM and GRU) in the proposed architecture are used for solving the problem of regression.

DRNN and ANFIS learning is carried out separately in two stages. At the first stage, DRNN is trained, at the second stage ANFIS is trained. Before learning, data are prepared and normalized. From the CSV file, the information is entered into the matrix: $MV = \{[V1 V2 V3 \gamma]i\}$, where $i = 0, 1, 2, \dots N_{mv}$, where N_{mv} —the number of rows in the table read from the file. From this matrix, learning and test sets are formed taking into account the following control parameters: lookback—the number of time intervals from the current moment, determining the number of rows in one learning data packet; delay—the interval of the forecast (if delay = 0, then the current condition is estimated); min_index and max_index—the indexes restricting data retrieval from MV; shuffle—a logic key, at shuffle = 1 rows are retrieved from MV with shuffling, at shuffle = 0 without shuffling; batch_size—a number of samples in one packet, according to which the network weights are adjusted; step—a period in intervals specifying the value of lines decimation from MV.

The LSTM/GRU unit (Fig. 1) uses several DRNN connected in parallel, which differ in the number of components in the input data vectors and the output parameter. For networks DRNN1–DRNN3 the input vector is the combined row vector [V1 V2], and the networks differ in what parameter is taken for them as the output one: r_1, ϵ , or $u_0: r_1$, respectively. For DRNN4–DRNN7 networks the sets of vectors [V2 V3] are the input parameters. DRNN4–DRNN7 are the output parameters in networks: r_2, σ_k, η , and γp respectively.

Without dwelling on the algorithms of the networks, we only note that the output y_k k -th DRNN, $k = 1, 2, \dots, 7$, is formed in accordance with the expression:

$$y_k = f(\text{state_}t_k \circ U_k + BV_k \circ W_k + b_k), \tag{2}$$

where $\text{state_}t_k, U_k, b_k$ —learning parameters of k -th LSTM for the current moment of time t , \circ —a symbol of Hadamard matrices (component-wise product), BV_k —the input packet of learning data.

It should be noted, that LSTM/GRU contains a sequentially located set of recurrence units and can only process a parameter row [20]. However, the learning algorithms provide for a packet supply of initial data to the network input (in accordance with the above-mentioned list of control parameters), therefore, state $state_t_k$, U_k , and b_k t_k , U_k , are matrices.

3 Application and Results

DRNN networks were trained in the mode of sequence to end, when not complete results sequences were returned for all time intervals, but only the last result for each input sequence. GRU application in the architecture shown in Fig. 1 allows reducing the computational cost for network learning due to their simpler structure, compared with LSTM, as noted above. The use of GRU together with LSTM is justified by the appropriateness of testing simpler solutions if they allow achieving the specified accuracy for TP condition estimation.

In the second stage, the ANFIS network is trained, this network has seven inputs (by the number of DRNNs) and one CL output having a range of values from 0 to 1. The network solves the problem of classifying the condition for TP based on the results of its evaluation of DRNN. It was accepted that the condition of the TP can be divided into four classes (depending on the value of the parameter γ_p): “nominal value”, “nominal value excess”, “small deviation down from the nominal value” and “big deviation down from the nominal value” (Table 1).

The entire range (from 0 to 100%) is a technologically permissible spread in values of the parameter γ_p , the exceeding of which is already monitored by instrumentation.

The program that implements the architecture provides a control parameter delay, depending on it the current condition can be evaluated (delay = 0) or forecasted (delay > 0). Unlike DRNN, ANFIS learning requires a significantly smaller training sample due to the relatively small number of adjustable network parameters [15].

To test the proposed neural network architecture simulation experiments were performed in MatLab 2019b environment, which has a specialized machine learning

Table 1 Classes numbers of the output parameter for the ore-thermal furnace

Class number	Class name	Interval of values for a parameter γ_p , %	ANFIS output, appropriate to class
1	Nominal value	40–60	0.75
2	Exceeding the nominal value	61–100	1.00
3	Small deviation down from the nominal value	30–39	0.50
4	Big deviation down from the nominal value	0–29	0.25



Fig. 3 Hybrid network layer scheme for one channel of data processing

library Deep Network Designer. Before learning, the data were normalized using the operations of subtraction the mean and roof-mean-square deviation. A simplified scheme of the channels layers for processing TP parameters is shown in Fig. 3.

Each of seven LSTM was trained during 250 epochs, the number of samples in the training dataset was 50,000, and in the testing one, it was 10,000. To avoid retraining the decimation mechanism was used. The training quality estimation (Fig. 4) was carried out with the use of two metrics: the root-mean-square error and loss function [21].

ANFIS configuration: the number of inputs—7; the number of membership functions for each input—2; the type of membership functions—trimf; the number of outputs—1; the type of membership functions—linear. In the process of ANFIS training ANFIS, a set of rules was generated, the structure of which is reflected in the fragment shown in Fig. 5.

The neural networks were trained on the following hardware: ASUS TUF Gaming FX705DT-AU039 notebook, AMD Ryzen 7 3750H CPU, 2.3 GHz, NVIDIA GeForce GTX 1650 4G GPU, 1024 CUDA cores (provide parallel computing). Classification results are presented in Fig. 5.

The crosses indicate the output of the hybrid architecture classifier, the dots indicate the levels corresponding to the true classes. The forecasting parameter delay = 0 was suggested, which means the recognition of the current condition, however,

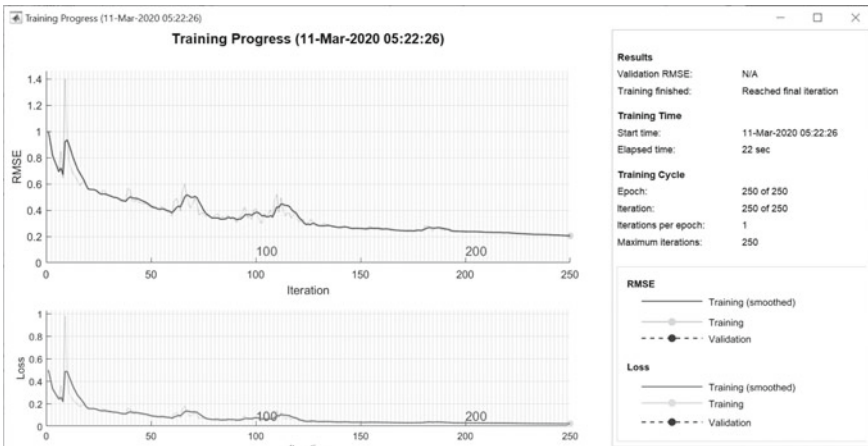


Fig. 4 LSTM metrics dynamics in the training process


```
1. If (input1 is in1mf1) and (input2 is in2mf1) and (input3 is in3mf1) and (input4 is in4mf1) and (input5 is in5mf1) and (input6 is in6mf1) and (input7 is in7mf1) then (output is out1mf1) (1)
2. If (input1 is in1mf1) and (input2 is in2mf1) and (input3 is in3mf1) and (input4 is in4mf1) and (input5 is in5mf1) and (input6 is in6mf1) and (input7 is in7mf2) then (output is out1mf2) (1)
3. If (input1 is in1mf1) and (input2 is in2mf1) and (input3 is in3mf1) and (input4 is in4mf1) and (input5 is in5mf1) and (input6 is in6mf2) and (input7 is in7mf1) then (output is out1mf3) (1)
4. If (input1 is in1mf1) and (input2 is in2mf1) and (input3 is in3mf1) and (input4 is in4mf1) and (input5 is in5mf1) and (input6 is in6mf2) and (input7 is in7mf2) then (output is out1mf4) (1)
5. If (input1 is in1mf1) and (input2 is in2mf1) and (input3 is in3mf1) and (input4 is in4mf1) and (input5 is in5mf2) and (input6 is in6mf1) and (input7 is in7mf1) then (output is out1mf5) (1)
6. If (input1 is in1mf1) and (input2 is in2mf1) and (input3 is in3mf1) and (input4 is in4mf1) and (input5 is in5mf2) and (input6 is in6mf1) and (input7 is in7mf2) then (output is out1mf6) (1)
7. If (input1 is in1mf1) and (input2 is in2mf1) and (input3 is in3mf1) and (input4 is in4mf1) and (input5 is in5mf2) and (input6 is in6mf2) and (input7 is in7mf1) then (output is out1mf7) (1)
8. If (input1 is in1mf1) and (input2 is in2mf1) and (input3 is in3mf1) and (input4 is in4mf1) and (input5 is in5mf2) and (input6 is in6mf2) and (input7 is in7mf2) then (output is out1mf8) (1)
9. If (input1 is in1mf1) and (input2 is in2mf1) and (input3 is in3mf1) and (input4 is in4mf2) and (input5 is in5mf1) and (input6 is in6mf1) and (input7 is in7mf1) then (output is out1mf9) (1)
10. If (input1 is in1mf1) and (input2 is in2mf1) and (input3 is in3mf1) and (input4 is in4mf2) and (input5 is in5mf1) and (input6 is in6mf1) and (input7 is in7mf2) then (output is out1mf10) (1)
```

Fig. 5 A fragment of ANFIS rules set

this does not affect the quality of the classification performed by ANFIS, since the LSTM/GRU unit is responsible for the forecast accuracy in this architecture (its accuracy characteristics are shown in Fig. 4). We note that in the experiment the replacement of LSTM by GRU practically did not affect the accuracy of the forecast, this fact can be due to a large number of training epochs or the features of the training data set.

The grouping of the classifier output values near the true class values in Fig. 6 can indicate the operability of the proposed hybrid architecture and the ability of its application to solve the problem for classifying the TP conditions. To obtain an integer class number from Table 1, it is possible to specify a valid range for the spread of the ANFIS output values. Some of the ANFIS outputs, underlined in Fig. 6, have

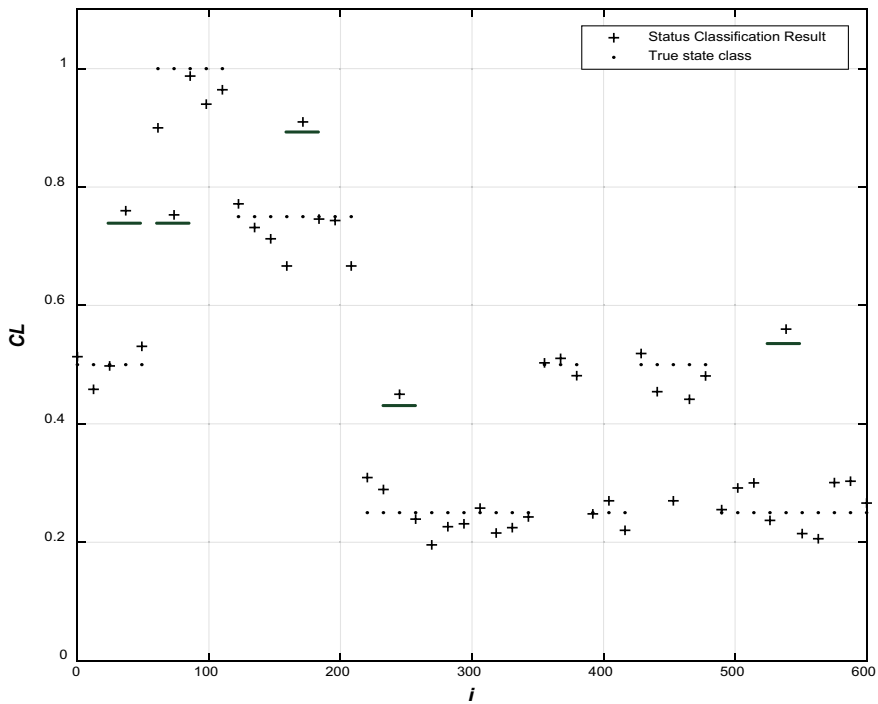


Fig. 6 Classification results

significant deviations from the true values, which reflect classification errors that can be reduced by modification of the hybrid architecture hyperparameters, for example, the number of ANFIS input membership functions can be increased to three.

4 Conclusion

The proposed hybrid architecture makes it possible to take advantage of two methodologies for constructing neural networks: to perform a retrospective analysis of time series using the DRNN ensemble and to generalize the results of their work with the ANFIS system providing an additional opportunity to make adjustments to the automatically created knowledge base in case of need.

The conducted simulation experiment showed the ability of the proposed hybrid architecture to carry out the classification of the process condition based on the stage-by-stage processing of the initial information using the DRNN and ANFIS systems.

The obtained results can be used in the development of knoware and software for systems of intelligent data analysis in various subject areas.

Acknowledgements The reported study was funded by RFBR according to the research projects No 18-29-24094 and No 19-01-00425.

References

1. Ivanavičius, A., Simonavičius, H., Gelšvartas, J., et al.: Real-time CUDA-based stereo matching using Cyclops2 algorithm. *J Image Video Proc.* **2018**, 12 (2018). <https://doi.org/10.1186/s13640-018-0253-2>
2. Moreno, J.J., Ortega, G., Filatovas, E., et al.: Using low-power platforms for evolutionary multi-objective optimization algorithms. *J Supercomput* **73**, 302–315 (2017). <https://doi.org/10.1007/s11227-016-1862-0>
3. Frazão X., Alexandre L.A.: Weighted Convolutional Neural Network Ensemble. In: Bayro-Corrochano, E., Hancock, E. (eds.) *Progress in Pattern Recognition, Image Analysis, Computer Vision, and Applications. CIARP 2014. Lecture Notes in Computer Science*, vol. 8827. Springer, Cham (2014)
4. Koitka S., Friedrich C.M.: Optimized convolutional neural network ensembles for medical subfigure classification. In: Jones, G., et al. (eds.) *Experimental IR Meets Multilinguality, Multimodality, and Interaction. CLEF 2017. Lecture Notes in Computer Science*, vol. 10456. Springer, Cham (2017)
5. Puchkov A., Dli M.I., Lobaneva E., Vasilkova M.: Choice of a deep neural networks architecture to monitor the dynamics of an object state. In: *Proc. of the 14th International Conference on Interactive Systems: Problems of Human–Computer Interaction (2019)*. <http://ceur-ws.org/Vol-2475/paper12.pdf>
6. Kulyasova, E.V., Kulyasov, N.S., Puchkov, A.Y.: The appliance of deep neural networks in the process of managing chemical enterprises. *IOP Conf. Ser.: J. Phys. Conf. Ser.* **1260**, 032024 (2019). <https://doi.org/10.1088/1742-6596/1260/3/032024>

7. Guo, Y., Wang, X., Xiao, P., et al.: An ensemble learning framework for convolutional neural network based on multiple classifiers. *Soft Comput.* **24**, 3727–3735 (2020). <https://doi.org/10.1007/s00500-019-04141-w>
8. Ståhl, N., Falkman, G., Mathiason, G., Karlsson, A.: A self-organizing ensemble of deep neural networks for the classification of data from complex processes. In: Medina J., Ojeda-Aciego, M., Verdegay, J., Perfilieva, I., Bouchon-Meunier, B., Yager, R., (eds.) *Information Processing and Management of Uncertainty in Knowledge-Based Systems. Applications. IPMU 2018. Communications in Computer and Information Science*, vol. 855. Springer, Cham (2018)
9. Lázaro, M., Herrera, F., Figueiras-Vidal, A.R.: Classification of binary imbalanced data using a Bayesian ensemble of Bayesian neural networks. In: Iliadis, L., Jayne, C. (eds.) *Engineering Applications of Neural Networks. EANN 2015. Communications in Computer and Information Science*, vol. 517. Springer, Cham (2015)
10. Dembski, J.: Multiclass AdaBoost classifier parameter adaptation for pattern recognition. In: Choraś, R. (ed.) *Image Processing and Communications Challenges 8. IP&C 2016. Advances in Intelligent Systems and Computing*, vol. 525. Springer, Cham (2017)
11. Lozhkin, A.G., Majorov, K.N.: The symmetry mechanism application in neural networks. In: *Conference Proceedings: Seventeenth National Conference on Artificial Intelligence with International Participation of CII-2019*, vol. 2, pp. 119–126. (2019)
12. Zhang, W., Jiang, J., Shao, Y., et al.: Snapshot boosting: a fast ensemble framework for deep neural networks. *Sci. China Inf. Sci.* **63**, 112102 (2020). <https://doi.org/10.1007/s11432-018-9944-x>
13. Puchkov, AYu., Dli, M.I., Lobaneva, E.I., Bliznyuk, O.A.: Optimization of energy consumption for a multistage phosphorus production process. *Conf. Proc.: Math. Meth. Technol. Tech.* **4**, 68–71 (2019)
14. Arun, K.S., Govindan, V.K.: A hybrid deep learning architecture for latent topic-based image retrieval. *Data Sci. Eng.* **3**, 166–195 (2018)
15. Tahmasebi, P., Hezarkhani, A.A.: Hybrid neural networks-fuzzy logic-genetic algorithm for grade estimation. *Comput. Geosci.* **42**, 18–27 (2012). <https://doi.org/10.1016/j.cageo.2012.02.004>. Accessed 09 Mar 2020
16. Liu, J., Chen, S.: Non-stationary multivariate time series prediction with selective recurrent neural networks. In: Nayak, A., Sharma, A. (eds.) *PRICAI 2019: Trends in Artificial Intelligence. PRICAI 2019. Lecture Notes in Computer Science*, vol. 11672. Springer, Cham (2019)
17. Althelaya, K.A., El-Alfy, E.M., Mohammed, S.: Stock market forecast using multivariate analysis with bidirectional and stacked (LSTM, GRU). In: *2018 21st Saudi Computer Society National Computer Conference (NCC)*, pp. 1–7. Riyadh (2018)
18. Ke, K., Hongbin, S., Chengkang, Z., et al.: Short-term electrical load forecasting method based on stacked auto-encoding and GRU neural network. *Evol. Intel.* **12**, 385–394 (2019). <https://doi.org/10.1007/s12065-018-00196-0>
19. Islam, M.M., Lam, A., Fukuda, H., et al.: An intelligent shopping support robot: understanding shopping behavior from 2D skeleton data using GRU network. *Robomech J.* **6**, 18 (2019). <https://doi.org/10.1186/s40648-019-0150-1>
20. Hochreiter, S., Schmidhuber, J.: Long short-term memory. *Neural Comput.* **9**(8), 1735–1780 (1997)
21. Boutaba, R., Salahuddin, M.A., Limam, N., et al.: A comprehensive survey on machine learning for networking: evolution, applications and research opportunities. *J. Internet Serv. Appl.* **9**, 16 (2018). <https://doi.org/10.1186/s13174-018-0087-2>

Fuzzy Rules Reduction in Knowledge Bases of Decision Support Systems by Objects State Evaluation



Maria Dagaeva and Aleksey Katasev

Abstract The problem of eliminating the redundancy of knowledge bases formed based on fuzzy neural networks is considered. To solve this problem, fuzzy rules reduction technology based on the principles of knowledge taxonomy and genetic optimization was proposed. A technique for clustering fuzzy rules in the initial knowledge base has been developed with obtaining an intermediate knowledge base. To minimize the number of fuzzy rules in the intermediate knowledge base and obtain the required knowledge base, a genetic algorithm has been developed. A software package was developed on the basis of the proposed mathematical methods. The research carried out based on the software complex showed the effectiveness of the technology of fuzzy rules reduction and the possibility of its practical use.

Keywords Knowledge base · Fuzzy rules reduction · Knowledge taxonomy · Genetic algorithm · Decision support · Object state evaluation

1 Introduction

Now in various fields of human activity, intellectual decision support systems on object state evaluation have become widespread [1–5]. The main component of such systems is the knowledge base [6]—a special repository of formalized knowledge of experts, characterizing the simulated objects, their external and internal relations, and regularities. Fuzzy production rules are often used as a model for the representation of expert knowledge [7]. Their usage allows the most accurate modeling of the expert's knowledge and inferences when solving practical problems. Besides, they have good linguistic interpretation, allowing us to evaluate the state of objects in conditions of uncertainty [8].

M. Dagaeva (✉) · A. Katasev
Kazan National Research Technical University Named After A.N. Tupolev-KAI, Karl Marx str.
10, Kazan 420111, Russia
e-mail: dagaevam@rambler.ru

A. Katasev
e-mail: Kat_726@mail.ru

© The Author(s), under exclusive license to Springer Nature Switzerland AG 2021
A. G. Kravets et al. (eds.), *Cyber-Physical Systems: Modelling and Intelligent Control*, Studies in Systems, Decision and Control 338,
https://doi.org/10.1007/978-3-030-66077-2_9

113

Construction of knowledge bases of intellectual systems is connected with questions selection and realization of knowledge reception strategy. It can be a traditional strategy for obtaining knowledge from an expert, as well as a strategy of forming knowledge-based on methods and algorithms of intellectual data analysis [9–12], in particular fuzzy neural networks [13–15]. In the case of the second strategy, there is an automatic construction of knowledge base by its parametrical adaptation to the analyzed data [16].

The result of training the fuzzy neural network is a system of fuzzy production rules that make up the knowledge base of the intellectual system. The formed knowledge base is complete, i.e. contains a full set of rules set by all combinations of input and output parameters of the object and their fuzzy gradations. In this case, not all the rules are equally important for object state evaluation. That is why the actual task of estimating the redundancy of the formed knowledge base and exclusion (reduction) of insignificant rules [17–19].

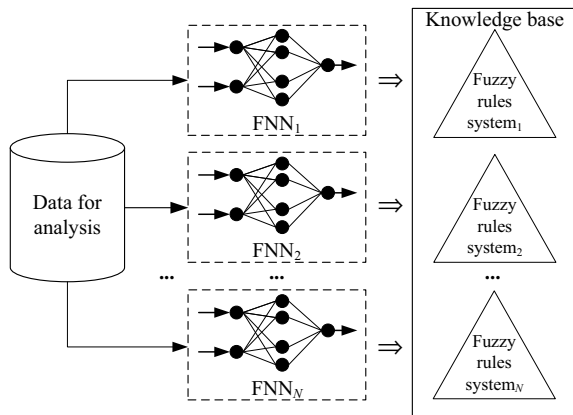
2 Fuzzy Rules Reduction Technology

In this work technology of fuzzy production rules reduction, formed based on model construction of collective of fuzzy neural networks [8] is offered (see Fig. 1).

As can be seen in the figure, fuzzy neural networks, learning from the available data, form a knowledge base for object state evaluation. In this case, fuzzy rules in the knowledge base have the following form [20]:

$$\text{If } x_1 = \overset{\leftrightarrow}{\underset{1}{A}}(w_1) \text{ and } x_2 = \overset{\leftrightarrow}{\underset{2}{A}}(w_2) \text{ and } \dots x_n = \overset{\leftrightarrow}{\underset{n}{A}}(w_n) \text{ Then } y = B[CF] \quad (1)$$

Fig. 1 Knowledge base formation diagram



where x_i —input parameters, $w_i \in [0,1]$ —weighting coefficient “ $x_i = Ax_i = \overset{\leftrightarrow}{A}_i$ ”, $A^{\leftrightarrow}_i = \{A_i, \overset{\leftrightarrow}{A}_i\}$, A_i —crisp value of input parameter, $\overset{\leftrightarrow}{A}_i = \{(x_i, \mu_{\overset{\leftrightarrow}{A}_i}(x_i))\}$ —fuzzy value of input parameter, $\mu_{\overset{\leftrightarrow}{A}_i}(x_i)$ —membership function of input parameters x_i to $\overset{\leftrightarrow}{A}_i$, y —output parameters, B —crisp value of output, $CF \in [0, 1]$ —rule confidence.

The automatically generated knowledge base has the following form [8]:

$$S_{Rule} \left\{ \begin{array}{l} \text{If } x_1 = \overset{\leftrightarrow}{A}_{11}(w_{11}) \& \dots x_i = \overset{\leftrightarrow}{A}_{i1}(w_{i1}) \& \dots x_n = \overset{\leftrightarrow}{A}_{n1}(w_{n1}) \text{ Then } y = B_1 [CF_{11}] \\ \dots \\ \text{If } x_1 = \overset{\leftrightarrow}{A}_{1j_1}(w_{1j_1}) \& \dots x_i = \overset{\leftrightarrow}{A}_{ij_i}(w_{ij_i}) \& \dots x_n = \overset{\leftrightarrow}{A}_{nj_n}(w_{nj_n}) \text{ Then } y = B_1 [CF_{1i_R}] \\ \dots \\ \text{If } x_1 = \overset{\leftrightarrow}{A}_{1m_1}(w_{1m_1}) \& \dots x_i = \overset{\leftrightarrow}{A}_{im_i}(w_{im_i}) \& \dots x_n = \overset{\leftrightarrow}{A}_{nm_n}(w_{nm_n}) \text{ Then } y = B_1 [CF_{1N_R}] \\ \dots \\ \text{If } x_1 = \overset{\leftrightarrow}{A}_{11}(w_{11}) \& \dots x_i = \overset{\leftrightarrow}{A}_{i1}(w_{i1}) \& \dots x_n = \overset{\leftrightarrow}{A}_{n1}(w_{n1}) \text{ Then } y = B_k [CF_{k1}] \\ \dots \\ \text{If } x_1 = \overset{\leftrightarrow}{A}_{1j_1}(w_{1j_1}) \& \dots x_i = \overset{\leftrightarrow}{A}_{ij_i}(w_{ij_i}) \& \dots x_n = \overset{\leftrightarrow}{A}_{nj_n}(w_{nj_n}) \text{ Then } y = B_k [CF_{ki_R}] \\ \dots \\ \text{If } x_1 = \overset{\leftrightarrow}{A}_{1m_1}(w_{1m_1}) \& \dots x_i = \overset{\leftrightarrow}{A}_{im_i}(w_{im_i}) \& \dots x_n = \overset{\leftrightarrow}{A}_{nm_n}(w_{nm_n}) \text{ Then } y = B_k [CF_{kN_R}] \\ \dots \\ \text{If } x_1 = \overset{\leftrightarrow}{A}_{11}(w_{11}) \& \dots x_i = \overset{\leftrightarrow}{A}_{i1}(w_{i1}) \& \dots x_n = \overset{\leftrightarrow}{A}_{n1}(w_{n1}) \text{ Then } y = B_K [CF_{K1}] \\ \dots \\ \text{If } x_1 = \overset{\leftrightarrow}{A}_{1j_1}(w_{1j_1}) \& \dots x_i = \overset{\leftrightarrow}{A}_{ij_i}(w_{ij_i}) \& \dots x_n = \overset{\leftrightarrow}{A}_{nj_n}(w_{nj_n}) \text{ Then } y = B_K [CF_{Ki_R}] \\ \dots \\ \text{If } x_1 = \overset{\leftrightarrow}{A}_{1m_1}(w_{1m_1}) \& \dots x_i = \overset{\leftrightarrow}{A}_{im_i}(w_{im_i}) \& \dots x_n = \overset{\leftrightarrow}{A}_{nm_n}(w_{nm_n}) \text{ Then } y = B_K [CF_{KN_R}] \end{array} \right. ,$$

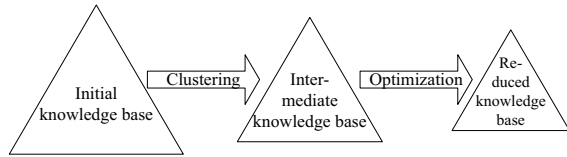
where x_i —rule’s input parameters, $i = 1 \dots n$, n —amount of input parameters, $A^{\leftrightarrow}_{ij_i}$ —values of input parameters, $j_i = 1 \dots m_i$, m_i —number of values i -th input parameters, y —rule’s output parameter, B_k —values of output parameter (object state), $k = 1 \dots K$, K —number of values of output parameter (number of object states), w_{ij_i} —weighting coefficient in rules, CF_{ki_R} —rule confidences, $i_R = 1 \dots N_R$, $N_R = \prod_{i=1}^n m_i$ —full number of rules for each object state.

Therefore, the total number of rules in the system is calculated by the form:

$$N_{Full} = K * N_R = K * \prod_{i=1}^n m_i .$$

Thus, even with a small number of input parameters, gradations, and object states, the knowledge base will include hundreds and thousands of rules, which in most cases is redundant.

Fig. 2 Diagram of the developed knowledge base reduction technology



The fuzzy rules reduction technology is based on the principles of knowledge taxonomy (clustering fuzzy rules) [21, 22] as well as genetic optimization [23]. The diagram of the developed technology is shown in Fig. 2.

Thus, the developed technology consists of two stages:

- (1) clustering of fuzzy rules in the initial knowledge base with obtaining an intermediate knowledge base consisting of rules corresponding to the centers of formed clusters;
- (2) genetic optimization of the intermediate knowledge base, which allows minimizing the number of rules and obtaining the required knowledge base.

Let's consider the implementation of these stages in more detail.

3 Clustering of Fuzzy Rules in the Initial Knowledge Base

To implement the first stage, there is proposed a method of clustering fuzzy rules in the initial knowledge base, which includes the following stages:

- (1) allocation of k rule groups in the initial knowledge base (clustering);
- (2) search for cluster centers (typical representatives of fuzzy production rules) R_{c_1}, \dots, R_{c_k} in each group;
- (3) formation of an intermediate knowledge base from the centers of constructed clusters R_{c_1}, \dots, R_{c_k} .

Figure 3 shows a diagram of the described method.

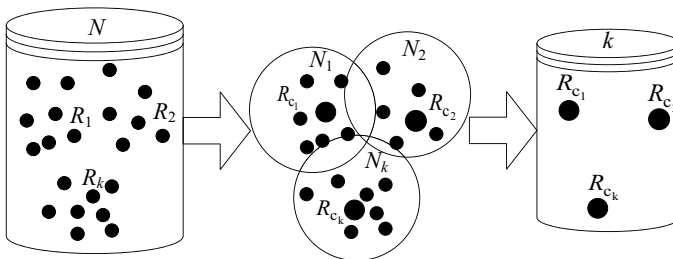


Fig. 3 Diagram of fuzzy rules clusterization

Therefore, the application of the proposed technique allows obtaining an intermediate knowledge base of N volume from the initial knowledge base of $k < N$ volume. Let's consider in more detail the realization of the proposed technique.

Let there be an initial knowledge base, formed on the basis of the model of the fuzzy neural network collective and consisting of the set of systems $R = \{R_1, \dots, R_i, \dots, R_m\}$ fuzzy production rules of the type (1), $i = 1 \dots m$. For a taxonomy of fuzzy rules (grouping of rules by similarity), it is necessary to present them in the derivative form suitable for the application of cluster analysis methods. One of such representations is a reflection of each fuzzy production rule in the format of corresponding fuzzy gradations of the following type:

$$(\tilde{A}_{11}, \tilde{A}_{12}, \dots, \tilde{A}_{1n}), (\tilde{A}_{21}, \tilde{A}_{22}, \dots, \tilde{A}_{2n}), \dots, (\tilde{A}_{m1}, \tilde{A}_{m2}, \dots, \tilde{A}_{mn}). \tag{2}$$

However, this type of rules is still not enough for the effective application of cluster analysis methods that work with numerical values. An effective way to transform fuzzy gradations into a numerical form is their defuzzification [24]. In this work the traditional defuzzification of fuzzy sets by the center of gravity method is used [25]:

$$x = \frac{\sum_i (\mu_{\tilde{A}}(x_i) * x_i)}{\sum_i \mu_{\tilde{A}}(x_i)},$$

where $\mu_{\tilde{A}}(x_i) \in [0, 1]$ is the function that determines the degree to which the x_i elements belong to an indistinct set \tilde{A} .

Usage the described defuzzification procedure allows transforming expression (2) to the following form:

$$(x_{11}, x_{12}, \dots, x_{1n}), (x_{21}, x_{22}, \dots, x_{2n}), \dots, (x_{m1}, x_{m2}, \dots, x_{mn}).$$

Thus, the knowledge base of the intellectual system is represented as a set of vectors of data points, each of which encodes fuzzy gradation in the corresponding rule. For the obtained n-dimensional data point space it is possible to apply the methods of cluster analysis after the normalization procedure according to the following rule:

$$x'_{ij} = \frac{x_{ij} - \min_{i=1,m}(x_{ij})}{\max_{i=1,m}(x_{ij}) - \min_{i=1,m}(x_{ij})},$$

where x_{ij} —initial value, x'_{ij} —normalized value.

As a result of normalization, we get numerical data reduced to the range [0, 1] of the following kind:

$$(x'_{11}, x'_{12}, \dots, x'_{1n}), (x'_{21}, x'_{22}, \dots, x'_{2n}), \dots, (x'_{m1}, x'_{m2}, \dots, x'_{mn}).$$

For this form of data representation, it is possible to use algorithms of cluster analysis [26]. The extended algorithm of k -average as the most effective algorithm of clustering is used in this paper [27], this allows us to work in spaces of large dimensionality.

In clustering, it is possible to obtain various cluster solutions. Classification error based on the appropriate intermediate knowledge base is used as a criterion of optimality of each cluster solution. The value of the classification error is calculated using a formula:

$$E = \left(1 - \frac{N_{\text{true}}}{N_{\text{total}}} \right) \rightarrow \min_k,$$

where N_{true} —number of correctly classified input patterns from the data test sample, N_{total} —test sample size, k —number of clusters formed in a particular cluster solution.

The final result of clustering fuzzy rules in the source knowledge base is an intermediate knowledge base consisting of rules corresponding to the centers of formed clusters. Further optimization of the number of remaining rules in the intermediate knowledge base is based on the use of a specially developed genetic algorithm.

4 Genetic Optimization of the Intermediate Knowledge Base

Let us consider the developed genetic algorithm for optimization of an intermediate knowledge base. Let's represent it as the following set of fuzzy rules: $R_c = \{R_{c_1}, \dots, R_{c_k}\}$. In this case, the knowledge base includes k rules R_c , $c = 1 \dots k$. To implement the genetic algorithm it was necessary to code the knowledge base in the form of a chromosome, consisting of «0» and «1»:

$$H_i = \{h_{ij}\},$$

where $h_{ij} = \begin{cases} 0, & \text{if } R_j \text{ not activ,} \\ 1, & \text{if } R_j \text{ activ.} \end{cases}$.

The zero chromosome gene means that there is no rule in the intermediate knowledge base, respectively, a single gene means there is a rule in it.

The work of the genetic algorithm includes such stages as the creation of the initial population of chromosomes, selection of parental chromosomes from the initial population for crossing and obtaining daughter chromosomes, their mutation, determination of adaptation in the population, and reduction. Each stage of the genetic algorithm is implemented in the framework of the corresponding mathematical methods are used in classical genetic algorithms [28].

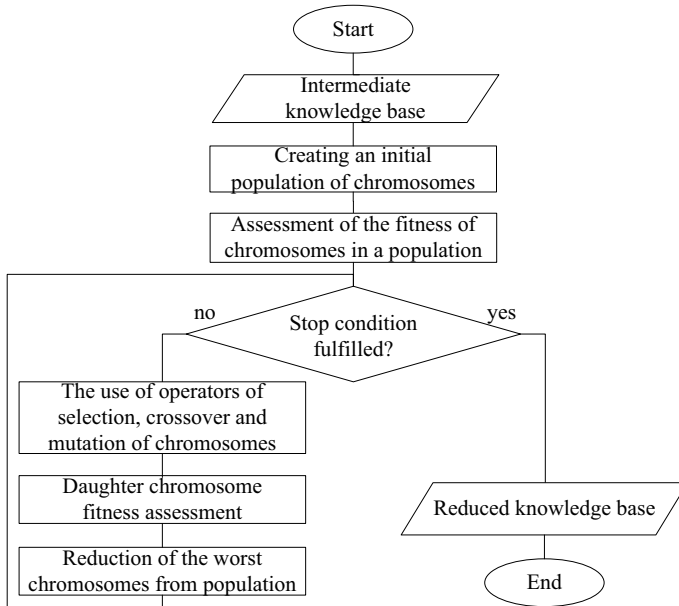


Fig. 4 Flowchart of the structural optimization algorithm

The peculiarity of the proposed algorithm is the way to create an initial population of chromosomes. Unlike traditional genetic algorithms, in which the initial population is formed randomly, in the developed algorithm, in addition to random selection, the initial population necessarily includes an individual (chromosome), encoding the intermediate knowledge base with all the fuzzy rules in it. This approach allows obtaining optimized knowledge bases with a classification ability not lower than that of the intermediate knowledge base.

Figure 4 shows a flowchart of the genetic algorithm.

The genetic algorithm is performed as long as chromosomes with better adaptability appear. The result is the best chromosome that matches the required knowledge base.

5 Fuzzy Rules Reduction Software

Software is developed on the basis of the offered mathematical methods the program complex implemented in the environment of modeling Matlab [29]. This software consists of two basic program modules, responsible for the reduction of initial knowledge base and evaluation of its classification ability. The reduction is carried out based on the proposed technology. Evaluation of classification ability of knowledge bases is performed based on a method of tenfold decimal cross-validation.

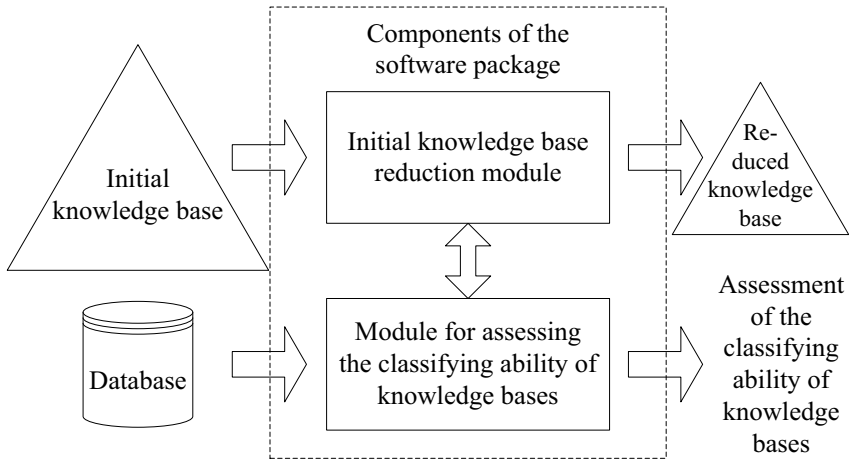


Fig. 5 Block diagram of the knowledge base reduction software

Figure 5 shows a block diagram of the developed software.

The software evaluates the classification ability of the initial knowledge base, produces its reduction based on the algorithm of clustering and genetic optimization, and determines the classification ability of the obtained knowledge base. The procedure of cross-validation is cyclically implemented for this purpose, which allows to accurately enough define the classification ability of the required knowledge base.

6 Researches Performed on the Basis of Software

Public data set from UCI Machine Learning Repository [30] was used for researches based on the developed software to solve the task of revealing non-standard transactions with bank cards. The characteristics of the data set are presented in Table 1.

The data sample included 690 records on 14 input parameters and 1 output with two solution classes (standard and non-standard transactions). The initial knowledge base was formed based on fuzzy neural networks training on these data groups. The reduction of the formed knowledge base was carried out on the basis of the developed software.

Table 1 Dataset characteristics for research

Name of dataset	Number of input parameters	Type of input parameters	Sample size	Number of solution classes
Australian credit approval	14	numerical, categorical	690	2

Table 2 Comparative characteristics of knowledge bases

Knowledge base	Number of fuzzy rules	Classification ability, %	Logic output execution time, s
Initial	13,608	88	0.43
Intermediate	973	88	0.08
Required	649	89	0.07

The results of the conducted researches have shown that the reduced knowledge base has better classification ability and speed of a logical conclusion in comparison with the initial knowledge base (see Table 2).

Thus, the reduction of fuzzy rules in the initial knowledge base has led to the elimination of its redundancy (the number of rules has decreased by 95%), higher classification ability (the accuracy of classification has increased by 1.13%), and the interpretability of the knowledge base, as well as reduced time for logical conclusion on the rules of the knowledge base (time has decreased by 83.7%).

7 Conclusion

The described in chapter technology of fuzzy rules reduction in databases of knowledge of intelligent cyber-physical systems on an object state evaluation, and also its mathematical methods and software have shown the possibility of essential reduction of dimensionality of the generated knowledge base, an increase of its classification ability and decrease of logic output execution time. Besides, the evaluation of redundancy has led to the improvement of the interpretability of the reduced knowledge base. This factor has a positive impact on the increase in human confidence in the decisions obtained from such knowledge bases.

Thus, the obtained results indicate the efficiency of the developed technology of fuzzy rules reduction and the possibility of its practical use for the optimization of knowledge bases in the decision support intellectual systems for the object state evaluation.

References

1. Radhi, A.M.: Risk assessment optimization for decision support using intelligent model based on fuzzy inference renewable rules. *Indonesian J. Electr. Comput. Sci.* **19**(2), 1028–1035 (2020)
2. Kizim, A.V., Kravets, A.G.: On systemological approach to intelligent decision-making support in industrial cyber-physical systems. *Stud. Syst. Decis. Control* **260**, 167–183 (2020)
3. Bolshakov, A.A., Kulik, A., Sergushov, I., Scripal, E.: Decision support algorithm for parrying the threat of an accident. *Stud. Syst. Decis. Control* **260**, 237–247 (2020)

4. Alekseev, A., Katasev, A., Kirillov, A., Khassianov, A., Zuev, D.: Prototype of classifier for the decision support system of legal documents. *CEUR Workshop Proc.* **2543**, 328–335 (2020)
5. Alekseev, A.A., Katasev, A.S., Khassianov, A.F., Tutubalina, E.V., Zuev, D.S.: Intellectual information decision support system in the field of economic justice. *CEUR Workshop Proc.* **2260**, 17–27 (2018)
6. Yang, W., Fu, C., Yan, X., Chen, Z.: A knowledge-based system for quality analysis in model-based design. *J. Intell. Manuf.* **31**(6), 1579–1606 (2020)
7. Bounabi, M., El Moutaouakil, K., Satori, K.: Association models to select the best rules for Fuzzy inference system. *Adv. Intell. Syst. Comput.* **1076**, 349–357 (2020)
8. Katasev, A.S.: Neuro-fuzzy model of fuzzy rules formation for objects state evaluation in conditions of uncertainty. *Comput. Res. Model.* **11**(3), 477–492 (2019)
9. Anufriev, D., Petrova, I., Kravets, A., Vasiliev, S.: Big data-driven control technology for the heterarchic system (building cluster case-study). *Stud. Syst. Decis. Control* **181**, 205–222 (2019)
10. Veshneva, I., Bolshakov, A., Kulik, A.: Increasing the safety of flights with the use of mathematical model based on status functions. *Stud. Syst. Decis. Control* **199**, 608–621 (2019)
11. Perfilieva, I.G., Yarushkina, N.G., Afanasieva, T.V., Romanov, A.A.: Web-based system for enterprise performance analysis on the basis of time series data mining. *Adv. Intell. Syst. Comput.* **450**, 75–86 (2019)
12. Yarushkina, N., Filippov, A., Moshkin, V., Namestnikov, A., Guskov, G.: The social portrait building of a social network user based on semi-structured data analysis. *CEUR Workshop Proc.* **2475**, 119–129 (2019)
13. Chupin, M.M., Katasev, A.S., Akhmetvaleev, A.M., Kataseva, D.V.: Neuro-fuzzy model in supply chain management for objects state assessing. *Int. J. Supply Chain Manage.* **8**(5), 201–208 (2019)
14. Jain, D.K., Kumar, A., Sharma, V.: Tweet recommender model using adaptive neuro-fuzzy inference system. *Future Gener. Comput. Syst.* **112**, 996–1009 (2020)
15. Anikin, I.V., Makhmutova, A.Z., Gadelshin, O.E.: Symmetric encryption with key distribution based on neural networks. In: 2nd International Conference on Industrial Engineering, Applications and Manufacturing, ICIEAM 2016—Proceedings, 7911640
16. Chakraborty, A., Martin, C.F.: Optimal measurement allocation algorithms for parametric model identification of power systems. *IEEE Trans. Control Syst. Technol.* **22**(5), 1801–1812 (2014)
17. Szabo, G., Kovacs, L.: Optimization of the morpher morphology engine using knowledge base reduction techniques. *Comput. Inf.* **38**(4), 963–985 (2019)
18. Zhang, Y., Deng, A.: Redundancy reduction algorithms in rule-based knowledge bases. *Int. J. Pattern Recogn. Artif. Intell.* **30**(9), 1660011 (2016)
19. Xiey, N.: Knowledge reduction in knowledge bases and its algorithm. *J. Comput. Anal. Appl.* **20**(6), 1127–1137 (2016)
20. Katasev, A.S., Kataseva, D.V., Emaletdinova, L.Yu.: Neuro-fuzzy model of complex objects approximation with discrete output. In: 2nd International Conference on Industrial Engineering, Applications and Manufacturing, ICIEAM 2016—Proceedings, 7911653
21. Fan, Z., Chiong, R., Hu, Z., Lin, Y.: A multi-layer fuzzy model based on fuzzy-rule clustering for prediction tasks. *Neurocomputing* **410**, 114–124 (2020)
22. Tan, M., Chaudhry, A.S., Lee, C.: Establishing the taxonomy of knowledge management: an analysis of the structural components of the discipline. *Int. J. Knowl. Cult. Change Manage.* **9**(3), 177–196 (2009)
23. Dykin, V.S., Musatov, V.Yu., Varezchnikov, A.S., Bolshakov, A.A., Sysoev, V.V.: Application of genetic algorithm to configure artificial neural network for processing a vector multisensor array signal. In: International Siberian Conference on Control and Communications, SIBCON 2015—Proceedings, 7147049
24. Peddi, P.B.R.: Defuzzification method for ranking fuzzy numbers based on centroids and maximizing and minimizing set. *Decis. Sci. Lett.* **8**(4), 411–428 (2019)

25. Allahviranloo, T., Saneifard, R.: Defuzzification method for ranking fuzzy numbers based on center of gravity. *Iran. J. Fuzzy Syst.* **9**(6), 57–67 (2012)
26. Kuo, R.J., Zulvia, F.E.: Multi-objective cluster analysis using a gradient evolution algorithm. *Soft. Comput.* **24**(15), 11545–11559 (2020)
27. Song, Y., Su, Y., Yang, H.: User power consumption cluster analysis based on cloud computing and improved K-means algorithm. In: *2nd International Conference on Information Systems and Computer Aided Education*, vol. 9075633, pp. 505–510. (2019)
28. Jantschi, L., Bolboaca, S.D., Sestras, R.E.: Classical approaches of genetic algorithms and their suitability. *Asian J. Chem.* **22**(3), 2275–2284 (2010)
29. Li, C., Zhang, Q.: Analysis and simulation on dynamical models of the magnetorheological damper based on Matlab/Simulink. *J. Mech. Strength* **42**(3), 734–740 (2020)
30. Amarnath, B., Balamurugan, S.: Review on feature selection techniques and its impact for effective data classification using UCI machine learning repository dataset. *J. Eng. Sci. Technol.* **11**(11), 1639–1646 (2016)

Conversion of CGA Models to Jordan Controlled Form for Design Significantly Nonlinear Control Systems



Rudolf Neydorf, Anatoly Gaiduk, Sergey Kapustyan, and Nikita Kudinov

Abstract Tasks, opportunities and prospects of converting the significantly nonlinear mathematical models, obtained for technical objects by the method of fragmentary, multiplicative-isolating approximation, to the Jordan controlled form are investigated. The equations of nonlinear objects in the Jordan controlled form and the algorithm of the analytical solution of the designing problem of the stabilizing control law on the basis of this model are considered. It is shown that the mathematical models of many significantly nonlinear objects can be obtained in the fragmentary form, but not in the analytical one. It is also shown that the method of Cut-Glue approximation allows us to provide these models with analytical properties. This gives a possibility for the analytical design of the nonlinear control laws with the property of “analytical adaptation” on the basis of the CGA models. The effectiveness of this approach is illustrated by the example of the analytical design of the nonlinear control system for the object with the fragmentary and considerably changing static characteristic on the base of the Jordan controlled form.

Keywords Online control · Jordan controlled form · Mathematical model · Experimental data · Fragmentary model · Multiplicative isolation · Cut-glue approximation · Analytical properties · CGA model

R. Neydorf · N. Kudinov
Don State Technical University, 1 Gagarin Square, Rostov on Don 344000, Russia
e-mail: ran_pro@mail.ru

N. Kudinov
e-mail: kudinov_nikita@mail.ru

A. Gaiduk (✉)
Southern Federal University, 44 Nekrasovsky, Taganrog 347928, Russia
e-mail: gaiduk_2003@mail.ru

S. Kapustyan
Southern Scientific Centre of the Russian Academy of Sciences, 41 Chekhova, Rostov on Don 344006, Russia
e-mail: kap56@mail.ru

1 Introduction

Now automatic control systems for different objects are created with use of their mathematical models (MM). Computer technologies stimulate development of analytical methods of the automatic control systems design. These methods allow to find the control laws, in particular, for nonlinear objects if the control objects MM are set of analytical algebraic and differential equations. In these cases, the control laws are found as a solution of the allowing equations systems in which both requirements to quality of designed ACS and control object properties are considered [1–5].

The MM of complex and poorly studied nonlinear objects are created by experimental methods. They are based on comparison of the special influences given on object inputs, and the corresponding its output reactions [6–9]. The obtained experimental data are described mathematically by the approximating functions which structure and properties depend on the applied approximation method.

Very often experimental data have very difficult nonlinear character therefore the uniform approximating function does not exist. In these cases, a “piecewise” (fragmentary) approach is applied [5, 10]. Received by these methods the fragmentary MM of a nonlinear object rather precisely describes required dependence only on separate intervals of change of her argument, but in general it is not analytical. Therefore, the majority of the known analytical methods of nonlinear control systems design cannot be applied. The new Cut-Glue method of approximation (CGA) was developed for overcoming this difficulty. It carries out multiplicatively additive association of fragmentary models in uniform analytical CGA model [10]. The property of analyticity of this model allows to transform it to some forms useful to design of nonlinear control laws by analytical methods.

Many analytical methods for nonlinear control system design are developed so far: feedback linearization [9, 10], method of conversions [1, 4], control on output [11–13]; methods of the quasilinear models and the Jordan’s controlled form [5, 14], backstepping [15, 16] and pacification [17–19]; position-trajectory control [20] etc. To apply each of these methods, the MM equations of the controllable object should have special forms; therefore, the MMs should be analytical. For example, to use the backstepping the right parts of the differential equations should be differentiable, since the time derivatives should be found from some auxiliary variables. Similarly, the feedback linearization requires finding partial derivatives from the right parts of the MM differential equations, i.e. the analytical nature of the MM is necessary.

However, the analyticity property is not the only condition to apply some methods stated above. Each analytical design method requires the MM of the special form. For example, in the paper [5] the MM of the nonlinear object, received using the CGA method, will be transformed to the quasilinear model. The last one is used for analytical design of nonlinear control systems. This chapter is devoted to the research of the opportunities to represent the MM models, obtained with the CGA method in the form, which is used when nonlinear control is designed with the method of Jordan controlled form (JCF) [14].

2 Research Objective and JCF Method

The task of the chapter is to investigate the possibility to convert the fragmentary MMs found for significantly nonlinear objects using the CGA method to such forms which are provided by the algorithm of the applied method of analytical design of the nonlinear ACSs. Nonlinear stabilization systems are considered as the simplest here. To solve this problem, it is necessary to follow these steps:

- consider the algorithm of the analytical nonlinear ACS design for the nonlinear controllable objects using the JCF method;
- select the method for the fragmentary models design which is the most adequate to the solvable task;
- create the fragmentary MM of the flight altitude control link of the airship using the selected method on the basis of the identification experiment data;
- create the analytical CGA model of this channel on the basis of its fragmentary model;
- transform the analytical CGA model into the JCF one;
- analytically design a nonlinear stabilization ACS of flight altitude of the airship;
- simulate the designed nonlinear ACS to study its properties.

To define the JCF model, let's consider the following system of differential equations:

$$\begin{aligned}\dot{x}_i &= \varphi_i(x_1, x_2 \dots x_{i+1}), \quad i = \overline{1, n-1}, \\ \dot{x}_n &= \varphi_n(x) + u,\end{aligned}\tag{1}$$

where $x = [x_1 \ x_1 \ \dots \ x_n]^T$ is a column vector of the state variables; $\varphi_i(x_1, x_2 \dots x_{i+1})$ is a nonlinear function, differentiated $n - i$ time on all arguments function, $i = \overline{1, n-1}$; u is a scalar control action.

Let $\tilde{\varepsilon}$ is some positive number. If the system of Eq. (1) meets the condition

$$\left| \frac{\partial \varphi_i(x_1, \dots x_{i+1})}{\partial x_{i+1}} \right| \geq \tilde{\varepsilon} > 0, \quad i = \overline{1, n-1},\tag{2}$$

that it is a Jordan controlled form (JCF), i.e. system (1), (2) is a JCF model [14].

Usually we assume that the state variables of object (1) are measured.

If the equations of some nonlinear object are JCF model, then the problem of analytical design of the nonlinear stabilizing control law for this object has a solution. To find this law, new state variables w_i are entered, according to the expressions:

$$\begin{aligned}w_1 &= x_1, \\ w_i &= \sum_{v=1}^{i-1} \frac{\partial w_{i-1}(x_1, \dots x_{i-1})}{\partial x_v} \varphi_v(x_1, \dots x_{v+1}) + \\ &+ \lambda_{i-1} w_{i-1}(x_1, \dots x_{i-1}), \quad i = \overline{2, n},\end{aligned}\tag{3}$$

where λ_i there are some constants. Besides, the support functions are defined by the next way:

$$\begin{aligned}\gamma_1(x) &= \prod_{i=1}^{n-1} \frac{\partial \varphi_i(x_1, \dots, x_{i+1})}{\partial x_{i+1}} \neq 0, \\ \gamma_2(x) &= \sum_{i=1}^{n-1} \frac{\partial w_n(x)}{\partial x_i} \varphi_i(x_1, \dots, x_{i+1}).\end{aligned}\tag{4}$$

Expressions (1)–(4) allow to find control:

$$u(x) = -\varphi_n(x) - [\gamma_2(x) + \lambda_n w_n(x)]/\gamma_1(x).\tag{5}$$

There λ_n is also some constant. The equations of closed are written as state variables w_i :

$$\dot{w} = \Lambda w, \quad \dot{w} = \begin{bmatrix} -\lambda_1 & 1 & \cdots & 0 & 0 \\ 0 & -\lambda_2 & \ddots & 0 & 0 \\ \vdots & \vdots & \ddots & \vdots & \vdots \\ 0 & 0 & \ddots & -\lambda_{n-1} & 1 \\ 0 & 0 & \dots & 0 & -\lambda_n \end{bmatrix} w,\tag{6}$$

where $w = [w_1 \ w_1 \ \dots \ w]^T$ there is a new state vector of system (1), (5). Apparently, the matrix Λ of system (6) matches an Jordan's cell if all $\lambda_i = \lambda$. It is obvious, if $\lambda_i > 0, i = \overline{1, n}$ then system (6) is asymptotically stable as λ_i are modules of the polynomial roots $\Lambda(s) = \det(sE - \Lambda)$ which is a characteristic polynomial of this linear dynamic system.

Conversion $x \rightarrow w$ can be presented in a vector–matrix form as $x = S(x)w$, and $\det S(x) = \gamma_1(x) \neq 0$. Therefore, this conversion is reversible, i.e. if system (6) is asymptotically stable, then system (1), (4) is also stable. By choice of the value $\lambda_i, i = \overline{1, n}$, it is possible to provide the desirable nature of transient of system (1), (4).

The expressions (3)–(5) are mathematical base of the nonlinear system design with using the JCF models. For given nonlinear object (1) meeting condition (2) they allow us to find required nonlinear stabilizing control (5). However, this method demands conversion of the object equations to JCF models (1), (2). Some approaches to a solution of this problem were considered in [14]. Very often this conversion can be executed by simple redesignation of the state variables, but the object MM should be analytical. This MM property is provided using the Cut-Glue approximation method to the fragmentary models of the significantly nonlinear objects. This fact will be shown in the following section on the example of the airship.

3 Experimental Creation of Fragmentary Airship Model

The main feature of the airship is the dependence of its lifting force on the attack angle [20–22]. This effect allows us to save power resources of propulsion systems of the aircraft. The specified dependence is significantly nonlinear, therefore a priori it cannot be described analytically and usually it is found experimentally.

In our case the dependence of the lifting force $F(\alpha)$ on the attack angle α is found as the result of experimental research of the airship 3D model [23, 24]. Numerical values of the attack angle α of the airship (in angular degrees) and the corresponding values of the lifting force $F(\alpha)$ (in kN) are given in Table 1, and the corresponding graph of $F(\alpha)$ is shown in Fig. 1 by the planimetric squares.

As you can see, the static characteristic $F(\alpha)$ of the control link of the airship flight altitude h consists of three considerably different branches (Fig. 1) in the range

Table 1 Dependence $F(\alpha)$

1st fragment		2st fragment		3rd fragment	
α°	$F_1^e(\alpha)$	α°	$F_2^e(\alpha)$	α°	$F_3^e(\alpha)$
- 36	- 166.7	0.0	00.00	40.767	185.4
- 30	- 156.7	6	38.95	48	113.4
- 24	- 143.9	12	76.34	54	67.55
- 18	- 125.0	18	111.1	60	34.31
- 12	- 96,81	24	141.3	66	13.73
- 6	- 55.97	30	165.0	72	5.824
0	00.00	36	180.4		
		40.767	185.4		

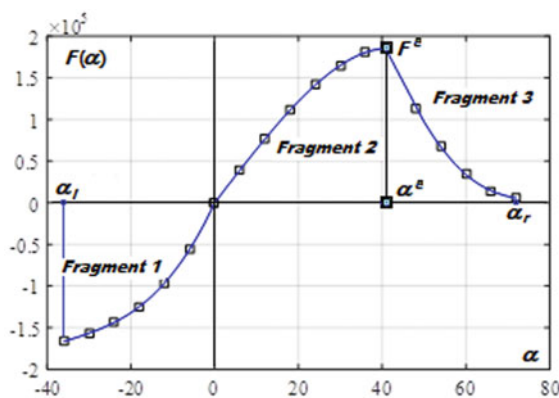


Fig. 1 Cut-Glue approximation of the airship characteristic

of attack angles $-36^\circ \leq \alpha \leq 72^\circ$. The characteristic branches corresponding to the different fragments are divided by “critical” points— $\alpha_{cr}^1 = 0^\circ$ and $\alpha_{cr}^2 = 40.767^\circ$.

If fragments 1 and 2 differ in the neighborhood point $\alpha_{cr}^1 = 0^\circ$ only in numerical value of the derivative $dF(\alpha)/d\alpha$, then fragments 2 and 3 have derivatives, opposite on the sign, in the point $\alpha_{cr}^2 = \alpha^e = 40.767^\circ$. It is caused by conditions of interaction of the incoming air of the airship body and its outside elements. The asymmetry of the lower and upper parts of the airship body affects at the point $\alpha = 0^\circ$; “stall” arises at the point $\alpha = \alpha^e = 40.767^\circ$.

As a result, the experimental static characteristic of the airship provided in Table 1 and Fig. 1 has shot points of the derivative. Therefore, it is not only nonlinear, but also not analytical in general.

The classical regression analysis allows us to find the polynomial approximation of each of three selected fragments [6–8]. Experimental values of lifting force in kN are specified in columns of Table 1. The regression equations are found for each fragment in the form of polynomials which describe this dependence (in N) rather precisely by the following expressions:

$$F(\alpha) = \begin{cases} \forall -36^\circ \leq \alpha \leq 0.0^\circ & \rightarrow F_1(\alpha); \\ \forall 0.0^\circ \leq \alpha \leq 40.767^\circ & \rightarrow F_2(\alpha); \\ \forall 40.767^\circ \leq \alpha \leq 72^\circ & \rightarrow F_3(\alpha), \end{cases} \quad (7)$$

where

$$\begin{aligned} F_1(\alpha) &= 10824.2\alpha + 259.371\alpha^2 + 2.42438\alpha^3, \\ F_2(\alpha) &= 6511.65\alpha + 0.979054\alpha^2 - 1.01816\alpha^3 - 0.00461\alpha^4, \\ F_3(\alpha) &= 43411\alpha - 1701.57\alpha^2 + 22.3751\alpha^3 - 0.0986265\alpha^4. \end{aligned} \quad (8)$$

Expressions (7), (8) are a fragmentary MM of the considered airship control channel. This model is nonlinear and not analytical.

4 Creation of Unified Analytical MM Using the CGA Method

Each polynomial $F_1(\alpha)$, $F_2(\alpha)$ and $F_3(\alpha)$ of fragmentary model (14) describes the studied dependence $F(\alpha)$ only in one of the specified ranges of change of the argument α . Expressions (7), (8) are not an analytical model in all range of the experimental research $-36^\circ \leq \alpha \leq 72^\circ$, since there are abrupt changes of the derivative $dF/d\alpha$ are at the critical values $\alpha = \alpha_{cr}^1 = 0^\circ$ and $\alpha = \alpha_{cr}^2 = 40.767^\circ$. As shown in [10], the distinctive feature of the Cut-Glue approximation method is its ability to give analytical properties to the fragmentary dependence, if the functions approximating fragments are analytical.

The analytical model of the channel “attack angle – lifting force” $F(\alpha)$ is created according to the CGA method for all interval $-36^\circ \leq \alpha \leq 72^\circ$. In this case, the fragmentary model (7), (8) includes three fragments therefore, according to the CGA model of this channel has the following form:

$$F(\alpha) = F_1(\alpha) \cdot E_1(\alpha, \alpha_{l1}, \alpha_{r1}, \varepsilon) + F_2(\alpha) \times \\ \times E_2(\alpha, \alpha_{l2}, \alpha_{r2}, \varepsilon) + F_3(\alpha) \cdot E_3(\alpha, \alpha_{l3}, \alpha_{r3}, \varepsilon). \quad (9)$$

Here the polynomials $F_1(\alpha)$, $F_2(\alpha)$, $F_3(\alpha)$ are defined still by expressions (8); according to the CGA method paradigm $E_i(\alpha, \alpha_{li}, \alpha_{ri}, \varepsilon)$ are one-dimensional multiplicative isolating functions (MIF) which are defined by the following expressions:

$$E_i(\alpha, \alpha_{li}, \alpha_{ri}, \varepsilon) = \frac{[\alpha - \alpha_{li} + R_l(z_{li})] \cdot [\alpha_{ri} - \alpha + R_r(z_{ri})]}{4 \cdot R_l(z_{li}) \cdot R_r(z_{ri})}, \quad (10)$$

where $R_l(z_{li}) = \sqrt{(\alpha - \alpha_{li})^2 + \varepsilon^2}$, $R_r(z_{ri}) = \sqrt{(\alpha_{ri} - \alpha)^2 + \varepsilon^2}$, $z_{li} = \alpha, \alpha_{li}, \varepsilon$, $z_{ri} = \alpha, \alpha_{ri}, \varepsilon$ $i = 1, 2, 3$.

In expressions (9) and (10) there are left and right borders of the i -interval of change of the variable α , respectively; ε is a setup variable of the MIF $E_i(\alpha, \alpha_{li}, \alpha_{ri}, \varepsilon)$ (10). It determines the regional accuracy of the functions allocation $F_i(\alpha)$ in their definition domain. Fragments $F_i^e(\alpha) \cdot E_i(\alpha, \alpha_{li}, \alpha_{ri}, \varepsilon)$ are isolated from each other more accurately if ε decreases [10]. Generally ε can be miscellaneous for the left and right borders, but need and expediency of it is not considered here.

In case of fragmentary dependences (7), (8) in (9), (10) these parameters have the following values: $\alpha_{l1} = -37^\circ$; $\alpha_{r1} = 0^\circ$, $\alpha_{l2} = \alpha_{r1}$; $\alpha_{r2} = 40.767^\circ$; $\alpha_{l3} = \alpha_{r2}$; $\alpha_{r3} = 73^\circ$; $\varepsilon = 0.01$. Values α_{l1} and α_{r3} are shifted on to the left and to the right, respectively, for exception of edge distortions of the joined functions $F_1(\alpha)$ and $F_3(\alpha)$.

The function $E_i(\alpha, \alpha_{li}, \alpha_{ri}, \varepsilon)$ is equal to 1 within the interval $\alpha_{li} < \alpha < \alpha_{ri}$; on the interval borders $E_i(\alpha_{li}, \alpha_{li}, \alpha_{ri}, \varepsilon) = E_i(\alpha_{ri}, \alpha_{li}, \alpha_{ri}, \varepsilon) = 0.5$, and it is equal to zero behind the borders of the interval. Distortion of edge values is mutually compensated on joint of fragments. Shift of the external limits of the argument values in the CGA model provides exception of the boundary distortions of the experimental data values [10].

The graph of the resulting analytical function $F(\alpha)$ (see Fig. 1) was made in all range of α change according to expression (9) using the MATHCAD package. Apparently, this graph is a continuous curve which has continuous derivatives, i.e. the CGA model is analytical.

The reviewed example shows that the CGA method can be applied to create analytical MMs of any nonlinear objects, on the experimental data having the fragmentary structure.

5 JCF Model of the Airship Controlled Movements

The JCF airship model should describe its movement with a constant speed towards the airflow when the height h of its flight does not influence the aero static component of the lifting force. A solid body at three-dimensional motion has 6 degrees of freedom, but in this case only 3 movements are considered: the longitudinal motion, the rotational motion in the planes “ $x-h$ ” and the vertical motion in this plane. The longitudinal motion is provided with special control system which is not considered here.

Thus, only two nonlinearly control movements of the airship should be described by the required model:

1. the vertical motion caused by the action of the aerodynamic force $F(\alpha)$ determined by expression (9). This force creates vertical acceleration of the airship:

$$\ddot{h} = (F(\alpha) - \mu \cdot v_h \cdot |v_h|) / m_D; \quad (11)$$

2. the rotational motion in the plane “ $x-h$ ” caused by the control action u_h of steering altitude of the airship. It is defined by the equation:

$$\ddot{\alpha} = M_u / J_D = L \cdot F_u / J_D = k_h \cdot u_h. \quad (12)$$

Let $x_1 = h_g - h = \Delta h$, i.e. x_1 is a deviation Δh of the present altitude h of the airship flight from given value of h_g ; $-x_2 = v_h$ is a speed of this motion, i.e. $x_2 = \dot{x}_1 = -\dot{h}$; μ is a coefficient of dynamic viscosity of the air at the vertical motion of the airship; $|\dots|$ is a designation of the module; m_D is a mass of the airship; $x_3 = \alpha$ is an attack angle, i.e. airship turning angle in the vertical plane and $x_4 = \dot{x}_3$ is an angular speed of change of this angle. In Eq. (12) J_D is an inertia moment of the airship concerning its horizontal transversal axis; $M_u = L \cdot F_u$ is a pitch moment created by the elevation rudder which is at distance L from center of mass and creates the force $F_u = k_F u_h$ where $k_h = L \cdot k_F / J_D \neq 0$.

The designations entered above and the additional ones $C_1(x_2) = -(\mu \cdot |x_2| x_2) / m_D$ and $C_2(x_3) = -F(x_3) / m_D$ allow us to write down Eqs. (11), (12) as the following system of the differential and algebraic equations:

$$\begin{aligned} \dot{x}_1 &= x_2, & \dot{x}_2 &= C_1(x_2) + C_2(x_3), \\ \dot{x}_3 &= x_4, & \dot{x}_4 &= k_h u_h, & h &= h_g - x_1. \end{aligned} \quad (13)$$

The coefficient $k_h \neq 0$, therefore we can replace the multiplication $k_h u_h$ by control action $\tilde{u} = k_h u_h$, and Eq. (13) to rewrite as follows, using obvious designations:

$$\begin{aligned} \dot{x}_1 &= x_2 = \varphi_1(x_2), & \dot{x}_2 &= C_1(x_2) + C_2(x_3) = \varphi_2(x_2, x_3), \\ \dot{x}_3 &= x_4 = \varphi_3(x_4), & \dot{x}_4 &= \tilde{u}, & h &= h_g - x_1. \end{aligned} \quad (14)$$

In Eq. (14) $\partial \varphi_1(x_2)/\partial x_2 = 1$, $\partial \varphi_2(x_2, x_3)/\partial x_3 = dC_2(x_3)/dx_3$, $\partial \varphi_3(x_4)/\partial x_4 = 1$. The derivative $dC_2(x_3)/dx_3 = -m_D^{-1}[dF(\alpha)/d\alpha] \neq 0$ at all $\alpha \in [-36^\circ \div 72^\circ]$, that follows from expressions (8) and (9). Therefore, differential Eq. (14) are the JCF model of the control channel of the airship flight altitude, and the problem of the control system design has the solution by the method stated in Sect. 2.

6 Design of the Control Law Airship Flight Height

To solve this task using the JCF model new state variable w_i are determined by expressions (3) at $n = 4$ taking into account Eqs. (14):

$$\begin{aligned} w_1 &= x_1, & w_2 &= \lambda_1 x_1 + x_2, \\ w_3 &= \lambda_1 \lambda_2 x_1 + (\lambda_1 + \lambda_2)x_2 + \varphi_2(x_2, x_3), \end{aligned} \quad (15)$$

$$\begin{aligned} w_4 &= \lambda_1 \lambda_2 \lambda_3 x_1 + (\lambda_1 \lambda_2 + \lambda_1 \lambda_3 + \lambda_2 \lambda_3)x_2 + \\ &+ \psi_1(x_2) \cdot \varphi_2(x_2, x_3) + C'_{23}(x_3)x_4, \end{aligned} \quad (16)$$

where $\lambda_i > 0$ is a constants, $i = 1, 2, 3$;

$$\begin{aligned} \psi_1(x_2) &= \lambda_1 + \lambda_2 + \lambda_3 + C'_{12}(x_2), \\ C'_{12}(x_2) &= dC_1(x_2)/dx_2, & C'_{23}(x_3) &= dC_2(x_3)/dx_3. \end{aligned} \quad (17)$$

Functions $\gamma_1(x)$ and $\gamma_2(x)$ are determined by formulas (4) also regarding Eq. (14):

$$\begin{aligned} \gamma_1(x) &= C'_{23}(x_3), \\ \gamma_2(x) &= \lambda_1 \lambda_2 \lambda_3 x_2 + [\lambda_1 \lambda_2 + \lambda_1 \lambda_3 + \lambda_2 \lambda_3 + \varphi_2(x_2, x_3)C''_{122}(x_2) \\ &+ \psi_1(x_2)C'_{12}(x_2)]\varphi_2(x_2, x_3) + [\psi_1(x_2)C'_{23}(x_3) + C''_{233}(x_3)]x_4. \end{aligned} \quad (18)$$

Here:

$$C''_{122}(x_2) = d^2C_1(x_2)/dx_2^2, \quad C''_{233}(x_3) = d^2C_2(x_3)/dx_3^2, \quad (19)$$

Comparing Eqs. (1) and (14) with $n = 4$, we conclude that $\varphi_4(x) = 0$ in this case. Therefore, control \tilde{u} from (14) is determined by formula (5) where $\varphi_4(x) = 0$ and some $\lambda_4 > 0$ taking into account expressions (16) and (18):

$$\tilde{u}(x) = -[\gamma_2(x) + \lambda_4 w_4(x)]/C'_{23}(x_3). \quad (20)$$

Derivative $C'_{23}(x_3)$ is defined regarding (8) and (9) by expression

$$C'_{23}(x_3) = -m_D^{-1}F'(\alpha) = -m_D^{-1}[F'_1(\alpha) \cdot E_1(\alpha, \alpha_{11}, \alpha_{r1}, \varepsilon) +$$

$$+ F_2'(\alpha) \cdot E_2(\alpha, \alpha_{l2}, \alpha_{r2}, \varepsilon) + F_3'(\alpha) \cdot E_3(\alpha, \alpha_{l3}, \alpha_{r3}, \varepsilon)] \Big|_{\alpha=x_3}. \quad (21)$$

where

$$\begin{aligned} F_1'(\alpha) &= 10824.2 + 518.742\alpha + 7.27314\alpha^2, \\ F_2'(\alpha) &= 6511.65 + 1.958108\alpha - 3.05448\alpha^2 - 0.01844\alpha^3, \\ F_3'(\alpha) &= 43411 - 3403.14\alpha + 67.1253\alpha^2 - 0.394506\alpha^3. \end{aligned} \quad (22)$$

Let's note that in expression (21) composed $F_i(\alpha) \cdot E_i'(\alpha, \alpha_{li}, \alpha_{ri}, \varepsilon)$ are lowered since derivatives $E_i'(\alpha, \alpha_{li}, \alpha_{ri}, \varepsilon) = dE_i(\alpha, \alpha_{li}, \alpha_{ri}, \varepsilon)/d\alpha$, $i = 1, 2, 3, 4$ have negligibly small values. The inequality $C_{23}'(x_3) \neq 0$ at all $\alpha \in [-36^\circ \div 72^\circ]$ follows from expressions (21), (22) with evidence.

The expression for function $C_{233}''(x_3) = d^2C_2(x_3)/dx_3^2 = dC_{23}'(x_3)/dx_3$ is easily defined from expressions (21), (22), therefore, here it is not brought.

The function $C_1(x_2) = -(\mu |x_2| x_2)/m_D$, therefore derivatives $C_{12}'(x_2)$ and $C_{122}''(x_2)$ are determined by expressions:

$$\begin{aligned} C_{12}'(x_2) &= -\frac{\mu}{m_D} \frac{d|x_2|x_2}{dx_2} = -\frac{2\mu}{m_D} x_2 \cdot \text{sign}(x_2), \\ C_{122}''(x_2) &= -\frac{2\mu}{m_D} \frac{d|x_2 \cdot \text{sign}(x_2)|}{dx_2} = -\frac{2\mu}{m_D} \cdot \text{sign}(x_2). \end{aligned} \quad (23)$$

In expression (12) coefficient $k_h \neq 0$, therefore, the required altitude control of the airship flight is determined according to expression (20) by the formula:

$$u_h(x) = -[\gamma_2(x) + \lambda_4 w_4(x)]/k_h C_{23}'(x_3). \quad (24)$$

So, the required control law of the airship flight altitude $h(t)$ described by Eqs. (13), is defined by expressions (16)–(18) and (21)–(24) with $\varphi_2(x_2, x_3) = C_1(x_2) + C_2(x_3)$.

The matrix $S(x)$ of transformation $w = S(x)x$ (15), (16) is defined in this case by expression

$$S(x) = \begin{bmatrix} 1 & 0 & 0 & 0 \\ \lambda_1 & 1 & 0 & 0 \\ \lambda_1 \lambda_2 & \psi_{32}(x_2) & C_{23}'(x_3) & 0 \\ \lambda_1 \lambda_2 \lambda_3 & \psi_{42}(x) & \psi_{42}(x) & C_{23}'(x_3) \end{bmatrix}. \quad (25)$$

where

$$\begin{aligned} \psi_{32}(x_2) &= \lambda_1 + \lambda_2 + C_{12}'(x_2), \quad \psi_{43}(x_2) = C_{23}'(x_3)\psi_1(x_2) + C_{233}''(x_3)x_4, \\ \psi_{42}(x_2) &= \lambda_1 \lambda_2 + \lambda_1 \lambda_3 + \lambda_2 \lambda_3 + C_{122}''(x_2)\varphi(x_2, x_3) + C_{12}'(x_2)\psi_1(x_2). \end{aligned}$$

Determinant $\det S(x) = (C_{23}'(x_3))^2$, i.e. $\det S(x) \neq 0$ at all $x_3 \in [-36^\circ \div 72^\circ]$ owing to expressions (21), (22), and transformation (15), (16) is reversible. In this case constants $\lambda_i > 0$, $i = 1, 2, 3, 4$, i.e. system (6) with $n = 4$ is asymptotically stable. Therefore, designed system (13), (24) is also asymptotically stable also, but

in the area $0 < x_i < \infty, i = 1, 2, 4$ and $x_3 \in [-36^\circ \div 72^\circ]$ due to the condition $\det S(x) \neq 0$.

If some perturbations change equilibrium state $x = 0$ of controlled airship (13), then its flight altitude $h(t)$ will be aspired to given value h_g as $t \rightarrow \infty$ under the influence of nonlinear control law (24).

7 Experimental results

The actual stability and quality of the designed system were investigated in all functioning range by simulating in GNU Octave. The values of modules of auxiliary polynomial roots $\Lambda(s)$, are chosen close to real indicators of the object dynamics and requirements to the fast response of the designed system: $\lambda_1 = 0.01; \lambda_2 = 0.03; \lambda_3 = 0.05$, and $\lambda_4 = 0.07$. These values provide the smooth nature of transients lasting no more than 600 s. Equilibrium barraging of the airship on the base altitude $h_g = 1895$ meters, is provided by the designed system at $\alpha = 0^\circ$. Perturbations were imitated by stepped variation of the attack angle α which can be caused, for example, by suddenly flown squall.

The transients shown in Fig. 2 arise in the designed system by the perturbation $\alpha_0 = -15^\circ$. The arisen deviations of the attack angle α the flight altitude h aim to the equilibrium values $\alpha = 0^\circ$ under the influence of the control u .

The transients have the similar character and at other perturbations. In Fig. 3 the graphs of the variables change α, h and control u which arise by the perturbation $\alpha_0 = 37^\circ$ are shown. Deviations fade and in this case.

The static characteristic $F(\alpha)$ has the critical points in which its character changes. Therefore, the behavior of the airship matters upon when the attack angle passes through the critical value during transient. The attack angle α aims to the equilibrium value $\alpha = 0^\circ$ on the provided graphs. At the same time, it passes through critical value $\alpha_{cr} = 0^\circ$ twice, but the transients remain smooth.

The simulation results allow us to conclude that the fast response of the perturbation suppression, and the transition to equilibrium state practically do not depend on perturbation value within available control resource. These facts are characterized

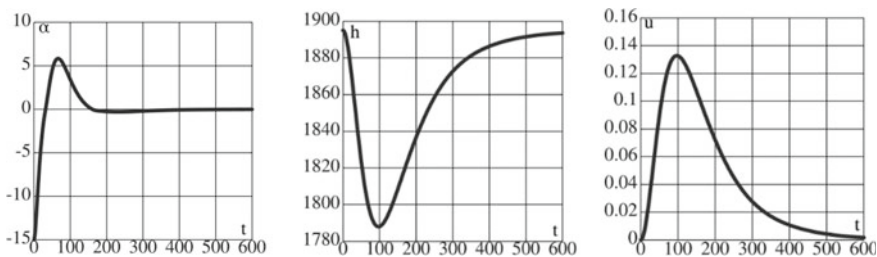


Fig. 2 The transients at perturbation $\alpha_0 = -15^\circ$

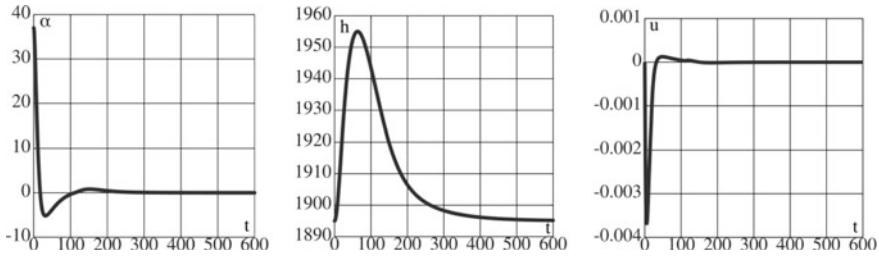


Fig. 3 The transients at perturbation $\alpha_0 = 37^\circ$

positively as the using method of the control systems design in relation to significantly nonlinear controlled objects, and efficiency of the mathematical models created by the CGA method.

8 Conclusion

The Cut-Glue approximation method allows us to create high-precision, analytical models of significantly nonlinear controlled objects on the fragmentary data of the identification experiments. It considerably expands the application range of the analytical design methods of nonlinear control systems. The design algorithm of nonlinear control systems on the basis of the Jordan controlled form is analytical. The choice of the root module values of the special stable polynomial enables us to provide the different nature of the nonlinear control systems transients.

Acknowledgements Chapter is prepared on the results of the projects creation with support of the RFBR grants No. 18-08-01178\20 in DGTU and No. 19-08-01226 in LLC “SRI MVUS”

References

1. Isidori, A.: Lectures in feedback design for multivariable systems. Advanced Textbook in Control and Signal Processing, p. 414. Springer, London (2016)
2. Moothedath, S., Chaporkar, P., Belur, M.N.: Minimum cost feedback selection for arbitrary pole placement in structured systems. *IEEE Trans. Autom. Control* **63**(11), 3881–3888 (2018)
3. Hua, C.-C., Li, K., Guan, X.-P.: Leader-following output consensus for high-order nonlinear multiagent systems. *IEEE Trans. Autom. Control* **64**(3), 1156–1161 (2019)
4. Lanzon, A., Chen, H.-J.: Feedback stability of negative imaginary systems. *IEEE Trans. Autom. Control* **62**(11), 5620–5633 (2017)
5. Gaiduk, A.R., Neydorf, R.A., Kudinov, N.V.: Application of cut-glue approximation in analytical solution of the problem of nonlinear control design. In: *Cyber-Physical Systems: Industry 4.0 Challenges*, pp. 117–132, Springer, (2020)
6. Ljung, L.: (1999) *System Identification: Theory for the User*, p. 315. PTR Prentice Hall, New Jersey (1999)

7. Chen, J., Zhang, K., Jia, B., Gao, Y.: (2018) Identification of a moving object's velocity and range with a static-moving camera system. *IEEE Trans. Autom. Control* **63**(7), 2168–2176 (2018)
8. Ahmed S., Huang B., Shah S.: Process identification from sinusoidal test data by estimating step response. In: *Preprints IFAC Symposium Systems Identification*, pp. 396–401, Saint-Malo, France (2009)
9. Kotenko, I., Parashchuk, I.: Determining the parameters of the mathematical model of the process of searching for harmful information. In: Kravets, A.G., Bolshakov, A.A., Shcherbakov, M.V. (eds.) *Cyber-Physical Systems: Industry 4.0 Challenges*, vol. 260, pp. 225–236. Springer (2019)
10. Neydorf, R., Neydorf, A., Vučinić, D.: Cut-glue approximation method for strongly nonlinear and multidimensional object dependencies modeling. *Adv. Struct. Mater.* **72**, 155–173 (2018)
11. Neydorf, R.A., Neydorf, A.R.: (2017) Modelling significant nonlinear technical systems by method of multiplicatively additive fragmentary approximation of experimental data. *Inf. Space* **1**, 47–57 (2019)
12. Yang, G., Liberzon, D.: Feedback stabilization of switched linear systems with unknown disturbances under data-rate constraints. In: *IEEE Transaction on Automatic Control*, vol. 63(7), pp. 2107–2122. C 49–60 (2018)
13. Yang, Y., Zhang, H.H., Voyles, R.M.: Rotary inverted pendulum system tracking and stability control based on input-output feedback linearization and PSO-optimization fractional order PID controller. In: *Automatic Control, Mechatronics and Industrial Engineering*, pp. 79–84. Taylor and Francis Group, London (2019)
14. Sun, H., Li, S., Yang, J., Zheng, W.: (2015) Global output regulation for strict-feedback nonlinear systems with mismatched nonvanishing disturbances. *Int. J. Robust Nonlinear Control* **25**(15), 2631–2645 (2015)
15. Gaiduk, A.R.: Control system design with disturbance rejection based on JCF of the nonlinear plant equations. *FACTA UNIVERSITATIS Ser: Autom. Control Robotics* **11**(2), 81–90 (2012)
16. Ascencio, P., Astolfi, A., Parisini, T.: (2018) Backstepping PDE design: a convex optimization approach. *IEEE Trans. Autom. Control* **63**(7), 1943–1958 (2018)
17. Furtat, I., Furtat, E., Tupichin, E.A.: Modified backstepping algorithm with disturbances compensation. *IFAC-Papers Online* **48**(11), 1056–1061 (2015)
18. Xia, M., Rahnema, A., Wang, S., Antsaklis, P.J.: Control design using passivation for stability and performance. *IEEE Trans. Control.* **63**(9), 2987–2993 (2018)
19. Wang, K., Chen, M.Z.Q., Li, C., Chen, G.: (2018) Passive controller realization of a biquadratic impedance with double poles and zeros as a seven-element series-parallel network for effective mechanical control. *IEEE Trans. Autom. Control* **63**(9), 3010–3015 (2018)
20. de Madeira, D.S., Adamy, J.: Feedback control of nonlinear systems using passivity indices. In: *Proceedings of IEEE Conference on Control Applications*, pp. 263–268. Sydney, Australia (2015)
21. Pshikhopov, V.Kh., Chernukhin, Yu.V., Medvedev, M.Yu.: Structural synthesis of dynamic regulators for position-trajectory adaptive mobile robot control system on base of mini-airships. In: *Proceedings of VII International SAUM Conference on Systems, Automatic Control and Measurements*, pp. 64–69. Vrnjачka Banja, Yugoslavia (2001)
22. Tairova, K., Shiskin, V., Kamalov, L.: Design automation of digital in-process models of parts of aircraft structures. In: Dolinina, O., Brovko, A., Pechenkin, V., Lvov, A., Zhmud, V., Kreinovich, V. (eds.) *Recent Research in Control Engineering and Decision Making: Studies in Systems, Decision and Control*, vol. 199, pp. 138–148. Springer (2019). <https://doi.org/10.1007/978-3-030-12072-6>
23. Grumondz, V.T.: Stability of the stationary motion of the airship. *Russ. Aeronaut.* **2016**(59), 29–35 (2016). <https://doi.org/10.3103/S1068799816010050>
24. Shen, S., Liu, L., Huang, B., Lin, X., Lan, W., Jin, H.: Wind speed estimation and station-keeping control for stratospheric airships with extended Kalman filter. In: *Proceedings of the 2015 Chinese Intelligent Automation Conference*, pp. 145–158. Springer-Verlag, Berlin, Heidelberg (2015). <https://doi.org/10.1007/978-3-662-46463-2>

25. Pshikhopov, V., Medvedev, M., Gaiduk, A., Neydorf, R., Fedorenko, R., Krukhmalev, V.: Mathematical model of robot on base of airship. In: Proceedings of the IEEE Conference on Decision and Control 2013, pp. 959–964. Article no. 6760006 (2013)

Searching and Selection of a Flexible Manufacturing System by Means of Frame Model



J. F. Mammadov, K. S. Abdullaev, U. H. Agaev, I. R. Aliev,
and G. G. Huseynova

Abstract In accordance with the topic of the chapter, to ensure the management and operation of archives of design work, a comparative analysis of information support algorithms was carried out, allowing you to choose flexible manufacturing systems (FMS), their standard elements, production modules, layout schemes and a set of information about their parameters or location of documents. The task was set and the model for creating algorithmic support based on the frame modeling for the effective search and selection of FMS, its production modules, and active elements by the scope of production and the purpose of each technical unit was implemented. To ensure the reliable functioning of the FMS automatic control system, an algorithm is proposed for the search for sensors based on frame slots and the values of the achievable positioning error of industrial robots and technological equipment. An algorithm for searching for sensors and controlling the active elements of the FMS production module is proposed. The software of an expert system of a frame type with fuzzy control of the shaft processing of a cylindrical gearbox for landing gear and bearings on a lathe in a flexible manufacturing module has been developed.

Keywords Frame modeling · Flexible manufacturing system · Search and selection algorithm · Frame slot · Graph diagram · Expert program

1 Introduction

The economic growth of developing countries largely depends on the introduction of industries with the most advanced technologies for automation and management into their industries. FMS is one of such innovative systems that ensure high-quality production of products for various purposes using flexible automated control technologies. The use of a sufficiently large number of enterprises in various fields of industry, interconnected corporations, and technology parks, due to the lack of their

J. F. Mammadov (✉) · K. S. Abdullaev · U. H. Agaev · I. R. Aliev · G. G. Huseynova
Sumgait State University, Sumgait, Azerbaijan
e-mail: cavan62@mail.ru

global information support, to some extent complicates the process of searching and selecting similar FMS projects, especially at the initial stages of their development.

Comparative analysis of existing methods for searching documents for FMS projects [1–3], pp. 123–210 showed that due to the versatility and complexity of such technical systems, difficulties arise with the correct selection of its technological equipment, industrial robots, manipulators, automated system of control (ASC) and their layout. In these works, the process of searching and selecting the active FMS elements is carried out by the user intuitively due to the accumulated experience in this area. For information retrieval, separate algorithms are used using production models [4], pp. 340–412 which do not provide an accurate search and selection of technical units for different applications because of the impossibility of a detailed description of the design object and the use of the number of products and, accordingly, the use of system memory. In this regard, the consideration of the creation of an algorithm for the automated search and selection of active FMS elements using the frame model, which provides step-by-step structural modeling depending on the field of application, is a scientifically relevant problem.

The purpose of this chapter is to develop algorithmic support based on the frame model for information retrieval and selection of FMS, its technical units, and the control system per the process flow diagram.

To achieve the goal, the following issues were identified:

1. Development of a frame modeling algorithm for the search and logical selection of such an FMS for its further design.
2. Creating an FMS search scheme, its equipment, layout, and ASC based on a graph—model frame diagram.
3. Construction of the layout diagram of the FMS in accordance with the results of the information search algorithm.
4. Creation of an algorithm for a reliable search for FMS sensors based on the frame model.
5. Creating a control algorithm using the example of FMS production module using logical transition conditions.
6. Software development of expert knowledge representation for the search, selection, and process control of a flexible manufacturing module for the manufacture of shafts of a cylindrical reduction tool.

2 Development of an Algorithm for the Frame Model for the Search and Selection of FMS, Its Control

To create an algorithm for searching and selecting complex technical systems, like a flexible production system, an intelligent method based on a modeling frame is used. The frame model is presented in the form of the following construction [5]:

$$f = [\langle r1, v1 \rangle, \langle r2, v2 \rangle, \dots, \langle rn, vn \rangle] \quad (1)$$

where f is the name of the frame; r_i is the name of the slot; v_i is the value of the slot. The names of other frames act as the values of the slots, which provide a link between the frames. The name of the frame (proto frame) is selected for the search keyword, which is written in the form:

$$fk_c \rightarrow \ll FMS \gg \tag{2}$$

In order to carry out a reliable search and exact selection of the design object (GPS using the example of a mechanical assembly shop), it is necessary to enter the name and value of the slot $\langle r_j, v_j \rangle$ in the form, respectively [6]:

$$\begin{aligned} f_{KC} = [& \langle r_1 \rightarrow \text{Application field, } v_{1j} \in \{v_{11}, v_{12}, \dots, v_{14}\} \rangle, \\ & \langle r_2 \rightarrow \text{Production, } v_{2i} \rightarrow \{v_{21}, v_{22}, v_{23}\} \rangle \\ & \langle r_3 \rightarrow \text{Equipment, } v_{3k} \in \{v_{31}, v_{32}, \dots, v_{37}\} \rangle \\ & \langle r_4 \rightarrow \text{FMS composes structure, } v_{4i} \in \{v_{41}, v_{42}, v_{43}\} \rangle \\ & \langle r_5 \rightarrow \text{Control system of FMS, } v_{5i} \in \{v_{51}, v_{52}, v_{53}\} \rangle, \end{aligned} \tag{3}$$

where v_{11} is the automotive industry; v_{12} —mechanical engineering; v_{13} —instrument making; v_{14} —metallurgy; v_{21} —car; v_{22} —truck; v_{23} —electric car; v_{31} —lathe; v_{32} —milled machine; v_{33} —drilling machine; v_{34} —grinding machine; v_{35} —bending machine; v_{36} —welding industrial robot; v_{37} —loading industrial robot; v_{41} —sequential layout; v_{42} —round layout; v_{43} —parallel layout; v_{51} —ASC based on SCADA TRACE MODE; v_{52} —ASC based on microprocessor control system (PLC Network); v_{53} —ASC based on PLC Simatic.

Based on the proposed proto-frame, from the established values of the r_i slots, a search engine for FMS and its modules for the manufacture of cars of various models is compiled with a further selection of the layout of flexible manufacturing modules, technological equipment, industrial robots and ASC (Fig. 1).

As can be seen from Fig. 1, the search and selection of FMS, its control system is carried out in stages, starting by entering the keywords as in expression (2). From the expression (3), the names of the slots r_i are selected which are converted into frame names (f21, f3k, f43, f51).

As can be seen from Fig. 1, the search and selection of FMS, its control system is carried out in stages, starting by entering the keywords as in expression (2). From the expression (3), the names of the slots r_i are selected which are converted into frame names (f21, f3k, f43, f51).

Based on frames f21, f3k, f43, f51, the search and selection of FMS, its control systems for the production of passenger cars, with all equipment, with their parallel layout and an automated control system based on SCADA TRACE MODE are implemented.

The frame model with the conclusions of the phased choice of the scope of production, the type of products, types of technological equipment, industrial robots, the

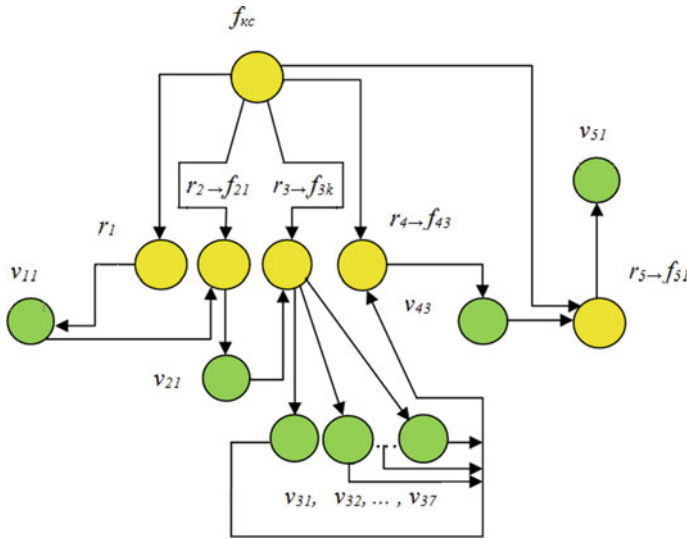


Fig. 1 The scheme of searching and selection of FMS, its equipment and ASC

layout of the FMS, and the automated control system is written in the form of logical expressions as follows:

If $\langle r_1, v_{11} \rangle$ then $\langle r_2, v_{21} \rangle$,
 where $r_2 \rightarrow f_{21} >$;
 If $\langle r_2, v_{21} \rangle$ then $\langle r_3, v_{3i} \rangle$,
 where $r_3 \rightarrow f_{3k} >$;

$\exists v_{3k} \in \{v_{31}, v_{32}, \dots, v_{37}\}$,

If $\langle r_3, v_{3k} \rangle$ then $\langle r_4, v_{43} \rangle$,
 where $r_4 \rightarrow f_{43} >$;
 If $\langle r_4, v_{43} \rangle$ then $\langle r_5, v_{51} \rangle$,
 where $r_5 \rightarrow f_{51} >$.

Based on the above algorithm, the flexible manufacturing module is formed with a parallel layout scheme, standard equipment, and an automated control system based on SCADA TRACE MODE [7] (Fig. 2).

The issue of choosing a technical solution for automated FMS control based on TRACE MODE is implemented in four stages: the choice of peripheral system hardware and network equipment; organization of the structure of information flows in the system; definition of information traffic regulations, setting up TRACE MODE servers [8]. The structure of information flows in the ASC of FMS should provide the necessary level of reliability and productivity.

The process of selecting the elements of the FMS control and monitoring system is formed based on the proposed layout diagram of the FMS production sites and their automation scheme. Based on the requirements for the accuracy of positioning of the handling facility on the working areas of the FMS production line, the total

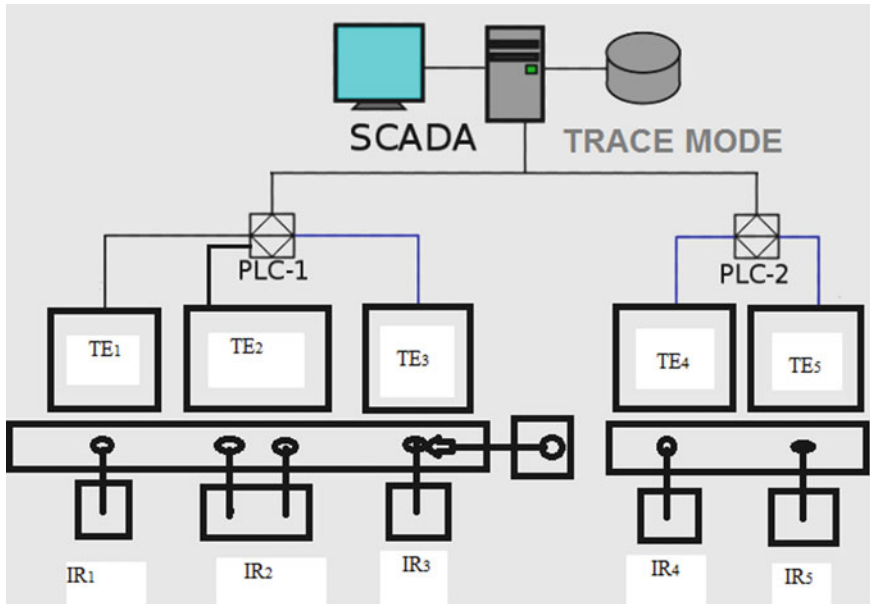


Fig. 2 Composes layout of FMS with ASC based on SCADA TRACE MODE

positioning error is determined. In this case, the error in the installation of the object in the equipment adaptation consists of two components: the error of the mismatch of the center of the shape of the part with a certain center in the equipment and the orientation error in the angle relative to some axis.

3 Creation of an Algorithm for Selecting Sensors and a Control Algorithm for FMS Manufacturing Module

The characteristics of manipulation objects in the FMS technological route influence the choice of the type and structure of sensing systems, the design of the actuator, and the functions of industrial robots in the flexible manufacturing module. The characteristics of the manipulation object determine the type of working zone of the active FMS elements.

Based on the assessment of the achievable positioning error, the sensors for the automatic control system of FMS are selected [9]:

$$\frac{S_i k_{\Delta}}{D_n} \leq \Delta_i \quad i = \overline{1, n}, \tag{4}$$

where S_i is the movement of the degree of mobility; $k_{\Delta} = 1.5, \dots, 3$ —coefficient taking into account the quality of the measuring circuits of the control system; Δ_i —positioning error of the robot, with three degrees of mobility, functioning in a flexible manufacturing module. The positioning error value is selected from the directory; D_n is the number of discrete inductive sensors measuring and angular displacement of an industrial robot.

In accordance with expressions (1) and (4), the values of the slots of the frame model for searching and selecting the elements of the FMS control system in the following form are determined:

FASC FMS = [r6 → application object, v6j ∈ {v₁₁, v₁₂, ..., v₁₄} {v6j, v6j, ..., v611}], where $j = 11$ —the quantity of technological equipment and industrial robots in FMS.

$$\langle r7 \rightarrow Si, v7j \in \{v_{11}, v_{12}, \dots, v_{14}\}, \{v7j, v7j, \dots, v711\} \rangle,$$

where for each active element's movement where the degree of mobility for each active element of FMS is taken into account.

$$\langle r8 \rightarrow k\Delta, v8j \in \{v_{11}, v_{12}, \dots, v_{14}\}, \{v8j, v8j, \dots, v811\} \rangle,$$

where the quality factor of the measuring circuits of the control system is taken into account for all active FMS elements.

$$\langle r9 \rightarrow \Delta i, v9j \in \{v_{11}, v_{12}, \dots, v_{14}\}, \{v9j, v9j, \dots, v96\} \rangle,$$

where the positioning error is taken into account for industrial robots of FMS. $j = 6$ is the number of industrial robots in the FMS.

$$\langle r10 \rightarrow \Delta n, v10j \in \{v_{11}, v_{12}, \dots, v_{14}\}, \{v10j, v10j, \dots, v106\} \rangle,$$

where the discrete number of the inductive sensor for measuring an angular displacement is taken into account for each industrial robot of FMS.

Based on the algorithm for searching for types of FMS sensors, an appropriate sensor is selected for particular equipment and industrial robot, which ensures reliable operation of the FMS automatic control system as a whole.

The database of sensors of the control system for active FMS elements is presented in the form of a recursive procedure, where the basis is the active FMS elements, their technologically functional characteristics, and parameters (Table 1) [10].

To select the parameter values from the database, a request is made from the expert system [11] for the designated symbols of the sensors in the following form:

$$|? - \text{sensor (Sfw, Parameter)}. \text{Parameter} = \Delta l.$$

Table 1 Technologically functional characteristics

#	Place of installation	Symbol	Fixing
Sensor	Gripper of IR	S_{gp_i}	The availability of workpieces
Sensor	Hand of IR	S_{u_i}	Up
Sensor	Hand of IR	S_{b_i}	Backward
Sensor	Hand of IR	S_{r_i}	Angular
Sensor	Hand of IR	S_{fw_i}	Forward
Sensor	Hand of IR	S_{d_i}	Down
Sensor	Technology equipment TE _i	S_{a_i}	The availability of workpieces
Sensor	Hand of IR	S_{up_i}	Up
Sensor	Hand of IR	S_{b_i}	Backward

where Δl is the movement of the hand of the industrial robot (IR_i) forward or backward along the X or Y axis of the three-dimensional coordinate axis; Δh is the movement of the hand of IR up or down along the Z-axis of the three-dimensional coordinate axis; $\Delta\varphi$ —the angular movement of IR hand around the Z-axis of the three-dimensional coordinate axis.

To determine other parameters from the database, similar queries are performed in the same way.

The next step in the creation of an automated FMS control system is the development of its control algorithm, which characterizes the logical conditions-transitions depending on the production cycle.

To develop a control algorithm, a step-by-step scheme of FMS automation is analyzed; initial parameters are set that characterize the displacements of the kinematic links IR and equipment, the workpiece numbers, the names of sensory and actuating elements in accordance with the functional purpose; Based on the recursive procedure [12], a control model for the manufacturing module is compiled.

The FMS control system functions as follows: information is received by the control microprocessor system about fixing the availability of the workpiece at the initial position of the automated transport system (ATS_i); sensory and executive organs IR are triggered; the technological functions of the servicing industrial robot IR begin, which ensures safe movement along with the established generalized coordinates, loading (the clamping force of the workpiece should not exceed the established norm to prevent rejection on its surface) and unloading the workpiece on equipment; Further, information on the completion of technological operations is transmitted to the control system of FMS which in turn, after processing current information from the device to determine product defects, sends a command to the executive body of the industrial robot to install the finished product or to exchange for finished products, or on a table for defective products [13].

In this case, the coordinates of the active elements are set according to previously de-fined parameters from Table 1.

As input data for the development of a control algorithm, types of sensors, actuators, and blanks are set. The generalized form of the FMS control algorithm is represented in the form of productions with true expressions and a logical consequence as follows [14]:

```
% variable names:
% AWi—workpieces
% Si—sensors with functional values
% Ai—actuators with functional purposes
% true expression (Si) logical consequence (Ai) AWi
if_then (Sl1 ∧ Sl2 ∧ ... ∧ Sln ⇒ Al1 ∧ Al2 ∧ ... ∧ Aln AWi)
if_then (S21i ∧ S22i ∧ ... ∧ S2ki ⇒ A21i ∧ A22i ∧ ... ∧ A2ni AWi)
...
...
...
If_then (Sm1i ∧ Sm2i ∧ ... ∧ Smki ⇒ Am1i ∧ Am2i ∧ ... ∧ Amni AWi).
```

The developed control algorithm for FMS sections allows you to analyze and describe the operating conditions of the actuator of each active element; synthesize control actions, programmatically automatically analyze current information about the state of the object, ensure maximum speed in management.

4 Creating Software for Searching and Selecting a FMS Project

To search and select FMS by region, types of products, types of equipment, and layout, we set the initial software window of the expert system [15]. The study of intelligent systems showed that in order to obtain reliable information about the process of automated search and the selection of complex technical systems like FMS, the development of an expert software environment based on ExpWin is required.

For this, on the basis of the frame method of modeling the search process and the selection of FMS, the key data are introduced (Fig. 3). In this case, the initial data are used according to expression (3).

When creating a new frame, at first the frame type is initially determined: “Class”, then a new slot is added by entering the name of the new slot in the “New slot name” field and activating the “Add slot”. The name of the new slot “Flexible manufacturing module (FMM)” is presented as one of the production units of FMS. It appears in the “Slots” field. The slot value, in this case, corresponds to the FMM for the production of machine tools [16].

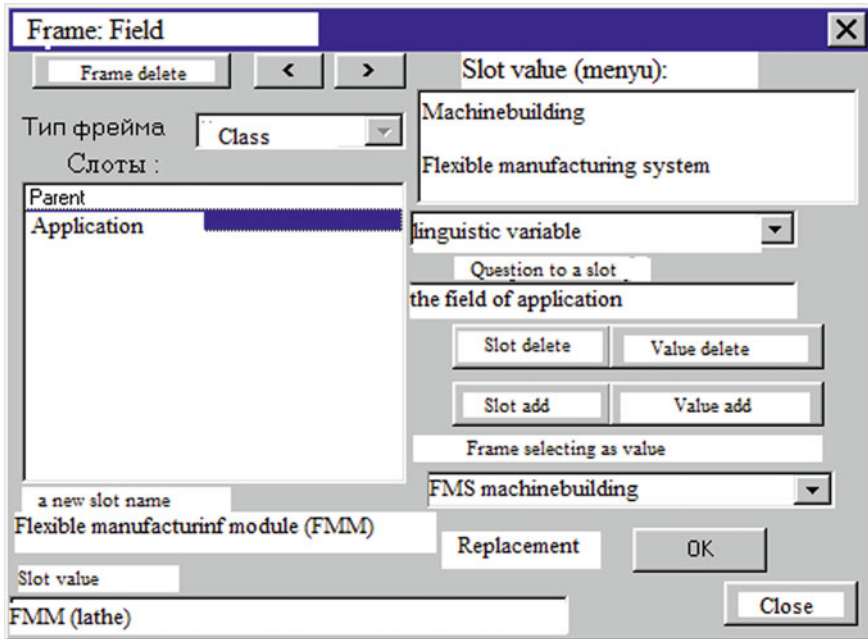


Fig. 3 Software window Frame-selection of FMS by field of application

For the selected slot, we introduce some parameters: the type of slot, the question of the slot, the slot values (Engineering, Flexible manufacturing system). This type of slot is expressed by a linguistic variable which is determined by choosing from the list “FMS in the field of mechanical engineering”. As a slot question, what is the scope? in the “Question to slot” field. The slot values are sequentially entered and added to the field “Slot values Machine-building, Flexible manufacturing system (FMM machine tool (CNC lathe)” using “Add value” [17]. To set the frame name as the slot value from the knowledge base there is a field “Select a frame as a name” After the creation of a new frame, the data is entered into the knowledge base.

When editing a frame, the ability to change the type of frame is blocked. To change any parameters of any of the slots, it is necessary to separate the name of the slot or its value, then in the corresponding field enter the new value of the parameter and make “Replace”. You can add a new slot to an existing frame. In this case, the sequence of actions does not differ from that in the case of creating a new one.

The knowledge base contains a set of frames and production rules for the automated search, selection, and design of the FMS production module. The format of the external representation of the knowledge base for the global search, selection, and design of FMS is presented in the form of the following software procedures [18]:

```
TITLE = <the name of expert system - searching and selecting FMM for FMS>
```

```

COMPANY = <enterprises name - FMM machine-building>
FRAME // frame <description of frame>
An example of knowledge bases:
TITLE = to select a method of knowledge bases presence FRAME =
purpose
a method of knowledge bases presence: ()
ENDF FRAME = Type
The solved tasks: (Computing select, searching and design of FMS)
ENDF FRAME = The field
Application [What is the field of application?]: (FMS of machine-
building)
ENDF FRAME = Quantity
Number of rules in the knowledge base (numerical): ()
Number of objects in the knowledge base (numerical): ()
ENDF FRAME = Action
Message: ()
ENDF RULE 1
> (Quantity. Number of objects in the knowledge bases; 120)
< (Quantity. Number of objects in the knowledge bases; 150)
< (Quantity. Number of objects in the knowledge bases; 90)
DO = (Type. The solved tasks; computing searching and selecting FMM
for FMS) 210
ENDR RULE 2
> (Quantity. Number of objects in the knowledge bases; 210)
> (Quantity. Number of objects in the knowledge bases; 120)
DO = (Type. The solved tasks; computing searching, selecting and
design) 210
ENDR RULE 3
= (The field. Application; machine-building FMS)
= (Type. The solved tasks; computing searching and selecting)
DO = (A method of knowledge presence; The rules-productions with
fuzzy of knowledge presence) 180
ENDR RULE 4
= (The field. Application; machine tool of FMM)
= (Type. The solved tasks; computing searching and selecting of
equipments for FMM)
DO
= (a method of knowledge presence; Frames) 210
= (A method of knowledge presence; Rules-productions with fuzzy
knowledge presence) 140
= (a method of knowledge presence; Semantically nets) 140
MS (Action. Message; a rule proven 8) ENDR.

```

The knowledge base consists of two parts: constant and variable. The variable part of the knowledge base is represented by the database and consists of facts obtained as a result of inference. The facts in the database are not permanent. Their number and value depend on the process and the results of the logical conclusion [19].

When working with this program shell, frames and production rules that were in a file with the *klb extension remain unchanged. The facts that were in the file with the *dtb extension can change in the process of inference, i.e. appear, be deleted, or change their meaning as a result of working out production rules or dialogue with the user.

The format for the external presentation of frames for automated search and selection of FMM for FMS is implemented according to the following algorithm:

```

FRAME (<frame type>) = <frame name - machine-building FMS>
PARENT: <frame name-ГПМ mechanical as-sembly >
<slot name 1 (manufactured product)> (<slot type (linguistically
variable)>) [<slot question (what is a product type)?>] {<slot
comment (*.txt)>}:
(<value 1 (spur gear)>); (<value 2 (body)>); (<value 2 (shaft)>); ...;
(<value k (helical gear)>)
<slot name 2 (equipment)> (<slot type>) [<what is an equipment?>]
{<slot comment слота (*.txt), (*.jpeg)>}:
(<value 1 (lathe)>);
(<value 2 (milling machine)>);
(<value 3 (drilling machine) >);
(<value 4 (grinding machine)>);
(<value 5 (industrial robot) >);
.....
<slot name 3 (computing system of control (ASC))> (<slot type
(linguistically variable ))>) [<slot question (what is ASC)?>]
{<slot comment (*.txt), (*.jpeg), (*.dtb)>}:
(<value 1 (PLC)>);
(<value 2 (positioning sensor)>);
(<sensor 3 (displacement sensor)>);
(<value 4 (executive mechanism)>)
ENDF

```

When forming a knowledge base for searching and selecting FMM from a flexible manufacturing system, linguistic variables are used as slots when describing fuzzy concepts. The linguistic variable allows you to set both the symbolic and numerical values of the slot of the expert program for fuzzy conclusions of the rules of the process of controlling the choice and design of FMS, its automated control system, and quality control of products [20].

A linguistic variable has one or more symbolic values. Each symbolic value is assigned a membership function, which determines the relationship between the numerical value of the linguistic variable and the reliability coefficient for a given numerical value (corresponding to the symbolic value). Each symbolic value of a linguistic variable has its membership function. The membership function is defined on a segment of the metric scale, the same for all symbolic values of the linguistic variable.

The description of linguistic variables is stored in a text file (*.lvd—Linguistic Variable Description). The first part of the file name must correspond to the names of files containing the knowledge base and database (*.klb and *.dtb). Format of the external representation of a linguistic variable [21]:

```

<Number of linguistic variables>
<Name of linguistic variable 1 (manufactured products - shaft of a
cylindrical gearbox)>
<Lower value of the border of the metric scale
below minimum shaft tolerance
Ø80-0.040.06 f7; eS=40 mkn; ei=-60 mkn for landing gear and bearing
Ø80-0.03-0.06 f7; eS=30 mkn; ei=60 mkn for landing gear and bearing
Ø80-0.020.06 f7; eS=20 mkn; ei=-60 mkn for landing gear and bearing
<Lower limit of the metric scale

```

minimum shaft tolerance

Ø80-0.02-0.04 f7; eS=20 mkn; ei=40 mkn for landing gear and bearing
 Ø80-0.01-0.04 f7; eS=10 mkn; ei=40 mkn for landing gear and bearing
 Ø80-0.000.04 f7; eS=0 mkn; ei=-40 mkn for landing gear and bearing
 <Middle limit of the metric scale

normal shaft tolerance

Ø80-0.020.06 f7; eS=20 mkn; ei=-60 mkn for landing gear and bearing
 Ø80-0.020.04 f7; eS=20 mkn; ei=-40 mkn for landing gear and bearing
 Ø80-0.03-0.06 f7; eS=30 mkn; ei=60 mkn for landing gear and bearing
 <Upper limit of the metric scale

maximal shaft tolerance

Ø800.030.00 f7; eS=30 mkn; ei=0 mkn for

normal shaft tolerance

Ø80-0.040.06 f7; eS=40 mkn; ei=-60 mkn for

normal shaft tolerance

Ø800.06-0.033 f7; eS=60 mkn; ei=33 mkn for

normal shaft tolerance

For providing a work regime on the determination of shaft by means of linguistical terms, the following expression will write as [21]:

Ø₁ → machine is not by a work status (Ø80^{-0.04}_{0.06} Ø80^{-0.03}_{-0.06} Ø80^{-0.02}_{0.06} (clearance and landing));

Ø₂ → machine is by a work status with minimal clearance and landing.

(Ø80^{-0.02}_{-0.04} Ø80^{-0.01}_{-0.04} Ø80^{-0.00}_{0.04});

Ø₃ → machine is by a work status with normal clearance and landing.

(Ø80^{-0.02}_{0.06} Ø80^{-0.02}_{0.04} Ø80^{-0.03}_{-0.06});

Ø₄ → machine is by a work status with maximal clearance and landing.

(Ø80^{0.03}_{0.00} Ø80^{-0.04}_{0.06} Ø80^{0.06}_{-0.033}).

In accordance with the created linguistic terms, a control algorithm for processing the shaft with acceptable landing gear and bearing is created:

```
IF «gear and bearing fit
below the minimum shaft tolerance;
THEN Ø1 «the machine is not in working condition
(Ø80-0.040.06 Ø80-0.03-0.06 Ø80-0.020.06
(clearance and landing))».
IF «landing gear and bearing with
minimal shaft tolerance;
THEN Ø2 «the machine is in working condition
(Ø80-0.02-0.04 Ø80-0.01-0.04 Ø80-0.000.04
(clearance and landing));
IF «gear and bearing seating with
normal shaft tolerance;
THEN Ø3 «the machine is in working condition
(Ø80-0.020.06 Ø80-0.020.04 Ø80-0.03-0.06
(clearance and landing));
IF «landing gear and bearing with
maximal shaft tolerance;
```



```
THEN Ø4 «the machine is in working condition
n(Ø800.030.00 Ø80-0.040.06 Ø800.06-0.033
(clearance and landing)).
```

5 Conclusion

This algorithm allows creating an expert software environment that provides flexible control for processing the shaft of a cylindrical gearbox for gears and bearings.

As a result of the study, the following conclusions can be drawn from the chapter:

- The developed algorithm for searching the FMS project based on the frame model allows you to accurately select its equipment, industrial robots, their layout scheme, and an automated control system from reliable sources in the global computer network, as well as suggest the final reliable layout and automation scheme.
- To ensure the reliable functioning of the FMS automatic control system and its production modules, an algorithm is proposed for searching for sensors and controlling the active elements of the FMS production module.
- To implement the proposed algorithms using frame models, the software was developed for an expert system of a frame type with fuzzy control of the shaft processing of a cylindrical gearbox for landing gear and bearings on a lathe in a flexible manufacturing module.

References

1. Kume, K.: Takao Fujiwara production flexibility of real options in daily supply chain. *Global J. Flexible Syst. Manage.* **3** (2016)
2. Spano, M.R., O'Grady, P.J., Young, R.E.: The design of flexible manufacturing systems. *Comput. Ind.* **21**(2), 185–198 (1993)
3. *Computer-Aided Design, Manufacturing, Modeling and Simulation III*. Trans Tech Publications Ltd, 2014, Zurich, Switzerland, ISBN10 3037859105, 776 p.
4. George, F.L.: *Artificial Intelligence, Strategies, and Methods for Solving Complex Problems*, p. 863. New Mexico University, Williams (2005)
5. David, C., Wynn, P.: John Clarkson process models in design and development. *Res. Eng. Design* **29**, 161–202 (2018)
6. The application of the geometric offset method to the rigid joint modelling in the differential quadrature element model updating of frame structures. *Mechanic* **50**(6) (2015). Springer. <https://doi.org/10.1007/S11012-015-0103-6>
7. *Encyclopedia of production and manufacturing management*. Kluwer Academic Publisher 2000. Springer Boston MA, Print ISBN: 978-0-7923-8630-8
8. Anzimirov, L.V.: Integrated SCADA and softlogic system TRACE MODE5, No. 1, pp. 15–22 (2002)
9. Mamedov, J.F., Aliev, R.A., Akhmedov, M.A.: Development of tools for computer-aided design of FMS control system. *Mechatron. Autom. Manage.* **9**, 27–35 (2005)

10. Mamedov, J.F., Huseynov, A.H.: Application of the intelligence and mathematical models for computing design of the flexible manufacturing module. *Appl. Comput. Math. Int. J.* **2**(1), 42–47 (2003)
11. Gero, J.S.: *Expert systems in computer-aided design* (2007). Elsevier Science Publishers B.V., North-Holland, Amsterdam, pp. 230–243
12. Trinh, M.T., Chu, D.H., Jaffar, J.: Model counting for recursively-defined strings. *Comput. Verif.* 399–418 (2018)
13. Bruccoleri, M., Sergio, N., Perrone, G.: An object-oriented approach for flexible manufacturing controls systems analysis and design using the unified modeling language. *Int. J. Flexible Manuf. Syst.* **15**(3), 195–216 (2003)
14. Hernandez-Matias, J.C., Hidalgo, A., Ríos, J.: Evaluation of techniques for manufacturing process analysis. *J. Intell. Manuf.* **17**(5), 571–583 (2006)
15. Cabrera, M.M., Edey, E.O.: Integration of rule based expert system and case based reasoning in an acute bacterial meningitis clinical decision support system. *Int. J. Comput. Sci. Inform. Sec.* **7**(2), 1947–5500 (2010)
16. Tan, C.F., Kher, V.K.: A fault diagnosis system for industry pipe manufacturing process. *Int. Rev. Mech. Eng.* **6**(6), 1292–1296 (2012)
17. Moorkherjee, R., Bhattacharyya, B.: Development of an expert system for turning and rotating tool selection in a dynamic environment. *J. Mater. Process. Technol.* **113**, 306–311 (2001)
18. Bradley, J.H., Hauser, R.D.: Framework for expert system implementation. *Expert Syst. Appl.* **8**(1), 157–167 (1995)
19. Al Ahmar, M.A.: Rule based expert system for selecting software development methodology. *J. Theoret. Appl. Inform. Technol.* 143–148 (2005)
20. Saritas, I.N., Allahverdi, N., Sert, U.: A fuzzy approach for determination of prostate cancer. *Int. J. Intell. Syst. Appl. Eng.* **1**(1), 01–07 (2013)
21. Syed-Abdullah, S., Omar, M., Mohd Idris, M.F.I.: Team achievements equality using fuzzy rule based technique. *World Appl. Sci. J.* **15**(3), 359–363 (2011)

Robust Autonomous Control of a Multiply Connected Technological Object with Input Delays



I. V. Gogol, O. A. Remizova, V. V. Syrokvashin, and A. L. Fokin

Abstract A synthesis technique of an autonomous multidimensional robust stabilization system based on a new structure for compensating cross-links of a multiply connected technological control object with delays in direct and cross-links is considered, which allows obtaining a physically realizable structure of the compensator for any relations between the values of delays indirect and reciprocal relationships and for any transfer functions inertial elements, which ensures the robustness of the system to the parametric uncertainty of the object and lag values in the presence of disturbances.

Keywords Combined control system · Robust system · System robustness · Perturbation

1 Introduction

When automating technological processes, the problem of controlling a multi-connected object with delay is important. This problem belongs to the class of completely unsolved problems of control theory, although a significant number of works have been devoted to this problem, for example [1–8]. In the presence of delays in direct and cross-connections, the qualitative indicators of the system sharply worsen, primarily indicators of stability due to the influence of cross-connections. The uncertainty of specifying model coefficients and lag values further complicates the problem. The coarseness of the system is also deteriorating, as they are related to the margin of stability.

This problem is relevant when solving the problems of stabilization of technological processes, as in the practice of automation more often consider single-circuit systems. In multiply connected systems, input delays in direct and cross-links are often present, and they also differ in the presence of significant uncertainty of the

I. V. Gogol · O. A. Remizova (✉) · V. V. Syrokvashin · A. L. Fokin
Saint-Petersburg State Institute of Technology, Saint-Petersburg, Russia
e-mail: remizova-oa@technolog.edu.ru

delay values (up to 50% of the nominal value) and parametric uncertainty of the inertial model terms.

To solve the problem of multiconnected control, an autonomous system is most often used [9, 10], the creation of which requires compensation for cross-links with delays. Indeed, it is known from the theory of multiply connected systems [9] that the dynamic quality of a multidimensional system is the higher, the more accurately it processes an input signal in each of the direct control channels for each output quantity and the less the influence of control in this channel on other output variables from due to mutual relations. From this point of view, an autonomous system is ideal in which due to the compensation of cross-links, the mutual influence of individual channels on each other is excluded. This approach is usually used in the automation of technological processes with delays.

The physical realizability of the compensator depends on the ratio of the delay values in direct and cross-links. Also, additional difficulties arise due to the parametric uncertainty of the inertial terms of the model and the values of delays. The traditional compensator circuit [9], unfortunately, does not have sufficient robustness concerning the uncertainty of the delay values. Therefore, the urgent task of the synthesis of the compensator with the necessary robustness [11].

2 Formulation of the Problem

Consider the mathematical model of the control object of the form in the form of a matrix transfer function

$$y(p) = W(p)u(p), \quad (1)$$

where $W(p)$ —is the square matrix $m \times m$ transfer functions with delays, $y(p)$, $u(p)$ —are m dimensional vectors.

In expanded form, model (1) will have the form

$$\begin{bmatrix} y_1(p) \\ y_2(p) \\ \vdots \\ y_m(p) \end{bmatrix} = \begin{bmatrix} W_{11}(p) & W_{12}(p) & \dots & W_{1m}(p) \\ W_{21}(p) & W_{22}(p) & \dots & W_{2m}(p) \\ \vdots & \vdots & \ddots & \vdots \\ W_{m1}(p) & W_{m2}(p) & \dots & W_{mm}(p) \end{bmatrix} \begin{bmatrix} u_1(p) \\ u_2(p) \\ \vdots \\ u_m(p) \end{bmatrix}, \quad (2)$$

where $W_{ij}(p) = \tilde{W}_{ij}(p) \exp(-\tau_{ij}p)$ —transfer functions linking control $u_j(p)$ with output $y_i(p)$, τ_{ij} —the value of delay in the channel (i, j) , $\underline{\tau}_{ij} \leq \tau_{ij} \leq \bar{\tau}_{ij}$, $\tilde{W}_{ij}(j\omega)$ —transfer functions defined with parametric uncertainty, e.g. $|\tilde{W}_{ij}(j\omega)| \leq |\bar{W}_{ij}(j\omega)|$, $0 \leq \omega < \infty$.

The well-known nominal model is also considered as one of the many models (1)

$$y(p) = W^0(p)u(p), \quad (3)$$

where is the matrix $W^0(p)$ is similar to $W(p)$ and consists of transfer functions $W_{ij}^0(p) = \tilde{W}_{ij}^0(p) \exp(-\tau_{ij}^0 p)$, $\underline{\tau}_{ij} \leq \tau_{ij}^0 \leq \bar{\tau}_{ij}$, $|\underline{\tilde{W}}_{ij}(j\omega)| \leq |\tilde{W}_{ij}^0(j\omega)| \leq |\overline{\tilde{W}}_{ij}(j\omega)|$.

To create an autonomous system, a compensator is usually used at the input of a nominal object so that a condition is satisfied that allows the main control channels to be independent of each other

$$W^0(p)W_K(p) = \text{diag}W^0(p) = \text{diag}\{\tilde{W}_{11}^0(p), \tilde{W}_{22}^0(p), \dots, \tilde{W}_{mm}^0(p)\}, \quad (4)$$

where $W_K(p)$ —compensator transfer matrix.

From (4) we obtain the transfer function of the compensator

$$W_K(p) = (W^0(p))^{-1} \text{diag}W^0(p). \quad (5)$$

When using compensator (5) at the input of a real object, complete compensation of mutual relations does not occur because the application of this approach is limited by accurate knowledge of the transfer functions, the presence of unstable and not minimally phase units, physical realizability (5), and the presence of delays in (3). In this way

$$W(p)W_K(p) = W(p)(W^0(p))^{-1} \text{diag}W^0(p) \neq \text{diag}W(p). \quad (6)$$

Here it is necessary to make a reservation that such compensation is always possible in the steady-state. But if there are delays, it is better to use the exact method of compensation [12], traditional for process automation, for cross-linking the object with the delay, which does not imply a reversal of the matrix $W^0(p)$. One of the possible structural schemes implementing this approach is shown in Fig. 1 for $m = 2$.

Here, to compensate for the effect of the cross-coupling $W_{ij}(p)$, $i \neq j$, a compensator $W_{Kj}(p)$ is used, at the input of which the control $\bar{u}_j(p)$ acts, and the output, which is fed to the i —input of the object $u_i(p)$. We assume that all the transfer functions of $W_{ij}(p)$, $i, j = 1, \dots, m$, but among them, at $i \neq j$ there may be not minimally phased. In this case, the transfer function of the compensator can be calculated from the condition

$$W_{Kj}(p) = (W_{ii}^0)^{-1}(p)W_{ij}^0(p). \quad (7)$$

For physical realizability (7), the following condition must be satisfied

$$\Delta\tau_{ij} = \tau_{ij}^0 - \tau_{ii}^0 \geq 0, \quad (8)$$

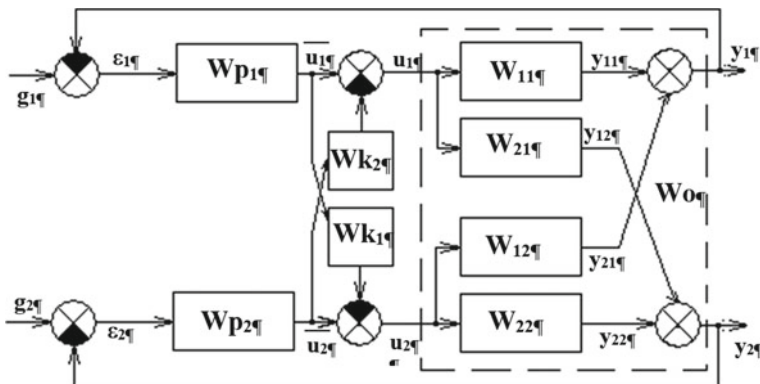


Fig. 1 Block diagram of a multidimensional system with delay, $W_{Pi}(p)$ —transfer functions of regulators, $W_{Ki}(p)$ —transfer functions of compensators

where τ_{ij}^0 —the nominal value of the delay in the cross-connection acting at the input of the link $W_{ij}(p)$, τ_{ii}^0 —delay in an element $W_{ii}(p)$.

Condition (8) means that the delay in the cross-coupling is greater than the delay in the diagonal element, at the output of which the cross-coupling acts. Besides, for the physical realizability of the transfer function (7), additional introduction of small-time constants may be necessary due to the inversion of the transfer function $\tilde{W}_{ii}^0(p)$. These factors, as well as the mismatch between the nominal and real transfer functions, determine the error of compensation. If condition (8) is not satisfied, then $\Delta\tau_{ij} = 0$, is accepted, otherwise, a predictor is needed.

Next, the task is to build a structural diagram of a multidimensional system with compensation free from these shortcomings.

3 Main Results

In an object without compensator $u_i = \bar{u}_i, i = 1, \dots, m$, therefore, in accordance with the structure in Fig. 1, at the output of i —channel of a multiply connected object, we obtain an additional signal from the effect of cross-connections

$$f_i = \sum_{\substack{j=1 \\ j \neq i}}^m W_{ij}(p)\bar{u}_j. \tag{9}$$

In an object with a compensator at the output of i —channel, taking into account (7), an additional compensating signal appears

$$z_i = W_{ii}(p) \sum_{\substack{j=1 \\ j \neq i}}^m W_{Kj}(p) \bar{u}_j(p) = W_{ii}(p) \sum_{\substack{j=1 \\ j \neq i}}^m (W_{ii}^0(p))^{-1} W_{ij}^0(p) \bar{u}_j(p). \quad (10)$$

As a result, we get the residual signal at the output

$$\phi_i = f_i - z_i = \sum_{\substack{j=1 \\ j \neq i}}^m [W_{ij}(p) - W_{ii}(p)(W_{ii}^0(p))^{-1} W_{ij}^0(p)] \cdot \bar{u}_j. \quad (11)$$

For the nominal i -channel of a multiply connected object at $W_{ii}(p) = W_{ii}^0(p)$, we get

$$\phi_i^0 = f_i - z_i = \sum_{\substack{j=1 \\ j \neq i}}^m [W_{ij}(p) - W_{ij}^0(p)] \cdot \bar{u}_j. \quad (12)$$

At the same time, real rather than nominal dynamics is considered as cross-links, since the presence of these links is the main reason for the deterioration of the quality of a multidimensional system.

This is a traditional result. Now, to obtain an alternative compensating signal, we use the results of [13, 14]. Consider the structural diagram in Fig. 2. Here, the internal model is used to construct an estimate of the response at the output of system \hat{f}_i , caused by the action of an additional signal from the influence of cross-links f_i at the output. Since the nominal transfer function of the i -channel of the object was used for estimation, the resulting estimate is generalized, since it additionally contains information about the parametric uncertainty of the transfer function of the real object in this channel.

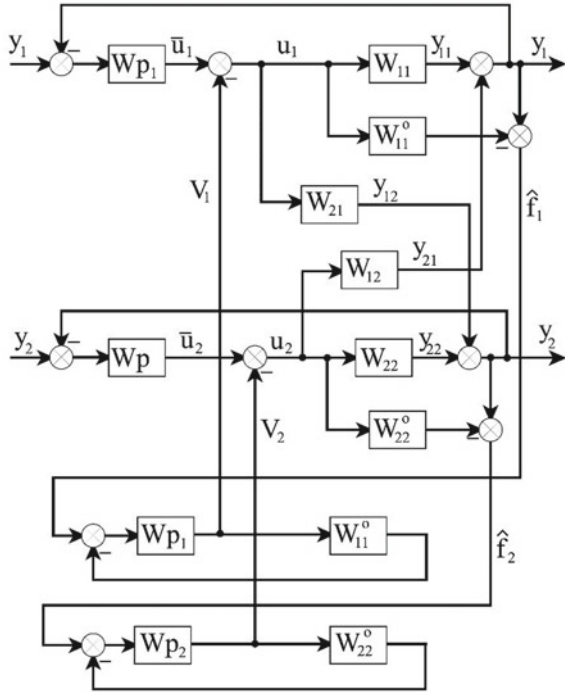
The variable \hat{f}_i enters the input of the servo system, which structurally coincides with the single-circuit system of i -channel, but instead of the transfer function $W_{ii}(p)$ the nominal transfer function $W_{ii}^0(p)$ is used here. If ideally we assume that the output of the servo system matches exactly \hat{f}_i and $W_{ii}^0(p) = W_{ii}(p)$, then it is accurate a model by which one can trace how a disturbance acts at any point in the structural diagram of a single-loop system. The variable H obtained in this way is used in the system to compensate for f_i .

An additional signal at the output of the i -channel of a multiply connected object from the influence of cross-links coincides with (9). We get a compensating signal. In accordance with the structural diagram, we obtain

$$\hat{f}_i = W_{ii}(p)u_i + f_i - W_{ii}^0(p)u_i = \Delta W_{ii}(p)u_i + f_i, \quad (13)$$

where $\Delta W_{ii}(p) = W_{ii}(p) - W_{ii}^0(p)$.

Fig. 2 Alternative compensation scheme



$$V_i = \frac{W_{Pi}(p)}{1 + W_{Pi}(p)W_{ii}^0(p)} \hat{f}_i,$$

$$u_i = \bar{u}_i - V_i = \bar{u}_i - \frac{W_{Pi}(p)}{1 + W_{Pi}(p)W_{ii}^0(p)} (\Delta W_{ii}(p)u_i + f_i).$$

From here provided $W_{ii}(p) = W_{ii}^0(p) + \Delta W_{ii}(p)$

$$u_i = \frac{1 + W_{Pi}(p)W_{ii}^0(p)}{1 + W_{Pi}(p)W_{ii}(p)} (\bar{u}_i + f_i).$$

The compensating signal will be

$$\begin{aligned} z_i &= W_{ii}(p)V_i = \frac{W_{Pi}(p)W_{ii}(p)}{1 + W_{Pi}(p)W_{ii}^0(p)} \hat{f}_i = \frac{W_{Pi}(p)W_{ii}(p)}{1 + W_{Pi}(p)W_{ii}^0(p)} (\Delta W_{ii}(p)u_i + f_i) \\ &= \frac{W_{Pi}(p)W_{ii}(p)}{1 + W_{Pi}(p)W_{ii}^0(p)} \left\{ \Delta W_{ii}(p) \frac{1 + W_{Pi}(p)W_{ii}^0(p)}{1 + W_{Pi}(p)W_{ii}(p)} (\bar{u}_i + f_i) + f_i \right\} \\ &= \frac{1 + W_{Pi}(p)W_{ii}^0(p)}{1 + W_{Pi}(p)W_{ii}(p)} \cdot \frac{W_{Pi}(p)W_{ii}(p)\Delta W_{ii}(p)}{1 + W_{Pi}(p)W_{ii}^0(p)} (\bar{u}_i + f_i) + \frac{W_{Pi}(p)W_{ii}(p)}{1 + W_{Pi}(p)W_{ii}^0(p)} f_i. \end{aligned} \tag{14}$$

The residual signal at the output will be

$$\begin{aligned}
 \phi_i &= f_i - z_i = \left\{ 1 - \frac{W_{Pi}(p)W_{ii}(p)}{1 + W_{Pi}(p)W_{ii}^0(p)} \right\} f_i \\
 &\quad - \frac{1 + W_{Pi}(p)W_{ii}^0(p)}{1 + W_{Pi}(p)W_{ii}(p)} \cdot \frac{W_{Pi}(p)W_{ii}(p)\Delta W_{ii}(p)}{1 + W_{Pi}(p)W_{ii}^0(p)} (\bar{u}_i + f_i) \\
 &= - \frac{W_{Pi}(p)\Delta W_{ii}(p)}{1 + W_{Pi}(p)W_{ii}^0(p)} \left\{ 1 + \frac{1 + W_{Pi}(p)W_{ii}^0(p)}{1 + W_{Pi}(p)W_{ii}(p)} W_{ii}(p) \right\} f_i \\
 &\quad - \frac{1 + W_{Pi}(p)W_{ii}^0(p)}{1 + W_{Pi}(p)W_{ii}(p)} \cdot \frac{W_{Pi}(p)W_{ii}(p)\Delta W_{ii}(p)}{1 + W_{Pi}(p)W_{ii}^0(p)} \bar{u}_i. \tag{15}
 \end{aligned}$$

For the nominal i -channel of a multiply connected object with $W_{ii}(p) = W_{ii}^0(p)$, we get

$$\phi^0 = 0, \tag{16}$$

This shows that the quality of compensation, in this case, is better than in (12). Also for the nominal i -channel, the compensating signal (14) will be

$$z_i^0 = \frac{W_{Pi}(p)W_{ii}^0(p)}{1 + W_{Pi}(p)W_{ii}^0(p)} f_i. \tag{17}$$

Statement Within the framework of the proposed structure (Fig. 2), the nominal compensation system f_i is described by the transfer function, which coincides with the transfer function of the closed nominal system of the main i -circuit.

Consequence The compensation system and the single-circuit system of the i -circuit have the same robustness, which is numerically evaluated using the H^∞ -norm of the sensitivity function [15]. The robustness of the system is understood as the low sensitivity of the output quantities to the parametric uncertainty of the model of a multidimensional object.

Thus, the problem of system coarseness is solved simultaneously at the stage of controller synthesis for a single-circuit system with autonomous control, as well as for the proposed compensation method. Robust control algorithms for single-loop systems in the class of PID laws were considered in [16, 17]. Algorithms obtained on the basis of qualitative exponential stability can also be used here [18, 19].

For the traditional compensation scheme for the nominal i -channel, instead of (17), based on (9), (10), we obtain

$$z_i = W_{ii}^0(p) \sum_{\substack{j=1 \\ j \neq i}}^m (W_{ii}^0(p))^{-1} W_{ij}^0(p) \bar{u}_j(p)$$

$$= \sum_{\substack{j=1 \\ j \neq i}}^m W_{ij}^0(p) \bar{u}_j(p) = f_i - \sum_{\substack{j=1 \\ j \neq i}}^m \Delta W_{ij}(p) \bar{u}_j(p), \quad (18)$$

where $\Delta W_{ij}(p) = W_{ij}(p) - W_{ij}^0(p)$.

From (18) it is seen that the compensating signal directly depends on the uncertainty of the assignment of the transfer functions of the cross-links. This can reduce the robustness of the system.

4 Example 1

Consider, as an example, the transfer matrix of a distillation column [20]

$$W_0(p) = \begin{bmatrix} \frac{0.66 \exp(-2.6p)}{6.7p+1} & -\frac{0.61 \exp(-3.5p)}{8.64p+1} & -\frac{0.0049 \exp(-p)}{9.06p+1} \\ \frac{1.11 \exp(-6.5p)}{3.25p+1} & -\frac{2.36 \exp(-3p)}{5p+1} & -\frac{0.01 \exp(-1.2p)}{7.09p+1} \\ -\frac{34.68 \exp(-9.2p)}{8.15p+1} & \frac{46.2 \exp(-9.4p)}{10.9p+1} & \frac{0.87(11.61p+1) \exp(-p)}{(3.89p+1)(18.8p+1)} \end{bmatrix}. \quad (19)$$

The transfer functions of the regulators by deviation [16, 17] have the following form

$$\begin{aligned} W_{P11}(p) &= \frac{0.343}{2.6 \cdot 0.66} \frac{6.7p+1}{p}, & W_{P22}(p) &= -\frac{0.343}{3 \cdot 2.36} \frac{5p+1}{p} : \text{PI laws} \\ W_{P33}(p) &= \frac{0.343}{0.87} \frac{(3.89p+1)(18.8p+1)}{p(11.61p+1)} : \text{PID law} \end{aligned} \quad (20)$$

First, consider the traditional compensation scheme (Fig. 1). Compensating constraints for which condition (8) is satisfied in accordance with Formula (7) in the first-order Padé approximation will be

$$\begin{aligned} W_{K12}(p) &= \frac{0.61}{0.66} \frac{6.7p+1}{8.64p+1} \exp(-0.9p) \approx \frac{0.61}{0.66} \cdot \frac{6.7p+1}{8.64p+1} \cdot \frac{1-0.45p}{1+0.45p}, \\ W_{K21}(p) &= \frac{1.11}{2.36} \frac{5p+1}{3.25p+1} \exp(-3.5p) \approx \frac{1.11}{2.36} \cdot \frac{5p+1}{3.25p+1} \cdot \frac{1-1.75p}{1+1.75p}. \end{aligned}$$

At the initial moment of time ($t = 0$, $p = \infty$), when approximating the delay unit using the Padé formula, a nonzero signal value is obtained. With large values of the coefficients in cross-linking, this creates computational problems. In this case, for approximation, it is better to use the link, which at $t = 0$ has a transmission coefficient equal to zero

$$\exp(-\tau p) = \frac{1}{\exp(\tau p)} = \frac{1}{[\exp(\tau p/k)]^k} \approx \frac{1}{\left[1 + \frac{\tau p/k}{1!} + \dots + \frac{(\tau p/k)^l}{l!}\right]^k}. \tag{21}$$

Therefore, in accordance with Formula (21) for $l = 3$ and $k = 2$, we obtain

$$W_{K31}(p) = \frac{34.68}{0.87} \cdot \frac{3.89p + 1}{8.15p + 1} \cdot \frac{18.8p + 1}{11.61p + 1} \cdot \frac{1}{(11.487p^3 + 8.4p^2 + 4.1p + 1)^2},$$

$$W_{K32}(p) = -\frac{46.2}{0.87} \cdot \frac{3.89p + 1}{10.9p + 1} \cdot \frac{18.8p + 1}{11.61p + 1} \cdot \frac{1}{(12.348p^3 + 8.82p^2 + 4.2p + 1)^2}.$$

For cross bonds $W_{13}(p)$ and $W_{23}(p)$ condition (8) is not satisfied, and therefore there is no delay link in the compensating bonds. Accordingly, we obtain

$$W_{K23}(p) = -\frac{0.01}{2.36} \frac{5p + 1}{7.09p + 1}, \quad W_{K13}(p) = \frac{0.0049}{0.66} \frac{6.7p + 1}{9.06p + 1}.$$

An alternative compensation scheme is shown in Fig. 2, it is completely physically feasible unlike the traditional ones and does not require special construction of the transfer functions of the compensators.

Figure 3 shows the transition characteristic for the output of the first channel $y_1(t)$ for a multiply connected system with a traditional compensator (Fig. 1), and in Fig. 4 for the proposed system (Fig. 2)

It can be seen that the qualitative characteristics of the traditional system are better in speed and oscillation, the same applies to the development of perturbations at the

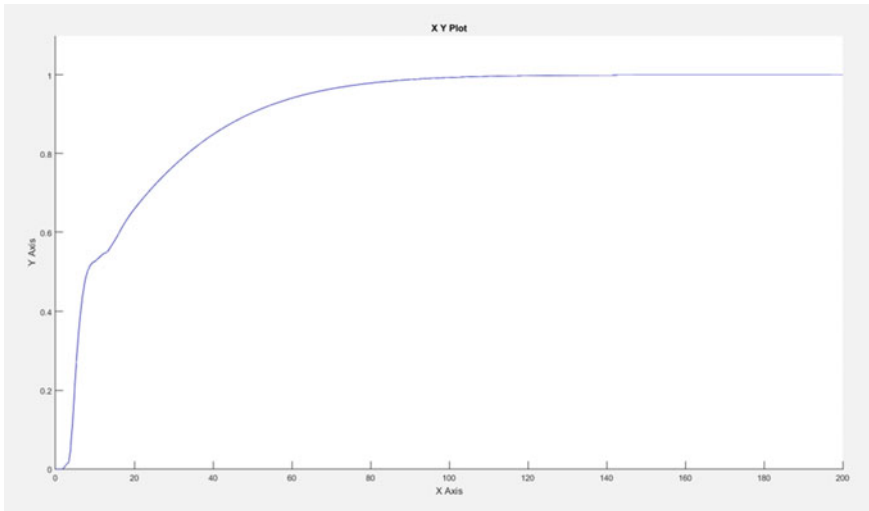


Fig. 3 Transient response $y_1(t)$ of a traditional system

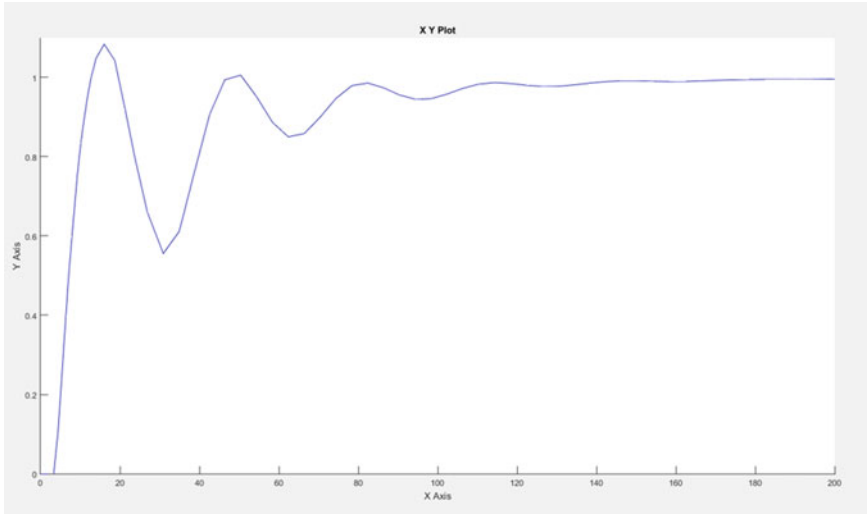


Fig. 4 Transient response $y_1(t)$ of the proposed system

input and output of the object, but the proposed system has a significantly greater coarseness (about two times) in relation to delay variations.

5 Example 2

Let us consider a distillation column [20] as a control object for separating methanol from the water with a nominal transfer function of the form

$$\begin{bmatrix} y_1 \\ y_2 \end{bmatrix} = \begin{bmatrix} -\frac{0.1153(10p+1)\exp(-0.1p)}{(4p+1)^3} & \frac{0.2429\exp(-2p)}{(33p+1)^2} \\ -\frac{0.0887\exp(-12.6p)}{(43p+1)(22p+1)} & \frac{0.2429\exp(-13.4p)}{(53.1p+1)} \end{bmatrix} \begin{bmatrix} u_1 \\ u_2 \end{bmatrix}. \quad (22)$$

For the transfer function of the first main channel, an approximation of the following form is possible

$$W_{11}(p) = -\frac{0.1153(10p+1)\exp(-0.1p)}{(4p+1)^3} \approx -\frac{0.1153(10p+1)\exp(-1.6p)}{(6.5p+1)(4p+1)}. \quad (23)$$

Accordingly, one can write two transfer functions for the robust controller in the first channel [16, 17] of the second (PID law) and third-order

$$W_{P1}(p) = -\frac{0.343}{0.1153 * 1.6} \frac{(4p+1)(6.5p+1)}{p(10p+1)}, \quad (24)$$

$$W_{P1}(p) = -\frac{0.343}{0.1153 * 0.1} \frac{(4p + 1)^3}{p(10p + 1)(0.1p + 1)}. \tag{25}$$

The robust controller in the second channel has the transfer function of the PI control law

$$W_{P2}(p) = \frac{0.343}{0.2429 \cdot 13.4} \frac{53.1p + 1}{p}. \tag{26}$$

First, consider the compensation scheme shown in Fig. 1. Here, the transfer functions (25), (26) are considered as regulators. The transfer functions of the compensators will be

$$\begin{aligned} W_{K1}(p) &= \frac{0.2429}{0.1153} \frac{(4p + 1)(6.5p + 1)}{(10p + 1)(33p + 1)^2} \exp(-0.4p) \\ &\approx \frac{0.2429}{0.1153} \frac{(4p + 1)(6.5p + 1)(1 - 0.2p)}{(10p + 1)(33p + 1)^2(1 + 0.2p)}, \\ W_{K2}(p) &= -\frac{0.087}{0.2429} \frac{53.1p + 1}{(43p + 1)(22p + 1)}. \end{aligned} \tag{27}$$

The transfer function $W_{K2}(p)$ does not contain delay since in (8) $\Delta\tau_{21} = \tau_{21} - \tau_{22} = 12.6 - 13.4 = -0.8$, it can be implemented only approximately without delay. The transient response of the 2nd channel is shown in Fig. 5

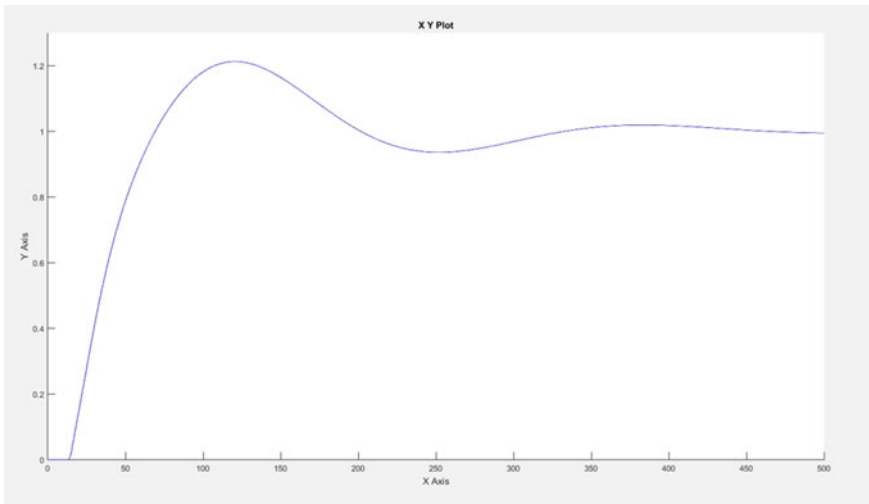


Fig. 5 Transient response on channel 2 in a traditional system

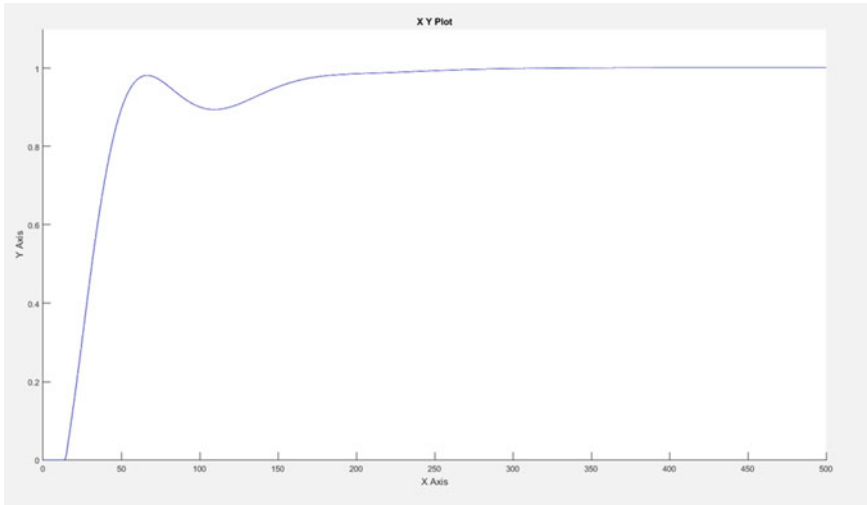


Fig. 6 Transient response on channel 2 in the proposed system

Note that if we use the reduced transfer function (24) as the regulator of the first channel, then the system is close to the loss of stability. This indicates high sensitivity to structural uncertainty.

As an alternative, the structural diagram in Fig. 6 is considered. Here, the reduced transfer function (24) was used as the regulator of the first channel.

It is seen that the quality of control has improved. The same applies to the problem of parrying disturbances at the input and output of an object. In addition, coarseness somewhat increases with respect to parametric uncertainty and decreases with respect to a change in the delay value. Thus, we obtained a result directly opposite to example 1—an improvement in the quality of regulation with approximately the same roughness with respect to parametric uncertainty and a decrease in x v /roughness with respect to delay. Therefore, the final choice of the system is determined by comparison in the simulation.

6 Conclusion

The chapter proposes a new scheme for compensating for the cross-connections of a multiply connected control object with control delays, which is no alternative to the traditional one and differs from it in that:

- it is always physically feasible,
- in some cases, allows you to get the best quality indicators of the transition process,
- provides rudeness concerning changes in the values of delays and coefficients of the model of the object.

References

1. Luyben, W.L.: Simple method for tuning SISO controllers in multivariable systems. *Ind. Eng. Chem. Process Des. Dev.* **25**, 654–660 (1986)
2. Shen, S.H., Yu, C.C.: Use of relay-feedback test for automatic tuning of multivariable systems. *AIChE J.* **40**(4), 627–646 (1994)
3. Bao, J., Forbes, J.F., McLellan, P.J.: Robust multiloop PID controller design: a successive semidefinite programming approach. *Ind. Eng. Chem. Res.* **38**, 3407–3419 (1999)
4. Vlachos, C., Williams, D., Gomm, J.B.: Genetic approach to decentralised PI controller tuning for multivariable processes. *IEE Proc. Control Theory Appl.* **146**(58), 58–64 (1999)
5. Hovd, M., Skogestad, S.: Improved independent design of robust decentralized controllers. *J. Process Control* **3**(4) (1993)
6. Xiong, Q., Cai, W.-J.: Effective transfer function method for decentralized control system design of multi-input multi-output processes. *J. Process Control* **16**, 773–784 (2006)
7. Xiong, Q., Cai, W.-J., He, M.-J.: Equivalent transfer function method for PI/PID controller design of MIMO processes. *J. Process Control* **17**, 665–673 (2007)
8. Kariwala, V.: Fundamental limitation on achievable decentralized performance. *Automatica* **43**, 1849–1854 (2007)
9. Pupkov, K.A., Egupov, N.D.: *Metody klassicheskoy i sovremennoy teorii avtomaticheskogo upravleniya: Uchebnik v 5 tomah. Tom 3. Sintez reguljatorov sistem avtomaticheskogo upravleniya* [Methods of classical and modern theory of automatic control: Textbook in 5 volumes. vol. 3. Synthesis of regulators of automatic control systems]. M.: BMSTU, pp. 616. (2004) (in Russ.)
10. Gajduk, A.R.: *Teorija i metody analiticheskogo sinteza sistem avtomaticheskogo upravlenija (polinomial'nyj podhod)* [Theory and methods of analytical synthesis of automatic control systems (polynomial approach)]. In: Fizmatlit, M. (ed.) pp. 300. (2012) (in Russ.)
11. Cykunov, A.M.: *Robastnoe upravlenie s kompensaciej vozmushhenij* [Robust control with disturbance compensation]. In: Fizmatlit, M. (ed.) pp. 300. (2012) (in Russ.)
12. Dudnikov, E.G.: *Avtomaticheskoe upravlenie v himicheskoy promyshlennosti* [Automatic control in the chemical industry]. In: Himija, M. (ed.) pp. 368. (1987) (in Russ.)
13. Remizova, O.A., Fokin, A.L.: *Robastnoe upravlenie ustojchivym tehničeskim obektom pri nalichii zapazdyvanija po upravleniju s kompensaciej vozmushhenij* [Robust control of a stable technical object in the presence of a control delay with compensation of disturbances]. *Izv. vuzov. Priborostroenie* **59**(12), 10–17 (2016). (in Russ.)
14. Gogol, I.V., Remizova, O.A., Syrokvashin, V.V., Fokin, A.L.: *Upravlenie tehničeskimi sistemami s zapazdyvaniem pri pomoshhi tipovyh reguljatorov s kompensaciej vozmushhenij* [Control of technical systems with delay using standard controllers with disturbance compensation]. *Izv. vuzov. Priborostroenie* **60**(9), 882–890 (2017). (in Russ.)
15. Egupov, N.D.: *Metody robastnogo, nejro-nechetkogo i adaptivnogo upravlenija* [Methods of robust, neuro-fuzzy and adaptive control]. M.: BMSTU, pp. 744. (2002) (in Russ.)
16. Remizova, O.A., Syrokvashin, V.V., Fokin, A.L.: *Sintez robastnyh sistem upravlenija s tipovymi reguljatorami* [Synthesis of robust control systems with standard controllers]. *Izv. vuzov. Priborostroenie* **58**(12), 12–18 (2015). (in Russ.)
17. Gogol, I.V., Remizova, O.A., Syrokvashin, V. V., Fokin, A. L.: *Sintez robastnyh reguljatorov dlja upravlenija tehnologičeskimi processami v klasse tradicijonnyh zakonov regulirovanija* [Synthesis of robust controllers for control of technological processes in the class of traditional control laws]. *Izv. Spbsti(TU)* **44**, 98–105 (2018)(in Russ.)
18. Grigorev, V.V.: *Kachestvennaja jeksponencial'naja ustojchivost nepreryvnyh i diskretnyh dinamicheskikh sistem* [Qualitative exponential stability of continuous and discrete dynamical systems]. *Izv. vuzov. Priborostroenie* **43**(1), 18–23 (2000). (in Russ.)
19. Grigorev, V.V., Bojkov, V.I., Bystrov, S.V., Rjabov, A.I., Mansurova, O.K.: *Issledovanie processov pozitivnyh sistem na osnove kachestvennoj jeksponencial'noj ustojchivosti* [Research of processes of positive systems on the basis of qualitative exponential stability]. *Izv. vuzov. Priborostroenie* **43**(4), 15–20 (2013). (in Russ.)

20. Sporjagin, K.V.: Matematicheskoe modelirovanie, razrabotka metodov i programmogo kompleksa dlja nastrojki parametrov tipovyh zakonov regulirovanija dinamičeskikh sistem s zapazdyvanijem [Mathematical modeling, development of methods and a software package for setting the parameters of typical control laws of dynamic systems with delay]. SPb, GOUVPO « Sankt-Peterburgskij gosudarstvennyj politehničeskij universitet » , pp. 237. (2010) (in Russ.)

Bee-Inspired Algorithm for Groups of Cyber-Physical Robotic Cleaners with Swarm Intelligence



Oleg Yu. Maryasin 

Abstract This chapter dwells upon the control of groups of autonomous cyber-physical robotic cleaners designed for wet cleaning of rooms in large public or commercial buildings. It presents various strategies to control the movements of a robot group or those of robots within a group. It also discusses the factors affecting the intragroup behavior of robots. The author offers a method for building robot formations, which is based on using the wet trails of the leading robot. To control groups of cyber-physical robotic cleaners, the chapter proposes an algorithm that combines a global strategy based on the bees search algorithm with elements of swarm intelligence, and a local formation-building method for orientation to the leading robot and its neighbors. The author has simulated some robot group control and formation tasks in NetLogo. The results can be used to solve other similar problems, such as harvesting, deactivating the area from radioactive substances, disinfecting the area from viruses and others.

Keywords Cleaning robots · Robot groups · Swarm robotics · Bees algorithm · NetLogo

1 Introduction

Autonomous household robotic vacuum cleaners have long been used to clean small rooms up to a few dozens of square meters. Unlike there, robotic cleaners are still a rare sight in larger commercial or public buildings: supermarkets, shopping malls, entertainment centers, sports venues, airports, etc. Operating in such a building may involve cleaning large spaces of complex shapes with multiple various obstacles. This is why such cleaning was, until recently, only performed by the human workforce using professional cleaning machines and floor cleaners equipped with large batteries for longer use as well as with capacious containers to collect garbage or to carry the detergents.

O. Yu. Maryasin (✉)
Yaroslavl State Technical University, Yaroslavl 150023, Russia
e-mail: maryasin2003@list.ru

© The Author(s), under exclusive license to Springer Nature Switzerland AG 2021
A. G. Kravets et al. (eds.), *Cyber-Physical Systems: Modelling and Intelligent Control*, Studies in Systems, Decision and Control 338,
https://doi.org/10.1007/978-3-030-66077-2_13

This has begun to change rapidly in recent years. Such equipment is yet to be produced on a large scale by major manufacturers; however, startups like Avidbots [1] have already begun to assemble autonomous robotic cleaners for large rooms. Robots.nu [2] shows promising models of cleaning robots. The industry is led by LG, TASKI Intellibot, and SoftBank Group Corp. Walmart plans to use robotic cleaning machines in its department stores [3]. That effort will involve Brain Corp., the company behind Brain OS, which is an artificial intelligence platform to control the machines. The platform will enable the robots to avoid collision with shelves and buyers while also improving their performance with every passing day. Technavio's analysts predict the professional cleaning robots market to grow by 17.35% per annum on average [4]. The global robotic cleaner market has the potential to grow by US dollars 3.70 billion during 2020–2024, and the market's growth momentum will accelerate throughout the forecast period.

Using groups of cleaning robots will enable even better performance time- and functionality-wise. A group can work in parallel to clean faster and over a greater area compared to a single robot. Since supermarkets today mostly use parallel shelving alignment, a group of robots could easily split to clean the aisles and then gather back together.

Intelligent mobile cleaning robots can be considered as mobile cyber-physical devices and a group of cleaning robots as a robotic cyber-physical system (RCPS). Such systems are based on the integration of robotics technology, wireless sensor networks and multi-agent systems [5]. RCPS is now actively developed and implemented in industry, energy, warehouse logistics, healthcare and other areas. In [5], RCPS was presented for managing a group of robots for monitoring overhead high-voltage transmission lines, and in [6] for managing warehouse operations.

Group control of autonomous mobile robots for a variety of applications has been covered in many papers [7, 8]. Of all algorithms used to that end, the most popular options as of recent years are bio-inspired algorithms (bees, ant colony, termite-hill, etc.) as well as swarm intelligence algorithms [9, 10]. The key advantages of swarm robotics are [11]:

- **Robustness.** A swarm remains functional even if it loses some of its members;
- **Flexibility.** A swarm can easily adapt to changes in the task or the roles of some of its members;
- **Scalability.** A swarm may consist of any number of robots, from a few to a few thousand.

This chapter discusses the control of groups of cyber-physical robotic cleaners for wet cleaning of larger commercial or public buildings: supermarkets, shopping malls, entertainment centers, sports venues, airports, etc. This is an area coverage task. Other area coverage tasks include harvesting, areal surveying, demining, etc. Paper [12] describes using a group of mobile robots to clean a supermarket, while paper [13] applies this approach to cleaning a large office building. However, these papers only consider using a single group of robots to clean the entire area, and the core problem of research, in either case, was to split the robots across the area. A good example of how a swarm intelligence algorithm handles an area coverage task

is presented in [14], a paper that proposes a swarm algorithm based on the collective behavior of chloroplasts in plant cells.

The general problem of controlling a group of mobile robots splits further into several subtasks: developing the group logic, developing the individual robot logic for operating in a group, developing the group hierarchy logic, developing the robot communication and coordination algorithms, etc. [15]. This chapter addresses the first two subtasks. To control a group of cleaning robots, it proposes a bee-inspired algorithm complemented with swarm intelligence.

2 How a Group of Robotic Cleaners Moves

Group movement uses a different set of algorithms compared to individual household robotic vacuums. Basic algorithms like random movement, zigzag movement, or spiral movement are secondary rather than primary in this scenario. Room cleaning is a regular periodic task covering a certain area. This is why a group of cyber-physical robotic cleaners has to follow a predefined route but might have to diverge. Such divergence may be due to the need to promptly clean some locations that are slightly off the route.

The route can be set by a variety of methods. Thus, Whiz robots (SoftBank) can be programmed by the demonstration method [2]. To that end, a supermarket employee drives the cleaning machine along the desired cleaning route, and the robot learns from it. This method can be used to control a group of cleaning robots provided there is a leader. The leading robot learns the route and follows it while the rest of the group follows the leader.

However, the author hereof believes a potentially better solution is to set a target for the group to follow. The target coordinates can be set dynamically in relation to the layout of the space to be cleaned. The target trajectory could be predetermined by any known graph traversal algorithm, such as breadth-first search, depth-first search, Dijkstra algorithm, A*, etc. [16, 17]. Analysis of such algorithms is beyond the scope hereof. The target trajectory could further be adjusted by the control system or by the human operator.

The group's task is to pursue the target, i.e. to shorten the group-to-target distance. The target coordinates are to be determined by the global or local positioning system. It communicates the coordinates to the entire group or to the leading robot only. In the latter case, the rest of the group must be aware of the leader's coordinates. Visual or sound-based communication will not suffice and is only suitable as an additional channel for the robots.

The target is adjustable by adding more tasks, i.e. specifying new locations for cleaning or spots to be cleaned again. Such locations or spots could be detected by human staff, CCTVs, or the so-called reconnaissance robots. Reconnaissance robots are special robots or dedicated cleaning robots programmed to detect unclean locations. They can traverse the building by random trajectories or following predefined routes based on where dirt is expected to appear. Once a spot is found that needs

cleaning, the reconnaissance robot may send a new task to the group and/or start cleaning it itself if the robot is also a cleaner.

3 Intragroup Movement of Robots

The intragroup movement of robots depends on whether the robots should maintain a specific formation or if the formation/positioning within the group is not critical. In the former case, referred as formation control, the controls are adjusted to keep a certain formation even if the group is moving. If that is not important, the intragroup movements can be based on that of bird flocks or fish schools, i.e. the robots should be capable of changing direction simultaneously while neither de-grouping nor colliding. To describe this behavior, Reynolds [18] formulated three basic principles each robot in a group should follow:

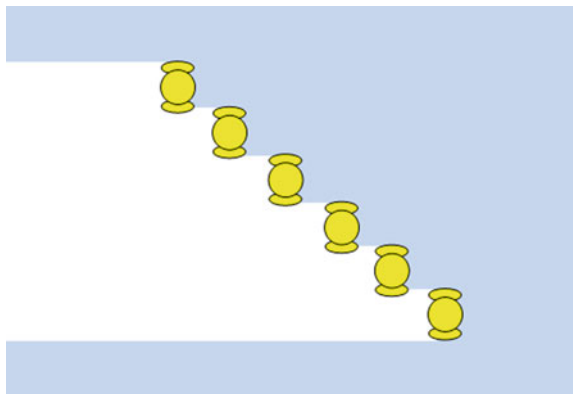
- Separation. Robots should travel at a specific minimum distance from each other to avoid a collision;
- Cohesion. Robots should flock together with their neighbors;
- Alignment. Robots should adjust their speed to the average speed of the group.

A variety of flocking algorithms have been developed based on these principles [19, 20].

The behavior of robots in a group is largely affected by what kind of area coverage tasks the robots are up to. On the one hand, good cleaning performance implies that robots should not move chaotically within a group. They should move in such manner as to get their cleaned areas partly overlap, see Fig. 1. A greater overlap will reduce the total cleaned area and jeopardize the cleaning performance. However, zero overlap may result in some of the areas remaining uncleaned.

On the other hand, the formation and the positioning of robots in relation to each other are not that important for cleaning. In a geometrically complex and cluttered

Fig. 1 A formation of cleaning robots



room where robots have to bypass multiple obstacles, the formation and the positioning in relation to each other cannot and should not be constant. Thus, swarm behavior principles above apply here. The key goals are to leave no untreated floor space behind the robots while also avoiding chaining or trailing.

To more accurately maintain a proper distance between robots' zones of responsibility, the author proposes using the wet path left from the robot in front. A cyber-physical robotic cleaner can be equipped with sensors to distinguish between dry and wet areas. The sensors must be sensitive enough to detect residual moisture that remained after vacuuming. The vacuum must be adjusted to leave enough moisture for the sensors to pick up while not leaving a wet floor.

When following the leader, each robot must strive to position itself in such a way as to have the edge of the leader-cleaned area between its wet-surface detector and the dry-surface detector. Thus, the distance maintenance task boils down to the well-known problem of the maze wall following. The robot must be capable of following either of or both edges of the wet trail.

The robots have to avoid collision with the interiors, people, sundry machines, or robots in the building, which further complicates the problem. The movement strategy will differ significantly depending on whether there are people in the room or not, i.e. whether the robots are running at night, during breaks, or when the room is full. The latter case is far more complex, as it requires better-equipped and smarter robots. At the same time, the route for the robots is subject to continual readjustment to minimize human encounters. Upon detecting an approaching person, the robot must issue an alarm and slow down or come to a full stop if a collision is likely. If the person attempts to tamper with the robot, the latter must issue an alarm to the maintenance staff.

4 Algorithm for Groups of Robotic Cleaners

As mentioned earlier, bio-inspired algorithms are an increasingly popular solution in robot control. The bees algorithm (the bee colony algorithm) is a popular optimization method [21, 22]. Its application to controlling a robot swarm is covered in [23]. The same paper proves the bee-inspired algorithm more efficient in foraging than the ant colony algorithm.

The author-proposed algorithm uses the following features of bees search: a topological distance or its analog; the combination of worker bees and scout bees; worker bees flying to the nectar source after it has been tracked; scout bees scouting the area for nectar.

Similarly to worker bees, cleaning robots split into groups. How many groups they split into depends on how many robots are available and on the floor space to be cleaned. Each group follows its own target. As said above, they can use a variety of strategies. Similarly to scout bees, reconnaissance robots can randomly search for new targets to further dispatch a group of robotic cleaners.

The objective function of a cleaning robot is the robot-to-target distance. When moving on a plane, the objective function is as follows

$$f_j(x_{rj}(k), x_{gi}(k)) = \sqrt{((x_{rj1}(k) - x_{gi1}(k))^2 + ((x_{rj2}(k) - x_{gi2}(k))^2), \quad (1)$$

where $x_{rj}(k)$ are the coordinates of the cleaning robot, $j = 1, \dots, m$, m is the number of robots in the group, $x_{gi}(k)$ are the target coordinates, $i = 1, \dots, n$, n is the number of targets, k is time. As the target coordinates keep changing, and the robotic cleaners are to pursue the target, minimizing the objective function (1) is a dynamic task.

To implement swarm behavior, modify the objective function (1) by adding a special term

$$\tilde{f}_j(x_{rj}(k), x_{gi}(k)) = f(x_{rj}(k), x_{gi}(k)) + \mu \sum_{k=1}^m h(|x_{rk}(k) - x_{rj}(k)|), \quad (2)$$

where μ is the weight, $h(\bullet)$ is a function that defines the robot-to-neighbor communications. The point of that function is to enable two robots to repulse if they come too close to each other, or to attract if they split too far away from each other [24]. The second term in the criterion (2) will have a minimum value if the robots stay within a specific zone (the group's coverage area) while not coming too close to each other.

The cyber-physical robotic cleaner control strategy can be formulated as follows:

1. If a cleaner is not in a formation or is outside the group's coverage area, its behavior is designed to handle the global task of pursuing the target using the criterion (2). As it moves towards the target, the robot will approach other members of its group. At the same time, the robot should continuously monitor the surroundings and track the wet trails to the left or to the right of itself.
2. If the robotic cleaner is within the group's coverage area, then it should switch to the local task of following the edge of the wet trail as soon as it detects the trail.
3. If the robotic cleaner is within the group's coverage area, but the floor under it is wet, i.e. there are no dry patches to either side of the robot, then the robot should drive to the left or the right (depending on the obstacles) until it detects the end of a wet floor. Then the robot switches to the local task of following the edge of the wet trail.
4. If the robot is within the group's coverage area but spearheads its formation, i.e. there no wet trail before the robot, then it should switch to the global task of pursuing the target, thus becoming the leader.
5. If the robot is within the group's coverage area but is a single robot to have no wet trail before it, then it should switch to the global task of pursuing the target.

Figure 2 shows different robot grouping scenarios based on this strategy. Figure 2a, f are robot groups, each with one leader. Figure 2b–f are groups with two or more leaders. Figure 2b–i are groups with robots tracking the wet trail on both sides.

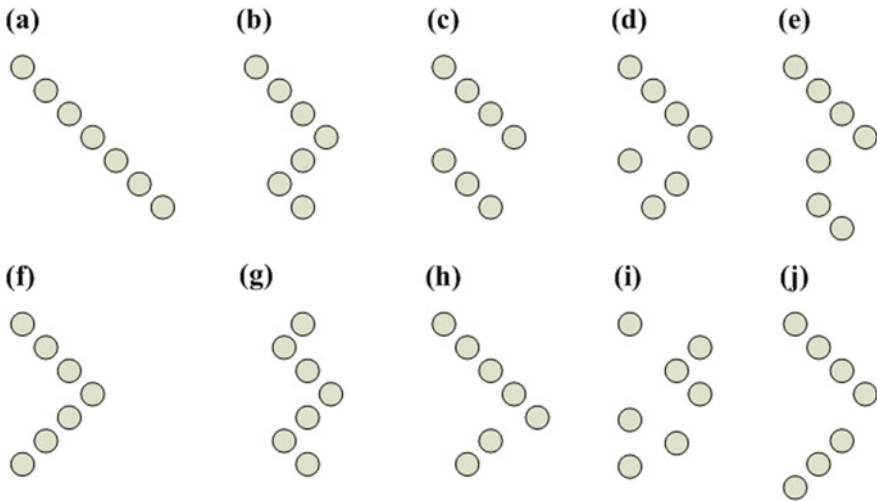


Fig. 2 Different grouping scenarios

Figure 2e, j show undesirable scenarios. In either case, the group splits into subgroups and leaves uncleaned space in-between. In such cases, the robots could be stimulated to attract each other by altering the parameters of the function h in (2). This will trigger a regroup and fill the unaffected gaps.

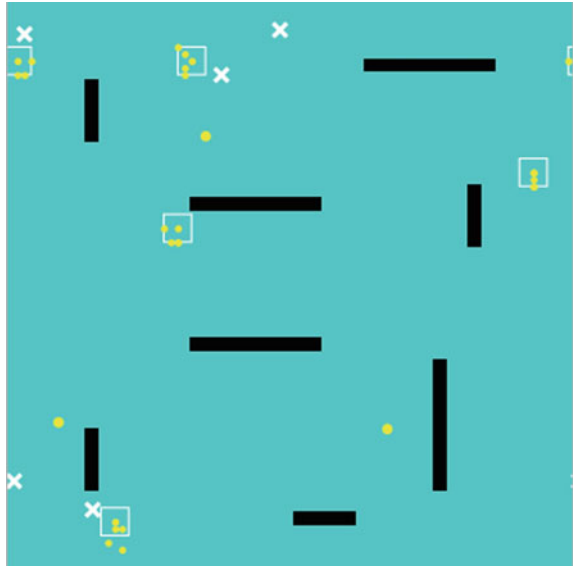
The proposed algorithm combines a global strategy based on the bees search algorithm with elements of swarm intelligence, and a local formation-building method for orientation to the leading robot and its neighbors.

5 Simulation

There are many simulation systems today that enable researchers to experiment with robot groups and swarm robotics. The most popular solutions are Gazebo, AnyLogic, Repast, and NetLogo. The latter is also the most suitable option for this research. NetLogo is relatively simple and has advanced tools for programming the agents and visualizing their behavior on a plane, which is why it is used in this research. Literature includes an article on how NetLogo helped solve an area surveying problem utilizing swarm robotics [25].

For simplicity, the algorithm proposed in Sect. 4 hereof was simulated in two stages. The first stage was to simulate the global task of pursuing the target (for each group, its own). That model was based on the bee-inspired model described in [24]. During the simulation, the robots sought to minimize their objective function expressed by the criterion (2). The experiments were designed to evaluate the robots' capability of flocking, reaching their target while bypassing the obstacles,

Fig. 3 NetLogo model for the first task



and switching to new targets identified by the reconnaissance robots. Figure 3 shows the NetLogo model for the first task after 20 iterations.

In Fig. 3, the white crosses stand for the robots' targets, the white squares are the group's coverage areas, and the black figures are obstacles the robots have to bypass. Smaller yellow dots are the cleaning robots, while larger dots are the reconnaissance robots. Experiments proved the proposed algorithm efficient. Robotic groups were capable of pursuing their targets steadily while bypassing the obstacles. The reconnaissance robots would find new targets and cause one group of cleaners to move to a new target.

The second stage was to simulate the local intragroup behavior. The goal here was to keep robots in a formation so as not to leave any patch of uncleaned floor space behind. The researcher also tested how obstacles could affect the formation. When encountering an obstacle, a robot would initiate a standard obstacle avoidance routine, i.e. the bug algorithm [26].

Figure 4a shows the NetLogo model for the second task at a time point when a formation of six cleaning robots approaches obstacles. The obstacles are shown as black rectangles, while the robots and the cleaned floor space behind them are shown in orange. During the simulation, Robot 2 and Robot 5 would encounter obstacles and bypass it, which would force them to follow the trails of their neighbors for some time. As soon as the obstacle was behind, the robots would go back to their positions in the formation as described in Step 3 of the proposed algorithm.

Figure 4b shows the NetLogo model after the robots have bypassed their obstacles. As shown in the Figure, the robots were able to keep their formation so as not to leave any uncleaned floor space behind. However, the formation did change somewhat, as some of the robots spent their time to bypass the obstacles and lagged a little behind

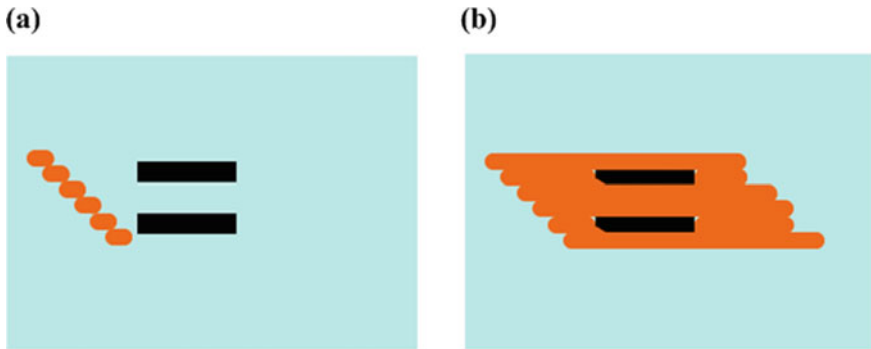


Fig. 4 NetLogo model: **a** a robot formation approaching an obstacle; **b** a robot formation has bypassed the obstacle

as a result. To reduce that gap, any robot with no obstacles in the path should slow down for some time.

6 Conclusions

Thus, this chapter discusses the control of groups of autonomous cyber-physical robotic cleaners for wet cleaning of larger commercial or public buildings: supermarkets, shopping malls, entertainment centers, sports venues, airports, etc. It presents various strategies to control the movements of a robot group or those of robots within a group. It also describes the factors affecting the intragroup behavior of robots.

The author offers a method for building robot formations, which is based on using the wet trails of the leading robot. To control groups of cyber-physical robotic cleaners, the chapter proposes an algorithm that combines a global strategy based on the bees search algorithm with elements of swarm intelligence, and a local formation-building method for orientation to the leading robot and its neighbors. The author has simulated some robotic group control and formation tasks in NetLogo. The simulation showed that the algorithm feasible and suitable for controlling groups of cyber-physical robotic cleaners.

The method for building robot formations and the algorithm for controlling groups of robots presented in the chapter can be used not only to solve the problem of wet cleaning of buildings but also for other similar tasks, such as harvesting, deactivating the area from radioactive substances, disinfecting the area from viruses and others. Common to these tasks is that robots can use the principles of swarm behavior and leave behind a trail visible to sensors, which can be used by other robots to form a group of robots.

References

1. Avidbots | Robot Scrubber, Auto Floor. <https://www.avidbots.com>. Accessed 25 Feb 2020
2. Robots in our life and work, find out which robot can help you. <https://robots.nu/en>. Accessed 25 Feb 2020
3. Robot janitors are moving into Walmart. <https://www.nbcnews.com/business/business-news/robot-janitors-are-moving-walmart-n943031>. Accessed 25 Feb 2020
4. Robotic Vacuum Cleaner Market by Application, End-users, Charging, and Geography—Forecast and Analysis 2020–2024. <https://www.technavio.com/report/robotic-vacuum-cleaner-market-industry-analysis>. Accessed 25 Feb 2020
5. Fan, F., Wu, G., Wang, M., Cao, Q., Yang, S.: Multi-robot cyber physical system for sensing environmental variables of transmission line. *Sensors* **18**, 1–29 (2018)
6. Lee, C.K.M., Lin, B., Ng, K.K.H., Lv, Y., Tai, W.C.: Smart robotic mobile fulfillment system with dynamic conflict-free strategies considering cyber-physical integration. *Adv. Eng. Inform.* **42**, 1–12 (2019). <https://doi.org/10.1016/j.aei.2019.100998>
7. Kalyaev, I.A., Gaiduk, A.R., Kapustyan, S.G.: Models and algorithms of collective behavior in groups of robots. Fizmatlit Publ, Moscow (2009)
8. Navarro, I., Matia, F.: A survey of collective movement of mobile robots. *Int. J. Adv. Robot. Syst.* **10**, 1–9 (2013)
9. Nedjah, N., Mourelle, L.M.: *Swarm Intelligent Systems*. Springer (2006)
10. Brambilla, M., Ferrante, E., Birattari, M., Dorigo, M.: Swarm robotics: a review from the swarm engineering perspective. *Swarm Intell.* **7**, 1–41 (2013)
11. Sahin, E.: Swarm robotics: From sources of inspiration to domains of application. In: 2004 International Workshop on Swarm Robotics, pp. 10–20 (2005)
12. Ahmadi, M. Stone, P.: A Multi-robot System for Continuous Area Sweeping Tasks. In: IEEE International Conference on Robotics and Automation, pp. 1724–1729 (2006)
13. Jager, M., Nebel, B.: Dynamic decentralized area partitioning for cooperating cleaning robots. In: IEEE International Conference on Robotics and Automation, pp. 3577–3582 (2002)
14. Hoshino, S., Takisawa, R., Kodama, Y.: Swarm robotic systems based on collective behavior of chloroplasts. *J. Robot. Mechatr.* **29**, 602–612 (2017)
15. Vasiliev, I.A., Polovko, S.A., Smirnova, E.Y.: Organization of group control of mobile robots for tasks of special robotics. Scientific and Technical Statements of SPbSPU. *Inform. Telecommun. Manage.* **1**, 119–123 (2013)
16. LaValle, S.M.: *Planning algorithms*. Cambridge University Press (2006)
17. Motorin, D., Popov, S., Glazunov, V., Chuvatov, M.: A study of a trajectory synthesis method for a cyclic changeable target in an environment with periodic dynamics of properties. *Cyber-Phys. Syst. Adv. Des. Model.* 121–134. Springer (2019). https://doi.org/10.1007/978-3-030-32579-4_10
18. Reynolds, C.W.: Flocks, herds, and schools: a distributed behavioral model. In: ACM SIGGRAPH 87 Conference, pp. 25–34 (1987). <https://doi.org/10.1145/37401.37406>
19. Turgut, A.E., Celikkanat, H., Gokce, F., Sahin, E.: Self-organized flocking in mobile robot swarms. *Swarm Intell.* **2**, 97–120 (2008)
20. Li, X., Ercan, M. F., Zhou, Y., Fung, Y.: Algorithm for swarm robot flocking behavior. In: 4th Int. Conf. on Autonomous Robots and Agents, pp. 161–165 (2009)
21. Karpenko, A.P.: *Modern search engine optimization algorithms. Algorithms inspired by nature*. Bauman MSTU Publ., Moscow (2014)
22. Amador, L., Castillo, O.: *Optimization of Type-2 Fuzzy Controllers Using the Bee Colony Algorithm*, Springer (2017)
23. Alers, S., Bloembergen, D., Hennes, D., de Jong, S., Kaisers, M., Lemmens, N., Tuyls, K., Weiss, G.: Bee-inspired foraging in an embodied swarm. In: 10th International Conference on Autonomous Agents and Multiagent Systems, pp. 1311–1312 (2011)
24. Ershov, N.M.: *Introduction to distributed modeling in NetLogo*. DMK Press Publ, Moscow (2018)

25. Bouraqadi, N., Doniec, A.: Flocking-based multi-robot exploration. In: 4rd National Conference on Control Architectures of Robots, pp. 1–9 (2009)
26. Oroko, J.A., Nyakoe, G.N.: Obstacle avoidance and path planning schemes for autonomous navigation of a mobile robot: a review. In: Mechanical Engineering Conference on Sustainable Research and Innovation, vol. 4, pp. 314–318 (2012)

Modeling the Highly Effective Object for Continuous Compaction Control of the Cyber-Physical Road-Construction System



Andrey Prokopev , Zhasurbek Nabizhanov , Rurik Emelyanov ,
and Vladimir Ivanchura

Abstract Compaction of hot mix asphalt (HMA) is one of the most important processes in the construction of road surfaces. The technologies of continuous compaction control (CCC) and intelligent compaction (IC) are based on algorithmic and software–technical means for processing informative signals and presenting the results of determining material compaction indicators. One of the possible reserves for increasing the efficiency of compaction is an increase in the compaction coefficient by the working bodies of stackers. The most effective management of road construction in real-time is carried out when asphalt pavers and road rollers interact as part of the existing cyber-physical system. In this chapter, using the state space method, a mathematical model of the HMA compaction process with a highly efficient stacker working body as an object of continuous nondestructive compaction control is obtained. The use of the state space method provided a clear formalization and automation of computational procedures, increasing the efficiency of theoretical research of the object using modern software. The model takes into account the design elements of the working body and the properties of the compacted material. The output parameters of the object model are intended for process dynamics analysis, continuous compaction monitoring, measurement, and control automation. The chapter presents a computer model of the object in the MATLAB/Simulink and the results of a computational experiment to model the workflow of the research object. The development of cyber-physical systems helps to increase the efficiency of managing sets of automated compacting machines at a construction site.

A. Prokopev (✉) · Z. Nabizhanov · R. Emelyanov · V. Ivanchura
Siberian Federal University, 79 Svobodny, Krasnoyarsk 660041, Russia
e-mail: prok1@yandex.ru

Z. Nabizhanov
e-mail: jasur150691@yandex.ru

R. Emelyanov
e-mail: ert-44@yandex.ru

V. Ivanchura
e-mail: ivan43ura@yandex.ru

Keywords Cyber-physical system · Paver · Highly effective working body · Dynamic model · State-space · Continuous compaction control

1 Introduction

Changes of requirements for asphalt pavement quality create conditions for the implementation of intelligent and “smart” technologies in the road building industry. The main stages of the asphalt pavements construction process affect coating performance [1]: manufacture, transportation from the plant to the facility, spreading, mixture placing, and compaction. Mixture compaction by pavers and road rollers eliminates up to 50% of the disadvantages of asphalt pavements and increases their service life [2].

Systems of continuous non-destructive compaction control of hot mix asphalt with intelligent compaction technologies, continuous compaction control [3–9], installed on vibratory rollers, and a neural network automatic control system [10, 11] are modern methods of compaction control of road surfaces.

Known methods and control means have a significant error, do not allow to evaluate the efficiency of the rolling process, and are not able to record the compaction characteristics [12]. These drawbacks are confirmed in many scientific papers [12–14].

Over the 40 years of the existence of the idea of continuous compaction control, the developers of automatic systems have not come up with effective means of reducing drawbacks in measuring the compaction degree of hot mix asphalt. The main variable of control systems is the acceleration of the vibratory roller. However, the material characteristics during compaction are not constant. The structure of the road-building mixture, humidity, temperature of the layer, stiffness of the base, layer thickness are changing. In well-known developments of continuous compaction control systems of leading companies such as Trimble, MOBA, Topcon, Hydac, etc., there are no data on the consideration of several significant factors in predicting the compaction effectiveness. Thus, the problem of increasing the efficiency of continuous non-destructive compaction control, taking into account significant factors of the changing properties of the material, strain–stress state, requires a solution.

The relevance of solving this problem increases in connection with the development of the scientific field—cybernetic physics [15]. The automation level of road-building machines—objects of cyber-physical systems (CPS), should be high. The performance of the entire CPS depends on the quality of measurements and forecasts of the parameters of the automated control system. We can state the presence of developed mathematical models of the compaction process by vibratory rollers [3–20], and oscillating rollers, which allows solving current issues of non-destructive technologies in the road construction field.

The set of road construction machines providing compaction of hot mix asphalt, in addition to road rollers, includes pavers that can compact the material to standard values when equipped with a highly effective working body. Depending on the

achieved compaction factor, we can reduce the number and types of road rollers, the number of passes after the stacker. These technological measures boost productivity and cost reduction of road construction. But it is impossible to completely exclude the use of existing road rollers with existing technologies isn't possible, because they are necessary to confirm the achieved compaction coefficient of the material and increase the structural strength of asphalt concrete. To increase the efficiency and productivity of the compaction processes of pavements, it is necessary to carry out continuous non-destructive compaction control and regulation of operating modes—tamping frequency, frequency of plate vibration, impulse movements frequency of the pressing bars, taking into account the technological capabilities of modern pavers. Currently, such automatic control and management systems for pavers are not available. Having such systems, it is possible to create a “smart” paver with a significant increase in productivity by optimizing the compaction process and reducing the workload of the driver. To increase the effectiveness of scientific research and the design of objects of cyber-physical systems, mathematical models of real processes are needed.

This work is devoted to the theoretical description of the object of continuous compaction control of a cyber-physical road-building system—an asphalt paver with a highly effective working body. Theoretical studies on the compaction of various materials (soils, asphalt mixtures) have been and are being carried out by many Russian [16] and foreign scientists [17–20]. The disadvantages of previously developed mathematical models are the problems of algorithmization of tasks, computational difficulties in the study of dynamic systems, the design of automatic control and management systems.

To eliminate these drawbacks and to increase the efficiency of theoretical research of the control object using the modern MATLAB/Simulink software, it is recommended to use the state space method, which allows making clear characterization and automation of computational procedures [21–23].

2 The Mathematical Formulation of the Problem

For research, a highly effective working body was taken in the following composition of the compacting units: tamper—vibration plate—two pressing bars. The compaction process of the mixture is carried out with constant contact of the vibrating plate with the mixture. The main compaction is performed by compressing the mixture with a horizontal platform of a tamping beam when moving in a vertical plane for 4–6 effects. A vibrating plate and pressing bars fix the achieved compaction result and improve the structure of the material. Pressing bars creates periodic impulse loadings with a frequency of 50–70 Hz and pressure in the hydraulic system from 5 to 15 MPa [24].

The dynamic parameters of compacting units and particles of material are frequency, amplitude, speed, and acceleration.

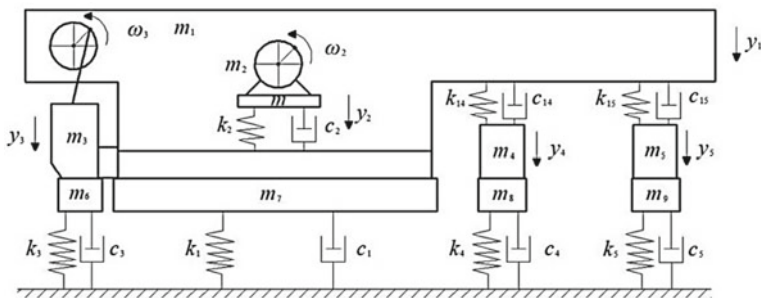


Fig. 1 The dynamic model of the mixture compaction process by the working body (tamper, vibration plate, two pressure bars) of the paver

A simulation model of a dynamic model of the compaction process of the mixture with a highly effective working body of the paver is obtained based on the technical documentation [24], Fig. 1.

On the Fig. 1 the following notation is used: m_1 —mass of the smoothing plate frame, kg; m_2 —weight of vibrator, kg; m_3 —weight of tamper, kg; m_4 —weight of the first pressure bar, kg; m_5 —weight of the second pressure bar, kg; m_6 —weight of the mix under the tamper, kg; m_7 —weight of the mix under the vibration plate, kg; m_8 —weight of mix under the first pressure bar, kg; m_9 —weight of the mix under the second pressure bar, kg; k_1 —coefficient of elastic resistance of the compacted mix under the plate, N/m; c_1 —damping coefficient of the compacted mix under the plate, N s/m; k_2 —coefficient of elastic resistance of the shock absorbers of the vibrator, N/m; c_2 —damping coefficient of shock absorbers of the vibrator, N s/m; k_3 —coefficient of elastic resistance of the compacted mix under the tamper, N/m; c_3 —damping coefficient of the compacted mix under the tamper, N s/m; k_4 —coefficient of elastic resistance of the compacted mix under the first pressure bar, N/m; k_5 —coefficient of elastic resistance of the compacted mix under the second pressure bar, N/m; c_4 —damping coefficient of the compacted mixture under the second pressure bar, N s/m; k_{14} and k_{15} —coefficient of elastic resistance of the first and second pressure bars, N/m; c_{14} and c_{15} —damping coefficient of the first and second pressure bars, N s/m; y_1 , y_2 , y_3 , y_4 and y_5 —the moving system elements, respectively, m.

We developed a mathematical model that presents both the vibration dynamics of structural elements and the rheological properties of the compacted material. Differential equations describing the movement of the first and second pressure bar

$$(m_4 + m_8) \cdot \ddot{y}_4 - c_{14} \cdot \dot{y}_1 + (c_4 + c_{14}) \cdot \dot{y}_4 - k_{14} \cdot y_1 + (k_4 + k_{14}) \cdot y_4 = F_4 + m_4 \cdot g + m_8 \cdot g, \quad (1)$$

$$(m_5 + m_9) \cdot \ddot{y}_5 - c_{15} \cdot \dot{y}_1 + (c_5 + c_{15}) \cdot \dot{y}_5 - k_{15} \cdot y_1 + (k_5 + k_{15}) \cdot y_5 = F_5 + m_5 \cdot g + m_9 \cdot g, \quad (2)$$

where F_4, F_5 is the force of the first and second pressure bar, respectively, N.

The differential equation of the smoothing plate vibrator

$$m_2 \cdot \ddot{y}_2 - c_2 \cdot \dot{y}_1 + c_2 \cdot \dot{y}_2 - k_2 \cdot y_1 + k_2 \cdot y_2 = m \cdot \omega_2^2 \cdot r \cdot \sin(\omega_2 \cdot t), \quad (3)$$

where F_3 is the force of tamping beam ram, N.

With allowance for the principle of relative motion, we obtain an additional equation

$$y_3 = y_1 + e \cdot \sin(\omega_3 \cdot t), \quad (4)$$

where e —tamper eccentricity size, m; ω_3 —the rotational speed of the tamper gear, rad/s.

Substituting Eq. (4) into (3) with transformations, we obtain the following equation

$$F_3 = (m_3 + m_6) \cdot \ddot{y}_1 + c_3 \cdot \dot{y}_1 + k_3 \cdot y_1 - (m_3 + m_6) \cdot e \cdot \omega_3^2 \cdot \sin(\omega_3 \cdot t) + k_3 \cdot e \cdot \sin(\omega_3 \cdot t) + c_3 \cdot e \cdot \omega_3 \cdot \sin(\omega_3 \cdot t + \pi/2) - m_6 \cdot g. \quad (5)$$

The differential equation of smoothing plate motion

$$(m_1 + m_7) \cdot \ddot{y}_1 + (c_1 + c_2 + c_{14} + c_{15}) \cdot \dot{y}_1 - c_2 \cdot \dot{y}_2 - c_{14} \cdot \dot{y}_4 - c_{15} \cdot \dot{y}_5 + (k_1 + k_2 + k_{14} + k_{15}) \cdot y_1 - k_2 \cdot y_2 - k_{14} \cdot y_4 - k_{15} \cdot y_5 = -F_3 - F_4 - F_5 + (m_1 + m_7) \cdot g. \quad (6)$$

Substituting Eq. (5) into (6), we obtain the following differential expression

$$(m_1 + m_7 + m_3 + m_6) \cdot \ddot{y}_1 + (c_1 + c_2 + c_3 + c_{14} + c_{15}) \cdot \dot{y}_1 - c_2 \cdot \dot{y}_2 - c_{14} \cdot \dot{y}_4 - c_{15} \cdot \dot{y}_5 + (k_1 + k_2 + k_3 + k_{14} + k_{15}) \cdot y_1 - k_2 \cdot y_2 - k_{14} \cdot y_4 - k_{15} \cdot y_5 = -F_4 - F_5 + ([m_3 + m_6] \cdot e \cdot \omega_3^2 - k_3 \cdot e) \cdot \sin(\omega_3 \cdot t) - c_3 \cdot e \cdot \omega_3 \cdot \sin(\omega_3 \cdot t + \pi/2) + (m_1 + m_6 + m_7) \cdot g. \quad (7)$$

3 Methods and Materials

The state-space method allows you to represent the control system in the form of an equations system [21, 22]:

$$\dot{x}(t) = A(t) \cdot x(t) + B(t) \cdot u(t), \quad (8)$$

$$y(t) = C(t) \cdot x(t) + D(t) \cdot u(t), \quad (9)$$

where $x(t)$ is the state vector of dimension $(n \times 1)$, whose components are state variables of the n -th order system, $x(t) = [x_1(t), x_2(t), \dots, x_n(t)]^T$, $y(t)$ is the dimension output vector $(p \times 1)$, whose components are the output variables of the system, $y(t) = [y_1(t), y_2(t), \dots, y_p(t)]^T$, $u(t)$ is the dimension input vector $(r \times 1)$, whose components are the output variables of the system $u(t) = [u_1(t), u_2(t), \dots, u_r(t)]^T$, $A(t)$ is the matrix of the system $(n \times n)$, $B(t)$ is the input matrix $(n \times m)$, $C(t)$ is the output matrix $(p \times n)$, $D(t)$ is the detour matrix $(p \times m)$, determining the direct dependence of the output on the input, p is the output quantity number.

The state parameters of a dynamic system are defined as follows: x_1 is the vertical movement of the vibrating plate, $x_1 = y_1$, x_2 is the vertical velocity of the vibrating plate, $x_2 = \dot{y}_1$, x_3 is the vibrator vertical movement, $x_3 = y_2$, x_4 is the vibrator vertical velocity $x_4 = \dot{y}_2$, x_5 is the first pressing bar vertical movement, $x_5 = y_4$, x_6 is the first pressing bar vertical velocity, $x_6 = \dot{y}_4$, x_7 is the second pressing bar vertical movement, $x_7 = y_5$, x_8 is the second pressing bar vertical velocity, $x_8 = \dot{y}_5$.

We get a mathematical formulation of the object dynamics in the form of Cauchy on the rearrangement of the equations system of (1)–(7):

$$x_2 = \dot{y}_1;$$

$$\dot{x}_2 = \frac{\begin{bmatrix} -(c_1 + c_2 + c_3 + c_{14} + c_{15}) \cdot x_2 + c_2 \cdot x_4 + c_{14} \cdot x_6 + c_{15} \cdot x_8 \\ + (k_1 + k_2 + k_3 + k_{14} + k_{15}) \cdot x_1 + k_2 \cdot x_3 + k_{14} \cdot x_5 + k_{15} \cdot x_7 - F_4 - F_5 \\ + ([m_3 + m_6] \cdot e \cdot \omega_3^2 - k_3 \cdot e) \cdot \sin(\omega_3 \cdot t) \\ + c_3 \cdot e \cdot \omega_3 \cdot \sin(\omega_3 \cdot t + \pi/2) + (m_1 + m_6 + m_7) \cdot g \end{bmatrix}}{m_1 + m_3 + m_6 + m_7},$$

$$x_4 = \dot{y}_2; \quad \dot{x}_4 = \frac{1}{m_2} \cdot (c_2 \cdot x_2 - c_2 \cdot x_4 + k_2 \cdot x_1 - k_2 \cdot x_3 + m \cdot r \cdot \omega_2^2 \cdot \sin(\omega_2 \cdot t)),$$

$$x_6 = \dot{y}_4; \quad \dot{x}_6 = \frac{1}{m_4 + m_8} \cdot (c_{14} \cdot x_2 - [c_4 + c_{14}] \cdot x_6 + k_{14} \cdot x_1 - [k_4 + k_{14}] \cdot x_5 + F_4 + [m_4 + m_8] \cdot g),$$

$$x_8 = \dot{y}_5; \quad \dot{x}_8 = \frac{1}{m_5 + m_9} \cdot (c_{15} \cdot x_2 - [c_5 + c_{15}] \cdot x_8 + k_{15} \cdot x_1 - [k_5 + k_{15}] \cdot x_7 + F_5 + [m_5 + m_9] \cdot g).$$

We can obtain the following results by moving these parameters into the corresponding vector and matrix.

Enter parameter value

$$M = m_1 + m_3 + m_6 + m_7,$$

$$K = k_1 + k_2 + k_3 + k_{14} + k_{15},$$

$$Q = c_1 + c_2 + c_3 + c_{14} + c_{15}.$$

Then the model of the process under study in the state space, in the vector–matrix form

$$y(t) = C \cdot x(t) + D \cdot u(t),$$

$$\begin{bmatrix} y_1(t) \\ y_2(t) \\ y_3(t) \\ y_4(t) \\ y_5(t) \\ y_6(t) \\ y_7(t) \\ y_8(t) \end{bmatrix} = \begin{bmatrix} 1 & 0 & 0 & 0 & 0 & 0 & 0 & 0 \\ 0 & 1 & 0 & 0 & 0 & 0 & 0 & 0 \\ 0 & 0 & 1 & 0 & 0 & 0 & 0 & 0 \\ 0 & 0 & 0 & 1 & 0 & 0 & 0 & 0 \\ 0 & 0 & 0 & 0 & 1 & 0 & 0 & 0 \\ 0 & 0 & 0 & 0 & 0 & 1 & 0 & 0 \\ 0 & 0 & 0 & 0 & 0 & 0 & 1 & 0 \\ 0 & 0 & 0 & 0 & 0 & 0 & 0 & 1 \end{bmatrix} \cdot \begin{bmatrix} x_1(t) \\ x_2(t) \\ x_3(t) \\ x_4(t) \\ x_5(t) \\ x_6(t) \\ x_7(t) \\ x_8(t) \end{bmatrix} + \begin{bmatrix} 0 & 0 & 0 & 0 \\ 0 & 0 & 0 & 0 \\ 0 & 0 & 0 & 0 \\ 0 & 0 & 0 & 0 \\ 0 & 0 & 0 & 0 \\ 0 & 0 & 0 & 0 \\ 0 & 0 & 0 & 0 \\ 0 & 0 & 0 & 0 \end{bmatrix} \cdot u(t),$$

$$\dot{x}(t) = A \cdot x(t) + B \cdot u(t),$$

$$\begin{bmatrix} \dot{x}_1(t) \\ \dot{x}_2(t) \\ \dot{x}_3(t) \\ \dot{x}_4(t) \\ \dot{x}_5(t) \\ \dot{x}_6(t) \\ \dot{x}_7(t) \\ \dot{x}_8(t) \end{bmatrix} = \begin{bmatrix} 0 & 1 & 0 & 0 & 0 & 0 & 0 & 0 \\ -\frac{K}{M} & -\frac{Q}{M} & \frac{k_2}{M} & \frac{c_2}{M} & \frac{k_{14}}{M} & \frac{c_{14}}{M} & \frac{k_{15}}{M} & \frac{c_{15}}{M} \\ 0 & 0 & 0 & 1 & 0 & 0 & 0 & 0 \\ \frac{k_2}{m_2} & \frac{c_2}{m_2} & -\frac{k_2}{m_2} & -\frac{c_2}{m_2} & 0 & 0 & 0 & 0 \\ 0 & 0 & 0 & 0 & 0 & 1 & 0 & 0 \\ \frac{k_{14}}{m_4+m_8} & \frac{c_{14}}{m_4+m_8} & 0 & 0 & -\frac{k_4+k_{14}}{m_4+m_8} & -\frac{c_4+c_{14}}{m_4+m_8} & 0 & 0 \\ 0 & 0 & 0 & 0 & 0 & 0 & 0 & 1 \\ \frac{k_{15}}{m_5+m_9} & \frac{c_{15}}{m_5+m_9} & 0 & 0 & 0 & 0 & -\frac{k_5+k_{15}}{m_5+m_9} & -\frac{c_5+c_{15}}{m_5+m_9} \end{bmatrix}$$

$$\cdot \begin{bmatrix} x_1(t) \\ x_2(t) \\ x_3(t) \\ x_4(t) \\ x_5(t) \\ x_6(t) \\ x_7(t) \\ x_8(t) \end{bmatrix} + \begin{bmatrix} 0 & 0 & 0 & 0 \\ \frac{1}{M} & 0 & 0 & 0 \\ 0 & 0 & 0 & 0 \\ 0 & \frac{1}{m_2} & 0 & 0 \\ 0 & 0 & 0 & 0 \\ 0 & 0 & \frac{1}{m_4+m_8} & 0 \\ 0 & 0 & 0 & 0 \\ 0 & 0 & 0 & \frac{1}{m_5+m_9} \end{bmatrix} \cdot u(t),$$

where

$$u(t) = \begin{bmatrix} -F_4 - F_5 + ([m_3 + m_6] \cdot e \cdot \omega_3^2 - k_3 \cdot e) \cdot \sin(\omega_3 \cdot t) \\ -c_3 \cdot e \cdot \omega_3 \cdot \sin(\omega_3 \cdot t + \pi/2) + (m_1 + m_6 + m_7) \cdot g \\ m \cdot \omega_2^2 \cdot r \cdot \sin(\omega_2 \cdot t) \\ F_4 + (m_4 + m_8) \cdot g \\ F_5 + (m_5 + m_9) \cdot g \end{bmatrix}.$$

4 Results and Analysis

A simulation model is obtained in the environment of the MATLAB/Simulink program. The initial data from scientific work [25] were used to simulate the process.

$$\begin{aligned}
 k_1 &= 4.2 \cdot 10^6 \text{ N/m}, k_2 = 10.3 \cdot 10^7 \text{ N/m}, k_3 = 1.68 \cdot 10^6 \text{ N/m}, \\
 k_4 &= 4.2 \cdot 10^6 \text{ N/m}, k_5 = 5 \cdot 10^6 \text{ N/m}, k_{14} = 1.1 \cdot 10^4 \text{ N/m}, \\
 k_{15} &= 1.1 \cdot 10^4 \text{ N/m}, c_1 = 1200 \text{ N} \cdot \text{s/m}, c_2 = 17600 \text{ N} \cdot \text{s/m}, \\
 c_3 &= 3160 \text{ N} \cdot \text{s/m}, c_4 = 1200 \text{ N} \cdot \text{s/m}, c_5 = 1200 \text{ N} \cdot \text{s/m}, \\
 c_{14} &= 200 \text{ N} \cdot \text{s/m}, c_{15} = 200 \text{ N} \cdot \text{s/m}, \\
 m &= 9.6 \text{ kg}, m_1 = 3000 \text{ kg}, m_2 = 80 \text{ kg}, m_3 = 260 \text{ kg}, m_4 = 260 \text{ kg}, \\
 m_5 &= 260 \text{ kg}, m_6 = 0.2 \cdot m_3, m_7 = 0.2 \cdot m_1, m_8 = 0.2 \cdot m_4, \\
 m_9 &= 0.2 \cdot m_5, r = 0,035 \text{ m}, e = 0,007 \text{ m}, f_2 = 20 \text{ Hz}, f_3 = 15 \text{ Hz}, \\
 f_4 &= 25 \text{ Hz}, f_5 = 25 \text{ Hz}, F_4 = 9000 \text{ N}, F_5 = 9000 \text{ N}.
 \end{aligned}$$

A simulation model of the studied process is presented in Fig. 2.

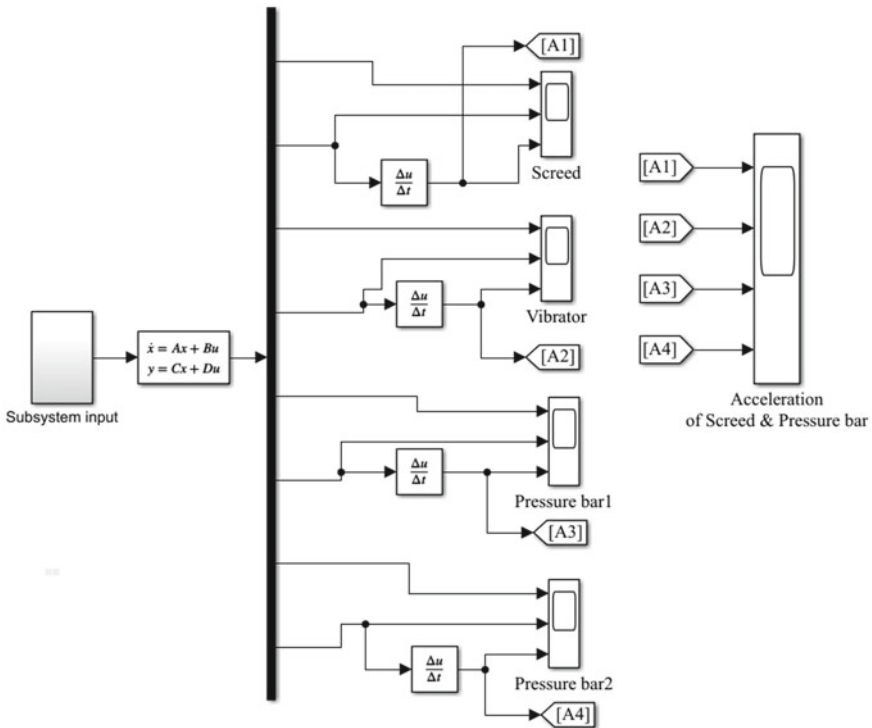


Fig. 2 Simulation model in the language of the program MATLAB/Simulink

The timing diagram of work process parameters was obtained by computer simulation: displacement, velocity, acceleration. Figure 3 shows the graphical dependencies for the vibration plate.

The obtained dependencies correspond to the oscillatory process, and stability features of a dynamic system are observed. The vibration plate acceleration with peak values up to 25 m/s^2 indicates a good correlation with the research results [1, 25].

The simulation results of the compaction process of the material by the second pressing bar are shown in Fig. 4.

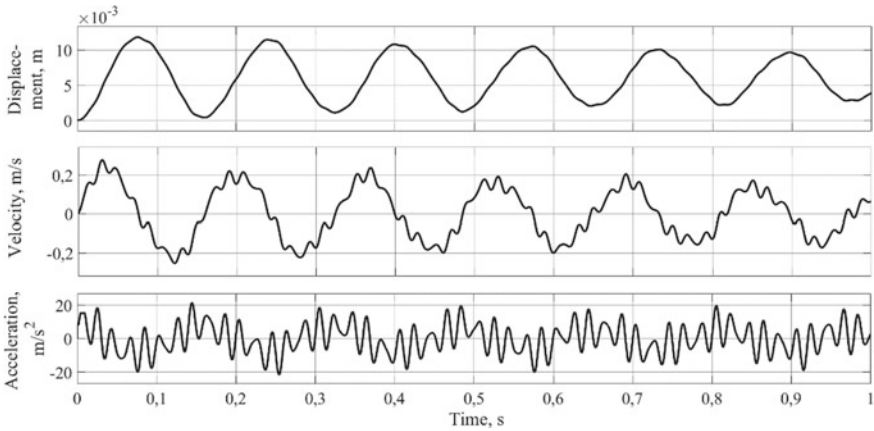


Fig. 3 The dependences of the oscillatory process parameters of the smoothing plate of the paver

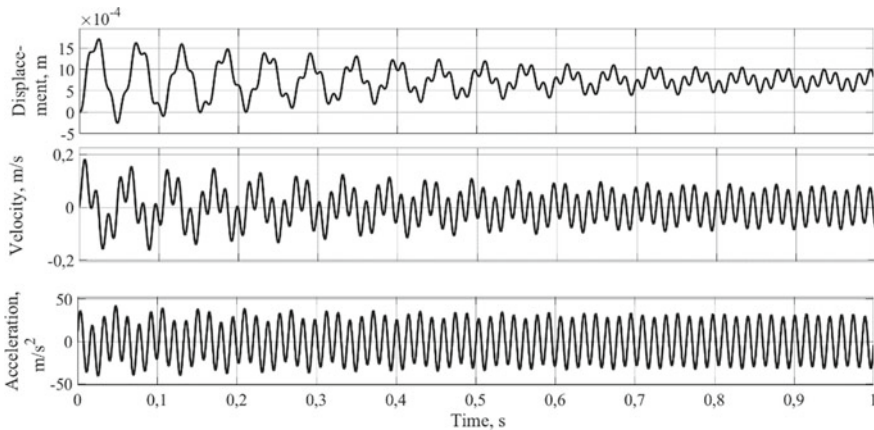


Fig. 4 The dependences of the oscillatory process parameters of the second pressing bar of the paver working body

The graphs in Fig. 4 show a significant decrease in the amount of the bar movement, a slight increase in acceleration due to gear vibration. Dependencies correspond to the nature of the physics of the workflow.

5 Determination of the Transfer Function of the Control Object

The transfer function was determined to conduct a study of a mathematical model using block simulation software. As a result of the MATLAB program tools implementation, we obtained advanced functions with the regulated variable—the angular frequency of vibration.

Transfer function regulated variable—vibrating plate displacement

$$W(s) = \frac{\begin{bmatrix} 0,0002556 \cdot s^6 + 0,05853 \cdot s^5 + 338,2 \cdot s^4 + 4890 \cdot s^3 \\ +1,119 \cdot 10^7 \cdot s^2 + 6,576 \cdot 10^7 \cdot s + 9,337 \cdot 10^{10} \end{bmatrix}}{\begin{bmatrix} s^8 + 234,7 \cdot s^7 + 1,351 \cdot 10^6 \cdot s^6 + 2,147 \cdot 10^7 \cdot s^5 + 4,667 \cdot 10^{10} \cdot s^4 \\ +3,446 \cdot 10^{11} \cdot s^3 + 4,391 \cdot 10^{14} \cdot s^2 + 8,324 \cdot 10^{14} \cdot s + 5,51 \cdot 10^{17} \end{bmatrix}},$$

transfer function regulated variable—vibrating plate velocity

$$W(s) = \frac{\begin{bmatrix} 0,0002556 \cdot s^7 + 0,05853 \cdot s^6 + 338,2 \cdot s^5 + 4890 \cdot s^4 \\ +1,119 \cdot 10^7 \cdot s^3 + 6,576 \cdot 10^7 \cdot s^2 + 9,337 \cdot 10^{10} \cdot s \end{bmatrix}}{\begin{bmatrix} s^8 + 234,7 \cdot s^7 + 1,351 \cdot 10^6 \cdot s^6 + 2,147 \cdot 10^7 \cdot s^5 + 4,667 \cdot 10^{10} \cdot s^4 \\ +3,446 \cdot 10^{11} \cdot s^3 + 4,391 \cdot 10^{14} \cdot s^2 + 8,324 \cdot 10^{14} \cdot s + 5,51 \cdot 10^{17} \end{bmatrix}}.$$

The obtained transfer functions correspond to the correct form since the degree of the numerator is less than the degree of the denominator. In further studies, when designing an automatic controller, it is necessary to take into account the high order of the mathematical model of the control object.

6 Conclusion

The chapter discusses the task of simulation as a highly efficient object of continuous compaction control of the cyber-physical system. A mathematical model of the mixture compaction process is obtained by a highly effective working body of the paver using the state space method. The obtained model was verified by simulation in the environment of the MATLAB/Simulink program. The results of the work are a stage of scientific research in the field of designing intelligent control and management systems for cyber-physical road-building systems.

Acknowledgements The reported study was funded by the RFBR project No. 19-37-90052.

References

1. Sun, J., Xu, G.: Dynamics modeling and analysis of paver screed based on computer simulation. *J. Appl. Sci.* **13**, 1059–1065 (2013). <https://doi.org/10.3923/jas.2013.1059.1065>
2. Prokopyev, A.P., Ivanchura, V.I., Emelianov, R.T., Palchikov, P.A.: Implementation of the concept of automation and intellectualization of management of road construction processes. *Vestnik MGSU*, **13**, 1(112), 61–70 (2018). <https://doi.org/10.22227/1997-0935.2018.1.61-70>
3. Xu, Q., Chang, G.K.: Adaptive quality control and acceptance of pavement material density for intelligent road construction. *Automat. Constr.* **62**, 78–88 (2015). <https://doi.org/10.1016/j.autcon.2015.11.004>
4. Anderegg, R., Kaufmann, K.: Intelligent compaction with vibratory rollers: feedback control systems in automatic compaction and compaction control. *Transp. Res. Board.* **1868**, 124–134 (2004). <https://doi.org/10.3141/1868-13>
5. Hu, W., Shu, X., Huang, B., Woods, M.: Field investigation of intelligent compaction for hot mix asphalt resurfacing. *Front. Struct. Civil Eng.* **11**(1), 47–55 (2017). <https://doi.org/10.1007/s11709-016-0362-x>
6. Fang, X., Bian, Y., Yang, M., Liu, G.: Development of a path following control model for an unmanned vibratory roller in vibration compaction. *Adv. Mech. Eng.* **10**(5), 1–16 (2018). <https://doi.org/10.1177/1687814018773660>
7. Bian, Y., Fang, X., Yang, M., Zhao, Z.: Automatic rolling control for unmanned vibratory roller based on fuzzy algorithm. *J. Tongji Univ. (Natural Science)* **45**(12), 1831–1838 (2017). <https://doi.org/10.11908/j.issn.0253-374x.2017.12.013>
8. Zhu, S., Li, X., Wang, H., Yu, D.: Development of an automated remote asphalt paving quality control system. *Transp. Res. Rec.* **2672**(26), 28–39 (2018). <https://doi.org/10.1177/0361198118758690>
9. Liu, D.H., Li, Z.L., Lian, Z.H.: Compaction quality assessment of earth-rock dam materials using rollerintegrated compaction monitoring technology. *Automat. Constr.* **44**, 234–246 (2014). <https://doi.org/10.1016/j.autcon.2014.04.016>
10. Barman, M., Nazari, M., Imran, S.A., Commuri, S., Zaman, M., Beainy, F., Singh, D.: Quality control of subgrade soil using intelligent compaction. *Innov. Infrastruct. Sol.* **1**(1), 23 (2016). <https://doi.org/10.1007/s41062-016-0020-0>
11. Barman, M., Imran, S.A., Nazari, M., Commuri, S., Zaman, M.: Use of intelligent compaction in detecting and remediating under-compacted spots during compaction of asphalt layers. In: Hossain, Z., Zhang, J., Chen, C. (eds.) *Solving Pavement and Construction Materials Problems with Innovative and Cutting-edge Technologies. GeoChina 2018. Sustainable Civil Infrastructures*. Springer, Cham, pp. 131–141 (2019). https://doi.org/10.1007/978-3-319-95792-0_11
12. Zakharenko, A.V., Permyakov, V.B., Molokova, L.V.: Road rollers: theory, calculation, application: monograph. SPb.: LAN Publishing House, 328 p. (2018) ISBN 978-5-8114-3201-1
13. Hua, T., Yang, X., Yao, Q., Li, H.: Assessment of real-time compaction quality test indexes for rockfill material based on roller vibratory acceleration analysis. *Adv. Mater. Sci. Eng.* **2018**, 1–15 (2018). <https://doi.org/10.1155/2018/2879321>
14. Liu, D., Gao, L.: Analysis and improvement of roller vibration behavior-based indexes for monitoring compaction quality of earth-rock dams. *J. Hydroelectr. Eng.* **37**(4), 111–120 (2018). <https://doi.org/10.11660/slfdbx.20180411>
15. Fradkov, A.L.: Horizons of cybernetical physics. *Philos. Trans. Math. Phys. Eng. Sci.* **375**(2088), 20160223 (2017). <https://doi.org/10.1098/rsta.2016.0223>

16. Miheyev, V.V., Saveliev, S.V.: Modelling of deformation process for the layer of elastoviscoplastic media under surface action of periodic force of arbitrary type. *J. Phys. Conf. Ser.* **944**(1), 012079 (2018). <https://doi.org/10.1088/1742-6596/944/1/012079>
17. Rinehart, R.V., Mooney, M.A.: Instrumentation of a roller compactor to monitor vibration behavior during earthwork compaction. *Autom. Constr.* **17**, 144–150 (2008)
18. Beainy, F., Commuri, S., Zaman, M.: Dynamical response of vibratory rollers during the compaction of asphalt pavements. *J. Eng. Mech.* **140**(7), 04014039 (2014). [https://doi.org/10.1061/\(asce\)em.1943-7889.0000730](https://doi.org/10.1061/(asce)em.1943-7889.0000730)
19. Imran, S.A., Commuri, S., Barman, M., Zaman, M., Beainy, F.: Modeling the dynamics of asphalt-roller interaction during compaction. *J. Constr. Eng. And Manag.* **143**(7), 1763–1770 (2017). [https://doi.org/10.1061/\(ASCE\)CO.1943-7862.0001293](https://doi.org/10.1061/(ASCE)CO.1943-7862.0001293)
20. Wang, J., Sha, A., Hu, L.: Modelling vibratory roller-soil system dynamics using discrete element method. *Int. J. Eng. Model.* **31**(3), 35–50 (2019). <https://doi.org/10.31534/engmod.2018.3.ri.03m>
21. Derusso, P.M., Roy, R.J., Close, C.M.: *State variables for engineers* (1965). Wiley, New York, 608 p.
22. Phillips, Ch.L., Harbor, R.D.: *Feedback Control Systems* (2010). Pearson, 784 p.
23. Prokopev, A.P., Nabizhanov, Zh.I., Ivanchura, V.I., Emelyanov, R.T.: Modeling the non-destructive control of road surfaces compaction. *J. Phys. Conf. Ser.* **1399**, 044094 (2019). <https://doi.org/10.1088/1742-6596/1399/4/044094>
24. WIRTGEN GROUP Concentrating on the essentials: high quality paving RoadNews. **7**, 28–47 (2019). https://media.voegele.info/media/03_voegele/aktuelles_und_presse/roadnews_magazin/roadnews_07/RadNews_07__en.pdf
25. Liu, G., Tian, J., Xiao, Z., Xu, L., Yu, Y.: Simulation of dynamic character of compacting mechanism of paver. *J. Agric. Mach.* **36**(11), 34–37 (2005)

Modelling and Intelligent Control for Space Exploration

Creation of a Simulation Model of Spacecrafts' Navigation Referencing to the Digital Map of the Moon



Alexey Andreev , Natalya Demina , Yury Nefedyev , Natalya Petrova , and Arthur Zagidullin 

Abstract Currently, at NASA significant attention is paid to the development of an initiative on simulating and studying cyber-physical systems (CPS) (Cyber-Physical Systems Modeling and Analysis (CPSMA) Initiative, https://www.nasa.gov/centers/ames/cct/office/studies/cyber-physical_systems.html). CPS are a new class of physical systems describing the complex models of the behavior of spacecrafts equipped with high-performance software complexes of control and navigation (DRAFT Modeling, Simulation, Information Technology & Processing Roadmap Technology Area 11, https://www.nasa.gov/pdf/501321main_TA11-MSITP-DRAFT-Nov2010-A1.pdf). CPS could therefore be characterized as both hybrid systems combining software and hardware and mechatronic complexes containing electronic and mechanic components. In particular, when implementing space missions, CPS include systems for transforming coordinates and algorithms of spatial navigation referencing that have competitive advantages in the accuracy of parameters, the stability of the interaction between various components of CPS, and the possibility of adaptation to the change in dynamic behavior (DRAFT Robotics, Tele-Robotics and Autonomous Systems Roadmap Technology Area 04, https://www.nasa.gov/pdf/501622main_TA04-Robotics-DRAFT-Nov2010-A.pdf). The creation of simulation models for space navigation that could be used further in CPS is an important and relevant task. This chapter considers the development of the navigation simulation model for the lunar space satellite (LSS) referencing the dynamic reference selenocentric system on the basis of coordinates transformation using the regression modeling. The transformation process includes the generation of a photogrammetrically corrected image and referencing the observed lunar objects to the ones included in the digital maps of the Moon. By the coordinate position of an object observed by the LSS and using the software developed by the authors one calculates and compares altimetry parameters of the given point in relation to known selenocentric reference objects.

A. Andreev (✉) · N. Demina · Y. Nefedyev · A. Zagidullin
Kazan Federal University, Kazan 420008, Russia
e-mail: alexey-andreev93@mail.ru

A. Andreev · N. Petrova
Kazan Power Engineering University, Kazan 420066, Russia

Keywords Simulation regression modeling · Lunar space navigation systems · Digital selenocentric maps

1 Introduction

To implement the upcoming missions on space exploration, the works on Cyber-Physical Systems Modeling and Analysis (CPSMA) have been initiated at NASA [1]. The development of CPSMA aims at creating software applications, technical approaches, and facilities for simulating states of a system and its predicting with the purpose of efficient control and navigation on the basis of physics and dynamic data. Concerning the latter one should mention the following. At the moment, despite the significant progress in determining selenographic parameters by means of spacecrafts, the problem of highly accurate provision of navigation support in the lunar orbit is not yet solved. According to [2], the topography and gravimetry produced during the “LRO” and “GRAIL” space missions, is currently the most accurate, are referenced neither to the terrestrial nor to the celestial coordinate systems, and are only oriented in relation to our natural satellite. The correctness of the results produced at the missions mentioned above was assessed by the value of a spacecraft’s orbits shift concerning the intersection points of these orbits [3]. Thus, it was the reliability of the spacecraft’s orbit model that was estimated, but the referencing was performed to different orbits of the spacecraft. In this connection, the need for data of another kind is quite obvious. One of the options is highly accurate referencing to stars [2]. The approach considered in this work, within which different topography data are brought to the single system and a catalog of lunar reference objects based on the results of modern space projects and referenced to stars is developed, allows creating the selenocentric dynamic reference system. The first results on coordinate referencing to the coordinate system, as which a catalog of craters on both sides of the Moon was used, were obtained by means of photogrammetry methods at the “LRO” project [4]. This chapter considers the opportunity to implement coordinate referencing of the near-Moon spacecrafts to the reference system using the coordinates of objects from the reference catalog.

Currently, the Moon is the subject of many studies in space experiments and the center of attention for scientists in the fields of astronomy and planetary science. The launch of American scientific satellites “Clementine” [5] and “KAGUYA” [6] swiftly and radically changed the situation in the study of the Moon. A powerful stream of high-precision and multi-parameter information received from boards of the modern spacecrafts generated a strong surge of interest and enthusiasm for industrial robotic exploration of the Moon by 2018, and a manned flight to Mars in 2025–2030 after the creation of long-term manned lunar bases. Modern space technologies require accurate coordinate-time support, including reference system construction, the establishment of mutual orientation between inertial and dynamical systems, and study of dynamics and geometry of celestial bodies. This concerns both dynamic and geometric selenocentric parameters.

However, space studies of the Moon performed not only for scientific purposes but for practical ones too, are not provided with the selenocentric coordinate network (catalog of reference objects), adequately covering the near and far sides of the Moon and having a center close to the center of mass. The catalog, based on observations from "Apollo" spacecraft, and the reference networks for the western hemisphere of the Moon, which were obtained by reducing the number of images of the far side of the Moon from "Zond-6" and "Zond-8" spacecrafts, cover only a part of the lunar surface. In work [7] was conducted a detailed analysis of the internal accuracy of the "Apollo" system. Based on this analysis, we can draw the following conclusions. In order to transform the topographical coordinates of the "Apollo" mission, 3 ALSEP stations were used. Since the mean square errors of the transformation were less than ± 80 m and the measurement error was about ± 60 m, one may consider, that the points, which are near and between these 3 ALSEP stations, have position errors less than ± 150 m. The displacement relative to the location of the ALSEP station increases the error up to ± 300 m, and this is a major part of the observed area. The errors of points, lying near the borders of the studied areas, positions can reach ± 300 m and even exceed ± 1000 m.

For the near side of the Moon, there are several coordinate systems, and among them, the most informative one is the dynamics selenocentric catalog (DSC), constructed in Engelhardt Astronomical Observatory (EAO) [8] on the basis of large-scale photographs of the Moon with the stars [9] and space observations. We should notice the 264 craters system, built by [10] in Engelhard Observatory of Kazan. In contrast to DSC, a built-in dynamical coordinate system, Kiev catalog is constructed in the quasi-dynamical coordinate system.

It should also be noted, although the Moon is investigated by spacecrafts, ground-based observations are still relevant, this is why an optimal way of performing selenodetic studies is a reasonable combination of space and ground methods of observations. Both ground and space astrometry is necessary since they complement each other.

When there are the basic selenocentric catalog of coordinates of reference objects from the near side of the Moon (DSC) and a number of catalogs of objects from the librational zone and the far side of the Moon, construction of a unified coordinate system with a center, coinciding with the lunar center of mass, and axes, coinciding with the lunar principal axes of inertia, includes the following steps:

- investigation of systematic and random errors in the DSC catalog;
- compression and expansion of the DSC catalog for the near and the far sides of the Moon as well as for the librational zone.

2 Creation of DSC Selenodetic Network

DSC reference selenodetic network on the surface of the Moon is based on large-scale photographs of the Moon and the stars, obtained by the unique method of separated astroplates [11]. Currently, an almost acceptable way of extending the well-known

selenocentric coordinates catalog DSC, constructed in the system with the lunar center of mass and axes, coinciding with the lunar axes of inertia, in Kazan, for a major part of the lunar surface or, under certain conditions, for its entire sphere, is the application of coordinates transformation matrixes. The elements of the matrixes and the displacement vectors can be obtained from common points for the DSC catalog and another one, being converted into the DSC system.

When extending the DSC (system X), the main problem is the precise determination of orientation matrix's elements and displacement vector of origins during the transition from Y coordinate system to another one by common points you can write a regression model:

$$X = AY + X_0, \quad (1)$$

where A—transition matrix, X_0 – displacement vector of the Y system's origin relative to the zero point of the X coordinate system. The relevance of the exact solution significantly increases, when performing coordinates extrapolation. In our case, it is especially important, since the objects of the far side of the Moon are outside the set of the control points.

Achievement of the highest possible accuracy of transformed system TS is provided by solving the following tasks:

- (a) Justification of the adaptive regression modeling (ARM-approach) application, involving:
 - quality control of the TS model;
 - diagnostics of the observance of the Ordinary Least Squares conditions (particularly, Gauss-Markov conditions);
 - numerical adaptation, when any of the conditions is violated;
- (b) Development of a method to apply the ARM-approach, including:
 - an accuracy criterion for the transition;
 - a set of competing mathematical models of TS;
 - a corresponding set of structural and parametric identification methods;
 - data processing algorithm, providing the model's predictive properties estimates, diagnostics of the conditions' violation, and adaptation in case of violation to achieve the required optical properties of the estimates (consistency, non-displacement property, efficiency).

Within the ARM-approach [12], it is postulated that the matrix model TS (1) is unknown for each pair of catalogs and it should be found among the set of competing ones. In relatively general form, for example, the first equation from (1) may be rewritten in form of the matrix equation of regression:

$$Y = X\beta + \varepsilon, \quad (2)$$

by adding the error matrices ε and considering the first row of the matrix as β vector. Obviously, when performing the structure identification, simultaneously the parameters of the equation, i.e. elements of the vector β in the simple case (2), are being estimated as well.

Due to the presence of errors at coordinates determination, and possible multicollinearity (interdependence) of estimates, the matrix A often does not satisfy the orthogonality condition of the transition from Y to X , written as:

$$ATA = E, \det A = 1. \quad (3)$$

In this regard, the basic deterministic transformation is the Eq. (1), considered together with the conditions (3). In the present chapter this task is solved by the numerical optimization method with an accuracy up to the difference between the centers of Y and X systems and the scale factor.

At this stage, as a competing approximating transformation the model (1) is applied without the conditions (3). Later, when the fundamental DSC is being transformed, the algebraic polynomials of second and third orders as well as two-component descriptions, in which the first component is the deterministic model (1) and conditions (3) and the second one is marked polynomials describing the remains after the first one, are planned to be used. The optimal models were obtained on the basis of ARM-approach.

3 Description of “Transformation Selenodesic Coordinates” (TSC) Software Package

The software package is developed in SharpDevelop 3.2 in C # using the modern programming technologies under OS Windows, such as the PLO, NET, and Windows Forms. The architecture of the program may be divided into two independent parts: the core and the graphical shells. In accordance with an object-oriented programming paradigm (OOP), the core contains classes implementing the basic functionality and graphical shells are responsible for user interaction. Such an architecture simplifies the interaction with other software complexes; for example, the core parts can be moved to other projects.

Graphical shells are based on using API Windows Forms. The shells interact with the user and fix a lot of bugs, related to the user's incorrect actions. Below there is a brief description of the modules forming the core.

Primary data processing modules. Data preparation for solving the basic problem is provided by three modules with the following assignments: the transformation of spherical coordinates into rectangular ones, the transformation of rectangular coordinates into spherical ones, the search for common objects in the rectangular coordinate system.

Deterministic models formation modules. With these modules, the elements of the orientation matrix and the displacement vectors of the centers of the coordinate systems for the model (1), considering the orthogonality conditions (3), are determined by analytical, numerical, and parametric methods.

TS module. It is designed to transform rectangular coordinates from the system Y into X by the orientation matrix A and the displacement vector X₀.

The “Search for optimal regression system” (SORS) package for obtaining approximate descriptions. SORS package in its latest modification is used to obtain approximate models of TS (operating procedures: multiple regressions, step by step regression, complete sorting out, etc.), perform diagnostics of the remains, and implement the adaptation algorithms.

4 Creation Global Catalog for the Full Sphere of the Moon in the DSC System

Catalog DSC was constructed in the system with the lunar axes, coinciding with the lunar axes of inertia and its center of mass. The method for extension DSC to the whole lunar sphere is coordinating transformation matrixes. DSC is based on large-scaled lunar astroplates in stars system obtained by the unique approach of separated images [5]. For transformed into DSC system the displacement vectors and elements of the matrixes should be obtained from common points for the researched catalog and DSC.

As result, 12 catalogs have been transformed into DSC system: AMS, ACIC, Baldwin, ARTHUR, Goloseevo-1 and -2, MILLS-2, Kiev, SCHRUTKA-1 and -2, ULCN 2005 [6] and the Valeev catalog [7] using displacement vectors X₀ (regression model (1) under conditions (3)) and orientation of A matrixes use the orthogonality conditions and the numerical approach. The efficiency of the orthogonal model TS has been obtained by comparing the results from the model (1) without orthogonality consideration. The model (1) is the regression approximating transformation as algebraic polynomial having the first order.

When solving a problem, the following steps have been made:

1. analysis and study of ULCN basic network accuracy;
2. determination of common objects for the coordinate systems being processed;
3. development of mathematical support for the TSC software package.

A regression method for creating the global system of selenographic coordinates. When developing a method for bringing selenographic data to the single system the following approaches were used. The observational data produced during the processing was estimated using the regression model [8]:

$$AX = AY + X_0 + \varepsilon, \quad (4)$$

where \mathbf{X} —matrix of the final transformed system of different observations; \mathbf{Y} —matrix of the initial observational system; \mathbf{A} —orientation matrix; \mathbf{X}_0 —shifts matrix; \mathbf{e} —errors' matrix.

The system of Eq. (4) was solved within regression adaptive modeling (RAM) at which LSM-conditions compliance is checked, and the applicability of numerical adaptive procedures is studied if the conditions are not observed. The robustness of the estimations produced was provided by the presence of a spectrum of regression models and by taking into account multiple scenarios of data processing depending on quality measures of the constructed models.

The transformation of the reference network and an increase in the number of reference objects are implemented according to the expression as follows:

$$A \times \theta + \vec{\varepsilon} = Z, \tag{5}$$

where $\mathbf{A}(A_{ij})$ —orientation matrix, $\Theta(\Delta\xi, \Delta\eta, \Delta\zeta)$ —origin's shift matrix in relation to $\vec{\varepsilon}$.

Within the RAM approach, it is postulated that the type of coordinate transformation for the model (5) is unknown for each pair of coordinate systems and could be determined according to the competing characteristics being set [9]. For the general case, the relation (5) could be brought to the regression type:

$$Y = X \vec{\beta} + \vec{\varepsilon}, \tag{6}$$

where $\vec{\varepsilon}$ —errors matrix, $\vec{\beta}$ —the first row of the orientation matrix \mathbf{A} .

The orientation matrix \mathbf{A} in many cases does not correspond to the orthogonality transformation criteria from \mathbf{Y} to \mathbf{X} due to errors arising when coordinates of the objects from both systems are determined. At the same time, the following condition must be satisfied:

$$A^T A = E, \det A = 1. \tag{7}$$

The relation (6) together with the condition (7) allows performing the general deterministic coordinates transformation. This problem may be solved by the method of mathematic programming.

The desired parameters $\Theta(\Delta\xi, \Delta\eta, \Delta\zeta)$ are determined as:

$$\Theta = (A^T P A)^{-1} (A^T P Z), \tag{8}$$

and their errors are determined by the expression:

$$D(\Theta) = \frac{V^T P V}{2n - 3} (A^T P A)^{-1}, \quad (9)$$

where V —residual deviations matrix.

5 Determination of the Position of the Moon's Center of Mass Concerning Its Figure Based on Expansion into Spherical Functions and the Use of Harmonic Multi-parameter Analysis

The next stage of the study was the analysis of the origin of DCLRO in relation to the Moon's center of mass (CM) and the center of symmetry (CS). Altimetry from DCLRO was expanded into a series of spherical functions:

$$h(\lambda, \phi) = \sum_{n=0}^N \sum_{m=0}^n \left(\bar{C}_{nm} \cos m\lambda + \bar{S}_{nm} \sin m\lambda \right) \bar{P}_{nm}(\cos\phi) + \varepsilon, \quad (10)$$

where λ, ϕ —selenocentric longitude and latitude of a reference object, $\bar{C}_{nm}, \bar{S}_{nm}$ —normalized harmonic parameters; \bar{P}_{nm} —normalized associated Legendre polynomials; ε —random regression error.

The shift in the geometric center of the Moon (GCM) in relation to its center of mass was calculated through harmonic parameters of the first order:

$$\Delta\xi = \sqrt{3}\bar{C}_{11}, \Delta\eta = \sqrt{3}\bar{S}_{11}, \Delta\zeta = \sqrt{3}\bar{C}_{10}, \quad (11)$$

where $\Delta\zeta$ —GCM shift along the axis directed to the Earth; $\Delta\xi$ —GCM shift along the axis perpendicular to ζ and lying in the equator plane; $\Delta\eta$ —GCM shift along the axis of lunar rotation; $\bar{C}_{11}, \bar{S}_{11}, \bar{C}_{10}$ —harmonic parameters of the first order in (10).

Based on (10) and (11) the positions of the origin for the systems built on the data from “Selene”, “Clementine”, and DCLRO are determined.

The results presented in Table 1 indicate that the parameters of DCLRO, “Clementine”, and “Selene” models match well. DCLRO is therefore dynamic and may be applied when selenographic navigation problems are solved.

Table 1 Coordinates of CS in relation to CM for 3 regression models

Shift	Clementine	Selene	DCLRO
$\Delta\xi$	-1.82	-1.78	-1.59
$\Delta\eta$	-0.72	-0.76	-0.79
$\Delta\zeta$	-0.62	0.25	0.43

6 The Method of Orbital Spacecraft Selenographic Referencing to the Selenocentric Coordinate System

The implementation of the method of orbital spacecraft selenographic referencing to the selenocentric coordinate system on the basis of DCLRO was performed within the simulation model of navigation support. The simulation model represents a software package providing an opportunity to form a digital model and compare it with the digital map of the Moon. The developed method is based on the assumption that reference points located close to each other are characterized by a higher similarity. The search for the altimetry component of the investigated point is based on the analysis of neighboring points located in the close vicinity of the desired point. Taking into account the uneven distance between neighboring points is implemented by assigning them weight coefficients:

$$\widehat{Z}(S_0) = \sum_{i=1}^N \lambda_i Z(S_i), \tag{12}$$

Where

- $\widehat{Z}(S_0)$ the investigated altimetry component of the point S_i ;
- λ_i points' weight coefficients decreasing when moving away from the investigated points;
- $Z S_i$ measured value of altimetry component at the point;
- N the number of points located in the vicinity of the investigated point and involved in the calculation.

The weight coefficients are calculated according to the expression:

$$\lambda_i = \frac{d_{i0}^{-p}}{\sum_{i=1}^N d_{i0}^{-p}}, \tag{13}$$

where d_{i0} —distance from the investigated point S_0 to the reference point with index i S_i .

The exponent p influences the weight assigned to the reference object (point): when the distance to the investigated point increases, the weight coefficient decreases exponentially.

Based on the method described above one may implement navigation referencing of the desired points on the lunar surface and the position of a spacecraft to the selenocentric dynamic coordinate system based on the catalog of reference point created within this work.

7 Conclusion

The analysis of the method for creating a navigation network in the lunar orbit has shown that the modern selenographic models are not equally accurate and the data presented in these models refer to different reference systems [13]. For these reasons, it seems necessary to apply complex approaches of CPS for the hybrid combination [14] of space photogrammetry and ground-based observational material under the condition of highly accurate accounting physical libration. The simulation model of coordinate support allows performing modeling for the determination of navigation positions of the desired objects on the Moon's surface using on-board goniometrical measurements with laser interferometer from the board of the spacecraft and the spacecraft itself using the measurements from the surface of the Moon [15, 16]. As a result, a digital catalog of lunar reference objects (DCLRO) is created using 12 catalogs of reference objects on the lunar surface. DCLRO contains over 274 thousand Cartesian coordinates for the reference points produced by means of various observation methods and brought to the single selenographic coordinate system. To work with DCLRO, a specialized software allowing the user to select altimetry and compare it with the digital map of the lunar surface is developed in Matlab. The user gets the data set being investigated as a cube or sphere covering the chosen area. It should be noted that the least number of objects from DCLRO corresponds to the areas that are close to the poles. The comparative analysis of the regression topography models constructed on the bases of data from the modern satellite lunar missions has allowed assessing the accuracy of coordinates of the desired objects on the lunar surface. It is revealed that navigation support for the near side of the Moon is more accurate than for the far side. The obtained results and advantages of using CPS [17] when developing navigation support for the lunar missions are (1) capacities on the control of spacecrafts and prediction of their physical and technical parameters over long time interval are extended; (2) the possibility of checking adaptation and stability for CPS of hybrid systems [18] for spacecraft is considered [19, 20]; (3) the creation of local systems for the work in complex environments remote from the Earth [21, 22]; (4) the recognition and use of local conditions without assistance; for achieving the high level of space missions safety [23].

Acknowledgements This work was partially supported by the Russian Science Foundation, grants no. 20-12-00105 (according to the grant, the method for data analysis was created) and 19-72-00033 (according to the grant, the numerical calculations were carried out). This paper has been supported by the Kazan Federal University Strategic Academic Leadership Program. This work was partially supported by the Russian Foundation for Basic Research grant 19-32-90024 and the Foundation for the Advancement of Theoretical Physics and Mathematics "BASIS".

References

1. Cyber-Physical Systems Modeling and Analysis (CPSMA) Initiative, https://www.nasa.gov/centers/ames/cct/office/studies/cyber-physical_systems.html. Accessed 05 Apr 2020
2. Nefedjev, Y., Valeev, S., Mikeev, R., Varaksina, N., Andreev, A.: Analysis of data of “CLEMANTINE” and “KAGUYA” missions and “ULCN” and “KSC-1162” catalogues. *Adv. Space Res.* **50**(11), 1564–1569 (2012)
3. Konopliv, A., Park, R., Yuan, D.N., Asmar, S., Watkins, M., Williams, J., Fahnestock, E., Kruizinga, G., Paik, M., Strelkalov, D., Harvey, N., Smith, D., Zuber, M.: The JPL lunar gravity field to spherical harmonic degree 660 from the GRAIL primary mission. *J. Geophys. Res. Planets* **118**(7), 1415–1434 (2013)
4. Binder, A.B.: Lunar prospector: overview. *Science* **281**(5382), 1475–1476 (1998)
5. Smith, D.E., Zuber, M.T., Neumann, G.A., Lemoine, F.G.: Topography of the moon from the clementine lidar. *J. Geophys. Res. Planets* **102**(E1), 1591–1611 (1997)
6. Araki, H., et al.: Lunar global shape and polar topography derived from Kaguya-LALT laser altimetry. *Science* **323**(5916), 897–900 (2009)
7. Selenocentric geodetic reference system, https://repository.library.noaa.gov/view/noaa/18063/noaa_18063_DS1.pdf. Accessed 05 Apr 2020
8. Rizvanov, N.G., Nefed'ev, Y.A., Kibardina, M.I.: Research on selenodesy and dynamics of the Moon in Kazan. *Solar Syst. Res.* **41**(2), 140–149 (2007)
9. Nefedjev, Y.A., Rizvanov, N.G.: The results of an accurate analysis of EAO charts of the Moon marginal zone constructed on the basis of lunar occultations. *Astronomische Nachrichten: Astronomical Notes* **323**(2), 135–138 (2002)
10. Habibullin, S.T., Risvanov, N.G.: Independent selenocentric system of coordinates by large-scale star-calibrated lunar photography. *Earth Moon Planet.* **30**(1), 1–19 (1984)
11. Rizvanov, N., Nefedjev, J.: Photographic observations of solar system bodies at the Engelhardt astronomical observatory. *Astron. Astrophys.* **444**(2), 625–627 (2005)
12. Valeev, S.G.: Regression modelling in selenodesy. *Earth Moon Planet.* **35**(1), 1–5 (1986)
13. Garcia, R.F., Gagnepain-Beyneix, J., Chevrot, S., Lognonné, P.: Very preliminary reference Moon model. *Phys. Earth Planet. Inter.* **188**(1–2), 96–113 (2011)
14. Michniewicz, J., Reinhart, G.: Cyber-physical robotics—automated analysis, programming and configuration of robot cells based on cyber-physical-systems. *Proc. Technol.* **15**, 566–575 (2014)
15. Bagrov, A.V., Leonov, V.A., Mitkin, A.S., Nasyrov, A.F., Ponomarenko, A.D., Pichkhadze, K.M., Sysoev, V.K.: Single-satellite global positioning system. *Acta Astronaut.* **117**, 332–337 (2015)
16. Shirenin, A.M., Mazurova, E.M., Bagrov, A.V.: Development of a high-precision selenodetic coordinate system for the physical surface of the Moon based on LED beacons on its surface. *Cosm. Res.* **54**(6), 452–457 (2016)
17. Potteiger, B., Zhang, Z., Koutsoukos, X.: Integrated moving target defense and control reconfiguration for securing cyber-physical systems. *Microprocess. Microsyst.* **73**, 102954 (2020)
18. Abdel-Aziz, H., Koutsoukos, X.: Data-driven online learning and reachability analysis of stochastic hybrid systems for smart buildings. *Cyber-Phys. Syst.* **5**(1), 41–64 (2019)
19. Unified Lunar Control Network 2005 and Topographic Model, <https://ntrs.nasa.gov/archive/nasa/casi.ntrs.nasa.gov/20050165143.pdf>. Accessed 05 Apr 2020
20. Valeev, S.G.: Coordinates of the Moon reverse side sector objects. *Earth Moon Planet.* **34**(3), 251–271 (1986)
21. Valeev, S., Samokhvalov, K.: The ARM-approach based local modelling of the gravitational field. In: *International Conference on Computational Science*, pp. 471–480. Springer, Berlin, Heidelberg (2003)

22. DRAFT Modeling, Simulation, Information Technology & Processing Roadmap Technology Area 11. https://www.nasa.gov/pdf/501321main_TA11-MSITP-DRAFT-Nov2010-A1.pdf. Accessed 05 Apr 2020
23. DRAFT Robotics, Tele-Robotics and Autonomous Systems Roadmap Technology Area 04. https://www.nasa.gov/pdf/501622main_TA04-Robotics-DRAFT-Nov2010-A.pdf. Accessed 05 Apr 2020

Information Technology Concept of Integration of Computing Resources and Physical Processes in Cyber-Physical Systems for Personalized Information About the Potential Danger of an Emergency Situation in High-Altitude Flight



Nikolai Markov, Alexey Bogomolov, Anatoly Shishov,
and Mikhail Dvornikov

Abstract The chapter presents an information technology concept for integrating aircraft computing resources into the physical processes of personalized informing passengers of civil aviation aircraft about the potential danger of an emergency in high-altitude flight, based on the calculation of estimates of the reserve time of consciousness preservation by a person in real time using technologies of the fourth industrial revolution.

Keywords Aviation cyber-physical system · Backup time of consciousness preservation · Hypoxia · Backup time indicator · Aviation oxygen mask · High-altitude flight emergency · Fourth industrial revolution

N. Markov (✉)

Scientific and Production Association “Topaz”, 16, 3rd Mytischinskaya street, Moscow 129626, Russia

e-mail: nikolya.markov.1987@mail.ru

A. Bogomolov

Saint Petersburg Institute of Informatics and automation of the Russian Academy of Sciences, 39, line 14 of Vasilievsky island, Saint Petersburg 199178, Russia

e-mail: a.v.bogomolov@gmail.com

A. Shishov

State Scientific Center of the Russian Federation-Institute of Medical and biological problems of the Russian Academy of Sciences, 76 a, Khoroshevskoe highway, Moscow 123007, Russia

e-mail: aashishov@yandex.ru

M. Dvornikov

Central Research Institute of the air force of the Russian Ministry of Defense, 12-A, Petrovsko-Razumovskaya alley, Moscow 127083, Russia

e-mail: dvormv@yandex.ru

© The Author(s), under exclusive license to Springer Nature Switzerland AG 2021

A. G. Kravets et al. (eds.), *Cyber-Physical Systems: Modelling and Intelligent*

Control, Studies in Systems, Decision and Control 338,

https://doi.org/10.1007/978-3-030-66077-2_16

1 Introduction

Solving the problem of ensuring the safety of passengers and crew in an emergency situation of high-altitude flight requires the development and implementation of alarm systems and information about the danger of an emergency in real time [1]. In accordance with the current level of scientific and technological progress, such systems should be implemented on the basis of an information technology concept that implies the integration of computing resources into physical processes—that is, they are implemented as cyber-physical systems [2–6]. In a cyber-physical system, sensors, equipment, and information components are connected throughout the chain of information collection and processing, interacting with each other to predict, self-tune, and adapt to changes in the situation [7–9].

To ensure the safety of aircraft passengers in high-altitude flight emergencies, cyber-physical alarm systems and real-time emergency notification systems must include protective equipment—primarily oxygen masks.

Numerous variants of aviation oxygen masks and sets of oxygen equipment for aircraft crews are known—their main drawback is that the design does not fully take into account the key technological trends underlying cyber-physical systems [10–14]. Such technologies will increase safety in high-altitude flight emergencies by providing personalized notification of aircraft passengers about the potential danger of a high-altitude flight emergency in the dynamics of its development.

Special cyber-physical systems have been developed to provide personalized information to passengers about the danger of an emergency situation on Board an aircraft in high-altitude flight. The personification of informing passengers of a civil aviation aircraft using such a system is provided by ensuring that individual anthropometric characteristics are taken into account when calculating the value of the reserve time for preserving consciousness by a person under hypoxic hypoxia.

2 Method for Calculating the Estimation of the Reserve Time of Consciousness Preservation in an Emergency High-Altitude Flight

Situations associated with the rapid impact on a person of an environment with a low oxygen content in the surrounding air lead to the development of hypoxic States in a person, which cause a high risk of loss of consciousness by a person until his death [1, 15].

The solution of this problem requires assessment of the risk of loss of consciousness of a person, taking into account the influence of the hypoxic environment on the human body. Well-known mathematical models allow us to calculate such an estimate under static conditions, that is, while maintaining a constant intensity of hypoxic exposure during the analyzed time interval, which significantly limits the

scope of their application. This disadvantage can be overcome by applying theoretical approaches to normalizing the impact of hypoxic gas environment on the human body and modeling hypoxic States based on the dose principle [1, 16–18].

It should ensure the integration of computing resources (no electronic computers) aircraft in the physical processes of personalized information about a potential hazard emergencies in high-altitude flight, implemented by using embedded sensors barometric pressure, information displays, microprocessors, LEDs, connected in the chain of collecting and processing information and interacting to predict self-adjustment and adaptation in the dynamics of development of emergency.

Analytically, “hypoxia dose” is defined by the expression

$$D(t) = \int_0^T [p_{6500}^m - p^m(t)] dt,$$

where $D(t)$ —exposure dose of hypoxic exposure, $p_{6500}^m = 37,8 \text{ кПа}$ —partial pressure of oxygen in the trachea at a barometric pressure of 44 kPa (corresponding to an altitude of 6.5 km above sea level), $p^m(t)$ —current value of partial pressure of oxygen in the trachea, T —integration interval.

The partial pressure of oxygen in the trachea is related to the barometric pressure dependence

$$p^m = F(p - p_{H_2O}),$$

where F —relative oxygen concentration in the atmosphere ($F = 0,21$), p —barometric pressure, p_{H_2O} —the partial pressure of saturated water vapor at a temperature of 310 K, equal to 6,27 кПа.

In numerical integration, the expression for hypoxia dose can be written as

$$D = \sum_{i=1}^n [0 - (t_i)] \Delta t,$$

where $t_i = i \Delta t$, a difference $p_{6500}^m - p^m(t)$ defined as the intensity of hypoxic exposure (U).

In altitude physiology [1, 16, 17], empirical results have been obtained that allow us to calculate estimates of the minimum (T_{min}^{nc}), average (T_{mean}^{nc}) and maximum (T_{max}^{nc}) reserve time for maintaining consciousness when a person is at different altitudes (at different barometric pressure).

Using these data, the Levenberg–Marquardt method synthesized regression equations describing the dependence of the time of consciousness preservation on the intensity of hypoxic exposure. These equations have the following form

$$T_{min}^{nc} = 186,15 U^{-1,0003}, T_{mean}^{nc} = 367,23 U^{-1,0008}, T_{max}^{nc} = 710,37 U^{-1,1557}.$$

The statistical significance of the synthesized equations according to the Fisher criterion corresponds to the significance level $p < 0.001$.

Taking into account the results of structural identification of the laws of distribution of reserve time of loss of consciousness analytical expressions are obtained for calculating estimates of probabilities of loss of consciousness W^{nc}_U depending on the time t of stay in a hypoxic gas environment, the intensity of which is constant, i.e. $U = const$:

$$W_U(t) = \begin{cases} 0,5 - \Phi \left[3,224 \frac{t_i - T_{i mean}^{nc}(U)}{T_{i mean}^{nc}(U) - T_{i min}^{nc}(U)} \right], & \text{if } (t_i - T_{i mean}^{nc}(U)) \leq 0 \\ 0,5 - \Phi \left[3,224 \frac{t_i - T_{i mean}^{nc}(U)}{T_{i max}^{nc}(U) - T_{i mean}^{nc}(U)} \right], & \text{if } (t_i - T_{i mean}^{nc}(U)) > 0; \end{cases}$$

where Φ —Laplace function.

The parameters of this mathematical model are determined under the condition of constant barometric pressure during the entire time of a person's stay in the gas environment, which makes it difficult to use it in relation to dynamic conditions. However, the dose approach allows us to overcome these difficulties due to the fact that, having determined the dose of hypoxia in accordance with the change p^m and dividing its value by the measurement time, the value is calculated

$$\Delta P = D / \sum_{i=1}^n i \Delta t,$$

equivalent to the received dose of hypoxia under the condition of constant partial pressure of oxygen in the trachea (flight at a constant altitude), and, therefore, uniquely associated with it by barometric pressure and altitude above sea level. Then the equivalent dose the value of the partial pressure of oxygen in the trachea is equal to

$$P_e^m = DP_e^m + P_0^m.$$

This value is used for dynamic calculations of estimates of the reserve time of consciousness preservation T^{nc}_{min} , T^{nc}_{mean} , T^{nc}_{max} at all stages of the flight.

By defining the values of these parameters and knowing the current time $t_i = i \Delta t$, estimates of the probability of loss of consciousness are calculated.

Coefficients of expressions approximating dependencies of quantities T^{nc}_{min} , T^{nc}_{mean} , T^{nc}_{max} from U , equal to the doses of hypoxic exposure corresponding to the specified tolerance times of hypoxic exposure. Taking these values into account, a model was synthesized that allows determining the probability of loss of consciousness depending on the hypoxia dose at any time t_i

$$W_D(t) = \begin{cases} 0, 5 - \Phi \left[\frac{3, 224 \sum_{i=1}^n U(t_i)^\alpha \Delta t - 367, 23}{181, 01} \right], & \text{if } \sum_{i=1}^n U(t_i)^\alpha \Delta t - 367, 23 \leq 0 \\ 0, 5 - \Phi \left[\frac{3, 224 \sum_{i=1}^n U(t_i)^\alpha \Delta t - 367, 23}{343, 14} \right], & \text{if } \sum_{i=1}^n U(t_i)^\alpha \Delta t - 367, 23 > 0 \end{cases}$$

$$\alpha = 1 + 0, 000454 \sum_{i=1}^n U(t_i) \Delta t - 367, 23,$$

where $\sum_{i=1}^n U(t_i)^\alpha \Delta t$ —current value of the hypoxia dose at a time t_i , Δt —the time interval after which the dose is determined, n —number of dose measurements.

The methodology of the dose approach and its mathematical support allow us to calculate the time of preservation of human consciousness in conditions of hypoxic hypoxia and its recovery after loss of consciousness caused by hypoxia. The time of the beginning of recovery of human consciousness is the moment when the sign of the hypoxia dose changes, and the time of full recovery of consciousness is the moment when the modulus of positive and negative doses of hypoxia is equal.

This approach provides the calculation of adequate estimates of the probabilities of the considered adverse effects at any values of the rates and profiles of changes in the partial pressure of oxygen in the trachea, multiplicity, and time of exposure to the hypoxic environment.

The developed method provides the possibility of communication between the computational and physical elements of a complex system for ensuring safety in emergency situations in high-altitude flights, providing the possibility of implementing a distributed cyber-physical system for personalized information about the danger of an emergency in high-altitude flight [19–22].

3 Cyber-Physical System for Personalized Information About the Danger of an Emergency in High-Altitude Flight

Cyber-physical system personalized on the dangers of emergency in high-altitude flight was developed in two versions: cyber-physical system integration aviation oxygen masks and cyber-physical systems integration of aircraft passenger seats. The construction of these cyber-physical systems is based on the information technology concept of integrating aircraft computing resources into the physical processes of personalized information about the potential danger of an emergency in high-altitude flight.

The functioning of the developed cyber-physical system, which combines barometric pressure sensors, a microprocessor, an information Board, a comparator, a wireless interface unit, a multi-mode led and an oxygen mask connected to oxygen equipment, is as follows. In an emergency situation of high-altitude flight, the oxygen mask falls out of a special compartment on Board the aircraft and “hangs” in front of the passenger. At the same time, the continuous supply of oxygen to the mask is

switched on and excessive pressure is created in it. The passenger “pulls” the mask and presses it to the face.

Due to the presence of excessive pressure in the mask, its obturator, acting on the principle of a petal, is pressed to the face and provides the necessary hermetic fit of the mask. During exhalation, the excess pressure in the mask increases to a value higher than the pressure exerted by the membrane on the saddle mask, so flap exhalation valve and the membrane valve exhalation away from the saddle, and exhaled mixture released to the environment. Since the horizontal bands of the human nose contour shaper in the mask are compressed according to the shape of the user’s nose, and due to the shape of the lower part of the frame, which deeply covers the chin, the thickness of the frame cloth ensures ergonomically comfortable use of the mask.

In the mask integrated indicator backup time of preservation of consciousness, including the body, the walls of which are flush the outer surface of the integrated barometric pressure sensor, and a display for presenting the backup time of preservation of the consciousness of man, and the outer wall of the housing opposite the outer wall with a built-in scoreboard, equipped with a mount, and the output of the barometric pressure sensor is connected to the storage devices connected to the computer, the output of which is connected to the comparator, which is connected to the scoreboard and block the wireless interface. The estimation of the reserve time of consciousness preservation is performed using the algorithms described above.

While using the indicator, the user is informed of the masks were-the rank of standby time saving consciousness without the use of a mask, which is displayed on the display part of the indicator and the built-in mask flush its external surface so that the indicator was visible to the user of the mask, and the barometric pressure in the surrounding gaseous environment to provide objective check the measured values of barometric pressure (the outer surface of the sensor must not overlap components, masks, etc.) [23–25].

In addition, to further inform the Maxi user about the danger of an emergency in high-altitude flight, an led with at least three modes of illumination (green, yellow, red) is embedded in the mask. The led is embedded in the mask sharp its outer surface so that it is visible to the user of the mask, and is connected to a computer that controls the modes of illumination of the led depending on the calculated value of the reserve time of consciousness preservation.

After the mask falls out, readings are taken from the barometric pressure sensor in the surrounding gas environment at a frequency of 10 Hz (10 times per second).

The values of the barometric pressure in the environment from the sensor are sent to the data storage device, which is a shift register of 300 cells. In other words, the storage device can store no more than 300 barometric pressure measurements at a time (which corresponds to measurements every second for 5 min)—301 measurements are recorded instead of the first, 302 measurements are recorded instead of the second, and so on.

After entering the information storage of the results of the first 300 measurements of barometric pressure in the surrounding gas medium in the dynamic calculator start calculating backup time preserving the consciousness of a person (t, s), taking into

account height, weight and width of the back, taken into account in estimating the reserve time of preservation consciousness as indicators of lung capacity.

The height estimation of the mask user is defined as the difference between the readings of the laser rangefinder (for example, based on the VL53L0X chip) in the absence and presence of a passenger in the seat, followed by recalculation of the sitting height to the standing height according to [16].

The body weight is estimated using the built-in strain gauge in the seat of the chair. The force of the body's impact on the seat causes the built-in spring or beam load cell to deform. The degree of this deformation gives information about the body weight.

The passenger's back width is estimated using pyroelectric infra-red sensors (for example, Diymore AM312), which are equidiscrately integrated into the passenger's seat back—the back width corresponds to the width of the strip of simultaneously “triggered” sensors.

The personalized estimate of the reserve time of consciousness preservation, calculated taking into account the height, body weight and back width, is displayed in the digital digits of the indicator Board and determines the led light mode.

The calculation of the reserve time estimation based on the mathematical apparatus for describing the hypoxia dose in the form of an integral of the intensity of hypoxic impact within the time of action of this flight factor allowed us to move into the dynamic field of research of the effects of hypoxic gas environment and assess its impact on the human condition when the intensity of hypoxic impact changes over time, which is essential in an emergency situation of high-altitude flight.

Based on the values of the reserve time of consciousness preservation and on the glow of the led, the passenger of an aircraft in an emergency high-altitude flight can assess the real danger of being without a oxygen mask, for example, when performing an action to help other passengers, moving around the cabin of the aircraft, etc.

Passengers' awareness of the real danger of an emergency in extreme conditions of high-altitude flight, in addition, contributes to maintaining calm, which is essential for ensuring safety in an emergency.

The functioning of the developed cyber-physical system, which combines barometric pressure sensors, a microprocessor, an information Board, a comparator, a loudspeaker, a wireless interface unit, a multi-mode led and an aircraft passenger seat, consists of the following.

An aviation passenger seat contains a seat, a back with a headrest, and armrests. To build a cyber-physical system, a tableau is built into the back of the seat, and a barometric pressure sensor and a loudspeaker are built into the headrest, which is flush with its surface, connected to a microprocessor fixed inside the seat, the output of which is connected to the tableau.

During the flight, as in the previous case, the readings are taken from the barometric pressure sensor in the surrounding gas environment at a frequency of 10 Hz (10 times per second). The values of barometric pressure via the information control bus are sent to the microprocessor, which calculates the estimate of the reserve time of preservation of consciousness by a person in hypoxia and generates audio information for playback through a loudspeaker.

If the calculated estimate of the reserve time of consciousness preservation is less than 300 s, then a signal is given to turn on the tableau and the speaker. At the same time, in digital digits, the indicator displays the calculated estimate of the initial time of preservation of consciousness by a person, which changes in real time with a discreteness equal to the frequency of measurement of barometric pressure in the surrounding gas environment. The inscriptions in Russian and English are highlighted simultaneously with the inclusion of the tableau and with the appearance of a calculated estimate of the reserve time of consciousness preservation. Audio information about the amount of time reserved for consciousness preservation is given out alternately in Russian and English via the loudspeaker. If the calculated estimate of the reserve time of consciousness preservation becomes greater than or equal to 300 s when the tableau and speaker are switched on, a signal is issued to turn off the tableau and speaker.

The passenger in the seat sees the information on the display Board that is part of the seat in front of him, and hears the information through a loudspeaker—this ensures that passengers are informed of the potential danger of the situation due to the risk of hypoxia.

The presence of a wireless interface block as part of cyber-physical systems (in the two described versions of their implementation) makes it possible to transfer estimates of the reserve time of consciousness preservation to the crew and ground services in order to develop and implement a rational strategy of actions in terms of planning the flight path of the aircraft, determining the need and level (first, qualified, specialized) of the required medical care, etc.

4 Conclusion

The results of the research allow for the first time to implement an innovative personalized approach to personalized riskmetry and personalized information about the potential danger of a high-altitude flight emergency in real time based on the concept of cyber-physical systems.

The developed approach and the cyber-physical systems implementing it will be used on aircraft that have a risk of depressurization of the cabin and/or cabin; when conducting tests in pressure chambers with the participation of volunteers, when staying in high-altitude conditions, and when solving other practical tasks related to ensuring the safety of human activity in conditions associated with hypoxia.

The described information technology concept of integrating aircraft computing resources into the physical processes of personalized information about the potential danger of an emergency in high-altitude flight undoubtedly has wide practical applications in the field of ensuring the safe operation of complex cyber-physical systems in extreme conditions.

Acknowledgements This work was supported by a grant from the President of the Russian Federation for state support of leading scientific schools of the Russian Federation (NSh-2553.2020.8).

References

1. Shishov, A.A., Bogomolov, A.V.: (2020) Physiological justification of an adequate way out of an emergency situation in high-altitude flight. *Aerospace and Environmental Medicine* **54**(2), 65–71 (2020)
2. Kravets, A.G., Bolshakov, A.A., Shcherbakov, M.V. (Eds.): *Cyber-Physical Systems: Advances in Design & Modelling* (2019). Springer, 340 p. <https://doi.org/10.1007/978-3-030-32579-4>
3. Kizim, A.V., Kravets, A.G.: On systemological approach to intelligent decision-making support in industrial cyber-physical systems. In: *Cyber-Physical Systems: Industry 4.0 Challenges. Studies in Systems, Decision and Control*, vol. 260 (2020). Springer, Cham, pp. 167–183
4. Chueshev, A.V., Melekhova, O.N., Meshcheryakov, R.V.: Cloud robotic platform on basis of fog computing approach. In: *Lecture Notes in Computer Science*, 11097 LNAI (2018), pp. 34–43. https://doi.org/10.1007/978-3-319-99582-3_4
5. Wang, F., Mei, X., Rodriguez, J., Kennel, R.: Model predictive control for electrical drive systems—an overview. *CES Trans. Electric. Mach. Syst.* **1**(3), 219–230 (2017)
6. Brown, D.E., Abbasi, A., Lau, R.Y.-K.: Predictive analytics: predictive modeling at the micro level. *IEEE Intel. Syst.* **30**(3), 6–8 (2015)
7. Kravets, A.G., Bolshakov, A.A., Shcherbakov, M.V. (eds.): *Cyber-physical systems: industry 4.0 challenges* (2019). Springer, 334 p. <https://doi.org/10.1007/978-3-030-32648-7>
8. Larkin, E., Bogomolov, A., Gorbachev, D., Privalov, A.: About approach of the transactions flow to Poisson one in robot control systems. In: *Lecture Notes in Computer Science*, vol. 10459 LNAI (2017). Springer, GmbH, pp. 113–122. https://doi.org/10.1007/978-3-319-66471-2_13
9. Meshcheryakov, R.: Control of hyperlinked cyber-physical systems. In: *Smart Innovation, Systems and Technologies* (2020). Springer, pp. 27–33
10. Elugachev, P., Shumilov, B.: Development of the technical vision algorithm. In: *MATEC Web of Conferences*, vol. 216, 04003 (2018); *Polytransport Systems* (2018), 7 p.
11. Mehcheryakov, R.V., Galin, R.R.: Review on human–robot interaction during collaboration in a shared workspace. In: *Interactive Collaborative Robotics ICR-2019. LNCS*, vol. 11659 (2019). Springer, Cham, Stambul, pp. 63–74
12. Mehcheryakov, R.V., Galin, R.R.: Human-robot interaction efficiency and human-robot collaboration. *Stud. Syst. Decis. Control* **272**, 55–63 (2020)
13. Bogomolov, A.V., Sviridyuk, G.A., Keller, A.V., Zinkin, V.N., Alekhin, M.D.: Information-logical modeling of information collection and processing at the evaluation of the functional reliability of the aviation ergate control system operator. In: *Proceedings of 2018 International Conference on Human Factors in Complex Technical Systems and Environments (ERGO)* (2018). Piscataway, NJ, United States, pp. 106–110
14. Kotenko, I.V., Parashchuk, I.B.: Analysis of the sensitivity of algorithms for assessing the harmful information indicators in the interests of cyber-physical security. In: *Cyber-Physical Systems*, Published: 4 March 2019 in *Electronics*, Special Issue, vol. 8, No. 3 (2019), pp. 1–15
15. Ushakov, I.B., Bogomolov, A.V., Kukushkin, Yu.A.: Methodological aspects of dynamic control of functional States of operators of dangerous professions. *Medico-Biol. Socio-Psychol. Probl. Saf. Emerg. Situations* **4–2**, 6–12 (2010)
16. Matyushev, T.V., Dvornikov, M.V.: (2017) Analysis of human respiratory reactions in a modified gas environment on a mathematical model. *Comput. Res. Model.* **9**(2), 281–296 (2017)
17. Matyushev, T.V., Dvornikov, M.V., Bogomolov, A.V., Kukushkin, Yu.A., Polyakov, A.V.: (2014) Mathematic modeling of the dynamics of human gas exchange indicators in hypoxia. *Math. Model.* **26**(4), 51–64 (2014)
18. Larkin, E., Bogomolov, A., Privalov, A.: Data buffering in information-measuring system. In: *Proceedings—2017 2nd International Ural Conference on Measurements, UralCon-2017* (2017), pp. 118–123
19. Ushakov, I.B., Bogomolov, A.V., Kukushkin, Yu.A.: (2014) Psychophysiological mechanisms of formation and development of functional states. *Russ. J. Plant Physiol.* **100**(10), 1130 (2014)

20. Jennings, N.R., Wooldridge, M.J. (eds.): *Agent Technology: Foundations, Applications, and Markets* (2012). Springer, Heidelberg, 325 p.
21. Vasiliev, S.S., Korobkin, D.M., Kravets, A.G., Fomenkov, S.A., Kolesnikov, S.G.: Extraction of cyber-physical systems inventions' structural elements of russian-language patents. *Cyber-Phys. Syst. Adv. Design Model.* **2020**, 55–68 (2020)
22. Schatz, B.: Predictive modeling in health informatics. *IEEE J. Biomed. Health Inform.* **19**(4), 1384–1384 (2015)
23. Ushakov, I.B., Bogomolov, A.V., Dragan, S.P., Soldatov, S.K.: Methodological foundations of personalized hygienic monitoring. *Aerosp. Environ. Med.* **51**(6), 53–56 (2017)
24. Alyokhin, M.D., Bogomolov, A.V., Kukushkin, Yu.A.: Methods for analyzing breathing patterns in non-contact monitoring of psychophysiological States of operators of ergatic systems. *Aerosp. Environ. Med.* **53**(2), 99–101 (2019)
25. Bychkov, E.V., Boogmolov, A.V., Kotlovanov, K.Y.: Stochastic mathematical model internal wave. In: *Bulletin of the South Ural state University. Series: Mathematical Modeling and Programming*, vol. 13, No. 2 (2020)

The Use of the Synthetic Method of Harmonic Analysis for Investigating the Structure of Space Natural Bodies



Natalya Demina  and Alexey Andreev 

Abstract This chapter considers a method for investigating the topographic model of the Moon’s surface based on harmonic multi-parameter analysis and fractal geometry. The data from the “Clementine”, “Kaguya” and “LRO” satellite space missions were used as observational material. The Russian plans include carrying out works that will provide referencing of the lunar surface images to the selenographic coordinate system. The implementation of those plans may bring selenodesy to a level comparable to the Earth’s geodesy. At the same time, data analysis in the projects mentioned above put increased demands on the description of the complex dynamic and gravity model of the Moon’s structure. The observations produced at space missions refer to the so-called quasi-dynamic system whose origin coincides with the lunar center of mass, but axes have a shift concerning the lunar axes of inertia. Many lunar maps have a quasi-dynamic system. The main purposes of this work are related to the construction of theoretical models of the physical surface based on modern satellite measurements. An analysis of fractal dimensions and self-similarity coefficients of both individual local zones and the global model of the entire lunar sphere was conducted. As a result, similar zones of the lunar surface formed at the same physical processes were determined. These results are significant for constructing a theory of the Moon’s evolution.

Keywords Multi-parameter analysis · Fractal geometry · Space satellite measurements digital maps of the lunar surface

N. Demina (✉) · A. Andreev
Kazan Federal University, Kazan, Tatarstan 420008, Russia
e-mail: vnu_357@mail.ru

A. Andreev
Kazan Power Engineering University, Kazan 420066, Russia

1 Introduction

The number of countries involved in the study of the Moon has significantly increased recently. Researchers from the European Space Agency (ESA), Japan, China, and India have joined the long-term programs implemented by Russia and the USA. Among the most interesting projects of the past years one should mention NASA “Clementine” (1994) [1] and “Lunar Prospector” (1998–1999) [2], Lunar Laser Ranging (1969–2010) [3], ESA “SMART-1” (2003–2006) [4], JAXA “Kaguya” (2007–2009) [5], Chinese probes “Chang’e-1” (2007–2009), “Chang’e-2” (2010), “Chang’e-3” (2014) [6], “Chang’e-4” (2018) [7], NASA “LRO” (2009–2010) [8], Indian satellites “Chandrayaan-1” (2008–2009), “Chandrayaan-2” (2013) [9], NASA “GRAIL” (2011–2012) [10]. The increase in the accuracy of coordinate measurements planned in the upcoming Russian missions to the Moon is supposed to provide a much higher level of modeling of digital lunar maps [11]. In so doing, the construction of digital lunar maps is a source basis for studying the Moon by spacecraft. Currently, the lunar spacecraft’ landing accuracy is within 30×15 km [12]. For geological investigations, one has to use lunar rovers to take rock samples or conduct their analysis on-site in scientifically interesting areas. The delivery of scientific equipment to a planned site of the investigation will reduce its cost and increase its efficiency significantly. The achievement of high accuracy of coordinate support for space activity on the Moon will be even more relevant when building a permanent lunar station of modules delivered from the Earth: one will either deliver the modules at their docking distance by flexible units or provide for the long-range transportation of heavy modules on the lunar surface [13]. The position of any point on the Moon’s surface is defined by 3 values—latitude, longitude, and radius-vector counted from the Moon’s center of mass. To increase the accuracy of coordinate and time support, it is necessary to develop a theoretical basis for both satellite observations conducted and the processing of their results.

The processing of the experimental data is performed using original numerical algorithms and computer programs that include the calculation and construction of the digital lunar map. On the one hand, the produced altimetry for the lunar physical surface describes the relief well but is not able to serve for creating the reference selenographic network [14]. On the other hand, lunar positional observations taken by ground-based methods refer to the corresponding selenographic systems including the selenocentric dynamic coordinate system, but on their basis, it is impossible to build a highly accurate model of the Moon’s relief [15].

When studying both the structural and evolutionary characteristics of celestial bodies, various approaches to statistical assessment are applied [16–18]. These include methods based on fractal geometry. Fractality implies a high degree of identity at scaling. In doing so, the key problems are the calculation of fractal dimension (FD) for datasets produced during an experiment and determining conditions at which a structure under investigation manifests fractality. As the basic property of fractal structures is their self-similarity, experimental datasets are characterized by FD and self-similarity coefficient (SC). The presence of fractality is found in dynamic

systems whose examples are surfaces of small (asteroids) and relatively large (Mars and Earth) celestial bodies. In this work, based on approaches introduced in [19], the author's method of highly accurate accounting SC and color FD by a set of properties of models analyzed is developed.

2 Creation of Digital Maps of the Lunar Surface

To create digital maps, the altimetry produced at “Clementine”, “Kaguya” and “LRO” missions was expanded into spherical functions by the Formula [20, 21] as follows:

$$h(\lambda, \beta) = \sum_{n=0}^N \sum_{m=0}^n (\bar{C}_{nm} \cos m\lambda + \bar{S}_{nm} \sin m\lambda) \cdot \bar{P}_{nm}(\cos \beta) + \varepsilon, \quad (1)$$

where $h(\lambda, \beta)$ —altitude function dependent on longitude and latitude;

λ, β —longitude, latitude (known parameters);

$\bar{C}_{nm}, \bar{S}_{nm}$ —harmonic normalized amplitudes;

\bar{P}_{nm} —Legendre functions, normalized and associated;

ε —regression error, random.

The basic method used for studying the lunar macro-relief is numerical and analytical one which implies the expansion of a catalog data in harmonic series of spherical functions. For this purpose, it is advisable to use methods of regression analysis. Among statistical methods, regression analysis is most often used for solving the tasks related to experimental data processing. Thus, regression analysis allows constructing mathematical models based on various observations. The simulation implies introducing the parametric interrelationships between processes observed and parameters corresponding to them. There are 4 aspects of regression analysis:

1. Representation of observations data based on mathematical methods;
2. Construction of models characterizing observed process;
3. Determining unknown parameters in the mathematical models using Least Square Method (LSM);
4. Finding and selecting the most reliable model based on the parameters being determined.

For solving the tasks of constructing a digital map of the Moon, the method based on regression simulation is used. For this purpose, the software package “Automated System of Transformation Coordinate” (ASTC) has been developed. There are several specialized software packages (SSP) constructed by Russian and foreign teams and focused on data processing by using methods of mathematical statistics. However, those (SSP) are not suitable for the tasks of selenodesy considered in the present work. ASTC software package is built on modular principles. The components of the given software package allow conducting researches in any field of selenodesy. In this case, the systematic approach based on mathematical systems

of data processing allowing automating both data processing itself and control is used. During the construction of the model of the Moon's macro-figure, there was an attempt of using another software package SORS ("Searching for Optimum Regression System") along with ASTC, since the regression simulation approach was implemented in SORS and its efficiency had been proved during astrophotographers processing. However, as it was proved again, the features of data on mega-relief and the lunar gravitational field (dimension and structure) and transformations methods for applying the regression approach did not allow using SORS. Thus, during the processing, only ASTC automated system representing a software package of special modules intended for conducting procedures of regression simulation and aimed at analyzing the processes taking place in astronomical and geodetic systems has been used. In particular, this software package allows studying the topography and gravitational field of the Moon. The main capabilities of the software package include the possibility of creating stochastic models with the following determining unknown parameters as well as the possibility of full control over the computational process. The present software complex has been developed due to the specific approach to the solution of the assigned tasks that required a large number of the solution options and using various methods of unknowns' errors detecting. The question of matching remainder with basic parameters of LSM, when determining parameters of the model, is relevant as well.

The software modules included in ASTC provide solutions to normal and overdetermined systems of linear algebraic equations. The solution of the latter is implemented based on LSM. Values of unknowns and their errors, values of correlation matrix elements, internal and external quality measures used for determining reliability, and receiving recommendations for structuring a model can take on the role of output. In most cases, the program contains one or the other procedure of searching for the most reliable structure of the model. There is a possibility of using step-by-step regression analysis, which is applied for obtaining model by less number of observations n than the number of coefficients p . This is possible since the terms are introduced in the model consecutively and the calculation procedure can end earlier than excess solutions appear.

3 Method for Analyzing Lunar Maps

Let us consider that a complex physical structure is presented as a partially ordered set $A(N^2)$, where N^2 —the number of elements $a_{ij} \in A(N^2)$, where $(i, j = 1 \dots N)$.

Let us also assume that the elements of the set have certain common properties $H_\xi(a)$ inherent only to these elements $\forall a_{ij} (\in \{a | H_\xi(a)\})$. In this case, if there is more than 1 property, the considered set will be characterized by a few values of FD. Let us define the upper and lower limits of the set $A(N^2)$ by all properties $H_\xi(a)$ as $G_\xi = \sup A(N^2)$ and $g_\xi = \inf A(N^2)$. Matching the upper and lower limits the values (R) and a_ζ , respectively, let us cover the studied set by a cubic structure.

Each subset of the studied set, whose number constitutes $\sup Q^{(k)}(n^2) \in Q^{(k)}(n^2)$, accounts for a cube of volume $\vartheta_\xi = \frac{V_\xi}{\alpha^3}$, and the total area of all the elements of the subset is $S_\xi(n^2) = s_\xi n^2$.

Now, let us determine FD D_ξ of the set $A(N^2)$ by the property $H_\xi(a)$ through the angle of the $\log \Gamma_\xi(n^2)$ dependence on $\log s_\xi n^2$, where $\Gamma_\xi(n^2)$ is the number of cubic structures' sides in contact that covers the set $Q^{(k)}(n^2)$:

$$D_\xi = \sum_\gamma \frac{\log \Gamma_\xi(n_{\gamma+1}^2) - \log \Gamma_\xi(n_\gamma^2)}{|\log S_\xi(n_{\gamma+1}^2)| - |\log S_\xi(n_\gamma^2)|} * \left(\frac{\alpha_{\gamma+1} - \alpha_\gamma}{N - 1} \right), \tag{2}$$

The self-similarity coefficient (SC) K_ξ is given as

$$K_\xi = \frac{D_\xi^0}{D_\xi} \tag{3}$$

where FD of the self-similar set is designated as D_ξ^0 :

$$D_\xi^0 = \frac{\log \Gamma_\xi(N^2) - \log \Gamma_\xi(1)}{|\log S_\xi(N^2)| - |\log S_\xi(1)|}. \tag{4}$$

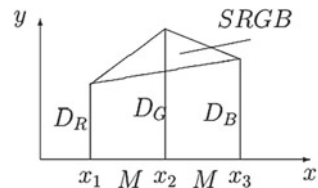
When analyzing fractal characteristics of the altimetric models of the Moon built based on ‘‘Selene’’ JAXA mission’s data, pixel color codes are used as ξ parameters: Red ($\xi = R$), Green ($\xi = G$), and Blue ($\xi = B$).

As a result, the considered surface structures are described by 3 FD–DR, DG, and DB. Using them, SRGB triangles are formed and their areas, that characterize the studied areas of the surface with a high sensitivity to change in color indicators, are determined (Fig. 1).

As a result of processing the altimetry, the images of self-similarity coefficients’ variations are formed (Fig. 2) and 3D-model of FD values (Fig. 3) for various areas of the Moon’s surface digital model is built.

In Fig. 2 the model of the surface is divided into square areas with a side of 15° in selenographic longitude and latitude. In Fig. 2 it is shown that SC varies between 0.8 and 1, which confirms the fractality of the considered model. In Fig. 3 are presented the values of SRGB area for square zones with a side of 15° for the considered model.

Fig. 1 SRGB system



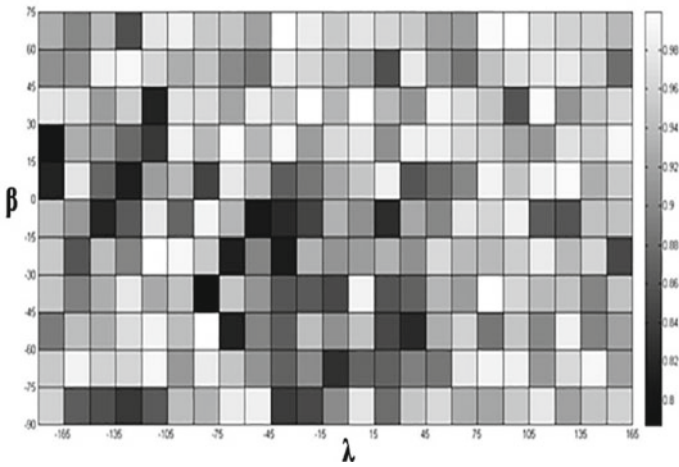


Fig. 2 Variations of SC depending on selenographic longitude and latitude

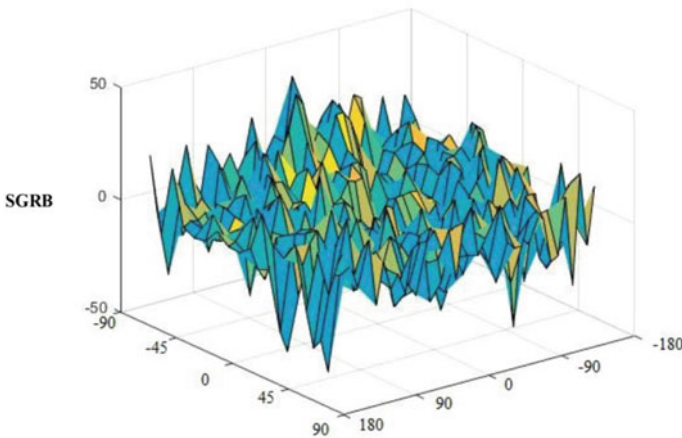


Fig. 3 Variations of SRGB area depending on selenographic longitude and latitude

The study of SRGB area distribution for zones of the lunar surface allows defining zones with a similar structure.

As an example, Fig. 4 provides a diagram of SRGB area variations in longitude at the fixed latitude ($45^\circ < \varphi < 60^\circ$).

The fact that SRGB values are equal for several zones of the lunar sphere indicates that those structures are similar.

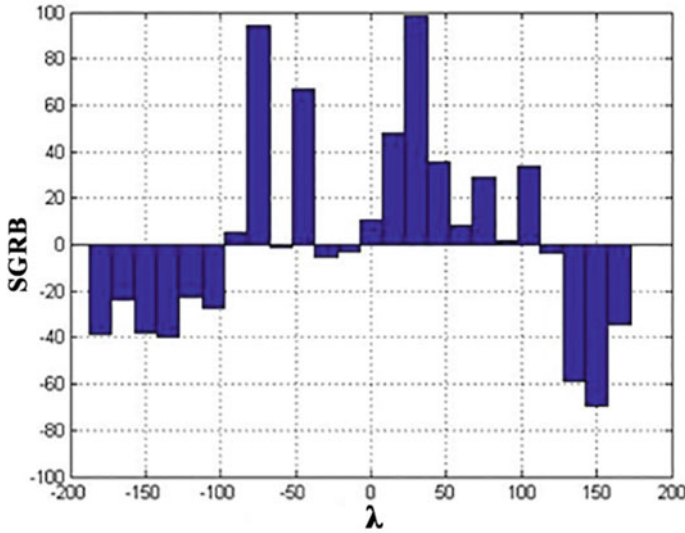


Fig. 4 Diagram of SGRB area distribution depending on longitude at fixed latitude ($45^\circ < \varphi < 60^\circ$)

4 Analysis of the Lunar Macro Figure

As a result, using the catalog “DSC” [22] the lunar harmonic model (LHM) (1) of the expansion of the 5th order was made. The next stages of constructing the LHM were performed. The robust analysis of the LHM for various orders of expansion was made; it was obtained that in this case further increase isn’t reasonable. After that, optimal structures for the given model were analyzed. In the end, the influence of the LHM structure overdetermination on parameters unknown values was studied.

The search for unknown parameters and analysis of the LHM was performed using LSM. Stepwise regressions were used to expand the LHM data in spherical functions. All the constructed LSM contained only the main elements. The studies were carried out to find the most reliable LHM expansion order. It was obtained that the 17th order of expansion was the most suitable for the given number of observations.

One of the methods of analyzing the LSM based on various lunar systems aimed at the studying of their reliability and matching is an approach of comparing topographic information isohypses. In this case reference surface for altitude, data is set by the “DSC” catalog.

It should be noted that at the present there is only one lunar surface macro relief model, which is constructed in JPL USA based on harmonic analysis and contains the coefficients up to the 70th order [23]. The model covers the lunar surface area limited by 750 by northern and southern latitude. But for the present study, the LHM of the 17th order appeared sufficient.

For the study we used the lunar macro-figure cross-section isohypses obtained during “Kaguya” [24], “LRO” [25], “Clementine” [26] lunar missions and “DSC”

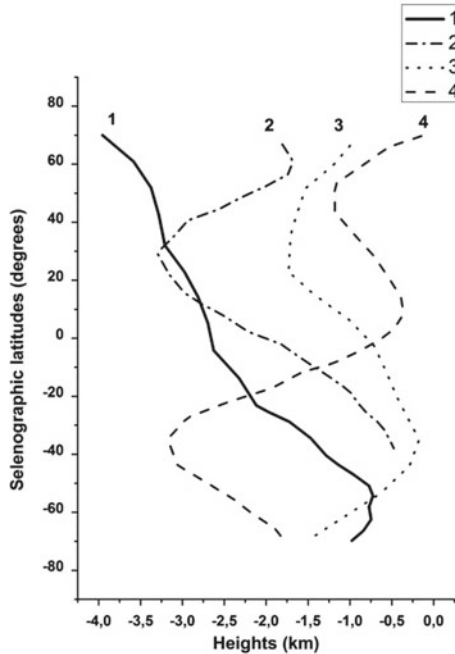


Fig. 5 Comparison of the lunar macro figure cross-sections from “DSC” catalogue (line 1), “Kaguya” (line 2), “Clementine” (line 3), and “LRO” (line 4) space missions for -20° . The X-axis corresponds to altitude in km; the Y-axis corresponds to latitude in degrees; the curves are represented for selenographic longitude -20°

[27] catalogue. The LSM was constructed in spherical functions up to the 5th order of expansion. The isohypses for the next listed lunar longitude values (40° ; 200° ; 0° ; -20° ; -40°) with 200 step by latitude. In Fig. 5 there are cross-sections of the lunar macro relief for 4 selenographic systems for longitude -20° . Here, the Y-axis corresponds to selenographic latitude; the X-axis corresponds to the isohypses’ altitudes relative to the basic latitude (1738 km).

Based on the study of the isohypses built for longitudes 400° ; 20° ; 0° ; -20° ; -40° we may conclude that:

1. The mean level of the surface of the Moon in the North is less than the level of the South hemisphere.
2. The view of elevation curves of “Clementine” lunar mission isohypses are like to the ones taken from the “DSC” catalog; “Kaguya”, “LRO” isohypses variations are significantly different from them.

5 Conclusion

In this work, the modern satellite optical observations from the lunar missions are investigated. The necessity to reprocess arrays of satellite measurements using the modern approaches to data processing is confirmed. For the model under investigation, more than 160 distribution of the values of (SRGB) area is analyzed. The regions characterized by a similar structure of surface are determined, which confirms the same conditions of their evolutionary parameters. Using the author's method, fractal properties for the multi-parameter model of our natural satellite's physical surface are determined. The constructed digital maps are going to be used when building the selenocentric system of navigation support [28, 29].

Acknowledgements This work was partially supported by the Russian Science Foundation, grants no. 20-12-00105 (according to the grant, the method for data analysis was created). This paper has been supported by the Kazan Federal University Strategic Academic Leadership Program. This work was partially supported by The Russian Foundation for Basic Research grant no. 19-32-90024 and the Foundation for the Advancement of Theoretical Physics and Mathematics "BASIS".





References

1. Smith, D.E., Zuber, M.T., Neumann, G.A., Lemoine, F.G.: Topography of the moon from the clementine lidar. *J. Geophys. Res. Planets* **102**(E1), 1591–1611 (1997)
2. Binder, A.B.: Lunar prospector: overview. *Science* **281**(5382), 1475–1476 (1998)
3. Löcher, A., Kusche, J.: Assessment of the impact of one-way laser ranging on orbit determination of the Lunar Reconnaissance Orbiter. *J. Geodesy* **93**, 2421–2428 (2019)
4. Foing, B.H., Racca, G., Marini, A., Koschny, D., Frew, D., Grieger, B., ... Grande, M.: SMART-1 technology, scientific results, and heritage for future space missions. *Planetary Space Sci.* **151**, 141–148 (2018)
5. Araki, H., et al.: Lunar global shape and polar topography derived from Kaguya-LALT laser altimetry. *Science* **323**(5916), 897–900 (2009)
6. Di, K., Xu, B., Peng, M., Yue, Z., Liu, Z., Wan, W., ... Zhou, J.: Rock size-frequency distribution analysis at the Chang'E-3 landing site. *Planetary Space Sci.* **120**, 103–112 (2016)
7. Wang, Q., Liu, J.: A Chang'e-4 mission concept and vision of future Chinese lunar exploration activities. *Acta Astronaut.* **127**, 678–683 (2016)
8. Keller, J.W., Petro, N.E., Vondrak, R.R.: The Lunar reconnaissance orbiter mission—six years of science and exploration at the moon. *Icarus* **273**, 2–24 (2016)
9. Elugachev, P., Shumilov, B.: On the application of the photogrammetric method to the diagnostics of transport infrastructure objects. In: *Cyber-Physical Systems: Industry 4.0 Challenges*, pp. 51–62 (2020). https://doi.org/10.1007/978-3-030-32648-7_5
10. Sood, R., Chappaz, L., Melosh, H.J., Howell, K.C., Milbury, C., Blair, D.M., Zuber, M.T.: Detection and characterization of buried lunar craters with GRAIL data. *Icarus* **289**, 157–172 (2017)
11. Lidong, W., Guanghui, W., Cheryl, A.A.: Big data and visualization: methods, challenges, and technology progress. *Digit. Technol.* **1**(1), 33–38 (2015)
12. Bogatyrev, V.A., Aleksankov, S.M., Derkach A.N.: The model of reliability of dabled real-time computers for cyber-physical systems. In: *Cyber-Physical Systems: Industry 4.0 Challenges*, pp. 11–21 (2020). https://doi.org/10.1007/978-3-030-32648-7_2

13. Bagrov, A.V., Leonov, V.A., Mitkin, A.S., Nasyrov, A.F., Ponomarenko, A.D., Pichkhadze, K.M., Sysoev, V.K.: Single-satellite global positioning system. *Acta Astronaut.* **117**, 332–337 (2015)
14. Andreev, A., Nefedev, Y., Demina, N., Petrova, N., Demin, S., Zagidullin, A.: Analysis of dynamical and quasidynamical space coordinate systems. *AIAA SPACE and Astronautics Forum and Exposition*. pp. 1–6 (2017)
15. Rizvanov, N., Nefedev, J.: Photographic observations of solar system bodies at the engelhardt astronomical observatory. *Astronomy Astrophys.* **444**(2), 625–627 (2005)
16. Valeev, S., Samokhvalov, K.: The ARM-approach based local modeling of the gravitational field. In: *International conference on computational science*, pp. 471–480. Springer, Berlin, Heidelberg (2003)
17. Chrysochoou, C., Rutishauser, C., Rauber-Lüthy, C., Neuhaus, T., Boltshauser, E., Supertifurga, A.: An 11-month-old boy with psychomotor regression and auto-aggressive behavior. *Europ. J. Pediatrics* **162**(7–8), 559–561 (2003)
18. Queffelec, H., Volný, D.: On martingale approximation of adapted processes. *J. Theor. Probability* **25**(2), 438–449 (2011)
19. Valeev, S.G.: Coordinates of the Moon reverse side sector objects. *Earth Moon Planet.* **34**(3), 251–271 (1986)
20. Nefedev, Y., Valeev, S., Mikeev, R., Varaksina, N., Andreev, A.: Analysis of data of “CLEMENTINE” and “KAGUYA” missions and “ULCN” and “KSC-1162” catalogs. *Adv. Space Res.* **50**(11), 1564–1569 (2012)
21. Andreev, A.O., Demina, N.Y., Nefedev, Y.A., Demin, S.A., Zagidullin, A.A.: Modeling of the physical selenocentric surface using modern satellite observations and harmonic analysis methods. *J. Phys. Conf. Ser.* **1038**(1) (2018)
22. Nefedev, YuA, Andreev, A.O., Petrova, N.K., Demina, N.Y., Zagidullin, A.A.: Creation of a global selenocentric coordinate reference frame. *Astron. Rep.* **62**(12), 1015–1019 (2018)
23. Veshneva, I.V., Bolshakov, A. A., Fedorova, A.E.: Organization of engineering education for the development of cyber-physical systems based on the assessment of competences using status functions. In: *Cyber-Physical Systems: Industry 4.0 Challenges*, pp. 277–288. Springer (2020). https://doi.org/10.1007/978-3-030-32648-7_22
24. Goossens, S., Mazarico, E., Ishihara, Y., Archinal, B., Gaddis, L.: Improving the geometry of Kaguya extended mission data through refined orbit determination using laser altimetry. *Icarus* **336**, 113454 (2020)
25. Williams, J.G., Konopliv, A.S., Boggs, D.H., et al.: Lunar interior properties from the GRAIL mission. *J. Geophys. Res. Planets* **119**(7), 1546–1578 (2014)
26. Kim, K.J., Wöhler, C., Berezhnoy, A.A., Bhatt, M., Grumpe, A.: Prospective ³He-rich landing sites on the Moon. *Planetary Space Sci.* **177**, 104686 (2019)
27. Andreev, A.O., Demina, N.Y., Nefedev, Y.A., Demin, S.A., Zagidullin, A.A.: Modeling of the physical selenocentric surface using modern satellite observations and harmonic analysis methods. *J. Phys. Conf. Ser.* **1038**(1) (2018)
28. Trigo, G.F., Maass, B., Krüger, H., Theil, S.: Hybrid optical navigation by crater detection for lunar pin-point landing: trajectories from helicopter flight tests. *Ceas Space J.* **10**, 567–581 (2018)
29. Nashivochnikov, N.V., Bolshakov, A.A., Lukashin, A.A., Popov, M.: The system for operational monitoring and analytics of industry cyber-physical systems security in fuel and energy domains based on anomaly detection and prediction methods. In: *Cyber-Physical Systems: Industry 4.0 Challenges*, pp. 261–273 (2020). https://doi.org/10.1007/978-3-030-32648-7_21

The Study of Geodynamic Parameters on the Basis of Adaptive Regression Modeling



Yury Nefedev , Regina Mubarakshina , Alexey Andreev ,
and Natalya Demina 

Abstract Many natural processes in space may be simulated and controlled by a computer using the corresponding methods and approaches. These processes include: geophysical phenomena, gravitational interactions, celestial bodies mechanics, and astrophysical events. In these cases, computer simulation directly interacts with physical systems. As it is well known, those models refer to cyber-physical systems (CPS). In the case of geophysical processes, there is the interaction between computer algorithms and complex physical systems, whose models are hard to develop and control. The practice of analyzing geophysical processes has shown one is able to control the behavior of such systems using the computer adaptive regression modeling which also allows performing prediction actions. The construction of the prediction dynamics of a physically complex system has a crucial value for the quality of processing geophysical information. At the same time, CPS could be complex, especially when it is necessary to combine cyber-physical systems. The application of adaptive regression modeling for analyzing geophysical parameters is considered. In this chapter, the variations of the Earth's pole position are investigated. Based on time series of observations of the Earth's pole an adaptive regression model (ARM) describing the pole's dynamics over 30 years is developed. Similar models were created earlier by other authors but their capabilities were limited for prediction. The ARM approach has provided a more accurate combination of observational and model parameters. As a result, the use of ARM has allowed constructing the predictive curve of the change in the Earth's pole motion and comparing the produced results with observations. The comparison shows a rather good agreement between the model parameters and the observations data.

Keywords Regression dynamic modeling · Automated software · Earth pole motion

Y. Nefedev (✉) · R. Mubarakshina · A. Andreev · N. Demina
Kazan Federal University, Kazan, Tatarstan 420008, Russia
e-mail: star1955@mail.ru

A. Andreev
Kazan Power Engineering University, Kazan 420066, Russia

© The Author(s), under exclusive license to Springer Nature Switzerland AG 2021
A. G. Kravets et al. (eds.), *Cyber-Physical Systems: Modelling and Intelligent Control*, Studies in Systems, Decision and Control 338,
https://doi.org/10.1007/978-3-030-66077-2_18

1 Introduction

Cyber-physical systems (CPS) are based on the interaction between calculation models, that are in direct connection with the real physical world and the processes occurring there, and allow to implement control over data processing systems [1]. The work [2] considers an approach based on CPS which allows efficient use of the entire flexibility of the created controlled local models which are automatically configured, programmed, and optimized on the basis of independent simulation requirements. Such a simulation representation of the system under investigation eliminates the disadvantage of information description and uncertainty in determining life cycles and CPS behavior prediction [3]. These requirements are achieved by the application of new methods and approaches to programming and adjustment of CPS, which allows reducing time costs significantly [4]. CPS are therefore capable of not changing only every step of the observations' analysis but also converging the two worlds—physical and virtual [5]. All of the above applies to geodynamic systems as well. The investigation of the polar region from the point of view of economic prospects has strengthened recently [6]. If photogrammetry of the Earth's surface is based on the existing large observational content and flexibility of model projection of a geodetic network and provides reliable and accurate results [7], then inaccuracy in the Earth's pole position does not allow referencing of the produced model to the geocentric coordinate system with the sufficient accuracy. At the same time, the necessary instruments for studying and analyzing terrestrial systems are models of various geodynamic processes. Although these models are rather diverse, one needs reliable and high-quality data for their description [8]. The status of analyzing geodynamic data is supposed to correspond to the level of theoretical modeling [9]. Such a simulation implies the expansion of latitude series of observations, that could be used at the investigations of isostasy dynamics, determination of gravimetric parameters [10], and most importantly—for analyzing the Earth's pole motion, into harmonic coefficients.

The method of time series of the Earth pole dynamic processing (TSDEP) includes the steps as follows: (1) transformation of the uneven TSDEP to even ones with the method of spectral windows or by data averaging [11]; (2) fractal analysis of TSDEP, trend selection [12]; (3) spectral and wavelet analysis; (4) harmonic components selection, application of the Kalman filter [13]; (5) building Generalized AutoRegressive Conditional Heteroskedasticity (GARCH model); (6) Autoregressive moving-average model (ARMA model) construction [14]; (7) smoothing of residues using the martingale approximation [15]. At each step reducing the “internal” and “external” sample standard deviation (SSD), the significance of the error changes is controlled, and analysis of the latitude observations data (TSDEP) model quality is performed. At each stage of application of the ARM approach [16], the construction and analysis of the corresponding components of the model are performed, approximation accuracy is estimated (σ) and model forecasting ($\sigma \Delta$), diagnosis of residues, and, if necessary, adaptation [17]. As a result, the TSDEP analysis was completed over a period from January 1985 to October 2015.

2 Modeling of the Earth Pole Dynamics

Model of the dynamics of the X coordinate of the North Pole

At the first stage of data analysis, within the ARM-approach, the hypothesis on series stationarity is rejected with a probability of 0.95.

The centering of the original series is performed ($\sigma = 0,1323, \sigma_{\Delta} = 0,14$).

According to the results of spectral analysis [18], there is a confirmed presence of harmonic components. To determine the carrier harmonics, the method of stepwise regression is used. 4 significant harmonics with periods of 363, 388, 433, 490 days are distinguished ($\sigma = 0,0831, \sigma_{\Delta} = 0,0962$).

As a result, ARMA model (6,0) with $\sigma = 0.0002$ and $\sigma_{\Delta} = 0,0094$ is built. The diagram for the combined model is given in Fig. 1, its form is demonstrated below.

The final model is represented as the sum of periodic component and the ARMA (6.0) model:

$$\begin{aligned}
 X = & 0, 1179 + 0, 080861 * \sin((2 * \Pi * t) / 363 + 171, 67) + 0, 024544 * \\
 & \sin((2 * \Pi * t) / 388 + 0, 75733) + 0, 15803 * \sin((2 * \Pi * t) / 433 + 72, 725) + 0, 019003 * \\
 & \sin((2 * \Pi * t) / 490 + 221, 37) + 2, 3691 * X_2(t - 1) - 1, 8415 * X_2(t - 2) \\
 & + 0, 43787 * X_2(t - 3) + 0, 049839 * X_2(t - 4) + 0, 061644 * X_2(t - 5) \\
 & - 0, 076996 * X_2(t - 6) + X_3(t),
 \end{aligned}
 \tag{1}$$

where $X_2(t)$ are residue after removal of the harmonic component, $X_3(t)$ are residue after the combined model.

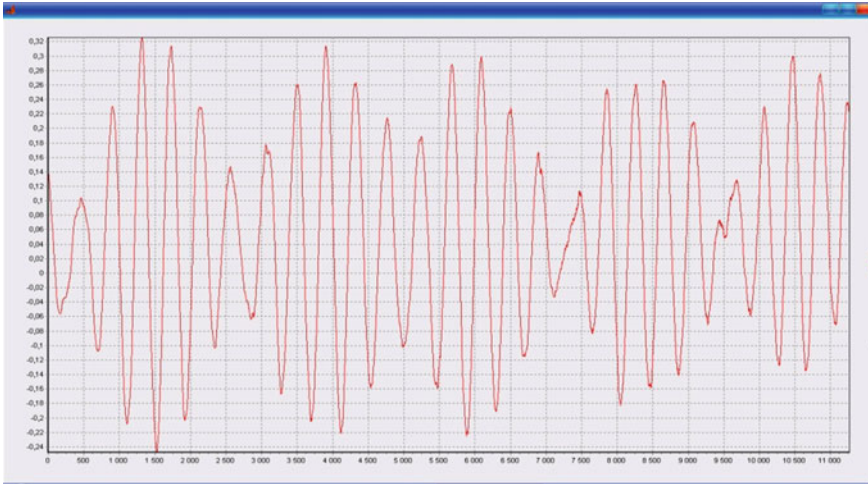


Fig. 1 Diagram of the combined model for TSDEP of the North Pole X-coordinate dynamics

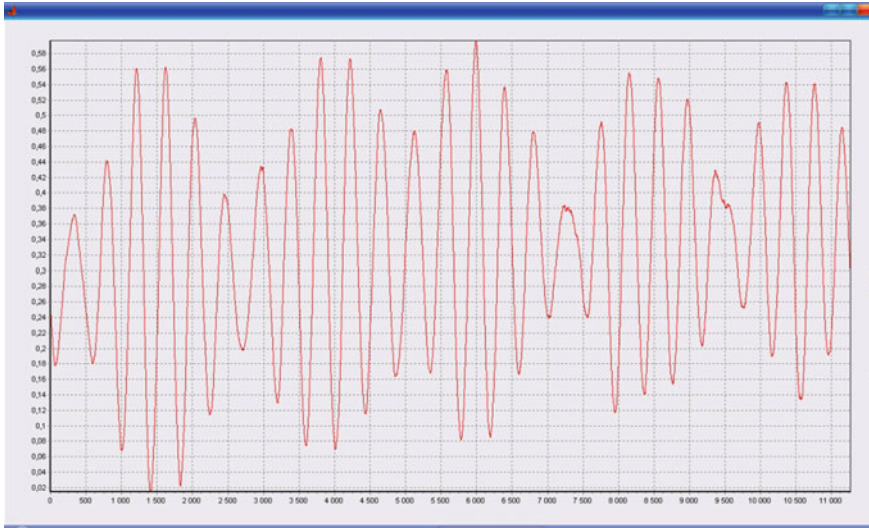


Fig. 2 Diagram of the combined model for TSDEP of the North Pole Y-coordinate dynamics

Model of the dynamics of the Y coordinate of the North Pole

The tested hypothesis of series stationarity is rejected with a probability of 0.95.

The centering of the original series is performed ($\sigma = 0,1306, \sigma_{\Delta} = 0,11$).

To determine the carrier harmonics, the method of stepwise regression is used [19]. This method selects four significant harmonics with periods of 363, 388, 433, 490 days. The dispersion (DS) of the models are respectively: $\sigma = 0,044, \sigma_{\Delta} = 0,043$.

ARMA (6,0) model is built with $\sigma = 0,000135$, and with $\sigma_{\Delta} = 0,0039$. The diagram of the complex model is given in Fig. 2. The final model is represented as the sum of the periodic component and the ARMA (6.0) model:

$$\begin{aligned}
 Y = & 0,322 + 0,072974 * \sin((2 * \Pi * t) / 363 + 260,65) + 0,024456 * \\
 & \sin((2 * \Pi * t) / 388 + 91,789) + 0,15762 * \sin((2 * \Pi * t) / 433 + 162,51) + 0,019638 * \\
 & \sin((2 * \Pi * t) / 490 - 44,806) + 2,4153 * Y_2(t - 1) - 1,9991 * Y_2(t - 2) \\
 & + 0,66257 * Y_2(t - 3) - 0,12927 * Y_2(t - 4) \\
 & + 0,16416 * Y_2(t - 5) - 0,11385 * Y_2(t - 6) + Y_3(t)
 \end{aligned}
 \tag{2}$$

3 Prediction of the Dynamics of the Earth Pole Coordinates

Using these models the prediction diagrams for X and Y coordinates of the North Pole of the Earth at 90 and 365 days are built.



Fig. 3 Diagrams of forecast **a** and observations **b** for the Earth North Pole X coordinate

A comparison of the obtained predictions with real data for the period from November 1, 2010, to February 2, 2011 (Fig. 3) is made.

Some predictions for the X coordinate are shown in Fig. 3, for the coordinate Y—in Fig. 4.

Similarly, a comparison of observations and predicted values of the polar coordinates of the Earth obtained by other researchers (<http://maia.usno.navy.mil/conv2010>) is made. Some predictions for the X coordinate are shown in Fig. 5, for the coordinate Y—in Fig. 6: diagrams of forecast **a** and observations **b** for the X coordinate and of Y coordinate the North Pole of the Earth obtained in US Naval Observatory.

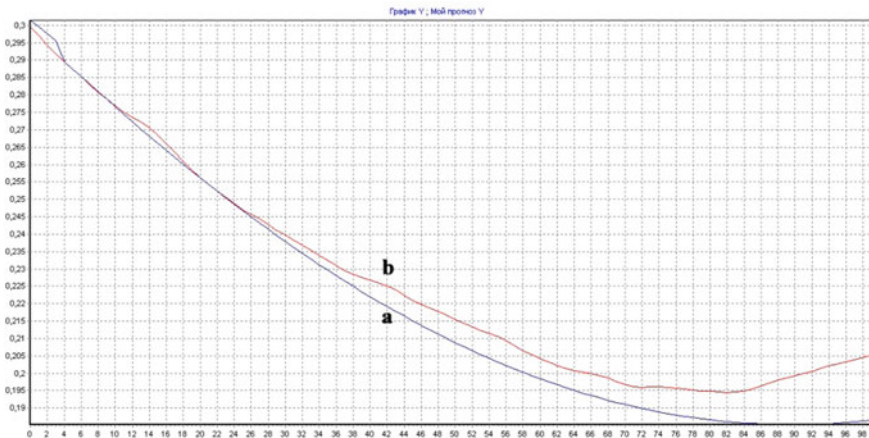


Fig. 4 Diagrams of forecast **a** and observations **b** for the Earth North Pole Y coordinate

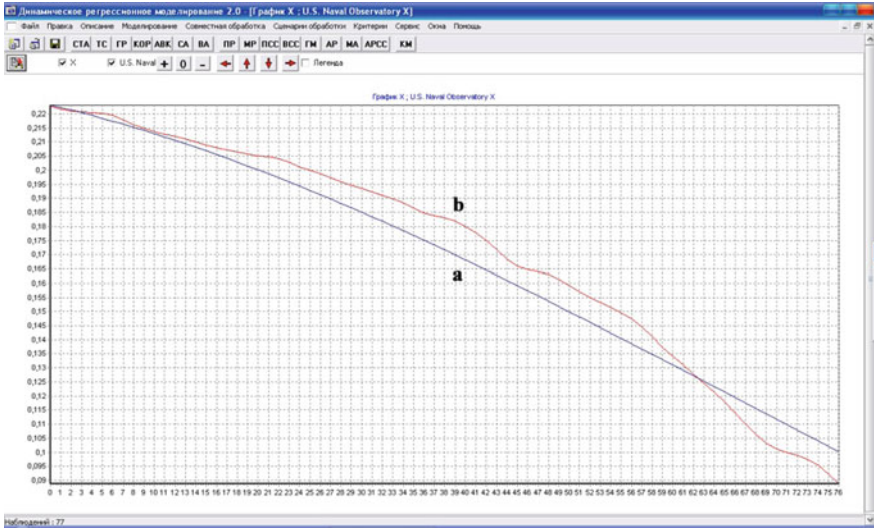


Fig. 5 Diagrams of forecast **a** and observations **b** for the X coordinate of the North Pole of the Earth obtained in US Naval observatory [20]

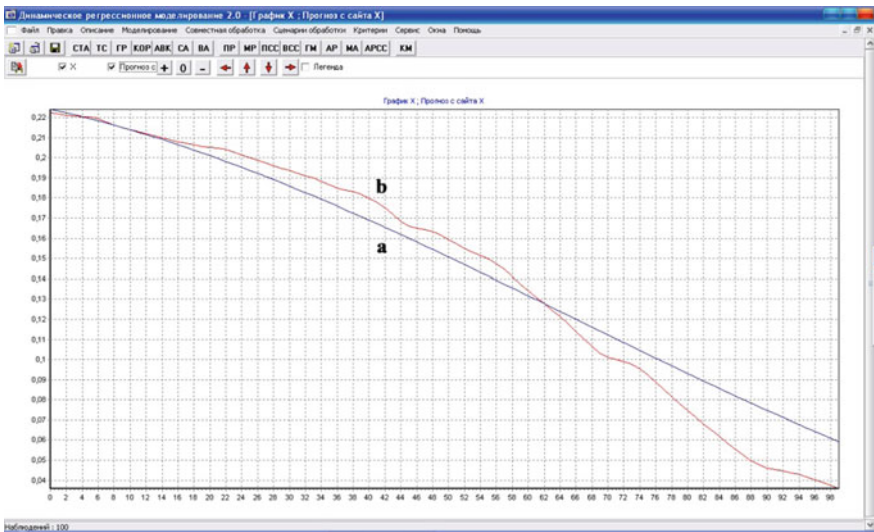


Fig. 6 Diagrams of forecast **a** and observations **b** for the Y coordinate of the North Pole of the Earth obtained in US Naval observatory [20]

Some predictions for the X coordinate are shown in Fig. 7, for the coordinate Y —in Fig. 8: diagrams of forecast **a** and observations **b** for the X coordinate and

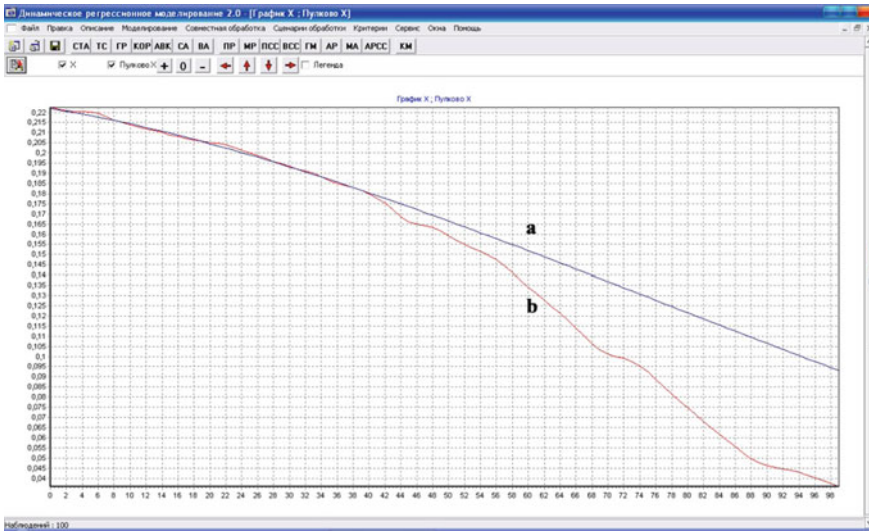


Fig. 7 Diagrams of forecast **a** and observations **b** for the X coordinate of the North Pole of the Earth obtained in the observatory in Pulkovo [21]

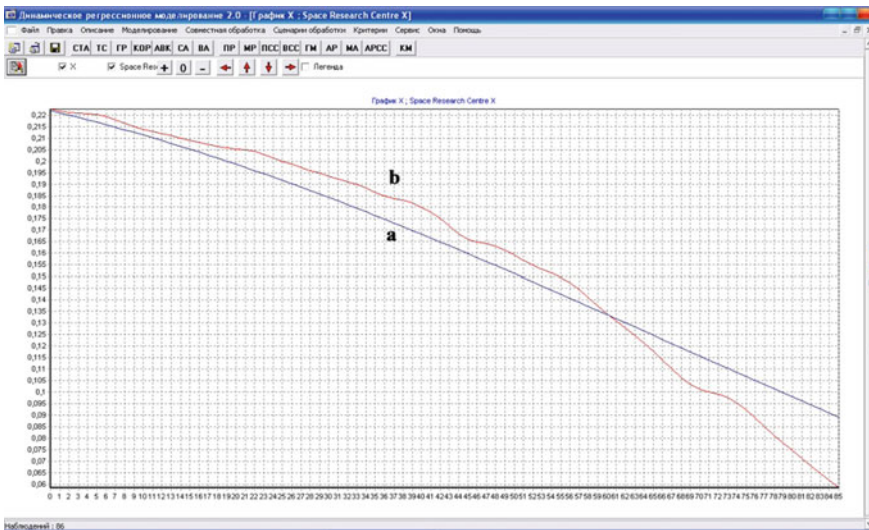


Fig. 8 Diagrams of forecast **a** and observations **b** for the Y coordinate of the North Pole of the Earth obtained in the observatory in Pulkovo [21]

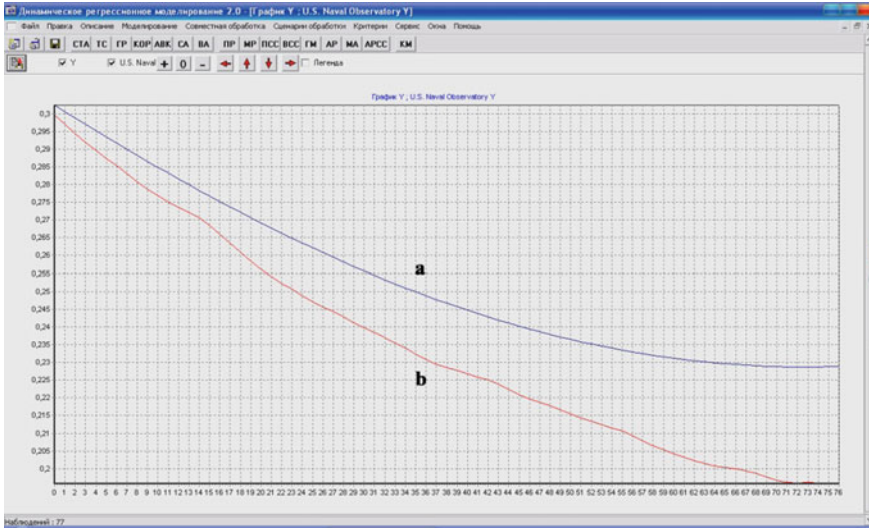


Fig. 9 Diagrams of forecast **a** and observations **b** for the X coordinate of the North Pole of the Earth obtained in the forecast from the site <http://www.iers.org>

for the Y coordinate of the North Pole of the Earth obtained in the Observatory in Pulkovo.

Some predictions for the X coordinate are shown in Fig. 9, for the coordinate Y—in Fig. 10: Diagrams of forecast **a** and observations **b** for the X coordinate and for Y coordinate the North Pole of the Earth obtained in the forecast from the site <http://www.iers.org>.

Some predictions for the X coordinate are shown in Fig. 11, for the coordinate Y – in Fig. 12: diagrams of forecast **a** and observations **b** for the X coordinate and for Y coordinate the North Pole of the Earth obtained in the Space Research Centre.

4 Conclusion

The results of this work are aimed at improving the accuracy of the regression dynamic model of the Earth’s pole motion. When performing these investigations, the modern methods for multi-parameter harmonic analysis, which allows solving practical problems of computational platforms of CPS in the field of geophysics, were used.

The deterministic mathematical model allows for a prediction of the studied characteristic value for future moments of time. Attempts to build such models have been made repeatedly, however, their predictive values turn out to be low. The development of statistical methods for time series (TSDEP) modeling allows us to hope

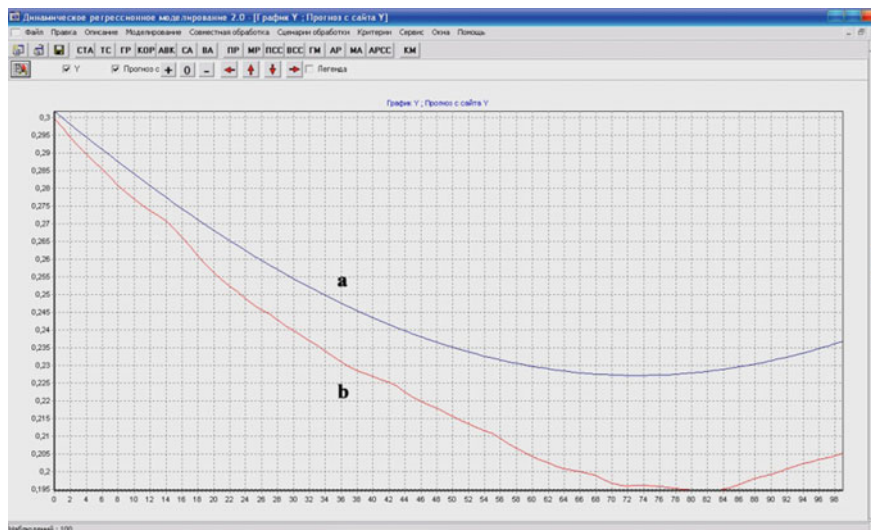


Fig. 10 Diagrams of forecast **a** and observations **b** for the Y coordinate of the North Pole of the Earth obtained in the forecast from the site <http://www.iers.org>

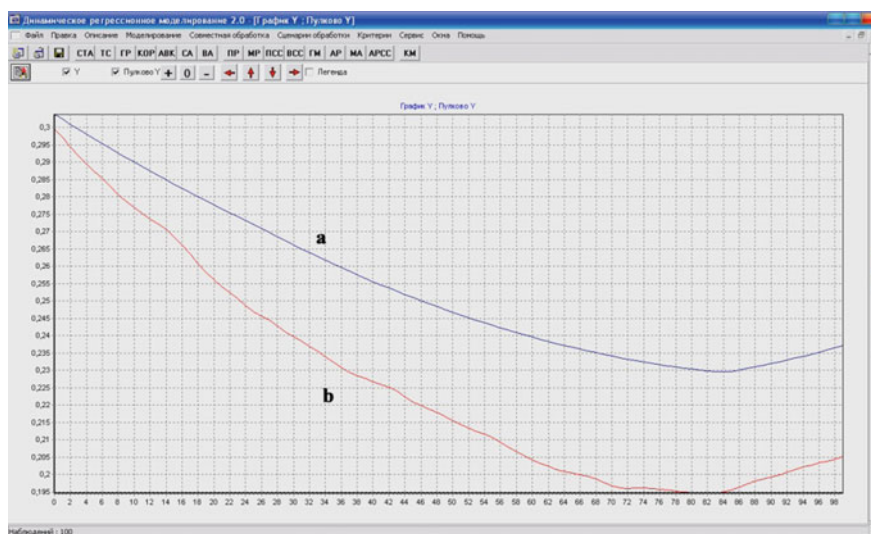


Fig. 11 Diagrams of forecast **a** and observations **b** for the X coordinate of the North Pole of the Earth obtained in space research centre [22]

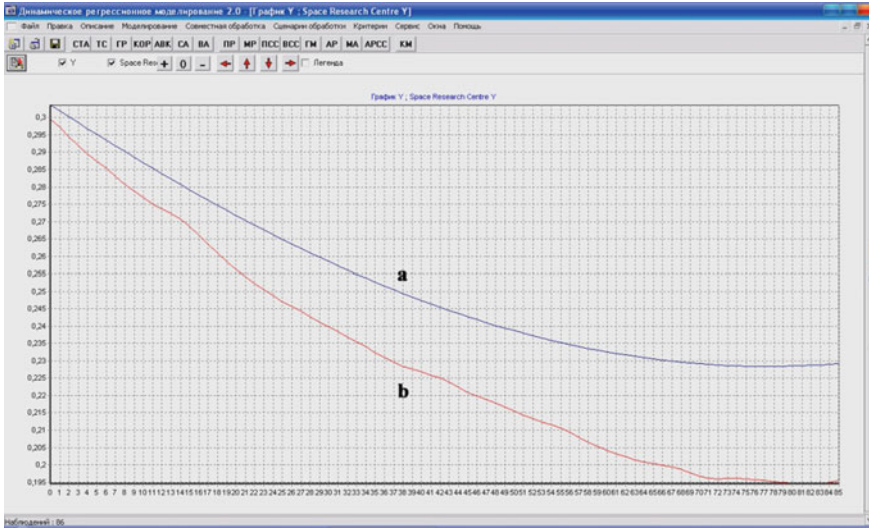


Fig. 12 Diagrams of forecast **a** and observations **b** for the Y coordinate of the North Pole of the Earth obtained in space research centre [22]

for the successful application of statistical models in the geophysical systems in the description of latitude variability in time.

Unlike deterministic models, statistical (regression) ones do not remain constant in structure and parameter values for the entire period of use. After getting the forecast for a step or several steps of discreteness in the future, the model is “updated” according to the current latitude values.

The regression dynamic modeling (ARM—approach) is a special case of the adaptive regression modeling approach (ARM approach). With its application, a complex TSDEP model is formed, consisting of a set of optimal mathematical structures, each describing the dependence of the “remnants” of its step on time. Let us call such a model of the regression dynamic modeling, keeping in mind that time is the main argument, and the final form of ARM is formed as a result of computational adaptation to the properties of the residuals of one or another step and violations of the conditions of application of the least-squares method (LSM).

Comparison with the work of other researchers of the North Pole dynamics has shown that the proposed models in the application of ARM-approach allow for a more accurate prediction of the coordinate Y while maintaining the accuracy of the coordinate X.

The results obtained in the chapter confirm the promise of using the so-called adaptive dynamic regressions, first proposed in [23] and being developed at present, for describing changes in latitudes. Their advantages, compared to the traditional approaches to the analysis of time series, in particular, to the analysis of the variability of geographical latitude, are: (1) expansion of the concept of the structure of the mathematical model describing the dynamics, (2) isolation of time-stable harmonics

of oscillations, (3) several times increased accuracy of forecasting the changes on a certain time interval forward, which might have practical consequences.

Acknowledgements This work was partially supported by the Russian Science Foundation, grants no. 20-12-00105 (according to the grant, the method for data analysis was created) and 19-72-00033 (according to the grant, the numerical calculations were carried out). This paper has been supported by the Kazan Federal University Strategic Academic Leadership Program. This work was partially supported by the Russian Foundation for Basic Research grant no. 19-32-90024 and the Foundation for the Advancement of Theoretical Physics and Mathematics “BASIS”.

References

1. Zong, X., Sun, Q., Yao, D., Du, W., Tang, Y.: Trajectory planning in 3D dynamic environment with non-cooperative agents via fast marching and Bézier curve. *Cyber-Phys. Syst.* **5**(2), 119–143 (2019)
2. Michniewicz, J., Reinharta, G.: Cyber-physical robotics—automated analysis, programming and configuration of robot cells based on cyber-physical-systems. *Proc. Technol.* **15**, 566–575 (2014)
3. Tran, T.B.L., Törngren, M., Nguyen, H.D., Paulen, R., Nancy Webster Gleason, N.W., Duong, T.H.: Trends in preparing cyber-physical systems engineers. *Cyber-Phys. Syst.* **5**(2), 55–91 (2019)
4. Abdel-Aziz, H., Koutsoukos, X.: Data-driven online learning and reachability analysis of stochastic hybrid systems for smart buildings. *Cyber-Phys. Syst.* **5**(1), 41–64 (2019)
5. Monostori, L.: Cyber-physical production systems: roots, expectations and R&D challenges. *Proc. Cirp* **17**, 9–13 (2014)
6. Li, W., Bhatia, V., Cao, K.: Intelligent polar cyberinfrastructure: enabling semantic search in geospatial metadata catalogue to support polar data discovery. *Earth Sci. Inf.* **8**(1), 111–123 (2014)
7. Forlani, G., Pinto, L., Roncella, R., Pagliari, D.: Terrestrial photogrammetry without ground control points. *Earth Sci. Inf.* **7**(2), 71–81 (2013)
8. Parsons, M.A.: Making data useful for modelers to understand complex Earth systems. *Earth Sci. Inf.* **4**(4), 197–223 (2011)
9. Borne, K.D.: Astroinformatics: data-oriented astronomy research and education. *Earth Sci. Inf.* **3**(1–2), 5–17 (2010)
10. Chen, W., Tenzer, R.: Harmonic coefficients of the Earth’s spectral crustal model 180—ESCM180. *Earth Sci. Inf.* **8**(1), 147–159 (2014)
11. Lapaeva, V.V., Nefedjev, Y.A., Meregin, V.P.: The study of the local fluctuations of the Earth’s crust using data of latitude observations. *Geophys. Res. Lett.* **32**(24) (2005)
12. Andreev, A.O., Demina, N.Y., Nefedyev, Y.A., Demin, S.A., Zagidullin, A.A.: Modeling of the physical selenocentric surface using modern satellite observations and harmonic analysis methods. *J. Phys. Conf. Ser.* **1038**(1) (2018)
13. Davoodabadi, I., Ramezani, A., Mahmoodik, M., Ahmadizadeh, P.: Erratum to: identification of tire forces using dual unscented kalman filter algorithm. *Nonlinear Dyn.* **78**(4), 2985–2985 (2014)
14. Chrysochoou, C., Rutishauser, C., Rauber-Lüthy, C., Neuhaus, T., Boltshauser, E., Superti-Furga, A.: An 11-month-old boy with psychomotor regression and auto-aggressive behavior. *Europ. J. Pediatrics* **162**(7–8), 559–561 (2003)
15. Queffelec, H., Volný, D.: On martingale approximation of adapted processes. *J. Theor. Probab.* **25**(2), 438–449 (2011)

16. Nefedyev, Y., Valeev, S., Mikeev, R., Varaksina, N., Andreev, A.: Analysis of data of “CLEMANTINE” and “KAGUYA” missions and “ULCN” and “KSC-1162” catalogues. *Adv. Space Res.* **50**(11), 1564–1569 (2012)
17. Rozovskii, L.V.: Accuracy of the normal approximation. *J. Soviet Math.* **61**(1), 1911–1918 (1992)
18. Madsen, C.K.: A novel optical vector spectral analysis technique employing a limited-bandwidth detector. *EURASIP J. Adv. Signal Process.* **2005**(10), 1566–1573 (2005)
19. Liu, Z., Huang, J., Shi, J., Tao, R., Zhou, W., Zhang, L.: Characterizing and estimating rice brown spot disease severity using stepwise regression, principal component regression and partial least-square regression. *J. Zhejiang Univer. Sci. B* **8**(10), 738–744 (2007)
20. Dick, S.: Observatory sciences and culture in the nineteenth century. *Metascience* **21**(1), 235–237 (2011)
21. Miller, N.O., Prudnikova, E.Y.: Early latitude observations at the Pulkovo observatory. *Kinematics Phys. Celestial Bodies* **27**(1), 30–37 (2011)
22. Drewes, H., Kuglitsch, F., Adám, J., Rózsa, S.: The Geodesist’s handbook 2016. *J. Geodesy* **90**(10), 907–1205 (2016)
23. Elmi, M., Talebi, H.A., Menhaj, M.B.: Robust adaptive dynamic surface control of nonlinear time-varying systems in strict-feedback form. *Int. J. Control Autom. Syst.* **17**(6), 1432–1444 (2019)

The Use of Huber's Method for Estimating Libration Selenographic Parameters



Konstantin Churkin  and Yury Nefedyev 

Abstract Currently, cyber-physical systems and technologies are successfully used while implementing space missions and creating coordinate and time reference systems. To solve the problems of spatial orientation and to apply on-board sight cameras and goniometers for this purpose, it is necessary to implement referencing to the visible limb of a celestial body and determine dynamic parameters from the long-term series of observations containing large data array and also erroneous measurements. In this process, the use of robust methods for assessing produced values of the desired parameters plays an important role. This chapter suggests a noise-immune Huber's method (Huber M estimator method—HMEM) for estimating selenographic and lunar libration parameters. In the investigations, we used positional observations of Mösting A crater concerning the lunar limb. Such observations represent unequal observations depending on the Moon's optical librations and conditions of observations. Such time series are therefore described by the complex system of conditional equations of desired parameters whose solution by the classic least squares method cannot eliminate erroneous observations from the processing. It is more plausible to estimate long-term observational series using HMEM. As a result, the values of lunar characteristics are obtained with high accuracy of their estimation.

Keywords Noise-resistant statistical analysis · The method of M-estimates · Selenodetic observations · The physical liberation of the moon

1 Introduction

Cyber-physical systems (CPS) include rather complex content [1]. A feature of CPS is the interaction and intersection of different spheres of modern technologies and scientific directions [2]. The main area of CPS is the development of methods and approaches to optimize innovative management processes [3]. The sphere of CPS activity also includes large databases, and their analysis, simulation of physical

K. Churkin (✉) · Y. Nefedyev
Kazan Federal University, Kazan, Tatarstan 420008, Russia
e-mail: kchurkin87@gmail.com

© The Author(s), under exclusive license to Springer Nature Switzerland AG 2021
A. G. Kravets et al. (eds.), *Cyber-Physical Systems: Modelling and Intelligent Control*, Studies in Systems, Decision and Control 338,
https://doi.org/10.1007/978-3-030-66077-2_19

237

processes, and creation of simulation physical and technical systems as well as many other directions [4]. CPS is therefore capable of covering the entire branches of space investigations including both the development of space missions and the creation of new observation methods from spacecraft and observations processing with a reliable assessment of desired parameters. The space industry has a wide production range, and it is, therefore, necessary to use the existing methods and approaches of CPS for higher mobility and productivity growth. Space technologies require high accuracy of all the activity lines and are therefore advantageous when CPS is applied for analyzing large electronic databases and their analytical processing [5]. Thus, more mobile, dynamic, and efficient methods for producing accurate and reliable results lead to cost reduction for implementing repeated space measurements that have a significant financial component [6].

The solution of the task on determining some parameters (physical, geometric, biological, economical, etc.) based on measurement results implies the processing of large arrays of information. These arrays are formed owing to the modern technologies and measuring systems at implementing space and ground-based physical and biological experiments, photogrammetric and geodetic, astrometric, navigational measurements, etc. This chapter considers an opportunity of applying the antijamming statistic analysis for processing a long-term series of selenodetic observations. The Development of this approach is caused by the active Moon exploration implying the creation of a precise coordinate and time support for the construction of selenocentric navigation reference system and lunar digital maps [7]. If to speak about combining observations taken by different methods and equipment, such investigations may lead to gross errors. For instance, combining the space observation taken at different spacecraft is currently one of the most complicated and not yet solved problems (due to difference in orbits, spacecraft's orientation errors).

It is well known that in astronomy, unlike other experiments in physics and chemistry, observations of many phenomena (events) cannot be repeated. Each of such measurements is therefore very valuable. On the other hand, some parts of astronomical observations, as well as experiments in other sciences, could be erroneous. The errors may be caused by several factors: astronomical climate at the moment of observation, the imperfection of equipment, human factor, etc. The accuracy of the final result is significantly influenced by the choice of an efficient method for reducing (processing) observations that could eliminate anomalous observations. At the moment, one knows some statistical methods for this purpose, in particular, the robust one. The modern robust methods for observation processing allow eliminating erroneous measurements that may distort the values of estimates when using the least-squares method (LSM). The method based on maximum plausibility is considered to be the most efficient. It was introduced by Huber [8]. He named the estimates by this method M-estimators. The technique was developed in a series of subsequent works [9, 10]. The M-estimators method is relatively simple compared to other ones. Under certain conditions (absence of anomalous measurements, independence of measurements, etc.) the results produced by this method and LSM are supposed to coincide. The M-estimators method finds a wide application in processing various observations containing gross errors. In fact, in this method all measurements produced at

the experiment are included in the processing; they are also assigned with weighting factors depending on the chosen Huber function.

Determination of lunar parameters is essential for:

- (a) the solution of the inverse photogrammetric problem, i.e. determination of the projection center and selenographic referencing of space and ground-based images of the Moon.
- (b) the lunar surface mapping;
- (c) the Moon’s figure and macro relief refining;
- (d) the study of the Moon’s physical libration.

We used the observations produced by the heliometer as observational data. However, recent studies have shown that a part of heliometric observations is anomalous. The estimation of the desired lunar parameters using the classic least squares method requires the elimination of erroneous measurements (editing), as the latter significant influence the LSM-estimates.

2 Creation of Heliometric Observations Regression Models

Determining the constants of the physical libration of the Moon is reduced to finding some vector A . For these purposes, the system of equations is compiled and solved.

$$Z = A\Delta q + \varepsilon, \tag{1}$$

where $Z - (n \times 1)$ —free member vector, $A - (n \times m)$ —coefficient matrix for unknowns, ε —vector of the errors by dimension n .

The calculation of vector component values Z , and also the component of matrix A is described in sufficient detail in [11].

Concerning the vector Δq , it should be noted that its specific form is determined by the approach to determining the parameter f . In the case of using the method of a_3 obtained can write

$$\Delta q = [\Delta H, \Delta\lambda, \Delta\beta, \Delta J, a_3, \Delta R_0] \tag{2}$$

where ΔH —correction to the initial value of the radius—vector h_0 of the crater Mesting A, $\Delta\lambda$ and $\Delta\beta$ —corrections to the initial values of the selenographic longitude of λ_0 and selenographic latitude β_0 , ΔJ —correction to the initial value of the J_0 of the lunar equator to the ecliptic, a_3 —harmonic in the expansion of physical longitudinal libration, ΔR_0 —correction to the radius of the Moon R_0 .

Parameter estimation using the least-squares method assumes that the model of measurement errors is described by a normal law with a given expectation $E(\varepsilon)$ and covariance matrix, known up to some positive multiplier σ^2 .

$$D = \sigma^2 R, \tag{3}$$

where R —a given positive definite matrix. If $E(\varepsilon)$ is given, then the problem of estimating by the least-squares method (LSM) can always be reduced to the form in which $E(\varepsilon) = 0$ [12]. So the challenge LSM is decided in the assumption that

$$F(\varepsilon) = N[0, \sigma^2, R], \quad (4)$$

where $N[E(\varepsilon), D]$ —known expression for the density of the normal distribution.

As is known, the formulas of the classical method of least squares have the form [13]:

$$\Delta \hat{q} = SA^T D^{-1} Z, \quad (5)$$

where $(SA^T D^{-1} Z)^{-1}$ —matrix, on the diagonal of which the dispersion estimates for the components of the vector are located $\Delta \hat{q}$.

A significant drawback of the classical least squares method is the excessive sensitivity of LSM—estimates to uncontrolled deviations from the accepted normal distribution law of measurement errors [14]. The importance of deviations from normality, similar to heavier tails in comparison with the normal distribution or simply anomalous measurement errors, was noted at the end of the last century by Newcomb (1886). Since the usual LSM does not take into account the possible appearance of emissions, in practice the various empirical and semi-empirical methods of preliminary cleaning information from coarse measurements are used. Observations of the Moon to determine the constants of physical libration are no exception in this regard. The issue of the audit of observational material has always occupied an important place. However, work with a large array of information does not exclude both erroneous emissions and erroneous conservation [15].

3 The Use of the Huber Method for Analyzing Observations Models

To obtain estimates of the lunar physical libration coefficients which are protected from possible anomalous measurement errors, it is proposed to apply a noise-resistant (robust) estimation method [16], for example, the HMEM method. The robust variant of a variation-weighted least squares method can be used, where the weight matrix B is searched for using the Huber function Ψ . The solution will be according to the following formulas:

$$\Delta \hat{q} = (A^T B A)^{-1} A^T B, \quad (6)$$

where

$$diag B = \Psi(\xi)/\xi, \quad (7)$$

$$\Psi(\varepsilon) = \begin{cases} \xi, & |\xi| \leq b, \\ b \operatorname{sign}(\xi), & |\xi| \geq b \end{cases}, \quad (8)$$

$$\xi = (Z_i - A_i \Delta q_0)/M. \quad (9)$$

In turn median among non-zero values $|Z_i - A_i \Delta q_0|/0.6745$

$$M = \operatorname{med}\{|Z_i - A_i \Delta q_0|/0.6745 \neq 0\}, \quad (10)$$

Δq_0 preliminary vector estimate Δq , b setting parameter.

Evaluation of the accuracy of the final result Δq is described by the covariance matrix of the form

$$\operatorname{Cov} = k(A^T A)^{-1}, \quad (11)$$

where

$$k = (Mn)^2 \sum_1^n \Psi^2(\xi)/(n-m) \left[\sum_1^n \Psi'(\xi) \right]^2. \quad (12)$$

In this case, in expressions (9) and (10), the final value Δq_0 of the vector is taken as Δq .

4 Analysis of the Results

The values of the Moon's physical libration [17] constants were obtained using the two approaches noted above. To qualitatively analyze the data taken for processing, the assessment was carried out with various amounts of information:

- (1) VARIANT 1—the system (4) of 616×6 size (global system) was solved,
- (2) VARIANT 1—solved the first half of the global system,
- (3) VARIANT 1—solved the second half of the global system.

The final values of LSM—estimates, and M—estimates of the constants of the physical libration of the Moon are given in Tables 1, 2, 3 (according to various amounts of information). Corrections to the initial physical libration values are given in Tables 4, 5, 6.

As the values of the constants of physical libration of the Moon [18], obtained from the processing of the lunar positional observations, it is recommended to adopt the following robust estimates (Table 7).

When estimating by the method of least squares, the hypothesis of equipotential measurements was adopted, i.e. $R = I$ in the expression (3). At the same time, the estimate $\Delta \hat{q}$ of the vector Δq was found by the formula:

Table 1 Constants of the physical libration of the Moon for VARIANT 1

Parameters	LSM—estimations	M—estimations	
		$b = 1.50$	$b = 1.345$
λ	$-5^{\circ}10'04.87'' \pm 15.13''$	$-5^{\circ}10'04.40'' \pm 8.96''$	$-5^{\circ}10'04.17'' \pm 8.72''$
β	$-3\ 12\ 24.70 \pm 8.64$	$-3\ 12\ 27.08 \pm 5.12$	$-3\ 12\ 27.47 \pm 4.98$
J	$1\ 31\ 48.99 \pm 17.74$	$1\ 31\ 44.15 \pm 10.51$	$1\ 31\ 44.02 \pm 10.22$
f	0.645 ± 0.051	0.633 ± 0.030	0.632 ± 0.029
R_C	$932.266'' \pm 0.034''$	$932.259'' \pm 0.021''$	$932.258'' \pm 0.020''$
H	933.489 ± 0.510	933.489 ± 0.302	933.581 ± 0.294

Table 2 Constants of the physical libration of the Moon for VARIANT 2

Parameters	LSM—estimations	M—estimations	
		$b = 1.50$	$b = 1.345$
λ	$-5^{\circ}09'40.92'' \pm 25.83''$	$-5^{\circ}09'33.43'' \pm 15.65''$	$-5^{\circ}09'31.44'' \pm 14.90''$
β	$-3\ 12\ 23.66 \pm 12.55$	$-3\ 12\ 23.62 \pm 7.60$	$-3\ 12\ 23.35 \pm 7.24$
J	$1\ 31\ 41.86 \pm 27.44$	$1\ 31\ 37.91 \pm 16.62$	$1\ 31\ 36.34 \pm 15.82$
f	0.665 ± 0.074	0.656 ± 0.045	0.658 ± 0.042
R_C	$932.220'' \pm 0.052''$	$932.215'' \pm 0.032''$	$932.217'' \pm 0.030''$
H	933.428 ± 0.893	933.637 ± 0.541	933.724 ± 0.515

Table 3 Constants of the physical libration of the Moon for VARIANT 3

Parameters	LSM—estimations	M—estimations	
		$b = 1.50$	$b = 1.345$
λ	$-5^{\circ}09'52.25'' \pm 21.18''$	$-5^{\circ}09'49.37'' \pm 11.75''$	$-5^{\circ}09'48.69'' \pm 11.19''$
β	$-3\ 12\ 27.65 \pm 12.60$	$-3\ 12\ 30.81 \pm 6.96$	$-3\ 12\ 31.08 \pm 6.66$
J	$1\ 32\ 02.37 \pm 26.76$	$1\ 31\ 53.20 \pm 14.77$	$1\ 31\ 53.50 \pm 14.13$
f	0.611 ± 0.076	0.602 ± 0.042	0.600 ± 0.040
R_C	$932.317'' \pm 0.051''$	$932.309'' \pm 0.028''$	$932.211'' \pm 0.027''$
H	933.416 ± 0.750	933.471 ± 0.414	933.468 ± 0.396

$$\Delta\hat{q} = (A^T A)^{-1} A Z. \tag{13}$$

Table 4 Corrections to parameters of the physical libration of the Moon for VARIANT 1

Parameters	LSM—estimations	M—estimations	
		$b = 1.50$	$b = 1.345$
ΔH	$19.66'' \pm 112.62''$	$38.11'' \pm 66.71''$	$39.99'' \pm 64.90''$
$\Delta \lambda$	2.13 ± 15.13	2.60 ± 8.96	2.83 ± 8.72
$\Delta \beta$	-82.70 ± 8.64	-85.08 ± 5.12	-85.47 ± 4.98
ΔJ	-31.01 ± 17.74	-35.85 ± 10.51	-35.98 ± 10.22
a_3	87.90 ± 14.29	91.24 ± 8.41	91.47 ± 8.19
ΔR_0	-0.314 ± 0.031	-0.321 ± 0.021	-0.322 ± 0.020

Table 5 Corrections to parameters of the physical libration of the Moon for VARIANT 2

Parameters	LSM—estimations	M—estimations	
		$b = 1.50$	$b = 1.345$
ΔH	$6.14'' \pm 197.45''$	$52.39'' \pm 119.62''$	$-71.50'' \pm 114.99''$
$\Delta \lambda$	26.08 ± 25.83	33.57 ± 15.65	35.56 ± 14.90
$\Delta \beta$	-81.66 ± 12.55	-81.62 ± 7.60	-81.35 ± 7.24
ΔJ	-38.14 ± 27.44	-42.09 ± 16.62	-43.66 ± 15.82
a_3	82.08 ± 20.50	84.73 ± 12.42	83.98 ± 12.08
ΔR_0	-0.360 ± 0.052	-0.365 ± 0.032	-0.363 ± 0.030

Table 6 Corrections to parameters of the physical libration of the Moon for VARIANT 3

Parameters	LSM—estimations	M—estimations	
		$b = 1.50$	$b = 1.345$
ΔH	$3.56'' \pm 165.64''$	$15.58'' \pm 91.42''$	$14.95'' \pm 87.51''$
$\Delta \lambda$	24.75 ± 21.18	27.63 ± 11.75	28.31 ± 11.19
$\Delta \beta$	-85.65 ± 12.60	-88.81 ± 6.96	-89.08 ± 6.66
ΔJ	-17.63 ± 26.76	-26.80 ± 14.77	-26.50 ± 14.13
a_3	97.79 ± 21.80	99.97 ± 12.03	100.62 ± 11.52
ΔR_0	-0.263 ± 0.052	-0.271 ± 0.028	-0.269 ± 0.027

Table 7 The recommended parameters of the physical libration of the Moon

$J =$	$1^\circ 31' 44.02'' \pm 10.22''$
$\lambda =$	$-5 \ 10 \ 04.17 \pm 8.72$
$\beta =$	$-3 \ 12 \ 27.47 \pm 4.98$
$f =$	0.632 ± 0.029
$H =$	$933.581'' \pm 0.294''$
$R_C =$	932.258 ± 0.020

5 Conclusion

The significant complexity of the modern models requires new approaches to systematic solutions for maintaining the necessary accuracy level [19], which could be achieved by the application of CPS-methods [20]. Besides, the demand for individual production by introducing various observations increases the diversity of computer systems, which makes their rearrangement labor-consuming and complex, and also requires the corresponding supercomputer facilities [21].

The noise-resistant estimates of the physical libration constants were found for two values of the tuning parameter (8): $b = 1.50$ and $b = 1.3457$. The first value corresponds to the exact normal distribution of measurement errors [22]. The second value of b allows one to obtain estimates with 95% efficiency (in the asymptotics) in the case of the normal distribution of interference. It is noted that a loss of 5% efficiency is a charge for achieving sustainability.

Theoretically, the M-estimates (for $b = 1.50$) and the estimates of the usual least-squares method should coincide in the case of a sample obeying the normal distribution law [23]. In our case, these estimates turned out to be different from each other (Tables 1, 2, 3). Therefore, it is fully justified to reject the hypothesis of equal measurement accuracy. In this case, it is fair to assume the presence of some deviations from the normal model of measurement errors, in particular, the presence of anomalous errors. Then the M—estimates of the physical libration constants of the Moon obtained with a setting value of 1.345 should be considered more reliable.

The results of this work can be used to analyze lunar physical parameters [24], study the internal structure of the Moon [25], and build maps of the physical surface of our natural satellite [26]. This is especially important because space missions and robotic exploration of the moon are planned.

Acknowledgements This work was partially supported by the Russian Science Foundation, grant no. 20-12-00105 (according to the grant, the method for data analysis was created and the numerical calculations were carried out). This paper has been supported by the Kazan Federal University Strategic Academic Leadership Program. This work was partially supported by the Russian Foundation for Basic Research grant no. 19-32-90024 and the Foundation for the Advancement of Theoretical Physics and Mathematics “BASIS”.

References

1. Bogatyrev, V.A., Aleksankov, S.M., Derkach A.N.: The model of reliability of dублиated real-time computers for cyber-physical systems. In: *Cyber-Physical Systems: Industry 4.0 Challenges*, pp. 11–21 (2020). https://doi.org/10.1007/978-3-030-32648-7_2
2. Jiang, W., Wen, L., Zhan, J., Jiang, K.: Design optimization of confidentiality-critical cyber-physical systems with fault detection. *Robot. Computer-Integr. Manuf.* **64**, 101956 (2020)
3. Nashivochnikov, N.V., Bolshakov, A.A., Lukashin, A.A., Popov M.: The system for operational monitoring and analytics of industry cyber-physical systems security in fuel and energy domains

- based on anomaly detection and prediction methods. In: *Cyber-Physical Systems: Industry 4.0 Challenges*, pp. 261–273 (2020). https://doi.org/10.1007/978-3-030-32648-7_21
4. Veshneva, I.V., Bolshakov, A.A., Fedorova, A.E.: Organization of engineering education for the development of cyber-physical systems based on the assessment of competences using status functions. In: *Cyber-Physical Systems: Industry 4.0 Challenges*, pp. 277–288. Springer, (2020). https://doi.org/10.1007/978-3-030-32648-7_22
 5. Monostori, L.: Cyber-physical production systems: roots, expectations, and R&D challenges. *Procedia CIRP* **17**, 9–13 (2014)
 6. Monostori, L., Kádár, B., Bauernhansl, T., Kondoh, S., Kumara, S., Reinhart, G., Sauer, O., Schuh, G., Sihm, W., Ueda, K.: Cyber-physical systems in manufacturing. *CIRP Ann.* **65**(2), 621–641 (2014)
 7. Nefedjev, Y.A., Rizvanov, N.G.: The results of an accurate analysis of EAO charts of the Moon marginal zone constructed based on lunar occultations. *Astron. Nachr.* **323**(2), 135–138 (2002)
 8. Huber, P.J., Kleiner, B., Gasser, T., Dumermuth, G.: Statistical methods for investigating phase relations in stationary stochastic processes. *IEEE Trans. Audio Electroacoustics* **19**(1), 78–86 (1971)
 9. Zhang, Z.: Parameter estimation techniques: a tutorial with application to conic fitting. *Image Vision Comput.* **15**(1), 59–76 (1997)
 10. Duchnowski, R.: Sensitivity of robust estimators applied in strategy for testing the stability of reference points. *EIF Approach Geodesy Cartography* **60**(2), 123–134 (2011)
 11. Nefedjev, Y., Valeev, S., Mikeev, R., Varaksina, N., Andreev, A.: Analysis of data of “CLEMENTINE” and “KAGUYA” missions and “ULCN” and “KSC-1162” catalogs. *Adv. Space Res.* **50**(11), 1564–1569 (2012)
 12. Yang, Y., Cheng, M.K., Shum, C.K.: Robust estimation of systematic errors of satellite laser range. *J. Geodesy* **73**(7), 345–349 (1999)
 13. Nefedjev, Yu.A., Andreev, A.O., Petrova, N.K., Demina, N.Yu., Zagidullin, A.A.: Creation of a global selenocentric coordinate reference frame. *Astron. Rep.* **62**(12), 1015–1019 (2018)
 14. Nowel, K., Kaminski, W.: Robust estimation of deformation from observations' differences (REDOD) for free monitoring networks. *J. Geodesy* **88**(8), 749–764 (2018)
 15. Wiśniewski, Z.: Estimation of parameters in a split functional model of geodetic observations (M split estimation). *J. Geodesy* **83**(2), 105–120 (2009)
 16. Huber, P.J.: Robust estimation of a location parameter. In: *Breakthroughs in Statistics*, pp. 492–518 (1992)
 17. Williams, J.G., Konopliv, A.S., Boggs, D.H., et al.: Lunar interior properties from the GRAIL mission. *J. Geophys. Res. Planets* **119**(7), 1546–1578 (2014)
 18. Petrova, N.K., Nefedjev, Y.A., Zagidullin, A.A., Andreev, A.O.: Use of an analytical theory for the physical libration of the moon to detect free nutation of the lunar core. *Astron. Rep.* **62**(12), 1020–1024 (2018)
 19. Nikolakis, N., Senington, R., Sipsas, K., Syberfeldt, A., Makris, S.: On a containerized approach for the dynamic planning and control of a cyber-physical production system. *Robot. Computer-Integr. Manuf.* **64**, 101919 (2020)
 20. Park, K.-J., Zheng, R., Liu, X.: Cyber-physical systems: milestones and research challenges. *Comput. Commun.* **36**(1), 1–7 (2012)
 21. Elugachev, P., Shumilov, B.: On the application of the photogrammetric method to the diagnostics of transport infrastructure objects. In: *Cyber-Physical Systems: Industry 4.0 Challenges*, pp. 51–62. Springer, (2020). https://doi.org/10.1007/978-3-030-32648-7_5
 22. Yang, Y., He, H., Xu, G.: Adaptively robust filtering for kinematic geodetic positioning. *J. Geodesy* **75**(2–3), 109–116 (2001)
 23. Bianco, A.M., Garcia Ben, M., Yohai, V.J.: Robust estimation for linear regression with asymmetric errors. *Canadian J. Stat.* **33**(4), 511–528 (2005)
 24. Kronrod, E.V., Kronrod, V.A., Kuskov, O.L.: Geochemical constraints for the bulk composition of the Moon. *Doklady Earth Sci.* **483**(1), 1475–1479 (2018)

25. Williams, J.G., Boggs, D.H.: Tides on the Moon: Theory and determination of dissipation. *J. Geophys. Res. E: Planets* **120**(4), 689–724 (2015)
26. Varaksina, N.Y., Nefedyev, Y.A., Churkin, K.O., Zabbarova, R.R., Demin, S.A.: Selenocentric reference coordinates net in the dynamic system. *J. Phys: Conf. Ser.* **661**(1), 012014 (2015)

Cyber-Physical Resolution Evaluation System for Digital Aerophotographic Systems



Evgeniy Chausov and Andrey Molchanov

Abstract The methodological support for the collection and processing of information in a cyber-physical system for evaluating the linear resolution of digital aerophotographic systems on the ground using the modulation transfer function is presented, which ensures the determination of the modulation transfer function according to the results of a flight experiment in an automated mode.

Keywords Cyber-physical system · Modulation transmission function · Linear resolution on the ground · Line-of-sight world · Digital aerophotographic system · Flight tests

1 Introduction

Flight tests are an important step in the creation of military digital aerophotographic systems (MDAPS) since it is the results of flight tests that evaluate the effectiveness of the system, on the basis of which a recommendation can be made to put the system into operation and put it into mass production. The main characteristic of the effectiveness of the MDAPS, evaluated during flight tests, is the linear ground resolution (LGR). Today, in accordance with the current regulatory and technical documents of the system of general technical requirements, the evaluation of LGR occupies at least 80% of the flight test program of the MDAPS, which amounts to 20 flights (launches) of aircraft (unmanned aerial vehicles) in depending on the complexity of the system and the requirements for it. On the one hand, this figure emphasizes the importance of the LGR indicator, but on the other hand, it shows the low efficiency of the existing methodological support for MDAPS flight tests.

E. Chausov (✉) · A. Molchanov
State Flight Testing Center Named After Chkalov, 12 Kharitonov Street, 416500 Akhtubinsk,
Russia
e-mail: ewhenig@ya.ru

A. Molchanov
e-mail: andryoe@yandex.ru

The search for ways and specific proposals for improving the methodological support of flight tests of the MDAPS is an urgent task. One of the main directions for intensifying tests and improving the quality of the results obtained is the use of special cyber-physical systems.

2 Methodic for Evaluation Linear Ground Resolution Based on the Modulation Transfer Function at the Stage of Flight Tests

The mathematical model of MDAPS can be represented as an analytical expression of the modulation transfer function (MTF), which reflects a decrease in the image (sharpness) properties of MDAPS due to losses and distortions both in the system and outside it, due to the influence of various factors (atmospheric, flight factors, decoder, etc.) [1–5]. Such a model makes it possible to evaluate the MDAPS LGR without performing part of the flights, which can significantly increase the effectiveness of the methodological support of MDAPS flight tests. However, the large number of assumptions used in constructing the mathematical model and the variety of approaches to the description of some parts of the MTF does not provide the reliability of the obtained LGR estimates, which is required for flight testing, which makes it difficult to use the analytical MTF in practice without taking steps to refine the mathematical model. The refinement of the model is to bring the analytical expression of the MTF to a form that ensures the convergence of the graph of the analytical MTF and the experimental MTF obtained during the flight experiment.

Thus, it is proposed to use the following methods for evaluation of the LGR of MDAPS based on the MTF:

1. The construction of a mathematical model (analytical MTF) MDAPS according to known mathematical dependencies [1–3].
2. The determination of the experimental MTF according to the results of the flight experiment.
3. Calibration of the mathematical model of MDAPS or the construction of a refined mathematical model (a posteriori MTF) based on a comparison of the analytical and experimental MTF and the further introduction of calibration coefficients to ensure the convergence of the analytical and experimental MTF.
4. Evaluation of the LGR using the refined MDAPS model in accordance with the known resolution indicators (Shade, threshold modulation characteristics, empirical indicators, etc.) [1–10].

The methodic issues of implementing paragraphs 1 and 4 of the proposed methodic are widely covered in the well-known works of domestic and foreign authors, however, the issues of determining the experimental MTF based on the results of a flight experiment and calibration of the model of MDAPS are not fully considered to date and deserve separate studies. The scope of this chapter addresses the issues

of determining the experimental MTF MDAPS according to the results of a flight experiment.

It is known [11–19] that with a decrease in the size of photographing objects, the brightness differences in their image decrease, i.e. their contrast in the image decreases. The characteristic of the relative distribution of illuminance E in the image of the object, determined by the expression

$$K_{im} = (E_{max} - E_{min}) / (E_{max} + E_{min}),$$

called image contrast. The ratio of the contrast of the K_{im} image to the contrast of the K_{ob} for a given spatial frequency ν is called the modulation transmission coefficient T :

$$T = K_{im} / K_{ob}.$$

The dependence of the modulation transmission coefficient T on the spatial frequency ν is a MTF:

$$W_{MDAPS} = T(\nu).$$

Thus, if you place a periodic test-object on the ground, consisting of alternating dark and light stripes, the width of which gradually decreases, and the brightness difference between the dark and light stripes remains constant and is characterized by the K_{ob} , and perform aerial photography of such a test-object by using MDAPS, then the instrumental analysis of the obtained aerial photographs will allow us to determine the experimental MTF of the MDAPS.

The test-object is a set of groups of black and white strokes with a constant width (spatial frequency) within the group and increasing (decreasing) from group to group (Fig. 1).



Fig. 1 Visible range test-object

3 The Automated Complex of Processing Digital Images in the Task of Determining the Linear Ground Resolution

The digital format of aerial photographs obtained by the MDAPS allows automating the process of determining the experimental MTF at an automated workstation with special software preinstalled on it. Therefore, for the purpose of determining the experimental MTF, a special cyber-physical system for digital image processing (ACPDPI) was developed. This automated complex operates on the basis of computers with the “Windows” operating system. In the dialogue mode, on the screen of the monitor through the menu system and prompts, the operator can automatically download digital images obtained using MDAPS, measure the illumination of the image sections of interest, calculate modulation transmission coefficients, carry out statistical processing of the results and plot the experimental MTF of the studied MDAPS [12–17].

ACPDPI structurally consists of 3 modules [4]:

- “Image analysis module”;
- “Calculation module”;
- “MTF construction module”.

The determination of the experimental MTF using ACPDI is carried out in accordance with the following algorithm:

1st stage: inputting the images of the test-object into the “Image Analysis Module”.

2nd stage: in the “Image Analysis Module”, the images of the test-object are decoded and the illuminances of the dark and light strokes of the test-object are measured.

Deciphering the image of the test-object is to visually determine the difference in the level of gray tone between each light stroke and the adjacent dark strokes. As long as the difference between light and dark strokes (sections of strokes) is visually perceived, measurements of illuminance of strokes (sections of strokes) are performed. Those groups of the test-object, according to the strokes of which the measurements were made, are taken as recognized groups. The subjective nature of the decryption results necessitates decryption not by one operator, but by k operators. Moreover, to ensure the reliability of decryption results, it is necessary $k \geq 3$ [18, 19].

Further, for each i -th image of the test-object, each k -th decryptor measures the illuminances of the test-object $E_{\max j i k}$ and $E_{\min j i k}$ for each j -th recognized group, where $E_{\max j i k}$ and $E_{\min j i k}$ are the illumination values of the bright and a dark stroke, respectively, of the j -th recognized group of the i -th image of the test object. Measurements of $E_{\max j i k}$ and $E_{\min j i k}$ are carried out in the values of the gray tone level 0 and 255 for dark and light strokes, respectively [20–26].

3rd stage: the measured values $E_{\max j i k}$ and $E_{\min j i k}$ are entered into the “Calculation module”, values of the width d_j of strokes of recognized groups (spatial frequencies) of the test-object, as well as the actual (passport) value of the modulation contrast of the test-object K_{ob} . After starting the calculation, the values of the

modulation transmission coefficients T_j are obtained for each j -th recognized group of test-object. The calculation algorithm ACPDI is constructed in such a way that when calculating T_j , the values $E_{\max j}$ and $E_{\min j}$ are used, obtained as the arithmetic average of the measurement results $E_{\max j i k}$ and $E_{\min j i k}$, respectively:

$$E_{\max j} = \left(\sum_{i=1}^n \sum_{k=1}^m E_{\max j i k} \right) / (n \cdot m), \quad E_{\min j} = \left(\sum_{i=1}^n \sum_{k=1}^m E_{\min j i k} \right) / (n \cdot m),$$

where n —is the number of images of the test-object, m —is the number of decoders.

4th stage: in the “MTF construction module”, based on the spatial frequencies of the test-object equal to $v_j = 1/d_j$ and the corresponding values of the modulation transmission coefficients T_j , the MTF graph is constructed.

4 Results of Experimental Verification of the Developed Methodological Support of a Cyber-Physical System for Processing Digital Images

Let us consider an example of determining the experimental MTF using ACPDI from images obtained during flight tests of a digital camera complex with an Orlan-10 UAV. As a test-object, a black canvas was used, which has 11 groups of white strokes. Aerial photography was carried out from a height of $H = 500$ m.

The initial data for determining the experimental MTF of the Orlan-10 UAV digital camera using ACPDI are:

1. stroke width of the test-object d : 0.066 m; 0.082 m; 0.102 m; 0.128 m; 0.16 m; 0.2 m; 0.25 m; 0.31 m; 0.39 m; 0.49 m; 0.61 m;
2. actual modulation contrast of the test-object $K_0 = 0.5$. The contrast of the test-object is determined by the formula $K_0 = (L_c - L_T) / (L_c + L_T)$, where L_T and L_c —are the results of measurements of the brightness of the dark and light strokes of the test object during aerial photography
3. total number of aerial photographs selected for analysis showing the test object: $n = 5$ (a fragment of one of the aerial photography is shown in Fig. 2)
4. the number of decoders decrypting the images of the test object and the automated measurement of the illuminance of the strokes of recognized groups using ACPDI software tools: $m = 3$

As a result of work at the first stage in the « Image Analysis Module », the results of measurements of the illumination of the dark and light strokes of the world were obtained. After entering the measurement results obtained at the first stage into the « Calculation module» and starting the computational process, the values of the modulation transfer coefficients T_j are obtained, shown in Table 1.

At the final stage in the “MTF construction module”, after the start of the charting function, obtained graphic view MTF, shown in Fig. 3.

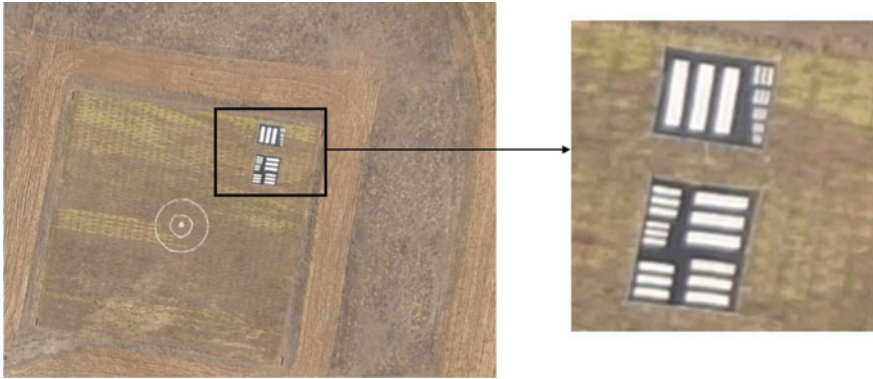


Fig. 2 A fragment of the image of the test object

Table 1 Values of modulation transmission coefficients

T	0.857	0.842	0.815	0.726	0.642	0.508	0.358	0.165	0.075	0.055	0.005
ν , 1/m	1.64	2.04	2.56	3.23	4	5	6.25	7.81	9.80	12.19	15.15

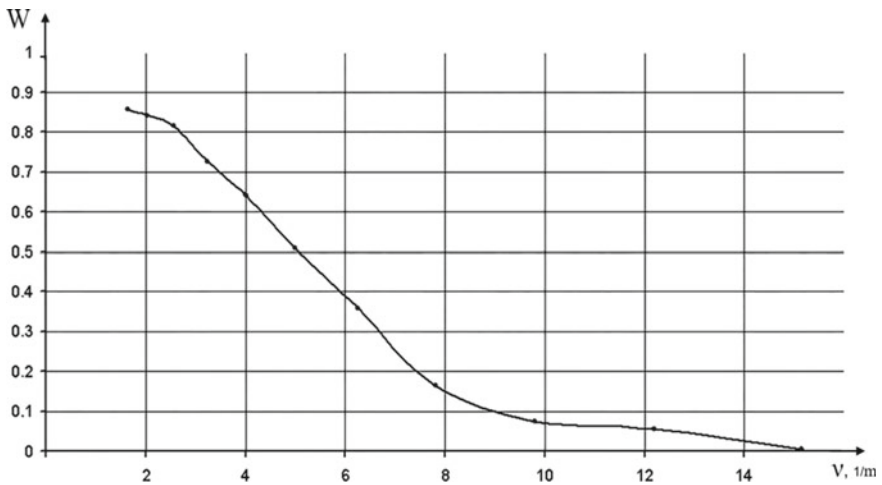


Fig. 3 Schedule of the experimental MTF of the digital camera UAV Orlan-10

The graph form of the experimental MTF of the digital camera complex with the Orlan-10 UAV obtained with the help of ACPDI practically coincides with the form of the typical photographic MTF given in [1, 2], which confirms the correctness of the functioning algorithm ACPDI.

The graphic view of the experimental MTF presented in Fig. 3, allows you to evaluate the LGR of a digital camera UAV « Orlan-10 » in accordance with known

indicators. When using one of the empirical resolution indicators, which corresponds to the MTF value $W_0 = 0.1$, the value of the limiting spatial frequency was $\nu_{\text{lim}} = 8.5 \text{ m}^{-1}$, which corresponds to the LGR value $L = 0.118 \text{ m}$. The visual LGR evaluation performed by the group of decoders for image of the test-object was $L = (0.128 \pm 0.052) \text{ m}$. Comparison of the LGR estimates obtained by the visual method and the experimental MTF, shows satisfactory convergence of the results, which confirms the reliability of the experimental MTF obtained using ACPDI.

5 Conclusion

The results obtained illustrate the performance of the developed cyber-physical system for assessing the resolution of digital aerophotographic systems, which makes it possible to effectively use it for evaluating the linear resolution on the ground during flight tests of aerophotographic systems of aerial reconnaissance and surveillance.

Acknowledgements The study was carried out with the financial support of the Russian Foundation for Basic Research within the framework of scientific project No. 20-013-00306.

References

1. Molchanov, A.S.: In: Theory of Building Iconic Aerial Reconnaissance Systems. pp. 224. Panorama, Volgograd (2017)
2. Perezyabov, O.A., Maltseva, N.K., Ilinski, A.V.: Optoelectronic system modulation transfer function measurement based on the method of summation over different frequencies harmonic functions. In: Proceedings of SPIE–The International Society for Optical Engineering. Optical Fabrication, Testing, and Metrology VI (2018)
3. Holst, G.C.: In: Electro-Optical Imaging System Performance. 2nd edn. pp. 120. SPIE Optical Engineering Press, Bellingham (2000)
4. Chausov, E.V., Molchanov, A.S.: Software and methodical complex for image processing during flight tests of iconic optical-electronic systems. *Geodesy and Cartography* **81**(1), 26–33 (2020). <https://doi.org/10.22389/0016-7126-2020-955-1-0-0>
5. Boreman, G.D.: In: Modulation Transfer Function in Optical and Electro-Optical Systems. pp. 110. SPIE, Bellingham (2001)
6. Yang, Z., Vorontsov M.A.: Impact of atmospheric turbulence and refractivity on the modulation transfer function of incoherent imaging system. *J. Opt.* (2017). <https://doi.org/10.1088/2040-8986/aa91f2>
7. Cyber-Physical Systems: Advances in Design and Modelling: In: Kravets, A.G., Bolshakov, A.A., Shcherbakov, M.V. (eds.) pp. 340. Springer (2019). <https://doi.org/10.1007/978-3-030-32579-4>
8. Agent Technology: Foundations, Applications, and Markets. In: Jennings, N.R., Wooldridge, M.J. (eds.) pp. 325. Springer, Heidelberg (2012)
9. Kizim, A.V., Kravets, A.G.: On systemological approach to intelligent decision-making support in industrial cyber-physical systems. In: Cyber-Physical Systems: Industry 4.0 Challenges. Studies in Systems, Decision and Control, vol. 260. pp. 167–183. Springer, Cham (2020)

10. Djite, I., Estribeau, M., Magnan, P., Rolland, G., Petit, S., Saint-Pe, O.: Theoretical models of modulation transfer function, quantum efficiency and crosstalk for CCD and CMOS image sensors. *IEEE Trans. Electron Devices* **59**(3), 729–739 (2012)
11. Larkin, E., Bogomolov, A., Privalov, A.: Discrete model of mobile robot assemble fault-tolerance. In: *Lecture Notes in Computer Science*. vol. 11659 LNAI, pp. 204–215 (2019). https://doi.org/10.1007/978-3-030-26118-4_20
12. Bychkov, E.V., Bogomolov, A.V., Kotlovanov, K.Y.: Stochastic mathematical model of internal waves. *Bullet. South Ural State Univer. Ser. Math. Modell. Program. Comput. Softw.* **13**(2), 33–42 (2020). <https://doi.org/10.14529/mmp200203>
13. Ishakova, A.O., Alekhin, M.D., Bogomolov, A.V.: Time-frequency transforms in analysis of non-stationary quasi-periodic biomedical signal patterns for acoustic anomaly detection. *Info. Manage. Syst.* **1**, 15–23 (2020). <https://doi.org/10.31799/1684-8853-2020-1-15-23>
14. Larkin, E., Bogomolov, A., Gorbachev, D., Privalov, A.: About approach of the trans-actions flow to poisson one in robot control systems. In: *Lecture Notes in Computer Science*. vol. 10459 LNAI. pp. 113–122. Springer-Verlag GmbH (2017). https://doi.org/10.1007/978-3-319-66471-2_13
15. Larkin, E.V., Bogomolov, A.V., Privalov, A.N., Dobrovolsky, N.N.: Discrete model of paired relay-race. *Bullet. South Ural State Univer. Ser. Mathe. Modell. Program. Comput. Softw.* **11**(3), 72–84 (2018). <https://doi.org/10.14529/mmp180306>
16. Vasiliev, S.S., Korobkin, D.M., Kravets, A.G., Fomenkov, S.A., Kolesnikov, S.G.: Ex-traction of cyber-physical systems inventions' structural elements of Russian-language patents. *Cyber-Phys. Syst. Adv. Design and Model.* **2020**, 55–68 (2020)
17. Dudzik, M.C.: The infrared and electro-optical systems handbook. In: *Electro-Optical Systems Design, Analysis, and Testing*. vol. 4. pp. 352. SPIE Optical Engineering Press, Bellingham (1993)
18. Ronald, W., Marwood, N.W.: *Electro-Optics Handbook*, 2nd edn, p. 1000. Food and Drug Administration Rockville, Maryland (2000)
19. Rebrin, Y.K.: In: *Optical-Electronic Reconnaissance Equipment for Aircraft*, pp. 450. VVAIU, Kiev (1988)
20. Gerald, F.M.: In: *Handbook of Optical and Laser Scanning*. pp. 784. Marcel Dekker Inc. (2004)
21. Meshcheryakov, R.: Control of hyperlinked cyber-physical systems. In: *Smart Innovation, Systems and Technologies*. pp. 27–33. Springer (2020)
22. Dragan, S.P., Bogomolov, A.V., Zinkin, V.N.: Methodical support of monitoring the acoustic safety of flight personnel. In: *AIP Conference Proceedings*, vol. 2140, pp. 020019. (2019). <https://doi.org/10.1063/1.5121944>
23. Larkin, E.V., Bogomolov, A.V., Gorbachev, D.V., Privalov, A.N.: Criteria investigation for the correspondence of events flow to a poisson flow. *Herald of Comput. Info. Technol.* **1**, 3–11 (2019). <https://doi.org/10.14489/vkit.2019.01>
24. Larkin, E.V., Bogomolov, A.V., Privalov, A.N.: A method for estimating the time intervals between transactions in speech-compression algorithms. *Autom. Document. Math. Linguistics.* **51**(5), 214 (2017). <https://doi.org/10.3103/S000510551705003X>
25. Liberovsky, N.Y., Chirov, D.S., Priputin, V.S.: Development of the two real signals blind separation method using fourth-order cumulants. *Bullet. South Ural State University. Ser. Math. Modell. Program. Comput. Softw.* **13**(2), 43–53 (2020). <https://doi.org/10.14529/mmp200203>
26. Rusetsky, V., Makukha, V.K.: Development of modulation transfer function test bench for image intensifier tubes. In: *Theses of the All-Russian Scientific-Practical Conference of Graduate Students and Undergraduates*, pp. 116–118 (2016)

Modelling and Intelligent Control Implementation

Configuring Systems Based on Petri Nets, Logic-Probabilistic, and Simulation Models



Irina Bondareva , Anna Khanova , and Yulya Khanova 

Abstract The presented conceptual solution enables the design of a complex system configuration and risk analysis using the example of a cargo port. A formal description of Petri net configuration graphs is presented. The sequential construction of risk scenarios, L-models, and B-models for each strategic goal is shown. The solution is based on the formal technique of goals definition, logical management of the sequence of operations, selection and issuance of management decisions, formalization of risk scenarios, and their interpretation based on the results of simulation modeling. The simulation model will make it possible to obtain a reasonable quantitative assessment of the risk of failure to achieve a strategic goal for making management decisions.

Keywords Petri nets · Configuration · Complex system · Logical-probabilistic models · Simulation models · Balanced scorecard system

1 Introduction

A promising direction of management in social and economic systems, including large transport logistics enterprises, is the focus on building configurations of complex systems (CS) based on the analysis and assessment of risk events and situations that arise during the course operation of these enterprises in order to prevent undesirable events by predicting the likelihood of their occurrence.

I. Bondareva (✉) · A. Khanova
Astrakhan State Technical University, 16 Tatishcheva St, Astrakhan 414056, Russia
e-mail: orange8@mail.ru

A. Khanova
e-mail: akhanova@mail.ru

Y. Khanova
Saint-Petersburg Electrotechnical University “LETI”, 5 Professora Popova St, 197376 St.
Petersburg, Russia
e-mail: yulya_khanova@mail.ru

The concept of the configuration of a complex system explored by Mintzberg et al. [1] implies a stable complex state corresponding to the period of its stable development and characterized by a combination of various factors: development strategy and the corresponding indicators, services provided, products produced, resources consumed, organizational structure, applied technologies, logistic schemes, methods and models, personnel, etc. Within the framework of the concept of configuration, the functioning of the CS is a cyclic process, which consists of the repetition of intra-configuration cycles (*IC*-cycles). *IC*-cycle has a time duration, for example, 1 year, 6 months, etc., determined by the *SG* development strategy, and consists of targeted actions – operations $p_i, i = 1, \dots, np$. For each configuration (each reiteration of the *IC*-cycle), a system of indicators is formed, with the corresponding hierarchy of goals $d_i, i = 15, \dots, md$ ($md = 25$ in the example in Fig. 2) taking into account the risk of their failure to be achieved [2]. The execution of operations is accompanied by the consumption of resources $r_i, i = 1, \dots, nr$ (raw materials, temporary, financial, labor, etc.) and the calculation of indicators of the CS $d_i, i = 1, \dots, nd$ ($nd = 13$ in the example in Fig. 2). Implementation of the *IC*-cycles depends on the impact of the external environment – exogenous factors $f_i, i = 1, \dots, nf$. In case of deviation of indicators from the planned values in the *IC*-cycle, a plurality of management decisions $u_i, i = 1, \dots, nu$ is formed in order to improve the situation. We should understand a “situation” as a set of indicator values and some events from the past.

One of the approaches to building the configuration of the complex systems (CS) is to build models based on Petri nets (PN) [3–5]. Due to the application of the logical-probabilistic (LP) approach, the possibilities of analyzing the parameters that affect the functioning of the system, as well as the risk of failure to achieve the set goals, are expanded [6, 7]. Simulation models are widely used to link the current state of the object and scenarios of management decisions with the future state of the object [8, 9]. The statistical data of the simulation models are generated as sets of indicators. In modern management, there is a number of indicator systems for the organization of effective management of complex systems [10]. In the Bain and Company’s study “Management Tools and Trends” [11], one of the most demanded, with a consistently high level of satisfaction from use in organizations is the balanced scorecard system (BSC) presented in the papers by Kaplan and Norton [12, 13]. Let us take a look at the integration of the presented approaches for building the CS configuration (Fig. 1). As the domain of the CS, we will choose a transport logistics enterprise—a cargo port (CP).

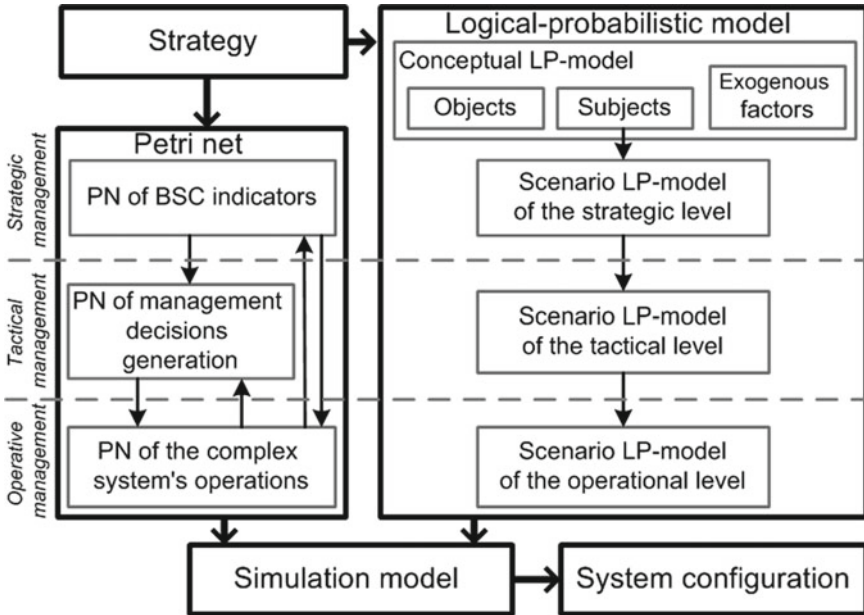


Fig. 1 CS configuration flow chart based on PN, LP, and simulation model

2 Configuration Model of a Complex System Based on the Petri Net

The PN-based CS configuration model (Fig. 1) is characterized by four interacting structures (Fig. 2) [14]:

1. the “vertical” structure of the BSC, including goals definition based on the “tree”-like acyclic SCs (graph of goals, Fig. 2a);
2. the “horizontal” structure of the BSC taking into account the mutual influence of deviations from the normal values of indicators based on “weighted” SCs (graph of indicators, Fig. 2b);
3. the process of acquisition of information about the complex system’s parameters, data analysis, and initialization of the management decisions – taking into account the parallelism and asynchrony of the decisions made, as well as their probabilistic nature based on the conventional SC (graph of operations, Fig. 2c);
4. the process of managerial response to probable deviations of the values of the BSC indicators from the standard values—taking into account the asynchrony of parallel processes based on the conventional SC (graph of management decisions, Fig. 2d).

The tree-like acyclic SCs of the BSC goals [15], as well as the “weighted” SCs, are logically united into a single network—colored SC [3]. The graph of operations is the coordinator of the SC-based CS configuration model. When the transition

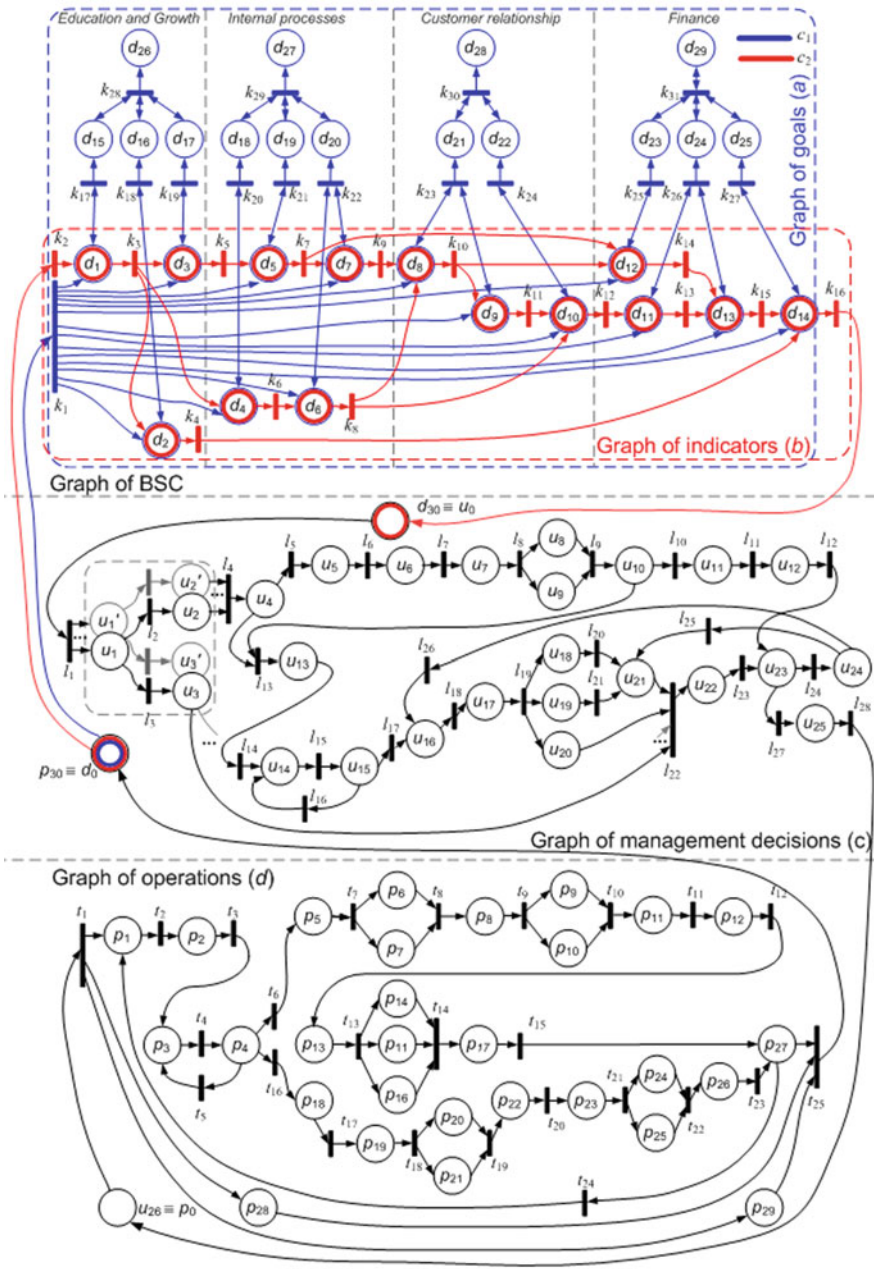


Fig. 2 PN-based CS configuration model

t_{25} of the operations graph is triggered (Fig. 2), markers are added to the initial empty positions of the BSC goals graph and certain positions of the BSC indicators graph. Initial increments are set for the inserted markers. At the time immediately preceding the t_{25} triggering, the model of the CS configuration was in equilibrium, and the increments (markings of BSC indicators graph positions) were zero. As a result, in the graphs of goals and indicators (BSC graph, Fig. 2), a transient process is initiated, and marker move during this process. During the course of the process execution, the values and, possibly, the signs of the indicators change in the BSC indicators column [16].

At the end of the transient process, equilibrium is established: in the BSC goals graph, due to its acyclicity, in the BSC indicators graph—with the obtained values of goals and indicators, and also taking into account external influences, permitting conditions are calculated that weigh the transitions of the operations graph. When the transition k_{16} is triggered, a PN is launched modeling the processes of assessing and recognizing the current situation, forming, ranking, classifying, parameterizing, and making managerial decisions based on the indicators and goals of the BSC (graph of management decisions, Fig. 2) [17].

The generated set of solutions is transferred to the operating network, and the intra-configuration simulation cycle is repeated (Fig. 2). Operating network transitions management $t_i, i = 1, \dots, nt$ is carried out by permitting conditions referenced with transitions.

3 LP-Model of the Goals Non-achievement Risk

The hybrid LP-model of risk (Fig. 1) combines two conceptual LP-models and one scenario model at three levels of management (strategic, tactical, and operational) (Fig. 3). The difference between the conceptual and scenario models, in this case, is that the LP-model of the risk of each conceptual process or development phenomenon is an L-union of the influencing events (factors, subjects) that are not quantitative characteristics [18]. Their risks as the events leading to a decrease in the efficiency of the functioning of the cargo port should be assessed using expert information [19].

The subjects S_{cep} , and exogenous random factors EF_{cep} are identified as conceptual components, object-goals G_{cep} are represented by the scenario LP-model. Failure to achieve the SG strategy depends on subjects $S_{cep} = (S_1, S_2, \dots, S_5)$ and object-goals $G_{cep} = (GN_1, GN_2, \dots, GN_4)$ detailing the main goal chosen as a complex problem.

Subjects S_{cep} determine who solves the problem posed, and objects—what smaller goals are associated with the SG problem. From the point of view of the implementation of the CS's managerial function and on the basis of the presence of one or another degree of involvement, as well as interest in solving the specified problem, we will single out the following subjects (using the CP example): S_1 —port's management, S_2 —port's clients, S_3 —local government authorities, S_4 —people who are not port's clients, S_5 —port's and facilities' staff. We will represent the subject failure event S_i

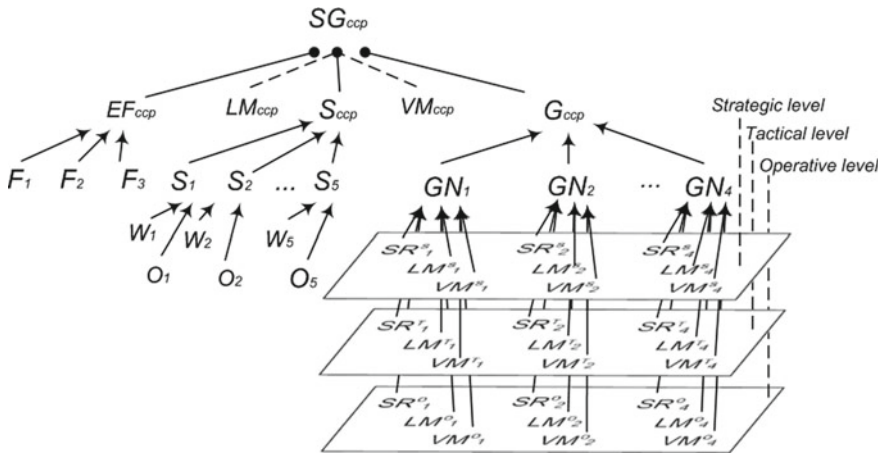


Fig. 3 Multilevel cascade hybrid LP-model of the CS strategic goal non-achievement risk

as complex events in the form of L-addition of the events of no “no will” W_i and “lack of opportunity” O_i having their probabilities.

The goals $G_{ccp} = (GN_1, GN_2, \dots, GN_4)$ correspond to the risk LP-model. Object-goals are the G_{ccp} components: GN_1 —reduce dependence on external loans, GN_2 —improve the efficiency of resources utilization, GN_3 —improve the level of social responsibility of the business, GN_4 —improve profitability and solvency. According to the concept of applying the hybrid risk LP-models for each i -th goal GN_i , it is necessary to build a scenario consistently.

Based on the possibility of simulation modeling, taking into account factors of a stochastic nature, the LP-model of the CS strategic goal non-achievement risk is supplemented by exogenous influencing factors EF_{ccp} . For the functioning of such a CS as a CP, these are, first of all, meteorological factors: freeze-up, wind speed above 15 m/s, and fog. Let us denote them by the corresponding logical variables F_1, F_2 , and F_3 . It is possible to expand the list of factors revealing not only the obstacles to the functioning of the port associated with weather conditions but also with interaction with counterparties, etc., suggest a more ramified classification, however, to represent the mechanism of interaction between logical-probabilistic and simulation modeling, only these three factors are named.

Verbally, the LP-model of the risk of each conceptual component of the cargo port’s functioning is formulated as follows: increase in the risk of suspension of the cargo port’s functioning occurs OR due to any single factor, OR due to any two factors,... OR due to all factors [20].

The L-model of the risk of the CS functioning suspension due to the presence of external random factors:

$$EF_{ccp} = F_1 \vee F_2 \vee F_3.$$

The P-model of the risk of the cargo port functioning suspension due to the presence of external random factors:

$$\begin{aligned} Pr\{EF_{ccp} = 0\} &= Pr\{F_1 = 0\} + Pr\{F_2 = 0\}(1 - Pr\{F_1 = 0\}) + \dots \\ &+ Pr\{F_3 = 0\} \times (1 - Pr\{F_1 = 0\})(1 - Pr\{F_2 = 0\}). \end{aligned}$$

When introducing a conceptual LP-model for external random factors into the model, it is necessary to correct the logical and probabilistic models of the cargo port strategic goal non-achievement risk:

$$\begin{aligned} SG_{ccp} &= S_{ccp} \wedge G_{ccp} \wedge EF_{ccp}; \\ Pr\{SG_{ccp} = 0\} &= Pr\{S_{ccp} = 0\} + Pr\{G_{ccp} = 0\}(1 - Pr\{S_{ccp} = 0\}) + \dots \\ &+ Pr\{EF_{ccp} = 0\} \times (1 - Pr\{S_{ccp} = 0\})(1 - Pr\{G_{ccp} = 0\}). \end{aligned}$$

The presented models together represent a toolkit and a mechanism that makes it possible to comprehensively assess the likelihood of risk situations in the port, interpret the results of simulation modeling, and identify possible causes of the occurrence of undesirable events in order to have them eliminated and prevented, and therefore, improve the management efficiency by means of generation of sound managerial decisions.

4 Simulation Model

The simulation model in the CS configuration scheme (Fig. 1) defines its specificity within a particular domain. Let us consider the features of the CS using the example of a CP. The complexity of control of the technological processes in the cargo port is determined by the variety of transshipment operations in terms of nature and labor intensity, stochastic nature of the transshipment processes intensity and the time spent by vehicles in the cargo port, the continuity of transshipment, the dependence of the cargo port on the traffic of the transport fleet. The competition between the transshipment facilities for the seizure of the cargo base requires them to improve the quality of cargo handling, increase the intensity of cargo handling, warehousing, and other operations. A feature of the processes in the port is their continuous development, due to both changing needs for the processing of certain cargo, and the constantly changing situation inside the port and in the regions it serves. These factors lead to the impossibility of analytical description and building of formal models, which significantly reduces the efficiency of control of such poorly formalized processes, and often makes it impossible [21]. Simulation modeling was chosen as a tool for analyzing port operations.

In simulation modeling [22], the algorithm that implements the model reproduces the process of functioning of the system under consideration in time, and the elementary phenomena that make up the process are simulated, while preserving their

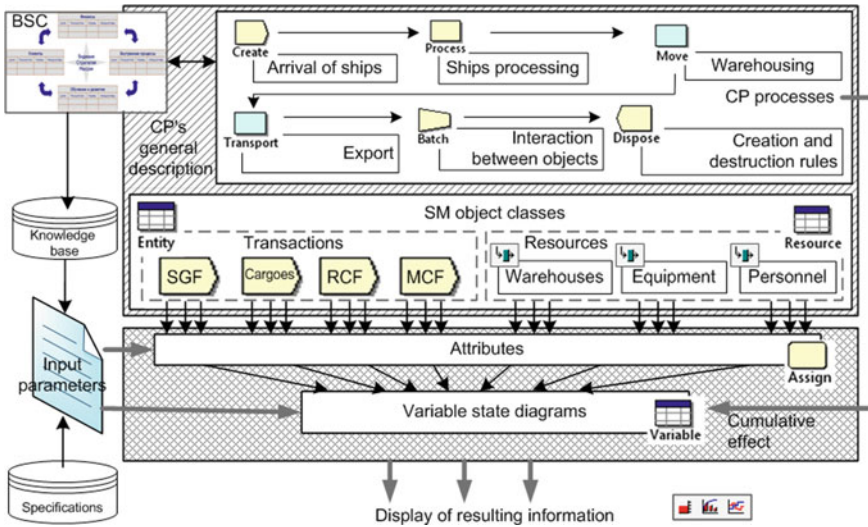


Fig. 4 Generalized structure of the CS SM (using the CP example) in terms of SIMAN

logical structure and sequence of flow in time, which allows using the initial data to acquire information about the states of the process at certain points in time, making it possible to evaluate the characteristics of the system. The generalized structure of the CS simulation model is shown in Fig. 4.

The modeled system represents the process of servicing the flow of applications (transactions): ships (SGF—sea cargo front), diesel locomotives (RCF—railway cargo front), motor vehicles (MCF—motor cargo front) with cargoes. At the same time, it is characterized by the random appearance of service requests, as well as the completion of loading/unloading processes by cranes and loaders at random times.

The simulation computer program has been verified using the following methods: the simulation model program was written and debugged by submodels; the model has been run with different input parameters [23].

In order to improve the model confidence: tracing was carried out using the Arena software; Simulation model runs have been accomplished under simplified assumptions to prove that the model data are changing in the correct order; based on the acquired statistical data, the probability distributions of the randomness factors of the model have been determined using the Input Analyzer; an animation scheme of the model has been built, which allows viewing the operation of the model dynamically, thereby identifying certain errors in the model.

The simulation model in the CS configuration scheme is a tool for testing and adapting the mechanisms and system interconnections obtained on the basis of PN and LP models to changing situations.

5 Conclusion

The structure of the CS configuration system has been developed based on a set of models:

- The PN-based CS configuration model allows for the structuring, formalization, and algorithmization of the process of making managerial decisions in complex systems based on BSC.
- The LP-model represents, on the one hand, a set of parameters that must be included in the simulation model during its development. It makes it possible to identify the cause-and-effect relationships of the occurrence of certain events in order to implement and adjust the strategy for conducting experiments with the model. The LP-model is necessary to identify favorable scenarios for the CS's behavior under the given conditions.
- A simulation model is a tool for checking the structure and algorithms of the system configuration, as well as for the numerical assessment of the probability of risk events on the basis of experiments within the specified intra-configuration cycles (*IC*-cycles).

Acknowledgements The chapter was prepared using the results of the project with the support of the RFBR grant No. 20-010-00465.

References

1. Mintzberg, H.: Die Ableitung von Konfigurationen: Kombination der Basismerkmale von Organisationen. In: Mintzberg über Management. Gabler Verlag, Wiesbaden (1991). https://doi.org/10.1007/978-3-322-91041-7_7
2. Orlova, E.: Approach for economic risks modeling and anti-risk decision making in a transport company (2019). <https://doi.org/10.2991/cmdm-18.2019.8>
3. Jensen, K., Kristensen, L.M.: In: Coloured Petri Nets—Modelling and Validation of Concurrent Systems. Springer, Heidelberg (2009). <https://doi.org/10.1007/b95112>
4. Dworzański, L.W., Lomazova, I.A.: CPN tools-assisted simulation and verification of nested Petri nets. *Aut. Control Comp. Sci.* **47**, 393–402 (2013). <https://doi.org/10.3103/S0146411613070201>
5. Zhao, J., Chen, Z., Liu, Z.: A novel matrix approach for the stability and stabilization analysis of colored Petri nets. *Sci. China Inf. Sci.* **62**, 192202 (2019). <https://doi.org/10.1007/s11432-018-9562-y>
6. Solozhentsev, E.: Logic and probabilistic risk models for management of innovations system of country. *Int. J. Risk Assessment Manage.* **18**(3-4), 237-255 (2015). <https://doi.org/10.1504/IJRAM.2015.071211>
7. Solozhentsev, E., Mityagin, S.: Logical and probabilistic risk models for assessment and analysis of the drug addiction problem in a region. *Int. J. Risk Assessment Manage.* **18**(1–20) (2015). <https://doi.org/10.1504/IJRAM.2015.068153>
8. Durán, J.M.: What is a simulation model?. *Minds and Mach.* (2020). <https://doi.org/10.1007/s11023-020-09520-z>

9. Protalinskiy, O., Andryushin, A., Shcherbatov, I., Khanova, A., Urazaliev, N.: Strategic decision support in the process of manufacturing systems management. In: Eleventh International Conference Management of Large-Scale System Development, pp. 1–4. MLSD, Moscow (2018). <https://doi.org/10.1109/MLSD.2018.8551760>
10. Niven, Paul R.: The balanced scorecard step by step: the maximum increase of efficiency and fixing received results. Balance Business Books (in Russian), Moscow (2003)
11. Rigby, D., Barbara, B.: In: Management Tools and Trends (2018). https://www.bain.com/contentassets/f8361c5cd99e4f40bbbf83c17d6a91b9/bain_brief-management_tools_and_trends.pdf. Last Access 16 Aug 2020
12. Kaplan, R.: Conceptual foundations of the balanced scorecard. *Handbooks of Manage. Accounting Res.* **3**, 1253–1269 (2009). [https://doi.org/10.1016/S1751-3243\(07\)03003-9](https://doi.org/10.1016/S1751-3243(07)03003-9)
13. Kaplan, R.S., Norton, D.P.: Using the balanced scorecard as a strategic management system. *Harvard Bus. Rev.* **74**(1), 75–85 (1996)
14. Yuditskii, S.A.: Operational-objective modeling of dynamics of organizational systems development via Petri nets. *Autom. Remote Control* **69**, 105–113 (2008). <https://doi.org/10.1134/S0005117908010104>
15. Theriou, N.G., Demitriades, E., Chatzoglou, P.: A proposed framework for integrating the balanced scorecard into the strategic management process. *Oper. Res. Int. J.* **4**, 147 (2004). <https://doi.org/10.1007/BF02943607>
16. Strohhecker, J.: Factors influencing strategy implementation decisions: an evaluation of a balanced scorecard cockpit, intelligence, and knowledge. *J. Manage. Control* **27**, 89–119 (2016). <https://doi.org/10.1007/s00187-015-0225-y>
17. Sandkuhl, K., Seigerroth, U.: Method engineering in information systems analysis and design: a balanced scorecard approach for method improvement. *Softw. Syst. Model.* **18**, 1833–1857 (2019). <https://doi.org/10.1007/s10270-018-0692-3>
18. Solozhentsev, E., Karaseva, E.: Data structures, logical-probabilistic models and digital management of the safety and quality of systems in the economics. *Int. J. Risk Assessment Manage.* **23**(1), 27–53 (2020). <https://doi.org/10.1504/IJRAM.2020.106162>
19. Orlova, E.: In: Synergetic Synthesis of the Mechanisms and Models for Coordinated Control in Production and Economic System. pp. 783–788 (2019). <https://doi.org/10.1109/CSCMP4.5713.2019.8976801>
20. Solozhentsev, E., Karasev, V.: Hybrid logical and probabilistic models for management of socioeconomic safety. *Int. J. Risk Assess. Manag.* **21**(1–2), 89–110 (2018). <https://doi.org/10.1504/IJRAM.2018.090258>
21. Parygin, D., Malikov, V., Golubev, A., Sadovnikova, N., Petrova, T., Finogeev, A.: Categorical data processing for real estate objects valuation using statistical analysis. *IOP Conf. Series: J. Phys. Conf. Series* **1015**, 032102 (2018). <https://doi.org/10.1088/1742-6596/1015/3/032102>
22. Ramírez-Nafarrate, A., González-Ramírez, R.G., Smith, N.R., et al.: Impact on yard efficiency of a truck appointment system for a port terminal. *Ann. Oper. Res.* **258**, 195–216 (2017). <https://doi.org/10.1007/s10479-016-2384-0>
23. Protalinsky, O.M., Khanova, A.A., Bondareva, I.O.: Simulation model of technological processes of cargo port. *Vestnik of Saratov State Technical University* **4**(50), 134–144 (2010). (in Russian)

Intelligent Robots Coalition Formation in Cyberphysical Space for Emergency Response



Alexander Smirnov, Nikolay Teslya , and Anna Motienko

Abstract Coalitions of robots equipped with a set of special sensors and actuators can be used for rescuing injured people in emergency situations. These sets will vary depending on the type of emergency and the activity of the environment, which, in turn, also affects the options for the interaction of robots and their tasks. In this chapter, the use of cyber-physical systems concept is proposed to form a common information-physical space in which robots will perform joint actions for eliminating the consequences of an emergency. Each robot in the coalition takes into account the specific of the emergency and the developing situation at the emergency site. Robots consider parameters of developing situations through their ontological description. The total functionality of the coalition covers the requirements of the tasks. Monitoring a developing situation allows making a timely decision on changing the composition of the coalition if the conditions change in such a way that the current composition becomes ineffective. The interaction of robots and the implementation of the rules for changing the coalition is carried out through smart contracts in a distributed ledger. This provides the opportunity to control the actions of the coalition and reduce the likelihood of being incorporated into the coalition in order to disrupt the coherence of the actions of its individual members.

Keywords Emergency · Cyberphysical space · Robot · Coalition · Smart contract · Intelligent agent

A. Smirnov (✉) · N. Teslya · A. Motienko
SPIIRAS, 14th Line 39, St.Petersburg, Russia
e-mail: smir@iias.spb.su

N. Teslya
e-mail: teslya@iias.spb.su

A. Motienko
e-mail: anna.gunchenko@gmail.com

1 Introduction

Every year, a large number of emergency situations occur in the world [1]. Their causes are both natural and human factors. Natural factors include earthquakes, floods, hurricanes, storms, and droughts. Human factors include everything that is the result of human activity: industrial accidents, domestic accidents, violation of a complex technological process, failure of control systems. An emergency caused by each of them can lead to human casualties and require the use of sophisticated equipment to deal with the consequences and search for victims.

In situations with a high risk for the human rescue team, robotic tools are increasingly being used [2]. Their main characteristics and requirements for them are off-road wheels, equipped with specific equipment, protection against aggressive environmental factors. Many emergencies are also characterized by a sufficiently large area. This makes it necessary to use a group of robots for various purposes, capable of interacting with each other. The interaction is carried out both in the information (cyber) world, with the aim of exchanging current information about the dynamics of the development of the situation, and in the physical world to perform joint actions on physical objects.

This chapter presents a mechanism for forming a coalition of autonomous robots for organizing a rescue operation in an emergency. The mechanism is based on the use of cyber-physical space and smart contract technology in a distributed registry environment to exchange information about the environment and organize a work plan. For interaction in the cyber-physical system the smart space technology is used, which allows providing ontology-based information sharing between different services of the system [3]. This technology aims for the seamless integration of different devices by developing ubiquitous computing environments, where different services share information and interact for joint task solving.

The coalition model provides a complex interaction between intelligent agents based on the assessment of the gain in achieving the final goal. It includes the implementation of the distribution model of the gain and the description of the actions required to obtain it [4]. These implementations allow agents to form coalitions that best meet the requirements of the task, plan the order of their own actions, and make decisions in case of unforeseen impacts.

The fuzzy cooperative game mechanism is using to provide a dynamic adaptation to the situation development [5]. To store the rules of the game, competencies, and requirements of intelligent agents, as well as information about the current state of the coalition and task distribution between the agents, it is proposed to use smart contracts with blockchain technology [6, 7]. The contract code, as well as the current state of the problem solution, is stored in a blockchain-based distributed ledger. This allows providing a trusted information source for the agents to store and searching for information about the stage of task solving and the current coalition state.

The rest of the chapter is organized as follows. Chapter two gives an overview of the current situation regarding the use of robots in rescue operations and cyber-physical systems for organizing collaboration between robots. Chapter 3 presents the

formalization of the task of analyzing the current environment for the formation of the initial action plan of a coalition of robots. Chapter 4 presents the use of cyberspace to exchange information between robots. Chapter 5 shows the mechanism for adapting robots to changing environmental conditions using smart contracts. Chapter 6 shows the example of rescuing operation with the usage of the proposed approach.

2 Related Work

2.1 Robots for Injured Human Rescue

There are a variety of robots for human rescue in emergency situations. They are different in autonomy level, passability, equipment for scanning and rescuing, etc. The following are an overview of existing rescue robots.

ICARUS Project [8]

The ICARUS project is focused on the development of unmanned search and rescue technologies for the detection, localization, and rescue of people. Remote-controlled search and rescue vehicles act as the first scouts of the territory, along with other participants, to ensure the safety of human personnel. The main goal of the ICARUS project is to reduce the risk of harm and the consequences of this harm to humans. It includes two types of automated platforms: a small BNTS intended for penetration into destroyed buildings to search for injured; and a large unmanned ground vehicle, which is used as a mobile base for a small unmanned vehicle, and equipped with extensive sensing capabilities, transmitting collected data to operators to increase their situational awareness.

BEAR robot nurse (Battlefield Extraction-Assist Robot) [9]

BEAR can load and transport injured people with robot's "hands", in contrast to the more commonly used method of placing the injured on the platform of an unmanned vehicle. It is able to rescue a wounded human from a dangerous environment to a safe zone; search and rescue (including in hazardous areas: in mines; areas with biological, nuclear or chemical wastes contamination; in non-hazardous buildings after an earthquake, fire, landslide, or explosion); transportation of supplies; elimination of obstacles; lifting heavy objects; hazardous material handling; intelligence service; inspection of mines and improvised explosive devices.

Mini Robocue [10]

Is a type of nurse robot capable of loading operations and placing the injured inside a special protective safe box with a built-in oxygen container on the robot's platform that the injured person can use. The robot can climb the stairs inside the building. Navigation is carried out using ultrasonic sensors and infrared cameras.

«*FEDOR*» [11]

The prototype of the Russian anthropomorphic robotic system *FEDOR*. An extended list of medical and technical requirements includes the ability to wade through the rubble of a destroyed building, search and transport the injured, deliver water, administer pain medication, and organize communication in the emergency area.

Rescue robot CHIMP [12]

CHIMP is an anthropomorphic robot equipped with hands with three fingers, with which it can use various tools. The arms and legs of the robot are also equipped with rubber-coated caterpillars for moving, using all four limbs for stability. If necessary, *CHIMP* can move only on two limbs. The robot generates a full 3D-model of the surrounding space, using various sensors on the head, and transmits this model to the human operator to provide situational awareness without delay. *CHIMP* can move independently from an operator, keeping balance and avoiding collisions with other objects. In the case of special needs, the operator can control the robot directly.

HUBO Robot [13]

The open platform humanoid robot, *HUBO*, is being developed jointly by several teams. An important point is a way to remotely control the robot. The *HUBO* robot accurately copies any movements performed by the operator on another similar robot.

Atlas Robot [14]

Atlas is a humanoid robot designed to travel over rough terrain. It is equipped with two vision systems—a lidar and stereo video cameras, which are controlled by the on-board computer. *Atlas* can build a model of the surrounding space using the sensors installed on it. In addition, the robot can evaluate its body size and plan a route so that it passed through all the narrow openings. Table 1 presents the comparison between the main characteristics of the robots mentioned above.

Table 1 A comparative analysis of rescue robots' characteristics

Characteristics	Rescue robots				
	BEAR	CHIMP	DRC-HUBO	Atlas	FEDOR
Size	1.8 m 227 kg	1.5 m 181 kg	1.8 m 80 kg	1.75 m 82 kg	1.84 m 106–160 kg
Carrying capacity	270 kg	N/A	30 kg	4.5 kg	10 kg
Autonomous work with a single charge [min]	N/A	90 min	130 min	60 min	N/A
Remote interaction with the operator	+	+	+	+	+
Operator decision support features	+	+	+	+	+
The ability to monitor the condition of the injured (with appropriate sensors)	+	+	+	+	+
Copy mode of execution of manipulations	–	–	+	–	+

2.2 *Interaction Between Robots*

All rescue robots described above are equipped with different hardware and software. Therefore, it is important to consider the heterogeneity and provide a common model to reach consensus during task decomposition and resolution. Each robot shares its own competencies and goals, which he aims to achieve after the problem solving. In this case, the coalition can be considered as a union of agents with their interests, which through the negotiation decide on a joint solution of the problem and the distribution of the reward.

The solution to robots' interaction problem is usually carried out by using the cyber-physical systems concept [15]. Robots are viewed as intelligent agents equipped with sensors and actuators for interacting with the physical environment. They are also equipped with communication and information processing tools for exchanging available data and making decisions about their own actions. The development of computer technology, as well as artificial intelligence technologies and cooperative work mechanisms also provide a certain level of robots' autonomy and the possibility of forming and coordinating complex plans for joint actions in a cyber-physical environment.

Regarding the organization of robots' interaction, the blockchain is mostly used as immutable storage for information exchange and a platform for smart contracts. Information stored in the blockchain could contain records about task and consumables distribution [16, 17], smart contracts, and reward transactions [18], as well as global knowledge about coalition previous actions [19]. In combination with cooperative games, blockchain technology can provide trust for communication between robots, due to storing information about transactions in the immutable log that are verified by every coalition participant. The blockchain is used to provide safe and trustiness logging of tasks and winnings distribution between robots during task solving.

It is also should be noted that the combination of the peer-to-peer network and the cryptographic algorithms used in blockchain technology allow for a negotiation process and consensus building without the presence of any controlling authorities [19]. At the same time, due to blockchain, the security of the transmitted data is ensured (garbage data can affect the achievement of a common goal), distributed decision making (creating a distributed voting system for the solution), separation of robots behavior (switching between behavior patterns depending on the role in the swarm), the emergence of new business models using the swarm.

3 **Response to an Emergency**

The overall response to an emergency by robot coalition can be divided into two groups depending on operation types (Table 2). Rescue operations show the main steps that have to be done for rescuing injured people from the emergency area. Other

Table 2 Classification of rescue operations types

Rescue operations	Other emergency work, including lesions
<ul style="list-style-type: none"> • Exploration routes of formations and areas of upcoming work • Localization and extinguishing of fires on the paths of movement and work sites • Search for victims and removing them from the rubble, damaged and burning buildings, gassed, smoked, and flooded rooms • Air supply to blocked protective structures with damaged ventilation. • Autopsy of destroyed, damaged, and littered protective structures, the rescue of people there • Providing first aid to injured in the emergency zone, at the point of collection of the injured, and in preparing them for medical evacuation • Export (withdrawal) of the population from dangerous places to safe areas • Sanitary treatment of people, disinfection of their clothes, territory, structures, equipment, water, and food 	<ul style="list-style-type: none"> • Laying of column ways and arrangement of driveways (passages) in the rubble and on infected areas • Localization of accidents on public utilities and technological networks • Strengthening or collapse of buildings threatening a collapse on the ways of movement to the work sites • When conducting emergency rescue and other emergency operations in the lesions formed as a result of hostilities, additionally carried out: <ul style="list-style-type: none"> – Detection, disposal, and destruction of unexploded ordnance in conventional equipment; – Repair and restoration of damaged protective structures; – Disinfection of lesions; – Collection of material assets; – Providing food for the population in need; – Disposal of contaminated food to prevent an epidemy

work includes all supporting operations that will help rescue teams to successfully carry out the rescue.

A model for analyzing emergencies and predicting the injures can be described using a Bayesian network (Fig. 1). The result of moving through the network is the probability of specific injuries depending on the type of emergency.

These injuries correspond to certain types of robots that have the appropriate equipment for manipulating specific injures. The model is represented by the following expression:

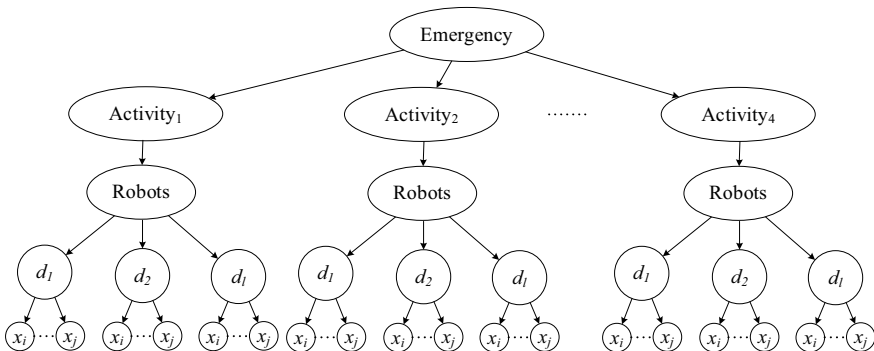


Fig. 1 Bayesian network for injures prediction

$$\langle \mathbf{R}, \mathbf{PAR}_R \rangle,$$

where \mathbf{R} is an acyclic directed graph; \mathbf{PAR}_R are parameters that define a Bayesian network.

Vertices of the graph \mathbf{R} are described with the following parameters:

1. Discrete variables denoting:
 - most common injuries— x_1, \dots, x_{18} ;
 - signs of injury— x_{19}, \dots, x_k ;
 - methods for identifying signs of injury (examination, interrogation, manipulation)— d , which are associated with variables x_{19}, \dots, x_k . Here, if the sign of the injury is not detected by one of the methods for determining injury, the relationship between them is not available. For example, an indication of injury “Tinnitus” has no connection with the “inspection” and “manipulation”;
 - environment activity— A (“high”, “medium”, “low”, “absent”), on which the application of methods for determining injuries depends;
2. The top of the emergency that describes its type— y_1, \dots, y_l , where l is a number of emergencies.
3. The top of the “robots” describing the number of robots— r_1, \dots, r_p .

Parameters of \mathbf{PAR}_R network are the following:

1. For the node of an emergency without parental variables, there are a priori probabilities (unconditional probabilities) that the emergency is “transport accidents”, “accidents with the release (threat of release) of chemically hazardous substances”, etc.— $P(\tilde{y}_L)$, $L = 1 \dots l$.
2. For the node A , conditional probabilities of environment activity type (“high”, “medium”, “low”, “absent”) are set depending on its parameters (temperature, concentration of chemical hazardous substances, seismic scale points, Beaufort points, INES international relative scale of nuclear events, calculation of zones of possible chemical infection, etc.):— $P(\tilde{A}_m | a_S)$, $m = 1 \dots 4$, $S = 1 \dots s$. Sign « \sim » denotes a positive or negative value of a variable \tilde{x} .
3. For the robot nodes, conditional probabilities of the dependence of the number of robots on the type of emergency and environmental activity are set $P(\tilde{r}_p | \tilde{y}_L \tilde{A}_m)$, $P = 1 \dots p$ (p —the maximum number of robots available in the system), $L = 1 \dots l$, $m = 1 \dots 4$.
4. For nodes x_{19}, \dots, x_K conditional probabilities of the dependence of signs of injuries on methods for determining injuries are set— $P(\tilde{x}_K | \tilde{d}_n)$, $K = 19 \dots k$; $n = 1 \dots 3$.
5. For nodes x_1, \dots, x_{18} conditional probabilities of injury dependence on signs of injury are set— $P(\tilde{x}_j | \tilde{x}_K)$, $j = 1 \dots 18$, $K = 19 \dots k$.

Robots are interacting through the cyber-physical framework presented in [20]. The framework is based on the smart cyber-physical space created by extending of smart space concept (based on the “blackboard”) with a distributed ledger based

on blockchain. This combination provides the ability to organize basic interaction of robots in the physical and cyber (virtual) spaces by storing the history of each robot’s actions sequence in an immutable blockchain structure. The interaction includes solo and joint manipulations with physical objects, information exchange about the current state of robots, and objects for planning further joint actions during the coalition formation. Each robot is presented in the cyber-physical space with his Knowledge processor (KP) that is responsible for gathering data from the robot sensor, transmitting it to the cyber-physical space, and receive data from other robots through the cyber-physical space.

To provide semantic interoperability through the used framework each robot is described with generalized ontology, based on the IEEE Standard Ontology for Robotics and Automation [21]. For the precision farming scenario, it was extended with descriptive entities that are used in the creation of fuzzy rules knowledge base. A “State” class that presents the complete state of a robot has been added. “DeviceCompleteness” is a class that summarizes complete robot specification on a functional level: percentage and state of charge, potential movement speed, set of sensors. “Goal-Reachability” is a class that summarizes the reachability of the task by a specific robot with respect to the physical characteristics of the target. The ontology is presented in Fig. 2.

To form a coalition, robots are using rules and coalition norms based on the fuzzy logic theory [20]. The cooperative game purpose in case of rescue task is to generate an effective structure of robot coalitions for rescuing as much injured people as possible with the estimation of surviving probability. In turn, the generated structure of robot coalitions for particular types of injures represents the optimal configuration of the grand coalition (set of coalitions) that responds to getting maximal surviving probability.

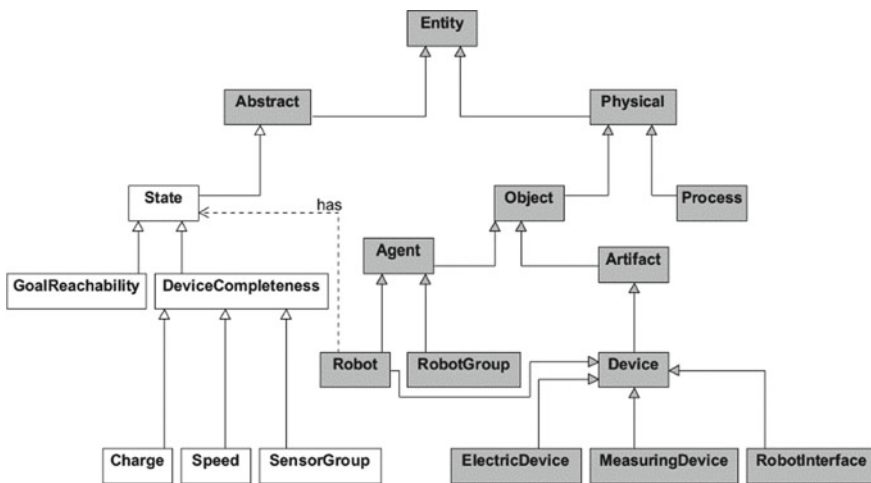


Fig. 2 Robot ontology for information sharing through the cyber-physical framework

Individual robots use the technique of nonlinear fuzzy regression to estimate the parameters of utility functions for their payments [22]. A “coalition robot” is enabled for constructing membership functions (MF) of coalitions and generating the game core (fuzzy-number generator). The algorithm of fuzzy number summation for obtaining coalition membership functions represents an important element of the model. The sum operation is based on Zadeh extension principle [23] for fuzzy numbers a and b (which are convex sets normalized in \mathbf{R}):

$$\mu_{a(*b)}(Z) = \sup_{z=x*y} \min(\mu_a(x), \mu_b(y)) \quad (1)$$

where $*$ can designate the sum \oplus or the product \bullet of fuzzy numbers. Each fuzzy set is decomposed into two segments, a non-decreasing and non-increasing one. The operation $*$ is performed for every group of n segments (one segment for each fuzzy set) that belong to the same class (non-decreasing or non-increasing one). Thus, a fuzzy set is generated for every group of n segments. The summation result is derived as a superposition of these sets, which gives the membership function as the sum of n fuzzy numbers.

4 Robot Coalition Formation for Emergency Response

Joint problem solving requires coordination of participants’ actions during the coalition formation. The coalition task solving is viewed as a two-stage process: scheduling and execution. At the first stage, the coalition is forming, and the execution plan is building in a static or dynamic way by analyzing the task requirements, robot competencies, and environmental characteristics. The following stages can be viewed through the first stage considering rescue in an emergency.

1. Definition of the emergency type

At this stage, the scale of the emergency, the number of robots, and their type are determined (robots with powerful manipulators for parsing debris, scouts for finding people, “medics” to determine injuries, transport robots). When determining the scale of an emergency, it is also necessary to have at least approximate information on the number of potential’s injures people in order to take into account how many robots of which types should be in each group.

2. Determination of environment activity (high, low, medium, absent).

- determining the configuration of robots depending on environment activity;
- distribution of functions depending on the environment activity. With a high activity, for example, a greater number of robots is sent for search than with a low one.

3. Division of emergency area into sectors.

Each sector has a separate group; if necessary, regrouping takes place. For example, in one of the sectors a large number of injured, while in the other there are none or fewer, resources are transferred to a more loaded sector.

4. The work of individual groups in sectors.

Regular assessment of environmental activity. Detection of the injured person, identification of signs of injury, sorting, calling the robot for transportation, or transportation using available means. Transportation in different poses can be carried out by different robots or by a robot capable of reconfiguration. For example, one robot for transportation human on the back and the stomach, a completely different one for transportation human in sitting or half-sitting manner.

The plan contains a list of sub-tasks for each robot with execution order and timestamps when each sub-task should be solved. Robots are negotiating with each other by distributing their own functions and efficiency estimations through cyber-physical space. The benefit is estimated based on the functions, winning expectations, and efficiency of the robot. Since some sub-tasks should be solved consequentially, all robots have to track the current status of task solving and coordinate their activities with the others.

After the coalition was formed, the execution stage is starting. During this stage, all robots perform their actions and report to the others about the progress on each task. After the task solving all earned profit is sharing between agents. Efficiency can be estimated based on the number of survived people after an emergency related to the expected number of people in the area before it, and energy spent. The most efficient coalition structure should provide a higher number of survived humans and minimum energy spent.

During the negotiations for coalition formation robots also take into account the ontological representation of the coalition norms, which describe the basic rules for the joint solution of the problem, like the logic of selecting or replacing coalition participants when their characteristics coincide.

The rules for selecting or replacing robots determine the choice of a specific executor for a task if their characteristics coincide, which are required to solve the problem (2). This type of behavior is based on the analysis of secondary parameters with respect to the task, which, however, affect the overall efficiency of the coalition, for example, the current energy supply or the number of hours worked (which affects equipment wear and possible downtime losses during repair).

The following logical expression describes the rule for replacing robots (2):

$$\forall i \forall j (\neg F(r_i, K) \wedge \neg F(r_j, K)) \wedge (\exists k : (f_k(r_i) > f_k(r_j))) \rightarrow F(r_i, K), \quad (2)$$

where r_i, r_j are robots, K is a coalition, $F(r_i, K)$ is a membership function, $f_k(r_i)$ is a value of resource k for robot r_i .

All robots interact through the cyber-physical platform using the ontology created via the Protégé tool and uploaded to every robot (Fig. 3).

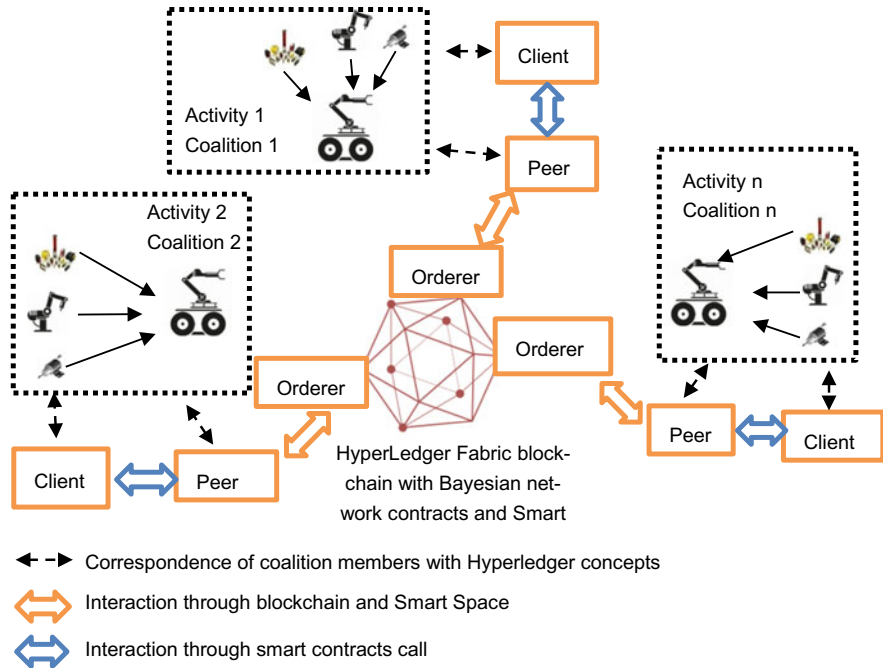


Fig. 3 Cyber-physical framework with blockchain support [24]

The blockchain network for the case study has been implemented based on the open-source Hyperledger Fabric platform. The platform provides a wide range of configurations: changing of a core database for transactions and block storing, changing of consensus mechanisms, and changing signature algorithms for peers' interaction with the blockchain. For the case study presented in the chapter, the default configuration has been used since it provides processing of more than 3500 transactions per second with a latency of hundred milliseconds. The architecture of the platform corresponds to the architecture of the proposed approach for multi-robot coalition formation.

Two kinds of chains are using for robot interaction: (i) resource state storage (ii) contract storage. All system resources including consumables, energy, reward, which are represented by tokens, are stored in the resources chains [25]. Contracts chain stores the rules of cooperative games, which are used by the coordinators during the coalition forming and the distribution of tasks. The first contracts in the chain of contracts are rules for processing tasks and assigning coalition core. The new task is formed with a program interface outside a coalition by the problem manager, or by the cores of another coalition in case of obtaining a new context that cannot be processed by the existing coalition. New tasks are stored in the contract chain of the blockchain, from where they become available for all coalition cores. Tasks contain

a formalized description of the goal, the initial parameters, and the amount of reward for the solution.

Following this chain, each robot can check the current state of task processing and adjust its own activity to provide better performance. Going further after the harvesting each customer can check a growing process and make a decision about product quality based on the history of operations.

5 Earthquake Emergency Coalition Formation Case

Let's consider the earthquake example for coalition formation. Some buildings in a city are collapsed after an earthquake. The first step of rescue is scouting. This work is carried out with drones equipped with video cameras and thermal imagers. All gathered information is shared through the proposed framework in the form of ontology. In parallel, dispatcher or special program service in smart space requests information about a number of people in the affected regions from the city authorities or information sources. According to scouting results, a decision is made with the Bayesian network of most probable injures in the area (Fig. 4). Injures types lead to the composition of robotic equipment that will help to eliminate blockages and fires and rescue injured people. For example, Fig. 4 shows part of the network where the environment shows low activity after the earthquake and the following injures probabilities are calculated (yellow boxes): bones broke (99%), spinal fracture (100%), concussion (98%). And for these injures the following rescue operations are required (blue boxes): position: on the back (100%), on the abdomen (89%), on the right side (75%), sitting (99%), half-sitting (73%). For each type of rescue operation, the robot is choosing that meet the requirements.

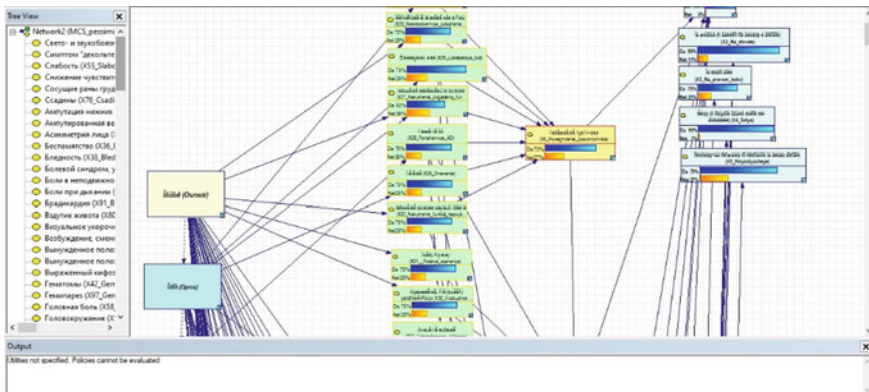


Fig. 4 Example of injures probability estimation depending on environmental with Bayesian network

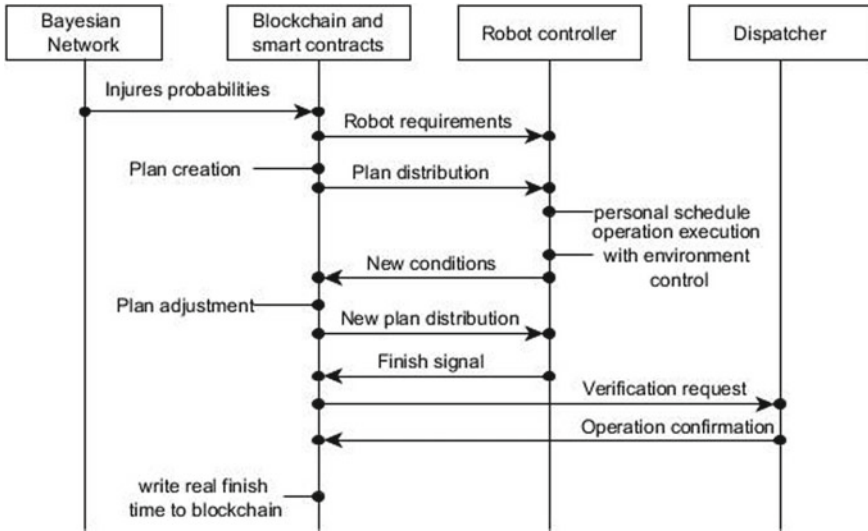


Fig. 5 Robot coalition formation timeline

While clearing the rubble, several paths are laid, to the injured ones, who find themselves in the destroyed and dilapidated sectors. Tiny robots or a swarm of robots can be sent to search for those injured at the very beginning of emergency rescue operations, just for the detection of survived people in the area (Fig. 5).

After eliminating huge interferences, the area is divided into sectors. A coalition of robots consisting of various rescuing robots that determine the position for transportation and robots that directly transport the injured is sent to each sector, based on regularly checked activity of the environment. All locations and injures types are processed with smart contract to find robots for solving rescue task (Listing 1).

Listing 1 Example of a chain code for coalition formation

```

var robots[]           // Robots with parameters
var environment_params[] // Current context
var rescue_tasks[]     // Rescue task parameters
var injures            // Injures' characteristics
func robots_select(stub shim.ChaincodeStubInterface, args
[]string) (string, error) {
    for task in rescue_tasks
    for robot in robots
        if task.requirements == robot.competences &&
        injure.type in robot.competences:
robot_contract_chain.put(rescue_task, robot);
    schedule_and_run_tasks(robot_contract_chain,
        environment_params)
    }
}
    
```

Those in general, the task boils down to the following: detecting an emergency, determining its type (based on which the composition of the coalition designed to

provide for the affected is determined), determining the activity of the environment to understand the composition of the parts of robotic tools that determine the position for transportation and the quantitative composition of the group (how many robots for transportation, or determine the position are needed). In parallel, scouts are sending to find the shortest paths to the affected and their delivery to a safe area.

6 Conclusions

The study of coalition forming for the injured human rescue in emergency situation tasks is difficult. It requires the prediction of possible injuries forming rescue teams and adaptation for environment activity. In some cases, it is too dangerous to send human teams for rescuing therefore a coalition of robots should be formed.

A set of problems should be solved in the case of forming coalitions of robots for rescuing operations, such as: coalition structure, task distribution, information exchange, synchronization of actions. To solve them, it was proposed to use the cyber-physical space with blockchain technology integrated into it.

To form the first structure of the coalition, the Bayesian network has been proposed. If robots evaluate their costs and expected gain using fuzzy sets stored in smart contracts for the blockchain platform, after which they negotiate to agree on an action plan, guided by the norms of action in the coalition. This approach allows us to consider the basic requirements when forming an action plan and to ensure the adaptation of robots to emergency situations. The introduction of a blockchain with smart contracts makes it possible to provide unchangeable process logs by which one can trace the history of operations and, if necessary, find a weak point, to enhance the effectiveness of future coalitions. Hyperledger platform is used to organize the blockchain and implement smart contracts for coalition formation and plan execution control.

Acknowledgements The present research was supported by the Russian Foundation for Basic Research, project number 17-29-07073 in the field of dynamic coalition formation for emergency medicine, and by Russian State Research No. 0073-2019-0005 for creating a cyberphysical space for intelligent robot interaction.

References

1. Fisher, D. (IFRC), Hagon, K. (IFRC), Lattimer, C., O'Callaghan, S., Swithern, S., Walmsley, L.: World Disasters Report 2018. In: *Leaving No One Behind: The International Humanitarian Sector Must Do More to Respond to the Needs of the World's Most Vulnerable People* (2018)
2. Tadokoro, S., Kimura, T., Okugawa, M., Oogane, K., Igarashi, H., Ohtsubo, Y., Sato, N., Shimizu, M., Suzuki, S., Takahashi, T., Nakaoka, S., Murata, M., Takahashi, M., Morita, Y., Rooney, E.M.: *The World robot summit disaster robotics category—achievements of the 2018*

- preliminary competition. *Adv. Robot.* **33**, 854–875 (2019). <https://doi.org/10.1080/01691864.2019.1627244>
3. Korzun, D., Kashevnik, A., Balandin, S.: Novel design and the applications of smart-M3 platform in the internet of things. IGI Global (2018). <https://doi.org/10.4018/978-1-5225-2653-7>
 4. Guerrero, J., Oliver, G.: Multi-robot coalition formation in real-time scenarios. *Robot. Auton. Syst.* **60**, 1295–1307 (2012). <https://doi.org/10.1016/j.robot.2012.06.004>
 5. Mareš, M.: In: *Fuzzy Cooperative Games*. Physica-Verlag HD, Heidelberg (2001). <https://doi.org/10.1007/978-3-7908-1820-8>
 6. Cong, L.W., He, Z., Zheng, J.: Blockchain disruption and smart contracts. *SSRN Electron. J.* **48** (2017). <https://doi.org/10.2139/ssrn.2985764>
 7. Delmolino, K., Arnett, M., Kosba, A., Miller, A., Shi, E.: Step by step towards creating a safe smart contract: lessons and insights from a cryptocurrency lab. In: Grossklags, J., Preneel, B. (eds.) *Financial Cryptography and Data Security*. FC 2016. pp. 79–94. Springer, Berlin, Heidelberg (2016). https://doi.org/10.1007/978-3-662-53357-4_6
 8. Armbrust, C., De Cubber, G., Berns, K.: ICARUS Control systems for search and rescue robots. In: *Field and Assistive Robotics—Advances in Systems and Algorithms*. pp. 1–16 (2014)
 9. Levinger, J., Hofmann, A., Theobald, D.: Semi-autonomous control of an emergency response robot. *AUVSI Unmanned Syst. North Amer. Conf.* **2008**(2), 914–927 (2008)
 10. Robot! Mini Robocuel Robotics Today. <https://www.roboticstoday.com/robots/mini-robocue>. Last Accessed 09 Jul 2020
 11. Bogdanov, A., Dudorov, E., Permyakov, A., Pronin, A., Kutlubaev, I.: Control system of a manipulator of the anthropomorphic robot fedor. In: *Proceedings-International Conference on Developments in eSystems Engineering, DeSE*. pp. 449–453. Institute of Electrical and Electronics Engineers Inc. (2019). <https://doi.org/10.1109/DeSE.2019.00088>
 12. Haynes, G.C., Stager, D., Stentz, A., Vande Weghe, J.M., Zajac, B., Herman, H., Kelly, A., Meyhofer, E., Anderson, D., Bennington, D., Brindza, J., Butterworth, D., Dellin, C., George, M., Gonzalez-Mora, J., Jones, M., Kini, P., Laverne, M., Letwin, N., Perko, E., Pinkston, C., Rice, D., Scheffle, J., Strabala, K., Waldbaum, M., Warner, R.: Developing a robust disaster response robot: CHIMP and the robotics challenge. *J. Field Robot.* **34**, 281–304 (2017). <https://doi.org/10.1002/rob.21696>
 13. Park, I.W., Kim, J.Y., Lee, J., Oh, J.H.: Mechanical design of humanoid robot platform KHR-3 (KAIST humanoid robot-3: HUBO). In: *Proceedings of 2005 5th IEEE-RAS International Conference on Humanoid Robots*. pp. 321–326 (2005). <https://doi.org/10.1109/ICHR.2005.1573587>
 14. Feng, S., Whitman, E., Xinjilefu, X., Atkeson, C.G.: Optimization based full body control for the atlas robot. In: *IEEE-RAS International Conference on Humanoid Robots*. pp. 120–127. IEEE Computer Society (2015). <https://doi.org/10.1109/HUMANOIDS.2014.7041347>
 15. Smirnov, A., Kashevnik, A., Ponomarev, A.: Multi-level self-organization in cyber-physical-social systems: Smart home cleaning scenario. In: *Procedia CIRP*. pp. 329–334. Elsevier B.V. (2015). <https://doi.org/10.1016/j.procir.2015.02.089>
 16. Verma, D., Desai, N., Preece, A., Taylor, I.: A block chain based architecture for asset management in coalition operations. In: Pham, T., Kolodny, M.A. (eds.) *Proceedings SPIE 10190, Ground/Air Multisensor Interoperability, Integration, and Networking for Persistent ISR VIII*. pp. 101900Y (2017). <https://doi.org/10.1117/12.2264911>
 17. Dorri, A., Kanhere, S.S., Jurdak, R.: Towards an optimized blockchain for IoT. In: *Proceedings of the Second International Conference on Internet-of-Things Design and Implementation-IoTDI'17*. pp. 173–178. (2017). <https://doi.org/10.1145/3054977.3055003>
 18. Zhang, Y., Wen, J.: The IoT electric business model: using blockchain technology for the internet of things. *Peer-to-Peer Netw. Appl.* **10**, 983–994 (2017). <https://doi.org/10.1007/s12083-016-0456-1>
 19. Ferrer, E.C.: The blockchain: a new framework for robotic swarm systems. *Adv. Intell. Syst. Comput.* **881**, 1037–1058 (2019). https://doi.org/10.1007/978-3-030-02683-7_77

20. Smirnov, A., Sheremetov, L., Teslya, N.: Fuzzy cooperative games usage in smart contracts for dynamic robot coalition formation: approach and use case description. In: ICEIS 2019- Proceedings of the 21st International Conference on Enterprise Information Systems. pp. 349–358. SCITEPRESS-Science and Technology Publications (2019). <https://doi.org/10.5220/0007763003610370>
21. IEEE Robotics and Automation Society: In: IEEE Standard Ontologies for Robotics and Automation (2015). <https://doi.org/10.1109/IEEESTD.2015.7084073>
22. Haekwan, L., Tanaka, H.: Fuzzy approximations with non-symmetric fuzzy parameters in fuzzy regression analysis. *J. Oper. Res. Soc. Japan* **42**, 98–112 (1999)
23. Zadeh, L.A.: Similarity relations and fuzzy orderings. *Inf. Sci.* **3**, 177–200 (1971). [https://doi.org/10.1016/S0020-0255\(71\)80005-1](https://doi.org/10.1016/S0020-0255(71)80005-1)
24. Smirnov, A., Sheremetov, L., Teslya, N.: Fuzzy cooperative games usage in smart contracts for dynamic robot coalition formation: Approach and use case description. In: ICEIS 2019- Proceedings of the 21st International Conference on Enterprise Information Systems. pp. 349–358 (2019)
25. Teslya, N.: Industrial socio-cyberphysical system’s consumables tokenization for smart contracts in blockchain. In: *Lecture Notes in Business Information Processing*. pp. 344–355. Springer, Cham (2019). https://doi.org/10.1007/978-3-030-04849-5_31

Aircraft Flight Safety Control Methodology



Aleksey Kulik 

Abstract The chapter presents the concept of aircraft flight safety management, which is based on a certain system of principles. The principles proposed by the author (intelligence, information, speed, safety), as well as methods and algorithms for their implementation, are a methodology for managing the flight safety of an aircraft. The chapter presents a new class of control object, an intelligent aviation system, which belongs to the class of cyber-physical systems and is characterized by the presence in its structure of the aircraft flight safety control subsystem, on the basis of which the proposed concept is implemented. In addition, the chapter shows a study of the efficiency of the algorithm for supporting decision-making by the crew to parry the threat of an aviation accident, which can be implemented based on the aircraft flight safety management system.

Keywords Flight safety · Expert system · Decision support

1 Introduction

In recent years, domestic and foreign aviation enterprises have paid great attention to improving the safety of aircraft flight. As a rule, to achieve this goal, various onboard software and hardware are used, the action of which is aimed at preventing the threat of an aviation accident, as well as procedures for improving the quality of development and operation of aviation equipment [1–4].

This is a known method of supporting the aircraft operator in emergencies [5], which allows an expert system to assess the performance of on-Board equipment and the actions of the crew, followed by predicting an emergency and notifying the crew of its presence. However, this method does not allow us to accurately assess the degree of occurrence of a catastrophic situation due to the lack of modeling of the development of a dangerous situation in the flight of an aircraft.

A. Kulik (✉)

National Research University Moscow Power Engineering Institute, 111250 Moscow, Russia
e-mail: kulikalekse@yandex.ru

Another option for ensuring the safety of aircraft flight is the “Automated highly intelligent system for ensuring the safety of aircraft flights” [6], proposed by employees of the Federal state unitary enterprise “Flight research Institute named after Gromov”. The system allows you to parry a catastrophic situation in the control of the vehicle based on predicting changes in conditions and assessing the excess of operational limits of its flight using an expert system for determining the threat of a catastrophic situation and a mathematical model of the control object. At the same time, the disadvantages of such a system are the need for high computational power for the qualitative functioning of the mathematical model of aircraft movement, as well as the prediction of changes in variables that affect the safety of the flight, including the psychophysical state of the engine.

The implementation of aircraft flight safety functions is carried out within the framework of the organizational and technical system, which is the aviation transport system (ATS) [1]. The aviation transport system is a complex of interacting systems whose functions are aimed at ensuring the life cycle of an aircraft. The ATS contains a “Crew-Aircraft” system, an air traffic control system, and a flight support system.

The “Crew-Aircraft” system ensures the operation of the aircraft. The main task of the crew is to perform a flight task taking into account the state of aviation equipment and external factors. The effectiveness of the crew depends on the professional level and psychophysical state of the crew. In this case, the functional efficiency of the aircraft is determined by its design, technology, and survivability. Design and technological excellence of the aircraft is created in the course of research of the vessel at the stages of its development, production of prototypes, and serial production. The main characteristics formed at the stages of development of the vessel are its reliability and reliability.

The air traffic control system ensures the aircraft’s flight along this route, as well as on the approach to the airfield. The perfection, reliability, and reliability of technical means, as well as the professional training of dispatchers and service personnel, determine the effectiveness of the system.

The flight support system determines the flight and technical operation of the aircraft. In the first case, the activity of the crew and other subsystems of the ATS is carried out in accordance with the recommendations of the preparation and execution of the fields. In the second case, maintenance is performed on the aircraft aimed at the timely prevention of failures of its functional systems and the most important elements.

Based on the description of the structural elements of the ATS, it can be concluded that the main work to ensure the safety of aircraft flight is performed at the stages of design, production, and preparation of the vessel for flight. At the same time, directly in flight, the greatest load on counteracting the threat of an aviation accident falls on the pilot, whose actions in extreme conditions can lead to a deterioration of flight conditions and the development of a catastrophic situation. Therefore, the improvement of ATS in terms of improving the safety of aircraft flight using the concept of designing cyber-physical systems is an urgent scientific and technical problem.

2 Problem Statement

The purpose of this work is to develop a methodology for managing aircraft flight safety, which is provided by the use of an intelligent decision support system as part of the aviation transport system.

To achieve this goal, it is necessary to: (a) analyze a new class of control object—the aviation intellectual system; (b) develop and test a set of methods, methods, and algorithms to ensure the safety of aircraft flight; (c) investigate the performance of the decision support system for parrying the threat of an accident.

3 Analyze the Aviation Intellectual System

To support the actions of the crew under the threat of an accident when controlling an aircraft, it is necessary to use an **intelligent decision support system and fuzzy logic** [7–15, 17–22] as part of aviation transport systems, which allows you to introduce the concept of an **intelligent aviation system**, which is the cyber-physical system. The block diagram of the intelligent aviation system is shown in Fig. 1. A distinctive feature of such a system in comparison with the ATS is the presence of a safety management system in its composition. The aircraft flight safety management system is a complex of control and management, the functioning of which is associated with

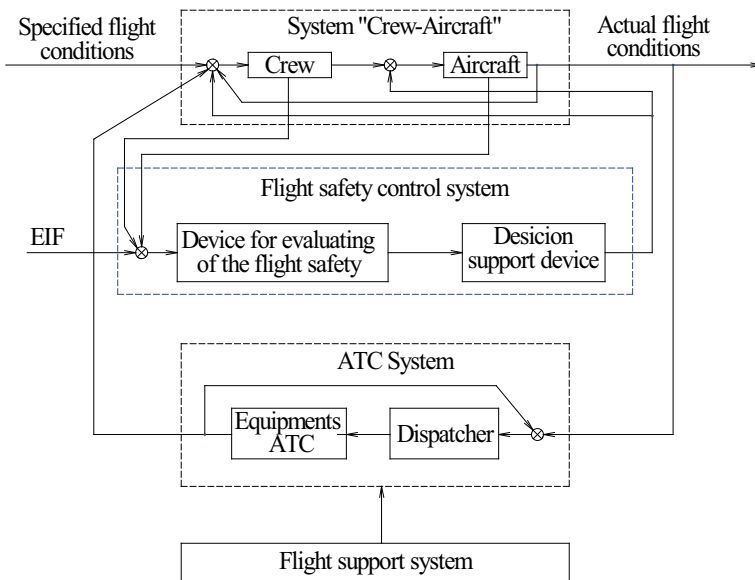


Fig. 1 IAS block diagram

the detection and elimination of flight accidents under the influence of internal and external factors on the ground and in the air.

where EIF—external influencing factors, DS—decision support, ATC—air traffic control

Based on the required properties of ATS and intelligent systems, the following principles of IAS operation are proposed:

1. **The intelligence** of the IAS is due to the presence of a crew, a dispatcher, and a decision support system in its structure. In this case, the decision support system is able to provide auxiliary actions to the crew and control actions in relation to the aircraft. In this case, the intelligence of the AIS will be understood as a relative value in terms of the functions performed by the decision support system. The quantitative evaluation of this function is an indicator of the system's intelligence.
2. **Informativity** The information content of the aviation-intellectual system is determined by the completeness and reliability of its input data (conditions for preparing and performing an aircraft flight, the state of the crew, aircraft and air traffic control facilities), as well as the output data of the decision support system. Along with the input and output data of the IAS, the completeness and reliability of the decision support system database are important.
3. **Speed.** The control system must have such a speed of information processing that ensures the functioning of the aviation system in real-time. Therefore, it is important for them to obtain and analyze current information in order to develop appropriate management actions.
4. **The interconnectedness of subsystems** provides for the participation of all elements of the system in ensuring the management of aircraft flight processes, as well as the exchange of data between them at the stages of flight preparation and execution.
5. **Aircraft flight safety** is a set of measures aimed at recognizing the threat of an accident and preventing it. The safety of the aircraft provides:
 - identification of the threat of an accident, which involves a qualitative and quantitative assessment of the flight conditions of the aircraft, as well as determining the type of threat of an accident (accident or catastrophic situation);
 - predicting the threat of an accident involves predicting changes in variables of external and internal factors that affect the flight conditions of the aircraft and, as a result, the safety of this process;
 - parrying the threat of an aviation accident is a complex of actions of the crew, aircraft onboard equipment, flight support systems, and intelligent decision support systems aimed at preventing the development of the threat of an aviation accident;
6. **The controllability** of the system implies the effective implementation of the aircraft flight process, which is provided by the signals of the crew management, the intelligent decision support system, and flight support tools.

Thus, the main task of an intelligent aviation system is to ensure a high level of safety of aircraft operation, which is achieved by using a flight safety management system in its structure, which implements the main properties of the IAS.

4 Develop and Test a Set of Methods, Methods, and Algorithms to Ensure the Safety of Aircraft Flight

The implementation of the principles that form the methodology for managing the safety of an intelligent aviation system is shown in Fig. 2. The block diagram represents the relationship of principles, methods, and algorithms aimed at improving the flight safety of an aircraft.

where P1-P6—principles of AIS functioning, M1-M4—methods of aircraft flight safety management, A1-A4—algorithms for aircraft safety management, SCS—aircraft flight safety control system

From Fig. 2 it can be seen that the intelligent method of assessing the threat of an accident (M1) is based on the principles of system intelligence (P1), identification of the threat of an accident (P5.1), informativeness (P2), and speed of the control system (P3). In turn, the method of predicting the threat of an accident (M2) contains the principles of system intelligence (P1), system performance (P2), and predicting the threat of an accident (P5.2). The method of crew decision support in the event of an accident threat (M3) contains the principles of parrying the AP threat (P5.3), as well as the principles of intelligence (P1), informatively (P2), and the relationship of

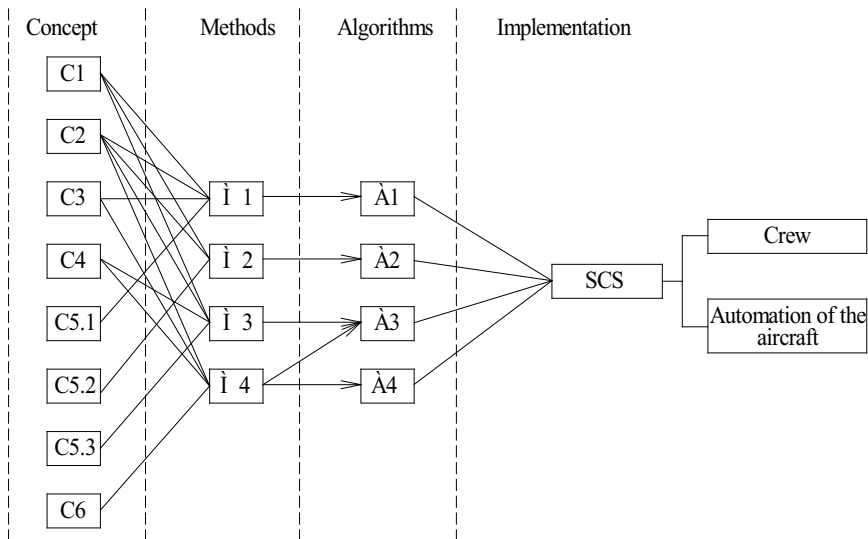


Fig. 2 The methodology of safety management IAS

the IAS subsystems (P4). The method of synthesis of the law of control of parrying the threat of AP (M4) is based on the principles of informativeness (P2), speed (P3), the interconnection of subsystems (P4), and system manageability (P6).

The proposed methods are implemented by software and hardware of the aircraft flight safety management system, which implements the following algorithms [16]:

1. Algorithm for assessing the threat of an accident and aircraft flight conditions (A1);
2. Algorithm for predicting the threat of an accident (A2);
3. Algorithm for parrying the threat of an aviation accident (A3);
4. Algorithm for reconfiguration of the integrated aircraft control system (A4).

Thus, the concept of building the functioning of an intelligent aviation system presented in this chapter is aimed at improving the safety of aircraft flight. A distinctive feature of this concept is the combination of methods and algorithms for identifying the threat of an aviation accident and its parrying, taking into account the psychophysical state of the crew, the technical condition of the control object, and external factors. At the same time, the implementation of methods and algorithms should be carried out on the basis of artificial intelligence tools and using the concept of building the cyber-physical systems, which form the aircraft flight safety management system [23, 24].

5 Experiment

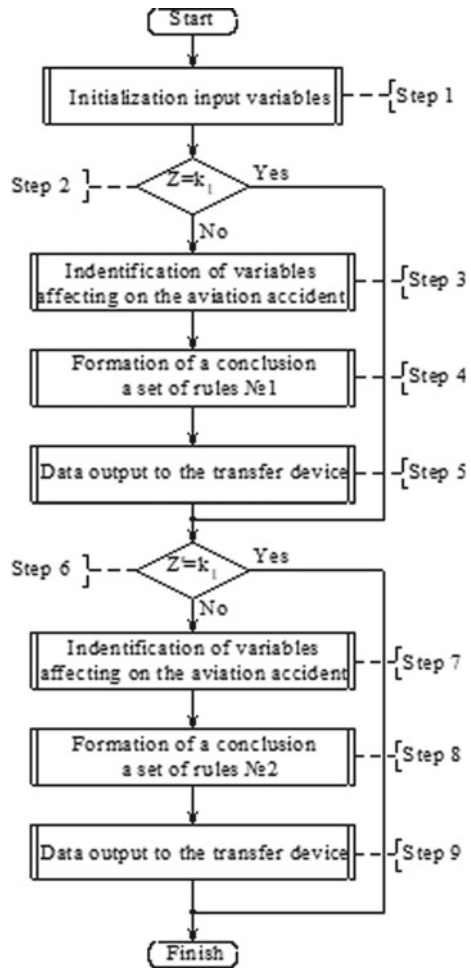
As an example of methods, techniques, and algorithms for improving the safety of aircraft flight, let's consider the algorithm for supporting the decision-making of the crew when parrying the threat of an aviation accident. The block diagram of the algorithm is shown in Fig. 3 [25].

where Z -aircraft flight conditions, k_1 -accident-free flight conditions.

The algorithm contains the following steps:

- Step 1. Initialization of input variables that characterize the state of the flight condition of the aircraft based on the results of preliminary processing of external and internal influencing factors.
- Step 2. Determining whether there is no threat of an accident. If there is no threat of an accident, then the analysis of the results of the forecast of changes in the controlled variables and flight conditions of the vehicle is carried out.
- Step 3. If the condition for block 2 is not met, the procedure is performed to determine the variables that affect the accident, compare them with the reference values, as well as with the values of the aircraft flight condition variable.
- Step 4. A method for parrying an incident threat is formed in accordance with the set of rules for the current threat (rule set 1), followed by the output of recommendations and management commands to the systems of the onboard equipment complex.

Fig. 3 Block diagram of decision support algorithm for parrying the threat of aviation accident



- Step 5. Data is transmitted by the method of parrying the threat of an accident under the influence of the current values of variables that affect flight safety, presented in the form of a command that is sent to the input of the warning and control systems of the AIRCRAFT's onboard equipment complex.
- Step 6. Determination of the absence of a predicted threat of an aviation accident. If the condition is met, the program goes to the end of the program.
- Step 7. If the condition is not met, the procedure is implemented to determine the variables that affect the AP threat based on the forecast results.
- Step 8. Formed a method is Formed for parrying a potential threat of an aviation accident in accordance with the set of rules No. 2.

Step 9. Data is transmitted on the method of parrying the threat of an aviation accident, taking into account the predicted values of variables that affect flight safety, presented in the form of a command that is sent to the input of the warning and control systems of the aircraft onboard equipment complex.

The algorithm was tested under the following flight conditions:

- the value of the flight conditions is “0.8”, which corresponds to an accident-free flight mode;
- the value of the flight conditions is “ - 0.8”, which corresponds to a catastrophic flight condition, i.e. under the influence of a combination of influencing factors, a threat of a catastrophic accident is created.

Based on the received data on the threat of an accident, the crew decision support algorithm, implemented on the basis of the high-level artificial intelligence program Prolog, was tested, the results are shown in Figs. 4 and 5.

From the information presented in Figs. 4, 5, it follows that the decision support device is able to form recommendations to the crew on actions under the threat of an aviation accident through the means of aircraft display and signaling.

Based on the results of tests of the safety control system of the aircraft, it can be concluded that its software is capable and can be used in the further development of the system, as well as devices of this class.

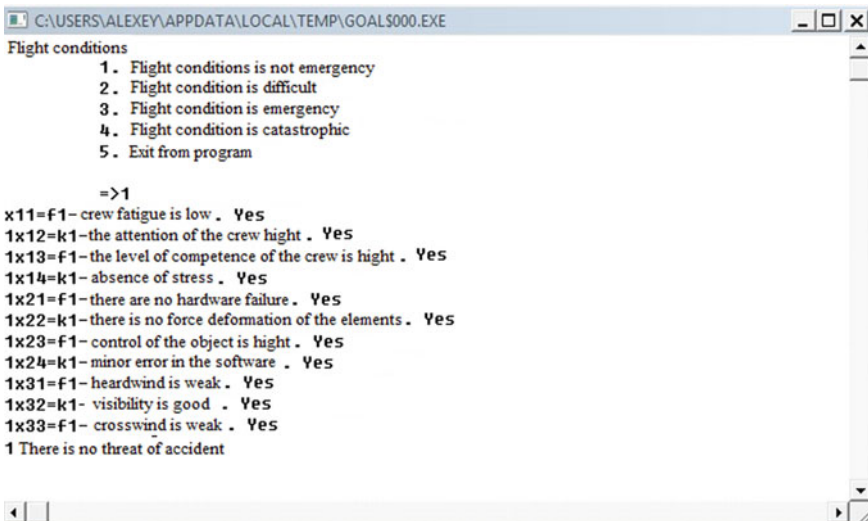


Fig. 4 Characteristics of the research results of the decision support algorithm for non-emergency flight conditions of aircraft

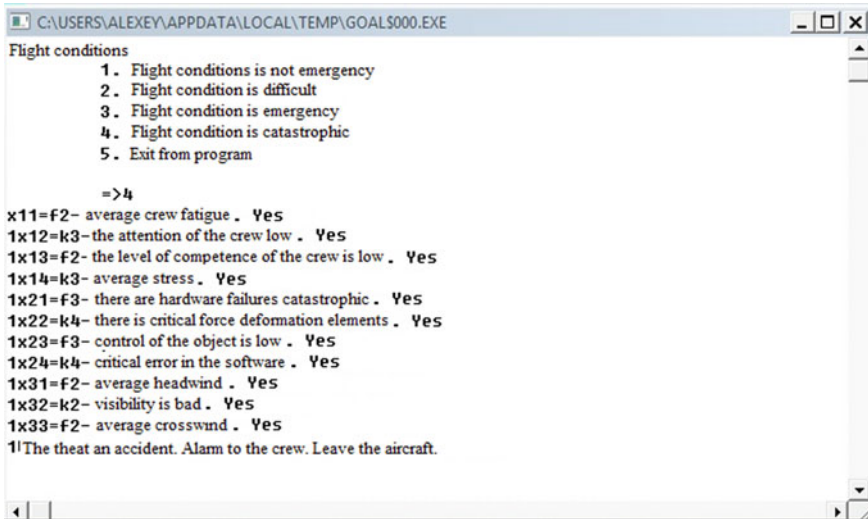


Fig. 5 Characteristics of the research results of the decision support algorithm under catastrophic flight conditions

6 Conclusion

In the course of the work, a set of methods, techniques and algorithms based on the design of cyber-physical systems is proposed, based on which a methodology aimed at improving the safety of aircraft flight is developed. This methodology is implemented by an intelligent aviation system, which differs from the existing aviation transport system by having an intelligent decision support system in its structure.

The chapter also presents the results of an experimental study of the software of the crew decision support system for parrying the threat of an accident, which confirms its operability and the possibility of further testing as part of the aircraft's onboard equipment.

Acknowledgements The work was performed using the results obtained from the implementation of the RFBR grant No. 15-07-07930 A.

References


1. Popov, Y.V.: The safety indicators for aviation flights. Electron. J. Technol. Techno Field Secur. **6(58)** (2014)
2. Sapogov, V.A., Anisimov, K.S., Novozhilov, A.V.: Fail-safe computer system for complex of aircraft flight control systems. Electron. J. Proceed. MAI. **45** (2008)

3. Glubokay, M.D.: Onboard decision support system at the take-off stage of the passenger aircraft. *Air Fleet Technol. LXXXII* 1(690), 21–30 (2008)
4. Shevchenko, A.M., Nachinkina, G.N., Solonnikov, Y.I.: Modeling of information support of the pilot on the take-off phase of the aircraft. In: *Proceedings of Moscow Institute of Electromechanics and Automatics (MIEA)*, vol. 5. pp. 54–64 (2012)
5. Suholitko, V.A.: Way to support the operator in dangerous situations. The patent for the invention RF № 220544 G05D 1/00. (2017)
6. Berestov, L.M., Harin, E.G.: Highly intelligent automated system for ensuring the flight safety of the aircraft. The patent for the invention RF № 2339547 B64D 45/00. (2008)
7. Reece Clothier the safety risk management of unmanned aircraft systems (2020). http://www.researchgate.net/publication/255853556_The_Safety_Risk_Management_of_Unmanned_Aircraft_Systems. Accessed 8 Jul 2020
8. James T.L., Trefor, P.: Williams Integrated decision support for aviation safety inspectors. *Finite Elements in Anal. Des.* **23**, 381–403 (1996)
9. Khaitan et. al.: Design Techniques and application of cyber physical systems: a survey. *IEEE Syst. J.* (2014)
10. Lee, E.A., Seshia, S.A.: In: *Introduction to Embedded Systems—A Cyber-Physical Systems Approach*. LeeSeshia.org (2011)
11. *Cyber-Physical System Driving force for innovation in mobility, healthy, energy, and production*. ACATECH (2011)
12. Wolf, W.: Cyber-physical system. *Computer* **3**, 88–89 (2009)
13. Crop: A cyber-physical system architecture model in the field of precision agriculture. In: *Conference Agriculture for Life, Life for Agriculture*. vol. 6. pp. 73–79 (2020)
14. Lee J., Bagheri B., Kao H.-A.: A cyber-physical systems architecture for industry 4.0-based manufacturing systems. *Manuf. Lett.* **3**, 18–23 (2015). <https://doi.org/10.1016/j.mfglet.2014.12.001>
15. Chuprynousky, V.P., Namiot, D.E., Sinyakov, S.A.: A cyber-physical system as the basis for the digital economy. *Int. J. org Open Info. Technol.* **4**(2), 18–25 (2016). ISSN: 2307-8162
16. Bolshakov, A.A., Kulik, A.A., Sergushov, I.V., Skripal, E.N.: Method of aircraft accident prediction. *Mechatron. Autom. Control* **19**(6), 416–423 (2018)
17. Fedunov, B.E., Prokhorov, M.D.: Conclusion on precedent in knowledge bases of onboard intelligent systems. *Artif. Intell. Decision-Making* **3**, 63–72 (2010)
18. Kosko, B.: Fuzzy systems as universal approximators. *IEEE Trans. Comput.* **43**(11), 1329–1333 (1994)
19. Cordon, O., Herrera, F.A.: General study on genetic fuzzy systems. In: Periaux, J., Winter, G. (eds.) *Genetic Algorithms in Engineering and Computer Science*, pp. 33–57. (1995)
20. Averchenkov, V., Miroshnikov, V., Podvesovsky, A., Korostelyov D.: Fuzzy and hierarchical models for decision support in software systems implementation. In: Kravets, A.G., Shcherbakov, M.V., Kultsova, M., Iijima, T. (eds.) *Knowledge-Based Software Engineering*, pp. 410–422 (2014)
21. Denisov, M., Kozin, A., Kamaev, V., Davydova, S.: Solution on decision support in determining of repair action using fuzzy logic and agent system. In: Kravets, A.G., Shcherbakov, M.V., Kultsova, M., Iijima, T. (eds.) *Knowledge-Based Software Engineering*, pp. 433–541. (2014)
22. Bazhanov, A., Vashchenko, R., Rubanov, V., Bazhanova, O.: Development of an automated system for monitoring and diagnostic a guided robotic vehicle. In: Kravets, A.G., Bolshakov, A.A., Shcherbakov, M.V. (eds.) *Cyber-Physical Systems: Industry 4.0 Challenges*, pp. 93–107. Springer, (2019)
23. Bolshakov, A.A., Kulik, A.A., Sergushov, I.V., Skripal, E.N.: Intelligent method for assessing the threat of an accident. *Bullet. Comput. Inf. Technol* **5**(167), 3–9 (2018)
24. Kulik, A.A., Bolshakov, A.A., Veshneva, I.V.: Increasing the safety of flights with the use of mathematical model based on status functions. In: *International Conference on Information Technologies ICIT 2019: Recent Research in Control Engineering and Decision Making* Springer. 29 January 2019. pp. 608–621. (2019)

25. Bolshakov, A.A., Kulik, A.A., Sergushov, I.V., Scripal, E.N.: Decision Support Algorithm for Parrying the Threat of on Accident. In: Kravets, A.G., Bolshakov, A.A., Shcherbakov, M.V. (eds.) *Cyber-Physical Systems: Industry 4.0 Challenges*, pp. 237–247. Springer, (2019)

The Applying of the Formalism of Cyber-Physical Systems in the Description of Hydrodynamic Cavitation in a Direct-Flow Valve



A. B. Kapranova , A. E. Lebedev, A. M. Melzer, S. V. Neklyudov, and A. S. Brykalov

Abstract The chapter provides a description of the bubble energy during its stochastic movement under conditions of hydrodynamic cavitation in the flow part of a direct-flow valve with a turn of the external shut-off shell depending on the throughput of the device from the standpoint of the energy method. The results of this description form the basis of stochastic modeling of the formation of the macrosystem of bubbles in this region and rely on the formalism of cyber-physical systems.

Keywords Cyber-physical system · Direct-flow valve · Separator · Cavitation · Bubble · Model · Energy · Parameters

1 Introduction

For pipeline control valves, the appearance of cavitation in flow areas is an accompanying effect, and its consequences in any form not only cause additional losses in various industries but also pose a potential risk of failure of this equipment and

A. B. Kapranova (✉) · A. E. Lebedev
Yaroslavl State Technical University, Moskovsky Prospect, 88, Yaroslavl 150023, Russian Federation

e-mail: kapranova_anna@mail.ru

A. E. Lebedev
e-mail: lae4444@gmail.ru

A. M. Melzer · S. V. Neklyudov · A. S. Brykalov
JSC “Regulyator”, Gagarin street, 68a, Yaroslavl 150023, Russian Federation
e-mail: meltzer.a@mail.ru

S. V. Neklyudov
e-mail: neklydov.s@nporeg.ru

A. S. Brykalov
e-mail: brykalov.a.s@nporeg.ru

the creation of accident conditions during operation. Given the scope of application of control valves in critical areas of oil production and oil refining purposes, the requirements for design projects are constantly increasing. Providing the operating mode of regulatory equipment while reducing the intensity of the cavitation phenomenon is one of the urgent design problems [1–4]. The formation of a theoretical base for calculating the parameters of the throttling process of selection of the working medium flows in the direct-flow valves is a necessary design stage and is associated with many factors that determine the behavior of the resulting cavitation cavities in the flowing areas of this type of control valves. Note that with the expansion of the scope of application of ready-made software products for calculating the main characteristics of liquid throttling, there is no loss of interest [5] in the development of analytical methods for determining cavitation indicators [6–8], including for choosing effective ranges of variation of the parameters of direct-flow valves [9]. The aim of this work is to study the dependence of the main parameters of the stochastic model of hydrodynamic cavitation on the valve capacity for the formation of cyber-physical systems, which further determine the engineering method for calculating a new control direct-flow valve based on the principle of rotation of an external locking shell [10]. It is proposed to apply a stochastic approach using the energy method [11].

Currently, known methods of dealing with these unwanted effects use the principle of throttling fluid flows [1–4, 9], which can be implemented in devices with various constructive solutions, for example, when changing the shape, location, and the number of throttle openings. Leading manufacturers of pipe fittings [1–4] pay special attention to the design of direct-flow regulating devices, in the working areas of which a significant decrease in local hydraulic resistance is possible in comparison with the values of this coefficient for valves of other body shapes (three-way, z-shaped, etc.), which contributes to an increase in the flow capacity of the valve. The main idea of the designers of leading companies when throttling fluid flows is to, firstly, warn cavitation bubbles from appearing near the valve's internal flow surfaces to prevent their possible erosion at the developed stages of cavitation due to the almost simultaneous collapse of these bubbles. Secondly, the resulting bubbles should be removed into the central flowing part for removal along with the flow of the working medium. For example, in single-flow valves, single-tier [12] and multi-tier [13] separator systems, channel chokes in flow dividers [4] are organized, including to achieve the effect of axial swirling of the fluid flow [3], etc. [1–4].

Thus, the design of new direct-flow type valves requires the solution of multifactor problems to achieve a decrease in the intensity of hydrodynamic cavitation, the solution of which is facilitated by a system-structural analysis of the process of formation of cavitation bubbles at the initial stages of cavitation evolution [14–17].

2 On the Choice of a Method for Modeling Hydrodynamic Cavitation in a Direct-Flow Valve in the Formalism of a Cyber-Physical System

In describing the phenomenon of cavitation, as a rule, the following are used: the traditional deterministic approach [18–20], be implemented for a single bubble; stochastic approach [6, 21–23] in the form of descriptions of homogeneous [21, 22] and heterogeneous (with the introduction of the heterogeneity factor) [6, 23] nucleation. As well as successful attempts to combine the first two methods with applying the Euler–Lagrange coordinates are known [24, 25]. However, the multifactorial nature of the formulation of the problem of modeling hydrodynamic cavitation depending on the valve capacity for the formation of the corresponding cyber-physical systems is difficult when using the classical deterministic approach, and in the indicated stochastic or combined models, the construction of distribution functions for the bubble macro system is based on experimental data. In the present work, it is proposed to use the energy method [1–4] for stochastic modeling of hydrodynamic cavitation in a direct-precision valve with the rotation of an external locking shell [10], which was tested in the description of the initial stage of bubble cavitation in a control device with an external shutter arrangement [15–17, 26].

The general formalism of constructing a cyber-physical system for assessing the main characteristics of control valves is presented in [14] and includes the step of describing a schematic diagram for calculating the throttling of a fluid flow with a partition of information variables $z = \{x, y, a, b\} = \{z_{\text{mod}}, z_{\text{reg}}, z_{\text{opt}}\}$ into groups:

- the calculated z_{mod} (determined from the model);
- the regulated by z_{reg} (consist of constructive a and mode b);
- optimizing z_{opt} (with possible replacement by rational ones).

The contents of the sets of variables x, y, a, b reflect the main stages of the process of throttling the flow of the working fluid in the direct-flow valve with the rotation of the external locking shell [10]. A feature of the separator is the change in the degree of its opening by turning the outer shell, also perforated by round holes. Thus, throttle openings have a variable area when the shape varies from a double segment to a circle if the valve is fully open. In particular, as the object of stochastic modeling, the process of hydrodynamic cavitation in the working volume of the main unit “separator-external rotary locking shell” (as two coaxial perforated cylinders) of the direct-flow valve [10] was selected.

The set of characteristics of this technological operation includes the following main parameters: input $x = \{x_{k_1} = \text{const}\} = \{Q_{1\text{max}}, \delta_{1\Delta P_{\text{min}}}, \delta_{2\Delta P_{\text{min}}}, t_1, w\}$, $k_1 = \overline{1, s_1}$; weekend $y = \{y_{k_2}\} = \{K_{vy}\}$, $k_2 = \overline{1, s_2}$; constructive $a = \{a_{k_3} = \text{const}\} = \{d_0, \lambda_1, \lambda_2, q_1, q_2, \delta_1, \delta_2, D_j, D_{\text{out}}, L\}$, $k_3 = \overline{1, s_3}$; mode $b = \{b_{k_5}\} = \{x_{k_1}, x_{k_4}\}$, $k_5 = \overline{1, s_5}$, where the condition $\Delta p_{\text{min}} \in \{b_{k_5}\}$; is fulfilled for the last set; $\{x_{k_4}\}$, $k_4 = \overline{1, s_4}$ is the set of parameters of the system of cavitation bubbles.

Here the notation is accepted: Q_{lmax} is maximum achievable fluid flow rate; $\delta_{1\Delta P_{min}}, \delta_{2\Delta P_{min}}$ are the limits of the change in the minimum pressure drop ΔP_{min} ; t_1 ($^{\circ}C$) is the temperature of the working medium; w is the fluid velocity in the pipeline; K_{vy} is the regulatory value of valve capacity; d_0 is the diameter of the radial throttle holes; λ_1, λ_2 are the distances, respectively, between the rows of throttle holes and holes in the same row; q_1, q_2 are the number of holes in one radial row and the number of these rows; δ_1, δ_2 are wall thicknesses of the separator and valve bodies $D_j, j = \overline{1, s_6}$ are characteristic diameters of the parts of the body; D_{out} is the inner diameter of the separator; L is the length of its perforated section.

In addition to information variables, it is necessary to take into account the physico-mechanical characteristics of the working fluid and the gas–vapor system in the resulting cavitation cavity $\varphi = \{\varphi_{k_3}\} = \{\rho_l, \rho_g, p_s, v_1, \sigma, \gamma, k\}, k_7 = \overline{1, s_7}$, where ρ_l, ρ_g, p_s are the densities of the liquid, gas, and vapor; v_1 is the kinematic viscosity of the liquid at a temperature t_1 ($^{\circ}C$); σ is the coefficient of surface tension; γ is the volumetric weight of the working fluid; k is the adiabatic exponent.

3 Features of Modeling the Energy of Stochastic Motion of a Cavitation Bubble

The application of the energy method [11] involves examining the states of an energetically closed macrosystem of randomly generated cavitation bubbles from the standpoint of the A. A. Markov process as homogeneous, stationary, Gaussian. Representation of a set of phase variables in the composition of the velocity of the center of mass of the bubble V and its radius R is sufficient to describe the energy of the indicated cavitation cavity $E(V, R)$ during its stochastic movement under conditions of hydrodynamic cavitation in the flow part of the direct-flow valve with the rotation of the external locking shell depending from the capacity of the device K_{vy} . The input of dimensionless variables (specific velocity $\nu = V/V_l$ and specific radius $\rho = R/R_k$) is reflected in the representations for the energy of a single bubble $E(V, R) = E(\nu, \rho)$ and the phase volume element $d\Psi = dVdR = V_l R_k d\nu d\rho$, where V_l, R_k are the given constants of the process under study, for example, the fluid flow rate and the minimum value of the radius of the spherical bubble R_{min} .

The energy closure of the macrosystem of bubbles makes it possible to obtain a stationary solution of the Fokker–Planck equation in the form of a decreasing exponential dependence for the distribution function of the number of cavitation bubbles over the specific radius ρ :

$$g(\rho) = N^{-1}dN/d\rho \quad (1)$$

depending on the parameters of the information variables described above, taking into account additional characteristics for the physico-mechanical properties of the working fluid and the gas–vapor system. Then the number of bubbles is determined

by the expression:

$$N = A \int_{\Psi} \exp[E(v, \rho)/E_0] dN \quad (2)$$

where the energy parameter E_0 and the constant A can be calculated using the system of energy balance equations and the normalization equation.

The main difficulties in modeling the functional dependence for the energy of the cavitation bubble are related to the conditional stages of the initial evolution of the cavitation phenomenon:

- cavitation cavity formation ($E_{bub} = 4\pi\rho_l R^3/3$);
- the design of its spherical shape ($E_{\sigma} = 4\pi\sigma R^2$);
- filling the internal cavity with a gas–vapor system ($E_{1g-p} = 4\pi P_s R^3$);
- the vortex movements of the latter system according to the Hill-type, taking into account the random component of the angular momentum M (if $E_{2g-p} = M^2/(2I)$);
- participation in interaction with the surrounding working fluid ($E_{bL} = k_{\zeta} \Delta P/(2R)$);
- the motion in the fluid flow ($E_{mot} = 2\pi(\alpha_g \rho_g + \alpha_s \rho_s) R^3 V^2/3$).

Here, we used a set of physicommechanical characteristics of the working fluid and the gas–vapor system in the resulting cavitation cavity = $\{\varphi_{k_3}\}$, $k_7 = \overline{1, s_7}$. In addition, the following notation is accepted: σ is the coefficient of surface tension of the liquid; I is an axial moment of inertia; P_s is the saturated vapor pressure; α_g, α_s is a fraction of gas and vapor in the cavity of the bubble; k_{ζ} is the coefficient of proportionality; $\Delta P = \zeta_{12} \rho_l V^2/2$ is the pressure drop associated with the Weisbach formula with the hydraulic resistance coefficient ζ_{12} in the transition section of the fluid flow when the Reynolds criterion changes within $0 < Re < 10^4$ according to [27].

In particular, the empirical relationship [27] between the values of the hydraulic resistance coefficient ζ_{12} and the capacity of the control valve K_{vy} in the form $\zeta_{12} = (1.26 \times 10^4 \pi D_y^2 / K_{vy})^2$ is known. Here, the conditional bore diameter D_y is set by the value of the conditional bore section of this device in accordance with the set of design parameters $a = \{a_{k_3} = const\}$, $k_3 = \overline{1, s_3}$ from Sect. 2. Note that the maximum value of the capacity of this device K_{vymax} also has an experimentally established connection with the set of input parameters of the process under study $x = \{x_{k_1} = const\}$, $k_1 = \overline{1, s_1}$, also introduced in Sect. 2. For example, the expression $K_{vymax} = Q_{1max}[\gamma/(1.5 \times \Delta P_{min})]^{1/2}$ is valid, where the following dimensions of quantities are assumed: for the valve capacity value $[K_{vymax}] = \text{m}^3/\text{h}$; for the volumetric weight of the working fluid $[\gamma] = \text{g} \times \text{cm}^3$; for its maximum achievable flow rate $[Q_{1max}] = \text{m}^3/\text{h}$; for a minimum pressure drop $[\Delta P_{min}] = \text{kPa}$. Thus, by analogy with the previously proposed models [15, 16] for the process of hydrodynamic cavitation in the control valve, we obtain the expression for the desired

dependence

$$E(V, R) = E_{bub} + E_{\sigma} + E_{1g-p} + E_{2g-p} + E_{bL} + E_{mot}. \tag{3}$$

In view of (3), we have the following representation $E(v, \rho) = V_l^2 v^2 \mu_1(\rho) + \mu_2(\rho)$, where the functions $\mu_1(\rho), \mu_2(\rho)$ take into account the described features of modeling the energy of stochastic cavitation motion the bubble.

Further modeling of the hydrodynamic cavitation process in the “separator – external rotary locking shell” assembly [10] is associated with finding two characteristic parameters: E_0 from expression (2) and M from the expression for the term E_{2g-p} in (3). We note that the parameter E_0 has the physical meaning of the energy of motion of the cavitation bubble at the moment of stochastization of the macrosystem of cavitation cavities. In this case, the parameter M describes the angular momentum of the bubble, taking into account its random nature during the flow of the working fluid in the node “separator-external rotary locking shell” [10]. A general approach to estimating the parameters E_0, M was proposed by the authors in [15] and involves solving the following system of two equations.

First equation

$$E_{tot} = E_{fr} \tag{4}$$

reflects the energy balance between the total energy of the macrosystem of bubbles, determined by the dependence $E_{tot} = \int_{\Psi} E(v, \rho) dN$, and the energy E_{fr} necessary for hydrodynamic rupture of the liquid in the flow part of the valve over a certain period of time $\Delta\tau$.

It is believed that the three terms from expression (3) make the main contribution to the energy E_{fr} when $E_{fr} = \int_{\Psi} [E_{\sigma}(\rho) + E_{bL}(\rho) + E_{mot}(v, \rho)] dN$. The ensemble average bubble volume $\langle V_b \rangle$ and the value of the time interval are taken into account

$$\Delta\tau = [16R_{min}^3 / (3V_l d_0^2 q_1 q_2 z)] \int_{\Psi} \rho^3 dN. \tag{5}$$

where the set of design parameters $\{d_0, q_1, q_2\} \in \{a_{k3} = const\}, k_3 = \overline{1, s_3}$ is described in Sect. 2; z is the degree of opening of the throttle holes.

The second equation [15] is a consequence of thermodynamic equality for the adiabatic process inside the bubble with respect to the gas–vapor system and has the form

$$(P_{max}/P_s)^{1/k} = (\langle R \rangle / R_{min})^3. \tag{6}$$

It is considered here that with a minimum bubble radius R_{min} , the maximum pressure at its center P_{max} is observed. With the ensemble bubble radius $\langle R \rangle$ averaged over the ensemble, the pressure value is P_s . The adiabatic exponent is denoted by k

and is included in the set $\varphi = \{\varphi_{k_3}\}$, $k_7 = \overline{1, s_7}$ for the physic mechanical characteristics of the working fluid and the gas–vapor system inside the cavitation cavity formed.

The desired solutions E_0, M for the described system of Eqs. (4), (6) were obtained taking into account (5) in the following approximations for the expansion of the Maclaurin series of the error function $\text{erf}(\eta) = 2\pi^{-1/2}\eta + O(\eta^3)$ and exponents $\exp(-\eta) = 1 - \eta + O(\eta^2)$

$$E_0 = \beta_0(\varepsilon_1 + \varepsilon_{10}\varepsilon_2)/(2\pi^2\varepsilon_{10}\varepsilon_3 - 20\varepsilon_4), \tag{7}$$

$$M = \left[3E_0\left(2\beta_9^{\frac{1}{3}} - 1\right) - u_4\right]R_{min}^5/(5\beta_3). \tag{8}$$

Expressions (7), (8) contain the following sets of parameters $\{\varepsilon_{j_1}, \varepsilon_{1j_{11}}\}$, $j_1 = \overline{1, 4}$, $j_{11} = \overline{0, 1}$; $\{u_{j_2}\}$, $j_2 = \overline{1, 7}$; $\{G_{1j_3}\}$, $j_3 = \overline{1, 2}$; $\{\beta_{j_4}\}$, $j_4 = \overline{0, 9}$, the calculation of which used the set of information variables $z = \{x, y, a, b\}$ from Sect. 2 and the notation:

$$\begin{aligned} \varepsilon_1 &= 60u_1u_2, \quad \varepsilon_{10} = (V_l^2 R_{min}/u_2)\text{erf}[u_2/(V_l^2 R_{min})]; \\ \varepsilon_{11} &= (V_l^2 u_5/u_2)\left\{\left[V_l/\left(\varepsilon_{10}\pi^{\frac{1}{2}}\right)\right] \exp\left(-u_2^{1/2}/R_{min}\right) - 1/2\right\}; \\ \varepsilon_2 &= 15u_3 R_{min}^3 + 3u_4 + G_{11}(u_4 - u_5 R_{min}); \\ \varepsilon_3 &= 2u_4\left(\beta_6^{\frac{1}{3}} - 1\right)(3 + \varepsilon_{11}); \\ \varepsilon_4 &= R_{min}(1 + u_6). \end{aligned} \tag{9}$$

$$\begin{aligned} u_1 &= \beta_1 R_{min}^3 G_{11} + \beta_2 R_{min}^{-1} G_{12}; \quad u_2 = (\beta_1 R_{min}^4 + \beta_2) V_l^2; \\ u_3 &= (32\pi)^{\frac{1}{2}}/(3D_y^2) - \beta_5; \quad u_4 = R_{min}^2(2\beta_4 + 3R_{min}\beta_5); \quad u_5 = 3\beta_1 R_{min}^4 - \beta_2; \\ u_6 &= 3R_{min}(5\beta_4 + R_{min}\beta_6); \quad u_7 = 2^{5/2}(\pi/3)^2 \beta_6 \beta_7 \beta_8^{3/2}. \end{aligned} \tag{10}$$

$$G_{11} = \int_0^1 \rho^4/(\beta_1 R_{min}^4 \rho^4 + \beta_2) d\rho; \quad G_{12} = \int_0^1 1/(\beta_1 R_{min}^4 \rho^4 + \beta_2) d\rho. \tag{11}$$

$$\begin{aligned} \beta_0 &= u_4 u_7 / \left[3(2\pi^{1/2})^3\right]; \quad \beta_1 = (2\pi/3)(\alpha_g \rho_g + \alpha_s \rho_s); \quad \beta_2 = k_\zeta \zeta_{12} \rho_l / 4; \\ \beta_3 &= 5\beta_1 / 8; \quad \beta_4 = 4\pi \sigma; \quad \beta_5 = 8\pi P_s / 3; \\ \beta_6 &= 1 + (3^3/\pi^4/4)(1 - \beta_8); \quad \beta_7 = 1 - (R_{min}/D_y)(K_{vy}/Q_{1max})^{1/2}; \\ \beta_8 &= (K_{vy}/K_{vymax})(D_{ymax}/D_y)^2; \quad \beta_9 = R_{min}^3 (P_{max}/P_s)^{1/k}. \end{aligned} \tag{12}$$

So, of particular interest for further studies is the dependence of the obtained parameters E_0, M according to expressions (7), (8) taking into account (9)–(12) on the main characteristics of the throttling process of the fluid flow in the node

“separator-external rotary locking shell” [10]. For example, such characteristics include the conditional bore diameter D_y for a direct-flow valve of the indicated type and its capacity K_{vy} .

4 An Example of Calculating the Main Parameters of a Stochastic Model of Hydrodynamic Cavitation for the Formation of Cyber-Physical Systems

As an example, we consider the calculation of the main parameters of the stochastic model of hydrodynamic cavitation E_0, M in the flow part of the valve with the rotation of the external locking shell [10]. It is believed that the physicomachanical properties of the working fluid for the set $\varphi = \{\varphi_{k_3}\}$, $k_7 = \overline{1}, s_7$ are determined by the properties of water with density $\rho_l = 10^3 \text{ kg/m}^3$ at a temperature $t_1 = 30^\circ\text{C}$, volumetric weight $\gamma = 0.995 \text{ g} \times \text{c/cm}^3$, surface tension coefficient $\sigma = 7.28 \times 10^{-4} \text{ N/m}$, kinematic viscosity $\nu_1 = 0.81 \times 10^{-2} \text{ cm}^2/\text{c}$. The vapor and air densities are equal to the values: $\rho_g = 1.205 \text{ kg/m}^3$ and $p_s = 1.44 \times 10^{-2} \text{ kg/m}^3$, the adiabatic parameter is $k = 1.3$. Characteristic factors for cavitation bubbles and their internal gas–vapor system are assumed to be similar to those adopted in [14–17]. In particular, with a minimum bubble radius $R_{min} = 10^{-3} \text{ m}$, the maximum pressure at its center is $P_{max} = 1, 3 \times 10^5 \text{ kPa}$, with an averaged radius, the value of this pressure corresponds to $P_s = 10^{-3} \text{ Pa}$.

Moreover, the choice of parameters from the described sets of input x , output y , structural a , and mode b corresponds to the following values. The set of input parameters $x = \{x_{k_1}\}$, $k_1 = \overline{1}, s_1$ includes the maximum attainable flow rate $Q_{1max} = 0.8 \text{ m}^3/\text{h}$ at the limiting values for the minimum pressure drop $\delta_{1\Delta P_{min}} = 1.10 \text{ kPa}$ and $\delta_{2\Delta P_{min}} = 1.50 \text{ kPa}$ at a temperature index of $t_1 = 30^\circ\text{C}$ and a value of the fluid velocity in the pipeline $w = 0.43 \text{ m/c}$. The mode parameter from the set $b = \{b_{k_5}\}$, $k_5 = \overline{1}, s_5$ is the average value from the given range $[\delta_{1\Delta P_{min}}; \delta_{2\Delta P_{min}}]$ for the minimum pressure drop $\Delta P_{min} = 1.30 \text{ kPa}$ at the indicated temperature t_1 .

The output parameter of the model from the set $y = \{y_{k_2}\}$, $k_2 = \overline{1}, s_2$ is the capacity of the control valve $K_{vy} = 7 \text{ m}^3/\text{h}$. In addition, the set $a = \{a_{k_3}\}$, $k_3 = \overline{1}, s_3$ for the design parameters of the throttling process of the fluid flow in the flow part of the valve with the rotation of the external locking shell [10] includes: $d_0 = 2.0 \times 10^{-3} \text{ m}$; $\lambda_1 = 1.0 \times 10^{-3} \text{ m}$; $\lambda_2 = 3.9 \times 10^{-4} \text{ m}$; $q_1 = 24$; $q_2 = 7$; $\delta_1 = 3.0 \times 10^{-3} \text{ m}$; $\delta_2 = 3.1 \times 10^{-3} \text{ m}$; $D_{out} = 3.4 \times 10^{-2} \text{ m}$; $L = 2.35 \times 10^{-2} \text{ m}$.

For the above values of the throttling process parameters, according to expressions (7), (8), the dependences $E_0(K_{vy}, D_y)$ and $M(K_{vy}, D_y)$ are obtained, shown in Figs. 1 and 2. The dashed lines in Figs. 1 and 2 for the indicated functions correspond to such values of their arguments K_{vy}, D_y , which are not included in the considered ranges of changes in the characteristics of the studied process. The limits of variation K_{vyj}, D_{yj} , $j = \overline{1, 4}$ are selected according to the following four values of the degree of opening of the throttle holes: 20, 50, 80, and 100%. These positions are determined

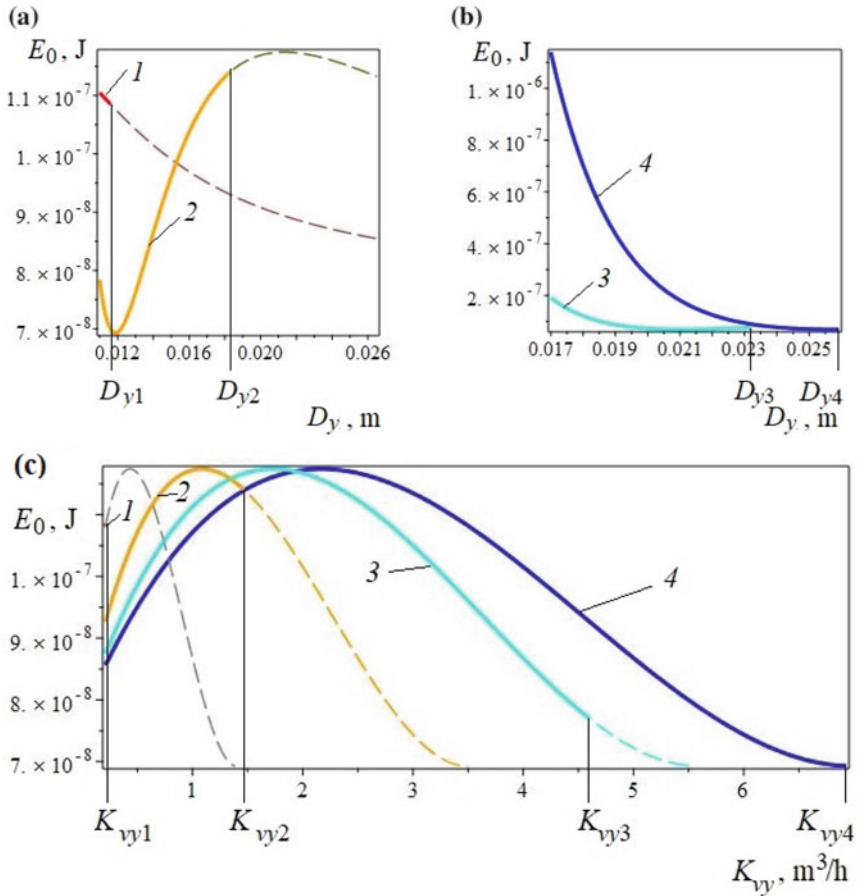


Fig. 1 Dependence of the parameter E_0 on the characteristics of the throttling process of the fluid flow: a, b $-E_0(D_y)$; c $-E_0(K_{vy})$; $D_{y1} = 1.16 \times 10^{-2}$ m, $K_{vy1} = 2.15 \times 10^{-1}$ m³/h (1); $D_{y2} = 1.83 \times 10^{-2}$ m, $K_{vy2} = 1.46$ m³/h (2); $D_{y3} = 2.13 \times 10^{-2}$ m, $K_{vy3} = 4.59$ m³/h (3); $D_{y4} = 2.59 \times 10^{-2}$ m, $K_{vy4} = 6.93$ m³/h (4); $\alpha_g = \alpha_s = 0.5$

by the radial rotation of the outer cylindrical perforated shell relative to the stationary cylindrical separator with round throttle openings. The combination of the diameters of the holes belonging to the shell and the separator leads to the complete opening of the valve (100% degree of its opening). Other positions of the shell provide separation of the fluid flow when flowing through open sections of throttle holes, which are in the form of segments (the degree of opening of the valve is less than 100%).

According to Fig. 1, initially, there is a slight increase in the values of the energy parameter E_0 for the values of the diameter of the conditional flow area from the range $D_y \in [D_{y1}, D_{y2}]$ (Fig. 1a) 1.04 times, and then its decrease by 0.55 times for $D_y \in [D_{y2}, D_{y3}]$ (Fig. 1a, b) and 0.9 times for $D_y \in [D_{y3}, D_{y4}]$ (Fig. 1b). In this

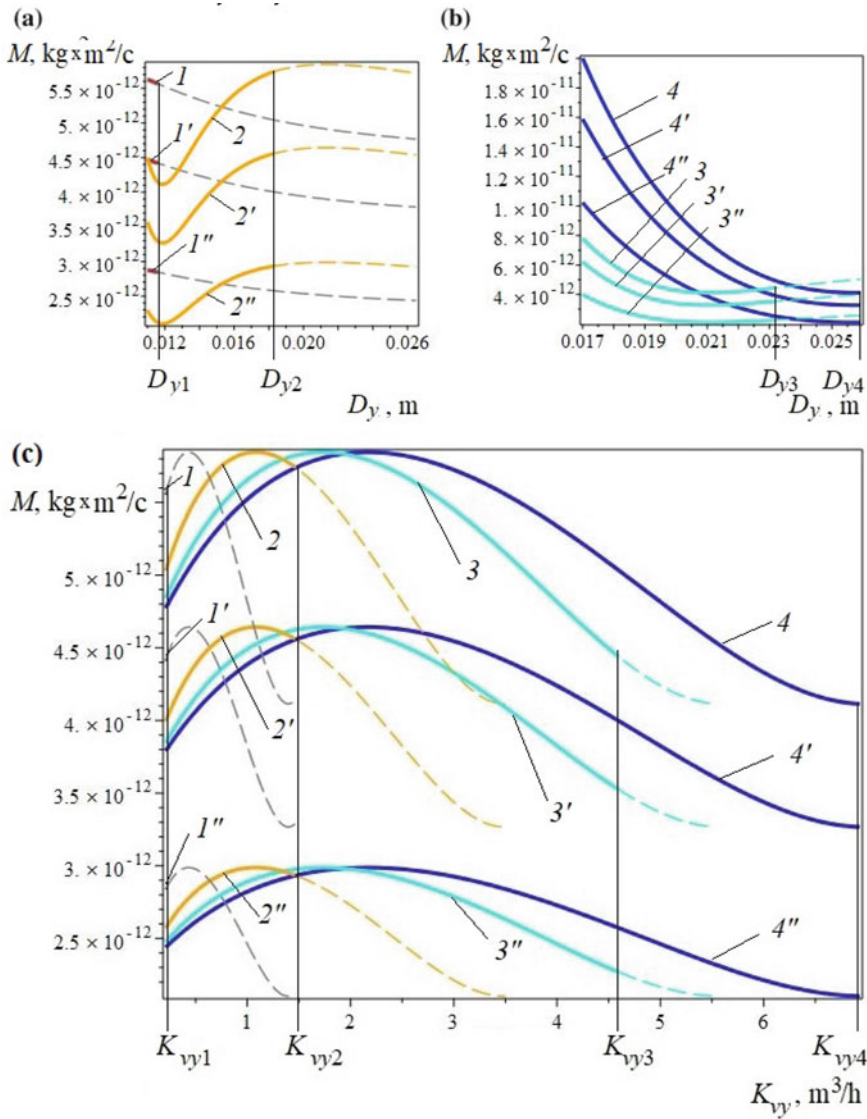


Fig. 2 Dependences of the parameter M on the characteristics of the throttling process of the fluid flow: a, b $-E_0(D_y)$; c $-E_0(K_{vy})$; $D_{y1} = 1.16 \times 10^{-2} \text{ m}$, $K_{vy1} = 2.15 \times 10^{-1} \text{ m}^3/\text{h}$ (1, 1', 1''); $D_{y2} = 1.83 \times 10^{-2} \text{ m}$, $K_{vy2} = 1.46 \text{ m}^3/\text{h}$ (2, 2', 2''); $D_{y3} = 2.13 \times 10^{-2} \text{ m}$, $K_{vy3} = 4.59 \text{ m}^3/\text{h}$ (3, 3', 3''); $D_{y4} = 2.59 \times 10^{-2} \text{ m}$, $K_{vy4} = 6.93 \text{ m}^3/\text{h}$ (4, 4', 4''); $\alpha_g = 0.8, \alpha_s = 0.2$ (1-4); $\alpha_g = \alpha_s = 0.5$ (1'-4'); $\alpha_g = 0.2, \alpha_s = 0.8$ (1''-4'')

case, the maximum drop in the value of the energy parameter by 0.61 times (Fig. 1c) corresponds to the transition from the 50% valve opening mode to the 100% mode (solid line endpoints for graphs 2 and 4, Fig. 1c), when the throughput K_{vy} increases 4.75 times (values K_{vy2} , K_{vy4} , Fig. 1c).

Similar behavior is noted for the random component of the angular momentum of the bubble $M(K_{vy}, D_y)$ in Fig. 2, both depending on the diameter of the nominal bore D_y (Fig. 2a, b), and on the flow capacity of the K_{vy} valve (Fig. 2c). In particular, for equal proportions of gas and vapor fractions α_g , α_s inside the bubble (family of graphs 1'-4', Fig. 2a, b), a maximum decrease in the value of the parameter M by 0.71 times corresponds to an increase in the diameter of the conditional passage D_y by almost 1.4 times and increase the K_{vy} value by 4.75 times when exiting from the 50% to 100% valve opening mode (endpoints of solid lines for graphs 2' и 4', Fig. 2a, b and c). Moreover, as a comparison of the positions of the endpoints of solid lines for each of the graph families 2, 2', 2'' and 4, 4', 4'' (Fig. 2c) shows, this is true for any ratio of gas and vapor fractions α_g , α_s inside the cavitation cavities.

5 Key Findings and Results

The use of the energy method [11] for stochastic modeling of hydrodynamic cavitation allowed the authors to construct appropriate models for the flow of working fluid in the flow part of the axial valve with the external location of the locking organ [15, 16]. In the present work, this approach is adapted for the case of fluid movement in the working volume of a direct-flow valve with the rotation of the external rotary locking shell of the valve [10].

We list the main conclusions and results of a study on the design of the cyber-physical system of the process of throttling the flow of a working medium in a direct-flow valve.

- A set of information variables of the studied throttling process of fluid has been identified, including input, output, structural, operational parameters, and additional physical and mechanical characteristics of the working medium. In particular, the most significant structural parameters include: the diameter of the throttle holes, their number in one radial row on the cylindrical surface of the separator, the number of these rows, the inner diameter of the separator.
- Two main parameters are identified for analyzing the behavior of the simulated dependencies for the main indicators of the process of throttling the working fluid in the flow part of the direct-flow valve: the diameter of the nominal pass and the capacity of the control device.
- One of the results of these studies is the functional dependence of the energy parameter of the model $E_0(K_{vy}, D_y)$ from (7) on the conditional capacity of the direct-flow valve of the indicated type K_{vy} and the diameter of the conditional bore D_y of the separator-external rotary locking shell assembly. For example, at the stage of transition from a mode with a valve opening degree of 50% to a mode

of its full opening, the maximum value of the energy parameter decreases by 0.61 times, which is accompanied by a 4.75 times increase in the capacity value.

- The obtained dependencies for the random component of the angular momentum of the bubble $M(K_{vy}, D_y)$ from (8) are of a similar nature taking into account the ratio of the gas and vapor fractions inside the cavitation cavity. In particular, with equal values of the latter, the maximum drop in the value of M by 0.71 times also occurs when 50% of the valve opening degree mode is changed to its 100% opening mode. At the same time, there is an increase in the diameter of the conditional passage by almost 1.4 times and the capacity value of 4.75 times.

6 Conclusion

Thus, for the designed cyber-physical system of the process of throttling the flow of the working medium in a direct-flow valve, the choice of information variables was made and the most significant design parameters from their number were identified. A stochastic simulation of the energy of movement of the cavitation bubble was performed using the energy method [11] to describe the process of hydrodynamic cavitation in the node “separator-external rotary locking shell” [10]. The nature of the change in the two main parameters of the system E_0, M was studied taking into account the corresponding ranges for the two main process indicators $K_{vyj}, D_{yj}, j = \overline{1, 4}$, which correspond to the following four values of the degree of opening of the throttle openings of the direct-flow valve: 20, 50, 80, and 100%.

In particular, an analysis was made of the behavior of the energy characteristic $E_0(K_{vy}, D_y)$ depending on the degree of opening of variable shape throttle holes when it changes from a double segment to a circle. In addition, the obtained dependencies for the random component of the angular momentum $M(K_{vy}, D_y)$ make it possible to analyze the state of the gas–vapor system inside the cavitation cavity.

The obtained results of this description form the basis of stochastic modeling of the formation of the macrosystem of bubbles during the formation of cyber-physical systems, which further determine the engineering method for calculating a new control direct-flow valve based on the principle of rotation of the external locking shell [10].

References

1. Emerson, F.: Available online at: <https://www.emerson.com/en-us/automation/fisher>. Accessed 21 Jan 2020
2. Mokveld. Axial flow valves by Mokveld. Available online at: <https://mokveld.com/en/home>. Accessed 21 Jan 2020
3. TALIS. ERHARD. [Электронный ресурс]. Режим доступа: <https://www.talis-group.com/brands/erhard.html>. Accessed 21 Jan 2020
4. Flowserve. Linear control valves. Available online at: <https://www.flowserve.com/en/products/valves/linear-control-valves>. Accessed 21 Jan 2020

5. Tang, T.F., Gao, L., Li B., Liao, L., Xi, Y., Yang, G.: Cavitation optimization of a throttle orifice plate based on three-dimensional genetic algorithm and topology optimization. *Structural and Multidisciplinary Optimization*. **60**(2), (2019). <https://doi.org/10.1007/s00158-019-02249-z>
6. Ellas, E., Chambre, P.L.: Bubble transport in flashing flow. *Int J. Multiphase Flow* **26**, 191–206 (2000)
7. Koch, S., Garen, W., Hegedűs, F., Neu, W., Reuter, R., Teubner, U.: Time-resolved measurements of shock induced cavitation bubbles in liquids. *Appl. Phys.* **108**, 345–351 (2012)
8. Seung, S., Kwak, H.Y.: Shock wave propagation in bubbly liquids at small gas volume fractions. *J. Mech. Sci. Technol.* **31**, 1223–1231 (2017). <https://doi.org/10.1007/s12206-017-0221-2>
9. Kapranova, A.B., Lebedev, A.E., Neklyudov, S.V., Melzer, A.M.: Engineering method for calculating of an axial valve separator with an external location of the locking part. *Front. Energy Res. Process Energy Syst.* **8**, 1–17 (2020). Article 32. <https://doi.org/10.3389/fenrg.2020.00032>
10. Lebedev, A.E., Kapranova, A.B., Melzer, A.M., Solopov, S.A., Voronin, DV, Neklyudov, V.S, Serov, E.M.: Utility Patent 2657371 Russian Federation (2018), IPC F16K 1/12. Direct-flow control valve. Publ. 06.13.2018, Bull. No. 17
11. Klimontovich, Y.L.: Turbulent motion and chaos structure: a new approach to the statistical theory of open systems, pp. 328. LENAND, Moscow, (2014)
12. Canjuga, S.: Utility Patent WO2019220153A2 (2019), IPC F16K 37/00, F16K 27/02. Axial valve of the modular concept of construction. Publ. 11.21.2019
13. Weevers, H.H.: Utility Patent US4327757 (2019) IPC F16K 47/14. Control Valve. Publ. **05**(04), 1982 (2019)
14. Kapranova, A.B., Lebedev, A.E., Melzer, A.M., Neklyudov, S.V.: About formation of elements of a cyber-physical system for efficient throttling of fluid in an axial valve. In: Kravets, A., Bolshakov, A., Shcherbakov, M. (eds.) *Cyber-Physical Systems: Advances in Design & Modelling. Studies in Systems, Decision and Control*, vol. 259, pp. 109–119. Springer, Cham (2020). https://doi.org/10.1007/978-3-030-32579-4_9
15. Kapranova, A., Lebedev, A., Melzer, A., Neklyudov, S.: Determination of the average parameters of cavitation bubbles in the flowing part of the control valves. *Int. J. Mech. Eng. Technol. (IJMET)* **9**(3), 25–31 (2018). Article ID: IJMET_09_03_003. Available online at <https://www.iaeme.com/IJMET/issues.asp?JType=IJMET&VType=9&IType=3>
16. Kapranova A., Neklyudov S., Lebedev A., Melzer A.: Investigation of the energy of the stochastic motion of cavitation bubbles in the separator of the axial valve, depending on the degree of its opening. *Int. J. Mech. Eng. Technol. (IJMET)* **9**(8), 160–166 (2018). Article ID: IJMET_09_08_017. Available online at <https://www.iaeme.com/ijmet/issues.asp?JType=IJMET&VType=9&IType=8>
17. Kapranova A., Neklyudov S., Lebedev A., Melzer A.: Qualitative evaluation of the coefficient of hydraulic resistance in the area of the divider of the fluid flow of the axial valve. *Int. J. Mech. Eng. Technol. (IJMET)* **9**(8), 153–159 (2018). Article ID: IJMET_09_08_016. Available online at <https://www.iaeme.com/ijmet/issues.asp?JType=IJMET&VType=9&IType=8>
18. Besant, W.H.: *Hydrostatics and hydrodynamics*. 185. Art. 158. Cambridge University Press, London (1916)
19. Baron Rayleigh, J.W.S.: *Scientific papers* **6** 1911–1919; Cambridge University Press, 1899–1920, reissued by the publisher, (2011) ISBN 978–0–511–70401–7
20. Plesset, M.S., Chapman, R.B.: Collapse of an initially spherical vapour cavity in the neighbourhood of a solid boundary. *J. Fluid Mech.* **47**(2), 125–141 (1971)
21. Volmer, V., Weber, A.: Keimbildung in uebersaetigen Daempfen. *Z. Phys. Chem.* **119**, 277–301 (1926)
22. Frenkel, Y.I.: *Kinetic theory of liquids*. 586 p. Nauka, Leningrad (1959)
23. Kedrinskii, V.K.: *Hydrodynamics of Explosion: Experiments and Models (Shock Wave and High Pressure Phenomena)*, Chap. 7, pp. 307–344. Springer, Berlin. (2005)
24. Petrov, N., Schmidt, A.: Effect of a bubble nucleation model on cavitating flow structure in rarefaction wave. *Shock Waves* **27**(4), 635–639 (2017). Springer. <https://doi.org/10.1007/s00193-016-0699-z>

25. Seung, S., Kwak, H.Y.: Shock wave propagation in bubbly liquids at small gas volume fractions. *J. Mech. Sci. Technol.* **31**, 1223–1231 (2017). <https://doi.org/10.1007/s12206-017-0221-2>.
26. Kapranova, A.B., Lebedev, A.E., Neklyudov, S.V., Melzer, A.M.: The ensemble-averaged characteristics of the bubble system during cavitation in the separator. In: *E3s Web of Conference*. 140, 06005. Published online December 18, 2019. (2019). <https://doi.org/10.1051/e3sconf/201914006005>.
27. Arzumanov, E.S.: *Hydraulic regulatory bodies of automated control systems*. 256 p. Engineering, Moscow (1985)

Analysis of Conjectural Variations in Nonlinear Stackelberg Duopoly Model for Cyber-Physical Systems in Telecommunications Markets



Mikhail Geraskin 

Abstract A duopoly model with a linear demand function and non-linear cost functions of agents is considered. We study a game with multi-level Stackelberg leadership. This game arises in the case of an oligopoly in the telecommunications market that connects consumers, services supply equipment, and management of the telecom operators, therefore, the market is related to cyber-physical systems. In this case, the decision-making mechanism of the management is based on the analysis of mutual assumptions of the operators about the possible strategies of competitors, taking into account the technical characteristics of the equipment. Conjectural variations (i.e., changes in the counterparty's actions assumed by the agent that optimize a utility function of the latter) are analyzed. Formulas for calculating the conjectural variations of agents are derived. Signs and boundaries of the variations for an arbitrary Stackelberg leadership level are investigated.

Keywords Duopoly · Stackelberg game · Power costs function · Multi-level leadership

1 Introduction

The solution to the firms' game in the duopoly market has the classical form of the Cournot-Nash equilibrium [1, 2], which is determined from the optimal agents' reactions system. However, due to the imperfection of the agent's awareness about the actions of the counterparty (i.e., environment), this equilibrium is not unique, because the optimal reaction of the agent depends on his assumption about the optimal reaction of the environment. Traditionally, these assumptions are described by a vector of conjectural variations [3]. In the case of the quantitative competition, the conjectural variation characterizes the agent's expected response to the counterparty's action (supply), which optimizes the utility function of the latter with the selected action of the former.

M. Geraskin (✉)

Samara National Research University, Moskovskoye shosse, 34, Samara 443086, Russia
e-mail: innovation@ssau.ru

If the counterparty ignores the agent in accordance with the Cournot model, then the agent becomes the Stackelberg leader [4]. In this case, the leader chooses the action taking into account the negative conjectural variation, i.e., he suggests that the counterparty's supply decreases relative to the leader's supply growth. As a result, the leader's supply volume increases, and the equilibrium aggregate volume increases. In addition, the game «struggle for leadership» [5] was investigated, when both agents choose actions taking into account the negative conjectural variations. In this case, both agents become the Stackelberg leaders, and their supply volumes increase. Consequently, in the equilibrium, the aggregate volume increases, and the price decreases.

Thus, the conjectural variation quantitatively expresses the mental reasoning of each agent about the environment's assumption: the assumption about the constancy of the agent's actions, the assumption about the best response of the agent to the environment's actions, the assumption about the agent's best response to the environment's best response, etc. As a result, this sequence of assumptions leads to multilevel Stackelberg leadership. In particular, if the counterparty assumes that the agent's actions are unchanged, the counterparty becomes the first level leader, if he assumes the best response from the agent, then the second level leader, etc. In the linear duopoly model, the classical results [4, 5] lead to the negative conjectural variation. Then the following question arises: does this uniqueness exist in a nonlinear model? To answer this question, our chapter develops a general method for calculating the conjectural variations.

In the linear oligopoly model [6–12], the inverse demand function and the agents' cost functions are linear, therefore, the calculation of the conjectural variations is not difficult. In the nonlinear model [13, 14], the inverse demand function is linear, and the agents' cost functions are nonlinear. In this model, in the analytical form, the conjectural variations were obtained only in the games with the first level Stackelberg leader (leaders) [15]. In the case of higher levels of leadership, the conjectural variations were determined implicitly from the system of nonlinear equations. The problem of multi-level leadership is relevant in the analysis of the reflexive games [16], in which various agents' assumptions lead to the differentiation of the game results.

In practice, the conjectural variations are applied in the study of equilibria in the telecommunications markets. On the one hand, these markets are classified as oligopolies [10, 15]. On the other hand, the service providers in these markets form networks that consist of the radar equipment and the administrative staff (i.e., management). Consequently, these man-machine networks belong to the cyber-physical systems [17, 18]. In this case, we investigate the cyber-physical system in terms of the influence of the mental management processes on such technical characteristics as the data transfer volumes.

We consider the problem of calculating the conjectural variations in an analytical form for an arbitrary Stackelberg leadership level, which enables us to study the influence of the leadership level on the players' behavior.

2 Formulation of Problem

In the cyber-physical system of the telecommunications market, in the case of the duopoly, the nonlinear model of choosing the optimal agent’s action has the following form:

$$\begin{aligned}
 Q_i^* &= \arg \max_{Q_i \geq 0} \prod_i (Q, Q_i) \\
 &= \arg \max_{Q_i \geq 0} \left\{ (a - bQ)Q_i - C_{Fi} - B_i Q_i^{\beta_i} \right\}, \quad i = 1, 2, \quad Q = Q_1 + Q_2, \quad (1)
 \end{aligned}$$

where Q_i, \prod_i are the action (the data transfer volume) and utility function (profit) of the agent i ; Q is the aggregate market volume of the data transfer; $C_{Fi} > 0, B_i > 0, \beta_i \in (0, 2)$ are the coefficients of the cost function of the type $C_i(Q_i) = C_{Fi} + B_i Q_i^{\beta_i}$, C_{Fi} is the fixed cost; $a > 0, b > 0$ are the coefficients of the inverse demand function; the symbol “*” indicates the optimal values. In the general case, the agents’ cost functions may be either concave at $0 < \beta_i < 1$, or convex at $1 < \beta_i < 2$. The first case corresponds to the positive effect of a return to scale, and it is observed at the stage of the firm appearance, the second case characterizes the negative effect of a return to scale, and it arises in great firms [19].

The Nash equilibrium in the model (1) is determined from the necessary extremum conditions of the following form

$$\frac{\partial \prod_i (Q_i, x_{ij})}{\partial Q_i} = 0, \quad i = 1, 2, \quad (2)$$

where $x_{ij} = Q'_{jQ_i}$ is the conjectural variation in the reaction equation of the agent i , i.e., the assumed change in the supply of the agent j in response to a unit increment in the supply of the agent i .

The Stackelberg leadership level of the agent is determined as follows. A zero level corresponds to the follower agent i , and it occurs if in the equation i of the system (2) $x_{ij(0)} = 0$, where the lower index in brackets indicates the leadership level r . The first leadership level of the agent i arises if in the equation i of the system (2) the variation $x_{ij(1)}$ is calculated by differentiation of another Eq. (2) with respect to Q_j , and in this equation $x_{ij(0)} = 0$. An arbitrary leadership level r of the agent i occurs if in the equation i of the system (2) the variation $x_{ij(r)}$ is calculated by differentiation of another Eq. (2) with respect to Q_j , and in this equation $x_{ij} = x_{ij(r-1)}$.

For model (1) of the actions’ choice of the agent i at the leadership level r , the solutions of system (2) satisfy the following equations [15]:

$$F_{i(r)} = a - bQ - bQ_i(1 + x_{ij(r)}) - B_i \beta_i Q_i^{\beta_i - 1} = 0, \quad Q_i > 0, \quad i = 1, 2, \quad (3)$$

subject to

$$g_{i(r)} = u_i - x_{ij(r)} < 0, i = 1, 2, \tag{4}$$

taking into account the following notation

$$u_i = -2 - \frac{B_i \beta_i (\beta_i - 1) Q_i^{\beta_i - 2}}{b} < 0, i = 1, 2 \tag{4a}$$

where $g_{i(r)}(\cdot)$ is a continuous and differentiable function, which characterizes the fulfillment of a sufficient maximum condition (i.e., unimodality condition) of function (1) of the agent i ; $u_i(\cdot)$ is function characterizing the influence of the nonlinearity of the cost function on the unimodality of the utility function of the agent i (when $u_i = -2$, system (3) is linear); $F_{i(r)}(\cdot)$ is a continuous and differentiable function.

In comparison to the linear model, in which condition (4) has the form $g_{i(r)} = -2 - x_{ij(r)} < 0$, in the nonlinear model (1) the utility function of the agent may not be unimodal due to the following reasons: (i) the influence of environmental actions, i.e. situations when $x_{ij(r)} < -2$; (ii) a result of the positive effect of a return to scale of the agent’s cost function. Therefore, we introduce the assumption that the rate of the marginal costs reduction with an increase in return to scale (i.e., $\beta_i < 1$) is less than the rate of decline in the price with an increase in the supply:

$$|MC'_{iQ_i}| = B_i \beta_i |\beta_i - 1| Q_i^{\beta_i - 2} < b \forall \beta_i < 1, \tag{5}$$

where $MC_i = C'_{iQ_i} = B_i \beta_i Q_i^{\beta_i - 1}$ are the marginal costs of the agent i . Assumption (5) guarantees the fulfillment of condition (4) if the condition $|x_{ij(r)}| < 1$ is satisfied, because under this assumption:

$$u_j < 0, |u_j| \geq 1 \forall \beta_j \in (0, 2). \tag{5a}$$

In the general case, if $|x_{ij(r)}| < |u_i|$, then condition (4) is satisfied.

We consider the problem of searching for the conjectural variation $x_{ij(r)}$ of the agent i in analytical form for an arbitrary value of r .

3 Analysis Results

The method of calculating the conjectural variations for different leadership levels is formulated in the form of the following assertion, and the proof is given in the Appendix.

Assertion. In the system of Eq. (3), which corresponds to the duopoly model (1) with a linear demand function and non-linear cost functions:

- (a) the conjectural variation in the equation of the agent i at the leadership level r is calculated by the following approximate formula:

$$\tilde{x}_{i(r)} = \frac{1}{u_j - x_{j(r-1)}}, x_{j(0)} = 0, i, j = 1, 2; \tag{6a}$$

- (b) the relative error $\delta x_{i(r)} = \frac{\Delta x_{i(r)}}{|x_{i(r)}|} = \frac{|x_{i(r)} - \tilde{x}_{i(r)}|}{|x_{i(r)}|}$ in the calculation of the conjectural variations according to formula (6a) for $r > 1$ in comparison with the exact value $x_{i(r)}$ is calculated by the following formula

$$\delta x_{i(r)} = \left| \frac{1 + \frac{\psi_{2(r-1)}}{\phi_{2(r-1)}} \tilde{x}_{1(r)}}{1 + \frac{1}{\phi_{2(r-1)}}} \right|, \text{ where, } \phi_{j(r-1)} = Q_j(x_{j(r-1)})'_{Q_i}, \tag{6b}$$

and, under conditions (i) $Q_i \geq \bar{Q}_i, i = 1, 2$ and (ii) $|x_{i(r)}| \leq X_{\max} \forall r > 1$, the relative error is limited to the following value

$$\delta x_{\max} = \left| \frac{1 + X_{\max}^2}{1 + \frac{1}{Q_{\max} \gamma}} \right|, \tag{6c}$$

where $Q_{\max} = \frac{a - \min_{i=1,2}(B_i \beta_i)}{b}$ if $\beta_i \geq 1$, or $Q_{\max} = \frac{a}{b}$ if $\beta_i < 1, \gamma = \frac{2\varepsilon}{Q}$,

$\bar{Q} = \max_{i=1,2} \bar{Q}_i, \bar{Q}_i = \left(\frac{B_i \beta_i |\beta_i - 1|}{\varepsilon b} \right)^{\frac{1}{2-\beta_i}}$; ε is a small positive number;

- (c) recurrence formula (6a) is equivalent to the following formula

$$\tilde{x}_{i(r)} = \frac{p(r)}{q(r)}, \tag{6d}$$

where τ is an ordinal number of a pair of natural numbers in the sequence (1,2), (3,4), (5,6), etc., which is calculated by the formula $\tau = \frac{f+2}{2}$ if $f < r \leq f + 2, f \in N$, N is a set of natural numbers, and $p(r) = \sum_{t=0}^{\tau-1} (-1)^t u_1^{r-\tau-t} u_2^{\tau-1-t} \frac{\prod_{\gamma=1}^t (r-\tau-\gamma+1)}{t!}$, $q(r) = \sum_{t=1}^{r-\tau+1} (-1)^{t+1} u_1^{r-\tau-t+1} u_2^{\tau-t+1} \frac{\prod_{\gamma=t-1}^{2-\gamma} (r-\gamma)}{(t-1)!}$.

Formula (6a) is intended to approximate the calculation of the conjectural variations in the reaction equations of agents at arbitrary leadership levels. The accuracy of the approximate calculation of the conjectural variations is determined by the formula (6b), and the accuracy estimation may be found by formula (6c). Formula (6d) gives an explicit form of the conjectural variations, and it is applicable for differentiation of the variations.

The values of a function (4a) affect the fulfillment of sufficient optimality conditions (4), and on the conjectural variations according to (6a). Function (4a) depends on the parameters of the agents' cost functions $B_i > 0, \beta_i \in (0, 2)$ and the parameter of the demand function b . An analysis [20] of the telecommunications companies of the Russian Federation showed that the coefficient $B_i \in (1, 3)$, if $Q_i \in (0, 500)$ billion min, parameter $b = 0.0009$ rubles/min, i.e., there is a relation $\sigma = \frac{B_i}{b} \approx 1000$. Therefore, we investigate the following two-parameter function

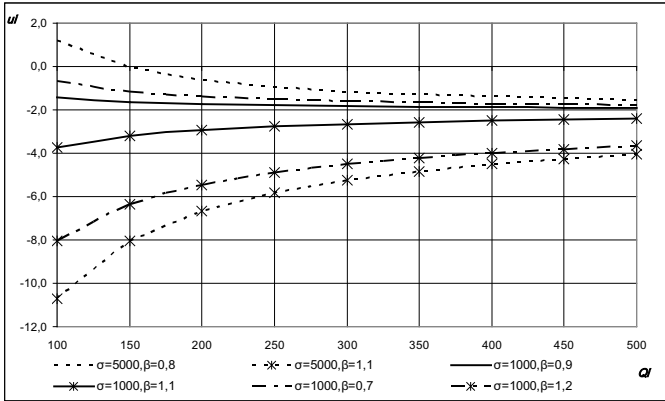


Fig. 1 Types of function $u_i(Q_i)$

$u_i(Q_i) = -2 - \sigma\beta_i(\beta_i - 1)Q_i^{\beta_i-2}$ in the range of $Q_i \in (100, 500)$ billion min at various values σ, β_i . An analysis of the graphs $u_i(Q_i)$ (Fig. 1) demonstrates that at great values of supply (i.e., $Q_i \geq 250$), and if the cost coefficients are close to the ratio $\sigma = 1000$, the function belongs to the range $-2,76 \leq u_i(Q_i) \leq -1,76$. In addition, in the case of the convex cost function (i.e., $\beta_i \geq 1$), the function $u_i(Q_i)$ to modulo is greater than 2, and in the case of the concave cost function (i.e., $\beta_i < 1$), the function $u_i(Q_i)$ to modulo is less than 2. With an increase in convexity, i.e. with the growth of β_i , and concavity, i.e. with a decrease in β_i , the module of $u_i(Q_i)$ grows. We study the conjectural variations with functions (6a) in the range of $-5 \leq u_i \leq -1$.

In the case of the convex cost function of the first agent and the linear cost function of the second agent (hereinafter, case (1), the dependencies of the conjectural variations on the leadership level are presented in Fig. 2. The analysis leads to the following conclusions. First, with an increase in the leadership level, the conjectural variations monotonically decrease, and they are limited in absolute value by a unity:

$$x_{i(r)} < 0 \wedge x'_{i(r)r} < 0 \wedge |x_{i(r)}| \leq 1, \text{ if } (u_1 < -2 \wedge u_2 = -2).$$

Second, the convexity of the agent cost function leads to an excess of the module of his conjectural variation in comparison with the module of the variation in the case of the linear cost function:

$$|x_{1(r)}| \geq |x_{2(r)}|, \text{ if } (u_1 < -2 \wedge u_2 = -2).$$

Third, in the case of the linear cost functions of both agents, the largest in absolute value conjectural variations are achieved in comparison with the non-linear costs:

$$|x_{i(r)}|_{u_i=-2} \geq |x_{i(r)}|_{u_i < -2}.$$

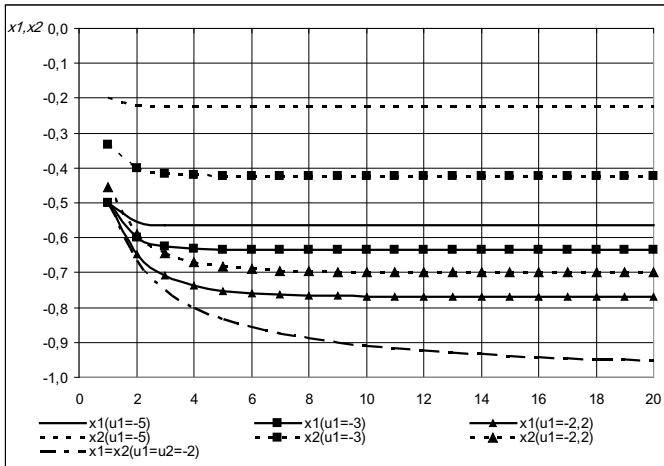


Fig. 2 Dependences of conjectural variations on leadership level with non-linear (convex) cost function of one agent in the case of $u_1 \leq -2, u_2 = -2$

Fourth, with a decrease in the convexity of the agent’s cost function (i.e., with a decrease in the module of u_1), the conjectural variations of both agents grow in absolute value:

$$|x_{i(r)}|_{\tilde{u}_i} \geq |x_{i(r)}|_{\tilde{u}_i}, \text{ if } |\tilde{u}_i| < |\tilde{u}_i|.$$

Hence, in the cyber-physical system of the telecommunications market, in the case of the convex or linear cost functions of the agents, despite an increase in the leadership level, a decrease in the data transfer volume remains the agent’s optimal response to an increase in the counterparty’s supply.

In the case of the concave cost function of the first agent and the linear cost function of the second agent (hereinafter, case 2), the dependencies of the conjectural variations on the leadership level are presented in Fig. 3. The situation is very different from the case of convexity. First, the conjectural variations are mostly negative, but it may be positive and are not limited in absolute value:

$$x_{i(r)} < 0 \vee x_{i(r)} > 0 \wedge |x_{i(r)}| < \infty, \text{ if } (u_1 > -2 \wedge u_2 = -2).$$

The positivity of the conjectural variation leads to the atypical behavior of the agent when the optimal agent’s response to an increase in the counterparty’s action is to increase its own effect. This reaction is paradoxical, because, as a result, the equilibrium price in the market is reduced. We discuss this paradox. This reaction is observed at the level (Fig. 3), which follows a series of levels when the conjectural variations of both agents are negative and very large in absolute value. As a result, the

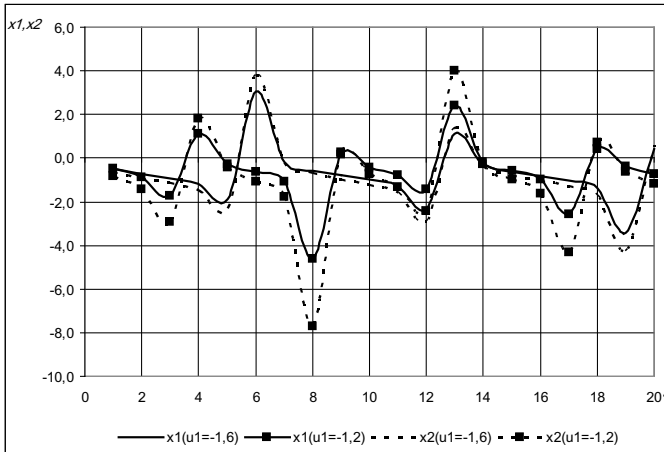


Fig. 3 Dependences of conjectural variations on leadership level with non-linear (concave) cost function of one agent in the case of $u_1 > -2, u_2 = -2$

equilibrium market volume increases excessively, and, as a consequence, the equilibrium price falls. A similar process was investigated by the classics in the «struggle for leadership» game [5]. Therefore, at the next level, the reverse process is optimal, for which the positive conjectural variations are necessary. As a result, the supply volumes decrease, and the equilibrium price rises. This process expresses market recovery (i.e., rebound), but a subsequent decrease in the conjectural variations shows that this rebound is not optimal.

Second, the trends of the conjectural variations $x_{1(r)}$ and $x_{2(r)}$ correlate, i.e., they increase and decrease mutually connected. Third, the amplitude of $x_{2(r)}$ exceeds the amplitude of $x_{1(r)}$, i.e., as in case 1, the following rule fulfills: with a decrease in the modulus of u_i , the conjectural variation of the agent i increases.

Consequently, in the cyber-physical system of the telecommunications market, in the case of the concave or linear cost functions of the agents, with an increase in the leadership level, the data transfer growth may be the agent’s optimal response to an increasing in the counterparty’s data supply.

In the case of concave or convex cost functions of agents (hereinafter, case 3), the dependencies of the conjectural variations on the leadership level are presented in Fig. 4. The situation is similar to cases 1 and 2. First, if the cost function of one agent is concave ($u_1 > -2$), and the cost function of another agent is convex ($u_2 < -2$), then the dynamics of the conjectural variations of both agents is similar to the case of the agent’s cost function concavity (case 2). Second, if the cost functions of both agents are concave ($u_1 > -2, u_2 > -2$), then the dynamics of the conjectural variations of both agents are similar to the previous case, but the period of oscillations is less, and the amplitude is greater. Third, if the cost functions of both agents are convex ($u_1 < -2, u_2 < -2$), then the dynamics of the conjectural variations of both agents is similar to case 1, i.e., these variations are monotonically decreasing, and they are

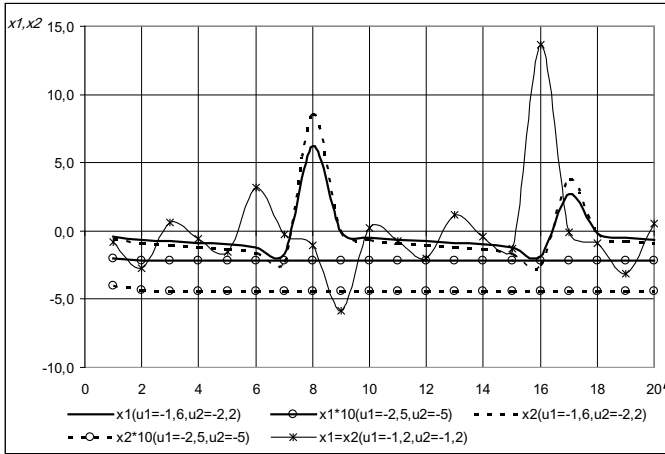


Fig. 4 Dependences of conjectural variations on leadership level for non-linear (convex and concave) cost functions of two agents

limited modulo unity, however, in contrast,

$$|x_{2(r)}| \geq |x_{1(r)}|, \text{ if } |u_2| > |u_1|.$$

4 Conclusion

The derived formula for the conjectural variation enables us to study the influence of the Stackelberg leadership level on the trends of these variations. Additionally, this formula allows us to analyze the influence of the convexity or concavity of the agents' cost functions on the dynamics of the conjectural variations in the process of an increase in the leadership level.

We investigate the agents' behavior in the cyber-physical system of the telecommunications market. The most important results of our analysis are as follows. The agents' behavior is significantly influenced by the technical characteristics of the cyber-physical system, which determine the type of the agent's cost function. The convex agents' cost functions, which are associated with a diminishing return on scale expansion, lead to stable downward dynamics of the conjectural variations with an increase in the leadership level. In the case of increasing returns to scale expansion, the concave agents' cost functions cause an abrupt change in these variations, which leads to the atypical positive reaction of the agent to an increase in the counterparty's action. We indicate the reason for this phenomenon. The increasing return to scale allows firms to dramatically increase the supply volumes that lead to lower prices and lower firms' profits. Then, this state encourages firms to contract the market.

Additionally, we show that such atypical reactions of both firms arise even if only one agent has the concave cost function.

Appendix

Proof of the assertion. Without loss of generality, we consider the first agent as the leader of the level r . To simplify the notation, we further designate: $x_{1(r)}$ is the conjectural variation of the first agent, $x_{2(r)}$ is the assumed variation of the second agent.

At the first leadership level ($r = 1$) of the first agent, the conjectural variation of the second agent is zero $x_{2(1)} = 0$, and Eq. (3) of the second agent has the form $F_{2(0)} = a - bQ - bQ_2 - B_2\beta_2 Q_2^{\beta_2-1} = 0$, therefore, the conjectural variation in the equation of the first agent, according to [21], is calculated by the formula $x_{1(1)} = -\frac{F'_{2(0)Q_1}}{F'_{2(0)Q_2}} = -\frac{-b}{-2b - B_2\beta_2(\beta_2-1)Q_2^{\beta_2-2}} = \frac{1}{u_2}$. By analogy, for $r = 1$, the conjectural variation in the equation of the second agent is equal to $x_{2(1)} = \frac{1}{u_1}$.

At the leadership level r , Eq. (3) of the second agent has the form $F_{2(r)} = a - bQ - bQ_2(1 + x_{2(r-1)}) - B_2\beta_2 Q_2^{\beta_2-1} = 0$. Therefore, the conjectural variation in the equation of the first agent is calculated by the following formula:

$$x_{1(r)} = -\frac{-b - bQ_2(x_{2(r-1)})'_{Q_1}}{-2b - B_2\beta_2(\beta_2 - 1)Q_2^{\beta_2-2} - b(Q_2x_{2(r-1)})'_{Q_2}}$$

$$= \frac{1 + Q_2(x_{2(r-1)})'_{Q_1}}{u_2 - x_{2(r-1)} - Q_2(x_{2(r-1)})'_{Q_2}}.$$

We denote $\phi_{2(r-1)} = Q_2(x_{2(r-1)})'_{Q_1}$, $\psi_{2(r-1)} = Q_2(x_{2(r-1)})'_{Q_2}$, then this variation may be written as follows:

$$x_{1(r)} = \frac{1 + \phi_{2(r-1)}}{u_2 - x_{2(r-1)} - \psi_{2(r-1)}}. \tag{A1}$$

If the values ϕ_2, ψ_2 are small, then an approximate recursive formula for calculating the conjectural variations of the agent i at the leadership level r has the following form:

$$\tilde{x}_{i(r)} = \frac{1}{u_j - x_{j(r-1)}}, x_{j(0)} = 0, i, j = 1, 2. \tag{A2}$$

The approximation error of formula (A2) is equal to:

$$\Delta x_{1(r)} = |x_{1(r)} - \tilde{x}_{1(r)}| = \left| \frac{\phi_{2(r-1)}(u_2 - x_{2(r-1)}) + \psi_{2(r-1)}}{(u_2 - x_{2(r-1)})(u_2 - x_{2(r-1)} - \psi_{2(r-1)})} \right|.$$

The relative approximation error of the formula (A2) is equal to:

$$\delta x_{1(r)} = \frac{\Delta x_{1(r)}}{|x_{1(r)}|} = \left| \frac{\phi_{2(r-1)}(u_2 - x_{2(r-1)}) + \psi_{2(r-1)}}{(u_2 - x_{2(r-1)})(1 + \phi_{2(r-1)})} \right| = \left| \frac{1 + \frac{\psi_{2(r-1)}}{\phi_{2(r-1)}} \tilde{x}_{1(r)}}{1 + \frac{1}{\phi_{2(r-1)}}} \right|. \quad (A3)$$

From formula (4a) it follows that $u'_{iQ_i} = \frac{(\beta_i - 2)(u_i + 2)}{Q_i}$. We introduce $Q_i \geq \bar{Q}_i$, where \bar{Q}_i is deduced from the condition $|u_i + 2| = \varepsilon$ and is equal to $\bar{Q}_i = \left(\frac{B_i \beta_i |\beta_i - 1|}{\varepsilon b}\right)^{\frac{1}{2 - \beta_i}}$, taking into account formula (4a), and ε is a small positive number. We denote $\bar{Q} = \max_{i=1,2} \bar{Q}_i$. Then $|u'_{iQ_i}| = \frac{(2 - \beta_i)|u_i + 2|}{Q_i} \leq \frac{2\varepsilon}{\bar{Q}} = \gamma$, where $\gamma = \frac{2\varepsilon}{\bar{Q}} < \varepsilon$.

We will perform the following conversion: $\frac{\phi_{2(r)}}{\psi_{2(r)}} = \frac{(x_{2(r)})'_{Q_1}}{(x_{2(r)})'_{Q_2}} = Q'_{2Q_1(r)} = x_{1(r)}$. We define an upper estimate for the modulus of the conjectural variation derivative. For simplicity, we assume that (i) the derivatives of these variations calculated by the exact formula (A1) and the approximate formula (A2) are equal; (ii) the difference in the derivatives of these variations at different levels may be neglected; (iii) the derivative of the first agent's variation opposite in sign to the derivative of another agent's variation:

$$(x_{i(r)})'_{Q_j} = (\tilde{x}_{i(r)})'_{Q_j}, \quad i, j = 1, 2,$$

$$\text{and } (\tilde{x}_{i(r)})'_{Q_j} = (\tilde{x}_{i(r-1)})'_{Q_j} = \chi_{ij}, \quad (\tilde{x}_{i(r)})'_{Q_j} = (\tilde{x}_{j(r-1)})'_{Q_j} \forall r > 0.$$

Then we calculate the derivative of the function (A2) as follows: $(\tilde{x}_{i(r)})'_{Q_j} = -\frac{u'_j Q_j - (\tilde{x}_{j(r-1)})'_{Q_j}}{(u_j - \tilde{x}_{j(r-1)})^2}$, and after a substitution $(\tilde{x}_{i(r)})'_{Q_j} = \chi_{ij}$, $(\tilde{x}_{j(r-1)})'_{Q_j} = -\chi_{ij}$, we deduce $\chi_{ij} = -\frac{u'_j Q_j}{(u_j - \tilde{x}_{j(r-1)})^2 + 1}$ from the equation $\chi_{ij} = -\frac{u'_j Q_j + \chi_{ij}}{(u_j - \tilde{x}_{j(r-1)})^2}$. Because, according to (5a), $|u_j| \geq 1$, and condition (4) requires that $|x_{ij(r)}| < |u_i|$ is satisfied, then the greatest absolute value χ_{ij} is achieved at $u_j = \tilde{x}_{j(r-1)}$, and it is equal to $\max |u'_j Q_j| = \gamma$. Therefore, the largest modulo value of $\phi_{i(r)}$ is equal to $Q_{\max} \gamma$. In this case, Q_{\max} is determined from the formula for the oligopoly market volume with an infinitely great number of firms [5]: $Q_{\max} = \frac{a - MC_{\min}}{b}$, where $MC_{\min} = \min_{i=1,2} MC_i$. In particular, taking into account the formula MC_i , $MC_{\min} = \min_{i=1,2} (B_i \beta_i)$, if $\beta_i \geq 1$ and $MC_{\min} = 0$, if $\beta_i < 1$. If the conjectural variations are limited in absolute value by X_{\max} , then the formula for the maximum error in the form (6c) follows from (A3).

We derive the analytical formula for the approximate calculation of the conjectural variations. Formula (A2) is a two-dimensional continued fraction [22] with

Table 1 Analysis of continued fractions $\tilde{x}_{1(r)}$

r	$p(r)$	$q(r)$
1	1	u_2
2	u_1	$u_1 u_2 - 1$
3	$u_1 u_2 - 1$	$u_1 u_2^2 - 2u_2$
4	$u_1^2 u_2 - 2u_1$	$u_1^2 u_2^3 - 3u_1 u_2 + 1$
5	$u_1^2 u_2^2 - 3u_1 u_2 + 1$	$u_1^2 u_2^3 - 4u_1 u_2^2 + 3u_2$
6	$u_1^3 u_2^2 - 4u_1^2 u_2 + 3u_1$	$u_1^3 u_2^3 - 5u_1^2 u_2^2 + 6u_1 u_1 - 1$
7	$u_1^3 u_2^3 - 5u_1^2 u_2^2 + 6u_1 u_2 - 1$	$u_1^3 u_2^4 - 6u_1^2 u_2^3 + 10u_1 u_2^2 - 4u_2$
8	$u_1^4 u_2^4 - 6u_1^3 u_2^3 + 10u_1^2 u_2 - 4u_1$	$u_1^4 u_2^4 - 7u_1^3 u_2^3 + 15u_1^2 u_2^2 - 10u_1 u_2 + 1$

a recursive record of the form: $\tilde{x}_{1(r)} = \frac{1}{u_2 - x_{2(r-1)}}$. One-dimensional continued fractions may be represented as a sequence of the convergent fractions $x_{1(r)} = \frac{p(r)}{q(r)}$, in which the numerator and denominator are calculated using the following recurrence formulas $p(r) = u_{(r)}p_{(r-1)} + p_{(r-2)}$, $q(r) = u_{(r)}q_{(r-1)} + q_{(r-2)}$ [23]. On the other hand, binomial coefficients are calculated as Stirling numbers of the first kind using the recurrence formula $S_{k(r+1)} = S_{k(r)} - rS_{k-1(r)}$ [21], where k is a serial number of Stirling numbers in the binomial expansion. Therefore, it can be assumed that a two-dimensional continued fraction may be represented by binomial decomposition. Indeed, the calculations of the numerator $p(r)$ and the denominator $q(r)$, of the fraction (A2), presented in Table 1, show the existence of a binomial regularity.

The analysis of the coefficients in the Table leads to the following formula $\tilde{x}_{1(r)} = \frac{p(r)}{q(r)}$, where $p(r) = u_1^{r-\tau} u_2^{\tau-1}$ for $r = 1, 2$, $q(r) = u_1^{r-\tau} u_2^\tau$ for $r = 1$,

$$p(r) = u_1^{r-\tau} u_2^{\tau-1} - (r - 2)u_1^{r-\tau-1} u_2^{\tau-2} \text{ for } r = 3, 4,$$

$$p(r) = u_1^{r-\tau} u_2^{\tau-1} - (r - 2)u_1^{r-\tau-1} u_2^{\tau-2} + \frac{1}{2}(r - 3)(r - 4)u_1^{r-\tau-2} u_2^{\tau-3}$$

for $r = 5, 6$ etc.,

$$q(r) = u_1^{r-\tau} u_2^\tau - (r - 1)u_1^{r-\tau-1} u_2^{\tau-1} \text{ for } r = 2, 3,$$

$$q(r) = u_1^{r-\tau} u_2^\tau - (r - 1)u_1^{r-\tau-1} u_2^{\tau-1} + \frac{1}{2}(r - 2)(r - 3)u_1^{r-\tau-2} u_2^{\tau-2}$$

for $r = 4, 5$ etc.

In general terms, these expressions are written in the form (6d).

References

1. Nash, J.: Non-cooperative Games. *Ann. Math.* **54**, 286–295 (1951)
2. Cournot, A.A.: *Researches into the Mathematical Principles of the Theory of Wealth*. Hafner, London (1960)
3. Bowley, A.L.: *The Mathematical Groundwork of Economics*. Oxford University Press, Oxford (1924)
4. Stackelberg, H.: *Market Structure and Equilibrium*, 1st edn. Translation into English, Springer, Bazar, Urch & Hill (2011)
5. Intriligator, M.D.: *Mathematical Optimization and Economic Theory*. Prentice-Hall, Englewood Cliff, New Jersey (1971)
6. Karmarkar, U.S., Rajaram, K.: Aggregate production planning for process industries under oligopolistic competition. *Eur. J. Oper. Res.* **223**(3), 680–689 (2012)
7. Ledvina, A., Sigar, R.: Oligopoly games under asymmetric costs and an application to energy production. *Math. Financ. Econ.* **6**(4), 261–293 (2012)
8. Currarini, S., Marini, M.A.: Sequential play and cartel stability in cournot oligopoly. *Appl. Mat. Sci.* **7**(1–4), 197–200 (2013)
9. Vasin, A.: Game-theoretic study of electricity market mechanisms. *Procedia Comput. Sci.* **31**, 124–132 (2014)
10. Sun, F., Liu, B., Hou, F., Gui, L., Chen, J.: Cournot equilibrium in the mobile virtual network operator oriented oligopoly offloading market. In: *IEEE International Conference of Communications, ICC*. No 7511340 (2016)
11. Naimzada, A.K., Sbragia, L.: Oligopoly games with nonlinear demand and cost functions: two boundedly rational adjustment processes. *Chaos, Solitons Fractals* **29**(3), 707–722 (2006)
12. Askar, S., Alnowibet, K.: Nonlinear oligopolistic game with isoelastic demand function: rationality and local monopolistic approximation. *Chaos, Solitons Fractals* **84**, 15–22 (2016)
13. Naimzada, A., Tramontana, F.: Two different routes to complex dynamics in an heterogeneous triopoly game. *J. Differ. Equ. Appl.* **21**(7), 553–563 (2015)
14. Cavalli, F., Naimzada, A., Tramontana, F.: Nonlinear dynamics and global analysis of a heterogeneous cournot duopoly with a local monopolistic approach versus a gradient rule with endogenous reactivity. *Commun. Nonlinear Sci. Numer. Simul.* **23**(1–3), 245–262 (2015)
15. Geraskin, M.I., Chkhartishvili, A.G.: Game-theoretic models of an oligopoly market with nonlinear agent cost functions. *Autom. Remote Control* **78**(9), 1631–1650 (2017)
16. Novikov, D.A., Chkhartishvili, A.G.: *Reflexion and Control: Mathematical Models*. CRC, London (2014)
17. Kravets, A.G., Bui, N.D., Al-Ashval, M.: Mobile security solution for enterprise network. *Commun. Comput. Inf. Sci.* **466**, 371–382 (2014)
18. Basinya, E., Rudkovskiy, A.: Automatic traffic control system for SOHO computer networks. *Stud. Syst. Decis. Control* **199**, 743–754 (2019)
19. Walters, A.A.: Production and cost functions: and econometric survey. *Econometrica* **31**(1), 23–44 (1963)
20. Geraskin, M.I.: Modeling reflexion in the non-linear model of the Stackelberg three-agent oligopoly for the Russian telecommunication market. *Autom. Remote Control* **79**(5), 841–859 (2018)
21. Korn, G., Korn, T.: *Mathematical Handbook for Scientists and Engineers: Definitions, Theorems, and Formulas for Reference and Review*. McGraw-Hill Book Company, N.-Y (1968)
22. Arnold, V.I.: Higher dimensional continued fractions. *Regul. Chaotic Dyn.* **3**(3), 10–17 (1998)
23. Jones, W.B., Thron, W.J.: *Continued Fractions: Analytic Theory and Applications*. Addison-Wesley, Reading, MA (1980)

Functional Model for the Formation of Individual Metal Control Programs of Boiler Equipment



V. D. Belov and E. R. Moshev

Abstract The study considers the flaws of the process of technical maintenance of boiler units of thermal power plants carried out with the use of non-specialized software and conducted as part of a set of engineering measures called an integrated logistics support. The results of the analysis of scientific and technical literature and regulatory and technical documentation governing the technical maintenance procedures of boiler units are presented. It is shown that it is possible to eliminate the flaws of the technical maintenance process by developing and applying a problem-oriented cyber-physical system. The goal and objectives of the study, necessary to automate the technical maintenance procedures of boiler units, including the intelligent decision-making procedures, are presented. A functional model is developed that formalizes the formation of individual metal control programs of boiler units as an organizational and technological process and describes the interconnections between the procedures of this process and the regulatory and technical requirements for its implementation.

Keywords Thermal power plants · Boiler unit · Cyber-physical system · Technical maintenance and repair system · Individual metal control program · SADT model · Functional model · Information model

1 Introduction

Nowadays, thermal power plants (TPPs) generate more than half of all thermal and electric energy of the Russian Federation. The main share of Russian TPPs is made up of steam turbine power plants, in which the potential energy of the steam is converted into kinetic energy of the spinning of the rotor of the turbine unit, and then

V. D. Belov (✉) · E. R. Moshev
Perm National Research Polytechnic University, Komsomolsky ave. 29, Perm 614990, Russia
e-mail: vladislav.belov.199@yandex.ru

E. R. Moshev
e-mail: erm@pstu.ru

© The Author(s), under exclusive license to Springer Nature Switzerland AG 2021
A. G. Kravets et al. (eds.), *Cyber-Physical Systems: Modelling and Intelligent Control*, Studies in Systems, Decision and Control 338,
https://doi.org/10.1007/978-3-030-66077-2_26

323

into electrical energy. One of the most important and critical types of engineering devices that ensure the operation of thermal power plants is boiler units (BU), the functional purpose of which is the generation of steam with high energy characteristics. Boiler units are operated at very large values of the technological parameters: the working temperature of the flue gases in the radiant zone is from 1700 to 1900 (°C); steam temperature up to 570 °C; steam pressure up to 15.0 MPa. The indicated operating conditions of boiler units place high demands on the quality of their technical maintenance TM, on which the reliability and economic efficiency of the entire TPP completely depend.

In industrial enterprises, the technical maintenance of the equipment is carried out in accordance with the requirements of the system of technical maintenance and equipment maintenance.

In accordance with the regulatory and technical documentation, technical maintenance of boiler units requires a large number of procedures, among which an important role is played by engineering and organizational and technological procedures. Currently, the implementation of these procedures is carried out with the use of software that does not require their automation, as well as information support for making necessary intelligent decisions. In addition, the performance of technical maintenance procedures is complicated by the state of technical documentation, which is presented at TPPs mainly in the form of paper or electronic, but not interactive documents. The above factors give rise to the following significant disadvantages of the technical maintenance process of boiler units:

- multiple duplications of search, input, and data processing operations;
- multiple creations of the same forms and schemes necessary to ensure the technical maintenance of the equipment;
- low speed of processing the results of instrumental diagnostics;
- the complexity of systematizing separate data;
- low speed and accuracy of engineering calculations;
- low speed of forming the technical documentation of technical maintenance;
- the complexity of information exchange between subjects of various stages in the lifecycle of boiler units;
- the complexity of performing intelligent procedures.

These flaws significantly increase the duration and labor-consuming of the technical maintenance process of boiler units. They also reduce the quality of the technical documentation, which negatively affects the efficiency and industrial safety of the performance of thermal power plants in general. The negative impact of the above flaws can be significantly reduced if we develop and implement a problem-oriented cyber-physical system (CPS) [1–4] that will allow automating the organizational and technological procedures of the technical maintenance of boiler units and the processing of their results, including those obtained by instrumental methods. The complexity of the development of CPS for this purpose lies in the fact that to date, the analysis of scientific and technical literature has not identified models [5–7],

algorithms [8–10], and software [11–15] that allow for the comprehensive automation of these procedures at the systemic level. The development of such models and algorithms is the ultimate purpose of the study.

To achieve the goal, the following objectives were formulated:

- to study the technical maintenance process of boiler units as an object of computerization;
- to develop a functional model formalizing metal control procedures of boiler units as an organizational and technological process;
- to develop models for the representation of knowledge about boiler units as a system of interconnected structural elements;
- to develop models for the representation of knowledge on procedures of assessing the technical condition of boiler units, including metal control procedures;
- to develop algorithms that automate the formation of metal control programs of boiler units with the use of the developed knowledge representation models.

This chapter presents the results of solving the first two problems.

2 Analysis of the Technical Maintenance Process of Boiler Units as an Object of Computerization

The study of the technical maintenance process of boiler units as an object of computerization was carried out on the basis of a thorough analysis of regulatory and technical documentation (RTD), scientific and technical literature, and the results of the staff survey of TPPs. As a result of the analysis, it was found that the following are the most important of all technical maintenance procedures of boiler units:

- analysis of the technological modes of performance of boiler units and the results of metal control of structural elements for the entire previous period of performance;
- strength calculations of equipment structural elements and steam pipelines;
- calculations of the residual life of elements in boiler units operating under creep flow and cyclic loading;
- continuous accounting of equipment operating time, temperature, and pressure of steam generated;
- the formation of individual metal control programs, metal control tasks, and reports on the results of metal control;
- formation and storage of passport-technical documentation.

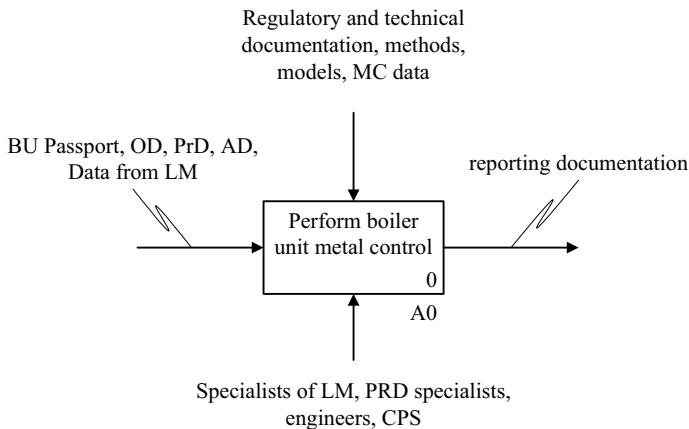
The analysis of the above procedures showed that many of them require the implementation of operations of search and processing of large amounts of information, as well as making intelligent decisions. In addition, they can be formalized with the use of models and algorithms of artificial intelligence theory [16, 17].

According to TPP specialists, one of the most time-consuming and intellectually complex procedures is the formation of individual control metal programs. A study of the subject area showed that this procedure can be formalized using the SADT model [18], an analog of which is known in the Russian Federation as a functional model (FM) [19–22].

3 Development of a Functional Model for Metal Control of Boiler Units

The context diagram of the upper level of the functional model of metal control is presented in Fig. 1, where the following documentation is used as the input information flow:

- boiler technical passport (BU Passport), which contains information on current operating parameters (pressure, the temperature in all subassemblies of the boiler unit), as well as data on repairs and results of previous BU diagnostics;
- operational documentation (OD), which includes a repair journal for each BU subassembly, shift protocol, schemes of various structures, a journal of thermal displacement of structural elements, repair schedules, forms;
- project documentation (PrD), which contains data on the main dimensions of the subassemblies, materials, calculated technological characteristics;
- assembly documentation (AD) containing data on welders, welding material, as well as schemes of welded joints;



Purpose: automation of the documentation formation of the boiler unit metal control

Viewpoint: planning and repair department

Fig. 1 Context diagram of the upper level of the functional model—block A0

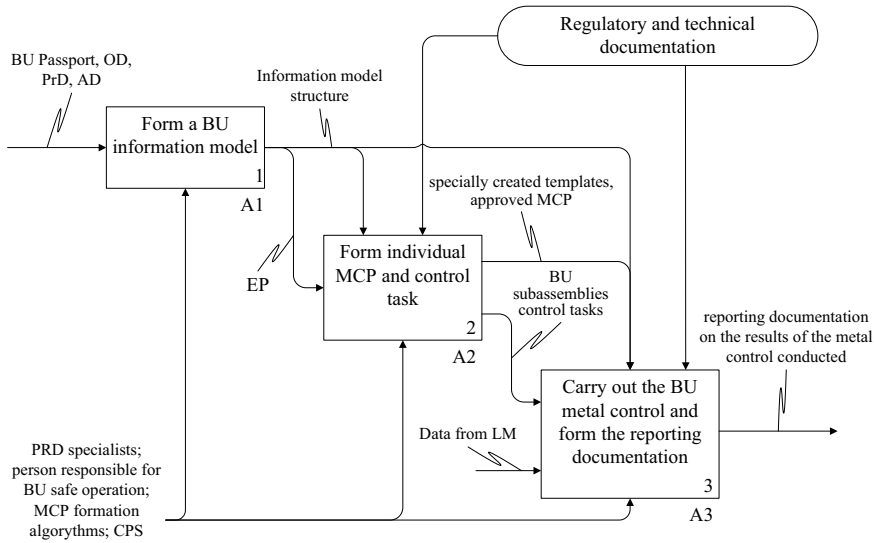


Fig. 2 Decomposition of block A0 of the functional model

- data from the laboratory of metals (LM) conducting metal controls. They contain basic information about the organization, specialists, and devices with which the metal control is carried out.

The output information flow is the reporting documentation on the results of the metal control conducted.

The decomposition of block A0 of the context diagram of the upper level of the FM is shown in Fig. 2 and includes three blocks (Fig. 2).

When performing the function given in block A1 with the use of the data contained in the input documentation, a primary model is created for representing knowledge about the structure and characteristics of structural elements, as well as about the parameters of the technological mode of BU performance (geometric dimensions; steel grades; various regulatory requirements; pressure; temperature and type of carried medium), hereinafter referred to as «BU information model».

In addition to the above characteristics and parameters, the information model contains special schemes of the structural subassemblies of the boiler unit, called forms. As a rule, at heat and power enterprises the forms of the following structural subassemblies of the boiler unit are formed: boiler drum; heating surfaces; superheaters; water economizer; feed pipeline within the boiler; main steam line within the boiler; recirculation pipelines; steam-circulating pipes.

When performing the function given in block A2, in accordance with the methods, guidance documents, and instructions, as well as using the BU information model, individual metal control programs (MCP) are formed. The formation of individual

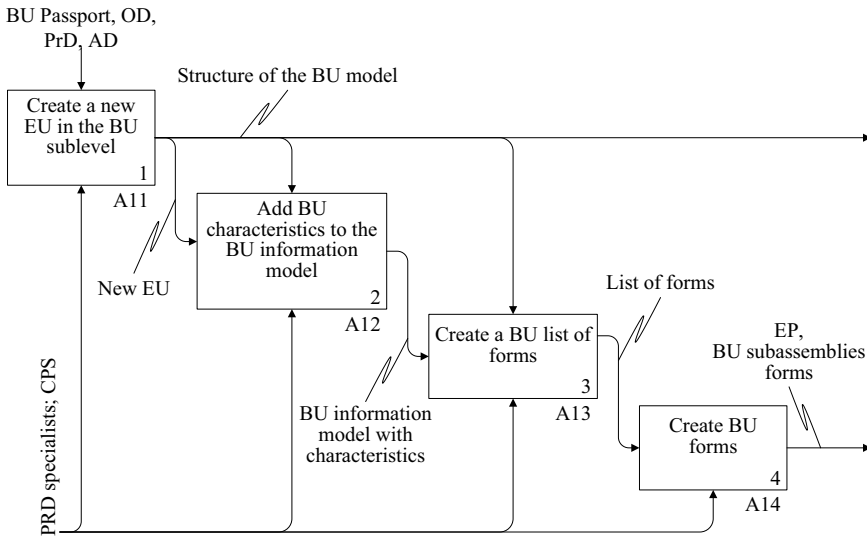


Fig. 3 Decomposition of block A1 of the functional model

MCPs is carried out on the basis of standard programs with the use of specially developed heuristic algorithms, knowledge representation models, and the BU information model created in block A1.

Block A3 completes the diagram, where the metal control of the BU subassemblies is carried out according to the approved task, putting the MC results in specially created templates and the formation of reporting documentation based on the results of the control.

The decomposition of block A1 (Fig. 2) of the functional model is shown in Fig. 3.

The input data for block A1 are the BU Passport, operational, project, and assembly documentation.

The output information flow is the electronic passport (EP) of the boiler unit, as well as the forms of the individual subassemblies of the boiler unit and the general structure of the model.

When performing the function in block A11 a specialist of the Planning and Repair Department (PRD) creates a new equipment unit (EU) within the hierarchical level «Equipment» in the BU sublevel. Functions A12, A13, and A14 describe the sequential introduction into the information model of the project, operational and assembly characteristics of the BU, as well as the formation of the list of forms and the creation of the forms themselves. During further work, a PRD specialist can add new forms to an existing model, as well as delete irrelevant forms.

Here, the input variables of block No. 1 are characteristics of the working medium (composition, temperature, pressure); technical data of the structural elements of the boiler unit (steel grade, typical size, characteristics of welded joints); BU passport data (date of an assemblage of elements, data on previous control); forms (simplified

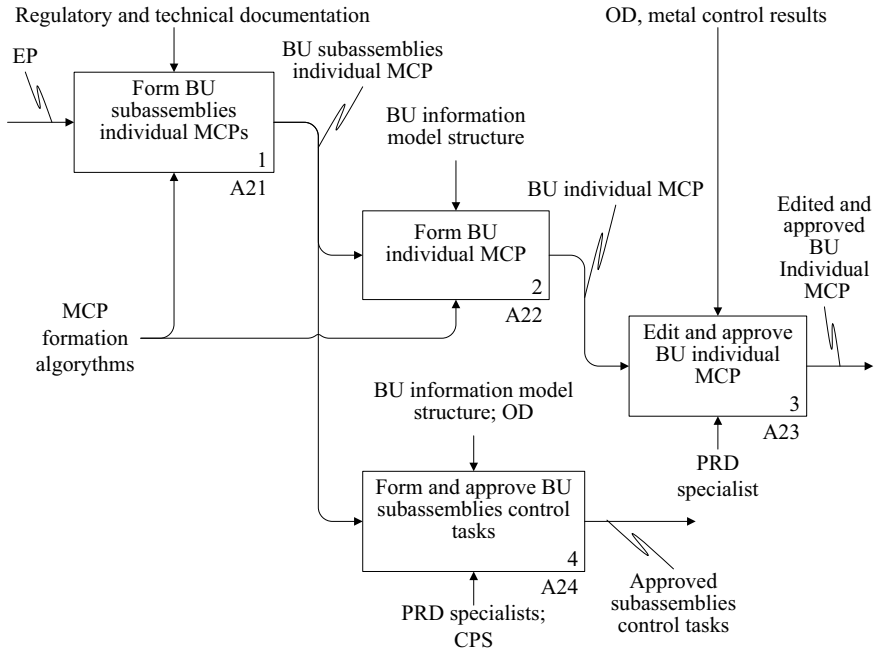


Fig. 4 Decomposition of block A2 of the functional model

graphic representation of the structural subassemblies of the boiler unit). All this data is stored in the database of the problem-oriented system (POS) after a PRD specialist has filled in all the attributes and rendered the forms, so the data is entered once and used at all subsequent stages of work.

The decomposition of block A2 (Fig. 2) is shown in Fig. 4 and describes the procedure for forming MC programs in a simplified form.

The output variables of block No. 1 are individual MC programs of subassemblies formed on the basis of standard programs indicated in the regulatory and technical documentation.

Input variables of block No. 2 are all input and output variables of block No. 1.

The output variable of block No. 2 is an individual MC program for all BU subassemblies.

For block No. 3, the input data is an individual metal control program of the boiler unit, and the output data is edited and approved MC program of the boiler.

When performing the function indicated in block No. 4, with the use of the product knowledge base (PNB) and problem-oriented system (POS), MC tasks of BU subassemblies are automatically generated—forms with a graphic image of specific control zones, as well as notes on the methods and scope of the metal control according to the generated individual MC programs. A PRD specialist edits if necessary and approves control tasks. The output data of block No. 4 are the tasks on the metal control of BU elements. The individual MC program formed in accordance

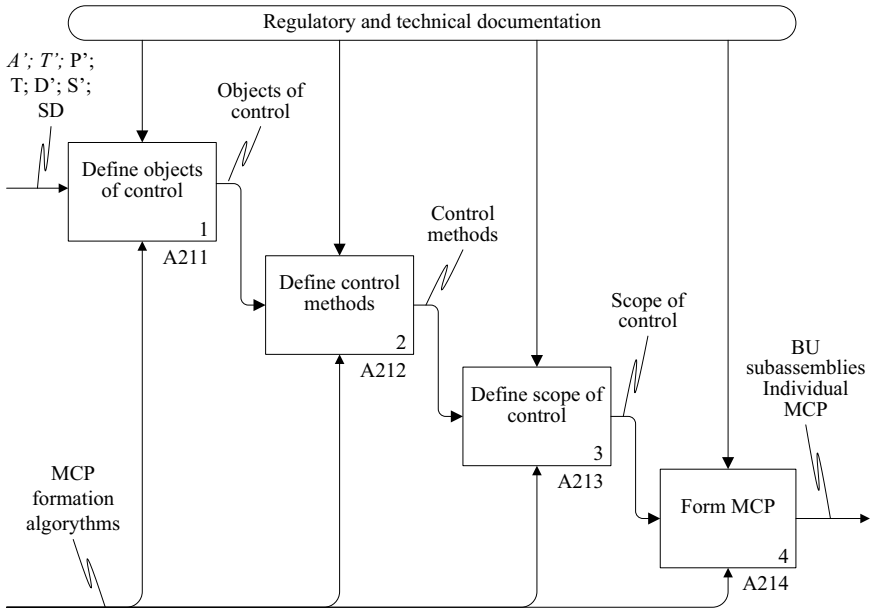


Fig. 5 Decomposition of block A21 of the functional model

with the described algorithm consists of tasks on the metal control of individual elements. The control task contains the methods and scope of control, as well as the number of sites that must be monitored.

Figure 5 shows the decomposition of block A21 (Fig. 4), where the procedure of the formation of individual MC programs for an individual BU subassembly is formalized.

Here, the input variables of block No. 1 are:

- technical characteristics of the structural elements of the boiler unit: type of the element (A'), diameter (D') and wall thickness (S') of the element, steel grade of the element (SD);
- operational characteristics of BU elements: hours of operation of an element (T'), working pressure (P'), and temperature (T).

The output variables of block No. 1 are the objects of control (structural elements, welded joints), which, in accordance with the regulatory and technical documentation, must be included in an individual metal control program.

The input variables of blocks Nos. 2, 3, and 4 are all input and output variables of the previous blocks.

The output variables of block No. 2 are object's control methods defined in accordance with the regulatory and technical documentation, and the output variables of block No. 3 are information about the scope of control for each control method.

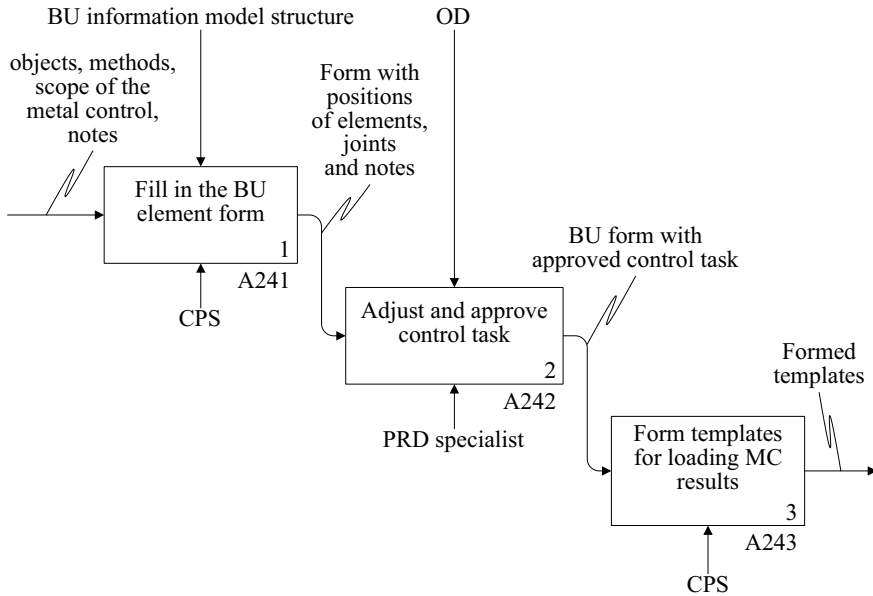


Fig. 6 Decomposition of block A24 of the functional model

The output parameter of block No. 4 is an individual MC program of the BU structural subassembly, which is a table with instructions on the methods and scope of control for each of the elements defined in block No. 1.

The decomposition of block A24 shown in Fig. 6 (Fig. 4) formalizes the procedure of the formation of tasks on the metal control for individual BU elements.

The input data for block No. 1 are the objects, methods, and the scope of the metal control—the output data of block A21.

As a result of the performed function given in block No. 1, the POS automatically generates a task for the metal control of an individual BU subassembly. The MC task is the form of the BU subassembly with marked positions of elements and joints, which should be monitored in accordance with the individual MC program, as well as notes on the methods and scope of control of elements.

The input data for block No. 2 is a form with positions of elements, joints, and notes. In block No. 2, a PRD specialist can adjust the positions of elements and joints, as well as notes on control methods and scope, on the basis of operational data.

The output data of block No. 2 is the MC task of individual BU subassemblies edited by a PRD specialist.

The input data of block No. 3 is the output data of block No. 2.

As a result of performing the function of block No. 3, the problem-oriented system automatically generates templates for loading MC results—interactive documents in Excel tables associated with the corresponding forms. Tables are formed on the basis of the approved MC tasks. After completing the metal control of a separate BU

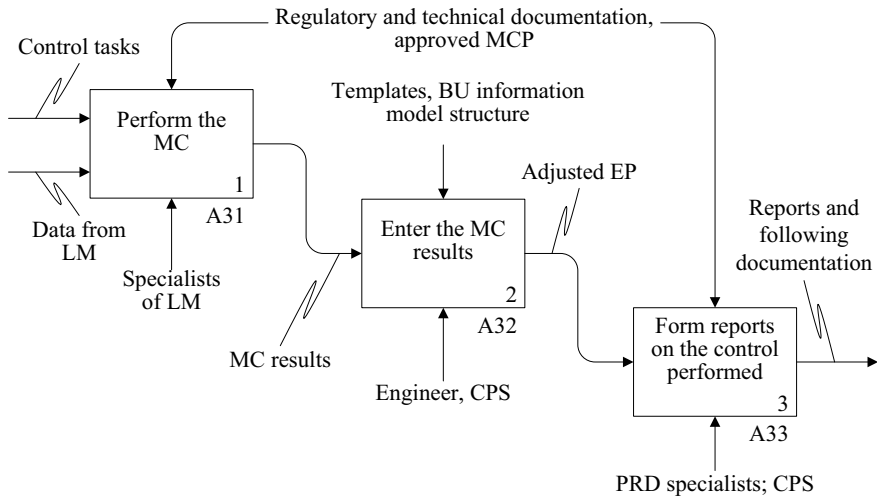


Fig. 7 Decomposition of block A3 of the functional model

subassembly, the results of this control are entered into the table, and the information is loaded into the database of the problem-oriented system.

The decomposition of block A3 shown in Fig. 7 (Fig. 4) formalizes the procedure of the automated formation of reporting documentation on the metal control.

The input data of block No. 1 are:

- the output data of block A24—approved MC tasks of individual BU subassemblies;
- data from the laboratory of metals: names of the specialists conducting the control, numbers, and characteristics of the devices used, dates of the MC execution.

The output information of block No. 1 is the result of metal control.

The input data of blocks No. 2 and 3 are the output data of the previous blocks.

When performing the function indicated in block No. 2, the engineer enters the MC results in the interactive templates for loading the results formed in block A243. The entered results are stored in the database of a problem-oriented system and are automatically entered in the EP of the equipment. Thus, the output information of block No. 2 is the adjusted EP of the boiler unit.

When performing the function specified in block No. 3, at the request of a PRD specialist, the following documents and reports on the control performed are automatically formed:

- conclusion on the control (separately for each type of metal control);
- protocols for individual types of MC;
- a list of all control results;
- a report on all measurements of the wall thickness of the elements.

To form the reports it is not necessary to enter additional information, as all data is already stored in the database of the problem-oriented system. Thus, the use of POS allows avoiding multiple data entry when generating reporting documentation on MC.

The presented information model describes the boiler unit as an element of the hierarchical structure of the enterprise and formalizes the knowledge about the boiler unit given in the project, passport and technological documentation. This model allows increasing the efficiency of the technical maintenance process of the boiler unit by automating the search, input, and output of information about the boiler unit, and compiling reporting documentation.

4 Conclusion

As a result of the analysis of scientific and technical literature, regulatory and technical, operational, and passport-technical documentation, as well as staff survey of TPPs, a functional model was developed for the formation of individual metal control programs of the boiler unit as an organizational and technological process. The developed FM is different in that it takes into account the systemic relationships between the operational and structural characteristics of the boiler unit on the one hand and the requirements of regulatory and technical documentation for monitoring these parameters on the other hand. This allows automating the procedure of forming individual control programs of the boiler unit as an organizational and technological process and creating a cyber-physical system for integrated logistics support of the boiler unit in thermal power plants.

References

1. Stepanov, M., Musatov, V., Egorov, I., Pchelintzeva, S., Stepanov, A.: Cyber-physical control system of hardware-software complex of anthropomorphous robot: architecture and models. In: Kravets, A., Bolshakov, A., Shcherbakov, M. (eds.) *Cyber-Physical Systems: Advances in Design and Modelling. Studies in Systems, Decision and Control*, vol. 259. Springer, Cham (2020)
2. Alekseev, A.P.: Conceptual approach to designing efficient cyber-physical systems in the presence of uncertainty. In: Kravets, A., Bolshakov, A., Shcherbakov, M. (eds.) *Cyber-Physical Systems: Advances in Design and Modelling. Studies in Systems, Decision and Control*, vol. 259. Springer, Cham (2020)
3. Moshev, E., Meshalkin, V., Romashkin, M.: Development of models and algorithms for intellectual support of life cycle of chemical production equipment. In: Kravets, A., Bolshakov, A., Shcherbakov, M. (eds.) *Cyber-Physical Systems: Advances in Design & Modelling. Studies in Systems, Decision and Control*, vol. 259. Springer, Cham (2020)
4. Buldakova T.I., Suyatinov S.I.: Assessment of the state of production system components for digital twins technology. In: Kravets, A., Bolshakov, A., Shcherbakov, M. (eds.) *Cyber-Physical Systems: Advances in Design and Modelling. Studies in Systems, Decision and Control*, vol. 259. Springer, Cham (2020)

5. Guo, F., Zou, F., Liu, J., Wang, Z.: Working mode in aircraft manufacturing based on digital coordination model. *Int. J. Adv. Manuf. Technol.* **98**, 1547–1571 (2018). <https://doi.org/10.1007/s00170-018-2048-0>
6. Kim, H., Han, S.: Interactive 3d building modeling method using panoramic image sequences and digital map. *Multimedia Tools Appl.* **77**(20), 27387–27404 (2018). <https://doi.org/10.1007/s11042-018-5926-4>
7. Moshev, E.R., Romashkin, M.A.: Development of a conceptual model of a piston compressor for automating the information support of dynamic equipment. *Chem. Petrol. Eng.* **49**(9–10), 679–685 (2014). <https://doi.org/10.1007/s10556-014-9818-9>
8. Meshnikov, V., Meshalkin, V., Obratsov, A.: Heuristic algorithms for 3D optimal chemical plant layout design. In: *Proceedings of 19th International Congress of Chemical and Process Engineering (CHISA-2010)*, vol. 4, pp. 1425. Prague (2010)
9. Lu, J., Zhu, Q., Wu, Q.: A novel data clustering algorithm using heuristic rules based on k-nearest neighbors' chain. *Eng. Appl. Artif. Intell.* **72**, 213–227 (2018)
10. Zakharova A., Savitskaya T., Egorov A.: Algorithm for calculating the reliability of chemical-engineering systems using the logical-and-probabilistic method in MATLAB. In: Kravets, A., Bolshakov, A., Shcherbakov, M. (eds.) *Cyber-Physical Systems: Advances in Design and Modelling. Studies in Systems, Decision and Control*, vol. 259. Springer, Cham (2020)
11. SAP Software and Solutions. <https://go.sap.com/index.html> (2015). Accessed 14 Apr 2020
12. Isogen@: Automatic piping isometrics from 3D plant design systems. https://www.alias.ltd.uk/ISOGEN_main.asp (2015). Accessed 21 Jan 2020
13. AVEVA: Software Solutions for the Plant Industries. <https://exchange.aveva.com/digital-interdisciplinary-engineering-and-design-for-sophisticated-power-generation-facilities> (2020). Accessed 15 May 2020
14. CEA Systems: Plant-4D-Plant Engineering Solution. <https://www.ceasystems.com/plant4d-asset-data-management-software-solution> (2014). Accessed 1 May 2020
15. iMaint.—CMMS Software—Service Management Software. <https://www.imaint.com/products/imaint/asset-management-software/> (2014). Accessed 5 Apr 2020
16. Wu, D., Olson, D.L., Dolgui, A.: Artificial intelligence in engineering risk analytics. *Eng. Appl. Artif. Intell.* **65**, 433–435 (2017)
17. Russell, S.J., Norvig, P.: *Artificial Intelligence: A Modern Approach*, 3rd edn. Prentice Hall, New Jersey (2010)
18. Protalinski, O.M.: *Application of Artificial Intelligence Techniques in the Automation of Technological Processes: Monograph*, 183 p. Publishing House of ASTU, Astrakhan (2004). (in Russian)
19. Sanchez-Marre, M., et al.: Intelligent environmental decision support systems. In: *Environmental Modelling, Software and Decision Support: State of the Art and Perspectives*, pp. 119–144. Elsevier, Amsterdam (2008)
20. Marca, D., C. McGowan, C.: *Structured Analysis and Design Technique*, p. 392. McGraw-Hill (1987)
21. Meshalkin, V.P., Moshev, E.R.: Modes of functioning of the automated system “pipeline” with integrated logistical support of pipelines and vessels of industrial enterprises. *J. Mach. Manuf. Reliab.* **44**(7), 580–592 (2015)
22. Moshev, E. R., Meshalkin, V. P.: Computer based logistics support system for the maintenance of chemical plant equipment. *Theor. Found. Chem. Eng.* **48**(6), 855–863 (2014)

Statistical Precision-Recall Curves for Object Detection Algorithms Performance Measurement



Anna A. Kuznetsova 

Abstract A statistical approach to the construction of Precision-Recall curves is proposed for analyzing the quality of algorithms for detecting objects in images. Statistical Precision-Recall curves, unlike traditional ones, are guaranteed to be monotonously non-increasing. At the same time, the statistical average accuracy of object detection algorithms on small test data sets turns out to be less than the traditional average accuracy. On relatively large test image sets, these differences are smoothed out.

Keywords Machine vision · Performance metrics · Precision · Recall · Precision-recall curve · Average precision

1 Introduction

The *Precision* and *Recall* metrics, proposed in 1955 in [1], have been used for many years to assess the performance of machine learning models (the term *Precision* itself was introduced later; in [1], this indicator was called *Relevance*). At the same time, in the models of classification, information retrieval, machine vision, etc., so-called *Precision-Recall* curves are often built, and the *Average Precision (AP)* of algorithms is calculated as the area under the *Precision-Recall* curve. This metric makes it possible to adequately compare the quality of models, including in the case of unbalanced classes, and has become a de facto standard, in particular, for comparing object detection algorithms.

Popular modern algorithms for object recognition in images are capable of recognizing objects from several classes. Thus, many contemporary two-stage and one-stage deep neural network models for object detection were trained on the COCO dataset [2] containing objects from 80 classes labeled in images. Benchmarking object detection algorithms on the COCO 2017 test dataset became the standard de facto.

A. A. Kuznetsova (✉)
Financial University Under the Government of the Russian Federation, Moscow, Russia
e-mail: AnAKuznetsova@fa.ru

Among two-stage object detectors, the C-Mask RCNN algorithm demonstrates $AP_{50} = 62.9\%$ on the COCO test dataset [3] The Grid R-CNN + shows $AP_{50} = 63.0\%$ [4], the DCN + R-CNN, SNIPER++, SNIP++, and TridentNet have $AP_{50} = 65.3\%$ [5], $AP_{50} = 67.0\%$ [6], $AP_{50} = 67.3\%$ [7], and $AP_{50} = 69.7\%$ [8] correspondingly.

Among one-stage object detectors, the ExtremeNet shows $AP_{50} = 55.5\%$ [9], the YOLOv3 demonstrates $AP_{50} = 57.9\%$ [10], the RetinaNet800 has $AP_{50} = 61.1\%$ [11], the CenterNet-HG and CenterNet511++ show $AP_{50} = 63.9\%$ [12] and $AP_{50} = 64.5\%$ [13] correspondingly. Finally, the most recent AB + FSAF, YOLOv4, YOLOv5, and EfficientDet-D7 algorithms demonstrate $AP_{50} = 65.2\%$ [14], $AP_{50} = 65.7\%$ [15], $AP_{50} = 67.4\%$ [16], and 72.4% [17] correspondingly.

At the same time, according to conceptual meaning, the *Precision-Recall* curve is non-increasing since a simultaneous increase in both *Precision* and *Recall* is impossible. However, in object detection tasks, *Precision-Recall* curves are almost always sawtooth, and researchers simply smooth them out using piecewise constant interpolation. This chapter proposes a statistical approach to the construction of *Precision-Recall* curves, in which these curves are guaranteed to be monotonously non-increasing.

2 Literature Review

In classification and information retrieval models, each object in ground-truth can belong to a positive or a negative class. At the same time, a machine learning system that predicts classes of objects can give correct predictions for some objects (calling positive objects positive, and negative ones negative). For other objects, it can make a type I error, calling negative objects positive, or a type II error, calling positive objects negative.

Thus, it is possible to construct a confusion matrix (Fig. 1), in which the following notation is used [18]:

- *TP* (True Positive)—the number of objects correctly classified by the machine learning system as positives;
- *TN* (True Negative)—the number of objects correctly classified by the machine learning system as negatives;
- *FP* (False Positive)—the number of type I errors, i.e., objects from the negative class, mistaken by the machine learning system for positives;

		Actual	
		Positive	Negative
Predicted	Positive	True Positive (<i>TP</i>)	False Positive (<i>FP</i>)
	Negative	False Negative (<i>FN</i>)	True Negative (<i>TN</i>)

Fig. 1 Confusion matrix

- *FN* (False Negative)—the number of type II errors, i.e., objects from the positive class, mistaken by the machine learning system for negatives.

Based on the confusion matrix, we can calculate:

$$Precision = \frac{TP}{TP + FP} \quad (1)$$

as the proportion of objects belonging to a positive class in ground-truth among all objects classified by a machine learning system as positives, and

$$Recall = \frac{TP}{TP + FN} \quad (2)$$

as the share of objects correctly classified by a machine learning system as positives among all objects, belonging to the positive class in ground-truth.

The importance of these indicators is determined by the fact that *Precision* characterizes the ability of the model not to make mistakes, giving a positive forecast, and *Recall*—the strength of the model not to miss positive objects.

As a rule, the classification system for each object gives the scored probability of assignment to the positive class, and it is possible to refer to the positive class those objects for which this probability is not less than the specified threshold.

By specifying different values for the threshold, we can change the relationship between *Precision* and *Recall*. As a result, by smoothly varying the threshold from one to zero, for each value of the cutoff threshold, we can calculate *Precision* and *Recall* and build a *Precision-Recall* curve.

At the same time, with an increase in the threshold, the machine becomes more “careful” so that it has fewer False Positives (which means that the *Precision* increases). At the same time, the number of objects called positive by the algorithm also becomes smaller (which leads to a *Recall* decrease).

The quality of an algorithm is considered good if *Precision* remains high with increasing *Recall*. In this case, when the threshold is changed, both the *Precision* and *Recall* will remain high.

In object detection problems, it is also possible to calculate *Precision* and *Recall* using (1, 2). In this case, *TP* is the number of objects in the image, the classes of which have been correctly detected by the algorithm, *FP* is the number of type I errors, that is, background objects in the image, erroneously assigned by the algorithm to one of the classes, and *FN* is the number of type II errors, i.e., objects not detected by the algorithm. Since there are infinitely many frames in the image that do not bound any object from the sought classes, the *TN* indicator is not analyzed in object detection tasks.

For each detection result, represented by the bounding box for the object detected, the IoU (Intersection over Union) metric is used—the percentage of overlapping of the detected bounding box according to the result of the algorithm, and the actual bounding box of the object. In Fig. 1, the blue bounding box is described around the ground-truth object, and the red bounding box is obtained as a result of applying the

algorithm. In this case,

$$IoU = \frac{\text{Area of Intersection}}{\text{Area of Union}}.$$

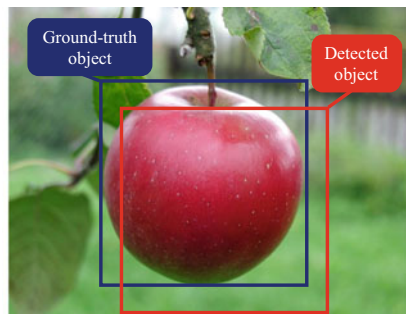
In addition to class probabilities, a confidence level is calculated for each recognized object (Fig. 2):

$$\text{Confidence} = \text{Class Probability} \cdot IoU.$$

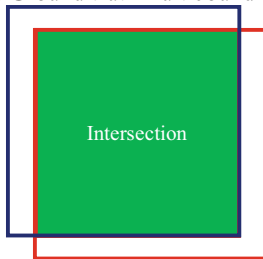
In object detection tasks, to build a *Precision-Recall* curve, the total number of objects in all images is first determined ($TP + FN$).

Then, all bounding boxes generated by the algorithm are sorted in descending order of confidence level. For each box, it is determined whether it bounds an object from the specified class (in this case $TP_i = 1, FP_i = 0$) or a background object ($TP_i = 0, FP_i = 1$). For each line k , the number of correctly detected objects is accumulated:

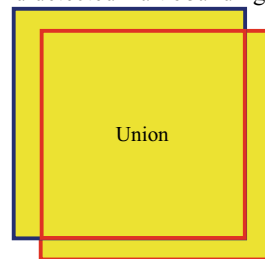
$$\text{Confidence} = \text{Class Probability} \cdot IoU.$$



(a) Ground truth fruit bounding box and detected fruit bounding box



(b) Intersection



(c) Union

Fig. 2 Intersection over Union for objects detection

$$Accumulated TP_k = \sum_{i=1}^k TP_i \tag{3}$$

and the total number of resulting objects:

$$Accumulated TP_k + Accumulated FP_k = \sum_{i=1}^k (TP_i + FP_i). \tag{4}$$

After that, we can calculate

$$Precision_k = \frac{Accumulated TP_k}{Accumulated TP_k + Accumulated FP_k} = \frac{\sum_{i=1}^k TP_i}{\sum_{i=1}^k (TP_i + FP_i)} \tag{5}$$

and

$$Recall_k = \frac{Accumulated TP_k}{TP + FN} = \frac{\sum_{i=1}^k TP_i}{TP + FN}. \tag{6}$$

Thus, the set of $(Recall_k; Precision_k)$ points defines the *Precision(Recall)* function whose graph forms the *Precision-Recall* curve. The area under this curve is called *Average Precision (AP)*.

Real *Precision-Recall* curves constructed in this way are almost always non-monotonous, and piecewise constant interpolation is used when calculating *AP*:

$$AP = \sum_k (Recall_{k+1} - Recall_k) Precision_{interpol.}(Recall_{k+1}),$$

where the interpolated *Precision* is defined as

$$Precision_{interpol.}(Recall_{k+1}) = \max_{r \geq Recall_{k+1}} Precision(r).$$

The nonmonotonicity of the *Precision-Recall* curves constructed in this way contradicts the meaning of the *Recall* and *Precision* metrics. The use of piecewise linear interpolation leads to an even more significant *AP* overestimation.

The main reason for the nonmonotonicity of traditional *Precision-Recall* curves is that the confidence level is used as a threshold. At the same time, in practical applications, it is not the confidence level itself that is important, but only its achievement of the minimum acceptable value. As a rule, in machine vision systems, an object is considered detected if its confidence exceeds 0.5 or 0.4.

3 Research Methodology

This chapter proposes an alternative approach to plotting *Precision-Recall* curves and calculating the average accuracy in object detection systems. This approach is based on calculating *Statistical Precision* and *Statistical Recall*.

As with the traditional *Precision-Recall* curve, the whole number of objects in all images is determined first ($TP + FN$). Further, in each image j , the number of correctly detected objects, the number of undetected objects, and the number of false alarms are determined:

$$\begin{aligned} \text{Integral } TP_j &= \sum_{l \in \text{Image}_j} TP_l, & \text{Integral } FN_j &= \sum_{l \in \text{Image}_j} FN_l, \\ \text{Integral } FP_j &= \sum_{l \in \text{Image}_j} FP_l. \end{aligned} \quad (7)$$

Then *Statistical Confidence* is calculated as the share of correctly detected objects in the image:

$$\text{Statistical Confidence}_j = \frac{\sum_{l \in \text{Image}_j} TP_l}{\sum_{l \in \text{Image}_j} TP_l + FN_l}. \quad (8)$$

After that, for each threshold level $t \in [0, 1]$, the total number of correctly recognized objects in all images is determined:

$$\text{Integral } TP^{(t)} = \sum_{j: \text{Statistical Confidence}_j > t} \text{Integral } TP_j, \quad (9)$$

the total number of background objects in all images mistakenly assigned by the algorithm to one of the classes:

$$\text{Integral } FP^{(t)} = \sum_{j: \text{Statistical Confidence}_j > t} \text{Integral } FP_j, \quad (10)$$

$$\text{Precision}^{(t)} = \frac{\text{Integral } TP^{(t)}}{\text{Integral } TP^{(t)} + \text{Integral } FP^{(t)}}, \quad (11)$$

and

$$\text{Recall}^{(t)} = \frac{\text{Integral } TP^{(t)}}{TP + FN}. \quad (12)$$

The resulting statistical *Precision-Recall* curve as a graph of the $\text{Precision}^{(t)}$ ($\text{Recall}^{(t)}$) function, in contrast to the traditional method, will be

monotonously non-increasing. We can calculate the area under this curve and consider this value as the Statistical Average Precision of object detection in images.

Let's consider a specific example. Our research group is developing an apple harvesting robot. Various apple detection methods based on the use of different modifications of the YOLO algorithm combined with pre- and post-processing procedures were sequentially tested in the machine vision system of this robot [19, 20].

As a test dataset, we use a set of 878 images with 5142 ripe apples, taken by employees of the VIM Federal Agroengineering Center in 2019 in an industrial apple orchard with different pixel resolutions, from different distances, and under different lighting conditions.

Figure 3 shows examples of such images. Apples that were correctly detected using the YOLOv3 algorithm with pre- and post-processing [19, 20] are framed by green bounding boxes (TP). Unrecognized apples are framed by red bounding boxes (FP).

Background objects mistaken by the algorithm for apples are framed by yellow bounding boxes (FN). Unique identifiers from A to Z6 are assigned to all bounding boxes. For each green and yellow bounding box, the confidence level is given. The results of detecting apples in these images are summarized in Table 1.

In Table 2, apple detection results are sorted in descending order of confidence level.

Further, in Table 2, *Accumulated TP_k* (3), *Accumulated FP_k* (4), *Precision_k* (5), and *Recall_k* (6) are calculated.

The blue line in Fig. 4 is a non-monotonous *Precision-Recall* curve constructed traditionally, and the red line is the result of its traditional piecewise linear interpolation.

Now let's move on to building the statistical *Precision-Recall* curve. The total number of ground-truth objects in all images $TP + FN = 28$.

Table 3 shows the number of correctly detected apples (*Integral TP_j*), the number of undetected apples (*Integral FN_j*), and the number of false positives (*Integral FP_j*) calculated by (7), as well as *Statistical Confidence_j* (8) for each image.

In Table 4, for each level $t \in [0, 1]$ of the threshold shows the calculations of the total number *Integral TP^(t)* of correctly recognized apples in all images (9), the total number *Integral FP^(t)* of background objects in all images, mistaken by the algorithm for apples (10), *Precision^(t)* (11) and *Recall^(t)* (12).

The green line in Fig. 5 represents the statistical *Precision-Recall* curve. For comparison, the traditional *Precision-Recall* curve (blue line) and its piecewise linear interpolation (red line) are also shown.

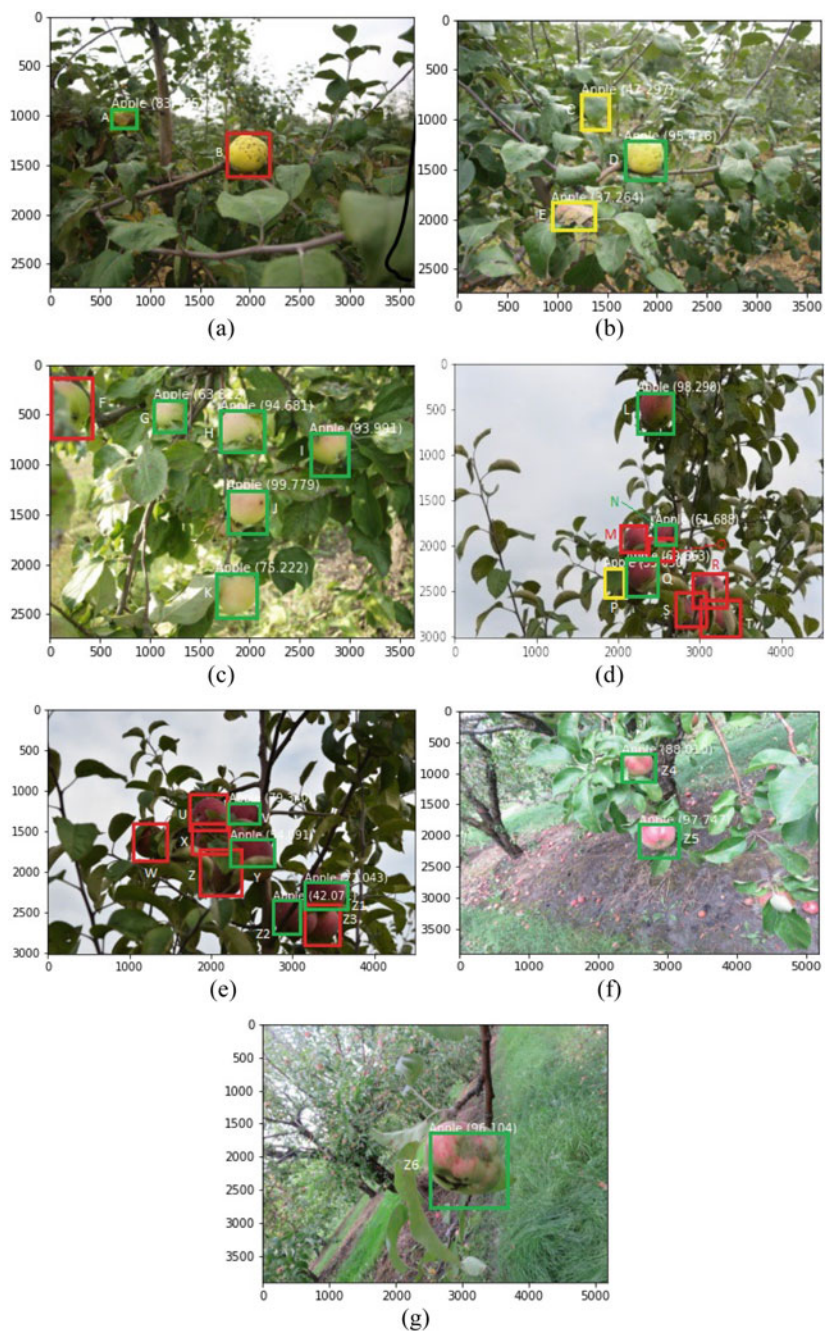


Fig. 3 Detecting apples in images

Table 1 Apple detections

Image	Object	Confidence	TP	FP	FN
a	A	83.47	1		
	B				1
b	C	47.29		1	
	D	95.42	1		
	E	37.26		1	
c	F				1
	G	63.82	1		
	H	94.68	1		
	I	93.99	1		
	J	99.78	1		
	K	75.22	1		
d	L	98.29	1		
	M				1
	N	61.69	1		
	O				1
	P	55.09		1	
	Q	69.63	1		
	R				1
	S				1
e	T				1
	U				1
	V	79.34	1		
	W				1
	X				1
	Y	54.09	1		
	Z				1
	Z1	52.04	1		
f	Z2	42.07	1		
	Z3				1
g	Z4	88.01	1		
	Z5	97.74	1		
	Z6	96.10	1		

Table 2 Traditional Precision-Recall curve construction

Image	Object	Confidence	TP	FP	FN	Acc.TP	Acc. FP	Precision	Recall
c	J	99.78	1			1	0	1.00000	0.03448
d	L	98.29	1			2	0	1.00000	0.06897
f	Z5	97.74	1			3	0	1.00000	0.10345
g	Z6	96.10	1			4	0	1.00000	0.13793
b	D	95.42	1			5	0	1.00000	0.17241
c	H	94.68	1			6	0	1.00000	0.20690
c	I	93.99	1			7	0	1.00000	0.24138
f	Z4	88.01	1			8	0	1.00000	0.27587
a	A	83.47	1			9	0	1.00000	0.31034
e	V	79.34	1			10	0	1.00000	0.34483
c	K	75.22	1			11	0	1.00000	0.37931
d	Q	69.63	1			12	0	1.00000	0.41379
c	G	63.82	1			13	0	1.00000	0.44828
d	N	61.69	1			14	0	1.00000	0.48276
d	P	55.09		1		14	1	0.93333	0.48276
e	Y	54.09	1			15	1	0.93750	0.51724
e	Z1	52.04	1			16	1	0.94118	0.55172
b	C	47.29		1		16	2	0.88889	0.55172
e	Z2	42.07	1			17	2	0.89474	0.58621
b	E	37.26		1		17	3	0.85000	0.58621
a	B				1	17	3	0.85000	0.58621
c	F				1	17	3	0.85000	0.58621
d	M				1	17	3	0.85000	0.58621
d	O				1	17	3	0.85000	0.58621
d	R				1	17	3	0.85000	0.58621
d	S				1	17	3	0.85000	0.58621
d	T				1	17	3	0.85000	0.58621
e	U				1	17	3	0.85000	0.58621
e	W				1	17	3	0.85000	0.58621
e	X				1	17	3	0.85000	0.58621
e	Z				1	17	3	0.85000	0.58621
e	Z3				1	17	3	0.85000	0.58621

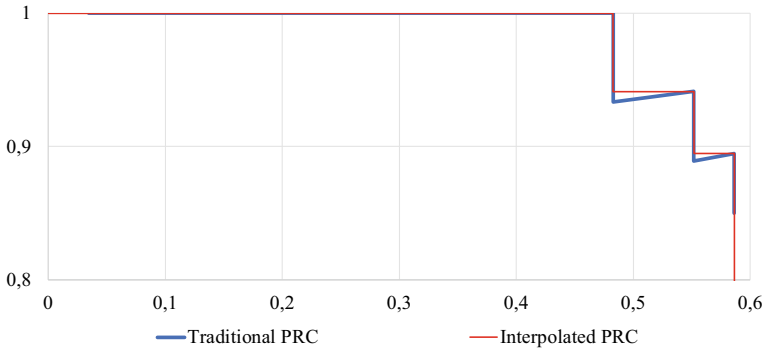


Fig. 4 Traditional precision-recall curve

Table 3 Statistical Confidence calculation

Image (<i>j</i>)	<i>Integral TP_j</i>	<i>Integral FN_j</i>	<i>Integral FP_j</i>	<i>Statistical Confidence_j</i>
a	0	1	1	0.00000
b	1	0	2	1.00000
c	5	1	0	0.83333
d	3	5	1	0.37500
e	4	5	0	0.44444
f	2	0	0	1.00000
g	1	0	0	1.00000

Table 4 Statistical Precision-Recall curve construction

<i>Threshold (t)</i>	<i>Integral TP^(t)</i>	<i>Integral FP^(t)</i>	<i>Precision^(t)</i>	<i>Recall^(t)</i>
0.000	16	11	0.59259	0.5714
...
0.370	16	11	0.59259	0.5714
...
0.375	13	6	0.68421	0.46429
...
0.440	13	6	0.68421	0.46429
0.445	9	1	0.90000	0.32143
...
0.830	9	1	0.90000	0.32143
0.835	4	0	1.00000	0.14286
...
0.995	4	0	1.00000	0.14286

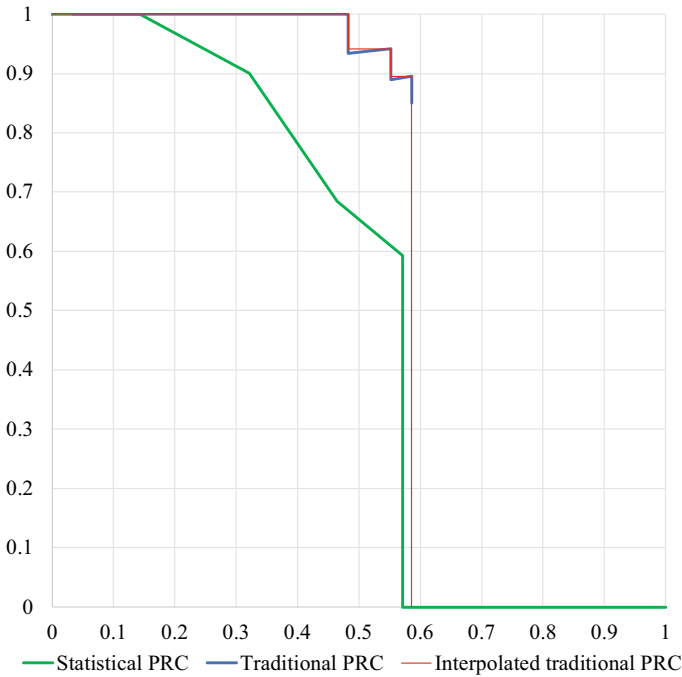


Fig. 5 Statistical and traditional precision-recall curves comparison

4 Results

Unlike traditional *Precision-Recall* curves, the statistical *Precision-Recall* curves proposed in this chapter are monotonously non-increasing. At the same time, *Statistical AP* of object detection algorithms calculated as the area under the statistical *Precision-Recall* curve always turns out to be less than *AP* calculated as the area under the traditional *Precision-Recall* curve.

It indicates that the proposed statistical approach assesses the performance of object detection models more realistically.

5 Discussion

In fact, although the proposed approach leads to a decrease in *AP* compared to the traditional approach, this decrease is not significant in algorithms' performance evaluation on relatively large test sets of images. For example, Fig. 6 shows statistical *Precision-Recall* curves for apple detection quality of the YOLOv3 algorithm combined with pre- and post-processing and the YOLOv5 without special pre- and post-processing on a full test dataset of 878 images with 5142 apples.

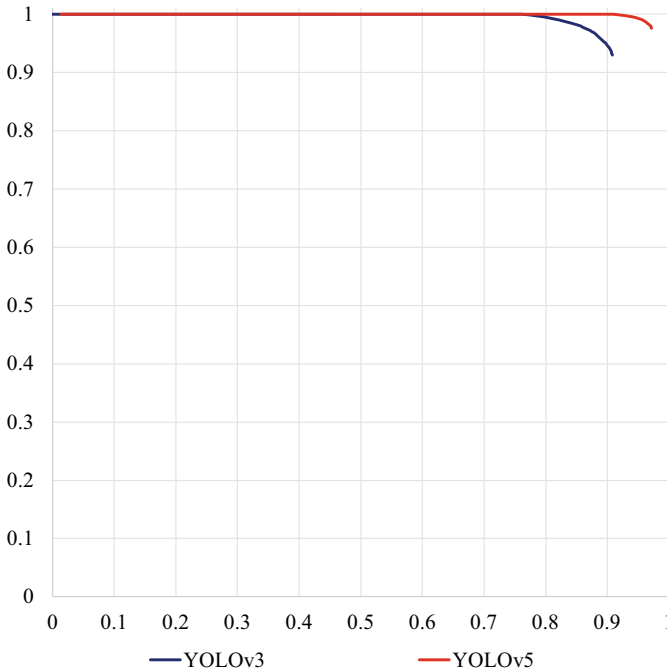


Fig. 6 Statistical precision-recall curves for apple detection using YOLOv3/YOLOv5

Both curves do not look pessimistic, although YOLOv5 has shown much better results than YOLOv3.

It seems that the proposed approach, based on the use of a statistical confidence level and guaranteeing the monotonicity of the *Precision-Recall* curves, is a good alternative to the traditional approach. However, for the widespread use of this approach in quality assessment of object detection algorithms, a more detailed study of the statistical *Precision-Recall* curves and the statistical *AP* is required.

Acknowledgements The reported study was supported by RFBR, research project 18-00-01103.

References

1. Kent, A., Berry, M.M., Luehrs Jr., F.U., Perry, J.W.: Machine literature searching VIII. Operational criteria for designing information retrieval systems. *Am. Doc.* **6**(2), 93–101 (1955). <https://doi.org/10.1002/asi.5090060209>
2. COCO: Common Objects in Context Dataset. <https://cocodataset.org/#overview> (2017). Accessed 10 July 2020
3. Chen, Z., Huang, S., Tao, D.: Context refinement for object detection. *Lect. Notes Comput. Sci.* **11212**, 74–89 (2018). https://doi.org/10.1007/978-3-030-01237-3_5

4. Lu, X., Li, B., Yue, Y., Li, Q., Yan, J.: Grid R-CNN plus: Faster and better. In: Proceedings of the IEEE Conference on Computer Vision and Pattern Recognition—CVPR 2019, pp. 7355–7364. Long Beach, CA, USA, 16–20 June 2019. <https://arxiv.org/abs/1906.05688>
5. Cheng, B., Wei, Y., Shi, H., Feris, R., Xiong, J., Huang, T.: Revisiting RCNN: on awakening the classification power of faster RCNN. *Lect. Notes Comput. Sci.* **11219**, 473–490 (2018). https://doi.org/10.1007/978-3-030-01267-0_28
6. Singh, B., M. Najibi, M., Davis, L.S.: SNIPER: Efficient multi-scale training. In: Proceedings of the 32nd Conference on Neural Information Processing Systems—NeurIPS 2018, pp. 1–11. Montréal, Canada, 2–8 December 2018. <https://arxiv.org/abs/1805.09300>
7. Singh, B., Davis, L.S.: An analysis of scale invariance in object detection—SNIP. In: Proceedings of the 31st IEEE Conference on Computer Vision and Pattern Recognition—CVPR 2018, pp. 3578–3587. Salt Lake City, UT, USA, 18–22 June 2018. <https://arxiv.org/abs/1711.08189>
8. Li, Y., Chen, Y., Wang, N., and Zhang, Z.: Scale-aware trident networks for object detection. In: Proceedings of the IEEE International Conference on Computer Vision—ICCV2019, pp. 6053–6062. Seoul, South Korea, 27 October—2 November 2019. <https://arxiv.org/abs/1901.01892>
9. Zhou, X., Zhuo, J., Krähenbühl, P.: Bottom-up object detection by grouping extreme and center points. In: Proceedings of the IEEE Conference on Computer Vision and Pattern Recognition—CVPR 2019, pp. 850–859. Long Beach, CA, USA, 16–20 June 2019. <https://arxiv.org/abs/1906.05688>
10. Redmon, J., Divvala, S., Girshick, R. Farhadi, A.: YOLOv3: an incremental improvement. In: Proceedings of the 31st IEEE Conference on Computer Vision and Pattern Recognition—CVPR 2018, pp. 1–6. Salt Lake City, UT, USA, 18–22 June 2018. <https://arxiv.org/abs/1804.02767>
11. Lin Ts.-Y., Goyal P., Girshick R., He, K., Dollar P.: Focal loss for dense object detection. In: Proceedings of the IEEE International Conference on Computer Vision—ICCV 2017, pp. 2980–2988. Venice, Italy, 22–29 October 2017. <https://arxiv.org/abs/1708.02002>
12. Zhou, X., Wang, D., Krähenbühl, P.: Objects as points. <https://arxiv.org/abs/1904.07850> (2019)
13. Duan, K., Bai, S., Xie, L., Qi, H., Huang, Q., Tian, Q.: CenterNet: keypoint triplets for object detection. In: Proceedings of the IEEE Conference on Computer Vision and Pattern Recognition—CVPR 2019, pp. 6569–6578. Long Beach, CA, USA, 16–20 June 2019. <https://arxiv.org/abs/1904.08189>
14. Zhu, Ch., He, Y., Savvides, M.: Feature selective anchor-free module for single-shot object detection. In: Proceedings of the IEEE Conference on Computer Vision and Pattern Recognition—CVPR 2019, pp. 840–849. Long Beach, CA, USA, 16–20 June 2019. <https://arxiv.org/abs/1903.00621>
15. Bochkovskiy, A., Wang, Ch.-Y., Liao, H.-Yu.M.: YOLOv4: optimal speed and accuracy of object detection. <https://arxiv.org/abs/2004.10934> (2020). Accessed 10 July 2020
16. Jocher, G., Nishimura, K., Mineeva, T., Vilariño, R.: YOLOv5. <https://github.com/ultralytics/yolov5> (2020). Accessed 10 July 2020
17. Tan, M., Pang, R., Le, Q.V.: EfficientDet: Scalable and efficient object detection. In: Proceedings of the IEEE Conference on Computer Vision and Pattern Recognition—CVPR 2020 pp. 10781–10790. Virtual, 14–19 June 2020. <https://arxiv.org/abs/1901.08043>
18. Fawcett, T.: An introduction to ROC analysis. *Pattern Recogn. Lett.* **27**(8), 861–874 (2006). <https://doi.org/10.1016/j.patrec.2005.10.010>
19. Kuznetsova, A., Maleva, T., Soloviev, V.: Using YOLOv3 algorithm with pre- and post-processing for apple detection in fruit-harvesting robot. *Agronomy* **10**(7), 1016 (2020). <https://doi.org/10.3390/agronomy10071016>
20. Kuznetsova, A., Maleva, T., Soloviev, V.: Detecting apples in orchards using YOLOv3. In: Gervasi, O., et al. (eds.) ICCSA 2020. LNCS, vol. 12249, pp. 923–934. Springer, Cham (2020). https://doi.org/10.1007/978-3-030-58799-4_66

YOLOv5 versus YOLOv3 for Apple Detection



Anna Kuznetsova , Tatiana Maleva , and Vladimir Soloviev 

Abstract The use of the YOLOv3 and YOLOv5 algorithms for apple detection in fruit-harvesting robots are compared. It is shown that the YOLOv5 algorithm could detect apples in orchards without additional pre- and post-processing with 97.8% Recall (fruit detection rate), and 3.5% False Positive Rate (FPR). It is much better than YOLOv3 that gives 90.8% Recall and 7.8 FPR when combined with special pre- and post-processing procedures, and then 9.1% Recall and 10.0% FPR without pre- and post-processing.

Keywords Computer vision · Fruit-harvesting robot · YOLOv3 · YOLOv5

1 Introduction

Over the past hundred years, several revolutions have taken place in agriculture. The two main ones related to the mechanization and use of chemical fertilizers have led to a significant increase in labor productivity. However, manual labor continues to be a vital cost component in agriculture [1, 2].

In horticulture, fruits are picked by hand; the share of manual labor in the total value of grown fruits is 40%. As a result of people's desire to move from rural areas to cities, it is becoming challenging to recruit seasonal workers for harvesting every year. At the same time, the crop shortage in horticulture reaches 40–50% [3].

A. Kuznetsova (✉) · T. Maleva · V. Soloviev
Financial University Under the Government of the Russian Federation, 38 Shcherbakovskaya,
Moscow 105187, Russia
e-mail: AnAKuznetsova@fa.ru

T. Maleva
e-mail: TVMaleva@fa.ru

V. Soloviev
e-mail: VSoloviev@fa.ru

The development of the use of intelligent robots for harvesting fruits can increase labor productivity significantly, reduce the share of heavy routine manual harvesting operations, and crop shortages [4, 5].

The development of prototypes of apple harvesting robots began back in the late 1960s. However, to this day, not a single prototype has entered the phase of practical use in agricultural enterprises. Prototypes of such robots cost hundreds of thousands of dollars, even though the speed of fruit-harvesting is deficient, and the share of unhandled fruits remains at a high level.

Recently, many new neural network-based models have been developed to recognize apples. However, the computer systems based on these models in the existing prototypes of harvesting robots work too slowly. These systems also take yellow leaves for apples, do not detect apples with a lot of overlapping leaves and branches, as well as darkened apples, green apples on a green background, etc.

Neural network algorithms of the YOLO family since 2016 demonstrate a high ability to detect various objects, including in real-time. The third version of the YOLO algorithm, YOLOv3 [6], which appeared in 2018, has already been used in several fruit-detection systems.

In March 2020, the EfficientDet—new fast and efficient neural network was published in open source [7], in April 2020, the open-source neural network YOLOv4 appeared [8], and in June 2020, the open-source YOLOv5 was released [9].

The research group of the Department of data analysis and machine learning of the Financial University under the Government of the Russian Federation and the Laboratory of machine technologies for cultivating perennial crops of the VIM Federal Scientific Agro-Engineering Center cooperate in an apple harvesting robot development.

The VIM Center develops the robot carriage and manipulators, while the Financial University is responsible for the apple detection and picking algorithms development.

We already used YOLOv3 in our machine vision system of the apple-picking robot [10, 11]. The results show that YOLOv3, with some special pre- and post-processing, gives a reasonable Fruit Detection Rate at 90.8% with 92.2% Precision, and at high speed.

In this chapter, we compare using YOLOv5 and YOLOv3 for apple detection in orchards.

The remainder of the chapter is structured as follows. The next section gives a review of related works on apple detection in orchards using intelligent algorithms. In Sect. 3, we present our methodology of using YOLOv3 and YOLOv5 for apple detection. The results are compared and discussed in Sect. 4.

2 Literature Review

2.1 Color-Based Fruit Detection Algorithms

Color is one of the main factors based on which the fruit can be detected in the image. Therefore, setting the color threshold makes it possible to determine for each pixel in the image, whether this pixel belongs to the fruit.

Clipping pixels by the color threshold was used to detect apples in [12–14].

The apparent advantage of fruit detection by color is the ease of implementation, but this method very poorly detects green and yellow-green apples. Also, bunches of red apples merge into one large apple.

2.2 Shape-Based Fruit Detection Algorithms

Apples, tomatoes, and other spherical fruits can be detected in images using algorithms based on the analysis of geometric shapes.

In [15–17], to detect fruits partially hidden by leaves or other fruits, various modifications of the Hough circular transformation were applied, in [18, 19], fruits were detected in images by identifying convex objects.

These systems are quite fast, but complex scenes, especially in uneven lighting, or when the fruits are overlapping by leaves or other fruits, as a rule, are not recognized effectively in such systems.

Many authors combined algorithms for analyzing color and geometric shapes of objects in images. As a rule, this led to an improvement in the recognition quality.

Analysis of geometric shapes for fruit detection has an advantage of its low dependence on the lighting level [17]. However, this method gives significant errors, since not only apples have a round shape, but also gaps between leaves, leaf silhouettes, spots, and shadows on apples.

2.3 Texture-Based Fruit Detection Algorithms

Fruits differ from the leaves and branches in texture, and these differences can be used to separate fruits from the background.

In [20], texture analysis, in combination with color analysis, was used to detect apples. In [21], apples were recognized in images using texture analysis in conjunction with geometric shapes analysis.

Fruits detection by texture only works in close-up images with good resolution and works very poorly in backlight. Texture-based fruit detection algorithms have too low speed and a too-high share of not-detected fruits. It leads to the inefficiency of such techniques in practical use.

2.4 Using Machine Learning for Fruit Detection

The first prototype of a fruit-picking robot that detects red apples against a background of green leaves using machine learning techniques was presented back in 1977 [22].

In [23], a linear classifier and KNN-classifier were used to detect apples and peaches. The authors of [24] used a linear classifier, and the authors of [25] used KNN-classifier was used to recognize apples. In [26], K-means clustering was used to detect apples.

All these early-stage machine learning techniques for fruit detection were tested on very limited datasets of several dozens of images, so the results cannot be generalized for practical use. For example, in [27], 92% apple detection accuracy was reported based on a test set of just 59 apples.

In 2012, the AlexNet deep convolutional neural network [28] was developed. Since then, machine vision and its use for detecting various objects in images, including fruits, received an impetus in development. In 2015, the VGG16 neural network was developed as an improved version of AlexNet [29].

In 2018, the authors of [30] built a robot for harvesting kiwi fruits with a machine vision system based on VGG16. In the field trials, 76% of kiwi fruits were detected.

In 2016, a new algorithm was proposed—YOLO (You Look Only Once) [31]. In this methodology, one neural network is applied to the whole image just once. The YOLO algorithm divides the entire image into regions and immediately determines the scope of objects and probabilities of classes for each object. In 2018, the third version of the YOLO algorithm was published as YOLOv3 [6].

The YOLOv3 algorithm is still one of the fastest, and it has already been used in robots for picking fruits. In [32, 33], modification of the YOLO algorithm was used to detect apples. The authors made the network tightly connected: each layer was connected to all subsequent layers, as the DenseNet approach suggests [34].

The authors of [35] compared the YOLOv3 and the DaSNet-v2 models for apple detection. They showed that DasNet-v2 performs slightly better.

In [36], the YOLOv3 was compared to the Faster-RCNN and the LedNet (the LedNet showed the best results).

In [10, 11], some special pre- and post-processing techniques were proposed to make a YOLOv3-based fruit detection system effective. As a result, combining the YOLOv3 with pre- and post-processing allowed to detect of 90.8% of apples in orchards while without this pre- and post-processing, the YOLOv3 was able to identify only 9.1% of apples.

Now the new version of the YOLO algorithm was released, the YOLOv5 [9]. In the next section, we will check how efficiently the YOLOv5 can detect apples in orchards, and compare the apple detection efficiency of the YOLOv3 and YOLOv5.

3 Research Methodology

3.1 Image Acquisition

As a test dataset, we use the same set of images, as in [10, 11]. This dataset consists of 878 images with 5142 ripe apples of different varieties, including red and green apples:

- 553 far-view images (4365 apples in total);
- 274 close-up images (533 apples in total).

The images were taken manually in the industrial plantation of the apple orchard in Zhilina, Oryol Region, Russia, during the 2019 harvesting season, by the VIM Center employees.

Images were taken Nikon D3500 AF-S 18–140 VR cameras equipped with Nikon Nikkor AF-P DX F 18–55 mm lenses.

Different pixel resolutions were used: 2528×4512 , 3008×4512 , 3888×5184 , and 4032×3024 . The images were collected during different weather conditions and under different lighting. Different distances for shooting were used from 0.2 to 2.0 m.

The ground-truth apples were labeled in the images manually by the authors.

3.2 Performance Measurement

To assess the algorithm performance, we use the traditional confusion matrix notation [37]:

- TP (True Positive)—the number of apples correctly detected by the algorithm;
- FP (False Positive)—the number of type I errors, i.e. background objects in the image, mistaken by the algorithm for apples;
- FN (False Negative)—the number of type II errors, i.e. not detected apples.
- Knowing TP , FP , and FN , we calculate
- $Recall_F = \frac{TP}{TP+FN}$ —the share of apples detected by the algorithm;
- $False\ Negative\ Rate = FNR = 1 - Recall = \frac{FN}{TP+FN}$ —the percentage of not detected apples, which affects the crop shortage;
- $Precision_F = \frac{TP}{TP+FP}$ —the share of ground-truth apples among all the objects that the algorithm called apples;
- $False\ Positive\ Rate = FPR = 1 - Precision = \frac{FP}{TP+FP}$ —the share of objects mistaken for fruits, which affects the harvesting speed;
- $F1 = \frac{2 \cdot Precision \times Recall}{Precision + Recall}$ —the harmonic mean of Precision and Recall.

3.3 Using YOLOv3 Without Pre- and Post-processing

In [10, 11], we used the standard YOLOv3 to detect apples in our test dataset. The results were not acceptable.

While Precision was at the 90.0% level, Recall was only 9.1%—the YOLOv3 was able to detect only 469 of 5142 apples. We also calculated $F1 = 16.5\%$, $FNR = 90.9\%$, and $FPR = 10.0\%$. False Negative Rate of 90.9% means that not less than 90.9% of apples will remain on trees (some detected apples could not be reachable by the robot, and some apples could be damaged during picking).

3.4 Using YOLOv3 with Pre- and Post-processing

To improve the apple detection efficiency, some image pre- and post-processing procedures were proposed in [10, 11].

First, we pre-processed images using adaptive histogram alignment, thickening of the borders, and slight blur. It led to the mitigation of such adverse effects as shadows, glare, minor damages of apples, and overlapping apples by thin branches.

Then, during pre-processing, we detected images with backlight by the prevailing average number of dark pixels and strongly lightened these images.

Images with spots on apples, perianth, as well as thin branches were improved during pre-processing by replacing pixels of brown shades with yellow pixels.

To detect apples in far-view canopy images, we divided such images into nine regions with the subsequent separate application of the algorithm to each region.

During post-processing, objects whose area of the circumscribed rectangle was less than the threshold were discarded—it helped not to take the gaps between the leaves for apples. Similarly, objects whose ratio of the larger side of the circumscribed rectangle to the smaller one was more than three were discarded—it made it possible not to mistake yellow leaves for apples.

In general, the YOLO-v3 algorithm, supplemented by the described pre- and post-processing procedures, detects both red and green apples quite accurately.

While Precision was equal to 92.2%, Recall has increased from 9.1 to 90.8%, and now 4671 of 5142 apples were detected in images.

We also calculated $F1 = 91.5\%$, $FNR = 9.2\%$, and $FPR = 7.8\%$.

3.5 Using YOLOv5 Without Pre- and Post-processing

Then we applied the standard YOLOv5 to detect apples in the test set of images. The results we obtained look extremely promising.

The standard YOLOv5, without any special pre- and post-processing, was able to detect 4998 of 5142 apples. The Recall was at the 97.2% level, Precision was equal to

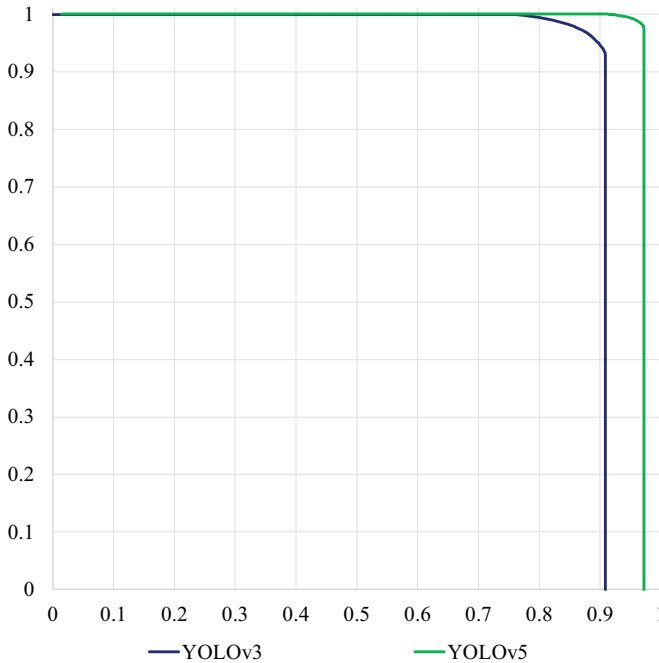


Fig. 1 Precision-Recall curves for YOLOv3 and YOLOv5

96.5%, and FI has increased to 96.9%. $FNR = 3.0\%$ means that the YOLOv5 is not able to detect only 3.0% of apples, $FPR = 3.5\%$ means that only 3.5% of detections are false.

In Fig. 1, the *Precision-Recall* curves are compared for the YOLOv3 with pre-and post-processing, and the YOLOv5. We can see that for the YOLOv5, Precision remains high as *Recall* increases up to 97.1%.

4 Results and Discussion

In Table 1, we compare the results of using the standard YOLOv5 without pre-and post-processing to the standard YOLOv3 without and with pre-and post-processing, and to other known fruit detection algorithms. We see that YOLOv5 performs much better than all the other algorithms.

The results show that the progress in deep convolutional network development leads to the inevitable introduction of robotic harvesting technology in horticulture in a very short time.

Table 1 Comparison to other models

Model	No. of images	Precision	Recall	F1	FNR	FPR
YOLOv3-Dense [32]	480	–	–	81.7%	–	–
DaSNet-v2 [35]	560	88.0%	86.8%	87.3%	12.0%	13.2%
YOLOv3 [35]	560	87.0%	85.2%	86.0%	13.0%	14.8%
YOLOv3 [36]	150	–	80.1%	80.3%	9.9%	–
Faster-RCNN [36]	150	–	81.4%	81.4%	8.6%	–
LedNet [36]	150	–	84.1%	84.9%	5.9%	–
YOLOv3 without pre- and post-processing [10]	878	90.0%	9.1%		90.9%	10.0%
YOLOv3 with pre- and post-processing [10]	878	92.2%	90.8%	91.5%	9.2%	7.8%
YOLOv5	878	96.5%	97.2%	96.9%	3.0%	3.5%

Acknowledgements The reported study was supported by RFBR, research project 18-00-01103.

References

1. Bechar, A., Vigneault, C.: Agricultural robots for field operations: concepts and components. *Biosyst. Eng.* **149**, 94–111 (2016). <https://doi.org/10.1016/j.biosystemseng.2016.06.014>
2. Sistler, F.E.: Robotics and intelligent machines in agriculture. *IEEE J. Robot. Autom.* **3**(1), 3–6 (1987). <https://doi.org/10.1109/JRA.1987.1087074>
3. Ceres, R., Pons, J., Jiménez, A., Martín, J., Calderón, L.: Design and implementation of an aided fruit-harvesting robot (Agribot). *Ind. Robot* **25**(5), 337–346 (1998). <https://doi.org/10.1108/01439919810232440>
4. Edan, Y., Han, S.F., Kondo, N.: Automation in agriculture. In: *Springer Handbook of Automation*, pp. 1095–1128. Springer, Berlin, Heidelberg (2009). https://doi.org/10.1007/978-3-540-78831-7_63
5. Grift, T., Zhang, Q., Kondo, N., Ting, K.C.: A review of automation and robotics for the bio-industry. *J. BioMechatron. Eng.* **1**(1), 37–54 (2008). <https://journal.tibm.org.tw/wp-content/uploads/2013/06/2.-automation-and-robotics-for-the-bio-industry.pdf>. Accessed 10 July 2020
6. Redmon, J., Divvala, S., Girshick, R., Farhadi, A.: YOLOv3: an incremental improvement. In: *Proceedings of the 31th IEEE Conference on Computer Vision and Pattern Recognition—CVPR 2018*, pp. 1–6. Salt Lake City, UT, USA, 18–22 June 2018. <https://arxiv.org/abs/1804.02767>
7. Tan, M., Pang, R., Le, Q.V.: EfficientDet: scalable and efficient object detection. In: *Proceedings of the IEEE Conference on Computer Vision and Pattern Recognition—CVPR 2020, Virtual*, pp. 10781–10790. 14–19 June 2020. <https://arxiv.org/abs/1901.08043>
8. Bochkovskiy, A., Wang, Ch.-Y., Liao, H.-Yu.M.: YOLOv4: optimal speed and accuracy of object detection (2020). <https://arxiv.org/abs/2004.10934>. Accessed 10 July 2020
9. Jocher, G., Nishimura, K., Mineeva, T., Vilariño, R.: YOLOv5 (2020). <https://github.com/ultralytics/yolov5>. Accessed 10 July 2020
10. Kuznetsova, A., Maleva, T., Soloviev, V.: Using YOLOv3 algorithm with pre- and post-processing for apple detection in fruit-harvesting robot. *Agronomy* **10**(7), 1016 (2020). <https://doi.org/10.3390/agronomy10071016>

11. Kuznetsova, A., Maleva, T., Soloviev, V.: Detecting apples in orchards using YOLOv3. In: Gervasi, O., et al. (eds.) ICCSA 2020. LNCS, vol. 12249, pp. 923–934. Springer, Cham (2020). https://doi.org/10.1007/978-3-030-58799-4_66
12. Mao, W.H., Ji, B.P., Zhan, J.C., Zhang, X.C., Hu, X.A.: Apple location method for the apple harvesting robot. In: Proceedings of the 2nd International Congress on Image and Signal Processing—CIPE 2009, pp. 17–19. Tianjin, China, 7–19 October 2009. <https://doi.org/10.1109/CISP.2009.5305224>
13. Bulanon, D.M., Kataoka, T.: A fruit detection system and an end effector for robotic harvesting of Fuji apples. *Agric. Eng. Int. CIGR J.* **12**(1), 203–210 (2010). <https://cigrjournal.org/index.php/Ejournal/article/view/1285/1319>. Accessed 10 July 2020
14. Wei, X., Jia, K., Lan, J., Li, Y., Zeng, Y., Wang, C.: Automatic method of fruit object extraction under complex agricultural background for vision system of fruit picking robot. *Optics* **125**(12), 5684–5689 (2014). <https://doi.org/10.1016/j.ijleo.2014.07.001>
15. Whittaker, A.D., Miles, G.E., Mitchell, O.R.: Fruit location in a partially occluded image. *Trans. Am. Soc. Agric. Eng.* **30**(3), 591–596 (1987). <https://doi.org/10.13031/2013.30444>
16. Xie, Z.Y., Zhang, T.Z., Zhao, J.Y.: Ripened strawberry recognition based on Hough transform. *Trans. Chin. Soc. Agric. Mach.* **38**(3), 106–109 (2007)
17. Xie, Z., Ji, C., Guo, X., Zhu, S.: An object detection method for quasi-circular fruits based on improved Hough transform. *Trans. Chin. Soc. Agric. Mach.* **26**(7), 157–162 (2010)
18. Kelman, E.E., Linker, R.: Vision-based localization of mature apples in tree images using convexity. *Biosyst. Eng.* **118**(1), 174–185 (2014). <https://doi.org/10.1016/j.biosystemseng.2013.11.007>
19. Xie, Z., Ji, C., Guo, X., Zhu, S.: Detection and location algorithm for overlapped fruits based on concave spots searching. *Trans. Chin. Soc. Agric. Mach.* **42**(12), 191–196 (2011)
20. Zhao, J., Tow, J., Katupitiya, J.: On-tree fruit recognition using texture properties and color data. In: Proceedings of the IEEE/RSJ International Conference on Intelligent Robots and Systems, pp. 263–268. Edmonton, Canada, 2–6 August 2005. <https://doi.org/10.1109/IROS.2005.1545592>
21. Rakun, J., Stajanko, D., Zazula, D.: Detecting fruits in natural scenes by using spatial-frequency based texture analysis and multiview geometry. *Comput. Electron. Agric.* **76**(1), 80–88 (2011). <https://doi.org/10.1016/j.compag.2011.01.007>
22. Parrish, E.A., Goksel, J.A.K.: Pictorial pattern recognition applied to fruit harvesting. *Trans. Am. Soc. Agric. Eng.* **20**(5), 822–827 (1977). <https://doi.org/10.13031/2013.35657>
23. Sites, P.W., Delwiche, M.J.: Computer vision to locate fruit on a tree. *Trans. Am. Soc. Agric. Eng.* **31**(1), 257–263 (1988). <https://doi.org/10.13031/2013.30697v>
24. Bulanon, D.M., Kataoka, T., Okamoto, H., Hata, S.: Development of a real-time machine vision system for apple harvesting robot. In: Proceedings of the Society of Instrument and Control Engineers Annual Conference, Sapporo, pp. 595–598. Japan, 4–6 August 2004. https://doi.org/10.11499/sicep.2004.0_108_5
25. Seng, W.C., Mirisae, S.H.: A new method for fruits recognition system. In: Proceedings of the 2009 International Conference on Electrical Engineering and Informatics—ICEEI 2009, vol. 1, pp. 130–134. Selangor, Malaysia, 5–7 August 2009. <https://doi.org/10.1109/ICEEI.2009.5254804>
26. Wachs, J.P., Stern, H.I., Burks, T., Alchanatis, V.: Low and high-level visual feature-based apple detection from multi-modal images. *Precis. Agric.* **11**, 717–735 (2010). <https://doi.org/10.1007/s11119-010-9198-x>
27. Tao, Y., Zhou, J.: Automatic apple recognition based on the fusion of color and 3D feature for robotic fruit picking. *Comput. Electron. Agric.* **142**(A), 388–396 (2017). <https://doi.org/10.1016/j.compag.2017.09.019>
28. Krizhevsky, A., Sutskever, I., Hinton, G.E.: ImageNet classification with deep convolutional neural networks. In: Advances in Neural Information Processing Systems 25—NIPS 2012, pp. 1–9. Harrahs and Harveys, Lake Tahoe, Canada, 3–8 December 2012. <https://papers.nips.cc/paper/4824-imagenet-classification-with-deep-convolutional-neural-networks.pdf>. Accessed 10 July 2020

29. Simonyan, K., Zisserman, A.: Very deep convolutional networks for large-scale image recognition. In: International Conference on Learning Representations—ICLR 2015, pp. 1–14. San Diego, CA, USA, 7–9 May 2015. <https://arxiv.org/abs/1409.1556>
30. Williams, H.A.M., Jones, M.H., Nejati, M., Seabright, M.J., MacDonald, B.A.: Robotic kiwifruit harvesting using machine vision, convolutional neural networks, and robotic arms. *Biosyst. Eng.* **181**, 140–156 (2019). <https://doi.org/10.1016/j.biosystemseng.2019.03.007>
31. Redmon, J., Divvala, S., Girshick, R., Farhadi, A.: You only look once: unified, real-time object detection. In: Proceedings of the 29th IEEE Conference on Computer Vision and Pattern Recognition—CVPR 2016, pp. 779–788. Las Vegas, NV, USA, 26 June–1 July 2016. <https://arxiv.org/abs/1506.02640>
32. Tian, Y., Yang, G., Wang, Zh., Wang, H., Li, E., Liang, Z.: Apple detection during different growth stages in orchards using the improved YOLO-V3 model. *Comput. Electron. Agric.* **157**, 417–426 (2019). <https://doi.org/10.1016/j.compag.2019.01.012>
33. Tian, Y., Yang, G., Wang, Zh., Li, E., Liang, Z.: Detection of Apple lesions in orchards based on deep learning methods of CycleGAN and YOLO-V3-Dense. *J. Sens., Special Issue, Sensors in Precision Agriculture for the Monitoring of Plant Development and Improvement of Food Production*, 1–14 (2019). <https://doi.org/10.1155/2019/7630926>
34. Huang, G., Liu, Zh., van der Maaten, L., Weinberger, K.Q.: Densely connected convolutional networks. In: Proceedings of the 30th IEEE Conference on Computer Vision and Pattern Recognition—CVPR 2017, pp. 1–9. Honolulu, HI, USA, 22–25 July 2017. <https://arxiv.org/abs/1608.06993>
35. Kang, H., Chen, C.: Fruit detection, segmentation and 3D visualization of environments in apple orchards. *Comput. Electron. Agric.* **171**, 105302 (2020). <https://doi.org/10.1016/j.compag.2020.105302>
36. Kang, H., Chen, C.: Fast implementation of real-time fruit detection in apple orchards using deep learning. *Comput. Electron. Agric.* **168**, 105108 (2020). <https://doi.org/10.1016/j.compag.2019.105108>
37. Fawcett, T.: An introduction to ROC analysis. *Pattern Recogn. Lett.* **27**(8), 861–874 (2006). <https://doi.org/10.1016/j.patrec.2005.10.010>